

Post-Tensioned Box Girder Design Manual



This page intentionally left blank.

1. Report No. FHWA-HIF-15-016	2. Government Accession No. XXX	3. Recipient's Catalog No. XXX	
4. Title and Subtitle Post-Tensioned Box Girder Design Manual Task 3: Post-Tensioned Box Girder Design Manual		5. Report Date June 2016	
		6. Performing Organization Code XXX	
7. Author(s) Corven, John		8. Performing Organization Report No. XXX	
9. Performing Organization Name and Address Corven Engineering Inc., 2864 Egret Lane Tallahassee, FL 32308		10. Work Unit No. XXX	
		11. Contract or Grant No. DTFH61-11-H-00027	
12. Sponsoring Agency Name and Address Federal Highway Administration Office of Infrastructure – Bridges and Structures 1200 New Jersey Ave., SE Washington, DC 20590		13. Type of Report and Period Covered XXX	
		14. Sponsoring Agency Code HIBS-10	
15. Supplementary Notes Work funded by Cooperative Agreement "Advancing Steel and Concrete Bridge Technology to Improve Infrastructure Performance" between FHWA and Lehigh University.			
16. Abstract This Manual contains information related to the analysis and design of cast-in-place concrete box girder bridges prestressed with post-tensioning tendons. The Manual is targeted at Federal, State and local transportation departments and private company personnel that may be involved in the analysis and design of this type of bridge. The Manual reviews features of the construction of cast-in-place concrete box girder bridges, material characteristics that impact design, fundamentals of prestressed concrete, and losses in prestressing force related to post-tensioned construction. Also presented in this Manual are approaches to the longitudinal and transverse analysis of the box girder superstructure. Both single-cell and multi-cell box girders are discussed. Design examples are presented in Appendices to this Manual. The document is part of the Federal Highway Administration's national technology deployment program and may serve as a training manual.			
17. Key Words Box girder, Cast-in-place, Multi-cell, Concrete, Top Slab, Cantilever Wing, Web, Bottom Slab, Prestressing, Post-tensioning, Strand, Tendon, Duct, Anchorage, Losses, Friction, Wobble, Elastic Shortening, Creep, Shrinkage, Force, Eccentricity, Bending moment, Shear, Torsion, Joint flexibilities, Longitudinal analysis, Transverse analysis		18. Distribution Statement No restrictions. This document is available to the public online and through the National Technical Information Service, Springfield, VA 22161.	
19. Security Classif. (of this report) Unclassified	20. Security Classif. (of this page) Unclassified	21. No of Pages 355	22. Price \$XXX.XX

SI* (MODERN METRIC) CONVERSION FACTORS

APPROXIMATE CONVERSIONS TO SI UNITS

Symbol	When You Know	Multiply By	To Find	Symbol
LENGTH				
in	inches	25.4	millimeters	mm
ft	feet	0.305	meters	m
yd	yards	0.914	meters	m
mi	miles	1.61	kilometers	km
AREA				
in ²	square inches	645.2	square millimeters	mm ²
ft ²	square feet	0.093	square meters	m ²
yd ²	square yard	0.836	square meters	m ²
ac	acres	0.405	hectares	ha
mi ²	square miles	2.59	square kilometers	km ²
VOLUME				
fl oz	fluid ounces	29.57	milliliters	mL
gal	gallons	3.785	liters	L
ft ³	cubic feet	0.028	cubic meters	m ³
yd ³	cubic yards	0.765	cubic meters	m ³
NOTE: volumes greater than 1000 L shall be shown in m ³				
MASS				
oz	ounces	28.35	grams	g
lb	pounds	0.454	kilograms	kg
T	short tons (2000 lb)	0.907	megagrams (or "metric ton")	Mg (or "t")
TEMPERATURE (exact degrees)				
°F	Fahrenheit	5 (F-32)/9 or (F-32)/1.8	Celsius	°C
ILLUMINATION				
fc	foot-candles	10.76	lux	lx
fl	foot-Lamberts	3.426	candela/m ²	cd/m ²
FORCE and PRESSURE or STRESS				
lbf	poundforce	4.45	newtons	N
lbf/in ²	poundforce per square inch	6.89	kilopascals	kPa

APPROXIMATE CONVERSIONS FROM SI UNITS

Symbol	When You Know	Multiply By	To Find	Symbol
LENGTH				
mm	millimeters	0.039	inches	in
m	meters	3.28	feet	ft
m	meters	1.09	yards	yd
km	kilometers	0.621	miles	mi
AREA				
mm ²	square millimeters	0.0016	square inches	in ²
m ²	square meters	10.764	square feet	ft ²
m ²	square meters	1.195	square yards	yd ²
ha	hectares	2.47	acres	ac
km ²	square kilometers	0.386	square miles	mi ²
VOLUME				
mL	milliliters	0.034	fluid ounces	fl oz
L	liters	0.264	gallons	gal
m ³	cubic meters	35.314	cubic feet	ft ³
m ³	cubic meters	1.307	cubic yards	yd ³
MASS				
g	grams	0.035	ounces	oz
kg	kilograms	2.202	pounds	lb
Mg (or "t")	megagrams (or "metric ton")	1.103	short tons (2000 lb)	T
TEMPERATURE (exact degrees)				
°C	Celsius	1.8C+32	Fahrenheit	°F
ILLUMINATION				
lx	lux	0.0929	foot-candles	fc
cd/m ²	candela/m ²	0.2919	foot-Lamberts	fl
FORCE and PRESSURE or STRESS				
N	newtons	0.225	poundforce	lbf
kPa	kilopascals	0.145	poundforce per square inch	lbf/in ²

*SI is the symbol for the International System of Units. Appropriate rounding should be made to comply with Section 4 of ASTM E380. (Revised March 2003)

Visit <http://www.fhwa.dot.gov/publications/convtbl.cfm> for a 508 compliant version of this table.

This page intentionally left blank.

Preface

This Manual contains information related to the analysis and design of cast-in-place concrete box girder bridges prestressed with post-tensioning tendons. The Manual is targeted at Federal, State and local transportation departments and private company personnel that may be involved in the analysis and design of this type of bridge. The Manual reviews features of the construction of cast-in-place concrete box girder bridges, material characteristics that impact design, fundamentals of prestressed concrete, and losses in prestressing force related to post-tensioned construction. Also presented in this Manual are approaches to the longitudinal and transverse analysis of the box girder superstructure. Both single-cell and multi-cell box girders are discussed. Design examples are presented in Appendices to this Manual. The document is part of the Federal Highway Administration's national technology deployment program and may serve as a training manual.

This page intentionally left blank.

Table of Contents

Chapter 1 – Introduction	1
1.1 Historical Overview.....	1
1.2 Typical Superstructure Cross Sections.....	2
1.3 Longitudinal Post-Tensioning Layouts.....	3
1.4 Loss of Prestressing Force.....	6
1.5 Post-Tensioning System Hardware.....	6
1.5.1 Basic Bearing Plates.....	6
1.5.2 Special Bearing Plates or Anchorage Devices.....	7
1.5.3 Wedge Plates.....	8
1.5.4 Wedges and Strand-Wedge Connection.....	8
1.5.5 Permanent Grout Caps.....	8
1.5.6 Ducts.....	9
1.5.6.1 Duct Size.....	9
1.5.6.2 Corrugated Steel Duct.....	9
1.5.6.3 Corrugated Plastic.....	10
1.5.6.4 Plastic Fittings and Connections for Internal Tendons.....	11
1.5.6.5 Grout Inlets, Outlets, Valves and Plugs.....	11
1.5.7 Post-Tensioning Bars Anchor Systems.....	11
1.6 Overview of Construction.....	12
1.6.1 Falsework.....	12
1.6.2 Superstructure Formwork.....	13
1.6.3 Reinforcing and Post-Tensioning Hardware Placement.....	15
1.6.4 Placing and Consolidating Superstructure Concrete.....	15
1.6.5 Superstructure Curing.....	16
1.6.6 Post-Tensioning Operations.....	17
1.6.7 Tendon Grouting and Anchor Protection.....	19
Chapter 2 – Materials	20
2.1 Concrete.....	20
2.1.1 Compressive Strength.....	20
2.1.2 Development of Compressive Strength with Time.....	21
2.1.3 Tensile Strength.....	22
2.1.4 Modulus of Elasticity.....	23
2.1.5 Modulus of Elasticity Variation with Time.....	24
2.1.6 Poisson’s Ratio.....	25
2.1.7 Volumetric Changes.....	25
2.1.7.1 Coefficient of Thermal Expansion.....	25
2.1.7.2 Creep.....	25
2.1.7.3 Shrinkage.....	29
2.2 Prestressing Strands.....	31
2.2.1 Tensile Strength.....	32
2.2.2 Modulus of Elasticity.....	32
2.2.3 Relaxation of Steel.....	33
2.2.4 Fatigue.....	34
2.3 Reinforcing Steel.....	34

Chapter 3 – Prestressing with Post-Tensioning	36
3.1 Introduction	36
3.2 Cross Section Properties and Sign Convention	37
3.3 Stress Summaries in a Prestressed Beam	37
3.4 Selection of Prestressing Force for a Given Eccentricity.....	39
3.5 Permissible Eccentricities for a Given Prestressing Force	46
3.6 Equivalent Forces Due To Post-Tensioning and Load Balancing	48
3.7 Post-Tensioning in Continuous Girders	50
3.9 Tendon Profiles—Parabolic Segments	54
Chapter 4—Prestressing Losses	60
4.1 Instantaneous Losses	60
4.1.1 Friction and Wobble Losses (AASHTO LRFD Article 5.9.5.2.2b)	60
4.1.2 Elongation	66
4.1.3 Anchor Set.....	67
4.1.4 Two-End Stressing	69
4.1.5 Elastic Shortening (AASHTO LRFD Article 5.9.5.2.3b)	71
4.2 Time-Dependent Losses	72
4.2.1 General (AASHTO Article LRFD 5.9.5.4.1)	72
4.2.2 Concrete Shrinkage (AASHTO Article LRFD 5.9.5.4.3a)	73
4.2.3 Concrete Creep (AASHTO Article LRFD 5.9.5.4.3b).....	75
4.2.4 Steel Relaxation (AASHTO Article LRFD 5.9.5.4.3c)	75
Chapter 5—Preliminary Design.....	76
5.1 Introduction	76
5.2 Establish Bridge Layout.....	77
5.2.1 Project Design Criteria.....	77
5.2.2 Span Lengths and Layout.....	78
5.3 Cross Section Selection	79
5.3.1 Superstructure Depth.....	79
5.3.2 Superstructure Width.....	79
5.3.3 Cross Section Member Sizes.....	80
5.3.3.1 Width and Thickness of Cantilever Wing	80
5.3.3.2 Individual and Total Web Thickness	81
5.3.3.3 Top Slab Thickness.....	82
5.3.3.4 Bottom Slab Thickness.....	85
5.3.3.5 Member Sizes for Example Problem	85
5.4 Longitudinal Analysis.....	87
5.4.1 Approach	87
5.4.2 Analysis by Method of Joint Flexibilities	87
5.4.3 Span Properties and Characteristic Flexibilities	87
5.4.4 Analysis Left to Right.....	88
5.4.5 Analysis Right to Left.....	88
5.4.6 Carry-Over Factors.....	89
5.5 Bending Moments	89
5.5.1 Effect of a Unit Uniform Load.....	89
5.5.2 Dead Load—DC (Self Weight and Barrier Railing).....	92
5.5.3 Dead Load—DW (Future Wearing Surface).....	92

5.5.4	Live Load—LL	93
5.5.4.1	Uniform Load Component	93
5.5.4.2	Truck—Positive Moment in Span 1 or 3	93
5.5.4.3	Truck—Positive Moment in Span 2	94
5.5.4.4	Truck—Negative Moment over Piers.....	95
5.5.4.5	Live Load Moment Totals	95
5.5.5	Thermal Gradient (TG)	97
5.5.6	Post-Tensioning Secondary Moments	98
5.6	Required Prestressing Force After Losses	101
5.7	Prestressing Losses and Tendon Sizing for Final Design (Pjack)	103
5.7.1	Losses from Friction, Wobble, and Anchor Set	103
5.7.2	Losses from Elastic Shortening	104
5.7.3	Losses from Concrete Shrinkage.....	105
5.7.4	Losses from Concrete Creep	107
5.7.5	Losses from Steel Relaxation	107
5.7.6	Total of Losses and Tendon Sizing.....	107
5.8	Service Limit State Stress Verifications	107
5.8.1	Service Flexure—Temporary Stresses (DC and PT Only)	108
5.8.2	Service Limit State III Flexure Before Long-Term Losses	109
5.8.3	Service Limit State III Flexure After Long-Term Losses	109
5.8.4	Principal Tension in Webs after Losses	110
5.9	Optimizing the Post-Tensioning Layout	112
Chapter 6—Substructure Considerations		115
6.1	Introduction	115
6.2	Bending Moments Caused by Unit Effects.....	116
6.2.1	Effect of a Unit Uniform Load.....	116
6.2.2	Effect of a Unit Lateral Displacement (Side-Sway Correction)	117
6.2.3	Effect of a Unit Contraction.....	117
6.3	Dead Load—DC (Self Weight and Barrier Railing)	118
6.4	Dead Load—DW (Future Wearing Surface)	118
6.5	Live Load—LL (Lane and Truck Components)	119
6.5.1	Envelope of Uniform Load Component	119
6.5.2	Truck—Positive Moment in Span 1 or 3.....	119
6.5.3	Truck—Positive Moment in Span 2.....	120
6.5.4	Truck—Negative Moment over Piers	120
6.6	Post-Tensioning Secondary Moments—Unit Prestressing Force.....	120
6.7	Thermal Gradient (TG)—20°F Linear	122
6.8	Moments Resulting from Temperature Rise and Fall.....	122
6.8.1	Temperature Rise—40°F Uniform Rise	122
6.8.2	Temperature Fall—40°F Uniform Fall	123
6.9	Moments Resulting from Concrete Shrinkage	123
6.10	Moments Resulting from Concrete Creep.....	125
6.11	Bending Moments Summaries.....	127
6.12	Post-Tensioning Force Comparison (after all losses, with thermal effects)	128
6.12.1	Side Span Positive Bending.....	128
6.12.2	Middle Span Positive Bending	128
6.12.3	Negative Bending at Piers	129

Chapter 7—Longitudinal Analysis & Design	130
7.1 Introduction	130
7.2 Modeling Concepts.....	130
7.2.1 Straight Bridges Supported on Bearings.....	131
7.2.1.1 Nodes	131
7.2.1.2 Elements.....	132
7.2.1.3 Post-Tensioning	134
7.2.2 Straight Bridges with Integral Piers.....	134
7.2.3 Curved Bridges.....	136
7.2.4 Other Three-Dimensional Analyses	143
7.3 Strength Limit Verification—Flexure	145
7.3.1 Factored Loads for Longitudinal Flexure.....	146
7.3.2 Flexural Resistance	148
7.3.2.1 Strain Compatibility	149
7.3.2.2 Material Stresses and Internal Forces	150
7.3.2.3 Internal Equilibrium	153
7.3.3 Resistance Factors (ϕ).....	155
7.3.4 Limits of Reinforcing	156
7.3.5 Procedure.....	157
7.4 Strength Limit Verification—Shear.....	163
7.4.1 LRFD Design Procedures for Shear and Torsion.....	163
7.4.2 General Requirements.....	164
7.4.3 Sectional Model Nominal Shear Resistance	165
7.4.3.1 Effective Web Width.....	166
7.4.3.2 Effective Shear Depth	168
7.4.4 Shear Resistance from Concrete (V_c).....	169
7.4.4.1 Method 2 (Simplified MCFT)	169
7.4.4.2 Method 3 (Historical Empirical).....	173
7.4.5 Shear Resistance from Transverse (Web) Reinforcing Steel (V_s).....	174
7.4.6 Shear Resistance from Vertical Component of Effective Prestressing (V_p) ..	175
7.4.7 Longitudinal Reinforcing	177
7.4.8 Torsion Reinforcing	178
Chapter 8—Transverse Analysis	179
8.1 Introduction	179
8.2 Methods of Analysis	179
8.3 Applicable AASHTO LRFD Specifications	180
8.3.1 Section 9—Deck and Deck Systems	180
8.3.2 Section 3—Loads	182
8.3.3 Section 4—Analysis.....	185
8.3.4 Section 13—Railing	188
8.4 Strip Method Analysis for a Multi-Cell Box Girder Superstructure	190
8.4.1 The Transverse Model.....	191
8.4.2 Transverse Bending Moment Results	192
8.4.3 Transverse Design Moments.....	194
8.5 Top Slab Transverse Bending Moment Results for a Single-Cell Box Girder.....	195
8.5.1 Introduction.....	195
8.5.2 Analysis for Uniformly Repeating Loads	197
8.5.3 Analysis for Concentrated Wheel Live Loads.....	199
8.5.4 Live Load Moments in Cantilever Wings.....	200

8.5.5	Negative Live Load Moments in the Top Slab.....	201
8.5.6	Positive Live Load Moments at Centerline of the Top Slab.	204
8.6	Transverse Post-Tensioning.....	206
8.6.1	Transverse Post-Tensioning Tendon Layouts.....	206
8.6.2	Required Prestressing Force	206
8.6.3	Transverse Post-Tensioning Tendon Placement and Stressing.....	208
Chapter 9—Other Design Considerations		210
9.1	Effects of Curved Tendons	210
9.1.1	In-Plane and Out-of-Plane Forces	211
9.1.2	AASHTO LRFD Design Approach	213
9.1.3	Regional Effects—Transverse (Regional) Bending.....	213
9.1.4	Local Shear and Flexure in Webs.....	216
9.1.4.1	Shear Resistance to Pull-out.....	217
9.1.4.2	Cracking of Concrete Cover	218
9.1.5	Out-of-Plane Force Effects	220
9.2	End Anchorage Zones.....	220
9.3	Diaphragms at Supports	222
9.3.1	Single-Cell Box Girder Transfer of Vertical Shear to Bearings.....	222
9.3.2	Single-Cell Box Girder Transfer of Torsion to Bearings	224
9.3.3	Multi-Cell Box Girder Diaphragms	225
Appendix A – Analysis of Two-Dimensional Indeterminate Structures by the Flexibility Method.....		227
Appendix B – Torsion		260
Appendix C – Example 1: Multi-Cell Box Girder Bridge		280
Appendix D – Example 2: Curved Two-Cell Box Girder Bridge		322

List of Figures

Figure 1.1	Cast-in-Place Post-Tensioned Box Girder Bridge for MARTA.....	1
Figure 1.2	Typical Span Ranges for Prestressed Concrete Bridge Types	2
Figure 1.3	Multi-Cell Box Girder Cross Section	3
Figure 1.4	Single-Cell Box Girder Cross Section	3
Figure 1.5	Typical Post-Tensioning Tendon Layout for Simple Spans.....	4
Figure 1.6	Tendon Layout for 4-Span Bridge, CIP on Falsework.....	4
Figure 1.7	Tendon Locations within Box Girder Cross Section	5
Figure 1.8	Possible Tendon Layout for Sequentially Cast Spans	5
Figure 1.9	Basic Bearing Plate Anchorage System	6
Figure 1.10	Multi-Plane Anchorage System (Courtesy of VSL)	7
Figure 1.11	Anchorage System for Flat Duct Tendon (Courtesy of DSI).....	7
Figure 1.12	Permanent Plastic Grout Caps (Courtesy of VSL)	9
Figure 1.13	Corrugated Metal Duct	10
Figure 1.14	Corrugated Plastic Duct.....	10
Figure 1.15	Typical High-Point Grout Vent	11
Figure 1.16	Post-Tensioning Bar Anchorage System (Courtesy of DSI).....	12
Figure 1.17	Modular Falsework Units for Cast-in-Place Construction.....	12
Figure 1.18	Steel Pipe Support Towers for Cast-In-Place Construction.....	13
Figure 1.19	Web and Cantilever Wing Formwork for a Single-Cell Box Girder	14
Figure 1.20	Web Formwork for a Multi-Cell Box Girder	14
Figure 1.21	Web and Bottom Slab Reinforcing, Tying Post-tensioning Ducts in Webs	15
Figure 1.22	Placing Deck Concrete and Finishing with a Roller Screed	16
Figure 1.23	Curing the Concrete Deck	17
Figure 1.24	Bundled Tendon Prepared for Pulling.....	18
Figure 1.25	Stressing Post-Tensioning Tendons.....	18
Figure 2.1	Concrete strength gain with time	22
Figure 2.2	Typical Stress-Strain Curve for Concrete	23
Figure 2.3	Concrete Modulus of Elasticity with Time	24
Figure 2.4	Creep of Concrete.....	25
Figure 2.5	Creep of Concrete (with no long-duration transient loads).....	26
Figure 2.6	Development of Concrete Creep with Time	29
Figure 2.7	Development of Concrete Shrinkage with Time.....	30
Figure 2.8	Rate of Concrete Shrinkage over Time.....	31
Figure 2.9	Stress-Strain Diagram for Prestressing Strand (Courtesy of PCI).....	33
Figure 2.10	Comparison of Typical Stress-Strain Relationships for Prestressing Strand and Mild Reinforcing.....	35
Figure 3.1	Prestressed Concrete Concepts.....	36
Figure 3.2	Cross Section Nomenclature and Sign Convention	37
Figure 3.3	Self Weight Flexure Stress in Simply-Supported Beam	38
Figure 3.4	Self Weight Plus Uniform Axial Compression	38
Figure 3.5	Self Weight, Axial and Eccentric Prestress Stresses	39
Figure 3.6	Efficiencies of Various Cross Sections	40
Figure 3.7	Internal Equilibrium for Positive Bending	41
Figure 3.8	Internal Equilibrium for Negative Bending.....	42
Figure 3.9	Limiting Eccentricities for Zero Tension Under Axial Force Only.....	43
Figure 3.10	Kern of a Cross Section for Bending About the Horizontal Axis	43
Figure 3.11	Example Concrete I-Girders	44
Figure 3.12	Limiting Eccentricities for the Example Bridge	48
Figure 3.13	Parabolic Tendon Profile for a Simple Span Girder	48

Figure 3.14	Equivalent Forces Resulting from Prestressing	49
Figure 3.15	Restraining Moments in Continuous Girders	51
Figure 3.16	Prestressing Moments for a Two-Span Continuous Girder	52
Figure 3.17	Total Prestressing Moments for a Two-Span Continuous	53
Figure 3.18	Tendon Profile Parabolic Segment	54
Figure 3.19	Typical End Span Tendon Profile for Continuous Superstructures	55
Figure 3.20	Typical Interior Span Tendon Profile for Continuous	55
Figure 3.21	Example Tendon Profile Parabolic Segments	56
Figure 3.22	Curvature Diagram for Prestressing	57
Figure 3.23	Curvature Diagram for Prestressing	57
Figure 3.24	Loaded Conjugate Beam	58
Figure 4.1	Friction and Wobble	60
Figure 4.2	Section of Tendon with Radial Alignment	61
Figure 4.3	Cross Section of Superstructure for Design Example 1	63
Figure 4.4	Tendon Profiles for Design Example 1	64
Figure 4.5	Tendon T2 Profile and Angular Deviations	64
Figure 4.6	Tendon Loss Calculations—Friction and Wobble	66
Figure 4.7	Anchor Set	68
Figure 4.8	Tendon Force Diagram after Anchor Set at End A	68
Figure 4.9	Tendon Force Diagram after Stressing from End B	70
Figure 4.10	Final Tendon Force Diagram (After Anchor Set at End B)	70
Figure 5.1	CIP Box Girder Bridge Preliminary Design Flow Chart	76
Figure 5.2	3-Span Box Girder Bridge for Preliminary Design	76
Figure 5.3	Existing, At-Grade Highway Cross Section to Be Spanned by Proposed Bridge	77
Figure 5.4	Span Layout for Preliminary Design Example	78
Figure 5.5	Bridge Width and Roadway Features	80
Figure 5.6	Cantilever Wing Dimensions	80
Figure 5.7	Top Slab Span and Thickness	84
Figure 5.8	Top Slab with Haunches	84
Figure 5.9	Example Cross Section Dimensions for Preliminary Design	86
Figure 5.10	Model of 3-Span Bridge for Example 1	87
Figure 5.11	Moment Diagram for a Unit Uniform Load	91
Figure 5.12	Moment Diagram for Dead Load (DC)	92
Figure 5.13	Moment Diagram for Dead Load (DW)	92
Figure 5.14	Uniform Live Load Moment Envelope	93
Figure 5.15	Simple Beam Rotations for a Concentrated Load	93
Figure 5.16	Moment Diagram for HL-93 Design Truck in Span 1 (Positive Bending)	94
Figure 5.17	Moment Diagram for HL-93 Design Truck in Span 2 (Positive Bending)	94
Figure 5.18	Moment Diagram for Two HL-93 Design Trucks about Pier 2 (Negative Bending)	95
Figure 5.19	Simple Beam Subjected to 20°F Positive Linear Gradient	97
Figure 5.20	Moment Diagram for a 20°F Positive Linear Gradient	98
Figure 5.21	Possible Tendon Locations at Mid-Span at over the Piers	99
Figure 5.22	Center of Gravity Profile of Prestressing (End Spans)	99
Figure 5.23	Center of Gravity Profile of Prestressing (Middle Span)	100
Figure 5.24	Conjugate Beam and Loads (End Spans)	100
Figure 5.25	Conjugate Beam and Loads (Main Span)	100
Figure 5.26	Secondary Prestressing Moments, M2(F)	101
Figure 5.27	Friction Diagram for the CG Profile Tendon	104
Figure 5.28	Mohr Circle for Location of Maximum Shear in Middle Span	112
Figure 5.29	Revised Center of Gravity Profile of Prestressing (End Spans)	113

Figure 5.30	Revised Conjugate Beam and Loads (End Spans).....	113
Figure 5.31	Revised Secondary Prestressing Moments, $M_2(F)$	114
Figure 6.1	Example CIP Box Girder Bridge Elevation.....	115
Figure 6.2	Bridge Cross Section at Piers.....	115
Figure 6.3	Effect of a Unit Uniform Load	116
Figure 6.4	Effect of a Unit Lateral Displacement (Side-sway Correction).....	117
Figure 6.5	Effect of a Unit Contraction.....	117
Figure 6.6	Effect of Dead Load (DC)	118
Figure 6.7	Effect of Dead Load (DW)	118
Figure 6.8	Uniform Live Load Moment Envelope	119
Figure 6.9	Moment Diagram for HS20 Truck in Span 1 or 3	119
Figure 6.10	Moment Diagram for HS20 Truck in Span 2	120
Figure 6.11	Moment Diagram for Two HS20 Trucks about Pier 2.....	120
Figure 6.12	Secondary Prestressing Moments, $M_2(F)$	121
Figure 6.13	Moment Diagram for a 20°F Positive Linear Gradient.....	122
Figure 6.14	Moment Diagram for 40° Temperature Rise	122
Figure 6.15	Moment Diagram for 40° Temperature Fall	123
Figure 6.16	Moment Diagram for Concrete Shrinkage	124
Figure 6.17	Moment Diagram for Concrete Creep.....	127
Figure 7.1	Example Straight Bridge on Bearings.....	131
Figure 7.2	Box Girder Superstructure Cross Section.....	131
Figure 7.3	Two-Dimensional Analysis Model.....	132
Figure 7.4	Typical Element Stiffness Matrix for a Plane Frame Member with 3DOF Nodes	133
Figure 7.5	Cross Section Properties for the Box Girder shown in Figure 7.2	133
Figure 7.6	Cross Section of Design Example 1 Bridge at the Piers	134
Figure 7.7	Two-Dimensional Analysis Model with Integral Piers.....	135
Figure 7.8	Detail of Model at Pier	135
Figure 7.9	Curved Bridge of Design Example 2.....	136
Figure 7.10	Design Example 2 Bridge	137
Figure 7.11	3D Model for Bridge in Design Example 2.....	137
Figure 7.12	Cross Section of Design Example 2 Bridge at the Piers	138
Figure 7.13	3D Model for Bridge in Design Example 2 at the Piers	138
Figure 7.14	Torsion in a Single Cell Box Girder.....	139
Figure 7.15	Torsion in a Two-Cell Box Girder.....	140
Figure 7.16	Cross Section of Bridge in Example 1, Appendix C	142
Figure 7.17	Grillage Model Development for Design Example 2.....	144
Figure 7.18	Grillage Model Design Example 2	144
Figure 7.19	Cross Section of Shell Element FEM Model for Design Example 2	145
Figure 7.20	Flexural Resistance by Strain Compatibility.....	149
Figure 7.21	Rectangular Stress Block to represent Concrete Compression	150
Figure 7.22	Comparison of Typical Stress-Strain Relationships for Prestressing Strand and Mild Reinforcing	151
Figure 7.23	Stress-Strain Relationships for Prestressing Strand	153
Figure 7.24	Flexural Resistance with Multiple Layers of Prestressing Steel and Mild Reinforcing.....	154
Figure 7.25	Transition of Resistance Factors from Compression to Tension Controlled	155
Figure 7.26	Flow Chart for Verification of Flexure at the Strength Limit State.....	158
Figure 7.27	Idealized Cross Section For Longitudinal Flexure.....	159
Figure 7.28	Location of Prestressing Reinforcing in Idealized Cross Section	159
Figure 7.29	Web Width based on Horizontal Widths	165

Figure 7.30	Web Width based on Horizontal Widths	166
Figure 7.31	Shear Flow in Single Cell Box Girder.....	167
Figure 7.32	Shear Stress and Shear Flow Around Ducts	168
Figure 7.33	Effective Depth for Shear Calculations	168
Figure 7.34	Actual vs. MCFT Girders	170
Figure 7.35	MCFT Forces and Longitudinal Strain	171
Figure 7.36	Types and Locations of Reinforced and Prestressed Girder Cracking.....	173
Figure 7.37	Contribution of Shear Reinforcing to Nominal Shear Resistance	174
Figure 7.38	Simple Span Beam with Parabolically Draped Tendon.....	176
Figure 7.39	Typical Tendon Profile for an End Span of a Continuous Unit	176
Figure 7.40	Typical Tendon Profile for an Interior Span of a Continuous Unit.....	177
Figure 7.41	Tendon Profile Parabolic Segment	177
Figure 8.1	Concrete Box Girder Cross Sections and Loads	179
Figure 8.2	AASHTO LRFD Design Truck and Design Tandem.....	182
Figure 8.3	Transverse Truck Placement.....	183
Figure 8.4	Tire Contact Area in the Transverse Direction	184
Figure 8.5	Alternate Vertical Loading for Overhang Design.....	184
Figure 8.6	Perspective of Multi-cell Box Girder.....	185
Figure 8.7	Transverse Strip for Approximate Design Method	186
Figure 8.8	Transverse Strip subjected to two Design Trucks.....	186
Figure 8.9	Critical Sections for Overhang Design to Develop Barrier Railing.....	189
Figure 8.10	Developing the Two-Dimensional Transverse Model.....	191
Figure 8.11	Transverse Self Weight Moments (ft-kip/ft).....	192
Figure 8.12	Transverse Barrier Railing Moments (ft-kip/ft)	192
Figure 8.13	Transverse Wearing Surface Moments (ft-kips/ft).....	192
Figure 8.14	Maximum Negative Design Truck Moment in Outer Web	193
Figure 8.15	Maximum Negative Design Truck Moment at Inner Web.....	193
Figure 8.16	Maximum Positive Design Truck Moment in Top Slab.....	193
Figure 8.17	Typical Single-Cell Box Girder Cross Section Defined at Mid-Span.....	195
Figure 8.18	Typical Single-Cell Box Girder Span with Cross Section Defined at Mid-Span.....	196
Figure 8.19	One-Foot Section of Typical Cross Section	196
Figure 8.20	Developing the Two-Dimensional Transverse Model.....	197
Figure 8.21	Transverse Bending Moments for Uniformly Repeating Loads	198
Figure 8.22	Truck Loads on a Single-Cell Box Girder Span	199
Figure 8.23	Truck Location for Maximum Transverse Bending Moment at Root of Cantilever.....	200
Figure 8.24	Loaded Influence Surface for the Cantilever Wing.....	200
Figure 8.25	Distribution of Cantilever Live Load Moments in the Cross Section	201
Figure 8.26	Final Bending Moments for Live Load in Cantilever.....	201
Figure 8.27	Truck Location for Maximum Transverse Bending Moment at Middle of Top Slab	202
Figure 8.28	Influence Surface for Maximum Negative Bending at the Left End of the Top Slab	202
Figure 8.29	Influence Surface for Maximum Negative Bending at the Right End of the Top Slab	202
Figure 8.30	Distribution of Fixed-End Live Load Moments for Maximum Negative Moment Case.....	203
Figure 8.31	Summed Live Load Moments for the Maximum Negative Moment Case.....	203
Figure 8.32	Live Load Position for Maximum Positive Bending	204
Figure 8.33	Maximum Positive Moment in the Top Slab for Fixed-End Conditions.....	205
Figure 8.34	Distribution of Fixed-End Live Load Moments for Maximum	

	Negative Moment Case	205
Figure 8.35	Summed Live Load Moments for the Maximum Positive Moment Case	205
Figure 8.36	Typical Transverse Tendon Layout	206
Figure 8.37	Transverse Duct Placement in Casting Machine	209
Figure 8.38	Mono-Strand Stressing of a 4 Strand Tendon and Anchorage After Stressing 2nd Strand.....	209
Figure 9.1	Curved Tendon Deviations	210
Figure 9.2	Tendons in Curved Superstructures	210
Figure 9.3	Cross Section of Multi-Cell Box Girder with Lateral Tendon Loads.....	211
Figure 9.4	Tendon Plane of Curvature	211
Figure 9.5	In-Plane and Out-of-Plane Tendon Forces	212
Figure 9.6	Hypothetical Concrete Member Completely Coincident with a Tendon.....	213
Figure 9.7	Post-Tensioning a Curved Plate	214
Figure 9.8	Web Flexure Restrained by Top and Bottom Slabs	214
Figure 9.9	Web Transverse (Regional) Bending Moments	215
Figure 9.10	Web Height for Equation 9.3	216
Figure 9.11	Parameters for Local Shear and Flexure Design	216
Figure 9.12	Effective Length of Failure Plane for Equation 9.6.....	217
Figure 9.13	Effective Length of Failure Plane for Equations 9.7 and 9.8	218
Figure 9.14	Local Bending Moments for Evaluating Cracking of Concrete Cover	219
Figure 9.15	Details of End of Post-Tensioned Box Girder Bridge	220
Figure 9.16	End Zone Design Development.....	221
Figure 9.17	Concentric Web/Bearing Orientation	222
Figure 9.18	Eccentric Web/Bearing Orientation.....	222
Figure 9.19	General Shear Friction and Localized Direct Tension.....	223
Figure 9.20	Vertical Force Transfer with Inclined Webs.....	223
Figure 9.21	Transverse Post-Tensioning in Diaphragms.....	224
Figure 9.22	Shear Flow Resulting from Torsional Forces	224
Figure 9.23	A-shaped Torsion Diaphragm.....	225
Figure 9.24	V-shaped Torsion Diaphragm.....	225
Figure 9.25	Possible Strut-and-Tie Layout for Diaphragm of Design Example 1	226
Figure 9.26	Strut-and-Tie Layout Considering Monolithic Column Connection	226
Figure A.1	Continuous Beam Load, Shear and Moment Diagrams.....	228
Figure A.2	Bending Moment and Rotation Sign Convention	229
Figure A.3	Equations for End Rotations of Simple Beams	229
Figure A.4	Bending Moment Diagram for Unit Moment at Node i.....	229
Figure A.5	Bending Moment Diagram for Unit Moment at Node j.....	230
Figure A.6	Simple Span Beam Characteristics	230
Figure A.7	Span ij in a Continuous Unit	231
Figure A.8	Isolating Span ij.....	232
Figure A.9	Compatible rotations of adjacent members.....	232
Figure A.10	Adjacent Member Flexibilities	233
Figure A.11	Member End Flexibility for Span hi	235
Figure A.12	Carry Over Factor from j to i.....	237
Figure A.13	Moment Equilibrium at Node i	239
Figure A.14	Model of 3-Span Bridge for Example 1	242
Figure A.15	Moment Diagram for a Unit Uniform Load	245
Figure A.16	Moment Diagram for a Unit Uniform Load	246
Figure A.17	Cantilever Column.....	246
Figure A.18	Column with Multiple Elements.....	248
Figure A.19	Column in a Rigid Frame.....	249
Figure A.20	Model of 3-Span Bridge for Example 1	250

Figure A.21	Moment Diagram for a Unit Uniform Load	257
Figure A.22	Moment Diagram for a Unit Lateral Side-Sway	259
Figure B.1	Circular Bar Subjected to Torsional Moment	260
Figure B.2	Segmented Circular Bar	261
Figure B.3	Kinematic Study 1	261
Figure B.4	Kinematic Study 2	262
Figure B.5	Kinematic Study 3	262
Figure B.6	Linear Twisting of the Circular Bar	263
Figure B.7	Shear Stresses and Shear Strains in the Circular Bar	263
Figure B.8	Element of the Circular Bar	264
Figure B.9	Closed Thin-Wall Shaft.....	266
Figure B.10	Segment of Closed, Thin-Wall Shaft.....	267
Figure B.11	Equilibrium in the Cross Section of the Thin Wall Closed Shaft	268
Figure B.12	Example Single Cell Box Girder	271
Figure B.13	Idealized Thin-Walled Members	272
Figure B.14	Two-Cell Box Girder Superstructure	274
Figure B.15	Example Two-Cell Box Girder	276
Figure B.16	Example Four-Cell Box Girder.....	278
Figure C.1	Elevation of Example 1 Bridge.....	280
Figure C.2	Cross Section through Example 1 Bridge	280
Figure C.3	Cross Section Dimensions	283
Figure C.4	Self Weight and Component Bending Moments	288
Figure C.5	Future Wearing Surface Bending Moments	288
Figure C.6	Concrete Creep Bending Moments	289
Figure C.7	Concrete Shrinkage Bending Moments	289
Figure C.8	Live Load Envelope Bending Moments	290
Figure C.9	Initial Post-Tensioning Bending Moments.....	290
Figure C.10	Bending Moments for Post-Tensioning Losses.....	291
Figure C.11	Final Post-Tensioning Moments	291
Figure C.12	Mohr's Circle	308
Figure C.13	State of Stress at Node 252	308
Figure C.14	Overhang Design Sections.....	314
Figure C.15	Equilibrium at Strength Limit State	315
Figure C.16	Length of Loaded Areas	317
Figure C.17	Live Load on Overhang	318
Figure D.1	Curved Bridge of Design Example 2.....	322
Figure D.2	Elevation of Example 2 Bridge.....	323
Figure D.3	Cross Section through Example 2 Bridge	323
Figure D.4	Cross Section Dimensions	325
Figure D.5	Frame Model for Transverse Analysis	327
Figure D.6	Load Location for Maximum Positive Flexure at Node 6.....	328

List of Tables

Table 3.1	Limiting Eccentricities for Example Girder	47
Table 4.1	Tendon Loss Calculations—Friction and Wobble	65
Table 4.2	Tendon Elongation	67
Table 5.1	Moment Components of Service Level III Loading at Three Locations	102
Table 5.2	Data for Friction Diagram for the CG Profile Tendon	103
Table 6.1	Bending Moments for Bridge on Bearings and Bridge with Fixed Piers	128
Table 7.1	Example Bridge 1 Bending Moments (ft-kips).....	148
Table 7.2	Example Bridge 1 Bending Moments (ft-kips).....	148
Table 8.1	Railing Loads for TL-4 Barrier (from AASHTO LRFD Table A13.2-1)	189
Table 8.2	Transverse Bending Moment Results from Frame Analysis	194
Table 8.3	Transverse Bending Moment Results from Frame Analysis	207
Table 8.4	Transverse Bending Moment Results from Frame Analysis	208
Table B.1	Coordinates of Points Defining the Thin-Walled Section.....	272
Table B.2	Thin-Walled Section Member Dimensions.....	272
Table C.1	Service Limit State Load Factors.....	292
Table C.2	Service Limit State Flexural Verifications.....	294
Table C.3	Strength Limit State Load Factors	295
Table C.4	Flexural Strength Design Verifications.....	299
Table C.5	Summary of Shear Design at Strength Limit State.....	306
Table C.6	Principal Tensile Stress Summary	309
Table C.7	Load Factors for Overhang Design.....	313
Table D.1	Fixed End Moments for Maximum Flexure at Node 6	328
Table D.2	Design Live Load Moments	329
Table D.3	Service Limit State Load Factors.....	329
Table D.4	Top Slab Stresses at Stressing of PT	330
Table D.5	Top Slab Stresses due to DC, DW, CR, SH after all losses.....	331
Table D.6	Top Slab Stresses From Service I (Compression) and Service III (Tension) Load Combinations	331
Table D.7	Strength I Load Factors for Transverse Analysis	332
Table D.8	Ultimate Moments for Transverse Design.....	332
Table D.9	Ultimate Capacity of the Top Slab	333
Table D.10	ϕM_n vs. $1.33 \cdot M_u$	333
Table D.11	Positive Bending Reinforcement, Bottom Slab and Webs.....	334
Table D.12	Negative Bending Reinforcement, Bottom Slab and Webs	334
Table D.13	Extreme Event II Load Factors	335
Table D.14	Number of Lanes per Web—Bending	340
Table D.15	Number of Lanes per Web—Shear	341
Table D.16	Service Load Combinations.....	342
Table D.17	Change in Superstructure Stresses over Time	344
Table D.18	Stress Summaries	345
Table D.19	Strength Limit State Design Factors	346
Table D.20	Factored Moments	349
Table D.21	Verification of Torsion Considerations	351
Table D.22	Ultimate Shear at Node 27	353
Table D.23	Verification of Torsion Considerations	355
Table D.24	Shear at Node 26	356
Table D.25	Ultimate Shear Forces.....	357
Table D.26	Concrete Shear Capacity, V_{ci}	358
Table D.27	Concrete Shear Capacity, V_{cw}	358
Table D.28	Required Web Reinforcing for Shear	359

Table D.29	Regional Web Bending Due to PT Moments and Required Reinforcing	360
Table D.30	Shear Reinforcing Requirements.....	362
Table D.31	Shear Reinforcing Design Regions.....	362
Table D.32	Web Bending Reinforcing Requirements.....	363
Table D.33	Final Web Reinforcing at Each Face of Each Web	364
Table D.34	Results of Principal Tension Check	367
Table D.35	Verification of Longitudinal Shear Reinforcing	368

Chapter 1—Introduction

The objective of this manual is to present design methodologies for cast-in-place concrete box girder bridges post-tensioned with internal post-tensioning tendons, within the framework of the AASHTO LRFD Bridge Design Specifications (2012). The target audience for this manual is a graduate civil engineer with one year of bridge design experience. The manual presumes that the target audience has been exposed to prestressed concrete concepts, but does not necessarily have prestressed concrete design experience.

1.1 Historical Overview

The origin of reinforced concrete bridge construction in the United States dates back to 1889 with the construction of the Alvord Lake Bridge in San Francisco, California. Though many advancements have been made, basic features of construction remain unchanged. The work requires construction of formwork to contain and provide shape to the wet concrete. Formwork is supported by falsework either resting on the ground or on prepared foundations, until the structure itself is self-supporting and formwork and/or falsework can be removed. Unfortunately, bridges constructed with reinforced concrete are only economical for relatively short spans. Superstructure types include flat slabs, beam with slabs, and box girders. At the time, longer spans were achieved by using arch construction.

Reinforced concrete box girder bridge construction flourished in the western part of the United States as a result of economy and local contractor experience. The California Department of Transportation (Caltrans) began constructing box girder bridges in the early 1950's. With the popularization of prestressed concrete technology in the early 1960's, Caltrans realized further economy through the construction of many post-tensioned concrete box girder bridges. Refinements to post-tensioned box girder bridge construction continued throughout the United States in the second half of the 20th century. Figure 1.1 shows two views of a cast-in-place post-tensioned box girder bridge.



Figure 1.1 – Cast-in-Place Post-Tensioned Box Girder Bridge for the Metropolitan Atlanta Regional Transit Agency (MARTA) – under construction (left), completed (right)

Today, cast-in-place post-tensioned box girder construction is used throughout the United States. The majority of this type of construction still occurs in western states, with much less frequency in other parts of the U.S. Reasons for this are varied, but stem from historical and regional developments—steel bridge construction in the northeast, precast prestressed beams in southern states, cast-in-place box girders in the west, etc. Though regional construction experience and expertise affect construction costs and consequently type selection, the need for further construction economy and alternate project delivery methods have led to a wider range of project specific bridge type evaluations.

Figure 1.2 shows a chart of applicable span ranges for the major types of prestressed concrete bridges. The span range for cast-in-place box girder construction is shown to vary from 100 feet to 250 feet. The lower end of the span range represents simple span bridges, shallow box girder bridges with depths restricted by vertical clearances, or bridges following highly curved alignments. The upper end of the span range represents continuous bridges, bridges with no restriction on box girder depth, or bridges on a tangent alignment. Longer span lengths can be achieved by using a variable depth structure, with deeper sections at piers to resist high negative moment demands.

The flexibility to accommodate a wide variety of span lengths and bridge geometries, over the most common range of highway bridge spans, is one of the excellent benefits of cast-in-place box girder construction. Other significant benefits include internal redundancy (multiple load paths), torsional stiffness and strength, and construction economy less sensitive to overall bridge size and aesthetics.

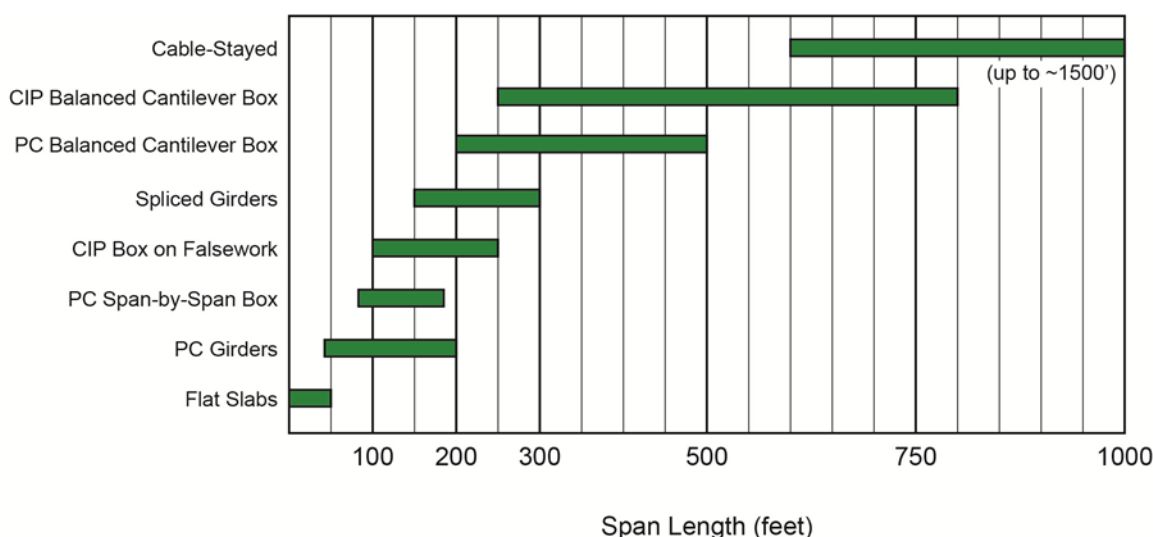


Figure 1.2 – Typical Span Ranges for Prestressed Concrete Bridge Types

1.2 Typical Superstructure Cross Sections

The superstructure cross sections of post-tensioned box girder bridges are typically multi-cell or single-cell box girders. A typical cross section of multi-cell box girder bridge is shown in figure 1.3. Figure 1.4 shows a typical cross section for a single-cell box girder superstructure.

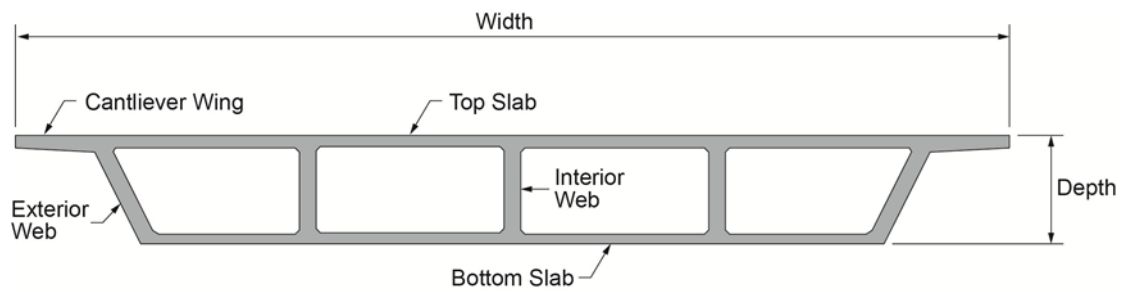


Figure 1.3 – Multi-Cell Box Girder Cross Section

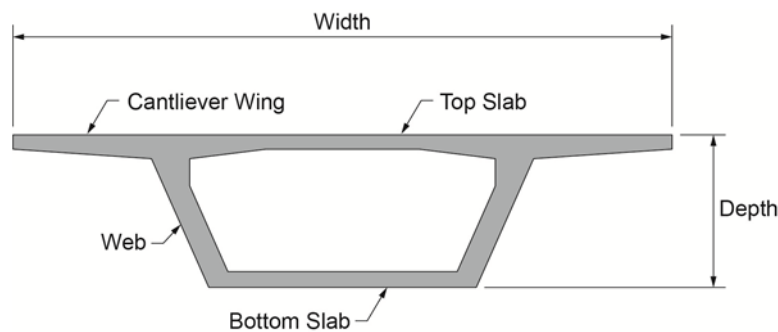


Figure 1.4 – Single-Cell Box Girder Cross Section

The basic components of the cross section are:

- Top slab—the entire width of concrete deck, including the portions between the webs and the overhangs outside of the webs.
- Overhangs (cantilever wings)—the overhanging portion of the top slab.
- Webs—vertical or inclined, exterior or interior.
- Bottom slab.

Multi-cell girder cross sections as shown in figure 1.3 can be used for bridges of nearly any width, by varying the spacing between, and/or, changing the number of webs. Widths of single-cell box girders typically range from 25 feet to 60 feet, though there are single-cell box girder cross sections as wide as 80 feet. This wide range of widths of single-cell box girders is achieved through the use of transverse post-tensioning within the top slab to control tensile stresses under the action of the permanent dead and live wheel loads plus impact effects.

1.3 Longitudinal Post-Tensioning Layouts

Cast-in-place box girder bridges are prestressed using post-tensioning tendons cast within the web concrete. These tendons are usually draped following parabolic profiles as shown in figure 1.5. The tendon profiles are low in the cross section at the center of the span and rise in elevation at the ends of the span. The vertical distance from the neutral axis of the bridge to the centroid of a post-tensioning tendon is called the tendon eccentricity (e). The force in the tendon multiplied by the eccentricity forms the *primary moment* due to post-tensioning. The primary moment, along with the axial compression induced by the post-tensioning, work to offset the longitudinal tensile stresses in the superstructure resulting from bridge self weight and

other applied loads. Vertical components of the prestressing force can offset or add to the shear demand of the webs.

Tendons for simple span bridges are grouped closely together at the bottom of the bridge web at mid-span to maximize tendon eccentricity. The spacing of the tendons increases at the ends of the span to appropriately locate the post-tensioning anchorages. Post-tensioning anchorages are cast into diaphragms constructed at the ends of the spans. The diaphragms, which are solid concrete sections, transfer and distribute the tendon forces acting on the anchorages to the typical cross section of the box girder.

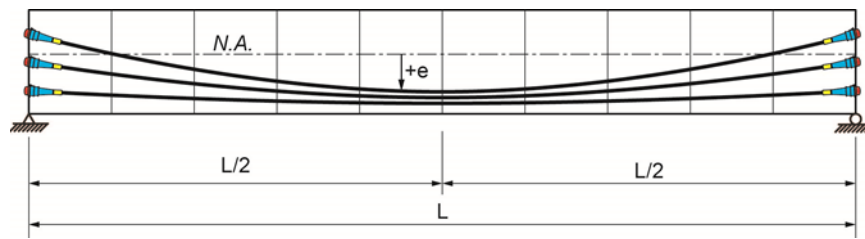


Figure 1.5 – Typical Post-Tensioning Tendon Layout for Simple Spans

Continuous post-tensioned box girder construction is achieved by stressing long tendons that reach the full length of the continuous unit. The tendons are anchored at either end of the unit with geometry similar to the ends of simple spans. Within the spans of the continuous unit, the tendons drape with geometry similar to that shown in figure 1.6. Tendon profiles are low in the section within the span and high in sections over interior piers. Figure 1.7 shows the tendons in the webs in cross section view at mid-span and over the piers.

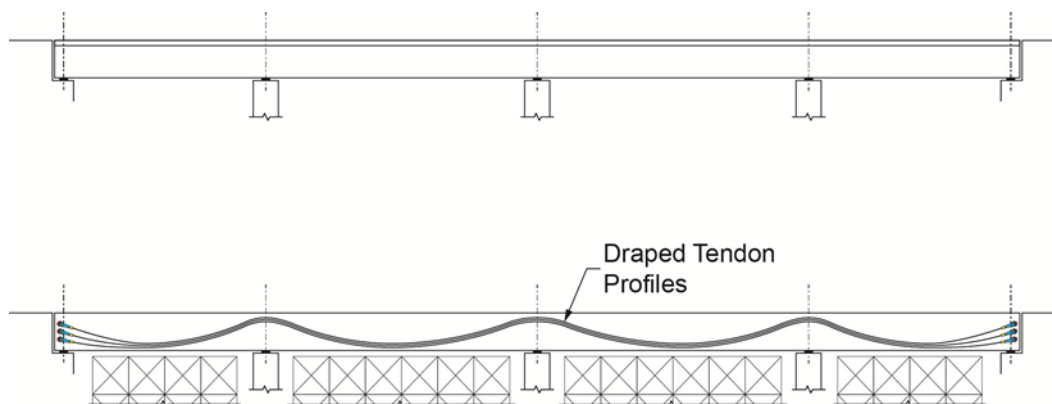


Figure 1.6 – Tendon Layout for 4-Span Bridge, CIP on Falsework

Primary moments resulting from the post-tensioning are the same in both simply supported and continuous structures. In a continuous superstructure, however, restraint of end rotations by adjacent spans and monolithic columns cause the development of secondary moments due to the post-tensioning. For tendon profiles similar to those shown in figure 1.6, the secondary moments reduce the effect of primary moments at mid-span sections and add to the effect of the primary moments over the piers. There are no secondary moments in a simply-supported

structure as the ends of the simple span are free to rotate and translate under the action of the post-tensioning.

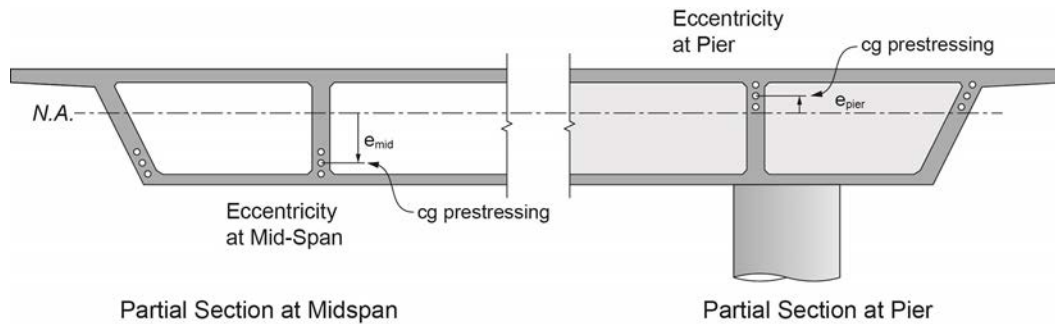


Figure 1.7 – Tendon Locations within Box Girder Cross Section

In very unique cases, an alternate to full length tendons in continuous spans is staged construction using shorter tendons that overlap at the piers. Figure 1.8 shows a concept of staged construction for the same four-span unit shown in figure 1.6. This approach can produce savings in falsework and formwork, but these savings may be offset by an increase in tendon and anchorage cost and by a slower rate of construction, as each span must gain sufficient strength prior to stressing the post-tensioning. The state of stress in bridges constructed in stages can be significantly different than those cast full length. Design calculations should consider the changing structural system as construction progresses and appropriate long-term bridge behavior.

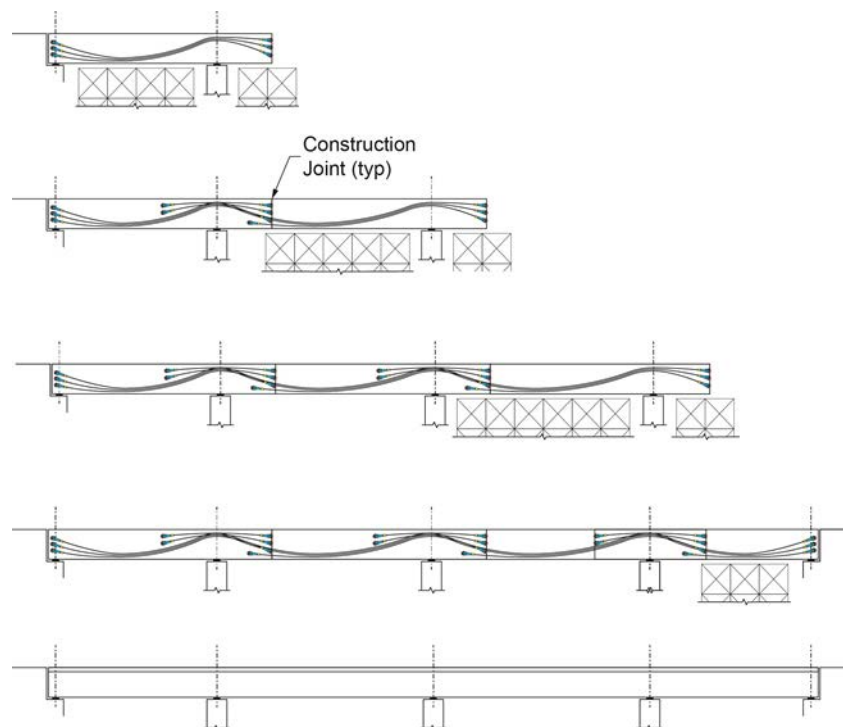


Figure 1.8 – Possible Tendon Layout for Sequentially Cast Spans

1.4 Loss of Prestressing Force

Post-tensioning tendon forces are established in design to provide precompression to offset undesirable tensile stresses in the concrete box girder. The engineer conveys the tendon force requirements in the contract drawings as either the required *jacking force* at the end of the tendon or the final *effective force* at some point along the length of the tendon. The differences between jacking forces and effective forces are called prestressing force *losses*. Prestressing force losses can be grouped into two families: 1) losses related to the material properties of the concrete and prestressing steel, and 2) losses related to the mechanics of the post-tensioning system and tendon geometry. These losses, summarized below, are presented in detail later in this Manual.

Losses Related to Material Properties

- Elastic shortening of concrete
- Shrinkage of concrete
- Creep of concrete
- Relaxation of prestressing steel

Losses Related to Physical Characteristics

- Duct friction due to curvature
- Wobble (unintentional friction)
- Wedge Set (or Anchor Set)

1.5 Post-Tensioning System Hardware

1.5.1 Basic Bearing Plates

A basic bearing plate is a flat plate bearing directly against concrete. This includes square, rectangular, or round plates, sheared or torch cut from readily available steel plate. Basic bearing plates are used in conjunction with galvanized sheet metal or plastic trumpets to transition from the strand spacing in the wedge plate to the duct (figure 1.9).

Basic bearing plate anchorages should comply with the requirements of section 10.3.2 of the AASHTO LRFD Bridge Construction Specifications (3rd Edition with Interims through 2015).

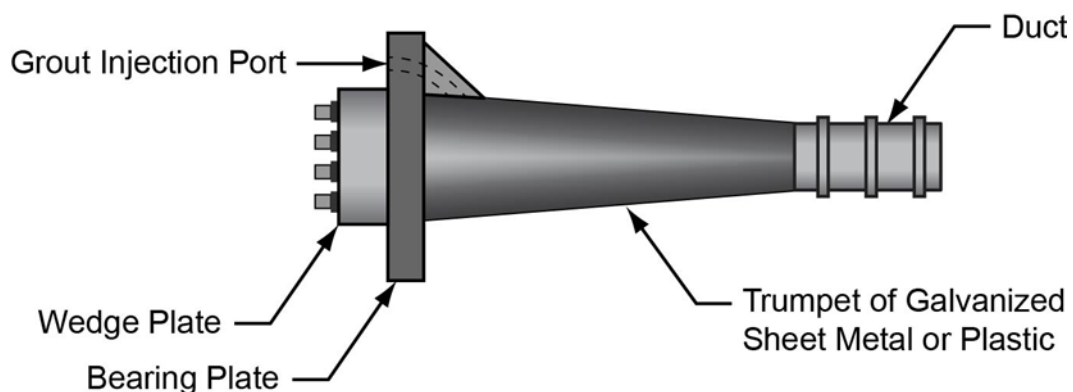


Figure 1.9 - Basic Bearing Plate Anchorage System

1.5.2 Special Bearing Plates or Anchorage Devices

A special bearing plate or anchorage device is any anchorage hardware that transfers tendon force into the concrete but does not meet normal analytical design requirements for basic bearing plates. Covered by this definition are devices having single or multiple plane bearing surfaces, and devices combining bearing and wedge plates in one piece. These anchorages typically require increased confinement reinforcement and should be accepted on the basis of physical tests. Figure 1.10 shows a cut-away view of a multi-plane anchorage system. Figure 1.11 shows the components of an anchorage system for a four strand tendon in flat duct, commonly used in slabs.

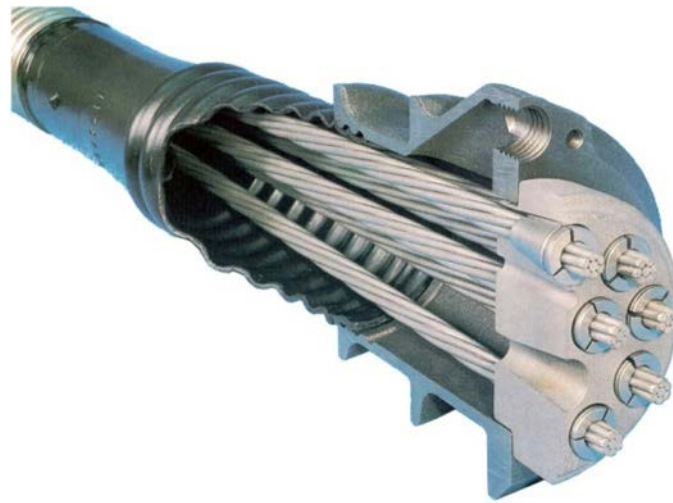


Figure 1.10 – Multi-Plane Anchorage System (Courtesy of VSL)



Figure 1.11 – Anchorage System for Flat Duct Tendon (Courtesy of DSI)

Use of a special bearing plate or anchorage device is acceptable if it complies with the testing requirements of section 10.3.2.3 of the AASHTO LRFD Bridge Construction Specifications.

1.5.3 Wedge Plates

Wedge plates, in conjunction with wedges, transfer the prestressing force in the strands to the anchorage. Wedge plates should comply with “Guide Specifications for Grouted Post-Tensioning, (PTI/ASBI M50.3-12, 2012)” section 4.3.2.

1.5.4 Wedges and Strand-Wedge Connection

Wedge performance is critical to the proper anchoring of strands. Different wedges have been developed for particular systems and applications such that there is no single standard wedge. However, wedges for post-tensioning systems should have the following characteristics:

- Wedge length at least 2.5 times the strand diameter.
- Wedge angle of 5 to 7 degrees.
- Internal serrated teeth for gripping the strand.
- Case-hardened low carbon or alloy steel.
- Two or three parts with a spring wire retainer clip or o-ring in a groove around the thick end of the wedge.

Wedges are case hardened with a ductile core to bite into the strand and conform to the irregularity between the strand and wedge hole. In so doing, the surface of the wedge may crack. This is normally acceptable and does not affect performance so long as wedge sections do not break completely into separate pieces. Often, it is only the portion outside the retainer ring that cracks.

Wedges should comply with “Guide Specifications for Grouted Post-Tensioning, (PTI/ASBI M50.3-12, 2012)” section 4.3.2.

1.5.5 Permanent Grout Caps

Permanent grout caps similar to those shown in figure 1.12 should be provided in accordance with Protection Levels specified in section 3.0 of “Guide Specifications for Grouted Post-Tensioning, (PTI/ASBI M50.3-12, 2012).” Project specific documents should specify when and where caps are required.

Permanent grout caps should be made of a non-corrosive material such as fiber reinforced plastic or stainless steel. To ensure an enduring, maintenance-free, life of 75 years fiber reinforced plastic caps should contain an anti-oxidant additive with an environmental stress cracking endurance of 192 hours per ASTM D1693; stainless steel caps should meet the requirements of ASTM A240 Type 316.

Grout caps shall meet the requirements of “Guide Specifications for Grouted Post-Tensioning, (PTI/ASBI M50.3-12, 2012)” section 4.3.3.



Figure 1.12 – Permanent Plastic Grout Caps (Courtesy of VSL)

1.5.6 Ducts

Ducts are used to form a continuous void through the concrete for later placement of the post-tensioning tendon steel. Originally, little attention was paid to the possible role of the duct as a barrier to corrosive agents. Today, strong emphasis is placed on the quality, integrity and continuity of the duct as a corrosion barrier in itself. This has resulted in a move toward the use of high density plastic ducts in some states. Nevertheless, more traditional metal ducts are still used.

1.5.6.1 Duct Size

Section 5.4.6.2 of the AASHTO LRFD Bridge Design Specifications calls for the inside cross-sectional area of the duct to be at least 2.0 times the net area of the strand tendon. The one exception cited by AASHTO is in the case where the tendons are to be placed by the pull-through method. In this case, the inside duct area should be 2.5 times the net area of the strand tendon. Section 4.3.5 of “Guide Specifications for Grouted Post-Tensioning, (PTI/ASBI M50.3-12, 2012)” standardizes the inside cross-sectional area of the duct to be at least 2.5 times the net area of the strand tendon cross-sectional area.

Oval “flat” ducts are commonly used for transverse tendons in deck slabs of concrete box girders. These transverse tendons have typically been made of up to 4 strands of 15 mm (0.6 in) diameter, though there are systems that will accept up to 5 strands. The internal clear dimensions of oval duct for a four strand tendon should be a minimum of 25 mm (1 in) vertically and 75 mm (3 in) horizontally.

1.5.6.2 Corrugated Steel Duct

Ducts are spirally wound to the necessary diameter from strip steel with a minimum wall thickness of 0.45 mm (26-gauge) for ducts less than 66 mm (2-5/8 in) diameter or 0.6 mm (24-gauge) for ducts of greater diameter. The strip steel should be galvanized to ASTM A653/A653M with a coating weight of G90. Ducts should be manufactured with welded or interlocking seams with sufficient rigidity to maintain the correct profile between supports during concrete placement (figure 1.13). Ducts should also be able to flex without crimping or

flattening. Joints between sections of duct and between ducts and anchor components should be made with positive, metallic connections that provide a smooth interior alignment with no lips or abrupt angle changes.



Figure 1.13 – Corrugated Metal Duct

1.5.6.3 Corrugated Plastic

Corrugated plastic ducts, as shown in figure 1.14, are also used for tendons internal to the concrete. These ducts should be seamless and fabricated from polyethylene or polypropylene meeting the requirements of section 4.3.5.2 of “Guide Specifications for Grouted Post-Tensioning, (PTI/ASBI M50.3-12, 2012).”



Figure 1.14 – Corrugated Plastic Duct

1.5.6.4 Plastic Fittings and Connections for Internal Tendons

All plastic duct splices, joints and connections to anchorages should be made with couplings and connectors that produce a smooth interior duct alignment with no lips or kinks. All fittings and connections between lengths of plastic duct and between ducts and steel components (e.g. anchors or steel pipe) should be made of materials compatible with corrugated plastic ducts. Plastic materials should contain antioxidant stabilizers and have an environmental stress cracking of not less than 192 hours as determined by ASTM D1693 “Standard Test Method for Environmental Stress-Cracking of Ethylene Plastics,” Condition C. Duct tape should not be used to join or repair ducts or make connections. See “Post-Tensioning Tendon Installation and Grouting Manual (2013),” available from the Federal Highway Administration, (<http://www.fhwa.dot.gov/bridge/pt/>) for further information on duct couplers.

1.5.6.5 Grout Inlets, Outlets, Valves and Plugs

Grout inlets, outlets, valves and plugs should be made of polypropylene or polyethylene meeting the requirements for plastic, corrugated ducts. Grout inlets, outlets, valves and plugs shall meet the requirements of “Guide Specifications for Grouted Post-Tensioning, (PTI/ASBI M50.3-12, 2012)” sections 4.3.12 and 4.4.4. Figure 1.15 shows a graphic depiction of grout vents extending from an embedded duct.

Tubes for inlets and outlets for strand tendons should have a minimum inside diameter of 20 mm (3/4 in). For bar tendons and for tendons comprising up to 4 strands, tubes should be at least 10 mm (3/8 in) internal diameter. Inlets and outlets should be closeable with suitable valves or plugs. For grouting of long vertical tendons, dual mechanical shut-off valves are usually necessary to facilitate intermediate stages of grouting and venting.

Inlets and outlets should be arranged and attached to ducts, anchorages and grout caps in a manner that allows all air and water to escape in order to ensure that the system is completely filled with grout. (See chapter 4 of “Post-Tensioning Tendon Installation and Grouting Manual (2013)” for examples of locations of inlets and outlets.)

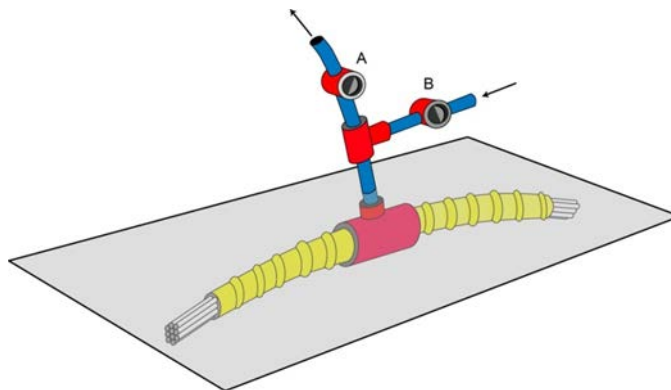


Figure 1.15 – Typical High-Point Grout Vent

1.5.7 Post-Tensioning Bars Anchor Systems

Anchorage systems for post-tensioning bars are comprised of bearing plates and anchor nuts similar to the components shown in figure 1.16. The anchorage system should comply with “Guide Specifications for Grouted Post-Tensioning, (PTI/ASBI M50.3-12, 2012)” section 4.3.2.



Figure 1.16 – Post-Tensioning Bar Anchorage System (Courtesy of DSI)

1.6 Overview of Construction

1.6.1 Falsework

Falsework is the structural system that supports the formwork onto which the concrete of the box girder will be cast. Falsework systems can be comprised of prefabricated modular shoring towers comprising well-braced interlocking frames in a square or rectangular arrangement of four legs as shown in figure 1.17. Multiple towers are located as necessary to support the falsework deck which in turn supports the superstructure formwork.



Figure 1.17 – Modular Falsework Units for Cast-in-Place Construction

Main vertical falsework supports may also consist of a series of individual columns made of structural steel sections or heavy section lumber. Poor ground conditions or the need to span an underlying roadway or waterway may limit the locations of falsework columns. Fewer but larger falsework columns, along with larger falsework beams, may be used to provide the needed clearances during construction. Figure 1.18 shows a network of falsework columns used to maintain navigational clearances during construction.



Figure 1.18 – Steel Pipe Support Towers for Cast-In-Place Construction

Depending on the nature of the site and the cost of temporary construction, falsework may be provided for the superstructure to be cast-in-place over the entire length of the bridge or continuous superstructure unit. If these costs are prohibitive, it may be necessary to move falsework from span to span as each is constructed and made self-supporting, provided that appropriate engineering analysis of intermediate states of construction is performed. In either case, careful consideration should be given to assuring that environmental clearances can be achieved for placing falsework.

For further guidance with regard to the design and construction of falsework, refer to the following publications:

- “Guide Design Specifications for Bridge Temporary Works”, (2008 Interim, AASHTO).
- “Construction Handbook for Bridge Temporary Works”, (2008 Interim, AASHTO).
- “Falsework Manual” (January 1988, Caltrans).

1.6.2 Superstructure Formwork

The falsework system provides supports for the superstructure formwork. Formwork may be made from lumber and plywood or prefabricated modular forming systems. Accuracy to line, level and thickness is essential to ensure the correct final shape and size of concrete members. External surfaces are usually formed of a high quality, smooth and dense finished plywood, metal or any required aesthetic texture, as necessary. Internal surfaces should be within

tolerance but are usually of a lesser quality finish and forming material. Figure 1.19 shows form components for a single-cell box girder.



Figure 1.19 – Web and Cantilever Wing Formwork for a Single-Cell Box Girder

Box girder sections can be constructed in stages, beginning with the bottom slab, webs and finally the top slab, as shown in figure 1.20. In this Figure, the bottom slab for this portion of the bridge has been cast, web reinforcing and longitudinal ducts for post-tensioning tendons have been tied and portions of the webs have been cast. Supports for top slab forming are being placed in the portion where webs are complete. Many bridges combine the casting of the bottom slab and webs into one stage.

Access to internal cells is usually necessary through diaphragms or manholes for future maintenance inspection which also provides a convenient way through which internal formwork can be removed after casting. Purpose-made, permanent, internal top slab soffit forms (lost deck forms) may remain in place provided that their weight and structural connectivity, if any, have been accounted for in the design.



Figure 1.20 – Web Formwork for a Multi-Cell Box Girder

1.6.3 Reinforcing and Post-Tensioning Hardware Placement

Reinforcing steel is placed in stages to coincide with the casting of the cross section components—i.e., bottom slab, webs, and top slab. Reinforcing should be detailed accordingly, giving attention to the location of bar splices to meet structural requirements and also facilitate forming and casting. Reinforcing steel should be installed to project construction tolerances.

All post-tensioning ducts, anchorage components and anchorage reinforcement should be installed in conjunction with the reinforcement. It is preferable that reinforcement and post-tensioning be designed and detailed free of conflicts. However, conflicts are not always evident in advance. Whenever a conflict is encountered between reinforcement and post-tensioning in the field, generally, the reinforcement should be adjusted locally as necessary to maintain the desired post-tensioning alignment. In cases of doubt, a decision should be sought from the Engineer of Record.



Figure 1.21 – Web and Bottom Slab Reinforcing (left), Tying Post-tensioning Ducts in Webs (right)

1.6.4 Placing and Consolidating Superstructure Concrete

Box girder superstructures can be cast in either two or three stages. When cast in two stages, the bottom slab and webs are poured at the same time. This is followed by the casting of the top slab. In three-stage casting the bottom slab, webs, and top slab are poured separately, with enough time between stages to permit sufficient concrete hardening. Longitudinal construction joints are normally located in the webs a few inches above the top of the bottom slab (three-stage casting) and a few inches above the top of the webs in the top slab fillets (two-stage and three-stage casting). This is mainly for convenience of construction and to provide a clean joint between components. In order to ensure proper structural integrity and function, joints should be prepared, cleaned and roughened prior to the next pour. This is usually sufficient for shear transfer. However, construction keyways may be necessary and should be shown on the plans where required. An approach to three-stage casting is presented in the following paragraphs.

The first stage of box girder construction is the casting of the bottom slab concrete. Placing typically commences at one side (usually the low side of grade and superelevation) and continues from there across the width of the slab and along the length of the bridge as necessary. The new open end face of the slab concrete face is kept fresh to facilitate consolidation with each new load of concrete. Concrete is consolidated using vibratory tools and then struck off to elevation by hand or mechanical screeds, followed by a float finish.

When the bottom slab concrete has set and sufficiently hardened the webs are formed. Web concrete is then placed and consolidated. The webs are placed in lifts of about two feet to control pressure on forms. Each fresh charge of concrete is consolidated and worked into the top of the previous lift—which must remain workable to receive the next load of concrete. Concrete in webs is typically consolidated by means of internal poker-type vibrators, though external form vibrators can be used. In the latter case, formwork must be sufficiently robust and braced to withstand the heavy vibration.

The top slab of the box section is cast last. Depending upon the profile of draped tendons, ducts may rise into the top slab at piers. All top slab reinforcing and, if necessary, transverse post-tensioning tendons must be in place and set to correct elevations and required clear covers before concrete is placed. Ducts for longitudinal tendons should be checked for obstructions before the top slab concrete is placed. Concrete is usually placed working across and longitudinally up hill. Slab concrete is consolidated, struck off to levels with screeds (figure 1.22) and usually floated to a final finish. Longitudinal or transverse traffic tines may be brushed or groove-cut into the deck surface after curing to improve vehicular traction.

The preceding paragraphs describe pouring the superstructure in three phases. Two-phased construction, in which bottom slab and webs are cast together, followed by the casting of the top slab, is also commonly used.

Longitudinally, vertical construction joints may be needed at various locations in a span or superstructure in order to keep the total volume of concrete placed to an amount which can be delivered, placed, consolidated and finished within a given work period. Vertical construction joints are typically not allowed in simple span bridges.



Figure 1.22 – Placing Deck Concrete and Finishing with a Roller Screed

1.6.5 Superstructure Curing

Proper concrete set and sufficient strength is required prior to releasing forms before the next stage of casting and especially prior to imposing high local anchorage forces from post-tensioning or releasing falsework.

For typical box girder construction, proper curing is accomplished using blankets, wet-burlap, moisture, fogging, and application of suitable curing compounds. Monitoring of internal concrete temperature using thermocouples or other devices at suitable locations over the curing period can be helpful in some cases, particularly for thick members and large pours. It provides a record of curing and can help avoid potential difficulties from a too rapid rise or fall from the heat of hydration. Protection of pours from adverse weather by enclosures and heating may be necessary in some situations (figure 1.23).



Figure 1.23– Curing the Concrete Deck

1.6.6 Post-Tensioning Operations

Multi-strand tendons are the most frequent choice for main longitudinal tendons in bridges. All the strands of one longitudinal tendon are simultaneously tensioned using a multi-strand jack. The sequence of stressing tendons should be clearly shown on the contract plans or approved shop drawings and must be followed on site.

Post-tensioning strands may be pushed or pulled through ducts to make a tendon. Pushing should be done with care using a protective plastic or metal cap provided by the post-tensioning system supplier so that the strands do not get caught by or introduce damage to the duct. Sometimes it may be easier to pull the entire tendon bundle of strands through the duct together using a special steel wire sock or other device securely attached to the end of the bundle (figure 1.24).



Figure 1.24– Bundled Tendon Prepared for Pulling

When a multi-strand tendon is stressed from one end it is often referred to as “single” or “one-end” stressing to distinguish it from tendons stressed from both ends. When a bridge has a number of similar, and often symmetrical, tendons that need only be stressed from one end, “alternate end stressing” can be used to keep the overall post-tensioning effect as symmetric as possible. In this case, tendons are stressed from one end only, but from opposite, alternate, ends of the bridge for similar tendon profiles.

When the tendons are very long, losses over the length of the tendon due to friction and wobble become large. Stressing the tendon from the second end results in a higher force in the tendon than if only stressed from one end. This is typically called “double” or “two-end” stressing. Also, for symmetrical tendons two-end stressing becomes effective when the effect of anchor set at the jacking end affects less than half of the tendon. Stressing from the second end should not be done if the calculated elongation is less than the length of the wedge grip. Re-gripping in a portion of the old grip length should be avoided.

It is important to also account for the staging of stressing across the width of the bridge. Individual tendon jacking forces (P_{jack}) must be selected to achieve a uniform distribution of stress across the width of the bridge.



Figure 1.25– Stressing Post-Tensioning Tendons

1.6.7 Tendon Grouting and Anchor Protection

After post-tensioning tendons have been installed and stressed, they must be properly grouted and anchorages sealed and protected to ensure long term durability. Grouting should proceed as soon as possible after installation and stressing of the tendons. Depending upon environmental conditions, temporary protection and sealing of open ducts may be necessary at anchorages, and temporary protection of the ends of the strands will be necessary.

For comprehensive information on the installation, stressing, grouting and protection of post-tensioning tendons and anchorages (including recommendations for the location of injection grout ports, vents, laboratory and field tests, quality control and records, etc.), refer to “Post-Tensioning Tendon Installation and Grouting Manual (2013)” available from the Federal Highway Administration (<http://www.fhwa.dot.gov/bridge/pt/>).

Chapter 2—Materials

The primary materials needed for the design of cast-in-place post-tensioned box girders are: concrete, prestressing steel, and mild reinforcing. This chapter presents the material characteristics for these three materials with respect to the design of this bridge type.

2.1 Concrete

2.1.1 Compressive Strength

Compressive strength (f'_c) is the characteristic that best gives an overall picture of the quality of a concrete.

The basic components of concrete are Portland cement, aggregates (coarse and fine) of varied gradation, water, and admixtures. Concrete sets and gains strength as a consequence of a hardening of the cement/water gel through the chemical reaction of hydration. The ratio of water to cement (water/cement ratio) is an important factor of resulting concrete strength. If too little water is used, not all of the cement will undergo hydration and the desired strength will not be obtained. Excessive water leads to overly dispersed hardened cement particles, again leading to less than desired strength. Water/cement ratios often range from 0.35 to 0.40.

Freshly placed, unconsolidated concrete contains excessive and detrimental voids. Unconsolidated concrete, if allowed to harden, will be porous and will poorly bond to the reinforcement. The resulting hardened concrete will have low strength, high permeability, and poor resistance to deterioration. Freshly placed concrete should be consolidated if it is to have needed characteristics of structural concrete.

Curing of the concrete is also important to producing high quality concrete. The main purpose of curing is to prevent unnecessary moisture loss, especially in the first few days of the initial hydration and strength development. In addition to moisture loss, control of the concrete temperature during curing is important. Hydration is an exothermic reaction, building up heat within the concrete member. This heat must be gradually dissipated in a controlled manner to offset excessive thermal gradients within the concrete that can lead to micro-cracking and diminished strength.

Admixtures are incorporated into concrete mixes to enhance the qualities of the hardened concrete. A controlled percentage (4–6 percent) of well-dispersed, microscopic air bubbles introduced by air-entraining agents enhances durability against freeze-thaw and improves workability for placement and consolidation. Super-plasticizers improve workability, facilitating reduced water/cement ratios and enhanced strength. Supplementary cementitious materials, such as pozzolans (most typically fly ash, silica fume, or granulated blast furnace slag), can be used in conjunction with or as a replacement to part of the cement to contribute to the properties of the hardened concrete. While increasing certain characteristics, excessive or poorly matched admixtures can have a negative impact on the resulting concrete.

Concrete compressive strength is determined by physical testing in accordance with AASHTO T22 (ASTM C39). Tests are performed at a standardized age of 28 days by compression tests to failure of sample cylinders 6 inches in diameter and 12 inches in length.

AASHTO LRFD Article 5.4.2.1 specifies that prestressed concrete shall not have a compressive strength less than 4.0 ksi. Typical 28-day concrete compressive strength for cast-in-place post-tensioned box girders range between 5.0 ksi to 6.0 ksi. Higher strength concrete can be used,

but local thickening of concrete members, such as bottom slabs near piers to control compressive stresses, are generally more cost effective than the increased cost of higher strength concrete throughout the bridge. In addition, higher strength concretes cast on site are more susceptible to environmental factors than high strength concrete produced in more controlled settings in casting yards.

Guidance as to the type or “Class of Concrete” for various applications is provided in AASHTO LRFD Article 5.4.2.1. Concrete mix characteristics, including strength, minimum cement content, maximum water cement ratio, range of air content and coarse aggregate per class of concrete, are given in AASHTO LRFD Table C5.4.2.1-1.

2.1.2 Development of Compressive Strength with Time

Standardized testing classifies strength at an age of 28 days. However, concrete continues to increase in strength over time. The increase in concrete compressive strength acts to increase other material characteristics that are related to strength (tensile strength, modulus of elasticity, time-dependent effects, etc.). As a result, it is important to be able to consider the change in concrete strength with time. The AASHTO LRFD specifications do not specifically address this feature of concrete, but other codes do. The Comité Euro-Internationale du Béton/Fédération Internationale de la Précontrainte (CEB-FIP) Model Code (1990) provides the following relationship for the change in concrete compressive strength over time:

$$\text{(Eqn. 2.1)} \quad f_{cm}(t) = \beta_{cc}(t) f_{cm}$$

$$\text{(Eqn. 2.2)} \quad \beta_{cc}(t) = \exp \left\{ s \left[1 - \left(\frac{28}{t/t_1} \right)^{1/2} \right] \right\}$$

Where, f_{cm} = 28-day compressive strength
 $f_{cm}(t)$ = concrete compressive strength at time t
 β_{cc} = time-dependent coefficient dependent on age of concrete
 t = age of concrete at which $f_{cm}(t)$ is computed (days)
 t_1 = 1 day
 s = cement rate of hardening coefficient
 (0.20 for rapid hardening high strength concretes, 0.25 for normal and rapid hardening cement, 0.38 for slow hardening cements)

Note that the 28-day compressive strength predicted by testing in accordance with the AASHTO LRFD specifications is used without modification in equation 2.1. This is as opposed to using the 28-day strength plus 8 MPa as in other CEB-FIP equations.

Figure 2.1 shows a plot of the ratio of concrete compressive strength to 28-day compressive strength (β_{cc}) for normal hardening cement.

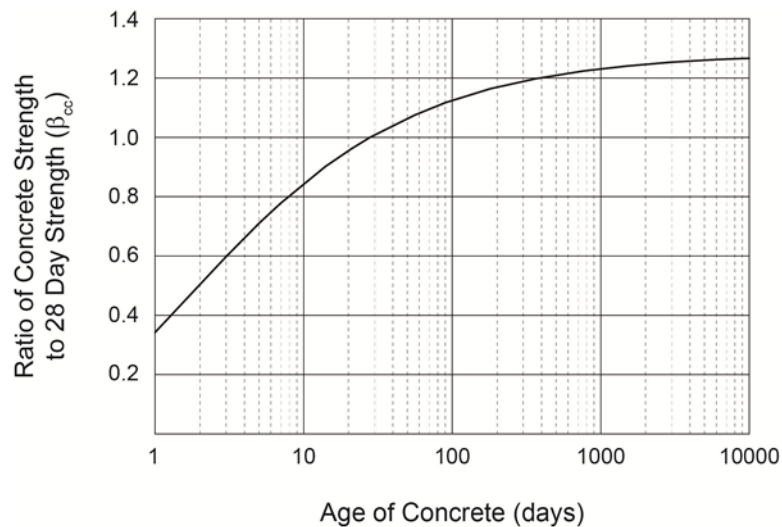


Figure 2.1 – Concrete strength gain with time

2.1.3 Tensile Strength

Concrete tensile strength greatly impacts prestressed concrete design as it forms the basis of the criteria for which post-tensioning force and layout is typically chosen. AASHTO LRFD specifies concrete tensile stress in two different ways: Modulus of Rupture and Direct Tensile Strength.

The Modulus of Rupture (f_r) is defined as the tensile stress in concrete developed by concrete flexure. For concrete compressive strengths up to 15 ksi and for normal-weight concrete, AASHTO LRFD Article 5.4.2.6 specifies the modulus of rupture in ksi to be:

$$\text{(Eqn. 2.3)} \quad f_r = 0.24\sqrt{f'_c}$$

The Modulus of Rupture is determined by standardized test AASHTO T97 (ASTM C78).

The Direct Tensile Strength, also designated as f_r , is specified in AASHTO LRFD Article 5.4.2.7. The commentary of this section specifies that for normal-weight concrete of compressive strengths up to 10 ksi, the direct tensile strength in ksi is:

$$\text{(Eqn. 2.4)} \quad f_r = 0.23\sqrt{f'_c}$$

Traditionally, testing for direct tensile strength is by the split cylinder tensile strength method performed in accordance with AASHTO T198 (ASTM C496). However, pull out methods specified in ASTM C900 may also be used.

The small difference in value between equations 2.3 and 2.4 is interesting to note. Most research indicates that, depending on the strength of the concrete, the modulus of rupture is significantly greater than the direct tensile stress (as much as two times as large). This is noted in the commentary to AASHTO LRFD Article 5.4.2.6., with rationale provided for the limit shown in equation 2.3. Of more practical importance are the allowable stresses established at service limit states for the particular behavior. For example, flexural tensile stresses in prestressed

concrete are most commonly limited to 40 percent of the modulus of rupture, where principal tensile stresses in webs of are limited to 50 percent of the direct tensile capacity of the concrete.

2.1.4 Modulus of Elasticity

The modulus of elasticity of a material, E_c , is the ratio of normal stress to corresponding strain in compression or tension. The modulus of elasticity is an integral feature of the stiffness based methods used to analyze structures. The modulus of elasticity is a part of the characteristic member stiffnesses which populate element stiffness matrices. Element stiffness matrices are transformed and assembled into a global stiffness matrix representing the entire structure. Member end (nodal) displacements are then computed by pre-multiplying the vector of applied fixed end member forces by the inverted stiffness matrix (or some more mathematically efficient matrix method). Member end forces are then back-computed from the nodal displacements.

Figure 2.2 shows a typical stress strain curve for concrete. The relationship of stress to strain as shown in this Figure is highly non-linear. However, within the range of stresses that define the service limit state for which bridges are designed, the relationship can be approximated by a linear relationship. Figure 2.2 also shows a line whose slope is the modulus of elasticity for the linear range. This modulus of elasticity is a secant modulus standardized by physical testing in accordance with ASTM C469. The two points that define the secant modulus are a strain of 50×10^{-6} (ϵ_1) and corresponding stress f_1 , and a strain ϵ_2 that corresponds to a stress of $0.4f'_c$.

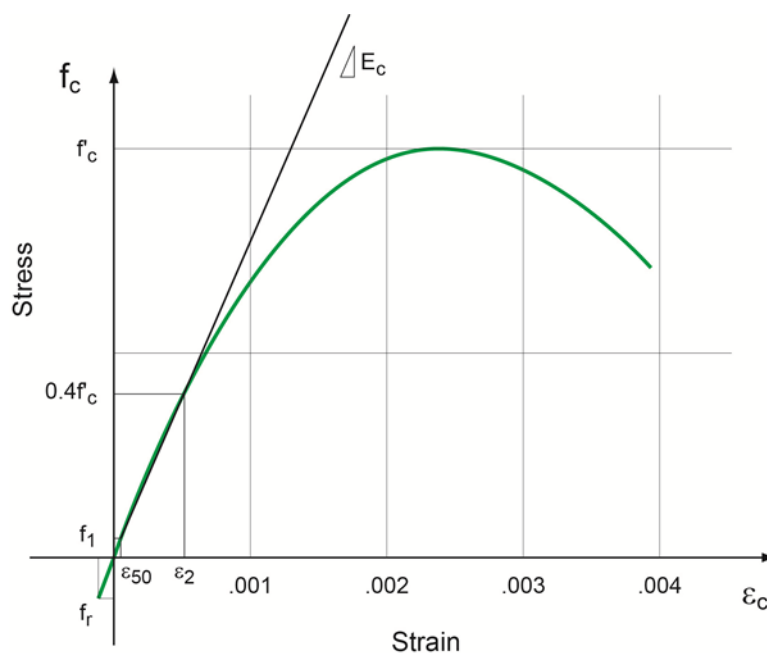


Figure 2.2 – Typical Stress-Strain Curve for Concrete

AASHTO LRFD Article 5.4.2.4 provides the equation for the concrete modulus of elasticity. This well-known equation, developed to fit physical testing, relates the modulus of elasticity of the concrete to the concrete unit weight and the concrete 28-day compressive strength. Equation 2.5 provides the equation for the modulus of elasticity in ksi:

(Eqn. 2.5)
$$E_c = 33,000K_1w_c^{1.5}\sqrt{f'_c}$$

where, f'_c = the 28-day compressive strength of concrete (ksi)
 w_c = the unit weight of concrete (kcf)
 K_I = correction factor for aggregate (equal to 1 unless determined by physical test and approved by authority of jurisdiction)

2.1.5 Modulus of Elasticity Variation with Time

Though the CEB-FIP Model Code 1990 is being used to estimate time-dependent characteristics, the AASHTO LRFD specification equation for Modulus of Elasticity as provided in Article 5.4.2.4 is used to estimate the 28-day Modulus of Elasticity.

The variation in Modulus of Elasticity with time is predicted by CEB-FIP Equations 2.1-57 and 2.1-58:

(Eqn. 2.6)
$$E_{ci}(t) = \beta_E(t) E_{ci}$$

(Eqn. 2.7)
$$\beta_E(t) = (\beta_{cc}(t))^{1/2}$$

Where, E_{ci} = the modulus of elasticity of concrete at an age of 28 days
 $E_{ci}(t)$ = the modulus of elasticity at time t
 β_e = coefficient depending on age of concrete, t (days)
 β_{cc} = coefficient defined by equation 2.2

Figure 2.3 shows a plot of the ratio of concrete modulus of elasticity to 28-day compressive strength (β_E) for normal hardening cement.

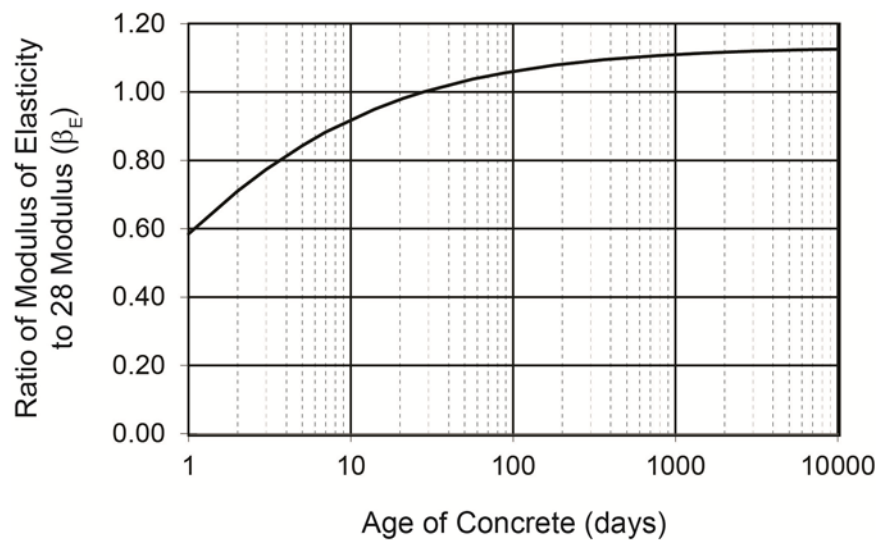


Figure 2.3 – Concrete Modulus of Elasticity with Time

2.1.6 Poisson's Ratio

Poisson's ratio of lateral to axial strain (μ) is prescribed in AASHTO LRFD Article 5.4.2.5 to be equal to 0.20.

2.1.7 Volumetric Changes

Volume changes in concrete arise from variations in temperature, shrinkage due to air-drying, and creep caused by sustained stress. These are influenced by environmental conditions such as temperature, humidity, and the maturity of the concrete, and by the time and duration of loading. Volume changes affect structural performance and must be properly accounted for when determining loss of prestress and long-term deflections.

2.1.7.1 Coefficient of Thermal Expansion

AASHTO LRFD Article 5.4.2.2 defines the coefficient of thermal expansion. For normal weight concrete the coefficient of thermal expansion (α) is 6×10^{-6} per $^{\circ}\text{F}$.

2.1.7.2 Creep

The creep of concrete is defined as the increase in concrete strain under a sustained stress. Figure 2.4 shows the influence of concrete creep on increased strain under the loading and unloading of a sustained load on a concrete element.

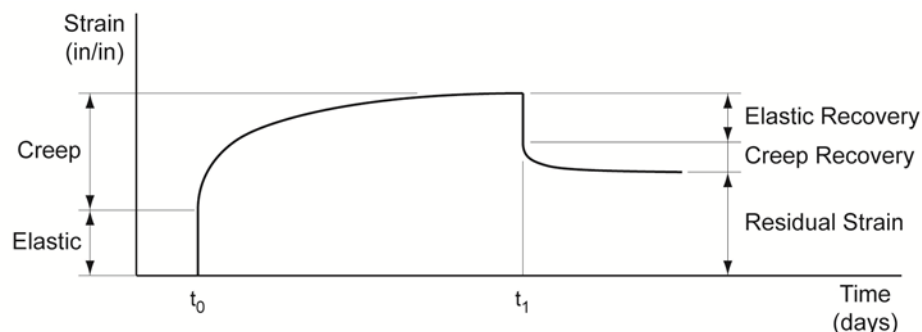


Figure 2.4 – Creep of Concrete

The concrete element is loaded at time t_0 and strains in proportion to the Modulus of Elasticity developed at that time. From time t_0 to time t_1 , the concrete creeps under the action of the sustained stress. At time t_1 the stress is removed and there is an elastic recovery in strain. The elastic recovery is less than the initial elastic strain because the Modulus of Elasticity has increased during the period of loading, as a function of concrete strength gain. Further reduction in strain is found at times greater than t_1 . This creep recovery strain is substantially smaller than the concrete creep, as it is proportional to the elastic recovery strain and occurs at a later age of the concrete's life than the original loading. At some time, the effects of creep recovery stop and the concrete element is left with a permanent residual strain.

Creep characteristics can vary greatly as a function of the mix design, member thickness, environment, and nature of loading. Some important factors influencing concrete creep are:

- Duration of Load—the longer the loading, the more creep realized.
- Initial Stress Level – the greater the level of initial stress, the more the concrete will creep.
- Concrete Age at Loading—the younger the concrete at loading, the more the concrete will creep.
- Relative Humidity—the higher the relative humidity of the loading environment, the lower the concrete will creep.
- Volume to Surface Ratio—the greater the volume to surface ratio, the less the concrete will creep.
- Concrete Strength—the greater the concrete strength the lower the creep.

Generally speaking, highway bridge loads are divided primarily into two types: permanent and live loads. There are typically no live loads that remain on the bridge for extended durations. As a result the strain versus time relationship of figure 2.4 is modified to that of figure 2.5.



Figure 2.5 – Creep of Concrete (with no long-duration transient loads)

The AASHTO LRFD specifications permits three models for estimating time dependent behavior of these materials. Article 5.4.2.3.1 permits three methods of computing the time-dependent creep behavior of concrete when mix-specific creep data is not available. The three methods permitted by code are:

- AASHTO LRFD Article 5.4.2.3.2.
- CEB-FIP Model Code.
- ACI 209.

The CEB-FIP Model Code 1990 is jointly produced by The Comite Euro-Internationale du Beton (The Euro-International Committee for Concrete) and the Federation Internationale de la Precontrainte (International Federation for Prestressing). The Model Code 1990 provides time-dependent material characteristics for concrete and prestressing steel. Along with its predecessor, the Model Code 1978, the CEB-FIP Model Code has been used extensively over the last 30 years in the United States for estimating the effects of material time-dependent behaviors.

This Chapter provides the CEB-FIP Model Code (1990) time-dependent characteristics required for the analysis of prestressed concrete bridges. These characteristics have been used in both of the example problems presented in this Manual. The equation numbers presented in this Chapter are those of the CEB-FIP Model Code (1990).

Within the elastic range, the creep strain at time t for a constant stress applied at time t_0 is given as:

$$\text{(Eqn. 2.8)} \quad \varepsilon_{cc}(t, t_0) = \frac{\sigma_c(t_0)}{E_{ci}} \phi(t, t_0)$$

Where, ε_{cc} = the creep strain at time $t > t_0$
 $E_{ci}(t)$ = the modulus of elasticity of concrete at an age of 28 days
 $\sigma_c(t_0)$ = compressive stress applied at time t_0
 $\phi(t, t_0)$ = the concrete creep coefficient

The creep coefficient is the product of the notional creep coefficient $\phi_0(t, t_0)$ (sometimes called the ultimate creep coefficient) and a time dependent coefficient $\beta_c(t-t_0)$.

$$\text{(Eqn. 2.9)} \quad \phi(t, t_0) = \phi_0 \beta_c(t-t_0)$$

Where, $\phi(t, t_0)$ = the creep coefficient
 ϕ_0 = the notional creep coefficient
 β_c = the coefficient to describe the development of creep with time after loading
 $\phi(t, t_0)$ = the concrete creep coefficient

The notional creep coefficient is a function of relative humidity, notional thickness, concrete strength, and age since loading, as per the following relationships:

$$\text{(Eqn. 2.10)} \quad \phi_0 = \phi_{RH} \beta(f_{cm}) \beta(t_0)$$

with,

$$\text{(Eqn. 2.11)} \quad \phi_{RH} = 1 + \frac{1 - RH / RH_o}{0.46(h / h_o)^{1/3}}$$

$$\text{(Eqn. 2.12)} \quad \beta(t_0) = \frac{1}{0.1 + (t_0 / t_1)^{0.2}}$$

$$\text{(Eqn. 2.13)} \quad \beta(f_{cm}) = \frac{5.3}{(f_{cm} / f_{cmo})^{0.5}}$$

Where, RH = the relative humidity of the ambient environment (%)
 RH_o = 100 percent
 f_{cm} = the mean concrete compressive strength at 28 days (MPa)
 f_{cmo} = 10 MPa
 t_0 = age of concrete at loading (days)
 t_1 = 1 day
 h_o = 100 mm

h = notional size of the member (mm) – see following equation where A_c is the cross section of the member and u is the perimeter in contact with the atmosphere.

In these expressions, the mean concrete compressive strength is a fixed number greater than the minimum compressive strength:

$$(Eqn. 2.14) \quad f_{cm} = f_{ck} + \Delta f$$

where, f_{cm} = mean compressive strength (MPa)
 f_{ck} = 28-day concrete compressive strength (MPa)
 Δf = 8 MPa

and the notional thickness is expressed as:

$$(Eqn. 2.15) \quad h = \frac{2A_c}{u}$$

where, A_c = cross-sectional area
 u = perimeter in contact with the atmosphere

For a closed box shape, where the environment inside the box girder can be markedly different than that outside the girder, standard practice has been to compute the perimeter in contact with the environment (u) as the outside perimeter plus one half of the interior perimeter.

The development of creep over time is given by:

$$(Eqn. 2.16) \quad \beta_c(t-t_0) = \left[\frac{(t-t_0)/t_1}{\beta_H + (t-t_0)/t_1} \right]^{0.3}$$

with,

$$(Eqn. 2.17) \quad \beta_H = 150 \left\{ 1 + \left(1.2 \frac{RH}{RH_o} \right)^{18} \right\} \frac{h}{h_o} + 250 \leq 1500$$

where, t_1 = 1 day
 RH_o = 100 percent
 h_o = 100 mm

Figure 2.6 shows a plot of the development of creep over time for a relative humidity of 75 percent and a notional thickness of 319 mm (conditions of examples 1 and 2 in this manual).

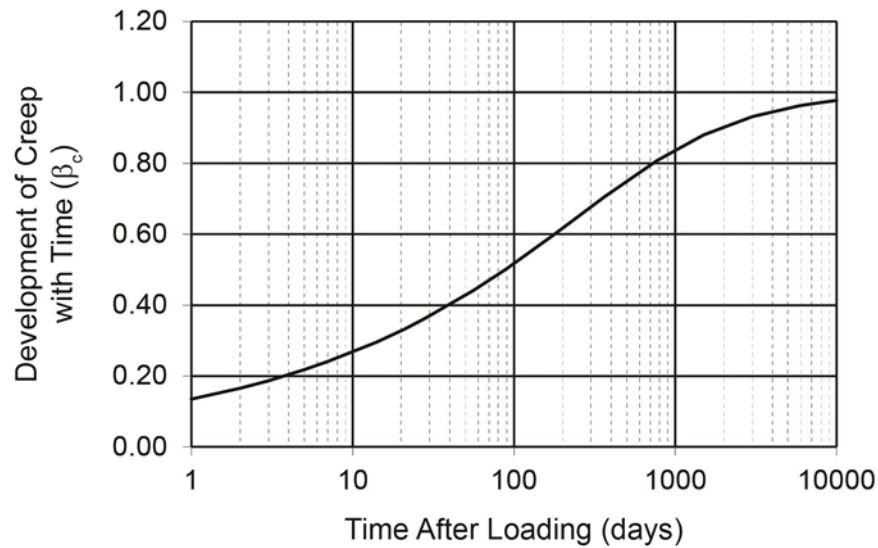


Figure 2.6 – Development of Concrete Creep with Time

2.1.7.3 Shrinkage

The total shrinkage strain at time t is calculated by:

(Eqn. 2.18)
$$\epsilon_{cs}(t, t_s) = \epsilon_{cso} \beta_s (t - t_s)$$

- Where,
- ϵ_{cso} = the notional shrinkage strain
 - β_s = coefficient to describe development of shrinkage with time
 - t = age of concrete (days)
 - t_s = age of concrete at beginning of shrinkage (days)

The notional shrinkage coefficient is determined by:

(Eqn. 2.19)
$$\epsilon_{cso} = \epsilon_s (f_{cm}) \beta_{RH}$$

with,

(Eqn. 2.20)
$$\epsilon_s (f_{cm}) = [160 + 10 \beta_{sc} (9 - f_{cm} / f_{cmo})] \times 10^{-6}$$

- where,
- f_{cm} = the mean concrete compressive strength at 28 days (MPa)
 - f_{cmo} = 10 MPa
 - β_{sc} = coefficient dependent on type of cement
(4 for slowly hardening cements, 5 for normal or rapid hardening cements, and 8 for rapid hardening high strength cements)

For relative humidity between 40 percent and 99 percent,

$$(Eqn. 2.21) \quad \beta_{RH} = -1.55\beta_{sRH}$$

For relative humidity greater than 99 percent,

$$(Eqn. 2.22) \quad \beta_{RH} = +0.25$$

where,

$$(Eqn. 2.23) \quad \beta_{sRH} = 1 - \left(\frac{RH}{RH_o} \right)^3$$

The development of shrinkage with time is:

$$(Eqn. 2.24) \quad \beta_s(t-t_s) = \left[\frac{(t-t_s)/t_1}{350(h/h_o)^2 + (t-t_s)/t_1} \right]^{0.5}$$

Figure 2.7 shows a plot of the development of shrinkage over time for a relative humidity of 75 percent and a notional thickness of 319 mm (conditions of examples 1 and 2 in this manual).

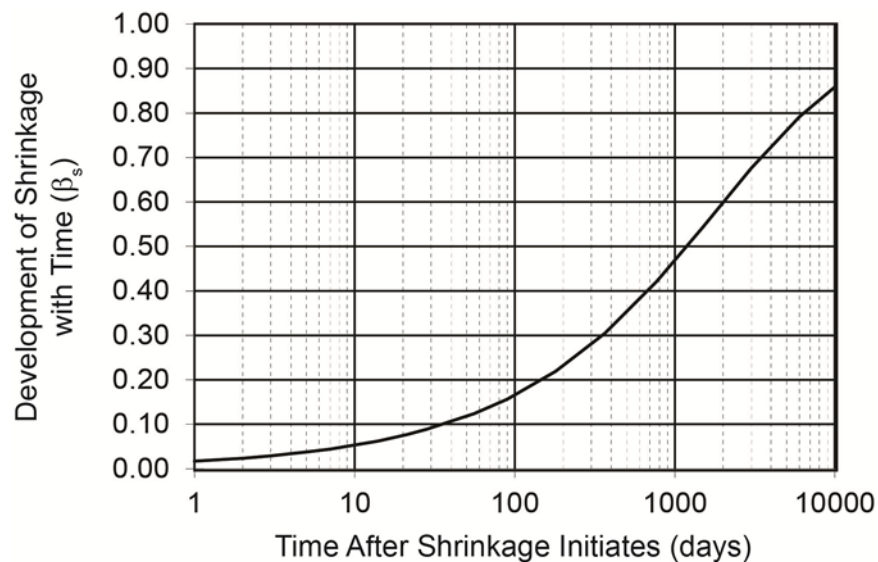


Figure 2.7 – Development of Concrete Shrinkage with Time

Shrinkage is primarily a result of sustained drying of the concrete as it is exposed to its surrounding environment. The majority of shrinkage occurs early in the life of the concrete, gradually slowing over time until ultimate shrinkage values are approached. This is seen in

figure 2.8, which plots the Time Development Factor (k_{td}) used to predict concrete shrinkage (as well as creep) over time as per as per AASHTO LRFD Articles 5.4.2.3.2 and 5.4.2.3.3.

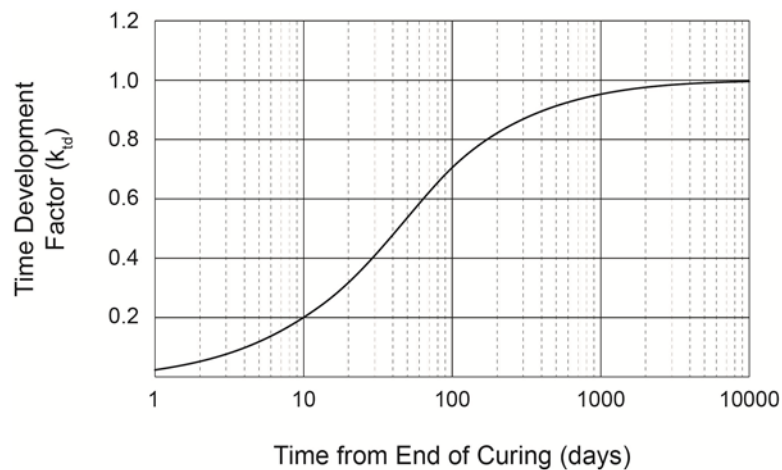


Figure 2.8 – Rate of Concrete Shrinkage over Time

As with concrete creep, AASHTO LRFD Article 5.4.2.3.1 permits three methods of computing time-dependent shrinkage behavior. It is important to note that the three methods should not be mixed. Inappropriately combined, the effects of for creep and shrinkage could be significantly miscalculated.

2.2 Prestressing Strands

Strands for post-tensioning are made of high tensile strength steel wire conforming to ASTM A416. A strand is comprised of 7 individual wires, with six wires helically wound to a long pitch around a center “king” wire. Strand is most commonly available in two nominal sizes, 0.5 inch and 0.6 inch diameter, with nominal cross-sectional areas of 0.153 in² and 0.217 in², respectively. Though the majority of post-tensioning hardware and stressing equipment is based on these sizes, the use of 0.62 inch diameter strand has been increasing.

Strand size tolerances may result in strands being manufactured consistently smaller than, or larger than nominal values. Recognizing this, “Acceptance Standards for Post-Tensioning Systems” (Post-Tensioning Institute, 1998) refers to the “Minimum Ultimate Tensile Strength,” which is the minimum specified breaking force for a strand. Strand size tolerance may also affect strand-wedge action leading to possible wedge slip if the wedges and strands are at opposite ends of the size tolerance range.

Strand conforming to ASTM A416 is relatively resistant to stress corrosion and hydrogen embrittlement due to the cold drawing process. However, since susceptibility to corrosion increases with increasing tensile strength, caution is necessary if strand is exposed to corrosive conditions such as marine environments and solutions containing chloride or sulfate, phosphate, nitrate ions or similar. Consequently, ASTM A416 requires proper protection of strand throughout manufacture, shipping and handling. Protection during the project, before and after installation, should be specified in project drawings and specifications.

2.2.1 Tensile Strength

All strands should be Grade 270 ksi low relaxation, seven-wire strand conforming to the requirements of ASTM A416 "Standard Specification for Steel Strand, Uncoated Seven Wire Strand for Prestressed Concrete." ASTM A416 provides minimum requirements for mechanical properties (yield, breaking strength, elongation) and maximum allowable dimensional tolerances. The AASHTO LRFD specifications do recognize the use of Grade 250 ksi prestressing steel, but this material is almost never used in major bridge construction, and is not addressed in this manual.

2.2.2 Modulus of Elasticity

Figure 2.9 shows a stress-strain diagram for prestressing strand. Up to a loading of approximately 90 percent of the ultimate strength of a strand, the stress-strain relationship is near linear. The slope of this stress-strain curve in this region is the Modulus of Elasticity of the prestressing strand within the elastic limit. AASHTO LRFD Article 5.4.4.2 specifies that the Modulus of Elasticity for prestressing strands to be used for design (E_p) is equal to 28,500 ksi.

The AASHTO LRFD specifications do not provide a stress-strain relationship other than within the elastic range as defined by E_p . The Precast Concrete Institute presents the stress-strain relationship up to the ultimate capacity of the strand. For 270 ksi strand, the relationships presented by PCI are:

For $\epsilon_{ps} \leq 0.0086$,

$$(Eqn. 2.25) \quad f_{ps} = 28,500(\epsilon_{ps})$$

For $\epsilon_{ps} > 0.0086$,

$$(Eqn. 2.26) \quad f_{ps} = 270 - \frac{.04}{\epsilon_{ps} - .007}$$

Figure 2.9 is a plot of the stress-strain diagram for prestressing strand using equations 2.25 and 2.26. The value of ultimate strain shown in figure 2.9 can vary with the source of the prestressing strand. Care should be used in selecting an appropriate value if excessive strains are required to provide ultimate capacity of a member.

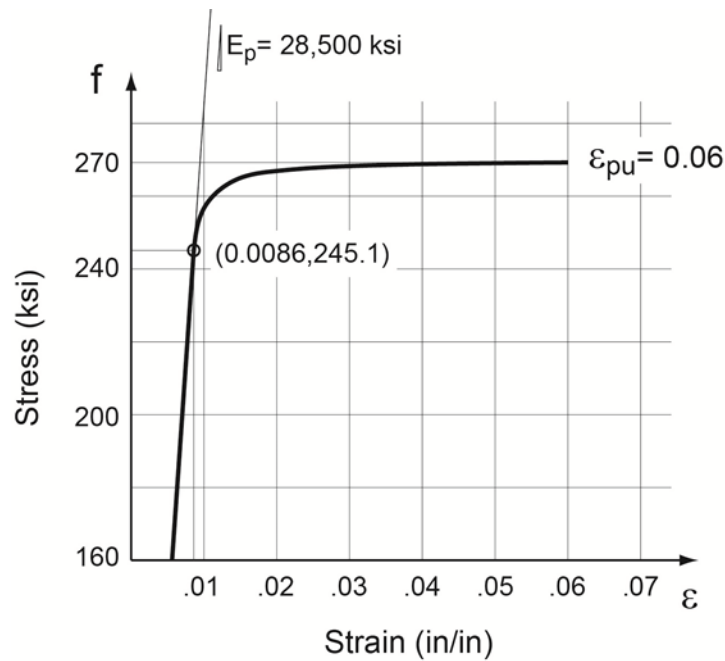


Figure 2.9 – Stress-Strain Diagram for Prestressing Strand (Courtesy PCI)

2.2.3 Relaxation of Steel

Relaxation of steel stress is a result of an increase in elongation over time while under an applied stress. The loss in prestressing stress due to steel relaxation for low relaxation steel over a time interval from (t_1) to (t) may be estimated as:

$$(Eqn. 2.27) \quad R_{lr} = f_{st} \left(\frac{(\log 24t - \log 24t_1)}{45} \right) \left(\frac{f_{st}}{f_y^*} - 0.55 \right)$$

With,

$$(Eqn. 2.28) \quad \left(\frac{f_{st}}{f_y^*} - 0.55 \right) \geq 0.05$$

And,

$$(Eqn. 2.29) \quad f_y^* = 0.90 f_{su}^*$$

- Where: f_{st} =steel stress level at beginning of time interval from (t_1) to (t) (psi)
- f_{su}^* = average stress in prestressed reinforcement at ultimate load (psi)
- f_y^* =yield point stress of prestressing steel (psi)
- t = end of time interval (days)
- t_1 = beginning of time interval (days)

Equations 2.27, 2.28 and 2.29 can be found in Article 10.4.1 of the Guide Specifications for Design and Construction of Segmental Concrete Bridges (2nd Edition 1999, with 2003 Interim Revisions). These equations do not appear in the AASHTO LRFD specifications in the form above, but are incorporated into predictions for prestressing force loss in AASHTO LRFD Article 5.9.5.4.2c.

2.2.4 Fatigue

Tendons in prestressed concrete structures do not experience stress cycling significant enough to induce fatigue problems. Fatigue in concrete bridges is a concern only in certain applications such as cable-stays in cable-stayed bridges where traffic loads significantly affect stress variations.

2.3 Reinforcing Steel

Reinforcing steel shall be in accordance with AASHTO LRFD Article 5.4.3. For this manual only reinforcing steel with a yield stress of 60 ksi is considered. AASHTO LRFD Article 5.4.3.1 permits the use of reinforcing steels with yield stresses greater than 60 ksi, up to 75 ksi, with the approval of the Owner. The modulus of elasticity of the reinforcing steel is 29,000 ksi as per AASHTO LRFD Article 5.4.3.2.

It is interesting to compare the stress-strain relationships for prestressing strands and mild reinforcing steel. Figure 2.10 provides a combined plot of stress-strain relationships used in this manual.

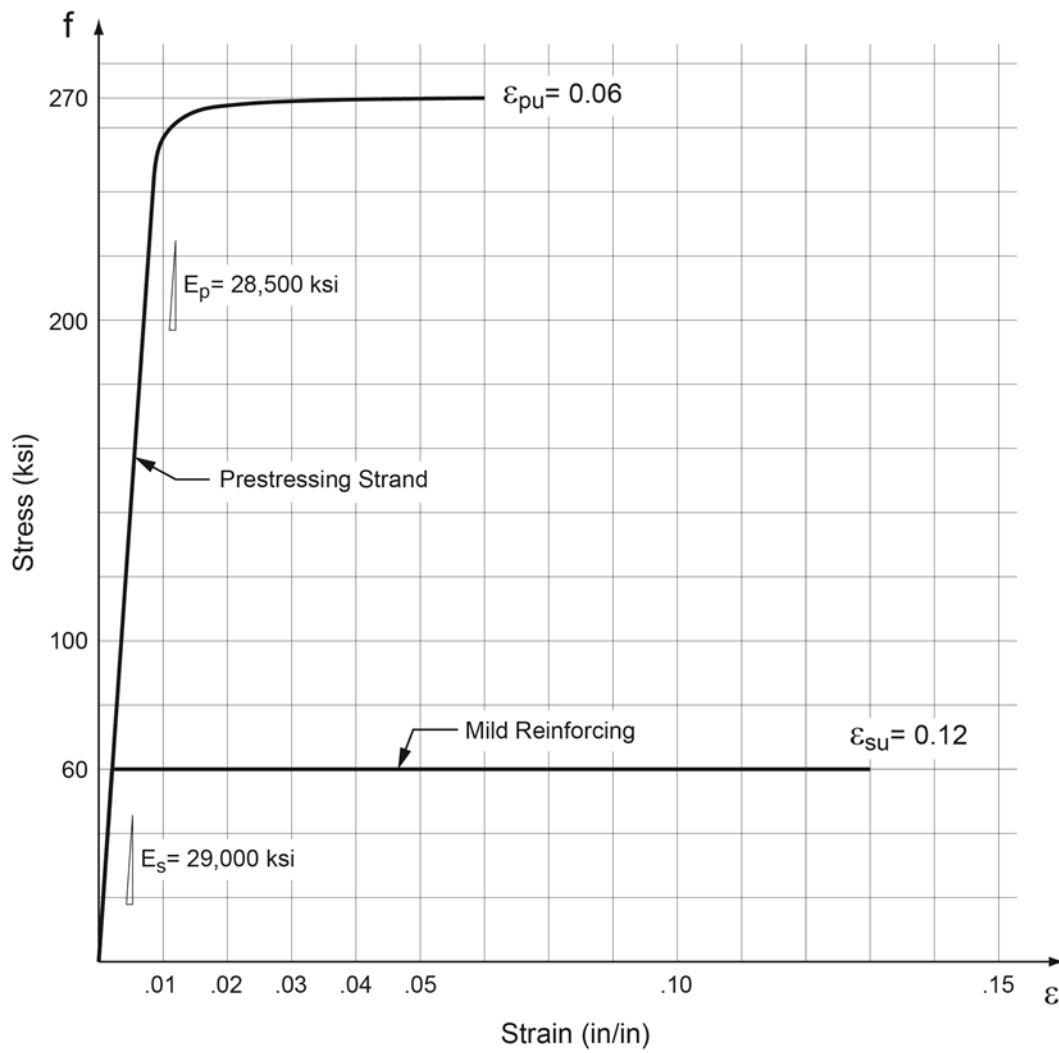


Figure 2.10 – Comparison of Typical Stress-Strain Relationships for Prestressing Strand and Mild Reinforcing

Chapter 3—Prestressing with Post-Tensioning

3.1 Introduction

Prestressing is the application of compressive force to a concrete member in order to offset tensile stresses resulting from other applied loads. Figure 3.1 illustrates the concept of prestressing for a simple span beam.

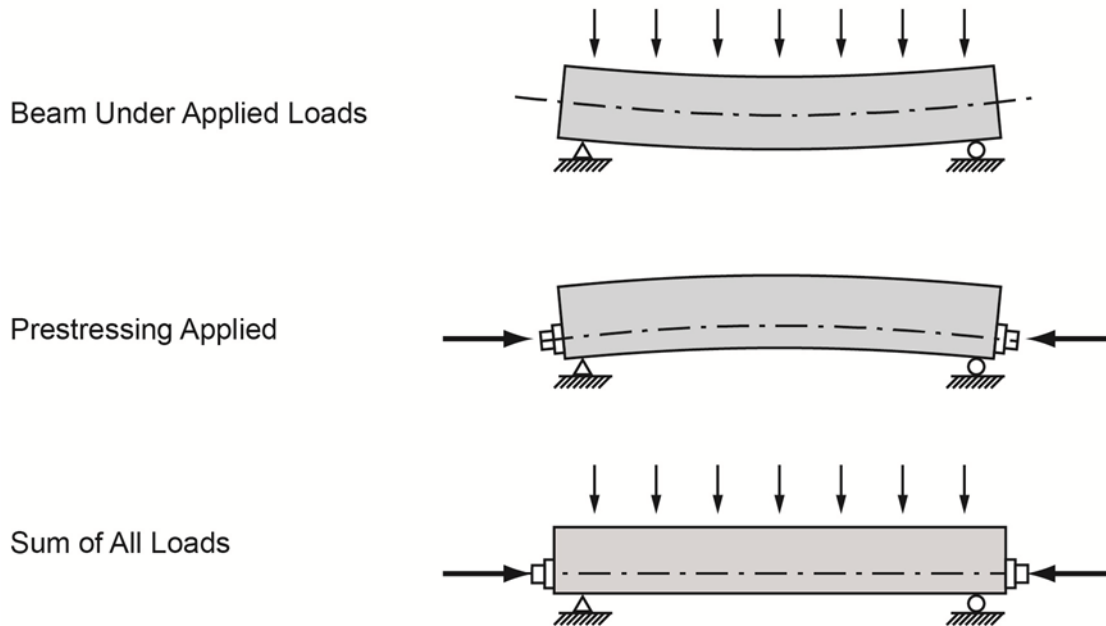


Figure 3.1 – Prestressed Concrete Concepts

Design of prestressed concrete involves optimizing member cross section and prestressing force and geometry to eliminate or offset concrete tension, enhance serviceability and reduce construction cost.

Prestressing is typically applied by means of tensioning high-strength steel strands or bars to react against and compress the concrete member. Prestressing concrete can be achieved in two ways:

- Pre-tensioning – In pre-tensioned members strands are installed along the length of a casting bed and tensioned against restraining bulkheads before the concrete is cast. After the concrete has been placed, allowed to harden and gain sufficient strength, the strands are released and their force is transferred to the concrete member by bond.
- Post-tensioning – Post-tensioned construction involves installing and stressing strand or bar tendons only after the concrete has been placed, cured and hardened. Ducts are placed inside the concrete so that the tendons can be threaded through them after the concrete hardens. Once in place, the tendons are tensioned by jacks and anchored against the hardened member using anchorage devices cast into the concrete.

The content of this manual deals with the application of prestressing through post-tensioning.

3.2 Cross Section Properties and Sign Convention

Depending on the approach taken to analyze a multiple-cell box girder bridge, cross section properties are computed for either the full box girder or idealized “line girders”. Figure 3.2 shows the girders for which cross section properties are typically computed: the full box girder, an internal “girder line,” and an external “girder line.”

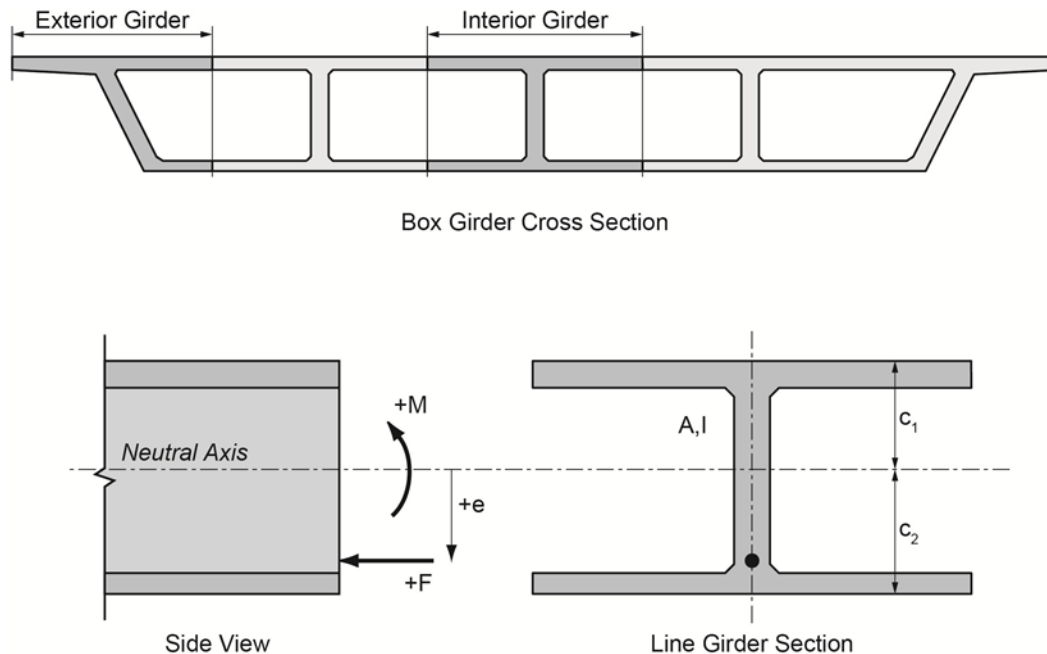


Figure 3.2 – Cross Section Nomenclature and Sign Convention

The cross section characteristics required for the analysis of the box girder are:

- A = Area of Box Girder or Girder Line (ft²)
- I = Moment of Inertia (ft⁴)
- c₁ = Distance from Neutral Axis to top Fiber (ft)
- c₂ = Distance from Neutral Axis to bottom fiber (ft)

The cross sections are assumed to be symmetrical about their vertical axes, and the prestressing is symmetrically applied so that there is no biaxial bending. Figure 3.2 also shows positive sign conventions for prestressing force (F), eccentricity of prestressing (e), and externally applied bending moments (M). For the conventions of this Manual, compressive stresses in the concrete are positive (+) and tensile stresses in the concrete are negative (-).

3.3 Stress Summaries in a Prestressed Beam

Consider the flexure of a simply-supported concrete beam section under the action of its own self weight as shown in figure 3.3. Top and bottom stresses are determined according to elastic beam theory. The top of the beam is in compression; the bottom is in tension. For plain concrete, the tensile stress could exceed the modulus of rupture, crack, and possibly cause failure of the beam.

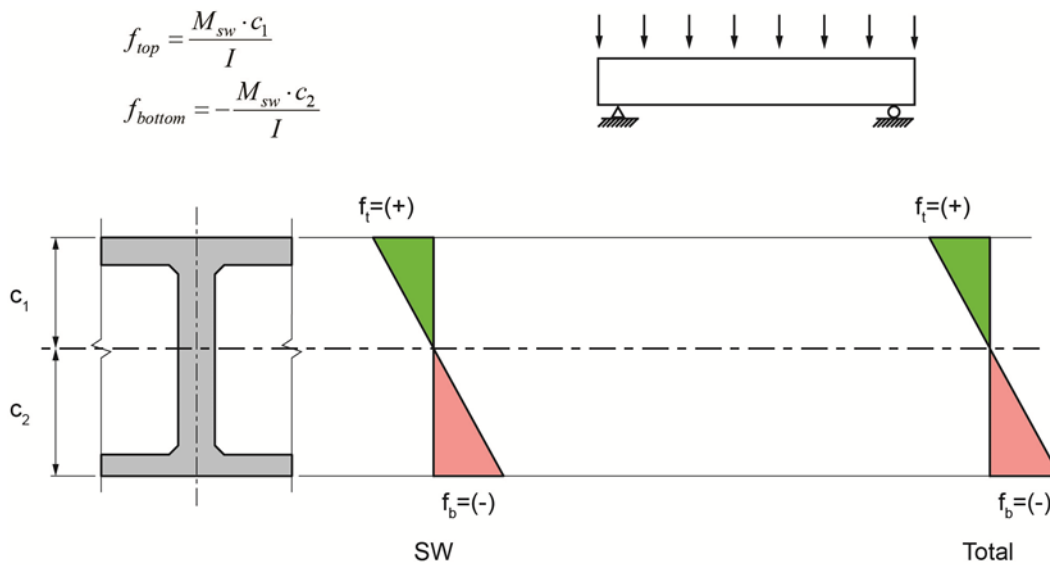


Figure 3.3 – Self Weight Flexure Stress in Simply-Supported Beam

If a purely axial compressive stress is applied through prestressing along the neutral axis of the beam as shown in figure 3.4, the sum of compressive stress at the top of the beam is increased while the tension at the bottom of the beam is reduced. The presence of a net bottom tension would indicate that the beam’s additional load carrying capacity is limited.

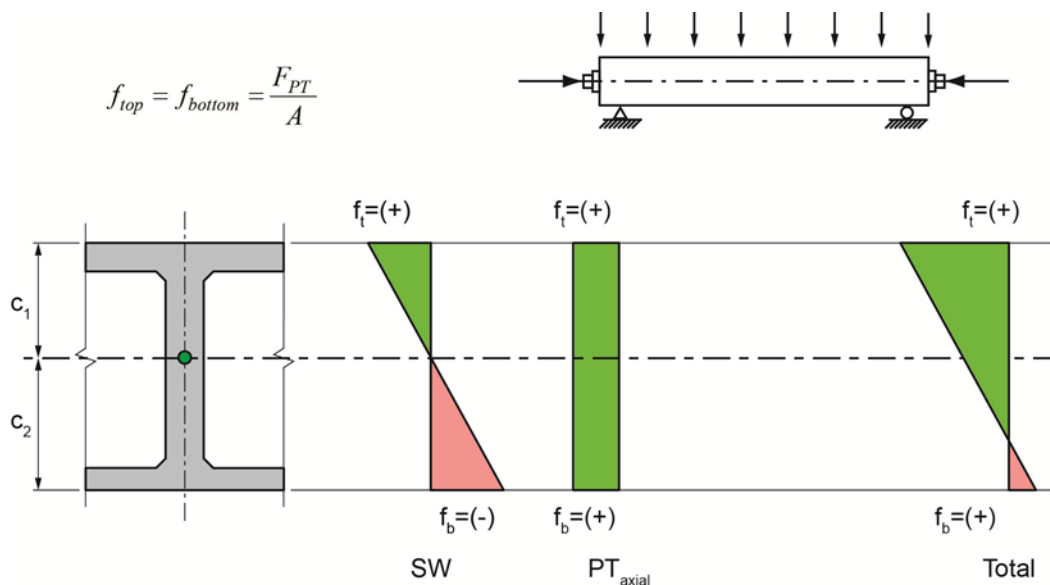


Figure 3.4 – Self Weight Plus Uniform Axial Compression

To improve the effects of the post-tensioning the elevation of the tendon is shifted vertically lower to make the prestressing force eccentric to the beam’s neutral axis (figure 3.5). In this case, in addition to the self-weight stress and the axial prestress effect, the eccentricity causes a resisting flexural moment that induces compression in the bottom of the beam and tension in the top.

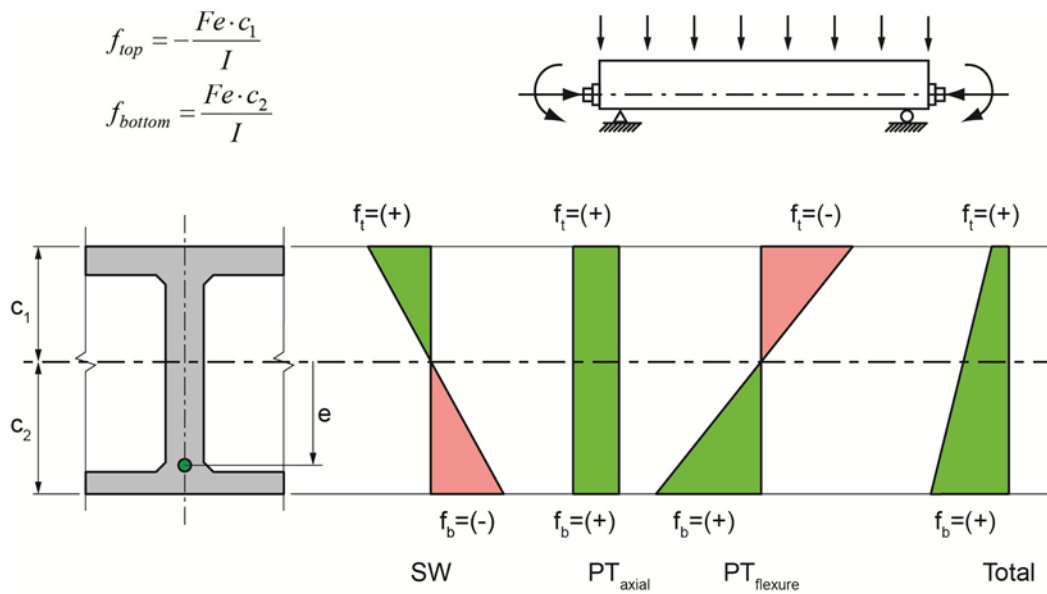


Figure 3.5 – Self Weight, Axial and Eccentric Prestress Stresses

The summation of these three load effects (i.e. self-weight with axial and eccentric prestress) as shown in figure 3.5, results in compressive stress throughout the depth of the beam. The additional compression at the bottom of the beam is available to offset tensile stresses caused by other load effects such as superimposed dead loads, highway traffic loadings, and temperature induced stresses.

Service limit state design of prestressed concrete bridges involves the summing of stresses at cross sections throughout the bridge, and verifying that the resulting stress totals are within allowable limits. In box girder bridges this also includes the summing of axial and shear stresses to verify principal tensile stresses in the webs are within limits.

3.4 Selection of Prestressing Force for a Given Eccentricity

Where service limit state flexural verification of prestressed members involves summing of stresses due to applied forces, it is often more convenient to work with internal forces and moments when designing prestressed members. This section develops expressions for prestressing based on force and eccentricity.

Stresses are determined at the extreme top and bottom fibers by the familiar equations:

(Eqn. 3.1)
$$f_t = \frac{F}{A} - \frac{Fec_1}{I} + \frac{Mc_1}{I}$$

(Eqn. 3.2)
$$f_b = \frac{F}{A} + \frac{Fec_2}{I} - \frac{Mc_2}{I}$$

These equations can be rearranged to express the required prestressing force as a function of the other equation variables.

Consider first the prestressing requirements for the bottom stress. The limiting prestressing force would be that which satisfies equation 3.2 when the bottom stress f_b is set to a permissible concrete stress f_a . Making this substitution and multiplying equation 3.2 through by the cross section inertia and dividing by the distance from the neutral axis to the extreme bottom fiber the equation becomes:

$$(Eqn. 3.3) \quad \frac{f_a I}{c_2} = \frac{FI}{Ac_2} + Fe - M$$

This equation can be reduced further by noting that the left hand side of the equation is a bending moment that produces the permissible stress in the concrete at the bottom of the girder:

$$(Eqn. 3.4) \quad M_{ab} = \frac{f_a I}{c_2}$$

Equation 3.3 now becomes:

$$(Eqn. 3.5) \quad M_{ab} = \frac{FI}{Ac_2} + Fe - M$$

Further simplification is made by defining the dimensionless parameter:

$$(Eqn. 3.6) \quad \rho = \frac{I}{Ac_1 c_2}$$

The parameter ρ is termed the Efficiency of the cross section with regard to prestressing. Cross section efficiencies for three typical shapes are shown in figure 3.6. As seen in this figure, cross section efficiency increases as material is moved away from the neutral axis and is located in top and bottom flanges.

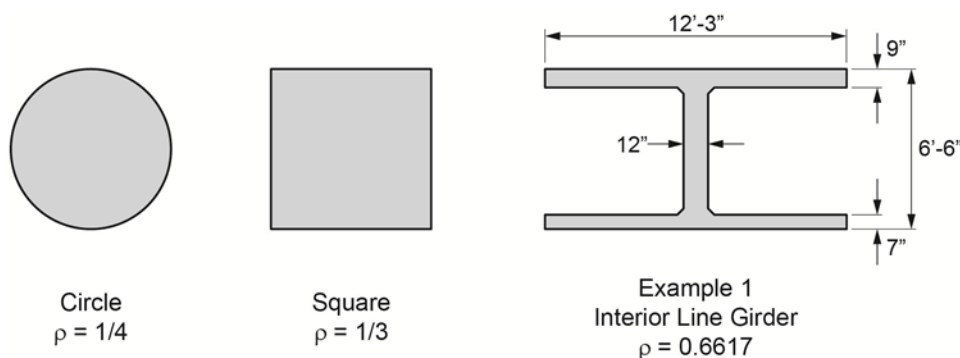


Figure 3.6 – Efficiencies of Various Cross Sections

Recognizing that:

$$(Eqn. 3.7) \quad \rho c_1 = \frac{I}{Ac_2}$$

Equation 3.5 is now simplified to:

$$(Eqn. 3.8) \quad M_{ab} = F \rho c_1 + Fe - M$$

Solving for the prestressing force:

$$(Eqn. 3.9) \quad F = \frac{M + M_{ab}}{\rho c_1 + e}$$

The numerator of this equation is the bending moment at the cross section under study, adjusted by the moment causing allowable stress. The sign of M_a is established by the sign of the allowable stress at the section. A permissible tension would cause M_a to be negative, reducing the required prestressing force. A requirement for a residual compressive stress would cause M_a to be positive, increasing the required prestressing force.

When M_a is established by the minimum allowable stress, equation 3.9 becomes the expression for minimum required prestress force. When maximum permissible compressive stress is controlling, equation 3.9 becomes the expression for maximum permissible prestress force.

This exercise can be repeated for limiting stress control at the top of a cross section. In this case, equation 3.1 can be rearranged to find:

$$(Eqn. 3.10) \quad F = \frac{M - M_{at}}{e - \rho c_2}$$

It is interesting to study equations 3.9 and 3.10 for additional implications. Figure 3.7 shows the internal equilibrium expressed by equation 3.9 for a positive bending moment. Figure 3.8 shows a similar diagram for the equilibrium expressed by equation 3.10.

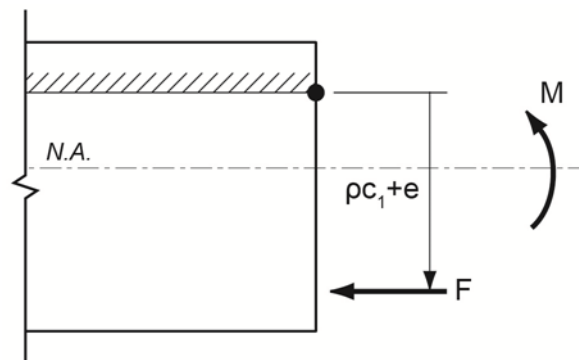


Figure 3.7 – Internal Equilibrium for Positive Bending.

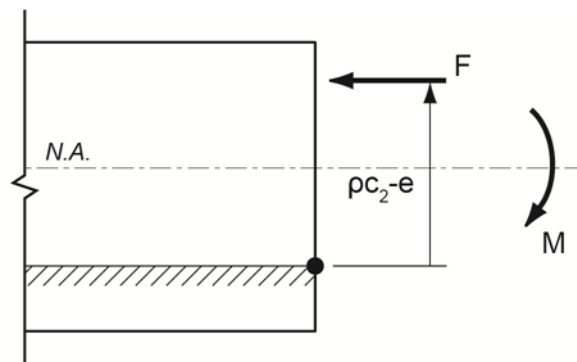


Figure 3.8 – Internal Equilibrium for Negative Bending.

Now consider the case of zero bending moment acting on the cross section. Equation 3.9 becomes:

$$\text{(Eqn. 3.11)} \quad F(\rho c_1 + e) = 0$$

This equation is satisfied in one of two conditions, either the prestressing force is equal to zero or:

$$\text{(Eqn. 3.12)} \quad e = -\rho c_1$$

Equation 3.12 shows that any prestressing force can be applied at a distance of ρc_1 above the neutral axis with the result being zero stress at the bottom of the cross section. Likewise, from equation 3.10:

$$\text{(Eqn. 3.13)} \quad e = \rho c_2$$

Equation 3.13 shows that any prestressing force can be applied at a distance of ρc_2 below the neutral axis with the result being zero stress at the top of the cross section. Graphically, these two limiting eccentricities are seen in figure 3.9.

Together, these limiting eccentricities define the upper and lower locations of the cross section kern—that portion of the cross section through which no tension occurs if the resultant compressive force is located therein. Figure 3.10 shows the layout of the upper and lower kern for a cross section with bending about the horizontal axis. Further analysis of the cross section could be undertaken to define the kern limits in any direction.

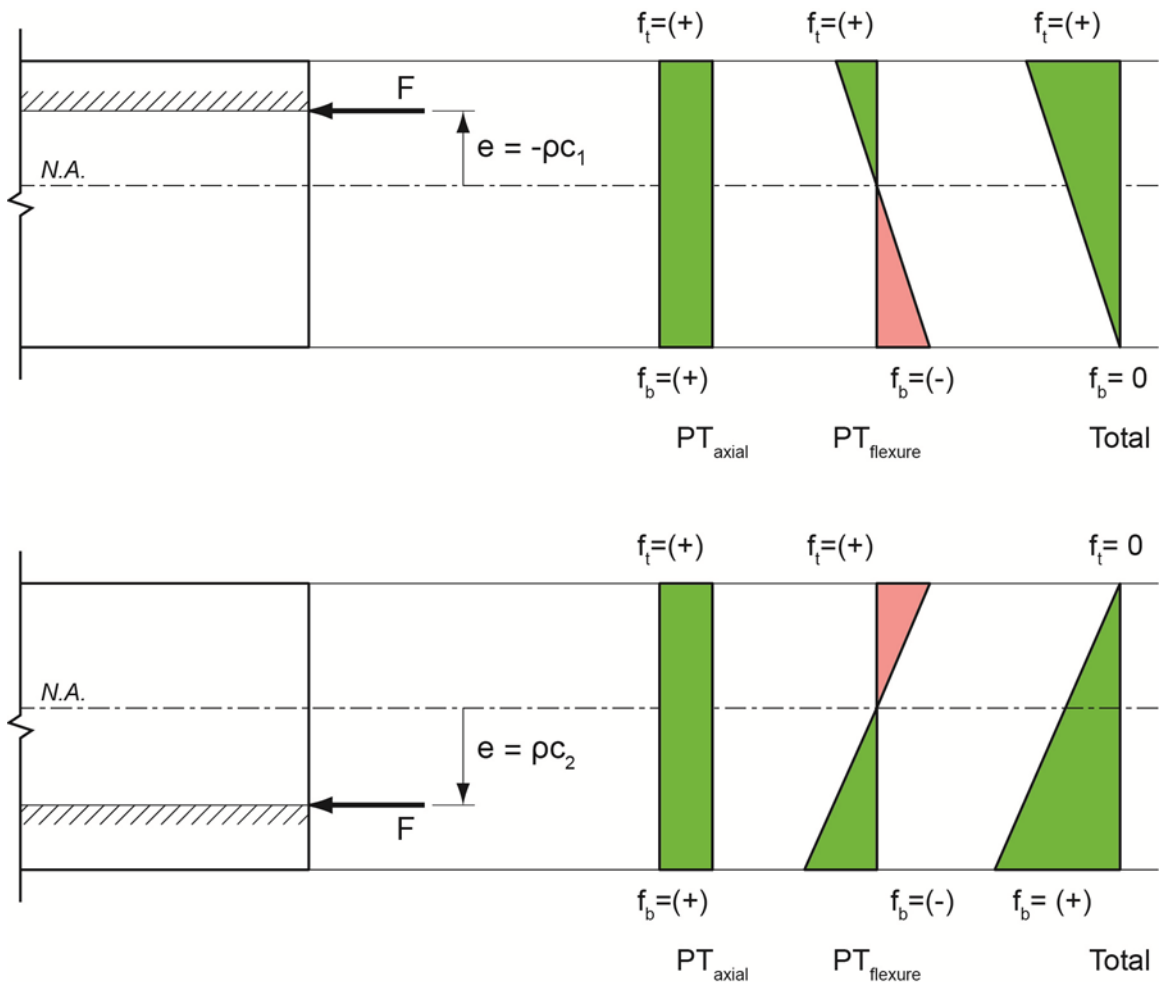


Figure 3.9 – Limiting Eccentricities for Zero Tension Under Axial Force Only

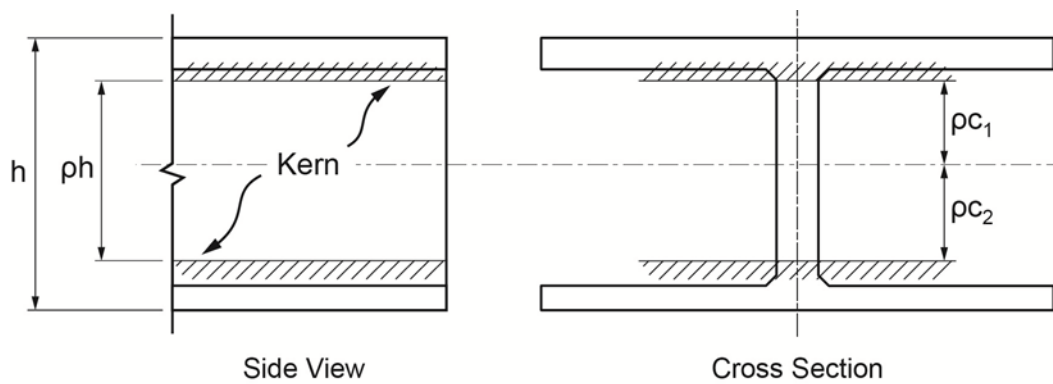


Figure 3.10 – Kern of a Cross Section for Bending About the Horizontal Axis.

Example: Consider the line girder segment of a concrete box girder bridge shown in figure 3.11. The girder is simply supported, with a span length of 120'. In addition to the girder self weight, the girder is subjected to a uniformly distributed load of 1.0 kip/ft. The concrete strength of the girder is 5000 psi. Determine the limiting values of prestressing for maximum and minimum stress at the top and bottom of the girder. The maximum permissible compressive stress is $0.6f'_c$. The minimum permissible tensile stress is $3\sqrt{f'_c}$.

The section properties of the girder are:

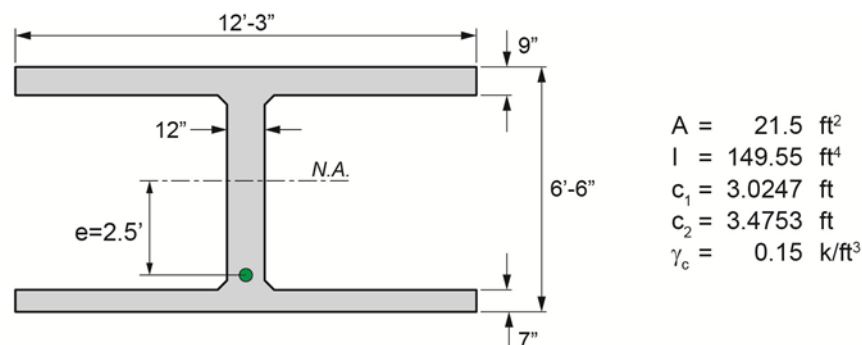


Figure 3.11 –Example Concrete I-Girders

The efficiency of the cross section is:

$$\rho = \frac{149.55}{21.5(3.0247)(3.4753)} = 0.6617$$

The moment required to produce the permissible tensile stress at the bottom-most fiber of the girder is:

$$M_{ab(T)} = -\frac{3\sqrt{f'_c}(I)}{c_2} = -\frac{3\sqrt{5000}(149.55)}{3.4753}(0.144) = -1,314.5 \text{ ft-kips}$$

The moment required to produce the permissible compressive stress at the bottom-most fiber of the girder with no axial force is:

$$M_{ab(C)} = \frac{0.6(f'_c)(I)}{c_2} = \frac{0.6(5000)(149.55)}{3.4753}(0.144) = 18,590 \text{ ft-kips}$$

The moment required to produce the permissible tensile stress at the top-most fiber of the girder is:

$$M_{at(T)} = -\frac{3\sqrt{f'_c}(I)}{c_1} = -\frac{3\sqrt{5000}(149.55)}{3.0247}(0.144) = -1,510.3 \text{ ft-kips}$$

The moment required to produce the permissible compressive stress at the top-most fiber of the girder is:

$$M_{at(C)} = \frac{0.6(f'_c)(I)}{c_1} = \frac{0.6(5000)(149.55)}{3.0247}(0.144) = 21,359 \text{ ft-kips}$$

The mid-span bending moment due to the applied load is:

$$w = 0.15(21.5) + 1 = 4.225 \text{ k / ft}$$

$$M = \frac{wL^2}{8} = \frac{4.225(120)^2}{8} = 7,605 \text{ ft-kips}$$

The minimum prestressing required to limit the bottom girder tension is:

$$F \geq \frac{M + M_{ab(T)}}{\rho c_1 + e} = \frac{7,605 + (-1,314.5)}{0.6617(3.0247) + 2.5} = 1,397.4 \text{ kips}$$

The maximum prestressing permissible to not overstress the bottom of the girder is:

$$F \leq \frac{M + M_{ab(C)}}{\rho c_1 + e} = \frac{7,605 + 18,590}{0.6617(3.0247) + 2.5} = 5,819.2 \text{ kips}$$

The maximum prestressing permissible to not exceed the minimum tension in the top of the girder is:

$$F \leq \frac{M - M_{at(T)}}{e - \rho c_2} = \frac{7,605 - (-1,510.3)}{2.5 - .6617(3.4753)} = 45,487 \text{ kips}$$

The minimum prestressing permissible to not over compress the top of the girder is:

$$F \geq \frac{M - M_{at(C)}}{e - \rho c_2} = \frac{7,605 - 21,359}{2.5 - .6617(3.4753)} = -68,635 \text{ kips}$$

Though the four limiting forces can be computed, the two limiting forces for top stress are not useful for this example. For the case of the maximum top tension, the limiting prestress force causes the bottom of the beam to exceed the maximum compressive stress. To reach the maximum top compression, the post-tensioning force would need to be negative. As a result, for this example, the prestressing force can vary between 1397.4 kips and 5819.2 kips without exceeding allowable stresses.

3.5 Permissible Eccentricities for a Given Prestressing Force

Equations for determining prestressing force for a given eccentricity were developed in the previous section. These equations can be used to solve for the prestressing force at a critical section. With the required prestressing force established, the tendon profile must be established such that the stress limitations are respected along the entire length of the member. Permissible ranges of eccentricity as a function of prestressing force can be determined in a fashion similar to those of the previous section.

Consider the condition of bottom stress in a simple span girder. As in the previous Section, equation 3.2 was simplified to equation 3.8, which is repeated here:

$$\text{(Eqn. 3.8)} \quad M_{ab} = F \rho c_1 + Fe - M$$

Solving for the eccentricity results in:

$$\text{(Eqn. 3.14)} \quad e = \left(\frac{M + M_{ab}}{F} \right) - \rho c_1$$

When the controlling bottom stress is minimum stress then equation 3.14 becomes the expression for minimum eccentricity. When the controlling bottom stress is compression, equation 3.14 is the expression for maximum eccentricity.

Likewise, the eccentricity limits established by allowable stress at the top of the girder can be expressed as:

$$\text{(Eqn. 3.15)} \quad e = \left(\frac{M - M_{at}}{F} \right) + \rho c_2$$

When the controlling top stress is minimum stress then equation 3.15 becomes the expression for maximum eccentricity. When the controlling bottom stress is compression, equation 3.15 is the expression for minimum eccentricity.

Using equations 3.14 and 3.15 along with maximum and minimum allowable stresses, we can define ranges of eccentricity. For stress control on the bottom of the girder:

$$\text{(Eqn. 3.16)} \quad \left(\frac{M + M_{ab(T)}}{F} \right) - \rho c_1 \leq e \leq \left(\frac{M + M_{ab(C)}}{F} \right) - \rho c_1$$

For stress control on the top of the girder:

$$\text{(Eqn. 3.17)} \quad \left(\frac{M - M_{at(C)}}{F} \right) + \rho c_2 \leq e \leq \left(\frac{M - M_{at(T)}}{F} \right) + \rho c_2$$

Where M_{at} represents the moment to cause the allowable tensile stress (or minimum compression), and M_{ac} represents the moment to cause allowable compression.

Example: Consider the concrete line girder analyzed in the previous example. Determine the limits of permissible eccentricity at tenth points along the girder for a prestressing force of 1200 kips.

Recall from the previous example:

$$M_{ab(T)} = -1,314.5 \text{ ft} - \text{kips} \quad M_{at(T)} = -1,510.3 \text{ ft} - \text{kips}$$

$$M_{ab(C)} = 18,590 \text{ ft} - \text{kips} \quad M_{at(C)} = 21,359 \text{ ft} - \text{kips}$$

The kern of the cross section is defined by:

$$\rho c_1 = 0.6617(3.0247) = 2.0014$$

$$\rho c_2 = 0.6617(3.4753) = 2.2996$$

The limits of eccentricity with regard to bottom of girder stress are defined as:

$$\left(\frac{M(x) + (-1314.5)}{1200} \right) - 2.0014 \leq e \leq \left(\frac{M(x) + 18590}{1200} \right) - 2.0014$$

The limits of eccentricity with regard to top of girder stress is defined as:

$$\left(\frac{M(x) - 21359}{1200} \right) + 2.2996 \leq e \leq \left(\frac{M(x) - (-1510.3)}{1200} \right) + 2.2996$$

For simple spans subjected to a uniform load:

$$M(x) = -\frac{px^2}{2} + \frac{pLx}{2} \quad p = 4.225 \text{ k} / \text{ft}$$

The resulting limiting eccentricities are:

kL	x	M(x)	Bottom Stress		Top Stress	
			e _{min}	e _{max}	e _{min}	e _{max}
0	0	0	-2.6275	6.8508	-7.8714	1.5805
0.1	12	2737.8	-1.3237	8.1546	-6.5677	2.8842
0.2	24	4867.2	-0.3097	9.1686	-5.5537	3.8982
0.3	36	6388.2	0.4145	9.8928	-4.8294	4.6225
0.4	48	7300.8	0.8491	10.3274	-4.3949	5.0570
0.5	60	7605	0.9940	10.4723	-4.2500	5.2019

Table 3.1 – Limiting Eccentricities for Example Girder

Graphically, these limiting eccentricities of this example are shown in figure 3.12. The tendon profile can lie within the shaded area in the sketch while respecting the minimum and maximum allowable flexural stresses in the girder.

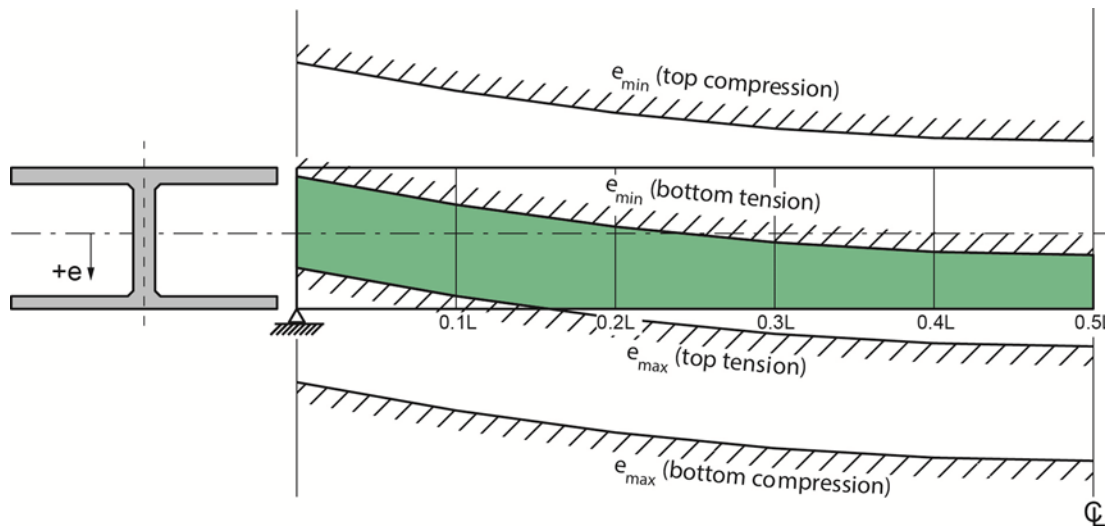


Figure 3.12 – Limiting Eccentricities for the Example Bridge

3.6 Equivalent Forces Due To Post-Tensioning and Load Balancing

Figure 3.13 shows a tendon profile that would satisfy the requirements permissible eccentricity in the previous example.

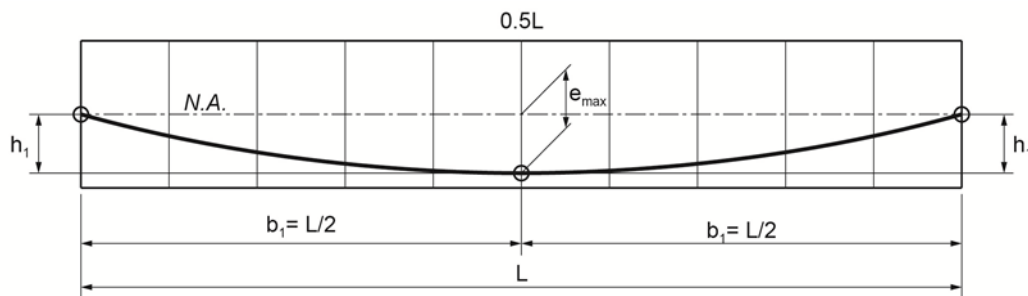


Figure 3.13 – Parabolic Tendon Profile for a Simple Span Girder

The profile of this tendon follows a parabolic trajectory, defined by the following equation for eccentricity:

(Eqn. 3.18)

$$e(x) = -\frac{4e_{\max}x^2}{L^2} + \frac{4e_{\max}x}{L}$$

The moment caused by the post-tensioning, assuming a constant force along the length of the tendon, would also be parabolic:

(Eqn. 3.19)
$$M_{PT}(x) = F \left(-\frac{4e_{\max} x^2}{L^2} + \frac{4e_{\max} x}{L} \right)$$

The parabolic bending moment caused by the post-tensioning can be equated to the bending moment created by the application of a uniform load distributed over the span length. For a load p , the simple span bending moment is:

(Eqn. 3.20)
$$M_p(x) = -\frac{px^2}{2} + \frac{pLx}{2}$$

Equations 3.19 and 3.20 can be equated and the equivalent uniform load determined:

(Eqn. 3.21)
$$-\frac{px^2}{2} + \frac{pLx}{2} = F \left(-\frac{4e_{\max} x^2}{L^2} + \frac{4e_{\max} x}{L} \right)$$

(Eqn. 3.22)
$$\frac{p}{2}(-x^2 + Lx) = \frac{4Fe_{\max}}{L^2}(-x^2 + Lx)$$

(Eqn. 3.23)
$$p_{\text{equivalent}} = \frac{8Fe_{\max}}{L^2}$$

Figure 3.14 shows the parabolic tendon layout and the resulting equivalent forces acting on the concrete girder. In this layout the tendon has no eccentricity at the ends of the span. If there were eccentricities at the ends of the span, these would be represented by end moments equal to the prestressing force times the end eccentricity. Note that the equivalent horizontal force in the lower diagram is made equal to the prestressing force. This approximation is typically used for simplicity in hand calculation, as tendon profiles are flat and that at any location $F \approx F \cos(\alpha)$, where α is the angle of the tendon relative to horizontal.

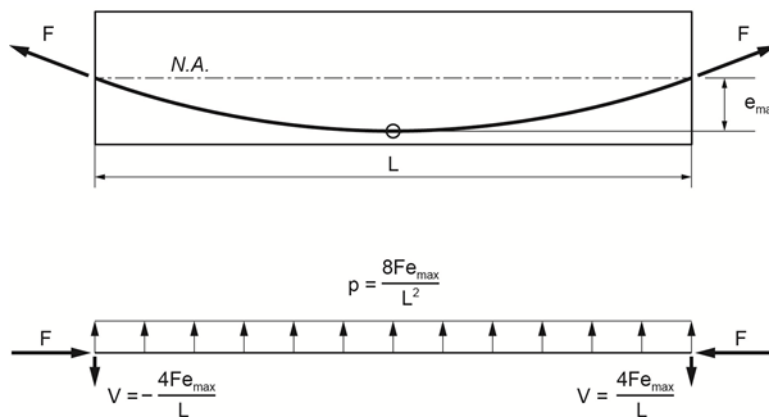


Figure 3.14 – Equivalent Forces Resulting from Prestressing

Rearranging equation 3.22, we can find the prestressing force required to offset an applied uniformly distributed load. The state of stress all along the length of the girder would be uniform compression over the depth of the girder ($F_{balancing}/A_{girder}$).

Eqn. 3.24

$$F_{balancing} = \frac{pL^2}{8e_{max}}$$

Load balancing has great merit in some prestressed concrete members. Most typically, however, the required quantity of prestressing is great, and cost effectiveness is found in reducing the applied prestressing to satisfy acceptable limits of tension in the concrete elements.

Example: For the girder of the previous examples, compare the prestressing force required for minimum bottom tension at mid-span and the prestressing required to balance the total applied load of 4.225 k/ft.

From Equation 3.9, the minimum prestressing force for the minimum bottom tension at mid-span is:

$$F \geq \frac{M + M_{ab(T)}}{\rho c_1 + e} = \frac{7605 + (-1314.5)}{0.6617(3.0247) + 2.5} = 1397.4 \text{ kips}$$

The prestressing force required to balance the applied load is found from equation 3.24

$$F_{balancing} = \frac{4.225(120)^2}{8(2.5)} = 3042 \text{ kips}$$

The post-tensioning force necessary to balance the applied loads is more than twice the force necessary to meet permissible tensile stress criteria.

3.7 Post-Tensioning in Continuous Girders

Up to this point we have been determining the values of prestressing force at cross sections and defining limits of eccentricities of tendons within simple span girders. These girders are free to rotate at their ends under the action of the prestressing. In continuous girders, adjacent spans restrain the rotations of each other. These restraining actions produce continuity moments along the length of the continuous girder.

Figure 3.15a shows a two-span girder, continuous over the middle support. The profile of the two-span post-tensioning tendon is comprised of two, simple span parabolic shapes described in figure 3.13. If the spans were simply supported, the two girders would deflect as in figure 3.15b, with the end rotations shown. Figure 3.15c shows the continuity moments produced to resist the simple span rotations.

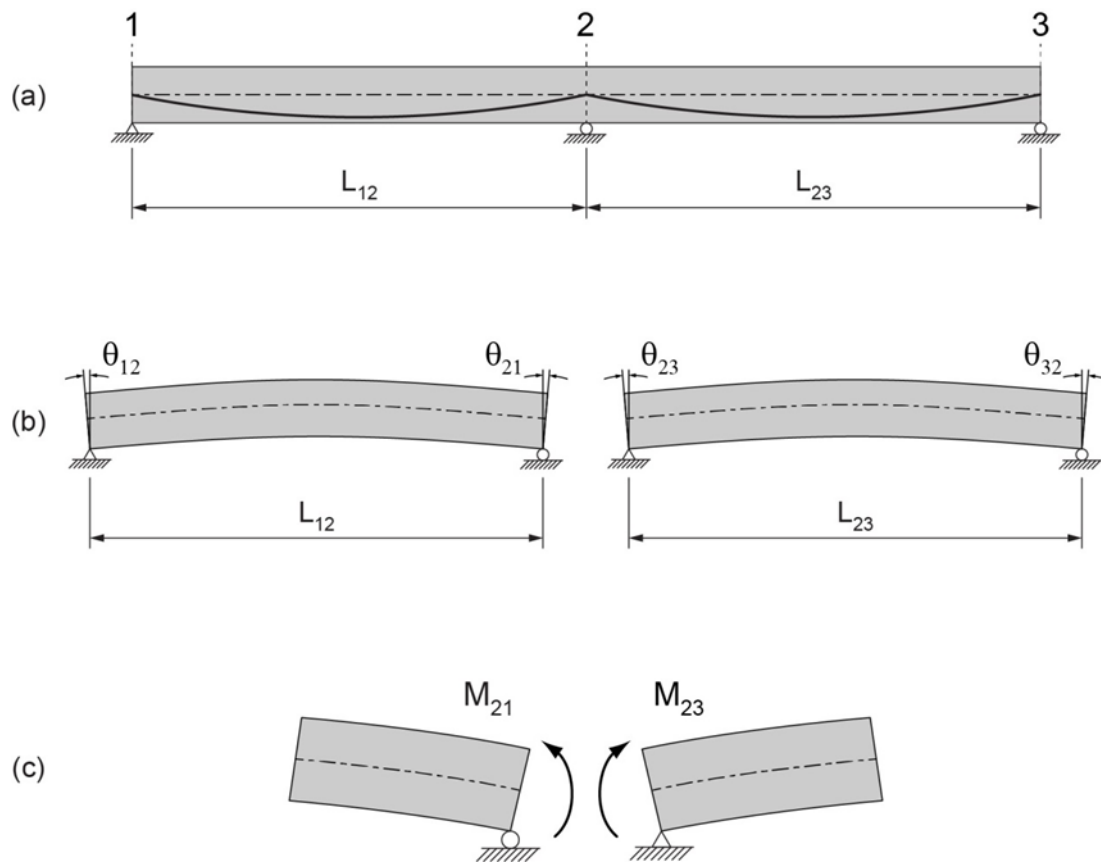


Figure 3.15 – Restraining Moments in Continuous Girders

The bending moment produced by the post-tensioning force acting at an eccentricity is called the *primary moment* due to the post-tensioning. The continuity moments produced in the continuous girders as a result of restraining the individual spans under the action of the post-tensioning are called the *secondary moments* due to post-tensioning.

Figure 3.16 shows the primary, secondary, and the *total moments* caused by the post-tensioning. The primary moment diagram is the result of the parabolically draped post-tensioning profile. The secondary moments are a result of restraining the rotations of the primary moment beam end rotations at the middle supports. The Total post-tensioning moment is the sum of the primary and secondary moments at each section along the length of the bridge.

It is interesting to consider the secondary moments as an effective adjustment to the tendon profile. Dividing the secondary moment at any location by the post-tensioning force at that section establishes a change in eccentricity from the original tendon geometry. Likewise, dividing the total prestressing moment by the axial force results in the effective eccentricity of the tendon profile.

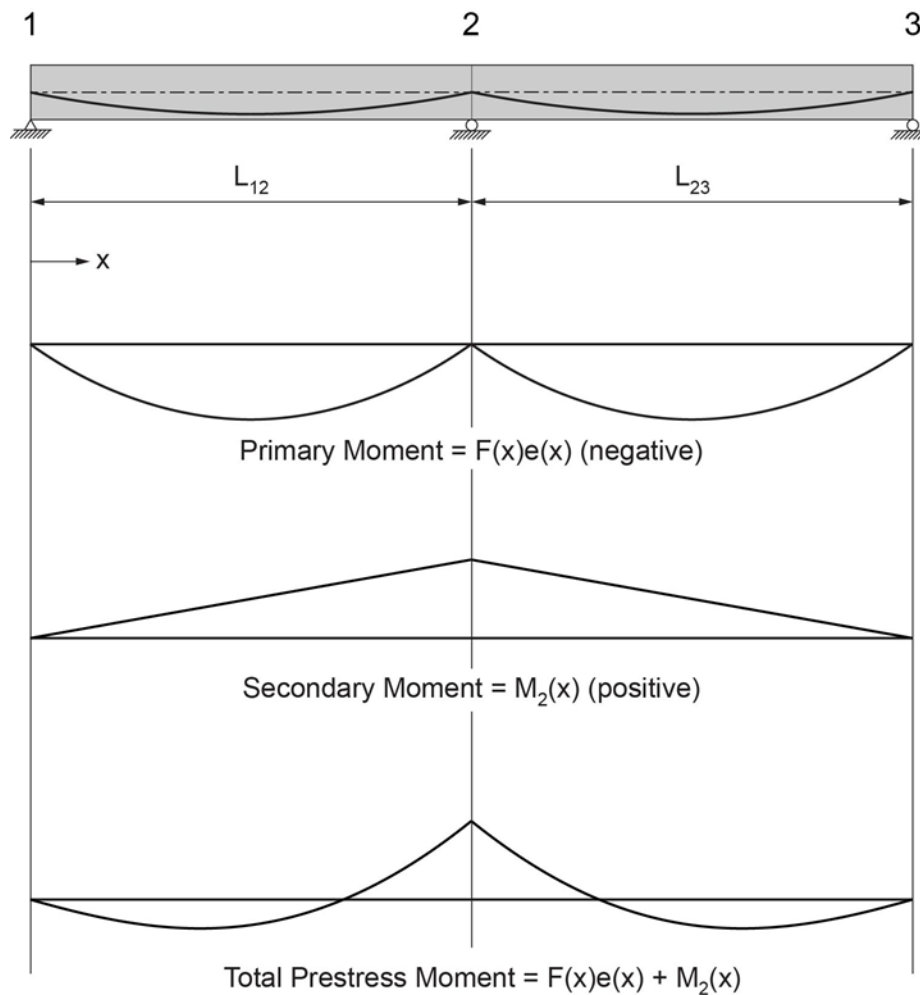


Figure 3.16 – Prestressing Moments for a Two-Span Continuous Girder

For the case of a structure symmetrical about the central support, the moments M_{21} and M_{23} shown in figure 3.15 would be those that would restore the cross section at the middle support to vertical (no net rotation). Considering the two span structure of the last section, the equivalent load of the tendon on the girder is a uniformly distributed load with a value of:

(Eqn. 3.25)
$$p = \frac{8Fe_{\max}}{L^2}$$

The simple beam end rotations caused by this uniform load are:

(Eqn. 3.26)
$$\theta = \frac{pL^3}{24EI} = \left(\frac{8Fe_{\max}}{L^2} \right) \frac{L^3}{24EI} = \frac{Fe_{\max}L}{3EI}$$

The rotation at the end of a beam with constant cross section properties, under the action of an end couple, is:

$$(Eqn. 3.27) \quad \theta = \left(\frac{L}{3EI} \right) M$$

By setting equations 3.26 and 3.27 equal to each other, the value of the continuity moment at the central support of the two span structure can be determined:

$$(Eqn. 3.28) \quad \frac{Fe_{\max} L}{3EI} = \left(\frac{L}{3EI} \right) M$$

$$(Eqn. 3.29) \quad M_{21} = M_{32} = Fe_{\max}$$

The bending moment diagram for the combined effects of primary and secondary prestressing moments is shown in figure 3.17.

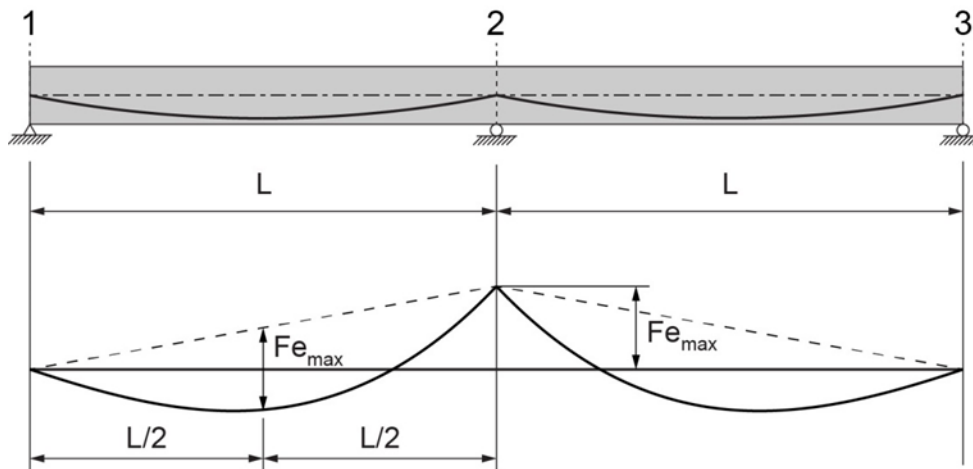


Figure 3.17 – Total Prestressing Moments for a Two-Span Continuous Girder

The impact of the secondary moments on the effective eccentricity for this example is:

- The effective eccentricity at the mid-span of the spans is reduced by half to $Fe_{\max}/2$.
- Though the tendon profile has no real eccentricity at the central support, the effective eccentricity is equal to the maximum eccentricity at the center of the spans.

Note: The preceding discussion considers a two span continuous bridge with a constant and symmetric post-tensioning force. In actual design there would be losses along the length of the tendon, and most likely, tendons of a two-span bridge would only be stressed from one end. See chapter 4 for a further discussion of post-tensioning losses

3.8 Tendon Profiles—Parabolic Segments

In section 3.6, a parabolic tendon was introduced to offset the effects of uniformly distributed applied forces. This is typically the case for cast-in-place concrete box girder bridges where the majority of the applied loads result from the uniformly distributed effects of girder self weight and barrier railing (DC), uniformly applied superimposed dead loads such as future wearing surfaces (DW) and the uniform load portion of the HL93 notional load. Rather than express the parabolic layout over its full length, the tendon geometry is typically subdivided into parabolic half-segments as shown in figure 3.18.

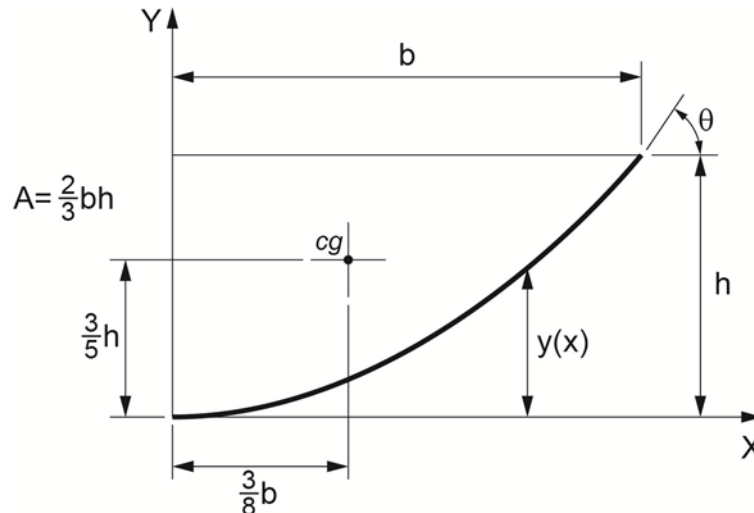


Figure 3.18 – Tendon Profile Parabolic Segment

The elevation of the tendon profile at a horizontal distance from the origin is given as:

(Eqn. 3.30)
$$y = \frac{h}{b^2} x^2$$

The slope of the tendon profile is:

(Eqn. 3.31)
$$\frac{dy}{dx} = \frac{2h}{b^2} x$$

And the angle of the tendon profile at the end of the parabolic segment is:

(Eqn. 3.32)
$$\theta = \frac{dy}{dx}(b) = \frac{2h}{b} (\text{radians})$$

The tendon profiles used for the two-span continuous girder in this Chapter were parabolically draped tendons similar to a simple span girder. Though these profiles were useful to demonstrate principles of the development of secondary moments, they are not efficient with regard to design and construction of continuous box girder bridges. The secondary moment in the positive bending region is excessive, and though effective eccentricity was developed over

the middle support, typically more effective eccentricity is needed to optimize post-tensioning quantities.

Using parabolic segments, tendon profiles can be developed which improve post-tensioning effectiveness. Figures 3.19 and 3.20 show the more typical layout of tendon profile for continuous bridges. Figure 3.19 shows the profile for an end span of a continuous unit. Figure 3.20 shows the profile for an interior span.

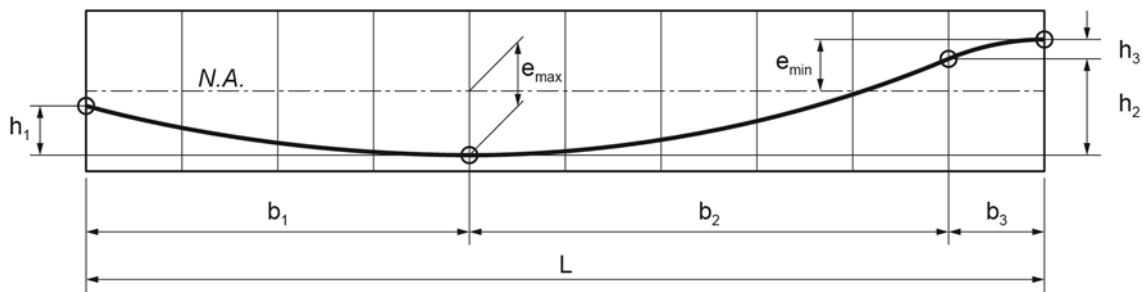


Figure 3.19 – Typical End Span Tendon Profile for Continuous Superstructures

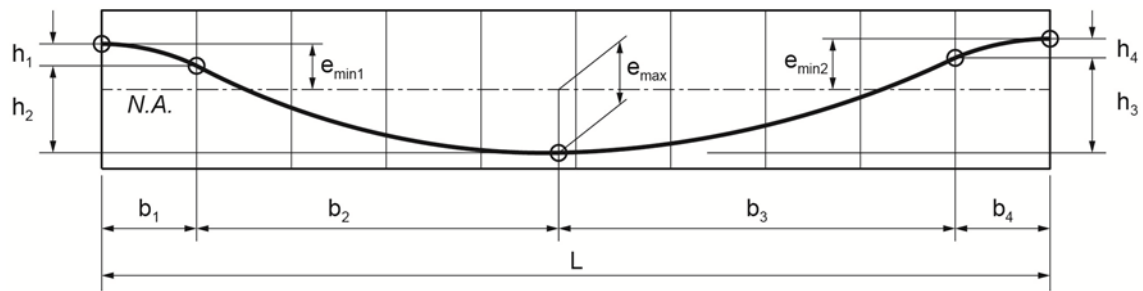


Figure 3.20 – Typical Interior Span Tendon Profile for Continuous Superstructures

When using parabolic segments to define tendons, it is required to maintain tendon slopes at junctions between the parabolic segments. Consider the common point of the parabolic segments within lengths b_2 and b_3 in figure 3.18. From Equation 3.32:

(Eqn. 3.33)
$$\theta_2 = \frac{2h_2}{b_2}$$

And,

(Eqn. 3.34)
$$\theta_3 = \frac{2h_3}{b_3}$$

Equating these two tendon slopes, we find relationships between parabolic segment run and rise:

(Eqn. 3.35)
$$\frac{h_2}{b_2} = \frac{h_3}{b_3}$$

Example: Using the two-span girder of the previous examples and the tendon profile shown in figure 3.21, compute the secondary moments for a post-tensioning force F .

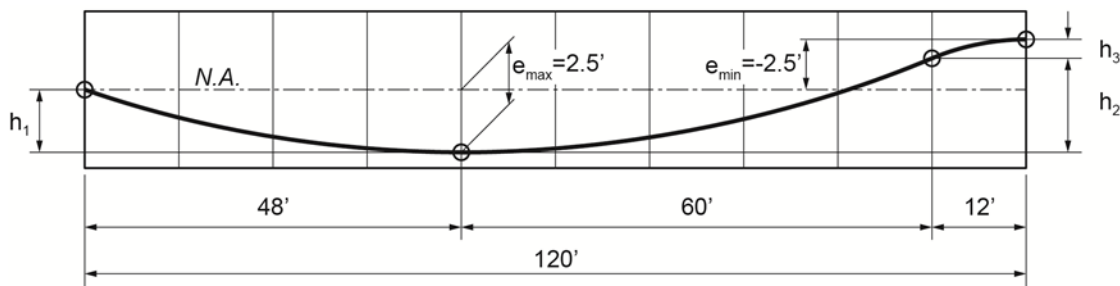


Figure 3.21 – Example Tendon Profile Parabolic Segments

The horizontal run of the tendon profiles are given. Complete the definition of the parabolic tendon segments by determining their rises. The first parabolic segment terminates at the neutral axis, so by inspection $h_1=2.5'$. The rises of the second and third parabolic segments are found by observing that:

$$h = h_2 + h_3 = e_{\max} - e_{\min} = 4.5'$$

Rearranging equation 3.35 leads to:

$$h_3 = h_2 \left(\frac{b_3}{b_2} \right)$$

Combining these expressions:

$$h = h_2 + h_2 \left(\frac{b_3}{b_2} \right) = 4.5'$$

Solving for h_2 :

$$h_2 = \frac{h}{1 + \left(\frac{b_3}{b_2} \right)} = \frac{4.5'}{1 + \left(\frac{12'}{60'} \right)} = 3.75'$$

And h_3 :

$$h_3 = h - h_2 = 4.5' - 3.75' = 0.75'$$

End rotations are found by the conjugate beam method, in which the end reactions of the conjugate beam, loaded with the curvature diagram (moment/EI), are equal to the end rotations. The bending moment for which rotations are to be computed is the primary prestressing moment. Prestressing force F , and beam stiffness, EI , are constant along the length of the structure in this example. Figure 3.22 shows curvature diagram due to the post-tensioning tendon.

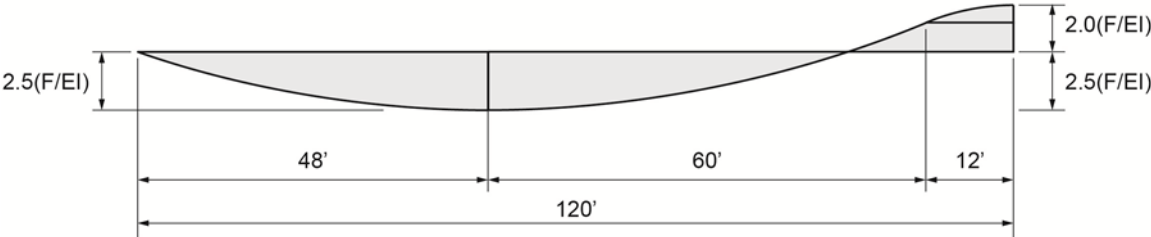


Figure 3.22 – Curvature Diagram for Prestressing

The forces acting on the conjugate beam are found by concentrating the curvature diagram into sections that can be easily expressed geometrically. For the tendon layout of this problem the curvature diagram is concentrated into four conjugate beam loads—the three parabolic segments and a rectangular segment which accounts for the fact that the transition between the positive and negative curvatures do not occur at the neutral axis. Figure 3.23 shows the four areas of concentrated curvature.

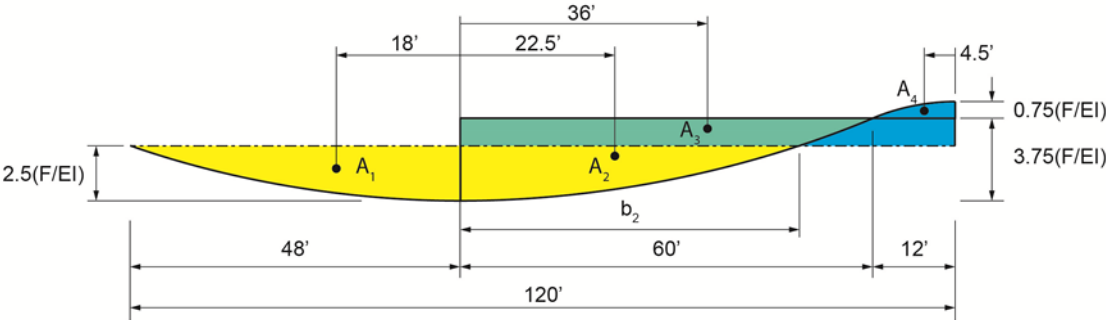


Figure 3.23 – Curvature Diagram for Prestressing

Working from left to right, the first load is the concentration of the first parabolic segment (A_1):

$$A_1 = \frac{2}{3}(48)(2.5)\left(\frac{F}{EI}\right) = 80\left(\frac{F}{EI}\right) \qquad x_{cg1} = 48 - \frac{3}{8}(48) = 30 \text{ ft}$$

The second parabolic segment (A_2) is concentrated to:

$$A_2 = \frac{2}{3}(60)(3.75)\left(\frac{F}{EI}\right) = 150\left(\frac{F}{EI}\right) \quad x_{cg2} = 48 + \frac{3}{8}(60) = 70.5 \text{ ft}$$

The third area, A_3 , is the rectangular area that when subtracted from A_2 results in the positive curvature between A_4 and the neutral axis.

$$A_3 = 72(2.5 - 3.75)\left(\frac{F}{EI}\right) = -90\left(\frac{F}{EI}\right) \quad x_{cg3} = 48 + \frac{60 + 12}{2} = 78 \text{ ft}$$

The fourth load is:

$$A_4 = \frac{2}{3}(12)(0.75) = -6\left(\frac{F}{EI}\right) \quad x_{cg4} = 120 - \frac{3}{8}(12) = 115.5 \text{ ft}$$

With the loads computed, the reaction on the conjugate beam can be found. Figure 3.24 shows the loaded conjugate beam

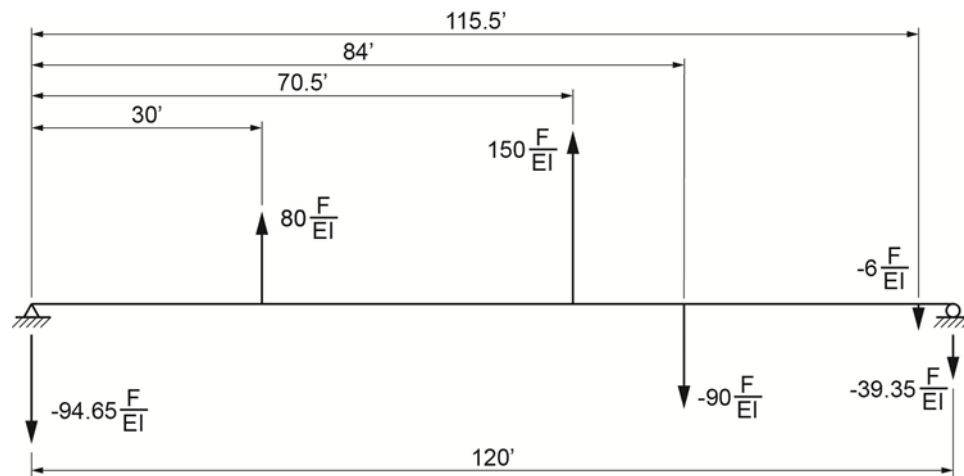


Figure 3.24 – Loaded Conjugate Beam

The reactions (end rotations) are:

$$\theta_{left} = 94.65\left(\frac{F}{EI}\right) \quad \theta_{right} = 39.35\left(\frac{F}{EI}\right)$$

As in the previous example, the secondary moment at the interior support is equal to the moment that restrains the rotation, returning the section to vertical.

$$\theta = \left(\frac{L}{3EI} \right) M = 39.35 \left(\frac{F}{EI} \right)$$

Solving for the secondary moment at the middle support (see Figure 3.16):

$$M_{21} = M_{23} = \left(\frac{3}{120} \right) 39.35 = 0.98F$$

It is interesting to compare the total prestressing moments in terms of effective eccentricity for this example (with parabolic segments and eccentricity at the middle pier) and the tendon profile shown in figure 3.17 (single parabola over the span lengths, with no eccentricity at the middle pier).

The effective eccentricities of this example at pier and mid-span are:

$$e_{pier} = -2.0' - 0.98' = -2.98' \quad e_{mid} = 2.35' - 0.49' = 1.86'$$

The effective eccentricities for the tendon profile shown in Figure 3.17 are:

$$e_{pier} = 0.0' - 2.5' = -2.5' \quad e_{mid} = 2.5' - 1.25' = 1.25'$$

The tendon profiles of this example are 20 percent more effective at the middle support and 50 percent more effective at mid-span

Secondary moments for the two-span girder in this Section were readily computed because of the structure's symmetry. More complex structures require a generalized approach to determine secondary moments using hand calculations. Appendix A of this manual presents a generalized flexibility-based hand method for solving continuous bridges. The method begins with the determination of span end rotations under the action of the applied loads. These end rotations are then used to determine continuity moments at the end of that span. This procedure is performed for all loaded spans, and the results summed to complete the analysis.

Chapter 4—Prestressing Losses

Post-tensioning tendon forces are established in design to provide precompression to offset undesirable tensile stresses in the concrete box girder. The engineer conveys the tendon force requirements in the contract drawings as either the required *jacking force* at the end of the tendon or the final *effective force* at some point along the length of the tendon. The differences between jacking forces and effective forces are the prestressing force *losses*. Prestressing force losses can be grouped into two families: 1) instantaneous losses related to the mechanics of the post-tensioning system and tendon geometry, and 2) time-dependent losses related to the material properties of the concrete and prestressing steel. The components of prestressing losses addressed in this chapter are:

Instantaneous Losses

- Duct friction due to curvature
- Wobble (unintentional friction)
- Wedge Set (or Anchor Set)
- Elastic shortening of concrete

Time-Dependent Losses

- Shrinkage of concrete
- Creep of concrete
- Relaxation of prestressing steel

4.1 Instantaneous Losses

4.1.1 Friction and Wobble Losses (AASHTO LRFD Article 5.9.5.2.2b)

Friction between the strands and duct during stressing is related to intended angular changes in the tendon geometry. The top sketch in figure 4.1 shows the trajectory of a tendon within a desired duct profile. As the tendon is stressed, friction where the tendon contacts the duct wall reduces the force in the tendon. The friction coefficient (μ), defined to predict losses of this type, is a function of the duct material.

Predicting friction losses along the length of a tendon using the friction coefficient alone has not proven to correlate well with field results. Another coefficient of friction loss, wobble (K), is used to account for unintended friction between strand and duct as a result of unintended duct misalignments. The concept of duct wobble is shown in the bottom sketch of figure 4.1.

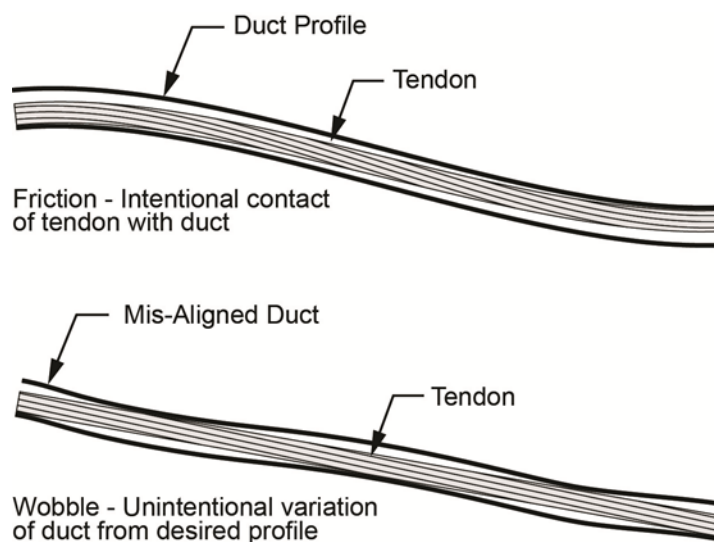


Figure 4.1 – Friction and Wobble

The equation to predict losses due to friction and wobble is found by considering a small section of tendon following a circular path as shown in figure 4.2.

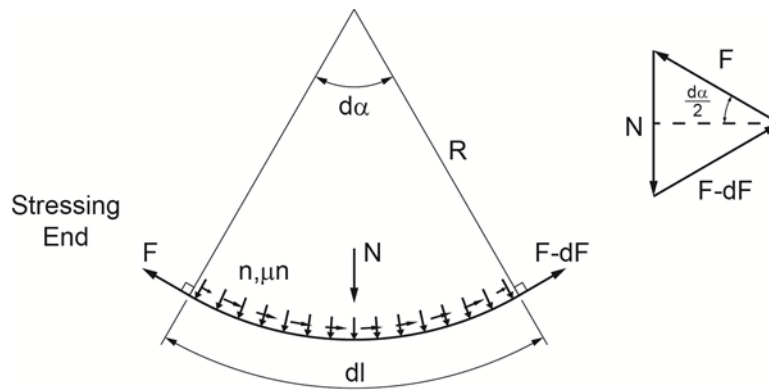


Figure 4.2 – Section of Tendon with Radial Alignment

The variables in figure 4.2 are defined as:

- $d\alpha$ = angle change
- dl = tendon length through angle $d\alpha$
- F = is the force at the stressing end of the section of tendon
- dF = loss in tendon force P resulting from friction and wobble
- n = distributed radial force resisting the angle change of the tendon force.
- N = resultant of distributed radial force, n
- μ = friction coefficient

For an infinitesimally small element of tendon, the vertical equilibrium can be expressed as:

$$(Eqn. 4.1) \quad N = F \sin\left(\frac{d\alpha}{2}\right) + (F - dF) \sin\left(\frac{d\alpha}{2}\right)$$

Or,

$$(Eqn. 4.2) \quad N = F \sin\left(\frac{d\alpha}{2}\right) + F \sin\left(\frac{d\alpha}{2}\right) - dF \sin\left(\frac{d\alpha}{2}\right)$$

For small angles,

$$(Eqn. 4.3) \quad \sin\left(\frac{d\alpha}{2}\right) \approx \frac{d\alpha}{2} \text{ (radians)}$$

And,

$$(Eqn. 4.4) \quad -dF \sin\left(\frac{d\alpha}{2}\right) \approx 0$$

So that Equation 4.1 can be reduced to,

$$(Eqn. 4.5) \quad N = Fd\alpha$$

Summing the forces horizontally,

$$(Eqn. 4.6) \quad \mu N = -F \cos\left(\frac{d\alpha}{2}\right) + (F - dF) \cos\left(\frac{d\alpha}{2}\right)$$

Again, for small angles,

$$(Eqn. 4.7) \quad \cos\left(\frac{d\alpha}{2}\right) \approx 1$$

Equation 4.6 then reduces to,

$$(Eqn. 4.8) \quad dF = \mu N$$

Combining expressions 4.5 and 4.8,

$$(Eqn. 4.9) \quad dF = \mu F d\alpha$$

We define the wobble coefficient, K , as a function of the prestressing force, per unit length, l , along the tendon so that the total loss in prestress force becomes:

$$(Eqn. 4.10) \quad dF = \mu F d\alpha + K dl$$

The change in prestress force as a function of the original force is,

$$(Eqn. 4.11) \quad \frac{dF}{F} = \mu d\alpha + K dl$$

Which can be integrated,

$$(Eqn. 4.12) \quad \int_{F_0}^{F_l} \frac{dF}{F} = - \left(\mu \int_0^{\alpha} d\alpha + K \int_0^l dl \right)$$

To find,

$$(Eqn. 4.13) \quad \ln\left(\frac{F_l}{F_0}\right) = -(\mu\alpha + Kl)$$

which can be expressed as,

$$(Eqn. 4.14) \quad F_l = F_0 e^{-(\mu\alpha + Kl)}$$

Or in terms of stress,

$$(Eqn. 4.15) \quad f_l = f_0 e^{-(\mu\alpha + Kl)}$$

Equation 4.15 relates tendon stress at a length along the tendon to the jacking force, tendon geometry, and the coefficients of friction and wobble. Expressions similar to equation 4.15 are found in AASHTO LRFD Article 5.9.5.2.2.

Design example 1 (Appendix C) presents the design of a three-span cast-in-place box girder bridge with span lengths of 120', 160' and 120'. The cross section of the box girder superstructure, shown in figure 4.3, has five webs, each containing three post-tensioning tendons, each comprised of 19, 0.6" diameter prestressing strands.

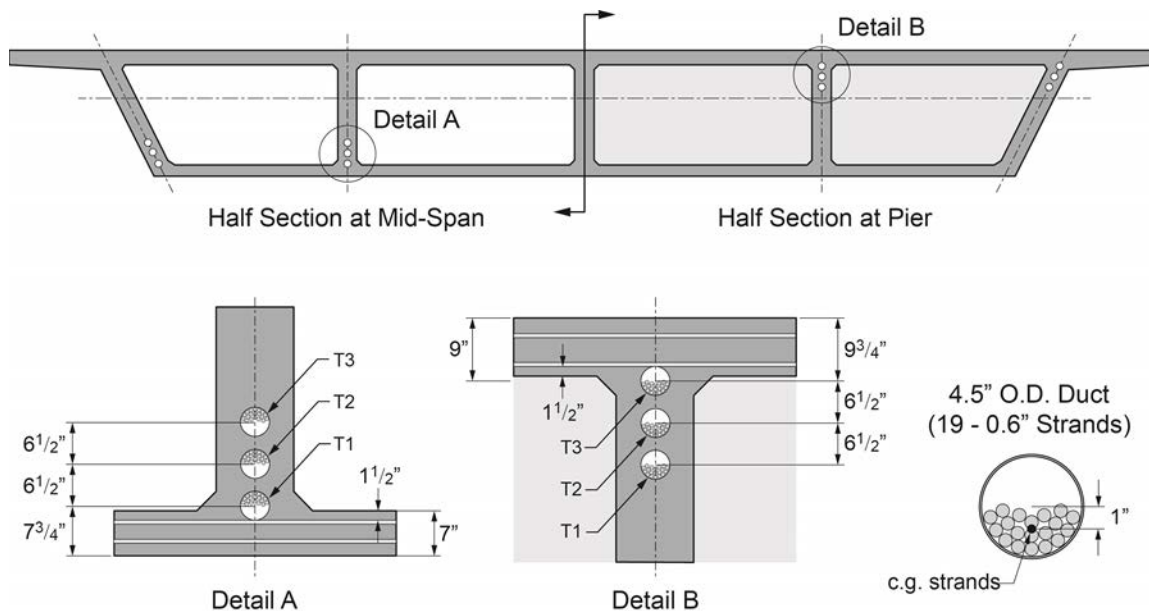


Figure 4.3 – Cross Section of Superstructure for Design Example 1

Figure 4.4 shows details of the tendon profiles of design example 1 in the end spans and center span. The profiles follow a series of parabolic segments as defined in the previous chapter. The tendon elevations shown take into account the location of the strands within the ducts as shown in the detail of figure 4.3. For this tendon size, a 1" offset from the center of the duct to the center of gravity of the strands is specified (AASHTO LRFD Article 5.9.1.6). When the tendon is low at mid-spans, the strands are pulled to the top of the duct and are 1" above the center of gravity of the duct. Over the piers the strands are pulled to the bottom of the duct and their cg is modeled 1" below the cg of the duct. At points between the parabolic segments, the tendons are modeled at the cg of the duct.

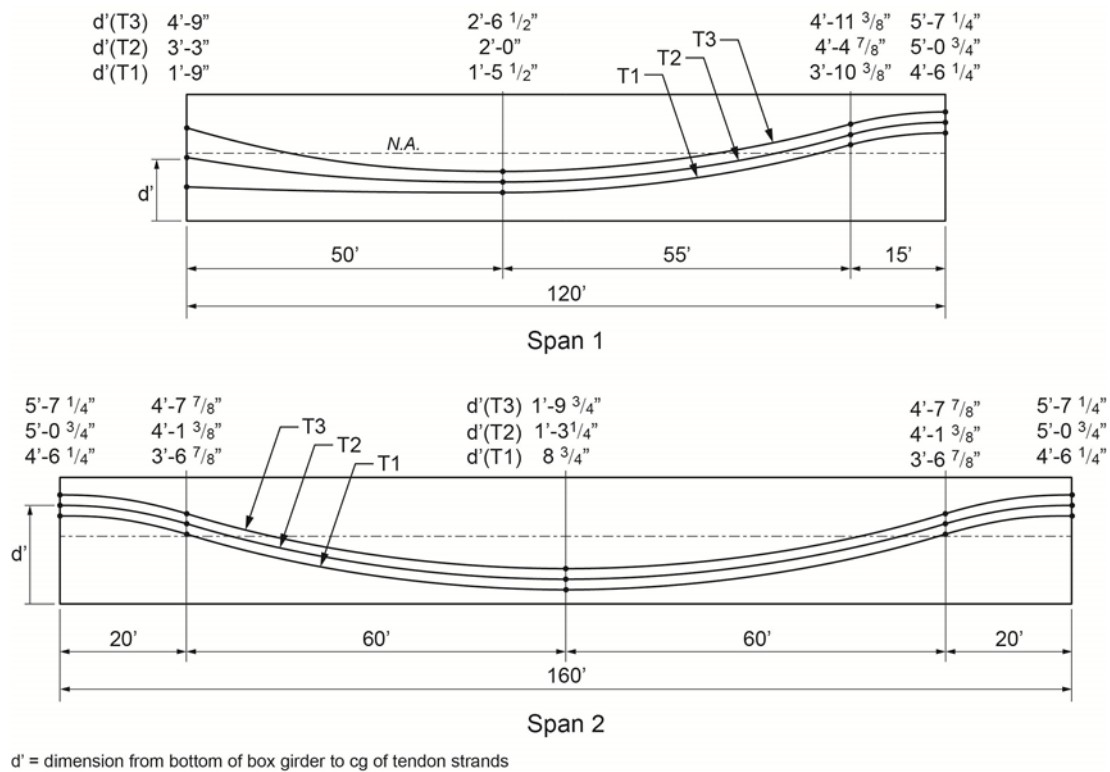


Figure 4.4 – Tendon Profiles For Design Example 1

Figure 4.5 shows the elevation of Tendon T2 only, highlighting the deviation angles that the tendon makes over the three spans. Assuming that the tendon is stressed from the left end, End A in figure 4.5, the calculation of the force along the length of the tendon can be made using equation 4.14. The coefficient of friction, μ , is assumed to be 0.25 (1/rad), and the wobble coefficient, k , is 0.0002 (1/ft).

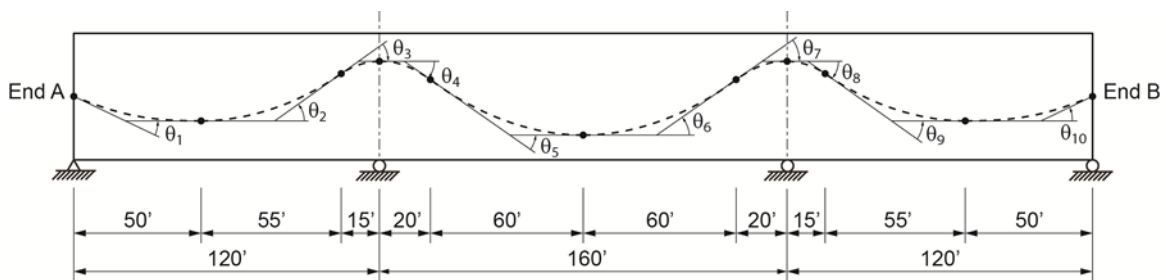


Figure 4.5 – Tendon T2 Profile and Angular Deviations

The calculation of the force along the length of Tendon T2 is summarized in the table shown in table 4.1. The steps taken to compute the values in this table are:

1. Define points, in this case points 1 through 11, at the beginning and end of the tendon and at transitions between parabolic segments.

2. Compute the lengths and heights of the parabolic segments from the tendon profile with appropriate adjustments for strand location within the ducts. The heights in this calculation are the absolute value of the difference in dimensions from the bottom fiber to the tendon centroid.
3. Compute the angular deviation that the tendon makes through each parabolic segment as computed using equation 3.32 from chapter 3.
4. Using equation 4.14 compute the incremental force coefficient as a fraction of the force at the beginning of the parabolic segment. (F_i/F_0).
5. Beginning with unit value at End A of the tendon, successively multiply the incremental force coefficients to determine the cumulative force coefficients at the end of each parabolic segment, in this case expressed as a fraction of the jacking force.
6. Multiply each cumulative force coefficient by the jacking stress. For this example the jacking stress was 75 percent of the ultimate strength of the tendon.
7. Find the tendon force along its length by multiplying the stress at that location times the area of the tendon. In this example the tendon is comprised of 19, 0.6" diameter strands. The area of the tendon is $0.217 \times 19 = 4.123 \text{ in}^2$.

Point	b (ft)	h (ft)	Angular Deviation $\theta=2h/b$ (rad)	Angular Force Coefficient	Cumulative Force Coefficient	Tendon Stress (ksi)	Tendon Force (kips)
1	0	0.0000	0.00000	0.0000	1.0000	202.50	835
2	50	1.2500	0.05000	0.9778	0.9778	197.99	816
3	55	2.4063	0.08750	0.9677	0.9461	191.59	790
4	15	0.6563	0.08750	0.9754	0.9229	186.88	771
5	20	0.9479	0.09479	0.9727	0.8977	181.78	749
6	60	2.8438	0.09479	0.9649	0.8662	175.04	723
7	60	2.8438	0.09479	0.9649	0.8358	169.25	698
8	20	0.9479	0.08750	0.9727	0.8130	164.63	679
9	15	0.6563	0.08750	0.9754	0.7930	160.58	662
10	55	2.4063	0.05000	0.9677	0.7674	155.39	641
11	50	1.2500	0.05000	0.9778	0.7503	151.93	626

Table 4.1 – Tendon Loss Calculations – Friction and Wobble

Figure 4.6 shows a graphical representation of the force along the length of Tendon T2 at full jacking force and with losses resulting from friction and wobble. The force at the left end of the tendon is equal to the jacking force of 835 kips. The force at the anchorage at End B is 626 kips.

Though the radii within the parabolic segment are changing over their lengths, the tendon force is assumed to vary linearly over the length of the parabolic segment. This results in the straight-line representation shown in figure 4.6.

It is important to note that the lengths used for computing losses for wobble in this example were the horizontal lengths of the parabolic segments. This simplification is made because the horizontal projection of the tendon length is not significantly different from the actual tendon length for most cast-in-place box girder bridges. When this assumption cannot be made, the losses should be computed along the length of the tendon.

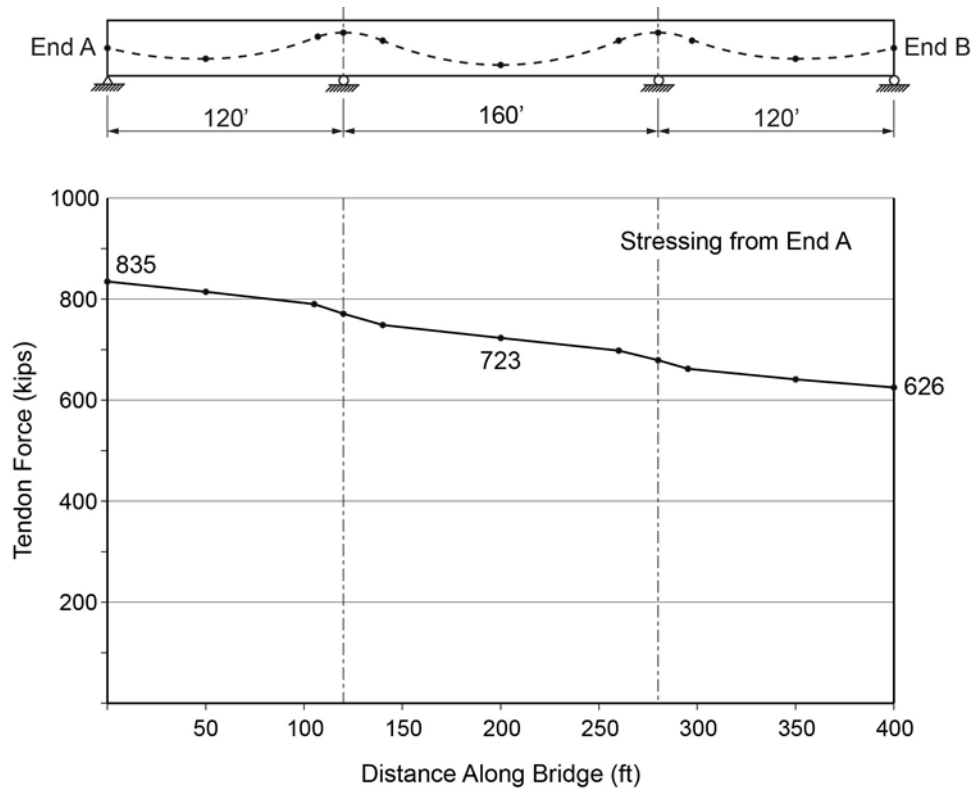


Figure 4.6– Tendon Loss Calculations – Friction and Wobble

4.1.2 Elongation

Post-tensioning tendons are stressed to a force chosen by the Engineer and presented in the contract drawings. Hydraulic jacks used to stress the tendons are fitted with gauges that relate hydraulic pressure to stressing force. Tendon elongations are measured during stressing as a secondary method of verifying force in the tendons.

Elongations are computed by considering the average force over a length of tendon:

(Eqn. 4.16)
$$\Delta_i = \frac{F_{i\text{ ave}} l_i}{A_s E_s}$$

Where $F_{i\ ave}$ is the average force over the length of tendon, l_i . The total elongation is obtained by summing the increments of elongation for each portion of the tendon, based on the average of the force at the beginning and end of that portion:

$$(Eqn. 4.17) \quad \Delta_{total} = \sum \frac{F_{i\ ave} l_i}{A_s E_s}$$

The table presented in table 4.2 shows the average length of each parabolic segment for Tendon T2 of design example 1, the average force over that length (found as the average of the force at the beginning and end of the segment), and the resulting elongation over each increment. The total elongation is the sum of the column of incremental elongations.

Point	b (ft)	Average Force (kips)	Incremental Elongation (in)
1	50	825.62	4.216
2	55	803.13	4.511
3	15	780.23	1.195
4	20	760.00	1.552
5	60	736.33	4.512
6	60	710.51	4.354
7	20	688.30	1.406
8	15	670.43	1.027
9	55	651.39	3.659
10	50	633.55	3.235
Total Elongation (in)			29.666

Table 4.2– Tendon Elongation

The area below the tendon force diagram in figure 4.7 represents the work done to elongate the tendon. This work divided by the tendon area and modulus of elasticity of the prestressing steel is equal to the total tendon elongation as demonstrated in figure 4.8.

4.1.3 Anchor Set

When the jacking force is reached at End A, the wedges are made snug and the tendon force released. The tendon draws the wedges, or seats them, into the wedge plate. The amount of movement that the wedges undergo is referred to wedge or anchor set. Values of anchor set vary with post-tensioning system, but typically vary from 1/4 to 3/8 of an inch. Figure 4.7 shows a depiction of the wedges before and after anchor set.

As the wedges are seated the tendon is shortened, reducing the tendon force. Often, only a portion of the length is affected as the work done in shortening the tendon is less than the work to elongate the tendon. Short tendons, however, requiring little elongation to achieve a desired force, can have the force affected along their entire length as a result of anchor set.

Figure 4.8 shows the effect of an anchor set of 3/8 inches on the forces along the length of the Tendon T2 of design example 1 after stressing at End A. The shaded area in figure 4.8 represents the work performed during the anchor seating. This area is determined by finding a point along the length of the tendon to a location where the anchor set does not impact the

tendon force (point of zero movement). Working back from the tendon force from that point to the anchorage, the loss in tendon force is related to the geometry of the tendon, friction and wobble, just as when originally stressed. A typical simplification is to mirror image the force loss diagram about a horizontal line passing through the point of zero movement.

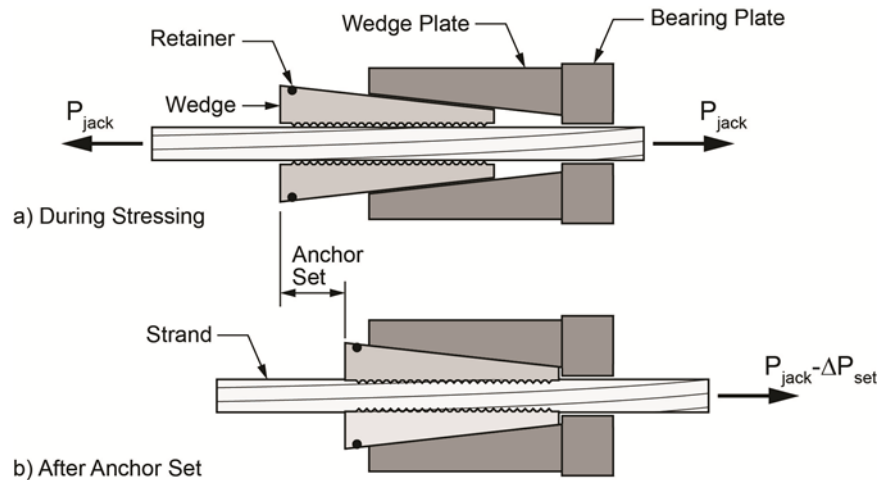


Figure 4.7– Anchor Set

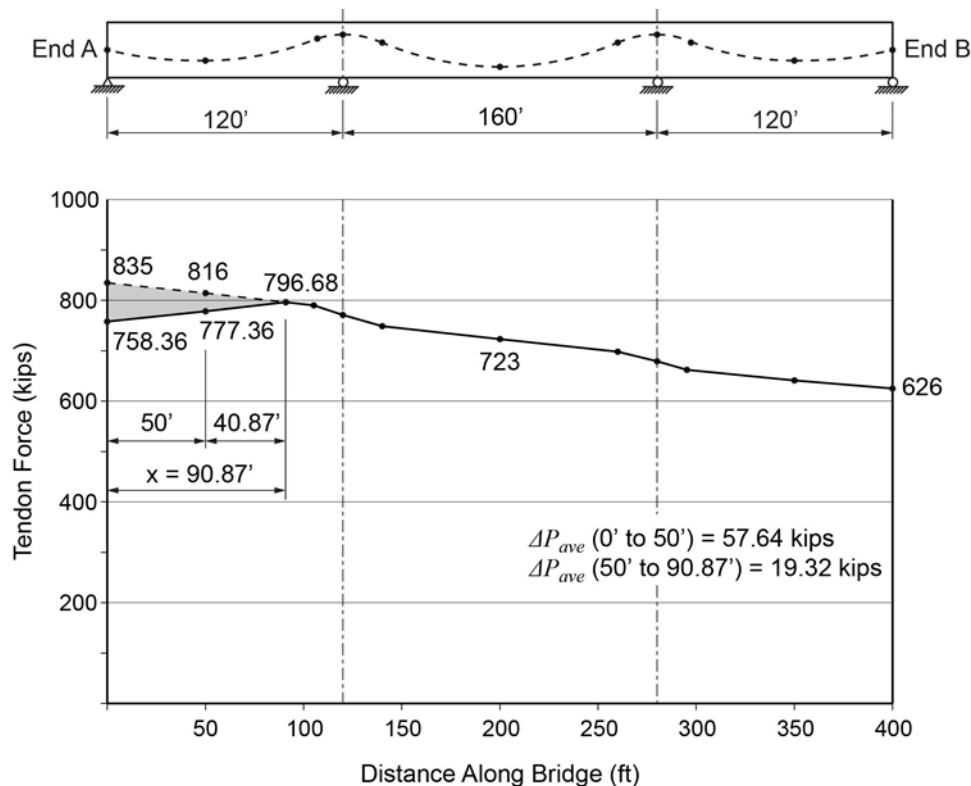


Figure 4.8 – Tendon Force Diagram after Anchor Set at End A

The point of zero movement was determined by trial and error to be 90.87' from the stressing end. The convergence on these values was found by equating the shaded area in Figure 4.8,

(average changes in force x length along tendon) divided by the tendon cross-sectional area and modulus of elasticity, to the anchor set of 3/8":

$$(Eqn. 4.18) \quad \Delta = \frac{\Delta P_{ave} l_{set}}{A_s E_s} = \frac{((57.64k \cdot 50') + (19.32k \cdot 40.87'))12}{(4.123in^2)(28,500ksi)} = 0.375"$$

The maximum force in the tendon at the point of zero movement is 796.68 kips. This force represents a stress in the tendon of 193.2 ksi, or 71.6 percent of GUTS, which is less than the permissible value of 74 percent specified by Table 5.9.3-1 of AASHTO LRFD Article 5.9.3. The force at the anchorage at End A is 758.36 kips. This force represents a stress of 183.9 ksi, or 68.1 percent of GUTS, which is less than the permissible value of 70 percent specified in the same AASHTO LRFD Table.

4.1.4 Two-End Stressing

For tendons that are relatively short, or for longer tendons with small vertical draping, single end stressing may provide sufficient force throughout the bridge superstructure. Stressing half of the tendons from their beginning and half from their end can help produce a more uniform level of force along the bridge.

Long tendons that are continuous over multiple spans, where friction losses are high, can be stressed at both ends to significantly increase the prestressing force in the bridge. The force in Tendon T2 of design example 1, which has been studied in the chapter, can be enhanced by this two-end stressing.

After stressing from End A, the force in Tendon T2 was found to be 626 kips (See figure 4.7 and 4.10). When jacking at End B, the tendon will not begin to elongate until this level of load is reached. The jack at End B will pick up load at 626 kips and continue to the final jacking force specified by the Engineer, which in this example is chosen to be 835 kips.

From symmetry of the structure and tendon geometry, the force along the length of the tendon when stressed from End B at the right would be the mirror image of that for stressing at End A as shown in figure 4.6. In this second stressing, however, the force along the tendon length would reduce as a result of friction and wobble, to a point where the force in the tendon is equal to the force from the first end stressing. No elongation, and therefore no force increase, will occur past that point. This is seen in figure 4.9, where the effects of stressing at End B elongate only the right half of the tendon. The point of zero movement of the second stressing is at the centerline of the main span of the bridge, where the forces from stressing at End A and End B both equal 723 kips.

The shaded area shown in figure 4.9 between the two tendon force diagrams is the work performed during the second stressing. This area, divided by the cross-sectional area of the tendon and modulus of elasticity is equal to the elongation due to stressing the tendon at End B. For the case of Tendon T2 of design example 1, the elongation due to second stage stressing is 2.3 inches.

The final change in tendon force is a result of the anchor set at End B. By symmetry of the tendon and jacking force, the resulting loss due to anchor set is the same as End A. This loss and the final tendon force diagram after stressing both ends and anchor set at End B is shown in figure 4.10.

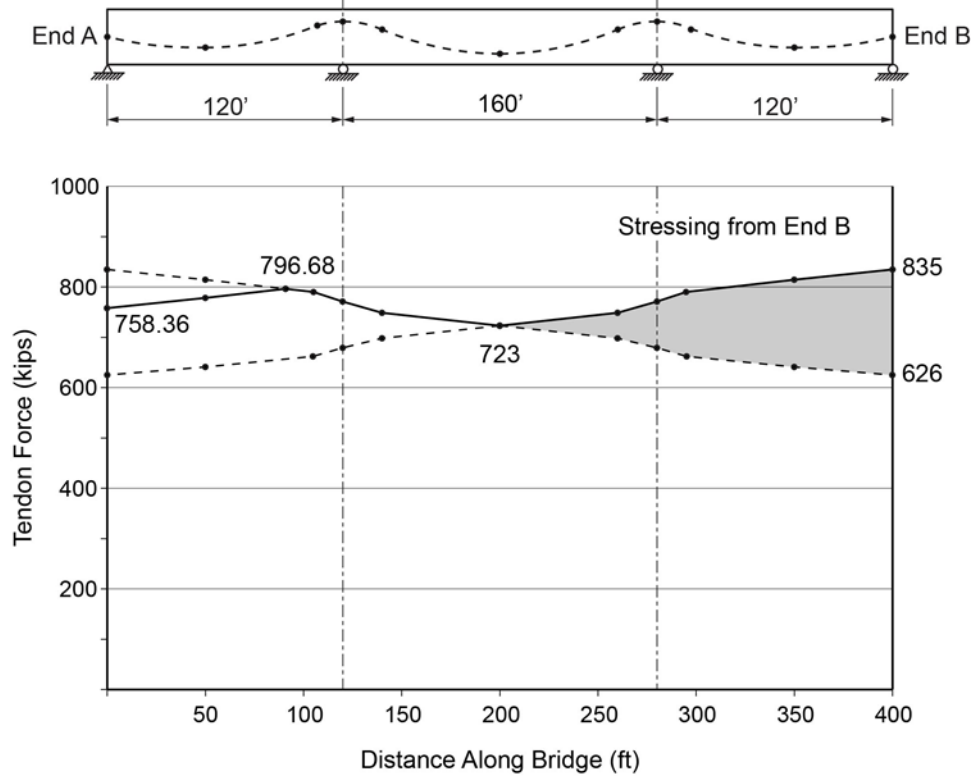


Figure 4.9 – Tendon Force Diagram after Stressing from End B

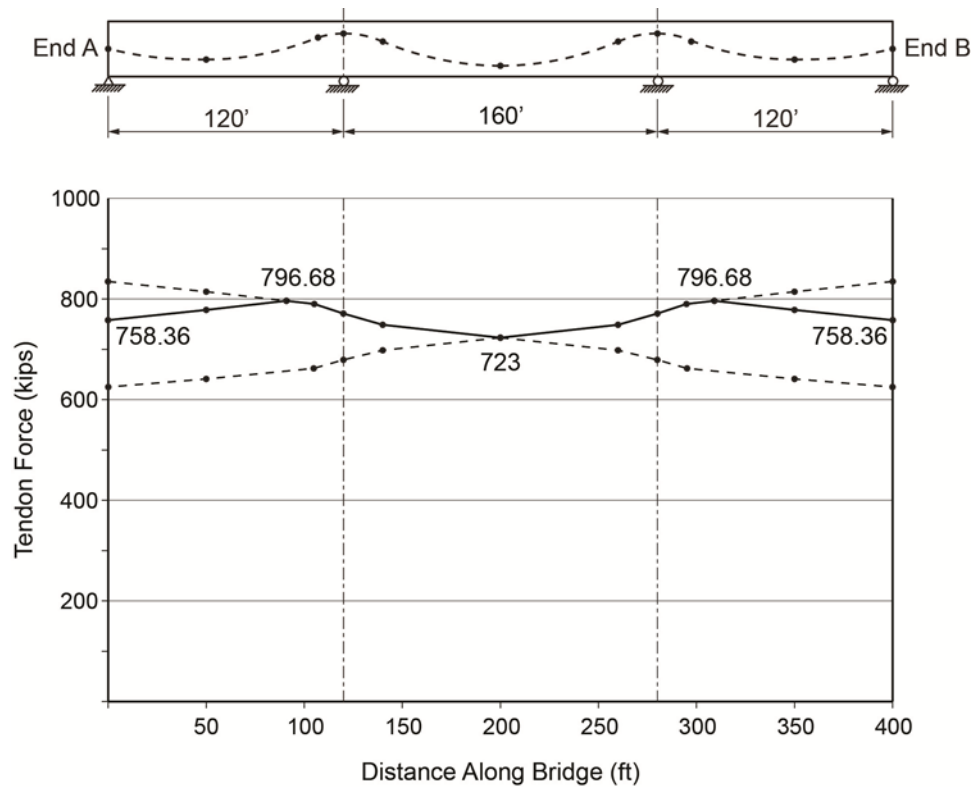


Figure 4.10 – Final Tendon Force Diagram (After Anchor Set at End B)

4.1.5 Elastic Shortening (AASHTO LRFD Article 5.9.5.2.3b)

Concrete box girder superstructures are post-tensioned with multiple tendons. When the first tendon is stressed, it is pulled to the specified jacking force and seated. The concrete box girder shortens as a function of the bridge length and axial stiffness.

The superstructure is further compressed when the second tendon is stressed, and shortens in proportion to the newly applied force. As the superstructure shortens, so does the tendon that was stressed first, reducing the force in that tendon. Subsequently stressed tendons incrementally reduce the force in all previously stressed tendons, until the last tendon is stressed and seated with the specified jacking force.

The difference between the sum of all tendon forces, as they have been affected by each other, and the total force, as if all tendons were stressed at the same time, is the instantaneous loss of prestress force due to elastic shortening.

Consider a structure that is incrementally prestressed with multiple post-tensioning tendons. The tendons are straight with no eccentricity. As the first tendon is stressed, the structure shortens an amount equal to:

$$\text{(Eqn. 4.19)} \quad \Delta_1 = \frac{F_1 L}{A_c E_{ci}}$$

Where, Δ_1 = Shortening of the superstructure under the force of stressing Tendon 1 (in)
 F_1 = Stressing force for Tendon 1 (kips)
 L = Length of bridge being prestressed (inches)
 A_c = Cross-sectional area of the box girder superstructure (in²)
 E_{ci} = Modulus of Elasticity of the concrete at the time prestressing is applied (ksi)

When the second tendon is stressed, the superstructure shortens more, and the first tendon shortens by the same amount. The resulting shortening of the superstructure at this phase of construction is:

$$\text{(Eqn. 4.20)} \quad \Delta_2 = \frac{F_2 L}{A_c E_{ci}} - \frac{\Delta F_{p1} L}{A_{p1} E_p}$$

Where, Δ_2 = Shortening of the superstructure under the force of stressing Tendon 2 (in)
 F_2 = Stressing force for Tendon 2 (kips)
 ΔF_{p1} = Change in force in Tendon 1 under the action of stressing Tendon 2
 A_{p1} = Cross-sectional area of Tendon T1 (in²)
 E_{ci} = Modulus of Elasticity of the concrete at the time prestressing is applied (ksi)
 E_p = Modulus of Elasticity of the prestressing steel (ksi)

Equation 4.20 can be rearranged to express the change in stress in Tendon 1 as Tendon 2 is stressed:

$$\text{(Eqn. 4.21)} \quad \Delta f_{p1} = \frac{\Delta F_{p1}}{A_{p1}} - \frac{E_p}{E_{ci}} f_{cg2}$$

Where, Δf_{p1} = Change in stress of Tendon 1 while stressing Tendon 2 (ksi)
 f_{cg2} = Stress at the center of gravity of the box girder superstructure as a result of stressing Tendon 2 (ksi)

Equations 4.20 and 4.21 were developed for the special case of a concentrically prestressed member where the center of gravities of the concrete and tendons coincide. More generally, the center of gravity of the post-tensioning is eccentric to the concrete superstructure center of gravity, and the stress is different from the axial value. Taking this into consideration, the total change in prestressing force in terms of the total stress in the concrete caused by all tendons, the expression is that of AASHTO LRFD Equation 5.9.5.2.3b-1:

$$\text{(Eqn. 4.22)} \quad \Delta f_{pES} = \frac{N-1}{2N} \frac{E_p}{E_{ci}} f_{cgp}$$

Where, Δf_{pES} = Change in stress of all tendons as a result of elastic shortening (ksi)
 N = the number of identical prestressing tendons
 f_{cgp} = sum of concrete stress at the center of gravity of the prestressing tendons due to the prestressing force after jacking and the self-weight of the member at the sections of maximum moment (ksi)

Comments on f_{cgp} :

- This stress may be computed considering losses in prestressing stress due to friction, early portions of steel relaxation, and an estimate of elastic shortening itself.
- Typically, all tendons are stressed prior to grouting. The tendons are then all unbonded and f_{cgp} should be calculated as an average stress at the level of the center of gravity of the prestressing steel, taken from several locations along the length of the bridge.

4.2 Time-Dependent Losses

Chapter 2 presented time-dependent characteristics for concrete and prestressing steel. The equations presented in that Chapter are those presented in the CEB-FIP Model Code (1990). The CEB-FIP equations are beneficial for computerized analyses of bridges that use time steps to evaluate phased bridge construction. The AASHTO LRFD Specifications provide equations for determining lump sum losses in prestressing. These equations are useful for preliminary design of complex structures and for the final design of bridges where a phased construction analysis is not required.

This section presents the AASHTO LRFD Specification equations for the refined lump sum approach for determining long term prestressing force losses. These equation are used chapter 5 for the preliminary design of the bridge of design example 1. The design example uses a computerized analysis that incorporates the CEB-FIP equations.

4.2.1 General (AASHTO LRFD Article 5.9.5.4.1)

Predictions for time-dependent losses presented in the AASHTO LRFD specifications are tailored to superstructures made of pretensioned girders with deck slabs made continuous after girder placement. The general equation for time-dependent losses is presented in AASHTO LRFD Equation 5.9.5.4.1-1:

$$\text{(Eqn. 4.23)} \quad \Delta f_{pLT} = \left(\Delta f_{pSR} + \Delta f_{pCR} + \Delta f_{pR1} \right)_{id} + \left(\Delta f_{pSD} + \Delta f_{pCD} + \Delta f_{pR2} - \Delta f_{pSS} \right)_{df}$$

The subscripts for the various changes in prestress stress, Δf_p , are:

- *id* refers to losses that occur between transfer of pretensioning force to the girder and placement of the concrete deck.
- *df* refers to losses that occur after deck placement (until final losses are realized).
- *SR*, *CR* and *R1* are losses associated with concrete shrinkage, concrete creep and prestressing steel relaxation between transfer of pretensioning force to the girder and placement of the concrete deck.
- *SD*, *CD* and *R2* are losses associated with concrete shrinkage, concrete creep and prestressing steel relaxation after deck placement.
- *SS* is a gain in prestressing stress as a result of the shrinkage of the composite deck slab

AASHTO LRFD Article 5.9.5.4.5 provides guidance for the application of the general equation for post-tensioned non-segmental girders. Recognizing that application of the prestressing and engaging of the self weight of the cast-in-place box girder happen at the same time, the part of AASHTO LRFD Equation 5.9.5.4.1-1 concerned with the time from transfer to deck placement is to be taken as zero. The construction of full cross sections of the box girders at the same time also causes the differential effects of the slab shrinkage relative to the webs and bottom slab also to be zero. As a result, equation 4.23 can be reduced to:

$$\text{(Eqn. 4.24)} \quad \Delta f_{pLT} = \left(\Delta f_{pSD} + \Delta f_{pCD} + \Delta f_{pR2} \right)_{df}$$

The subscript *df* refers to all losses that occur from initial loading until all time-dependent losses are realized. The remainder of this chapter presents the terms of equation 4.24 as applied to cast-in-place post-tensioned concrete box girders. Some bridge owners offer simplified approaches to determining time-dependent losses. Caltrans, for example, routinely forgoes detailed calculations and uses a lump sum loss of 20 ksi.

4.2.2 Concrete Shrinkage (AASHTO LRFD Article 5.9.5.4.3a)

The loss of prestress force resulting from shrinkage of the concrete superstructure is given by AASHTO LRFD Equation 5.9.5.4.3a-1 as:

$$\text{(Eqn. 4.25)} \quad \Delta f_{pSD} = \varepsilon_{bdf} E_p K_{df}$$

The strain ε_{bdf} , is the shrinkage strain from the time of prestressing to final time as provided by AASHTO LRFD Equation 5.4.2.3.3-1:

$$\text{(Eqn. 4.26)} \quad \varepsilon_{bdf} = k_s k_{hs} k_f k_{id} 0.48 \times 10^{-3}$$

The factors in Equation 4.26 are defined by AASHTO LRFD Equations 5.4.2.3.2-2, 5.4.2.3.3-2, 5.4.2.3.2-4, and 5.4.2.3.2-5:

$$\text{(Eqn. 4.27)} \quad k_s = 1.45 - 0.13 \left(\frac{V}{S} \right) \geq 1.0$$

$$\text{(Eqn. 4.28)} \quad k_{hs} = (2.00 - 0.014H)$$

$$\text{(Eqn. 4.29)} \quad k_f = \frac{5}{1 + f'_{ci}}$$

$$\text{(Eqn. 4.30)} \quad k_{td} = \left(\frac{t}{61 - 4f'_{ci} + t} \right)$$

Where, H = relative humidity (%)
 k_s = factor for the effect of the volume to surface ratio of the component
 k_{hs} = humidity factor for shrinkage
 k_f = factor for the effect of concrete strength
 k_{td} = time development factor
 t = age of concrete at the end of shrinkage (days)
 V/S = volume-to-surface ratio (in.)

The term K_{df} is given by AASHTO LRFD Equation 5.9.5.4.3a-2 as:

$$\text{(Eqn. 4.31)} \quad K_{df} = \frac{1}{1 + \frac{E_p}{E_{ci}} \frac{A_{ps}}{A_c} \left(1 + \frac{A_c e_{pc}^2}{I_c} \right) \left[1 + 0.7\psi_b(t_f, t_i) \right]}$$

Where, e_{pc} = eccentricity of the prestressing force with respect to the center of gravity of the concrete box girder (in.), positive in typical construction where prestressing force is below the centroid of the section
 A_c = area of the gross section of the concrete box girder (in.²)
 I_c = moment of inertia of the gross section of the concrete box girder (in.⁴)

The creep coefficient, ψ_b , is given by 5.4.2.3.2-1 as:

$$\text{(Eqn. 4.32)} \quad \psi_b(t_f, t_i) = 1.9k_s k_{hc} k_f k_{td} t_i^{-0.118}$$

Factors k_s , k_f , and k_{td} are defined above. Factor k_{hc} is defined by AASHTO LRFD Equation 5.4.2.3.2-3:

$$\text{(Eqn. 4.33)} \quad k_{hc} = 1.56 - 0.008H$$

Where, k_{hc} = humidity factor for creep
 t_i = age of concrete at time of load application (days)

4.2.3 Concrete Creep (AASHTO LRFD Article 5.9.5.4.3b)

The loss of prestress force resulting from the creep of concrete is defined by AASHTO LRFD Equation 5.9.5.4.3b-1:

$$\text{(Eqn. 4.34)} \quad \Delta f_{pCD} = \frac{E_p}{E_{ci}} f_{cgp} \left[\Psi_b(t_f, t_i) - \Psi_b(t_d, t_i) \right] K_{df} + \frac{E_p}{E_{ci}} \Delta f_{cd} \Psi_b(t_f, t_d) K_{df}$$

Deleting the terms that deal with time of transfer to time of deck placement, this equation can be simplified to:

$$\text{(Eqn. 4.35)} \quad \Delta f_{pCD} = \frac{E_p}{E_{ci}} f_{cgp} \Psi_b(t_f, t_i) K_{df}$$

Where, t_f = final age of concrete (days)

4.2.4 Steel Relaxation (AASHTO LRFD Article 5.9.5.4.3c)

The loss of prestress force resulting from the creep of concrete is defined by AASHTO LRFD Equation 5.9.5.4.3c-1 for pretensioned conditions, which assigns half of the relaxation from time of transfer to deck placement, and half from deck placement to final time:

$$\text{(Eqn. 4.36)} \quad \Delta f_{pR2} = \Delta f_{pR1}$$

This is evaluated by considering AASHTO LRFD Equation 5.9.5.4.2c-1:

$$\text{(Eqn. 4.37)} \quad \Delta f_{pR1} = \frac{f_{pt}}{K_L} \left(\frac{f_{pt}}{f_{py}} - 0.55 \right)$$

Where, f_{pt} = stress in prestressing strands immediately after transfer, but not less than $0.55f_{py}$
 K_L = 30 for low relaxation strands and 7 for other prestressing steels

As an option to evaluating prestress relaxation by the equations above, the AASHTO LRFD specifications permits a value of Δf_{pR1} equal to 1.2 ksi for low relaxation strand.

Considering relaxation from stressing to final time, the relaxation in cast-in-place box girder construction should be equal to two times Δf_{pR1} , or 2.4 ksi.

Chapter 5—Preliminary Design

5.1 Introduction

Previous chapters in this manual have introduced cast-in-place box girder construction and post-tensioning concepts. This chapter presents a preliminary design process for cast-in-place box girder bridge superstructures. The goal of the preliminary design is to select a bridge layout, box girder superstructure cross section, and preliminary longitudinal post tensioning arrangement in sufficient detail to assure an efficient final design phase. The flow chart shown in figure 5.1 outlines the steps of this preliminary design process.

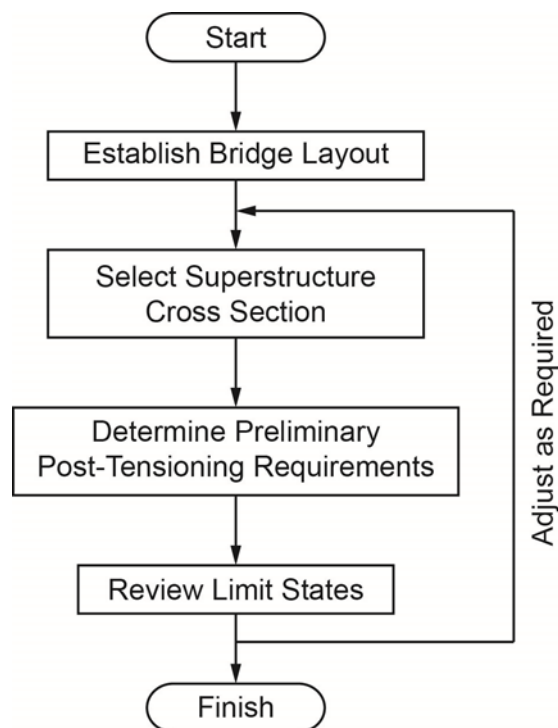


Figure 5.1 – CIP Box Girder Bridge Preliminary Design Flow Chart

The method of presenting this preliminary design process is to discuss influencing factors, and then apply them to an example bridge structure. Figure 5.2 shows an elevation view of a three span bridge that will be used to develop the preliminary design.



Figure 5.2 – 3-Span Box Girder Bridge for Preliminary Design

This bridge is planned as a part of a new highway passing through a relatively flat, developed urban area. The bridge is required to cross over an existing four-lane divided highway, with the travel lanes separated by 40' and having required side clear zones of 32'. Figure 5.3 shows the cross section of the existing highway lanes to be spanned.

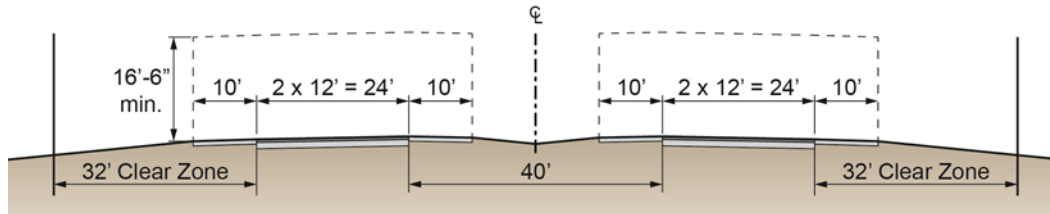


Figure 5.3 – Existing, At-Grade Highway Cross Section to Be Spanned by Proposed Bridge

5.2 Establish Bridge Layout

5.2.1 Project Design Criteria

Each bridge design project comes with a set of jurisdictional, technical and site specific criteria that need to be considered in establishing the bridge layout. Engineers and planners from various disciplines work to meet a wide range of owner requirements for the new facility. The most common of these are:

- Nature and function of the facility/geography to be spanned.
- Site topography.
- Required vertical and horizontal clearances.
- Horizontal alignment, profile grade, and superelevation of the proposed bridge.
- Number and widths of lanes and shoulders (highway bridges), dynamic clearance envelopes for trains (rail and transit bridges).
- Subsurface and geotechnical investigations.
- Environmental constraints.
- Bridge and Site drainage.
- Limits of Rights-of-Way.
- Utility requirements/conflicts.
- Permitting.
- Maintenance of Traffic.
- Applicable codes and regulations.

Working within the framework of the project design criteria, the bridge engineer begins preliminary design by selecting the following:

- Bridge type.
- Pier and abutment locations, resulting in bridge span lengths and overall bridge length.
- Length of bridge between expansion joints.
- Superstructure cross section.
- Pier and abutment types and dimensions.
- Probable foundation types and sizes.

Bridge type selection studies are often performed before the preliminary design phase. Various bridge types are compared using “order of magnitude” estimates, typically based on historic bridge cost information. For the purpose of this manual, it is assumed that the preferred bridge type is a cast-in-place post-tensioned concrete box girder.

5.2.2 Span Lengths and Layout

In the example project considered in this chapter, the following information has been provided to the bridge engineer:

- The bridge will lie on a tangent alignment, crossing the highway with zero skew.
- No permanent new construction is permitted within the clear zones or in the median of the underlying highway.
- Bridge depth should be minimized to reduce impacts on developed areas on either end of the bridge, height of fill, and length of retaining walls.
- There are no environmental restrictions at the bridge site with regard to the permanent bridge and the falsework required to build the bridge.
- The project lies within already procured right-of-way.
- No utility conflicts or future needs have been identified.
- A reduced vertical clearance of 14'-6" is permitted during construction.
- Falsework must span the clear roadways of the underlying highway, with temporary supports permitted in the median.

The out-to-out dimension of the clear zones of the highway being crossed is 152'. This length is the minimum clear span of the bridge crossing required to clear the underlying highway. With consideration for the width of supporting columns, a centerline-to-centerline span of 160' is selected.

A three-span continuous bridge is selected to minimize the depth of the superstructure of the example problem of this chapter. For cast-in-place post-tensioned concrete structures, efficient end span to main span ratios range from 0.75 to 0.80. Spans as short as 40 percent (requiring uplift restraining abutments) and as much as 100 percent of the main span length can be accommodated with appropriate post-tensioning design. For this example problem, an end span ratio of 0.75 is chosen. Expansion joints will be placed at the abutments.

The resulting span length and pier numbering for the example problem are shown in figure 5.4.

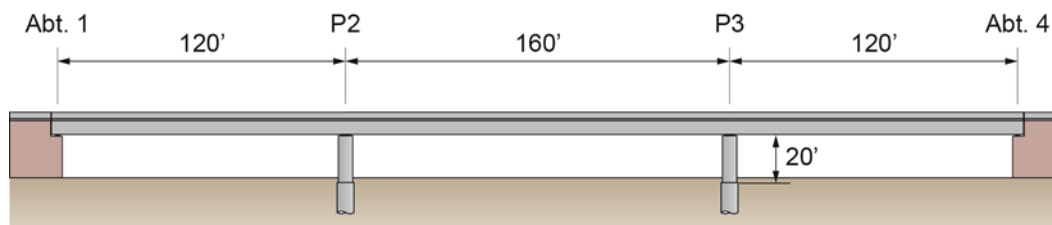


Figure 5.4 –Span Layout for Preliminary Design Example

Note: The example bridge analyzed in this chapter is supported at the piers and abutments by bearings. This facilitates demonstrating the preliminary design of the longitudinal post-tensioning. Often, the interior piers are cast monolithically with the superstructure. Chapter 7 presents considerations for design when monolithic construction is used.

5.3 Cross Section Selection

5.3.1 Superstructure Depth

Past editions of bridge design specifications presented depth to span ratios for various bridge types. The current AASHTO LRFD requirements focus on selecting superstructure stiffness to meet deflection criteria. AASHTO LRFD Article 2.5.2.6.3 does, however, present optional criteria for span-to-depth ratios for use if requested by the Owner.

AASHTO LRFD Table 2.5.2.6.3-1 presents the following traditional minimum depths for constant depth cast-in-place prestressed concrete box girder superstructures as a function of span length. For simple span girders the traditional minimum depth is:

$$\text{(Eqn. 5.1)} \quad D = 0.045L \quad (\text{simple spans})$$

$$\text{(Eqn. 5.2)} \quad D = 0.040L \quad (\text{continuous spans})$$

Expressed in terms of span-to-depth ratio, these equations become:

$$\text{(Eqn. 5.3)} \quad \left(\frac{L}{D} = 22L \right) \quad (\text{simple spans})$$

$$\text{(Eqn. 5.4)} \quad \left(\frac{L}{D} = 25L \right) \quad (\text{continuous spans})$$

Using the traditional span-to-depth ratio for continuous construction, the depth of the structure to begin preliminary design would be:

$$D = 0.040L = 0.040(160') = 6.4'$$

For convenience, the bridge depth carried into preliminary design is 6'-6".

Note—Other Owner Requirements: Occasionally, an Owner might require an internal minimum height within the concrete box girder for easy access of personnel and equipment for inspection and maintenance. This can be the case for long bridges with limited points of access, allowing longitudinal access along the entire length of the bridge. This can also be the case when the interior of the box girder is used to convey utilities such as power, water, and communications.

5.3.2 Superstructure Width

Highway and traffic studies performed for the example project have shown that the new bridge will carry three travel lanes in one direction only. The lane widths for the bridge are 12' and the two shoulder widths are 10' each. The Owner has standard concrete barrier railing that is 1'-9" wide. The resulting width of roadway is 59'-6" is shown in figure 5.5.

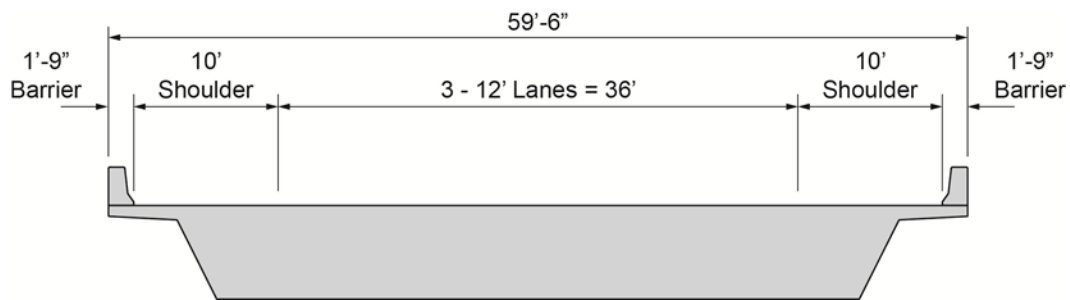


Figure 5.5 – Bridge Width and Roadway Features

5.3.3 Cross Section Member Sizes

This section provides guidance for the initial sizing of the members that comprise the box girder cross section. Members discussed are:

- Cantilever Wings.
- Webs.
- Top Slab.
- Bottom Slab.

The last part of this section applies the guidance to the example problem being developed in this chapter.

5.3.3.1 Width and Thickness of Cantilever Wing

Side overhangs, or cantilever wings, provide both structural and aesthetic benefits. Structurally, some length of overhang provides a development length for top slab reinforcing. Aesthetically, the cantilever wing presents a thin fascia and recesses the majority of the superstructure depth. Figure 5.6 shows a typical cantilever wing.

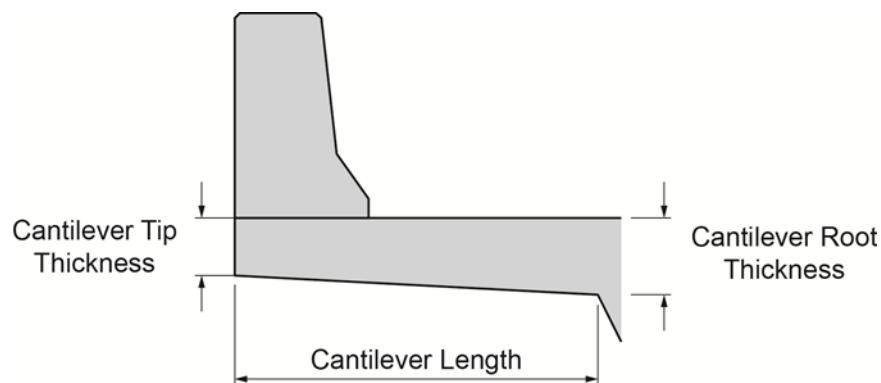


Figure 5.6 – Cantilever Wing Dimensions

Reinforced concrete cantilever wing lengths typically range from approximately 2' to 8' in length. Shorter lengths are controlled by the minimum length required to develop top slab and web reinforcing. Longer lengths can be achieved provided care is taken to assure durability by

controlling cracking under service level loadings. Transverse post-tensioning should be used to assure deck durability for cantilever wings greater than 8'.

A reinforced concrete cantilever wing typically needs a minimum thickness of 8" to 9" at the wing tip beneath the traffic barrier. This thickness is related to the level of crash testing associated with the barrier being used. The thickness of the root of the cantilever wing varies with cantilever length. The guidance provided in equation 5.5 and 5.6 may be used for initial box girder dimensioning.

For cantilever lengths less than 5' the root thickness can be approximated as:

$$\text{(Eqn. 5.5)} \quad t_c = \frac{L_c}{5} (12) \geq t_{tip}$$

For cantilever lengths between 5' to 8', the root thickness may be estimated as:

$$\text{(Eqn. 5.6)} \quad t_c = 12 + (L_c - 5)$$

where: L_c = length of the cantilever wing (ft)
 t_{tip} = thickness of the cantilever wing tip (in)
 t_c = thickness of the cantilever wing root (in)

5.3.3.2 Individual and Total Web Thickness

AASHTO LRFD Article 5.14.1.5.1c provides general criteria for the thickness of individual webs for box girder bridges:

"The thickness of webs shall be determined by requirements for shear, torsion, concrete cover, and placement of concrete."

The commentary to this article provides more definitive guidance:

"For adequate field placement and consolidation of concrete, a minimum web thickness of 8" is needed for webs without prestressing ducts; 12" is needed for webs with only longitudinal or vertical ducts; and 15" is needed for webs with both longitudinal and vertical ducts. For girders over about 8' in depth, these dimensions should be increased to compensate for increased difficulty of concrete placement."

The great majority of cast-in-place post-tensioned box girder bridges contain only longitudinal tendons. As a result, the 12" minimum thickness for individual webs thickness should be used.

Preliminary estimates of overall web thickness (number of webs at the selected thickness) are complicated by the various functions the webs play:

- Resisting shear resulting from vertical loads and torsion.
- Relationship between web spacing and top slab thickness.
- Providing sufficient pathways for post-tensioning to achieve desired eccentricities.

AASHTO LRFD does not provide a service limit state verification for shear stresses in webs. Approximated shear stresses can, however, help in the initial selection of total web thickness for

cast-in-place post-tensioned box girder bridges. As a starting point for total web thickness, calculate the shear stress from dead loads as:

$$(Eqn. 5.7) \quad \tau_{DL} = \frac{VQ_o}{Ib_{total}} = \frac{p_{DL}L_{max}}{2(0.8hb_{total})}$$

Where, p_{DL} = dead load of superstructure (kips/ft)
 L_{max} = maximum span length in bridge (ft)
 h = depth of box girder superstructure (ft)
 b_{total} = total width of web at neutral axis (ft)
 Q_o = first moment of the area above or below the neutral axis (ft)

The dead load of the superstructure can be estimated by using characteristic average thicknesses (cross-sectional area divided by bridge width). Multiplying the average thickness of the concrete cross section times the bridge width, times the unit weight of concrete produces the self weight of the bridge per foot of span length. The average thickness of cast-in-place box girder webs typically ranges from 1'-6" to 1'-9".

Including weights of barrier railing and wearing surface, the dead load per foot is:

$$(Eqn. 5.8) \quad p_{DL} = t_{ave}(B)(0.15kcf) + p_b + p_{ws}$$

Where, t_{ave} = average superstructure thickness - equal to cross-sectional area divided by bridge width (ft)
 B = overall bridge width (ft)
 p_b = weight of barriers (k/ft)
 p_{ws} = weight of wearing surface (k/ft)

Solving for b_{total} , and defining an allowable dead load shear stress:

$$(Eqn. 5.9) \quad b_{total} = \frac{p_{DL}L_{max}}{2(0.8h)\tau_{allow}}$$

Limiting the allowable shear stress in Equation 5.9 to between $5\sqrt{f'_c}$ and $7\sqrt{f'_c}$, typically produces a total web thickness that can be adequately reinforced in final design.

Note: AASHTO LRFD specifies limits for principal tension at service limit state only for segmental box girder bridges. Principal tension verifications of cast-in-place post-tensioned box girders do, however, have great merit.

5.3.3.3 Top Slab Thickness

Minimum thicknesses of decks are either directly or indirectly addressed by several Articles in AASHTO LRFD.

- AASHTO LRFD Article 9.7.1.1 states that, unless approved by the Owner, the minimum top slab thickness, excluding grinding and grooving, should be not less than 7”.
- Cover requirements in AASHTO LRFD Article 5.12.3 imply that the minimum thickness should be increased by ½” to 7 ½”, if the bridge deck is exposed to deicing salts, tire studs, or chains.
- AASHTO LRFD Article 5.14.1.5.1a provides three criteria for top slab thickness:
 - Requirements of AASHTO LRFD Section 9.
 - Sufficient to anchor and provide cover for transverse post-tensioning, if used.
 - Not less than the clear span between fillets, haunches, or webs divided by 20, unless transverse ribs or transverse post-tensioning are provided.
- If the Empirical Design Method is used for the top slab, AASHTO LRFD Article 9.7.2.4 requires that the ratio of effective length to top slab thickness be between 18.0 and 6.0, core depth of the reinforced slab not less than 4”, and effective lengths not greater than 13.5’.
- AASHTO LRFD Article 5.9.4.2.1 relates allowable compression limits to the slenderness ratio of the flanges of concrete box girders. The typical compressive stress limit of 0.6f’c is reduced by a factor (ϕ_w) when the slenderness ratio as defined in AASHTO LRFD Article 5.7.4.7.1 is greater than 15. The minimum reduction factor is 0.75.
- Section 5.3.3.2 describes the relationship between web spacing and top slab thickness. Additionally, the commentary of AASHTO LRFD Article 4.6.2.2.1, in presenting load distribution equations for “girder lines” in beam-slab bridges, recommends that cell width-to-height ratios should be approximately 2:1.
- AASHTO LRFD Article 2.5.2.6.2 provides limits on structure deflections if required by the Owner

Considering all of these requirements, the tendency is for top slabs of cast-in-place post-tensioned box girders to be on the more robust side of deck thicknesses. Monolithic connections to the webs produce higher negative deck moments, which in turn produce increased demands on the top-level slab reinforcement. In general, durability of these integral decks can be improved by increasing cover. However, excessive cover in thin slabs can be detrimental, as the larger covers can lead to larger crack widths. Increasing durability is better achieved by increasing the overall thickness of the slab while using appropriate concrete covers.

As a rule of thumb for initial box girder dimensioning, the following range of clear span to deck thickness ratio may be used:

$$(Eqn. 5.10) \quad 14 \leq \frac{L_{clear}}{t_{slab}} \leq 17$$

Expressing equation 5.10 in terms of the top slab thickness:

$$(Eqn. 5.11) \quad \frac{L_{clear}}{14} \geq t_{slab} \geq \frac{L_{clear}}{17}$$

The thickness of the top slab and clear span between webs or fillets are shown in figure 5.7.

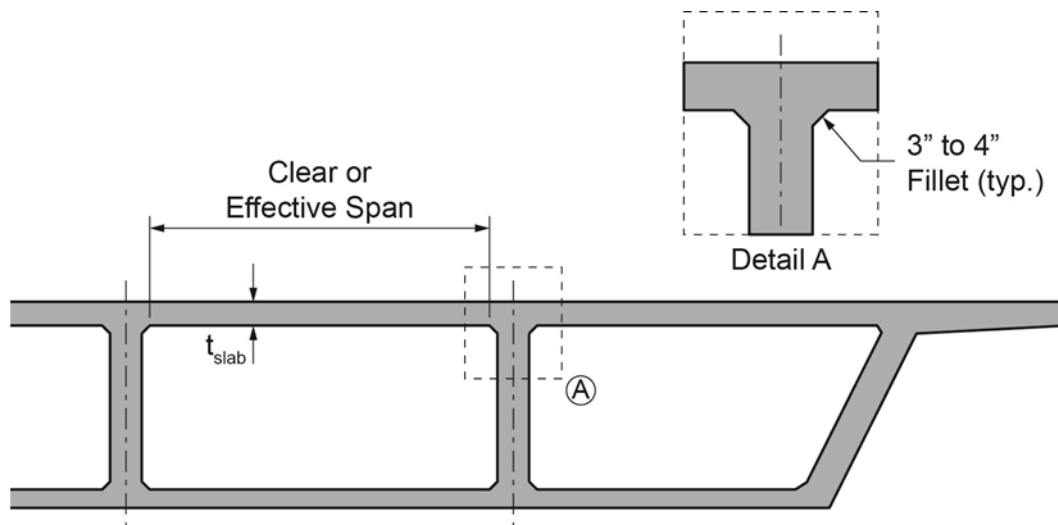


Figure 5.7 –Top Slab Span and Thickness

Small fillets (3" to 4"), shown in detail A of figure 5.7, are recommended at the top of webs/top slab interface. These fillets ease abrupt localized stresses and help facilitate placement and consolidation of concrete in the webs.

Using longer slab haunches, as shown in figure 5.8, can help optimize top slab concrete quantities and achieve longer slab spans. The haunch thickness at the face of the webs effectively accommodates negative flexure, while modifying the slab stiffness to help reduce the magnitude of positive moments. The benefits of reduced concrete quantities are sometimes offset by increased forming and reinforcing cost required to achieve the haunches.

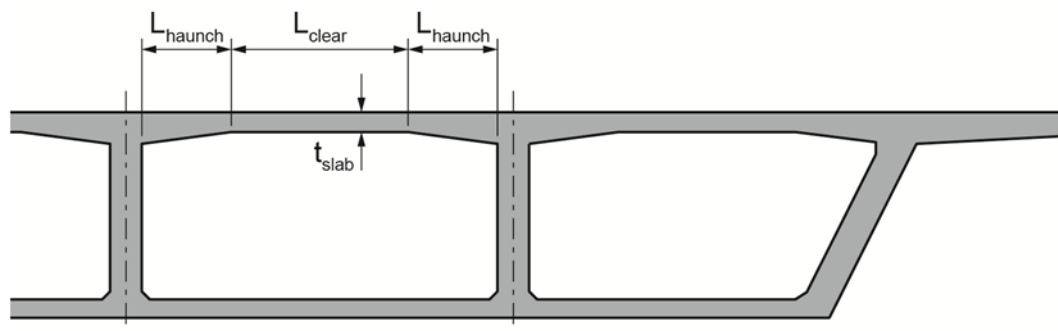


Figure 5.8 –Top Slab with Haunches

Transverse post-tensioning is typically required when clear spans in concrete box girder bridges are greater than 15' or when cantilever wing lengths are greater than 8'. The following adjustments to slab thicknesses should be considered for initial sizing when transverse post-tensioning is used:

- In order to accommodate post tensioning anchorages and local bursting reinforcement, use a cantilever wing tip of 9".
- For shorter cantilever wings, vary depth linearly from tip to root.

- For longer cantilever wings, maintain 9" thickness from tip for about 4' to 6', and then vary linearly to root.
- Use a cantilever wing root thickness of 9" plus ½" for each foot of cantilever length.
- Use a top slab haunch root thickness similar to the cantilever wing root.
- Use top slab interior haunch widths that are approximately 20 percent to 30 percent of the clear span between the webs.
- Do not require interior and exterior top slab haunches or fillets to be the same width.
- Use an 8" minimum top slab thickness between haunches. Increase the minimum top slab thickness as per equation 5.11.

5.3.3.4 Bottom Slab Thickness

AASHTO LRFD Article 5.14.1.5.1b provides criteria for the minimum thickness of bottom slabs:

- Bottom slab minimum thickness of 5.5 inches.
- The distance between fillets or webs of non-prestressed girders divided by 16
- The clear span between fillets, haunches, or webs for prestressed girders divided by 30, unless transverse ribs are used

The bottom slab between webs needs to be sufficient to carry its own self weight, superimposed loads such as utilities, while effectively participating in general bridge longitudinal and transverse behavior. If the bottom slab is to accommodate top and bottom cover and four layers of reinforcing (longitudinal and transverse bars in a top and bottom mat), the practical minimum thickness is approximately 7".

Note: Additional thickness may be needed for clearances for longitudinal post-tensioning ducts if placed in the bottom slab itself. Haunches at the webs can help provide extra clearance for such tendons, allowing for the remainder of the bottom slab to remain at a minimum thickness. Local effects of tendons in thin bottom slabs should be evaluated in final design for additional reinforcing needs.

5.3.3.5 Member Sizes for Example Problem

In this Section the guidelines for cross section member initial dimensioning are applied to the example problem being studied in this chapter.

- Cantilever Wings—Assume the use of a reinforced concrete deck with cantilever wing lengths of 4.75'. This leaves a 50'-0" top slab width between cantilever wings.
- Total Web Width and Spacing—Use an average cross section thickness of 1'-9", two barrier rails at 0.45 k/ft each, and a 2" overlay at 1.4 k/ft. The approximate dead load per foot of span is:

$$p_{DL} = 1.75(59.5)(0.15kcf) + 0.9 + 1.4 = 17.9 \text{ kips / ft}$$

The total width of all webs for a shear stress of $0.158\sqrt{f_c}$ is:

$$b_{total} = \frac{17.9(160)}{2(0.8(6.5))0.158\sqrt{5}(12)} = 65 \text{ inches}$$

Using $0.221\sqrt{f'_c}$ for the shear stress, the total of all web widths would be:

$$b_{total} = \frac{17.9(160)}{2(0.8(6.5))0.221\sqrt{5}(12)} = 46 \text{ inches}$$

Using a minimum web thickness of each web to be 12", the limits above would suggest either 5 or 4 webs. The centerline spacing of 5 webs would be $49.5/4 = 12.375'$. The spacing for 4 webs would be $49.5/3 = 16.5'$. Use 5 webs to keep the top slab as a reinforced concrete member.

- c. Top Slab thickness—Using 5 webs of 1' thickness and 3" fillets, the clear spacing between the webs would be $12'-4\frac{1}{2}" - 1' - 6" = 10'-10\frac{1}{2}"$. The range of top slab thicknesses to start preliminary design would be:

$$\frac{L_{clear}}{14} \geq t_{slab} \geq \frac{L_{clear}}{17}$$

$$0.78' \geq t_{slab} \geq 0.64'$$

Use a 9" top slab thickness for preliminary design.

- d. Bottom Slab Thickness—Use 7" to achieve cover and to fit mats of longitudinal and transverse reinforcing.

Note: This Section presented information for the preliminary sizing of a multi-cell concrete box girder superstructure. Dimensions for single cell box girders are similar to single cell segmental box girder. Information related to the sizing of segmental box girders is presented in LRFD Article 5.14.2.3.10.

Applying these initial dimensions with no interior haunches and making adjustments, such as sloping the outer webs, produces the preliminary design cross section shown in Figure 5.9.

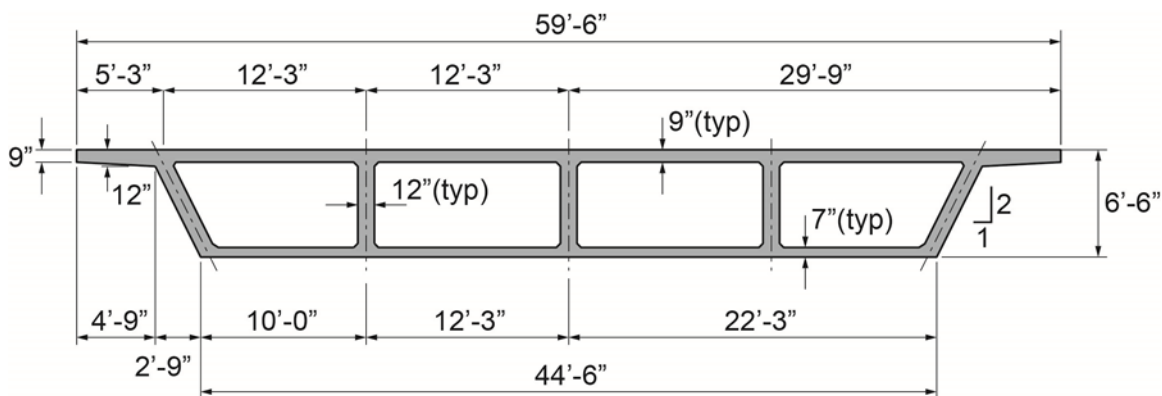


Figure 5.9 – Example Cross Section Dimensions for Preliminary Design

5.4 Longitudinal Analysis

5.4.1 Approach

Longitudinal analyses can be performed by any number of computerized solutions specifically for post-tensioned structures. General structural analysis programs can also be used with attentiveness to developing necessary load cases. Hand calculations like the Method of Joint Flexibilities presented in this manual are equally appropriate for longitudinal analysis, especially during preliminary design.

Analysis by the Method of Joint Flexibilities begins with the determination of span end rotations under the action of the applied loads. These end rotations are then used to determine continuity moments at the end of that span. This procedure is performed for all loaded spans, and the results summed to complete the analysis of the entire structure. This method is particularly helpful in evaluating load effects where the curvature diagram is readily determined, as is the case of prestressing primary effects (F_e). Appendix A of this manual presents the generalized flexibility-based hand method for solving continuous bridges.

5.4.2 Analysis by Method of Joint Flexibilities

The three-span example bridge being developed in this section is shown schematically in figure 5.10. The cross section of the superstructure of the box girder is shown in figure 5.9.

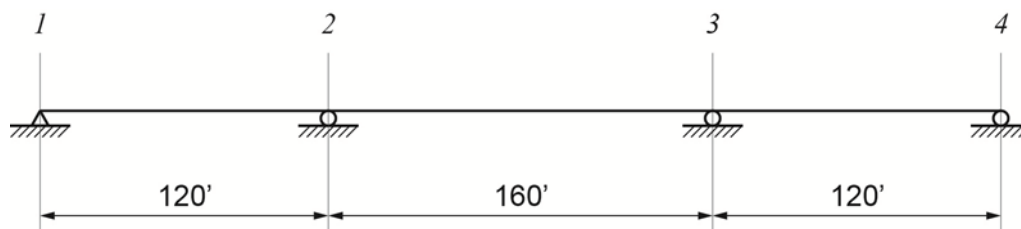


Figure 5.10 – Model of 3-Span Bridge for Example 1

5.4.3 Span Properties and Characteristic Flexibilities

The cross section properties of the box girder superstructure shown in figure 5.9 are:

$$I = 643.7 \text{ ft}^4$$

$$A = 99.45 \text{ ft}^2$$

$$c_1 = 2.732 \text{ ft}$$

$$c_2 = 3.768 \text{ ft}$$

$$\rho = 0.6288$$

$$Q_0 = 118.1 \text{ ft}^3$$

The characteristic flexibilities for the 120' Span are (See appendix A equations A.9 and A.10):

$$Ea = Ec = \frac{L}{3I} = \frac{120}{3(643.7)} = 0.06214$$

$$Eb = \frac{L}{6I} = \frac{120}{6(643.7)} = 0.03107$$

The characteristic flexibilities for the 160' Span are:

$$Ea = Ec = \frac{L}{3I} = \frac{160}{3(643.7)} = 0.08285$$

$$Eb = \frac{L}{6I} = \frac{160}{6(643.7)} = 0.041425$$

Note: For numerical ease, the modulus of elasticity of the concrete has been factored out of the flexibility coefficients. This will also be done for beam end rotation computations to produce a consistent solution.

5.4.4 Analysis Left to Right

Using equations A.28 and A.29 from appendix A:

$$K_{1/12} = \infty \quad k_{21/2} = c - \frac{b^2}{a + K_{1/12}} = 0.06214 - \frac{(0.03107)^2}{0.06214 + \infty} = 0.06214$$

$$K_{2/23} = \frac{1}{\frac{1}{0.06214}} = 0.06214$$

$$k_{32/3} = c - \frac{b^2}{a + K_{2/23}} = 0.08285 - \frac{(0.041425)^2}{0.08285 + 0.06214} = 0.07101$$

$$K_{3/34} = \frac{1}{\frac{1}{0.07101}} = 0.07101$$

5.4.5 Analysis Right to Left

Using equations A.28 and A.29 from appendix A:

$$K_{4/43} = \infty \quad k_{34/3} = a - \frac{b^2}{c + K_{4/43}} = 0.06214 - \frac{(0.03107)^2}{0.06214 + \infty} = 0.06214$$

$$K_{3/32} = \frac{1}{\frac{1}{0.06214}} = 0.06214$$

$$k_{23/2} = a - \frac{b^2}{c + K_{3/32}} = 0.08285 - \frac{(0.041425)^2}{0.08285 + 0.06214} = 0.07101$$

$$K_{2/21} = \frac{1}{\frac{1}{0.07101}} = 0.07101$$

5.4.6 Carry-Over Factors

For the Superstructure, using equations A.36 and A.37:

$$\phi_{12} = -\frac{b}{c + K_{2/21}} = -\frac{0.03107}{0.06214 + 0.07101} = -0.2333 \quad \phi_{21} = -\frac{b}{a + K_{1/12}} = -\frac{0.03107}{0.06214 + \infty} = 0.0$$

$$\phi_{23} = \phi_{32} = -\frac{b}{c + K_{3/32}} = -\frac{0.041425}{0.08285 + 0.06214} = -0.2857$$

$$\phi_{34} = -\frac{b}{c + K_{4/43}} = -\frac{0.03107}{0.06214 + \infty} = 0.0 \quad \phi_{43} = -\frac{b}{c + K_{3/34}} = -\frac{0.03107}{0.06214 + 0.07101} = -0.2333$$

5.5 Bending Moments

Bending moments are computed for the following loadings:

- Dead Load of Components (DC).
- Dead Load of Wearing Surface (DW).
- Live Loads (LL) – Truck and Uniform portions.
- Thermal Gradient (TG).
- Secondary Moments from Prestressing.

Several of these loadings are linearly scaled from the loading of a unit uniform load, which is solved first.

5.5.1 Effect of a Unit Uniform Load

The beam end rotations when loaded by a downward acting unit uniform load are:

$$E\omega_i = -E\omega_j = -\frac{L^3}{24I}$$

The beam characteristics of the 120' end spans are:

$$E\omega_i = -E\omega_j = -\frac{120^3}{24(643.7)} = -111.9$$

The beam characteristics of the 160' center span is:

$$E\omega_i = -E\omega_j = -\frac{160^3}{24(643.7)} = -265.1$$

The moments in Span 1 are:

$$M_{12} = 0.0 \qquad M_{21} = -\frac{\phi_{12}}{b}(\omega_2) = -\frac{0.2333}{.03107}(111.9) = -840 \text{ ft} - \text{kips}$$

The end moments in Span 2 are:

$$M_{23} = M_{32} = \frac{\phi_{32}}{b} \left(\frac{\omega_2 + \phi_{23}\omega_3}{1 - \phi_{23}\phi_{32}} \right) = \frac{0.2857}{0.041425} \left(\frac{-265.1 + 0.2857(265.1)}{1 - 0.2857(0.2857)} \right) = -1422 \text{ ft} - \text{kips}$$

The end moments in Span 3 (by symmetry),

$$M_{34} = -840 \text{ ft} - \text{kips} \qquad M_{43} = 0.0$$

The bending moments diagrams for the load in each span and the total of all moments is shown in figure 5.11.

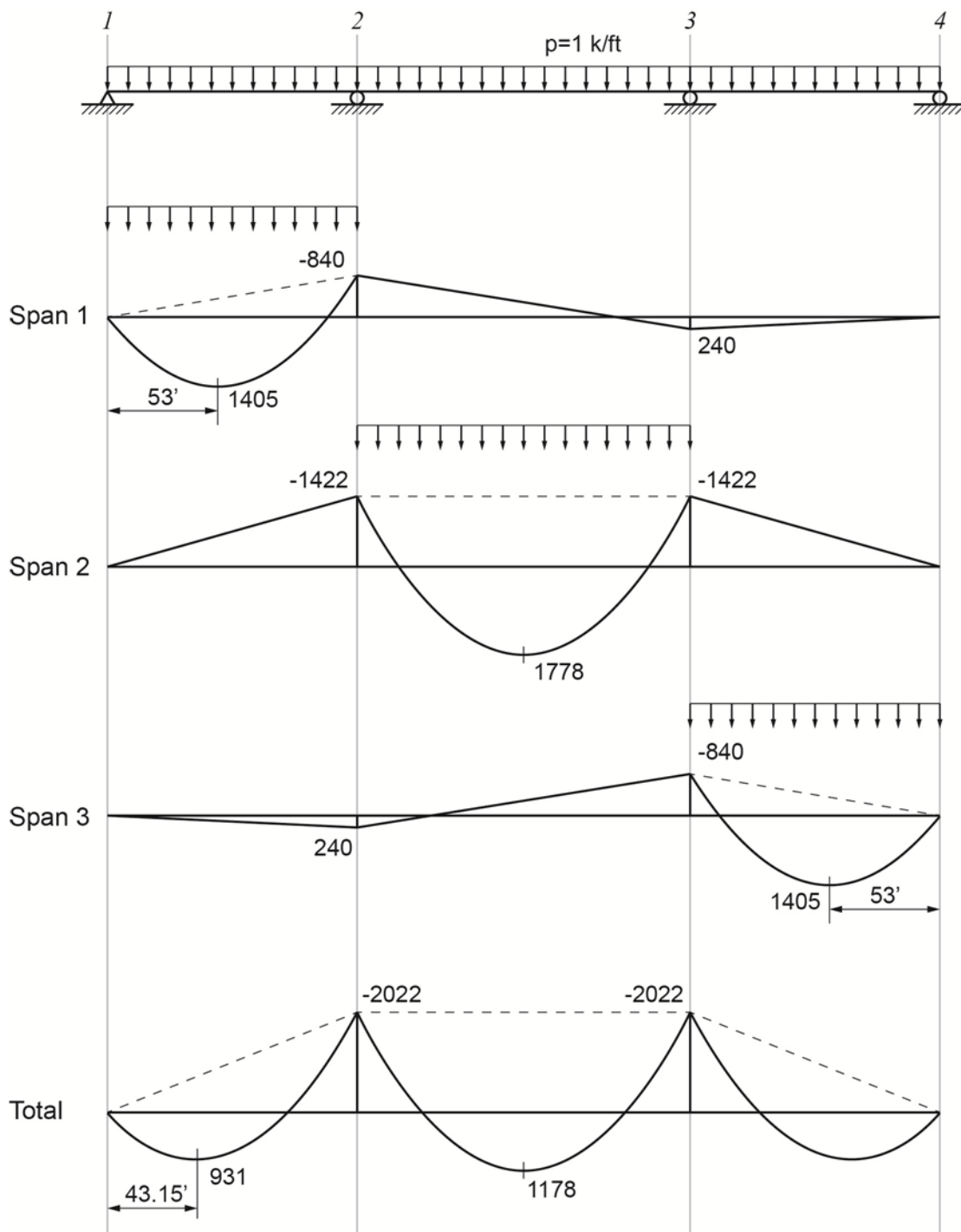


Figure 5.11 – Moment Diagram for a Unit Uniform Load

5.5.2 Dead Load—DC (Self Weight and Barrier Railing)

The gross area of the box girder superstructure is 99.45 ft². The unit weight of concrete for self weight computations is 150 lb/ft³. The resulting weight per foot of superstructure is 14.92 kips/ft. The weight of each barrier railing is 0.45 kips/ft. This results in a total dead load weight 15.82 kips/foot. Rounding up, use 16 kips/ft for finding bending moments. The DC moments are found as a linear scaling of the effects of a unit uniform load shown in Figure 5.11.

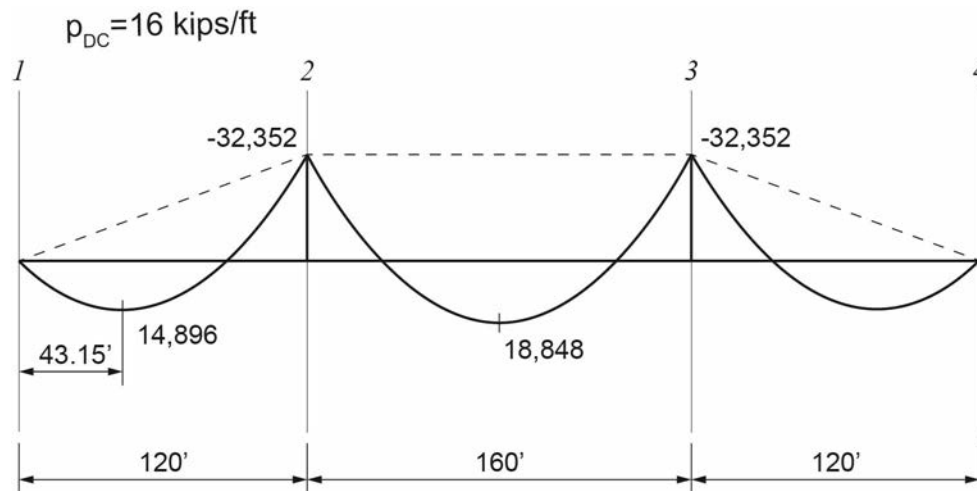


Figure 5.12 – Moment Diagram for Dead Load (DC)

5.5.3 Dead Load—DW (Future Wearing Surface)

The bridge is being designed to carry the weight of a 25 psf future overlay equal to 2" of concrete. Multiplying by the width of the roadway between barriers, the resulting weight per foot is 1.4 kips per foot. The DW moments are found as a linear scaling of the effects of a unit uniform load shown in figure 5.11.

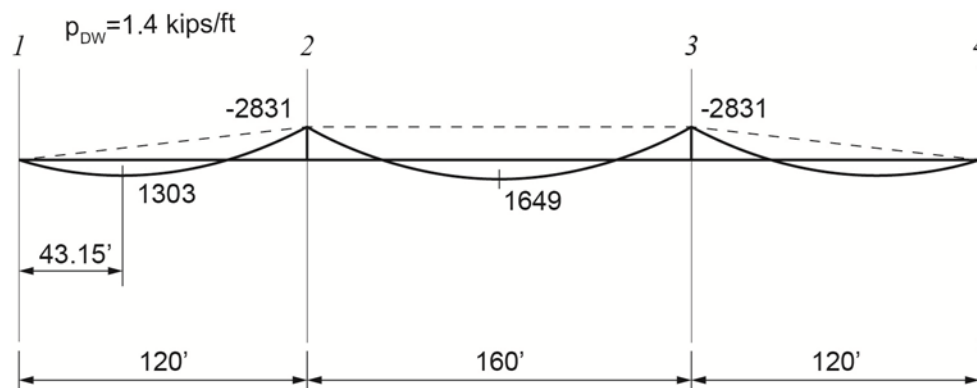


Figure 5.13 – Moment Diagram for Dead Load (DW)

5.5.4 Live Load—LL

Live load bending moments are computed for locations of maximum positive and negative moment. The HL-93 notional load contains the design truck and design lane load components. These are computed separately and combined later to determine maximum live load effects. The moments presented in this section are for a single lane. Total live load effects are calculated in section 5.5.4.5.

5.5.4.1 Uniform Load Component

The 0.64 kip/ft uniform lane load component of the AASHTO LRFD notional load can be applied in any combination of spans or partial spans to produce maximum and minimum effects. Figure 5.14 shows the bending moment envelope for the uniform load.

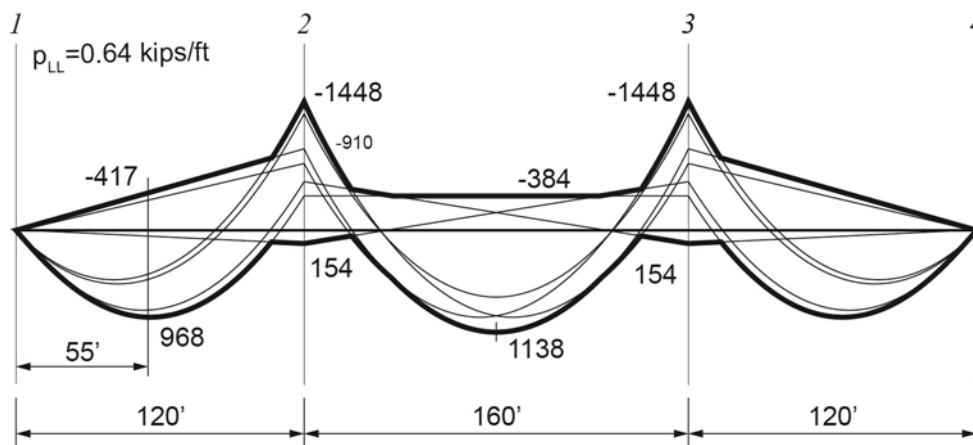


Figure 5.14 – Uniform Live Load Moment Envelope

5.5.4.2 Truck—Positive Moment in Span 1 or 3

Moments from truck axle loads are computed by determining and summing end rotations of the various axles and then solving for continuity moments. Figure 5.15 shows the end rotations for a beam subjected to a concentrated load. The rotations are defined in equation 5.12 and 5.13.

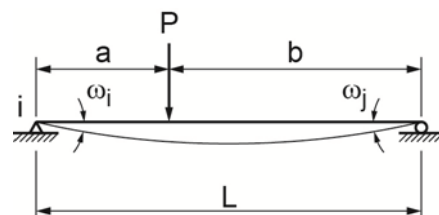


Figure 5.15 – Simple Beam Rotations for a Concentrated Load

(Eqn. 5.12)
$$E\omega_i = \frac{Pab}{6IL}(L+b)$$

(Eqn. 5.13)
$$E\omega_j = \frac{Pab}{6IL}(L+a)$$

The beam end rotation and end moment for the HL-93 design truck located 36' from the Abutment 1 are:

$$E\omega_j = 85.03$$

$$M_{21} = -\frac{\phi_{12}}{b}(\omega_2) = -\frac{0.2333}{.03107}(85.03) = -639 \text{ ft-kips}$$

Figure 5.16 shows the bending moment for a single truck with back axle located 36' from the beginning of the bridge.

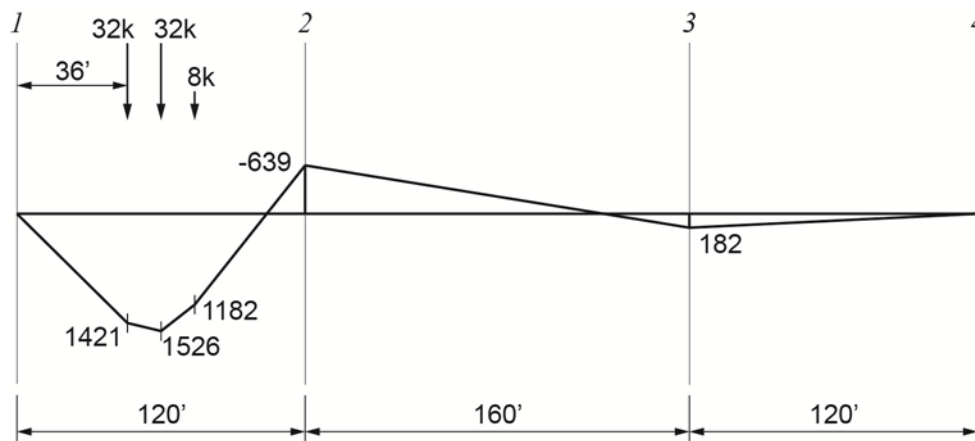


Figure 5.16 – Moment Diagram for HL-93 Design Truck in Span 1 (Positive Bending)

5.5.4.3 Truck—Positive Moment in Span 2

Figure 5.17 shows the bending moment for a single truck centered on Span 2.

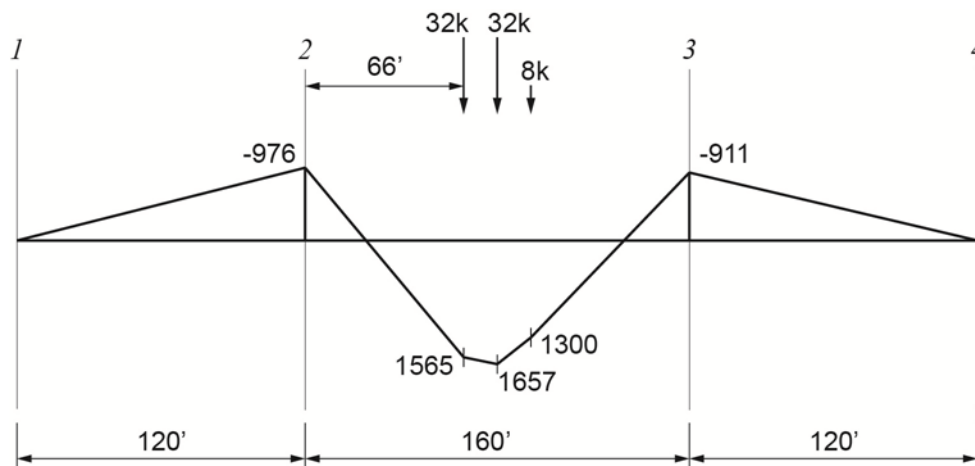


Figure 5.17 – Moment Diagram for HL-93 Design Truck in Span 2 (Positive Bending)

5.5.4.4 Truck—Negative Moment over Piers

AASHTO LRFD Article 3.6.1.3.1 calls for 90 percent of two trucks to be applied to produce negative moment results in continuous spans. Figure 5.18 shows the moment diagram for two HL-93 design trucks located about Pier 2 to generate maximum negative moment.

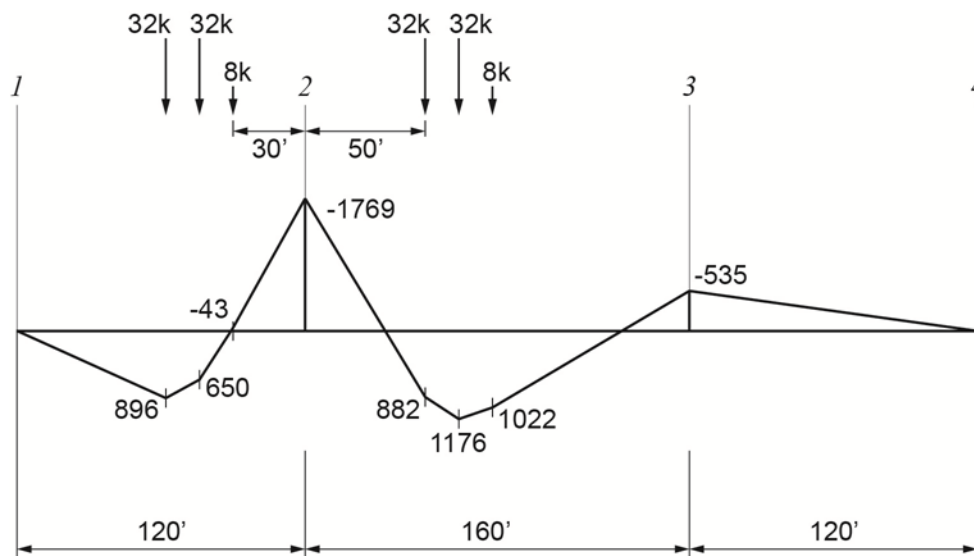


Figure 5.18 – Moment Diagram for Two HL-93 Design Trucks about Pier 2 (Negative Bending)

5.5.4.5 Live Load Moment Totals

AASHTO LRFD Article 4.6.2 provides approximate methods for determining live load distributions within bridge superstructures. AASHTO LRFD Article 4.6.2.2 provides live load distribution equations for beam-slab bridges. One of two approaches may be taken for determining live load distribution factors for cast-in-place multi-cell box girders. The first approach applies the distribution factors to each “girder line” individually. The effective cross section of each girder line consists of the web and the tributary areas of the top and bottom slabs. Two designs are then made, one for the interior girders and one for the exterior girders.

The second approach in applying the approximate method of live load distribution is the “whole-width” method. AASHTO LRFD Article 4.6.2.2.1 (paragraph 9) states:

Cast-in-place multi-cell concrete box girder bridge types may be designed as whole-width structures. Such cross sections shall be designed for the live load distribution factors in Articles 4.6.2.2.2 and 4.6.2.2.3 for interior girders, multiplied by the number of girders, i.e., webs.

AASHTO LRFD Table 4.6.2.2.1-1 identifies multi-cell box girder bridges as cross section type “d”. AASHTO LRFD Table 4.6.2.2.2b-1 provides live load distribution factor equations as a function of cross section type. For one design lane loaded, the equation for a type “d” section is:

$$(Eqn. 5.14) \quad DF = \left(1.75 + \frac{S}{3.6}\right) \left(\frac{1}{L}\right)^{0.35} \left(\frac{1}{N_c}\right)^{0.45}$$

The equation for two or more design lanes loaded is:

$$(Eqn. 5.15) \quad DF = \left(\frac{13}{N_c} \right)^{0.3} \left(\frac{S}{5.8} \right) \left(\frac{1}{L} \right)^{0.25}$$

where: DF = distribution factor
 L = length of span (ft) ($60 \leq L \leq 240$)
 N_c = number of cells ($N_c \geq 3$; use $N_c=8$ if $N_c \geq 8$)
 S = web spacing (ft) ($7.0 \leq S \leq 13.0$)

For positive moment, negative moment, and shear, L is the length of the span being considered. For negative moment between points of contraflexure under uniform loading, L is the average length of two adjacent spans.

In the case of the example problem being studied in this chapter, the distribution factors for two or more design lanes loaded govern over those for a one design lane loaded. The distribution factors are:

$$DF = \left(\frac{13}{4} \right)^{0.3} \left(\frac{12.25}{5.8} \right) \left(\frac{1}{120} \right)^{0.25} = 0.909 \quad (\text{Positive Moments in End Spans})$$

$$DF = \left(\frac{13}{4} \right)^{0.3} \left(\frac{12.25}{5.8} \right) \left(\frac{1}{160} \right)^{0.25} = 0.846 \quad (\text{Positive Moments in Middle Span})$$

$$DF = \left(\frac{13}{4} \right)^{0.3} \left(\frac{12.25}{5.8} \right) \left(\frac{1}{140} \right)^{0.25} = 0.874 \quad (\text{Negative Moments over Piers 2 and 3})$$

The number of design lanes is found from:

$$(Eqn. 5.16) \quad N_L = N_w \cdot DF$$

where: N_L = number of lanes
 N_w = number of webs

For the example problem:

$$N_L = 5(0.909) = 4.545 \quad (\text{Positive Moments in End Spans})$$

$$N_L = 5(0.846) = 4.230 \quad (\text{Positive Moments in Middle Span})$$

$$N_L = 5(0.874) = 4.370 \quad (\text{Negative Moments over Piers 2 and 3})$$

The resulting bending moments for preliminary design, including dynamic load allowance (impact) in accordance with AASHTO LRFD Article 3.6.2.1 are:

$$M_{LL+I} = (4.545)(1.33(1526) + 968) = 13,624 \quad (0.4167L \text{ Span 1})$$

$$M_{LL+I} = (4.230)(1.33(1657) + 1138) = 14,136 \quad (0.50L \text{ Span 2})$$

$$M_{LL+I} = 0.9(4.370)(1.33(-1769) + (-1448)) = -14,948 \quad (\text{At P2 \& P3})$$

5.5.5 Thermal Gradient (TG)

Continuous structures are subjected to stress distributions over the depth of the girder as a result of thermal gradients. AASHTO LRFD Article 3.12.3 shows the temperature distribution which should be applied to the depth of a concrete box girder. Preliminary design is simplified by assuming a 20 degree linear variation in temperature with depth for positive gradient, with the top slab 20 degrees warmer than the bottom slab. The resulting deformations of a simple beam subjected to a linear gradient are shown in figure 5.19.

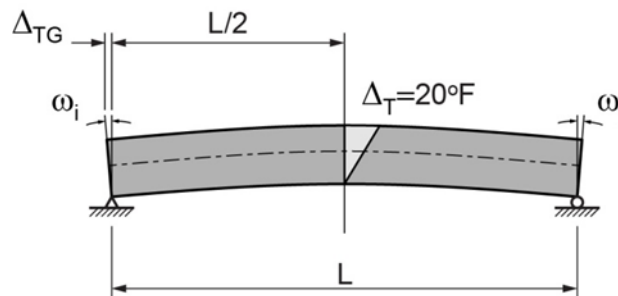


Figure 5.19 – Simple Beam Subjected to 20°F Positive Linear Gradient

The change in length of the top slab from the center of no movement (middle of beam) is equal to:

(Eqn. 5.17)

$$\Delta_{TG} = \frac{L}{2} \alpha \Delta T$$

The coefficient of thermal expansion for concrete, α , in equation 5.17 is equal to 6×10^{-6} . For small changes in length the beam end rotations are equal to this change in length divided by the depth of the beam. Considering our solution where E is included in the rotations,

(Eqn. 5.18)

$$E\omega_i = -E\omega_j = -\frac{\Delta_{TG}}{h} E = \frac{L\alpha\Delta T}{2h} E$$

For the example bridge being analyzed, the end rotations for the end spans and center span are:

$$E\omega_i = -E\omega_j = \frac{120'(6 \times 10^{-6})(20)}{2(6.5')} (617,300) = 683.8$$

$$E\omega_i = -E\omega_j = \frac{160'(6 \times 10^{-6})(20)}{2(6.5')} (617,300) = 911.7$$

The bending moments associated with these rotations are shown in figure 5.20.

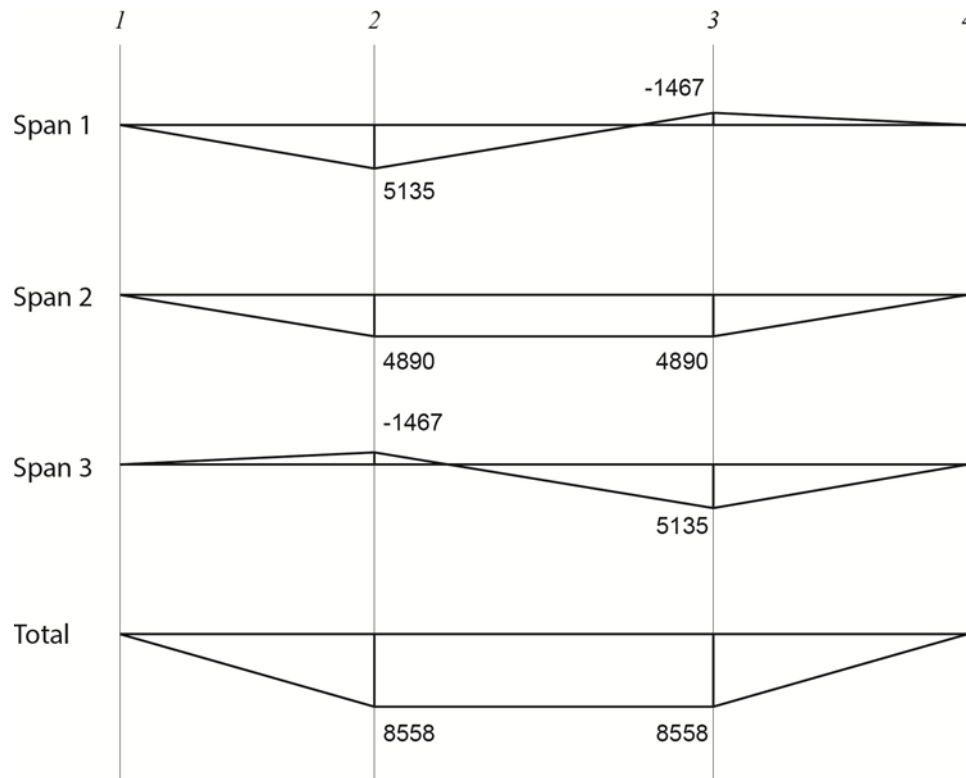


Figure 5.20 – Moment Diagram for a 20°F Positive Linear Gradient

5.5.6 Post-Tensioning Secondary Moments

Bending moments for DC, DW, LL, and TG have been computed directly from the applied loads or imposed deformations. Secondary moments from prestressing are, however, related to tendon geometries and prestressing forces, which are not yet determined. Using parabolic segments developed in chapter 3, a tendon profile that represents the center of gravity of all tendons can be assumed. The secondary moments can then be determined for a unit prestressing force (F=1 kip).

Figure 5.21 shows the cross section of the example bridge studied in this chapter. Detail A, detail B, and the position of the strands within the duct have been developed to find probable locations of tendons at the high and low points along their profiles. Assuming that three tendons per web will be used, the middle tendon profile will represent the center of gravity of all three tendons.

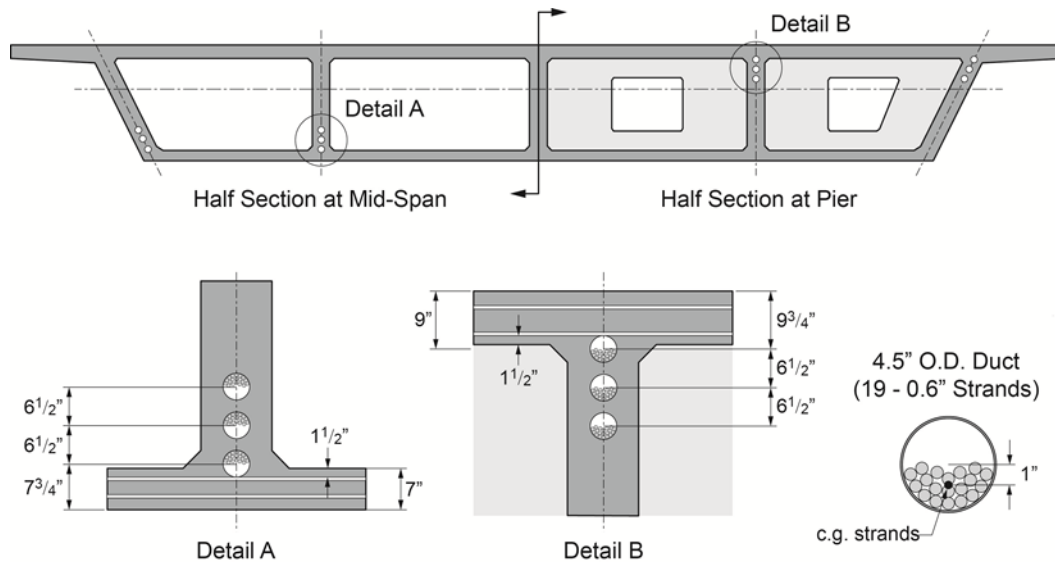


Figure 5.21 – Possible Tendon Locations at Mid-Span at over the Piers

For the cross section of the example problem, the distances from the neutral axis to the top and bottom most fibers of the beam are:

$$c_1 = 2.732'$$

$$c_2 = 3.768'$$

The minimum and maximum eccentricities are:

$$e_{\min} = -c_1 + 9 \frac{3}{4}'' + 6 \frac{1}{2}'' + 1'' = -1.29' \quad (\text{use } -1.25')$$

$$e_{\max} = c_2 - 7 \frac{3}{4}'' - 6 \frac{1}{2}'' - 1'' = 2.5'$$

Using the minimum and maximum eccentricities, the profile of the center of gravity (CG Profile) of the post-tensioning can be drawn. Figure 5.22 shows the CG Profile for the end spans. Figure 5.23 shows the CG Profile for the middle span. As a guide, the length of the parabolic segments at the piers is typically located from 0.10 to 0.15 of the span length. The low point of maximum eccentricity in the end spans is typically located from 0.35 to 0.45 of the span length measured from the end of the bridge.

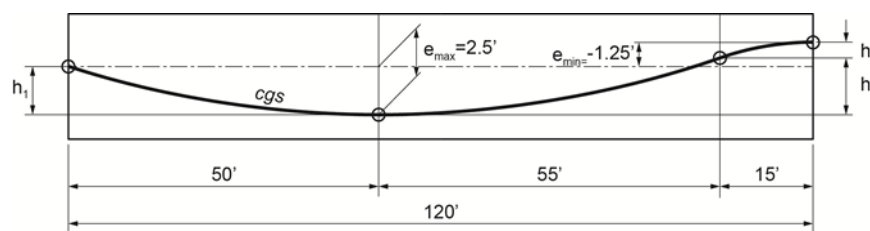


Figure 5.22 – Center of Gravity Profile of Prestressing (End Spans)

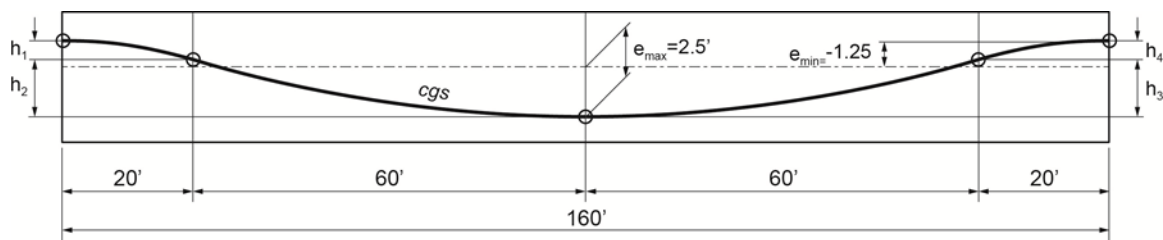


Figure 5.23 – Center of Gravity Profile of Prestressing (Middle Span)

Conjugate beam loads can be determined from the profiles using the methodology presented in chapter 3. Figures 5.24 and figure 5.25 show the conjugate beams and loads for a unit prestressing force ($F=1$).

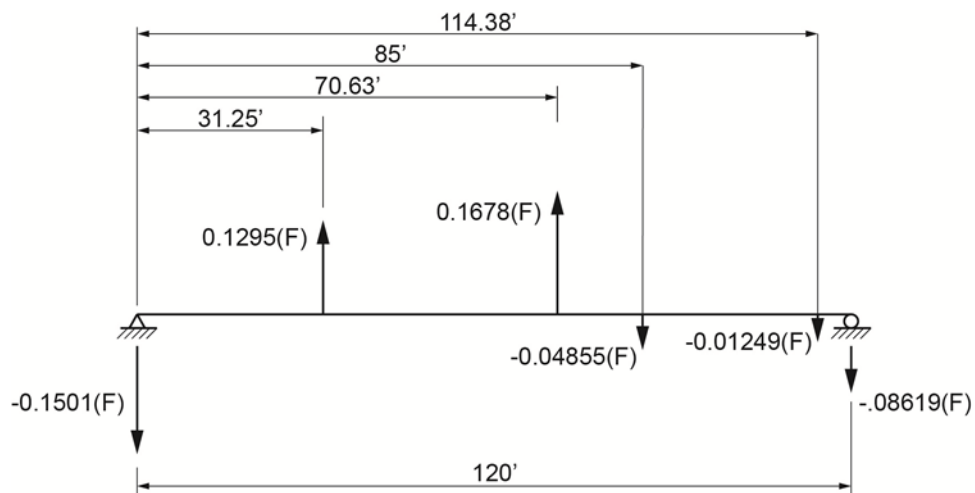


Figure 5.24 – Conjugate Beam and Loads (End Spans)

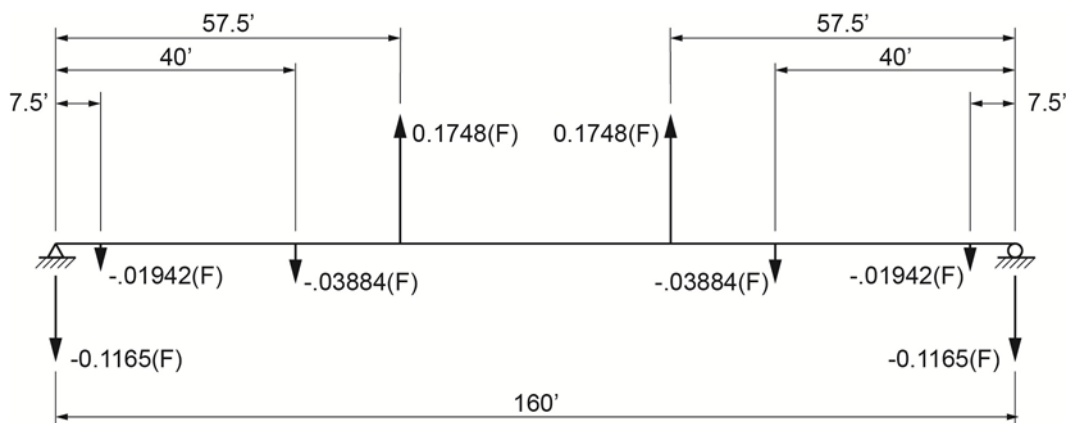


Figure 5.25 – Conjugate Beam and Loads (Main Span)

The conjugate beam reactions are equal to the simple beam end rotations. Continuity moments are found using these rotations flexibility analysis previously performed. The resulting moments for each span and the total secondary prestress moments are shown in figure 5.26.

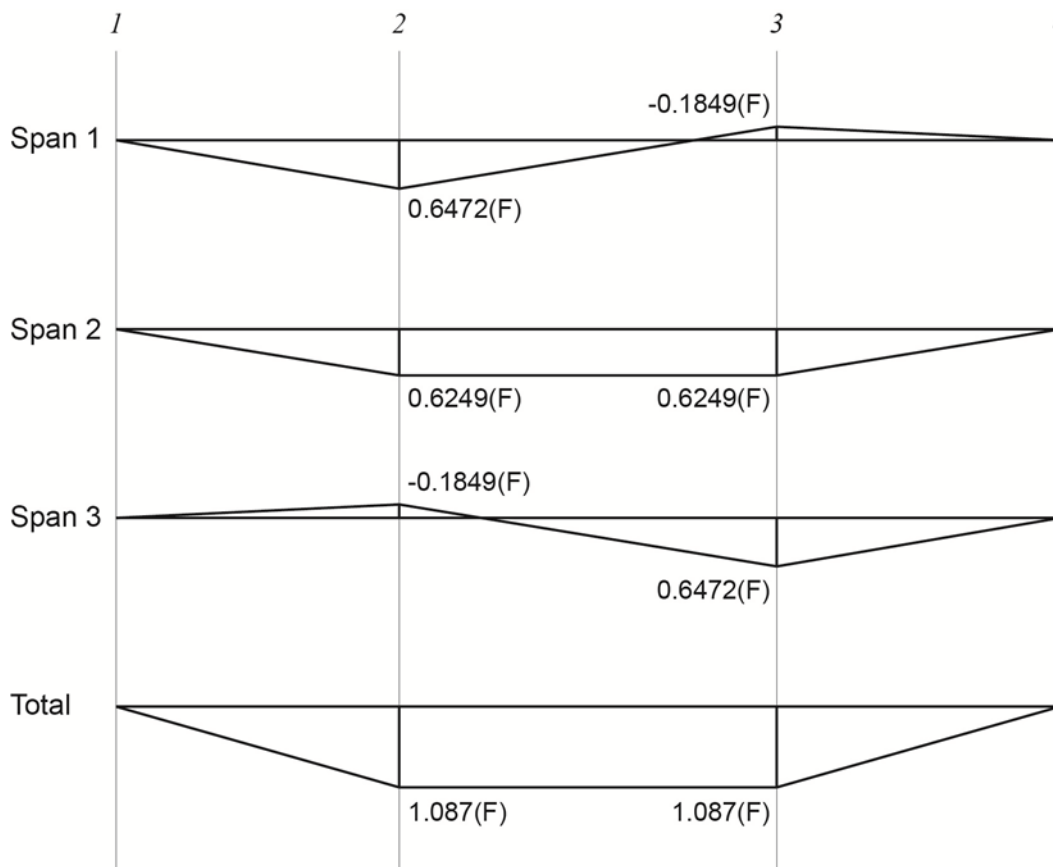


Figure 5.26 – Secondary Prestressing Moments, $M_2(F)$

5.6 Required Prestressing Force After Losses

In chapter 3 equations for determining post-tensioning requirements to limit tensile stresses in the concrete were developed. Equations 3.9 and 3.10 took the form:

(Eqn. 5.19)
$$F \geq \frac{M + M_{ab}}{\rho c_1 + e}$$

(Eqn. 5.20)
$$F \geq \frac{M - M_{at}}{e - \rho c_2}$$

The total bending moment, M , for checking tensile stresses is that corresponding to Service Level III. Using the load factors in AASHTO LRFD Table 3.4.1-1, total bending moment is:

(Eqn. 5.21)
$$M = M_{DC} + M_{DW} + 0.8M_{LL+I} + 0.5M_{TG} + M_2(F)$$

For convenience, equation 5.21 can be expressed as:

$$(Eqn. 5.22) \quad M = M_{sum} + M_2(F)$$

M_{sum} in this equation is the sum of all bending moments except the secondary moments from prestressing. Substituting equation 5.22 into equations 5.19 and 5.20:

$$(Eqn. 5.23) \quad F \geq \frac{M_{sum} + M_2(F) + M_{ab}}{\rho c_1 + e}$$

$$(Eqn. 5.24) \quad F \geq \frac{M_{sum} + M_2(F) - M_{at}}{e - \rho c_2}$$

These equations can be rearranged to:

$$(Eqn. 5.25) \quad F \geq \frac{M_{sum} + M_{ab}}{\rho c_1 + e - M_2}$$

$$(Eqn. 5.26) \quad F \geq \frac{M_{sum} - M_{at}}{e - \rho c_2 - M_2}$$

Table 5.1 shows the bending moments determined from the analyses presented earlier in this Chapter at three locations in the example bridge. The locations chosen for review are the points of maximum positive flexure within the spans and the point of maximum negative bending over the piers.

Section	DC	DW	0.8(LL+I)	0.5TG	Msum	M ₂
0.3596 L1	14,896	1303	10,899*	1539	28,637	0.391(F)
0.5 L2	18,848	1649	11,309	4279	36,085	1.087(F)
Pier 2/3	-32,352	-2831	-11,959	-1284**	-48,426	1.087(F)

*The maximum moment at 0.4167L (top of Page 24 of 41) was used for this example.

**Negative thermal gradient is -0.3 of the positive moment (LRFD Artivle 3.12.3).

Table 5.1 – Moment Components of Service Level III Loading at Three Locations

Assuming moderately corrosive conditions, AASHTO LRFD Table 5.9.4.2.2-1 states that the allowable stress in the concrete after all losses is $0.19\sqrt{f'_c}$, where f'_c has the units of ksi. This is equal to $6\sqrt{f'_c}$, where f'_c has the units of psi. The resulting moments producing allowable stresses are:

$$M_{ab} = -\frac{0.19\sqrt{f'_c}(I)}{c_2} = -\frac{0.19\sqrt{5}(643.7)}{3.768}(144) = -10,451 \text{ ft} - \text{kips}$$

$$M_{at} = -\frac{0.19\sqrt{f'_c}(I)}{c_1} = -\frac{0.19\sqrt{5}(643.7)}{2.732}(144) = -14,415 \text{ ft} - \text{kips}$$

The sign of these moments are consistent with the development of equations 3.9 and 3.10.

Using equations 5.25 and 5.26, the minimum prestressing force requirements at the three sections studied, after all losses, are:

$$F = \frac{28,637 + (-10,451)}{0.6288(2.732) + 2.5 - 0.391} = 4,752 \text{ kips} \quad (0.3596L \text{ Span 1})$$

$$F = \frac{36,037 + (-10,451)}{0.6288(2.732) + 2.5 - 1.087} = 8,172 \text{ kips} \quad (0.5L \text{ Span 2})$$

$$F = \frac{-48,426 - (-14,415)}{-1.25 - 0.6288(3.768) - 1.087} = 7,227 \text{ kips} \quad (\text{At Piers 2 and 3})$$

5.7 Prestressing Losses and Tendon Sizing for Final Design (Pjack)

The required prestressing force at the center of the middle span is 8,172 kips. Assuming three tendons in each of the five webs of the example problem cross section, the final post-tensioning force in each of the 15 tendons is 545 kips. The number of prestressing strands required in these tendons is a function of the amount of instantaneous and long-term prestressing force loss. Losses will be computed in accordance with the information presented in chapter 4.

5.7.1 Losses from Friction, Wobble, and Anchor Set

Using the CG Profile, the forces along the tendon after two-end stressing are computed. The assumed values for friction, wobble coefficient, and anchor set are 0.25, 0.0002/ft, and 0.375", respectfully. The geometry required for determining the losses is shown in table 5.2. The friction diagram, expressed in terms of stress is shown in figure 5.27.

Point	b (ft)	h (ft)	Angular Deviation $\theta=2h/b$ (rad)	Angular Force Coefficient	Cumulative Force Coefficient	Tendon Stress (ksi)
1	0	0.0000	0.00000	0.0000	1.0000	202.50
2	50	2.5000	0.10000	0.9656	0.9656	195.54
3	55	2.9464	0.10714	0.9629	0.9298	188.28
4	15	0.8036	0.10714	0.9707	0.9025	182.76
5	20	0.9375	0.09375	0.9729	0.8781	177.81
6	60	2.8125	0.09375	0.9652	0.8475	171.62
7	60	2.8125	0.09375	0.9652	0.8180	165.65
8	20	0.9375	0.09375	0.9729	0.7959	161.16
9	15	0.8036	0.10714	0.9707	0.7725	156.43
10	55	2.9464	0.10714	0.9629	0.7439	150.63
11	50	2.5000	0.10000	0.9656	0.7183	145.45

Table 5.2 –Data for Friction Diagram for the CG Profile Tendon

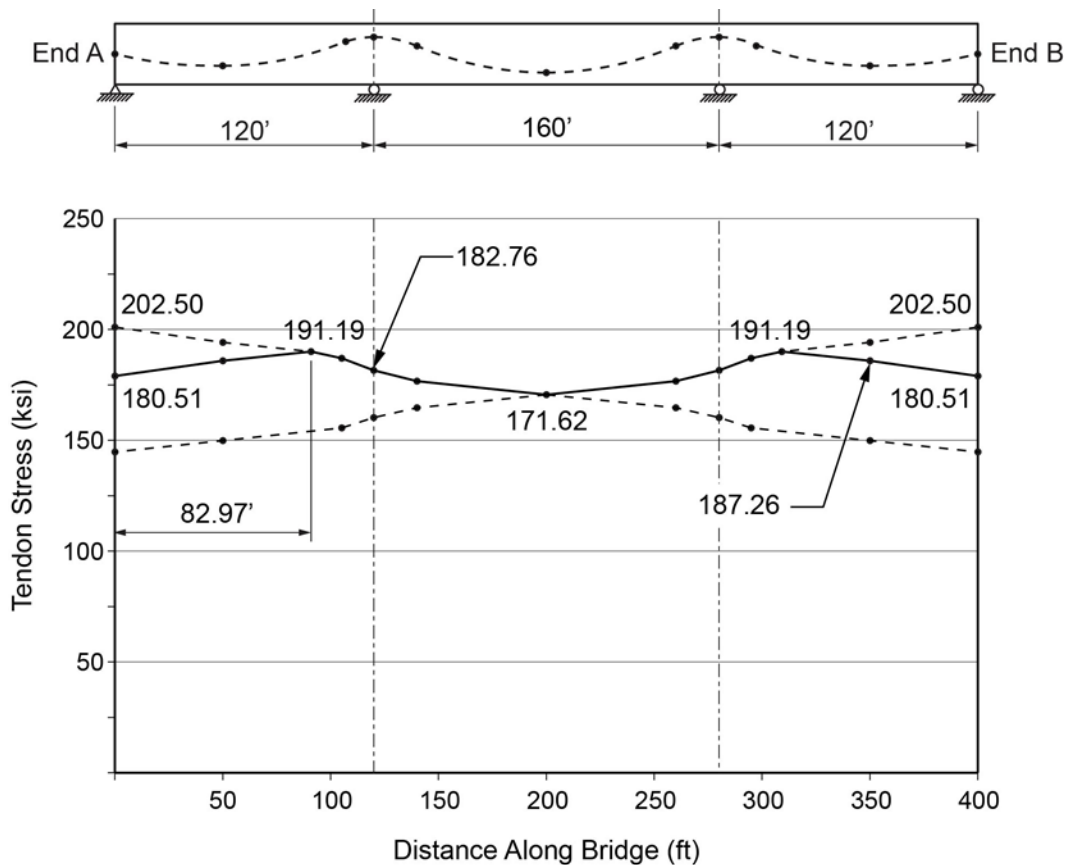


Figure 5.27 – Friction Diagram for the CG Profile Tendon

5.7.2 Losses from Elastic Shortening

Equation 4.24, repeated here, presented the AASHTO LRFD equation for losses from elastic shortening.

$$(Eqn. 5.27) \quad \Delta f_{pES} = \frac{N-1}{2N} \frac{E_p}{E_{ci}} f_{cgp}$$

Difficulty arises here, because the value of f_{cgp} , the concrete stress at the center of gravity of the prestressing, is computed after jacking and before any long-term losses. This requires an area of steel to be multiplied by the tendon stresses in figure 5.29, to produce a prestressing force by which concrete stresses can be computed.

This difficulty is overcome by making an initial assumption of all losses equal to 20 ksi. Subtracting this from the tendon stress at the center of the middle span (171.62 ksi) produces an estimate of final stress in the tendon at this location of 151.62 ksi (56 percent of f_{pu}). The estimate of final force per strand in the tendon, using 0.6" diameter strands with an area of 0.217 in² is 32.9 kips. Dividing the 550 kips per tendon by the force per strand results in 16.7 strands required in each tendon. Rounding up to 17 strands per tendon, forces after stressing can now be computed as the stresses in figure 5.29 times the tendon area of 0.217(17) = 3.689 in².

All of the post-tensioning tendons will be grouted within their ducts after installation and stressing. During construction, however, tendons are unbonded when elastic shortening occurs, assuming all tendons are stressed in one phase of construction.

AASHTO LRFD Article 5.9.5.2.3b states that:

For post-tensioned structures with unbonded tendons, the f_{cgp} value may be calculated as the stress at the center of gravity of the prestressing steel averaged along the length of the member.

Concrete stresses will be computed at four locations along the bridge and then a weighted average will be used for f_{cgp} . The equation used for computing the concrete stress is:

$$\text{(Eqn. 5.28)} \quad f_{cgp} = \frac{F}{A} \pm \frac{Fe^2}{I} \pm \frac{M_{sw}e}{I}$$

where: M_{sw} = bending moment from self weight only (ft-kips)

At end of bridge:

$$f_{cgp} = \frac{9,976}{99.45} = 100.3 \text{ksf}$$

At the point of maximum eccentricity in Span 1 and 3

$$f_{cgp} = \frac{10,362}{99.45} + \frac{10,362(2.5)^2}{643.7} - \frac{14,058(2.5)}{643.7} = 150.2 \text{ksf}$$

Over Piers 2 and 3

$$f_{cgp} = \frac{10,113}{99.45} + \frac{10,113(1.25)^2}{643.7} - \frac{30,532(1.25)}{643.7} = 66.9 \text{ksf}$$

At the center of the middle Span

$$f_{cgp} = \frac{9,497}{99.45} + \frac{9,497(2.5)^2}{643.7} - \frac{17,788(2.5)}{643.7} = 118.6 \text{ksf}$$

Using a straight-line average between the stresses at these locations, the average stress in the tendon is 106.4 ksf or 0.74 ksi. The loss associated with elastic shortening, using a concrete strength at the time of stressing of 4 ksi, is then:

$$\Delta f_{pES} = \frac{15 - 1}{2(15)} \frac{2,8500}{3,834} (.74) = 2.6 \text{ksi}$$

5.7.3 Losses from Concrete Shrinkage

The loss of prestress force resulting from shrinkage of the concrete superstructure is given by AASHTO LRFD Equation 5.9.5.4.3a-1 as:

$$\text{(Eqn. 5.29)} \quad \Delta f_{psD} = \varepsilon_{bdf} E_p K_{df}$$

The strain ε_{bdf} , is the shrinkage strain from the time of prestressing to final time as provided by AASHTO LRFD Equation 5.4.2.3.3-1:

$$\text{(Eqn. 5.30)} \quad \varepsilon_{bdf} = k_s k_{hs} k_f k_{td} 0.48 \times 10^{-3}$$

The factors in Equation 4.25 are defined by AASHTO LRFD Equations 5.4.2.3.2-2, 5.4.2.3.3-2, 5.4.2.3.2-4, and 5.4.2.3.2-5. Evaluating these for the example problem:

$$k_s = 1.45 - 0.13 \left(\frac{V}{S} \right) = 1.45 - 0.13(12.57) = -0.18 \quad (\text{Use } 1.0)$$

$$k_{hs} = (2.00 - 0.014H) = (2.00 - 0.014(75)) = 0.95$$

$$k_f = \frac{5}{1 + f'_{ci}} = \frac{5}{1 + 4} = 1$$

$$k_{td} = \left(\frac{t}{61 - 4f'_{ci} + t} \right) = \left(\frac{10,000}{61 - 4(5) + 10,000} \right) = 0.996$$

This results in a shrinkage strain of:

$$\varepsilon_{bdf} = (1.0)(0.95)(1.0)(0.996)0.48 \times 10^{-3} = 0.000454$$

Evaluation of the transformed section coefficient K_{df} requires computing the creep coefficient:

$$\Psi_b(t_f, t_i) = 1.9 k_s k_{hc} k_f k_{td} t_i^{-0.118}$$

$$k_{hc} = 1.56 - 0.008H = 1.56 - 0.008(75) = 0.96$$

$$\Psi_b(t_f, t_i) = 1.9(1.0)(0.96)(1.0)(0.996)(28)^{-0.118} = 1.226$$

The transformed section coefficient is then:

$$K_{df} = \frac{1}{1 + \frac{E_p}{E_{ci}} \frac{A_{ps}}{A_c} \left(1 + \frac{A_c e_{pc}^2}{I_c} \right) [1 + 0.7 \Psi_b(t_f, t_i)]}$$

$$K_{df} = \frac{1}{1 + \frac{28500}{3834} \frac{55.335}{99.45(144)} \left(1 + \frac{99.45(2.5)^2}{643.7(144)} \right) [1 + 0.7(1.226)]} = 1.054$$

Multiplying the components of equation 5.29, the loss of prestress stress resulting from the shrinkage of concrete is:

$$\Delta f_{pSD} = 0.000454(28500)(1.054) = 13.6 \text{ ksi}$$

5.7.4 Losses from Concrete Creep

The loss of stress in the prestressing steel resulting from the creep of concrete is:

$$\Delta f_{pCD} = \frac{E_p}{E_{ci}} f_{cgp} \Psi_b(t_f, t_i) K_{df} = \frac{28500}{3834} (.66)(1.226)(1.054) = 6.3 \text{ ksi}$$

5.7.5 Losses from Steel Relaxation

Using the AASHTO LRFD permissible value for low relaxation steel, the loss of prestressing stress is resulting from relaxation of the prestressing steel is:

$$\Delta f_{pR} = 2.4 \text{ ksi}$$

5.7.6 Total of Losses and Tendon Sizing

The total loss of prestressing force after jacking is the sum of elastic shortening, shrinkage, creep and relaxation:

$$\Delta f_p = 2.6 + 13.6 + 6.3 + 2.4 = 24.9 \text{ ksi}$$

The resulting stress in the prestressing steel at the center of the middle span is then:

$$f_p = 171.62 - 24.9 = 146.72 \text{ ksi}$$

The resulting force in a 0.6" diameter strand would be 31.9 kips. The number of strands in the 15 tendons, based on the force requirement at the center of Span 2 of 8,172 kips, would be 17.2. Therefore, use 18 strand tendons in final design. The jacking stressed assumed in the loss calculations was 75 percent of the ultimate strength of the strand. The resulting jacking force (Pjack) for each tendon would be 791 kips.

5.8 Service Limit State Stress Verifications

This Section presents stress summaries for important load cases at service limit states. Flexural stresses are verified after the tendons are stressed and before grouting, after the bridge is open to traffic and before long-term losses, and the bridge in operation after long-term

losses have occurred. A verification of principal stresses in the webs is made with the bridge in operation and after long-term losses have occurred.

5.8.1 Service Flexure—Temporary Stresses (DC and PT Only)

Longitudinal stresses in the concrete superstructure are verified at three locations along the bridge. The stresses are being verified after all post-tensioning tendons are stressed, but before grouting. The assumption for this example is that there is insufficient bonded mild reinforcing in the precompressed tensile zone to permit tension during this phase. Applied bending moments are taken from table 5.1.

Three post-tensioning tendons in each of the five webs of the box girder are stressed. Each of the tendons contains 18, 0.6" diameter strands. Tendon forces at the three study sections are based on stresses shown in figure 5.27, reduced for elastic shortening losses of 2.6 ksi as computed in section 5.7.2.

The allowable concrete stresses in the concrete before losses are presented in AASHTO LRFD Article 5.9.4.1. For a 28-day concrete strength of 5 ksi the allowable stresses are:

$$f_a = 0.60f_{ci}' = 0.60(4) = 2.4\text{ksi} = 345.6\text{ksf} \quad (\text{compression})$$

$$f_a = 0.0\text{ksf} \quad (\text{no tension when not considering bonded reinforcing})$$

At the point of maximum eccentricity in Span 1 and 3

$$f_{TOP} = \frac{10,819}{99.45} - \frac{10,819(2.5)(2.732)}{643.7} + \frac{19,126(2.732)}{643.7} = 75.2\text{ksf}$$

$$f_{BOT} = \frac{10,819}{99.45} + \frac{10,819(2.5)(3.768)}{643.7} - \frac{19,126(3.768)}{643.7} = 155.2\text{ksf}$$

Over Piers 2 and 3

$$f_{TOP} = \frac{10,556}{99.45} - \frac{10,556(-1.25)(2.732)}{643.7} + \frac{-20,879(2.732)}{643.7} = 73.5\text{ksf}$$

$$f_{BOT} = \frac{10,556}{99.45} + \frac{10,556(-1.25)(3.768)}{643.7} - \frac{-20,879(3.768)}{643.7} = 151.1\text{ksf}$$

At the center of the middle Span

$$f_{TOP} = \frac{9,903}{99.45} - \frac{9,903(2.5)(2.732)}{643.7} + \frac{29,613(2.732)}{643.7} = 120.2\text{ksf}$$

$$f_{BOT} = \frac{9,903}{99.45} + \frac{9,903(2.5)(3.768)}{643.7} - \frac{29,613(3.768)}{643.7} = 71.2\text{ksf}$$

The concrete stresses in the box girder superstructure are within permissible AASHTO LRFD limits. Stresses over Piers 2 and 3 could have been checked at the face of the support.

5.8.2 Service Limit State III Flexure Before Long-Term Losses

Longitudinal stresses in the concrete superstructure are verified at three locations along the bridge. The stresses are being verified when the bridge is first open to traffic. The assumption for this example is that there is insufficient bonded mild reinforcing in the precompressed tensile zone to permit tension during this phase. Applied bending moments are taken from table 5.1.

Three post-tensioning tendons in each of the five webs of the box girder are stressed. Each of the tendons contains 18, 0.6" diameter strands. Tendon forces at the three study sections are based on stresses shown in figure 5.27, reduced for elastic shortening losses of 2.6 ksi as computed in section 5.7.2.

The allowable concrete stresses in the concrete before losses are presented in AASHTO LRFD Article 5.9.4.2. For a 28-day concrete strength of 5 ksi the allowable stresses are:

$$f_a = 0.6\phi_w f'_c = 0.6(1)(5) = 3.0 \text{ ksi} = 432.0 \text{ ksf} \quad (\text{compression})$$

$$f_a = -0.19\sqrt{f'_c} = -0.19\sqrt{5} = -0.425 \text{ ksi} = -61.2 \text{ ksf} \quad (\text{tension})$$

At the point of maximum eccentricity in Span 1 and 3

$$f_{TOP} = \frac{10,819}{99.45} - \frac{10,819(2.5)(2.732)}{643.7} + \frac{32,867(2.732)}{643.7} = 133.5 \text{ ksf}$$

$$f_{BOT} = \frac{10,819}{99.45} + \frac{10,819(2.5)(3.768)}{643.7} - \frac{32,867(3.768)}{643.7} = 74.7 \text{ ksf}$$

Over Piers 2 and 3

$$f_{TOP} = \frac{10,556}{99.45} - \frac{10,556(-1.25)(2.732)}{643.7} + \frac{-36,952(2.732)}{643.7} = 5.3 \text{ ksf}$$

$$f_{BOT} = \frac{10,556}{99.45} + \frac{10,556(-1.25)(3.768)}{643.7} - \frac{-36,952(3.768)}{643.7} = 245.2 \text{ ksf}$$

At the center of the middle Span

$$f_{TOP} = \frac{9,903}{99.45} - \frac{9,903(2.5)(2.732)}{643.7} + \frac{46,850(2.732)}{643.7} = 193.3 \text{ ksf}$$

$$f_{BOT} = \frac{9,903}{99.45} + \frac{9,903(2.5)(3.768)}{643.7} - \frac{46,850(3.768)}{643.7} = -29.7 \text{ ksf}$$

The concrete stresses in the box girder superstructure are within permissible AASHTO LRFD limits. Stresses over Piers 2 and 3 could have been checked at the face of the support.

5.8.3 Service Limit State III Flexure After Long-Term Losses

Longitudinal stresses in the concrete superstructure are verified at three locations along the bridge. The stresses are being verified when the bridge is first open to traffic. The assumption for this example is that there is insufficient bonded mild reinforcing in the precompressed tensile zone to permit tension during this phase. Applied bending moments are taken from table 5.1.

Three post-tensioning tendons in each of the five webs of the box girder are stressed. Each of the tendons contains 18, 0.6" diameter strands. Tendon forces at the three study sections are based on stresses shown in figure 5.27, reduced by long-term losses of 24.9 ksi as computed in section 5.7.6.

The allowable concrete stresses in the concrete before losses are presented in AASHTO LRFD Article 5.9.4.2. For a 28-day concrete strength of 5 ksi the allowable stresses are:

$$f_a = 0.6\phi_w f'_c = 0.6(1)(5) = 3.0 \text{ ksi} = 432.0 \text{ ksf} \quad (\text{compression})$$

$$f_a = -0.19\sqrt{f'_c} = -0.19\sqrt{5} = -0.425 \text{ ksi} = -61.2 \text{ ksf} \quad (\text{tension})$$

At the point of maximum eccentricity in Span 1 and 3

$$f_{TOP} = \frac{9,513}{99.45} - \frac{9,513(2.5)(2.732)}{643.7} + \frac{32,357(2.732)}{643.7} = 132.0 \text{ ksf}$$

$$f_{BOT} = \frac{9,513}{99.45} + \frac{9,513(2.5)(3.768)}{643.7} - \frac{32,357(3.768)}{643.7} = 45.5 \text{ ksf}$$

Over Piers 2 and 3

$$f_{TOP} = \frac{9,249}{99.45} - \frac{9,249(-1.25)(2.732)}{643.7} + \frac{-38,372(2.732)}{643.7} = -20.8 \text{ ksf}$$

$$f_{BOT} = \frac{9,249}{99.45} + \frac{9,249(-1.25)(3.768)}{643.7} - \frac{-38,372(3.768)}{643.7} = 249.9 \text{ ksf}$$

At the center of the middle Span

$$f_{TOP} = \frac{8,596}{99.45} - \frac{8,596(2.5)(2.732)}{643.7} + \frac{45,429(2.732)}{643.7} = 188.0 \text{ ksf}$$

$$f_{BOT} = \frac{8,596}{99.45} + \frac{8,596(2.5)(3.768)}{643.7} - \frac{45,429(3.768)}{643.7} = -53.7 \text{ ksf}$$

The concrete stresses in the box girder superstructure are within permissible AASHTO LRFD limits. (Stresses checked over Piers 2 and 3 could have been checked at the face of the supporting pier.)

5.8.4 Principal Tension in Webs after Losses

AASHTO LRFD does not require principal tension verifications at service limit states for concrete box girders other than those built segmentally. These verifications are, however, useful for preliminary design, as an indicator whether the webs are sized appropriately. It is strongly recommended that principal tension be verified in cast-in-place concrete box girder construction when the box girder has only two webs.

Consider the cross section 0.72h (4.68') to the left of Pier 2 in Span 2. The shear forces acting are:

$$V_{DC} = 16(80 - 4.68) = 1,205 \text{ kips}$$

$$V_{DW} = 1.4(80 - 4.68) = 105 \text{ kips}$$

$$V_{LL(1 \text{ lane})} = 53 \text{ kips}$$

$$V_{LL(1 \text{ truck})} = 68 \text{ kips}$$

$$V_{LL+I} = 1.33(68) + 53 = 143 \text{ kips}$$

The live load distribution for shear is found by AASHTO LRFD Table 4.6.2.2.3a-1 for cross section type d and two or more design lanes loaded:

$$DF = \left(\frac{S}{7.3} \right)^{0.9} \left(\frac{d}{12(L)} \right)^{0.1} = \left(\frac{12.25}{7.3} \right)^{0.9} \left(\frac{78}{12(160)} \right)^{0.1} = 1.157$$

$$N_L = N_w \cdot DF = 5(1.157) = 5.785$$

$$V_{LL+I} = (0.8)5.785(143) = 662 \text{ kips}$$

$$\theta = \frac{2h}{b^2} x = \frac{2(-0.9375)}{(20)^2} (4.68) = -0.0219 \text{ rad} = -1.26 \text{ deg}$$

$$V_P = 9,249 \sin(-1.26) = -203 \text{ kips}$$

$$\sum V = 1205 + 105 + 662 + (-203) = 1769 \text{ kips}$$

The stresses acting on an element at the neutral axis are:

$$\sigma_x = \frac{9,249}{99.45} = 93.00 \text{ ksf}$$

$$\sigma_y = 0.0$$

$$\tau_{xy} = \frac{V(Q)}{I(B)} = \frac{1,769(118.1)}{643.7(5)} = 64.91 \text{ ksf}$$

The features of Mohr's Circle with these stresses are:

$$R = \sqrt{\left(\frac{\sigma_x}{2}\right)^2 + \tau_{xy}^2} = \sqrt{\left(\frac{93.00}{2}\right)^2 + (64.91)^2} = 79.85ksf$$

$$\sigma_{max} = \frac{\sigma_x}{2} + R = 126.35ksf$$

$$\sigma_{min} = \frac{\sigma_x}{2} - R = -33.35ksf = -231.6psi = -3.28\sqrt{f'_c} \quad (f'_c \text{ in psi})$$

The Mohr's Circle representation of stress at this location is then:

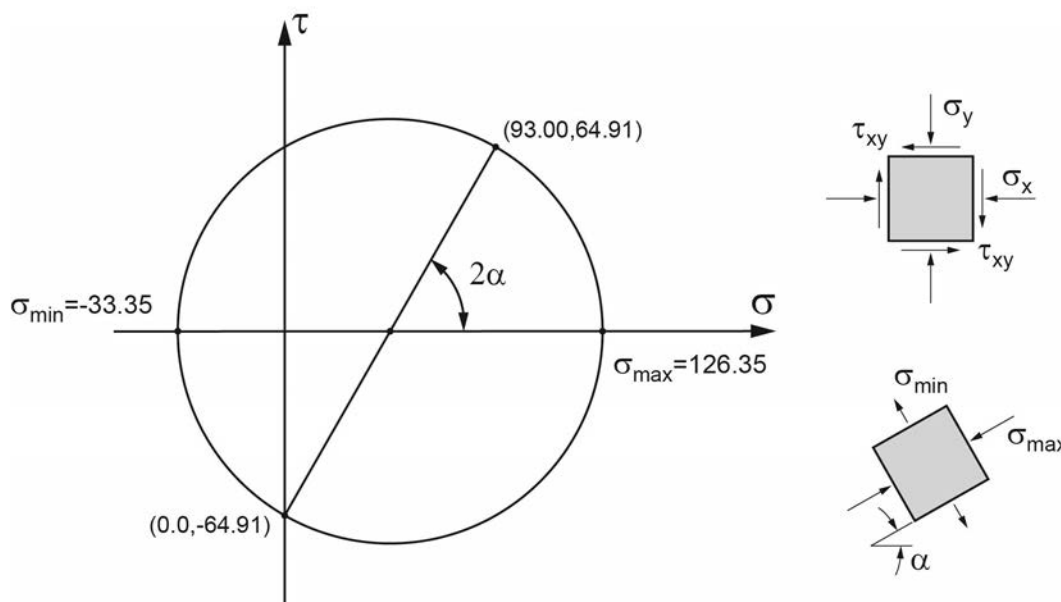


Figure 5.28 – Mohr Circle for Location of Maximum Shear in Middle Span

The maximum principal tension of -44 ksf is greater than what would be allowable for a segmental box girder, but does reflect a level of stress that can be adequately reinforced during final design.

5.9 Optimizing the Post-Tensioning Layout

Section 5.6 of this chapter showed the determination of the required post-tensioning forces at three sections in the example three-span bridge. The three final forces computed were:

- 4743 kips at 0.4167L of Spans 1 and 3.
- 8256 kips at mid-span of Span 2.
- 7169 kips over Piers 2 and 3.

The large disparity in the required post-tensioning force in the end spans versus the middle span indicates that some optimization of the post-tensioning layout is warranted. Decreasing the maximum positive eccentricity in Spans 1 and 3 will increase the post-tensioning demand

those spans. In Span 2, however, the effect of reducing the maximum positive eccentricity in Spans 1 and 3 will reduce the secondary moments, and the post-tensioning demand in that span.

Figure 5.29 shows a revised center of gravity post-tensioning layout for the end spans of the example bridge. The tendons have been raised to 2 feet from the bottom of the bottom slab. The resulting maximum positive eccentricity is 1.738'. The maximum eccentricity at the interior piers is unchanged.

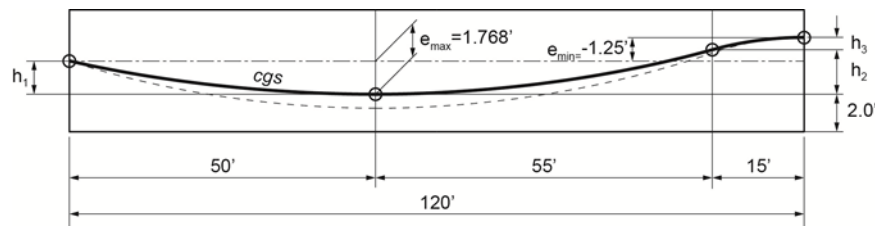


Figure 5.29 – Revised Center of Gravity Profile of Prestressing (End Spans)

Revised conjugate beam loads are determined from the revised profiles. Figure 5.30 shows the updated conjugate beams and loads in the end spans for a unit prestressing force ($F=1$). The conjugate beam loads for the middle span are unchanged.

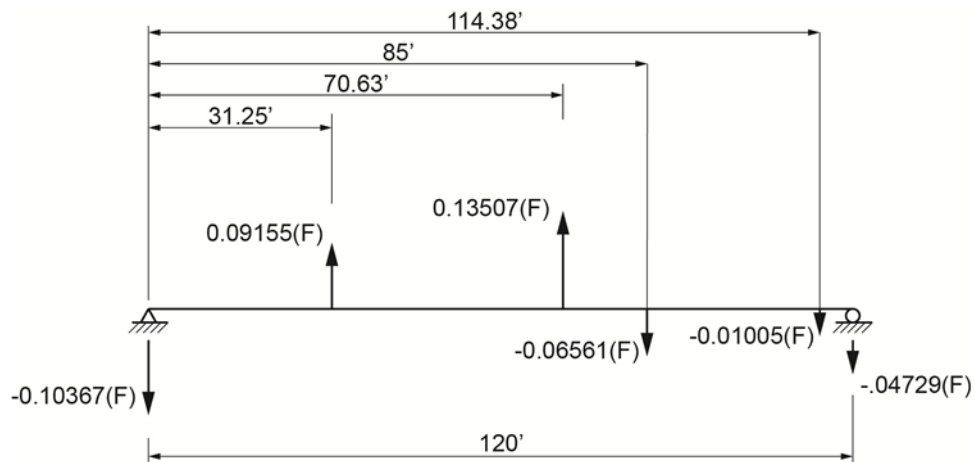


Figure 5.30 – Revised Conjugate Beam and Loads (End Spans)

The updated secondary prestress moments are shown in Figure 5.31.

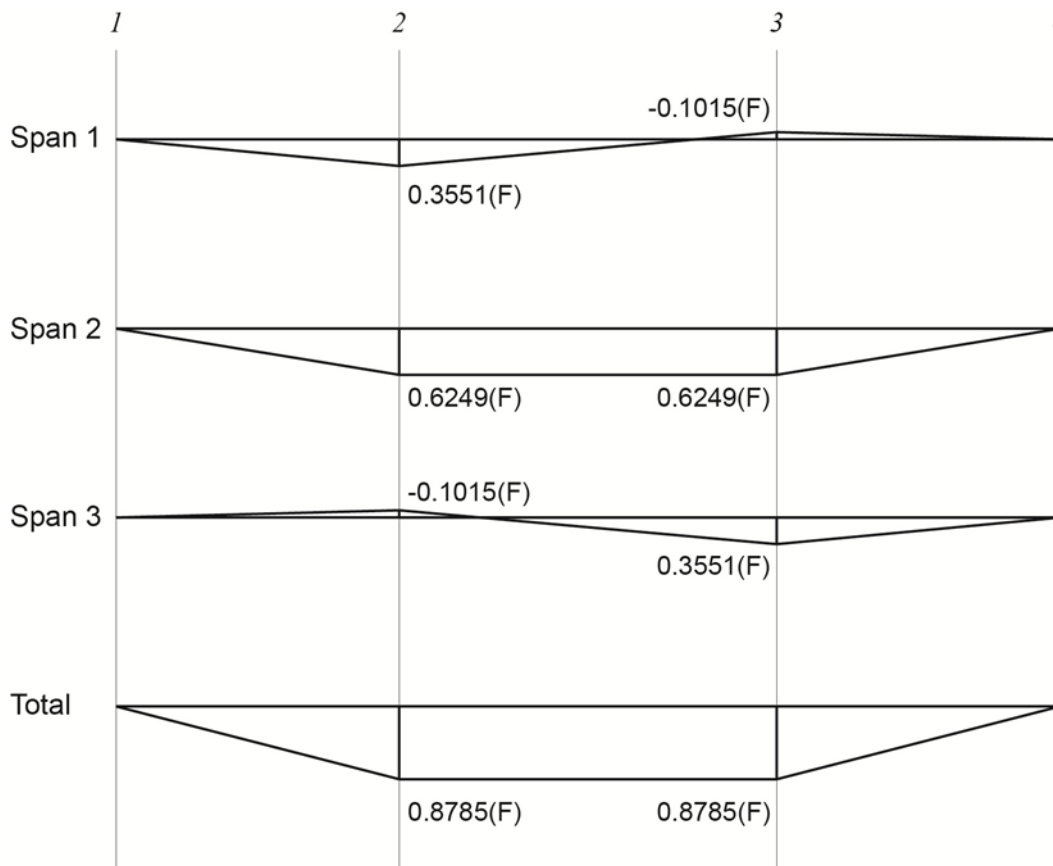


Figure 5.31 –Revised Secondary Prestressing Moments, $M_2(F)$

The minimum prestressing force requirements at the three sections studied, after all losses, are then:

$$F = \frac{28,637 + (-10,451)}{0.6288(2.732) + 2.5 - 0.316} = 5,633 \text{ kips} \quad (0.3596L \text{ Span 1})$$

$$F = \frac{36,037 + (-10,451)}{0.6288(2.732) + 2.5 - 0.8785} = 7,662 \text{ kips} \quad (0.5L \text{ Span 2})$$

$$F = \frac{-48,426 - (-14,415)}{-1.25 - 0.6288(3.768) - 0.8785} = 7,501 \text{ kips} \quad (\text{At Piers 2 and 3})$$

These force requirements are compared to those shown at the top of page 29 of 41. Raising the eccentricity in the side spans decreases the overall post-tensioning demand by 510 kips, or approximately 6 percent.

Chapter 6—Substructure Considerations

6.1 Introduction

Chapter 5 presented an approach to the preliminary design of cast-in-place post-tensioned box girder bridges. The approach was demonstrated by considering a three-span box girder bridge. To focus on superstructure concepts, the three-span example bridge was supported by bearings at the piers and abutments. Often, however, the supporting columns are cast integrally with the box girder superstructure. When this is the case, the analysis and design of the bridge should include the flexural stiffness of the supporting substructure.

This chapter presents bending moments for the same three-span example bridge of chapter 5, with the exception that the piers are integral with the superstructure. Figure 6.1 shows an elevation view of the example bridge. Figure 6.2 shows a cross section of the bridge supported at each pier with two 6' diameter columns. For this example, each column is supported by a 7' diameter drilled shaft, with an equivalent length to fixity of 10'. The flexibility analysis for this structure is provided in appendix A, beginning on page 25 of 33.

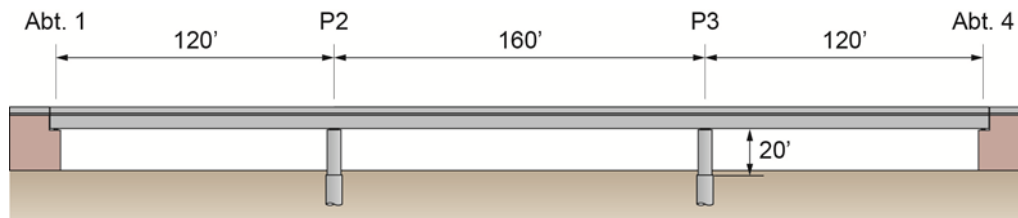


Figure 6.1 –Example CIP Box Girder Bridge Elevation

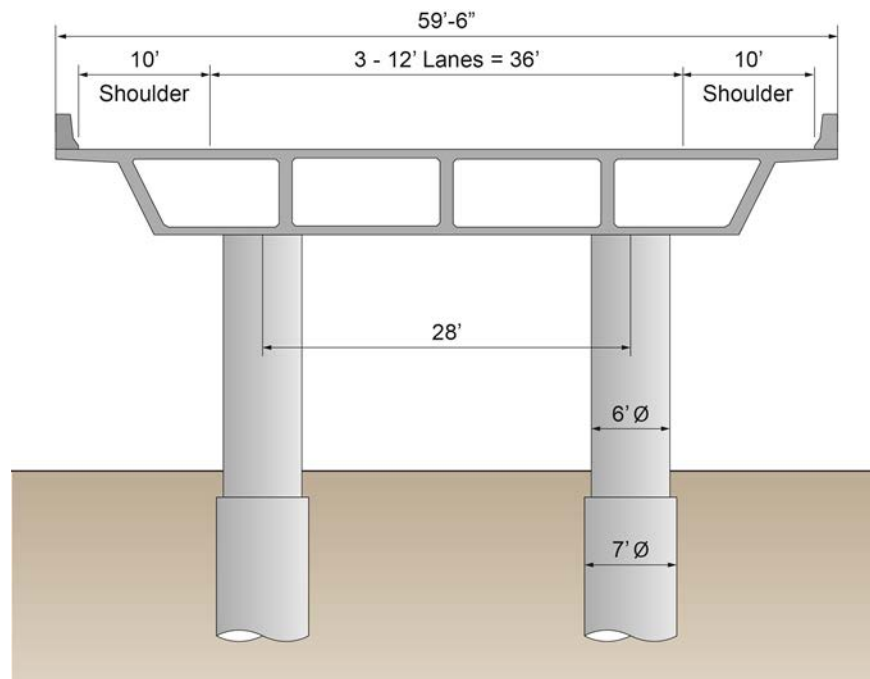


Figure 6.2 –Bridge Cross Section at Piers

6.2 Bending Moments Caused by Unit Effects

6.2.1 Effect of a Unit Uniform Load

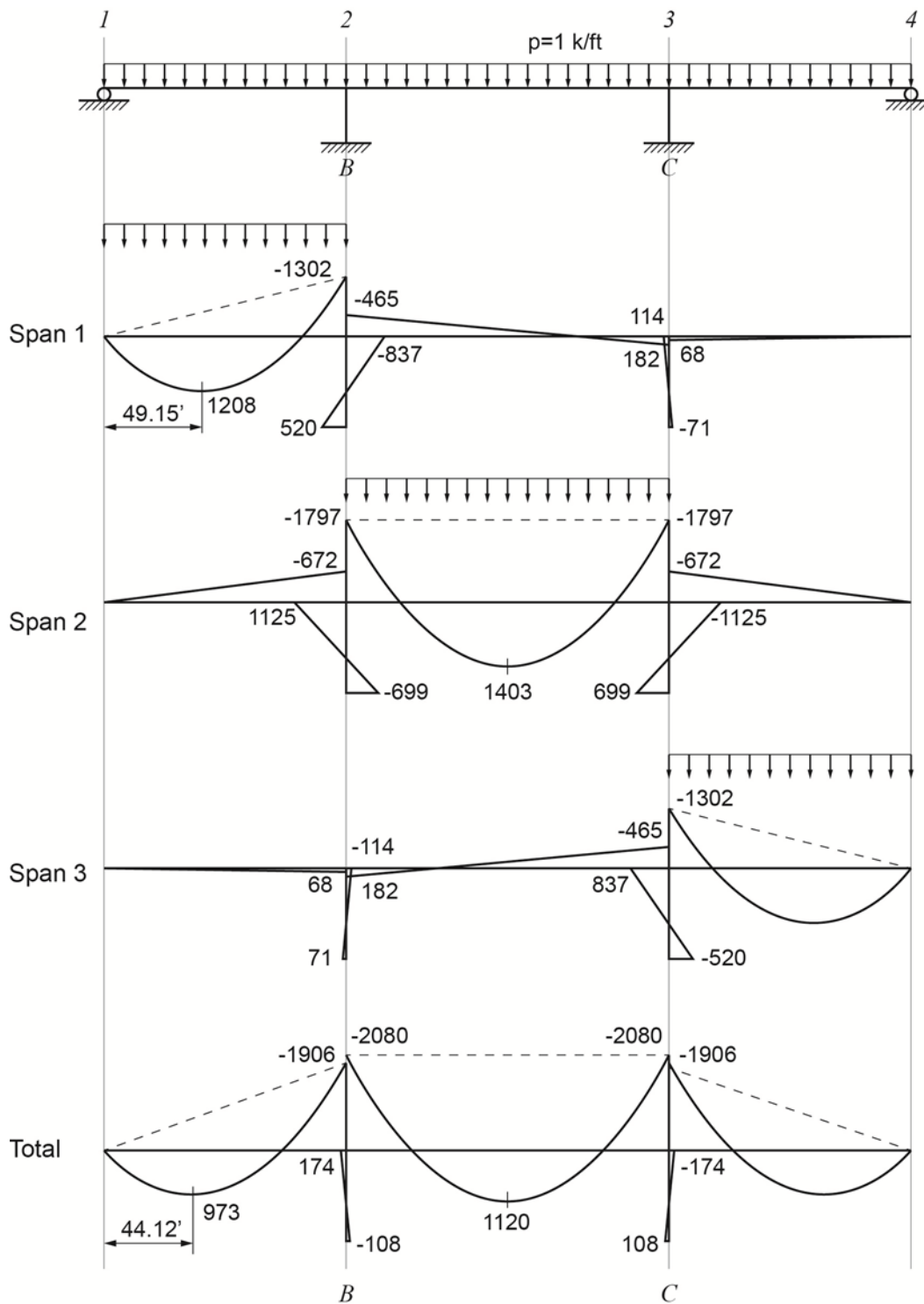


Figure 6.3 – Effect of a Unit Uniform Load

6.2.2 Effect of a Unit Lateral Displacement (Side-Sway Correction)

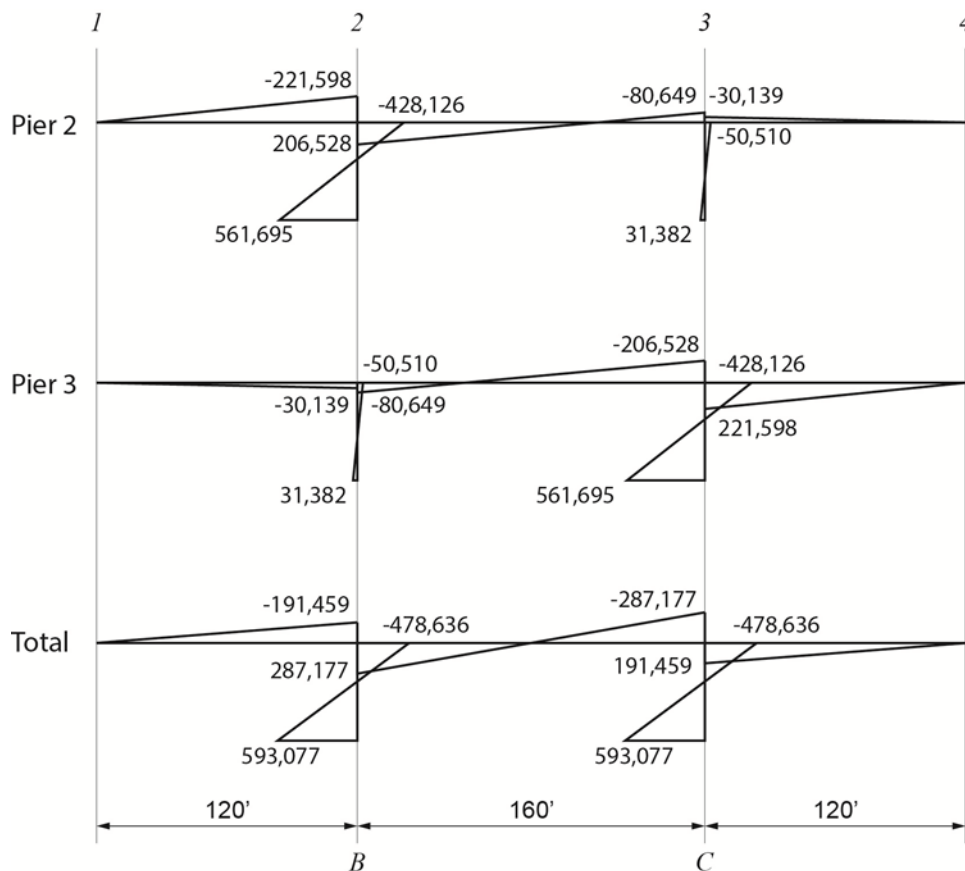


Figure 6.4 – Effect of a Unit Lateral Displacement (Side-sway Correction)

6.2.3 Effect of a Unit Contraction

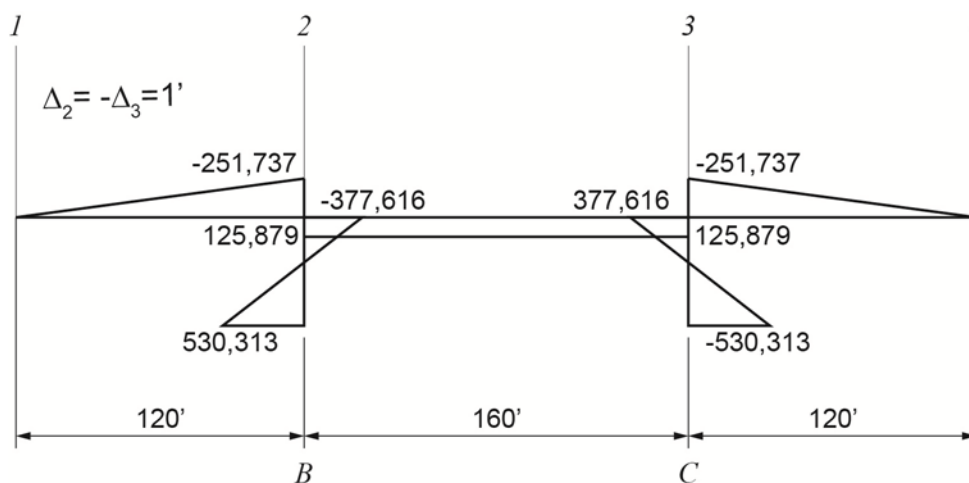


Figure 6.5 – Effect of a Unit Contraction

6.3 Dead Load—DC (Self Weight and Barrier Railing)

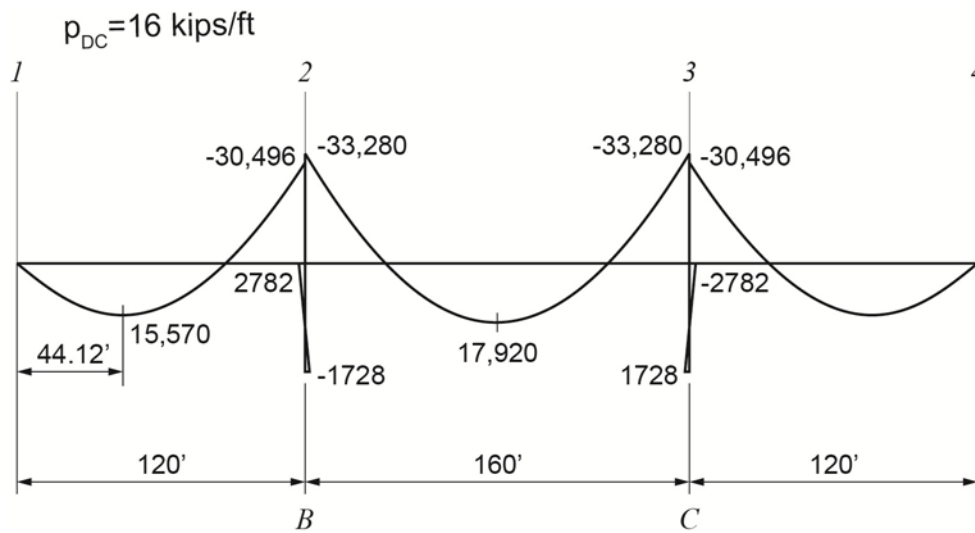


Figure 6.6 – Effect of Dead Load (DC)

6.4 Dead Load—DW (Future Wearing Surface)

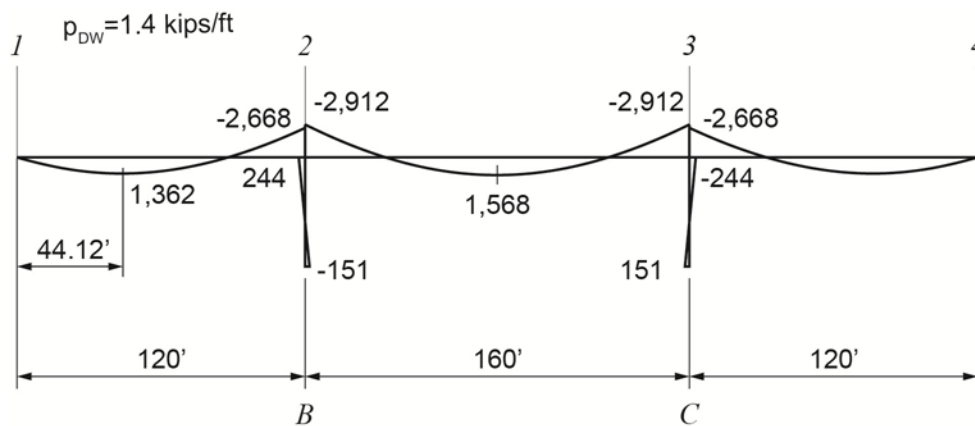


Figure 6.7 – Effect of Dead Load (DW)

6.5 Live Load—LL (Lane and Truck Components)

6.5.1 Envelope of Uniform Load Component

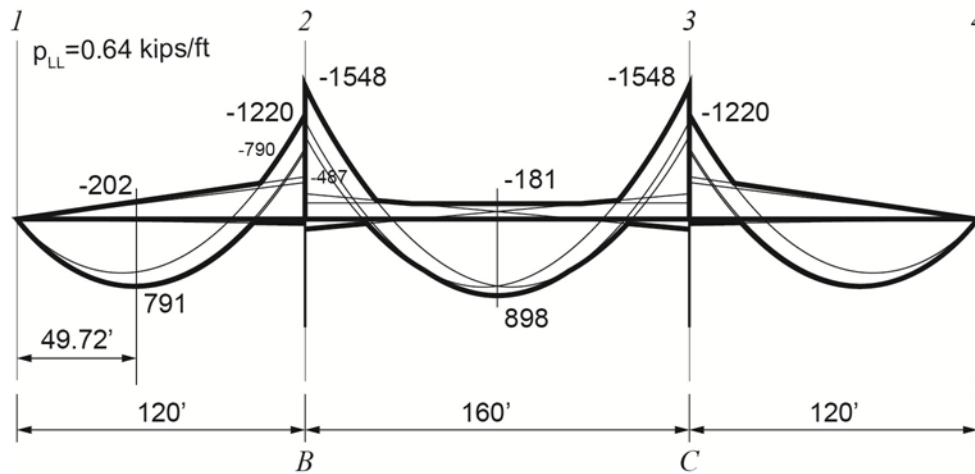


Figure 6.8 – Uniform Live Load Moment Envelope

6.5.2 Truck—Positive Moment in Span 1 or 3

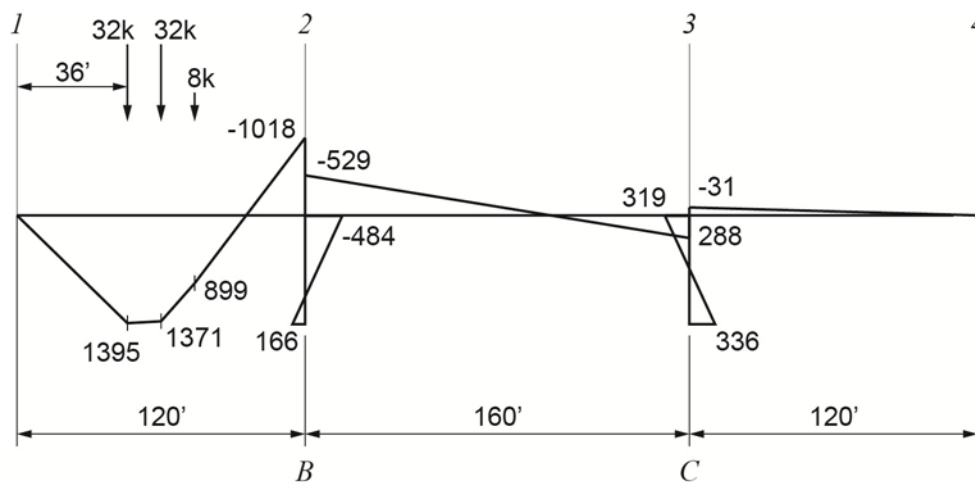


Figure 6.9 – Moment Diagram for HS20 Truck in Span 1 or 3

6.5.3 Truck—Positive Moment in Span 2

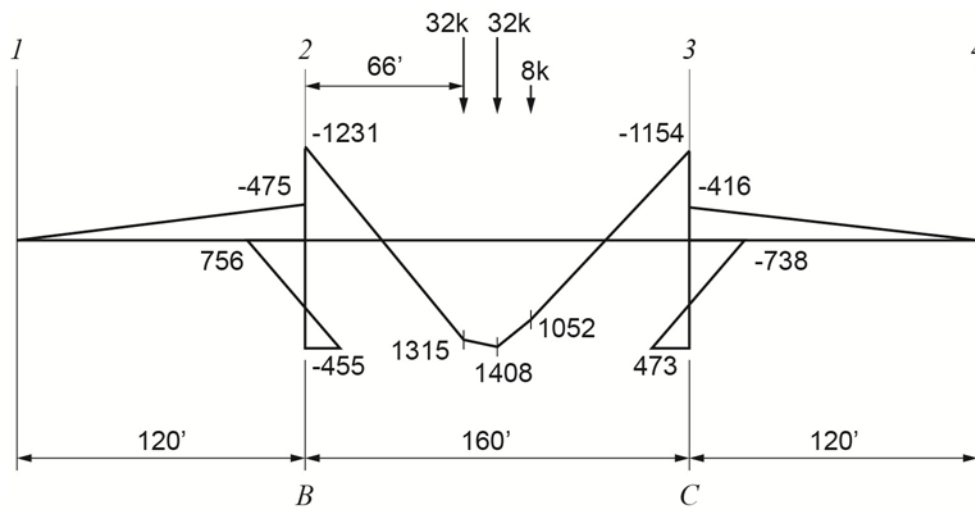


Figure 6.10 – Moment Diagram for HS20 Truck in Span 2

6.5.4 Truck—Negative Moment over Piers

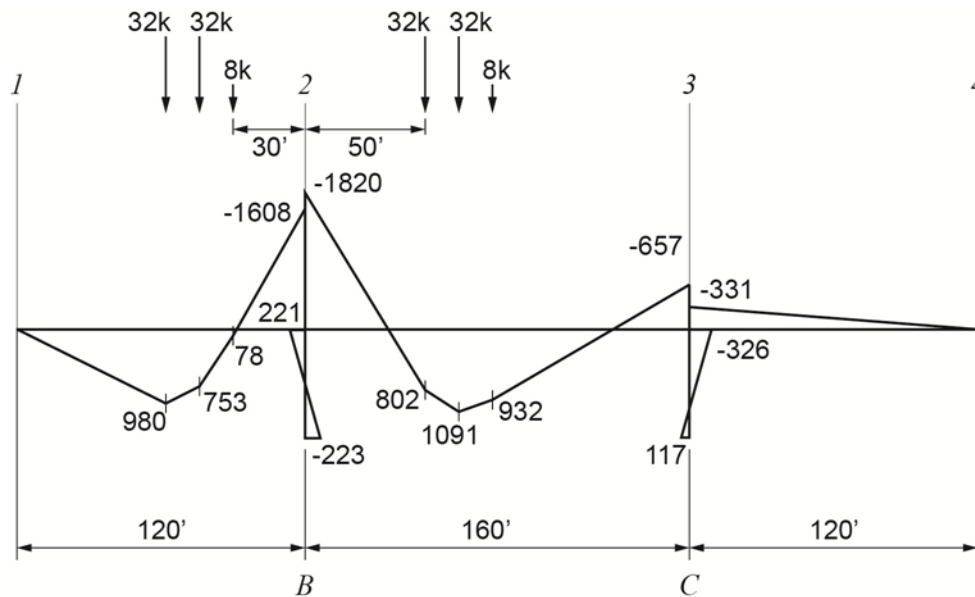


Figure 6.11 – Moment Diagram for Two HS20 Trucks about Pier 2

6.6 Post-Tensioning Secondary Moments—Unit Prestressing Force

Secondary moments from post-tensioning for the framed structure will be different from those of a similar bridge supported by bearings. The shortening of the superstructure under the prestressing induces bending moments in the columns which are distributed throughout the framed structure. The Flexibility Method solution for the frame considers a single rotational

degree of freedom at each member end. As a result, the effect of the axial shortening needs to be added to the flexural results to find the total secondary moments.

The top diagram in figure 6.12 shows the secondary moments considering the rotational restraint provided by the columns. The second diagram shows the secondary moments resulting from a unit force shortening the bridge. These moments are found by multiplying the results for the unit contraction (figure 6.5) times the shortening of the span between the columns under the action of a unit force, which is predicted as:

$$\Delta = \frac{PL}{AE} = \frac{(1)(80)}{(99.45)(617300)} = 1.3031 \times 10^{-6}$$

The modulus of elasticity is taken from equation 2.5 for a 28-day strength of 5 ksi and a unit weight of 150 lb/ft³.

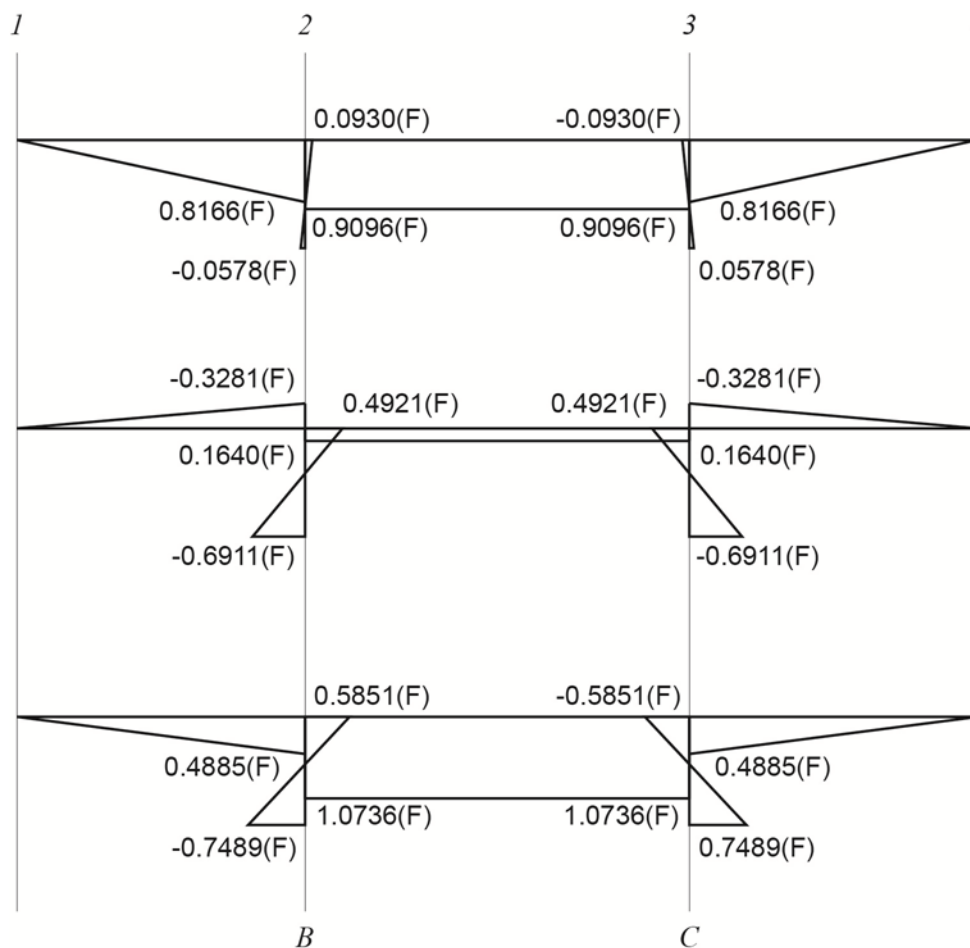


Figure 6.12 – Secondary Prestressing Moments, M2(F)

The component of the secondary moment resulting from axial shortening is slightly overestimated in this case as it does not consider the shear forces attracted by the columns. This approximation is not the case in a stiffness or flexibility solutions that consider rotational and displacement degrees of freedom simultaneously. The approximation could be refined by an iterative approach where the column top lateral displacement under the shear force is made

equal to the shortening of the span under the unit force, less the column shear force. For this example, the refinement reduces the secondary moments from axial shortening by about 4 percent.

6.7 Thermal Gradient (TG)—20°F Linear

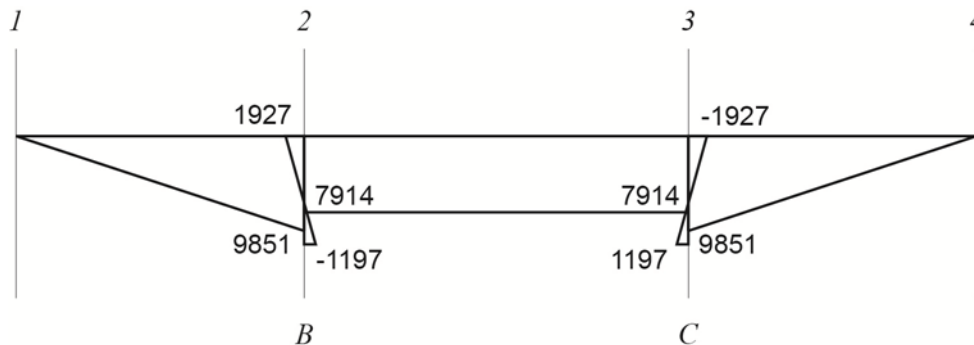


Figure 6.13 – Moment Diagram for a 20°F Positive Linear Gradient

6.8 Moments Resulting from Temperature Rise and Fall

6.8.1 Temperature Rise—40°F Uniform Rise

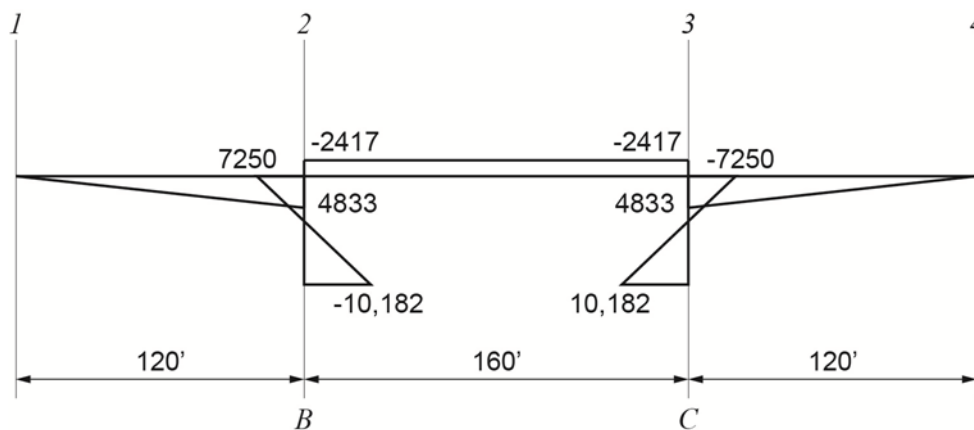


Figure 6.14 – Moment Diagram for 40° Temperature Rise

6.8.2 Temperature Fall—40°F Uniform Fall

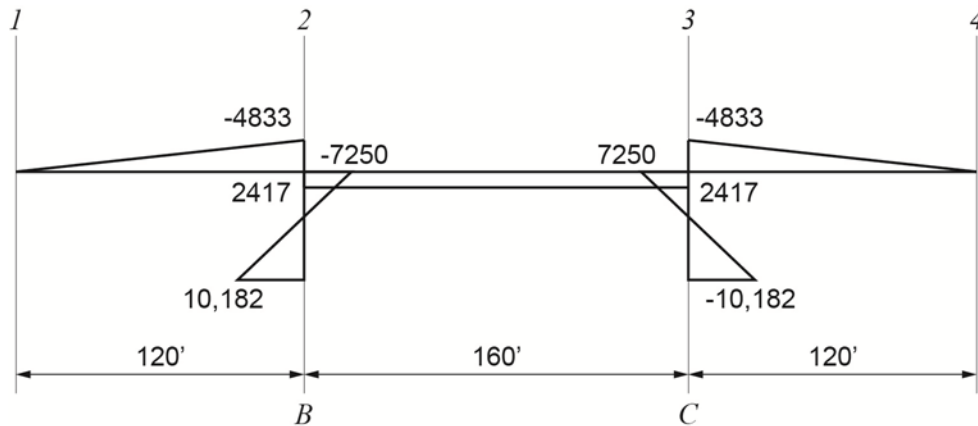


Figure 6.15 – Moment Diagram for 40° Temperature Fall

6.9 Moments Resulting from Concrete Shrinkage

Bending moments are produced in the rigid frame as the superstructure concrete shrinks and displaces the tops of the columns toward the center of stiffness of the structure. These bending moments can be estimated by factoring the load case for unit contraction (figure 6.5) by the pier top displacements. For the example structure, by inspection of its symmetry, the center of stiffness is located at the center of the middle span.

The shrinkage strain can be computed using the CEB-FIP Model Code presented in chapter 2. The total shrinkage strain at time t is calculated by:

$$\epsilon_{cs}(t, t_s) = \epsilon_{cso} \beta_s (t - t_s)$$

With,

$$\epsilon_{cso} = \epsilon_s(f_{cm}) \beta_{RH}$$

And,

$$\epsilon_s(f_{cm}) = [160 + 10\beta_{sc}(9 - f_{cm} / f_{cmo})] \times 10^{-6}$$

The values for the beta terms are computed first:

$$\beta_{sc} = 5$$

$$\beta_{sRH} = 1 - \left(\frac{RH}{RH_o} \right)^3 = 1 - \left(\frac{75}{100} \right)^3 = 0.5781$$

$$\beta_{RH} = -1.55\beta_{sRH} = -1.55(0.5781) = -0.8961$$

$$\beta_s(t-t_s) = \left[\frac{(t-t_s)/t_1}{350(h/h_o)^2 + (t-t_s)/t_1} \right]^{0.5}$$

Assuming day 10,000 to be the day when the concrete shrinkage is assumed to end, and considering the outside perimeter and half of the inside perimeter in computing the notional thickness (perimeter = 189.83’):

$$\beta_s(10000-1) = \left[\frac{(10000-1)/1}{350(319.36/100)^2 + (10000-1)/1} \right]^{0.5} = 0.8585$$

Substituting these values into the equations for concrete strain:

$$\epsilon_s(f_{cm}) = [160 + 10(5)(9 - 42.47/10)] \times 10^{-6} = 0.0003977$$

$$\epsilon_{cso} = \epsilon_s(f_{cm})\beta_{RH} = 0.0003977(-0.8961) = -0.0003564$$

$$\epsilon_{cs}(t, t_s) = \epsilon_{cso}\beta_s(t-t_s) = -0.0003564(0.8585) = -0.0003060$$

The resulting pier top deflection is:

$$\Delta = 0.0003060(80') = 0.02448'$$

The resulting bending moment diagram is:

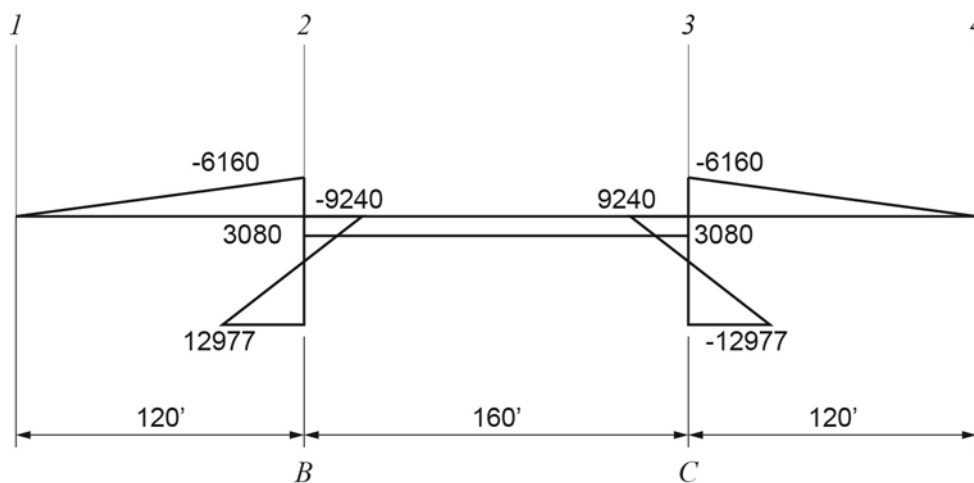


Figure 6.16 – Moment Diagram for Concrete Shrinkage

The bending moment diagram in figure 6.16 assumes that the same concrete mix is used for the superstructure and the substructure. Also, these results assume that the concrete of the

superstructure and substructure is poured at the same time (has the same age). Variations in these, or other, assumptions will impact the resulting bending moments. For example, the bending moments will increase if the columns are poured in advance of the superstructure, given that they are made of the same concrete. Oppositely, the bending moments will decrease if a lower strength of concrete is used in the columns, reducing their stiffnesses.

6.10 Moments Resulting from Concrete Creep

Cast-in-place post-tensioned concrete bridges will creep under the action of the permanently applied loads (typically self weight and post-tensioning). The bending moments determined in the elastic structure are compatible with member end rotations. These member end rotations will grow as a function of concrete creep, but no redistribution of bending moments will occur, as no new end restraints are applied, and the stiffness of the members, though changing with time, are relatively the same. Rotations and deflections will increase, but no change in bending moments.

Likewise, no creep moments will develop as a result of the continued top of pier displacement as a result of concrete creep. Lateral deflections will increase with no increase or decrease of bending moments. There will be a lessening of the prestressing force as the span shortens which will be opposite in direction to the moments produced during the axial shortening of the bridge during stressing.

Creep moments related to member end rotations will develop to reduce deformations induced by concrete shrinkage. These moments can be estimated as a percentage of the moments due to shrinkage, that percentage being a function of concrete creep characteristics.

A creep coefficient can be computed using the CEB-FIP Model Code presented in chapter 2. The relationship of creep strain to elastic strain is given by:

$$\varepsilon_{cc}(t, t_0) = \frac{\sigma_c(t_0)}{E_{ci}} \phi(t, t_0)$$

Where,

$$\phi(t, t_0) = \phi_0 \beta_c(t - t_0)$$

The notional creep coefficient is:

$$\phi_0 = \phi_{RH} \beta(f_{cm}) \beta(t_0)$$

With,

$$\phi_{RH} = 1 + \frac{1 - RH / RH_o}{0.46(h / h_o)^{1/3}} = 1 + \frac{1 - 75 / 100}{0.46(319.36 / 100)^{1/3}} = 1.3691$$

And,

$$\beta(t_0) = \frac{1}{0.1 + (t_0 / t_1)^{0.2}} = \frac{1}{0.1 + (28 / 1)^{0.2}} = 0.4884$$

And,

$$\beta(f_{cm}) = \frac{5.3}{(f_{cm}/f_{cmo})^{0.5}} = \frac{5.3}{(42.47/10)^{0.5}} = 2.5718$$

$$\phi_0 = \phi_{RH} \beta(f_{cm}) \beta(t_0) = 1.3691(2.5718)(0.4884) = 1.7197$$

The development of creep over time is given by:

$$\beta_H = 150 \left\{ 1 + \left(1.2 \frac{RH}{RH_o} \right) \right\} \frac{h}{h_o} + 250 \leq 1500$$

With,

$$\beta_H = 150 \left\{ 1 + \left(1.2 \frac{RH}{RH_o} \right) \right\} \frac{h}{h_o} + 250 = 150 \left\{ 1 + \left(1.2 \frac{75}{100} \right)^{18} \right\} \frac{319.36}{100} + 250 = 801$$

And,

$$\beta_c(t-t_0) = \left[\frac{(t-t_0)/t_1}{\beta_H + (t-t_0)/t_1} \right]^{0.3}$$

And,

$$\beta_c(t-t_0) = \left[\frac{(t-t_0)/t_1}{\beta_H + (t-t_0)/t_1} \right]^{0.3} = \left[\frac{(10000-1)/1}{801 + (10000-1)/1} \right]^{0.3} = 0.9771$$

Solving for the creep coefficient:

$$\varphi(t, t_0) = \phi_0 \beta_c(t-t_0) = 1.7197(0.9771) = 1.6804$$

The creep moment acts to reduce the moments induced by shrinkage. Consider the total strain under a sustained load.

$$\varepsilon_{total} = \varepsilon_{elastic} + \varepsilon_{cc} = \frac{\sigma_c(t_0)}{E_{ci}} + \frac{\sigma_c(t_0)}{E_{ci}} \varphi(t, t_0)$$

This expression can be rearranged to:

$$\varepsilon_{total} = \frac{\sigma_c}{E_{ci}} (1 + \varphi) = \frac{\sigma_c}{E'_{ci}}$$

Where E'_{ci} is an effective modulus of elasticity equal to the 28-day modulus adjusted by the creep coefficient,

$$E'_{ci} = \frac{E_{ci}}{(1 + \phi)}$$

Expressed in terms of bending moment, the total moment of shrinkage and the creep related to shrinkage is:

$$M_{total} = M_{sh} + M_{cr} = \frac{M_{sh}}{(1 + \phi)}$$

Solving for the creep moment:

$$M_{cr} = -M_{sh} \left(1 - \frac{1}{(1 + \phi)} \right)$$

For the example problem considered, the creep moment is estimated by the linear scaling of the shrinkage bending moment diagram.

$$M_{cr} = -0.6269M_{sh}$$

The bending moments resulting from creep of the concrete related to shrinkage are shown in figure 6.17.

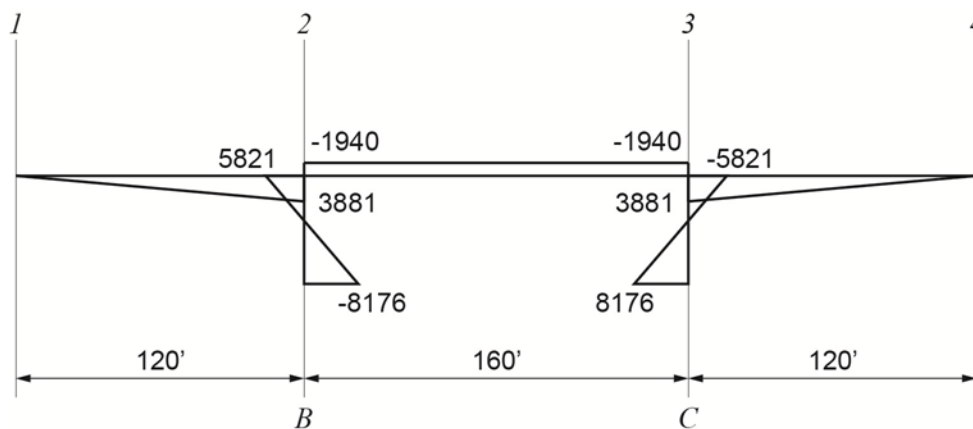


Figure 6.17 – Moment Diagram for Concrete Creep

Additional creep bending moments, in addition to those related to concrete shrinkage, can be generated in cast-in-place post-tensioned bridges even though the static scheme remains unchanged. These creep moments occur when relative creep characteristics of superstructure and substructure concrete are different, whether by being of different mix designs or of different casting dates. For example, if the substructure of the example bridge were made of the same concrete, but cast at a date earlier than the superstructure, the older substructure would resist the creep of the younger superstructure concrete. The moments to be considered in calculating this creep moment would be the summation of permanent loads (DC and PT). The moments would be estimated by scaling the sum of the permanent loads by a relative ratio of remaining creep coefficients of the two concretes.

6.11 Bending Moments Summaries

This Section presents bending moment diagrams for the two example bridges, one on bearings and one with integral piers. The moments were determined by Flexibility Analysis. The analysis for the bridge on bearings is found in chapter 5, section 5.4.2. The analysis for the bridge with integral piers is found in section A.13 of appendix A.

The “maximum” moments in the side spans are found at the location of maximum load under self weight. The location of the truck component of the live loads is the same within the spans of both the bridge on bearings and the bridge with integral piers. Though both a slightly larger truck component and therefore overall live load moment may be found, the values in figure 6.18 were chosen for the comparative exercise in this Chapter. (See section 5.5.4.5 for the number of design lanes.)

Load	Span 1 (“max”)		CL Span 2		CL Pier	
	Brg	Fixed	Brg	Fixed	Brg	Fixed
kL	0.3596L ₁	0.3677L ₁	0.5L ₂	0.5L ₂	0.0L ₂	0.0L ₂
DC	14896	15570	18800	17920	-32352	-33280
DW	1303	1362	1649	1568	-2831	-2912
LL _u	923	781	1138	898	-1448	-1548
LL _t	1475	1381	1657	1408	-1769	-1820
N _L	4.544	4.544	4.229	4.229	4.372	4.372
0.8(LL+I)	10487	9516	11306	9374	-11964	-12493
0.5GR	1539	1811	4279	3957	-1284	-1187
M ₂	0.3159F	0.1796F	0.8785F	1.0736F	0.8785F	1.0736F
T _r	0	1777	0	-2417	0	-2417
T _f	0	-1777	0	2417	0	2417
SH	0	-2265	0	3080	0	3080
CR	0	1427	0	-1940	0	-1940

Table 6.1 – Bending Moments for Bridge on Bearings and Bridge with Fixed Piers

6.12 Post-Tensioning Force Comparison (after all losses, with thermal effects)

6.12.1 Side Span Positive Bending

For the bridge on bearings:

$$F = \frac{28,225 + (-10,451)}{0.6288(2.732) + 1.768 - 0.316} = 5,607 \text{ kips}$$

For the bridge with integral piers:

$$F = \frac{29198 + (-10,451)}{0.6288(2.732) + 1.768 - 0.316} = 5,914 \text{ kips}$$

6.12.2 Middle Span Positive Bending

For the bridge on bearings:

$$F = \frac{36,034 + (-10,451)}{0.6288(2.732) + 2.5 - 0.8785} = 7,661 \text{ kips}$$

For the bridge with integral piers:

$$F = \frac{36,376 + (-10,451)}{0.6288(2.732) + 2.5 - 0.8785} = 7,763 \text{ kips}$$

6.12.3 Negative Bending at Piers

For the bridge on bearings:

$$F = \frac{-48,431 - (-14,415)}{-1.25 - 0.6288(3.768) - 0.8785} = 7,563 \text{ kips}$$

For the bridge with integral piers:

$$F = \frac{-51,149 - (-14,415)}{-1.25 - 0.6288(3.768) - 0.8785} = 8,167 \text{ kips}$$

Chapter 7—Longitudinal Analysis & Design

7.1 Introduction

The longitudinal analysis and design of post-tensioned concrete box girder bridge superstructures in accordance with AASHTO LRFD specifications culminates in the verification of superstructure cross sections at service and strength limit states. The loads for which the cross sections are verified under the various limit states are those determined by linear elastic analysis methods factored to achieve a desired reliability in design. Included in these elastic analyses is the appropriate consideration for the time-dependent characteristics of the superstructure concrete and post-tensioning.

Computerized solutions for post-tensioned structures are available from a number of software developers. These computer programs are typically based on either two or three-dimensional finite element methods using beam/column elements in the elastic range. Built around the finite element solutions are material characteristics that, through a series of time updates, allow the incorporation of effects such as concrete creep, concrete shrinkage, and relaxation of the post-tensioning. Most of these computer programs also allow for the input of post-tensioning tendons by geometric definition. The geometric definitions are transformed internally within the software into loads applied to the bridge model. Complete packages can include automatic generation of AASHTO LRFD live loads and limit state combinations to expedite cross section verifications.

Not having specialized software does not leave the engineer without the means to analyze and design post-tensioned concrete bridges. Hand calculations like those presented in this Manual, or those using general frame analysis software are adequate analysis tools for many bridges. More rigor is required in developing these analyses, but often they disclose valuable insights into the behavior of the bridge. The effects of post-tensioning are determined by applying equivalent loads to the stiffness based solution. The results are the total prestressing effects, from which primary effects are subtracted to find the secondary effects. Alternatively, flexibility solutions can produce secondary effects directly, which are then added to the primary effects to determine the total prestressing effects. Time-dependent effects of the concrete and prestressing steel are estimated by code equation and then applied in the form of forces or displacements to determine their effect on the bridge. This can be done conservatively by applying ultimate values at one time, or applying them incrementally to better estimate the diminishing of these effects as time progresses.

This manual utilizes both computer programs specifically developed to facilitate post-tensioned concrete bridge design along with supplementary hand calculations to verify limit states. The computer programs used are Bridge Designer 2 (BD2) and Bridge Designer 3 (BD3) by Interactive Design Systems. BD2, a two-dimensional analysis package, was used in the preparation of design example 1 provided in appendix C of this manual. Design example 2, provided in appendix D, uses BD3, a three-dimensional solution. The general-purpose finite element analysis program LARSA was used in design example 2 for the development of live load effects on the two-cell curved structure.

7.2 Modeling Concepts

Stiffness based finite element analyses model complex force-displacement behavior of a structure by dividing it into an assemblage of smaller members interconnected at nodes. Nodal locations are chosen so that a finite number of independent degrees of freedom will, with desired accuracy, capture the displacement characteristics of the structure. Relative

displacements of member connected nodes are established by idealized force-displacement, or “stiffness”, characteristics of the smaller finite members. The needed sophistication of stiffness characteristics for members in a finite element analysis is related to sophistication of force-displacement results needed for subsequent member design. Two-dimensional and three-dimensional beam-column elements represented by classic stiffness characteristics are elements with appropriate sophistication for the design of most cast-in-place box girder bridges.

7.2.1 Straight Bridges Supported on Bearings

The longitudinal design of straight concrete box girder superstructures can be made using two-dimensional analyses supplemented with hand calculations to estimate force effects out of the plane of the analysis. Figure 7.1 shows the elevation of a bridge similar to the one presented in design example 1 in appendix C. The bridge shown in figure 7.1 is different from the design example in that the superstructure is not integral with the piers, but rests on bearings. The cross section of this bridge, shown in figure 7.2, is the same as for design example 1.

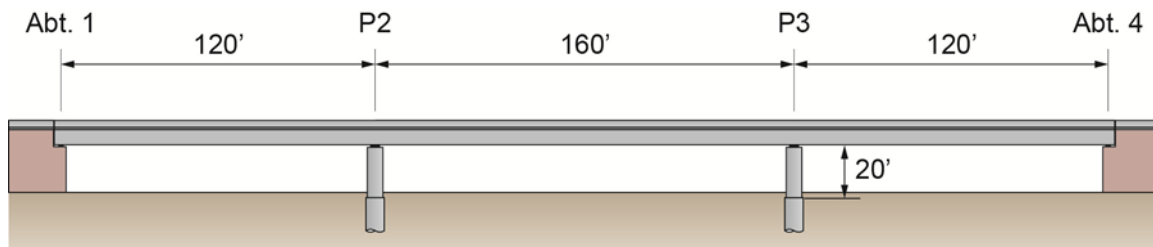


Figure 7.1 – Example Straight Bridge on Bearings

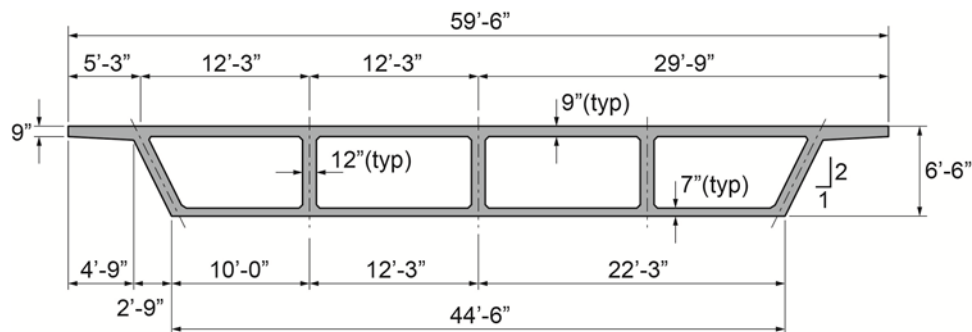


Figure 7.2 – Box Girder Superstructure Cross Section

7.2.1.1 Nodes

Figure 7.3 shows one layout for a two-dimensional model representation of the three-span bridge in figure 7.1. Nodes are defined by coordinates in an orthogonal coordinate system, such as x-coordinates in the longitudinal direction and y-coordinates in the vertical direction.

Longitudinally, nodes were first located at support locations and at even increments along the length of the bridge. The number of nodes defined along each span is the decision of the analyst, but should be sufficient to allow the analysis software member definitions to accurately model bridge behavior. A typical nodal spacing of 10' was used for the bridge model shown in figure 7.3. Additional nodes (3, 15, 17, 22, 35, and 47) were added for ease in using the results of the analysis. These nodes coincide with the design cross section for shear (d or $h/2$ from the centerline of pier, depending on the approach in finding nominal capacity). Two other nodes (1

and 49) were added behind the first and last bearing locations to facilitate the modeling of post-tensioning consistent with end anchor details

Nodes shown in figure 7.3 are defined vertically at the center of gravity of the superstructure cross section. The vertical location of the nodal coordinates changes with variations in cross section such as when a bottom slab is thickened near a pier to control compressive stresses, or in a variable depth structure used in longer spans. The vertical locations of the nodes are not adjusted for the profile of the bridge, except in the most extreme conditions. There are other bridge types, such as cable-stayed bridges, where horizontal forces are sufficiently large as to impose significant deck bending because of profile changes.

The analysis model is simply supported at all bearing locations in the vertical direction. A horizontal support is provided at Node 2 to assure model stability. Interior piers and bearing stiffnesses could be added to this model if the of long-term effects of concrete creep and shrinkage and prestressing steel relaxation are desired in the piers. Their effect is typically small on the results for the design of the superstructure (see chapter 6). If the bearings are flexible, such as for laminated elastomeric bearings, the horizontal stiffness can be input as a constraint between pier top and the superstructure. Rotational stiffnesses of these bearings should not be accounted for in the model. The very large rotational stiffnesses of these bearings rely on large vertical loads to remain active without uplift. The result is an inappropriately large attraction of bending moment to the pier if modelled, approaching that of integral piers. A rotationally free connection is more appropriate.

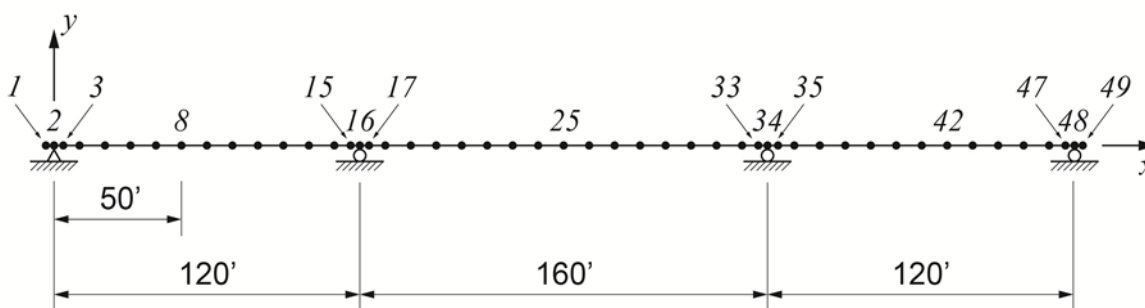


Figure 7.3 – Two-Dimensional Analysis Model

7.2.1.2 Elements

Nodes in the two-dimensional analysis model of the straight bridge are connected by idealized beam-column elements defined by appropriate stiffness matrices. Figure 7.4 shows a typical stiffness matrix for a beam element connecting nodes that have three degrees of displacement freedom (vertical, horizontal, and rotational).

Figure 7.4 shows that the information necessary to define the behavior of the beam-column element connecting two nodes includes:

- **Cross-Sectional Characteristics**—Area and Moment of Inertia about the horizontal axis passing through the centroid of the cross section. Typically the gross cross section characteristics of the concrete girder are considered. There may be instances where the cross-sectional area of the ducts is great enough to impact analysis results. When this happens, the net cross section should be used for superstructure construction and tendon stressing, and the gross properties used for loads applied after the tendons are grouted.

- Modulus of Elasticity—For the purposes of the verification of Service and Strength Limit States, cast-in-place post-tensioned bridges are analyzed with fully elastic behavior (LRFD C4.5.1). Within these elastic analyses, however, the time-dependent behaviors of concrete and prestressing steel must be incorporated (LRFD 4.5.2.2). Time-dependent behavior is most typically captured in commercially available software by a series of time updates, where changes in concrete dimension are estimated over a time step. Typically, the modulus of elasticity is based on the 28-day strength of the concrete (see chapter 2).

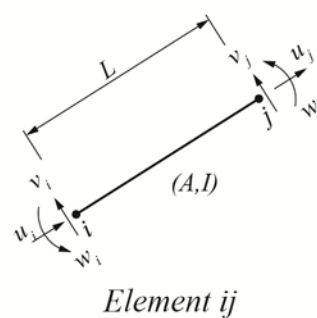
$$[k]_{ij} = \begin{bmatrix} \frac{AE}{L} & 0 & 0 & -\frac{AE}{L} & 0 & 0 \\ 0 & \frac{12EI}{L^3} & \frac{6EI}{L^2} & 0 & -\frac{12EI}{L^3} & \frac{6EI}{L^2} \\ 0 & \frac{6EI}{L^2} & \frac{4EI}{L^2} & 0 & \frac{6EI}{L^2} & \frac{2EI}{L} \\ \hline -\frac{AE}{L} & 0 & 0 & \frac{AE}{L} & 0 & 0 \\ 0 & -\frac{12EI}{L^3} & -\frac{6EI}{L^2} & 0 & \frac{12EI}{L^3} & -\frac{6EI}{L^2} \\ 0 & \frac{6EI}{L^2} & \frac{2EI}{L} & 0 & -\frac{6EI}{L^2} & \frac{4EI}{L^2} \end{bmatrix}$$


Figure 7.4 –Typical Element Stiffness Matrix for a Plane Frame Member with 3DOF Nodes

For the cross section shown in figure 7.2, the cross section characteristics are:

$$I = 643.7 \text{ ft}^4$$

$$A = 99.45 \text{ ft}^2$$

$$c_1 = 2.732 \text{ ft}$$

$$c_2 = 3.768 \text{ ft}$$

$$\rho = 0.6288$$

$$Q_0 = 118.1 \text{ ft}^3$$

Figure 7.5 –Cross Section Properties for the Box Girder shown in Figure 7.2

End and pier diaphragms are used at the supports to transmit shear forces from the webs to the supports and to stiffen the box girder with regard to torsion. End and pier diaphragms are typically solid sections of the bridge with small openings to allow for access between the spans after construction. It is important to incorporate the weight of these diaphragms into the design of the bridge. However, members containing small length diaphragms (up to approximately the depth of the box girder superstructure) should not be represented with cross section properties including the diaphragms. The typical cross section properties should be used for these members. Longer diaphragms could warrant a change in cross section characteristics.

7.2.1.3 Post-Tensioning

The effects of the post-tensioning tendons are modeled within the software as an equivalent set of forces acting on the elements of the bridge. Most post-tensioned bridge analysis software packages use a graphical interface so that the tendons can be defined by their desired geometry. Internal to the program, the geometry is used to compute fixed end element forces which then become the post-tensioning load case within the program. When loaded with the equivalent loads, the results are the combination of primary and secondary post-tensioning moments. The secondary moments are then determined by subtracting the primary moment, from the input tendon geometry, from the total post-tensioning moments.

The effect of time-dependent deformations of the concrete and steel are incorporated through time-steps where the long-term deformations are used to change the post-tensioning forces along the length of the tendons. Iterative solutions are often used to have the assumed and final time-dependent deformations converge over each time step.

General purpose software analysis packages without the capability to define post-tensioning tendons geometrically, or to track and update forces with time, can be used for the final design of cast-in-place bridge superstructures. An equivalent force approach could be taken with code predicted changes in the post-tensioning forces in order to capture appropriately long-term behavior. Design Aids 11.1.4 and 11.1.5 in chapter 11 of the Precast/Prestressed Concrete Institute Design Handbook, 7th Edition, are good resources for determining equivalent prestressing loads.

7.2.2 Straight Bridges with Integral Piers

The superstructure of the straight bridge modeled in section 7.2.1 is the same superstructure used in design example 1 in appendix C without integral piers. The cross section of the bridge used in design example 1 with integral piers is shown in figure 7.6. The integral pier shown consists of twin circular pier columns, each supported by a single drilled shaft foundation.

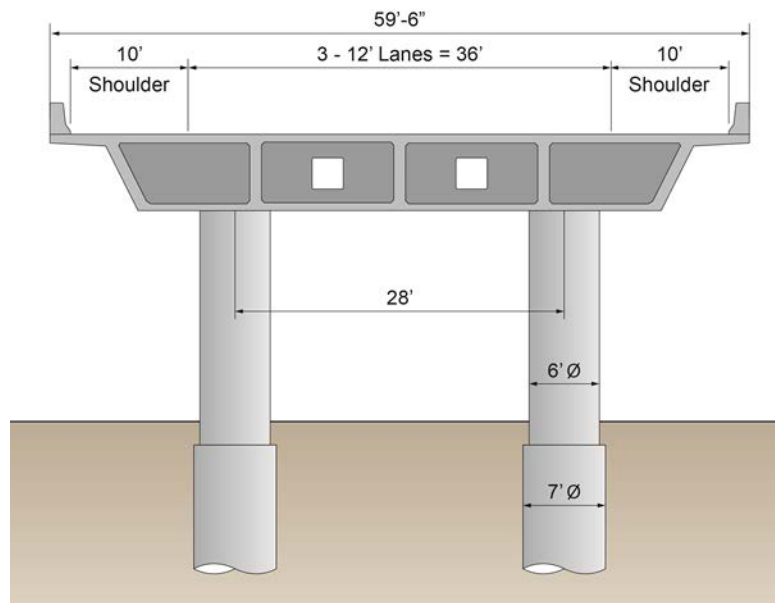


Figure 7.6 – Cross Section of Design Example 1 Bridge at the Piers

Figure 7.7 shows the model for the bridge with integral piers. The layout of nodes and members in the superstructure are the same as those for the straight bridge on bearings (section 7.2.1).

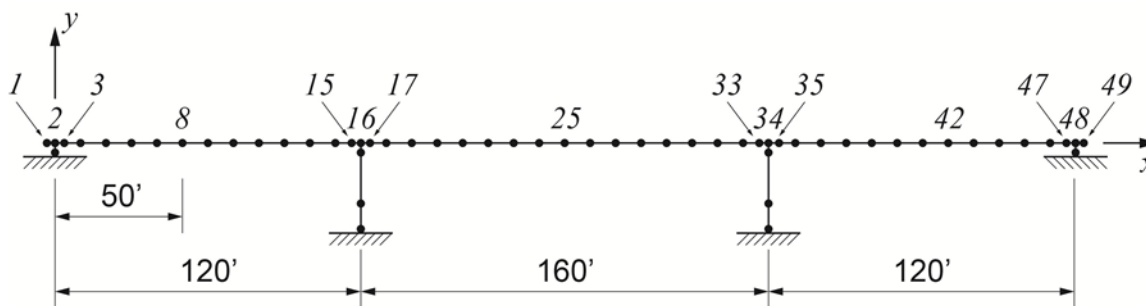


Figure 7.7 – Two-Dimensional Analysis Model with Integral Piers

Details of the modeling of the pier and foundation elements are shown in figure 7.8:

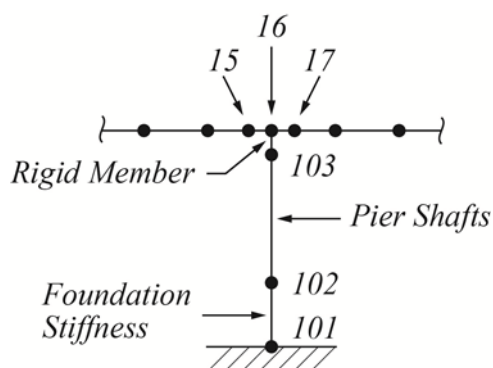


Figure 7.8 – Detail of Model at Pier

The model shown in figure 7.7 differs from that of figure 7.3 in three ways:

Pier Elements—The piers are modeled as the combination of the pier shaft properties participating in the longitudinal flexure of the bridge superstructure. In this example, the piers are modeled with twice the area and twice the inertial of two 6'-diameter pier columns.

Foundation Stiffnesses—In this example problem, the drilled shaft foundations are represented by two 7'-diameter concrete drilled shafts in the same way the piers were modeled. An equivalent member length to a point of fixity determined by soil-pile interaction was used to locate Node 101 relative to Node 102. Depending on the computer program used, the foundation could also be modeled with a user defined stiffness matrix determined by a study of soil-pile interaction.

Rigid Members—Members from the superstructure center of gravity to the top of the pier have been added. This element, modeled as rigid, facilitates the direct output of force and moment results at the tops of the piers. The rigid extensions at the end bents are added for dimensional consistency with the pier modeling.

7.2.3 Curved Bridges

LRFD Article 4.6.1.2.3 provides guidelines for including horizontal bridge curvature in the analysis and design of concrete girder bridges. Three categories of consideration, related to the ratio of span length to horizontal curve radius expressed in terms of span length central angle, are presented in the LRFD. The parameters for the evaluation are shown in figure 7.9

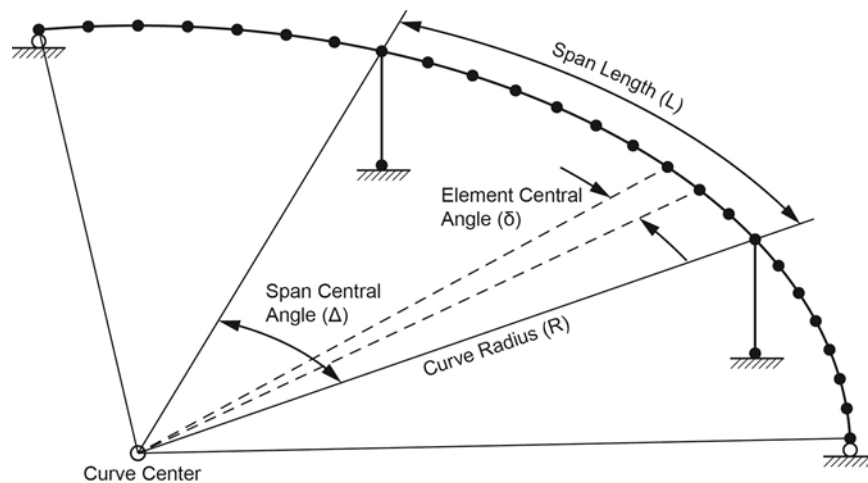


Figure 7.9 – Curved Bridge of Design Example 2

The three categories for consideration of horizontal curvature in LRFD are:

- Central Angle ≤ 12 degrees—A bridge whose largest span length has a central angle not greater than 12 degrees ($L/R \leq 0.2$) may be designed as straight. No consideration for bridge curvature is necessary for the longitudinal design of the concrete box girder superstructure.
- 12 degrees $<$ Central Angle ≤ 34 degrees—A bridge whose largest span has a central angle greater than 12 degrees ($L/R \leq 0.2$) and not greater than 34 degrees ($L/R \leq 0.6$) must include the horizontal curvature of the bridge in analysis and design. The analysis may be comprised of idealized beam-column elements defined between nodes at the center of gravity of the cross sections as it follows the horizontal curve. The girder elements may themselves be straight between nodes and should include stiffness characteristics that relate forces and displacements in 6 degrees of freedom (three translational and three rotational). The maximum length of the straight girder elements between nodes shall be such that the central angle between adjacent nodes shall not exceed 3.5 degrees ($L_{nodes}/R \leq 0.06$). The assemblage of these elements is sometimes referred to as a spine beam.
- Central Angle > 34 degrees—A bridge whose largest span has a central angle greater than 34 degrees ($L/R \leq 0.6$) shall be analyzed by a proven three-dimensional analysis method such as: grillages, folded plates, finite strips, or shell element finite elements.

The bridge presented in design example 2 in appendix D is a three span bridge with the same span lengths as the bridge presented in design example 1 in appendix C. Different from design example 1, however, is that the design example 2 bridge lies on a horizontal alignment with a radius of 600' over the full length of the bridge. Figure 7.10 shows the bridge of design example 2. The span lengths of the bridge are 120', 160', and 120'. The central angles of the spans are

11.5 degrees, 15.3 degrees, and 11.5 degrees. The central angle of the middle span is such that a curved girder analysis comprised of straight beam elements is appropriate. The model used in design example 2 is shown in figure 7.11.



Figure 7.10 – Design Example 2 Bridge

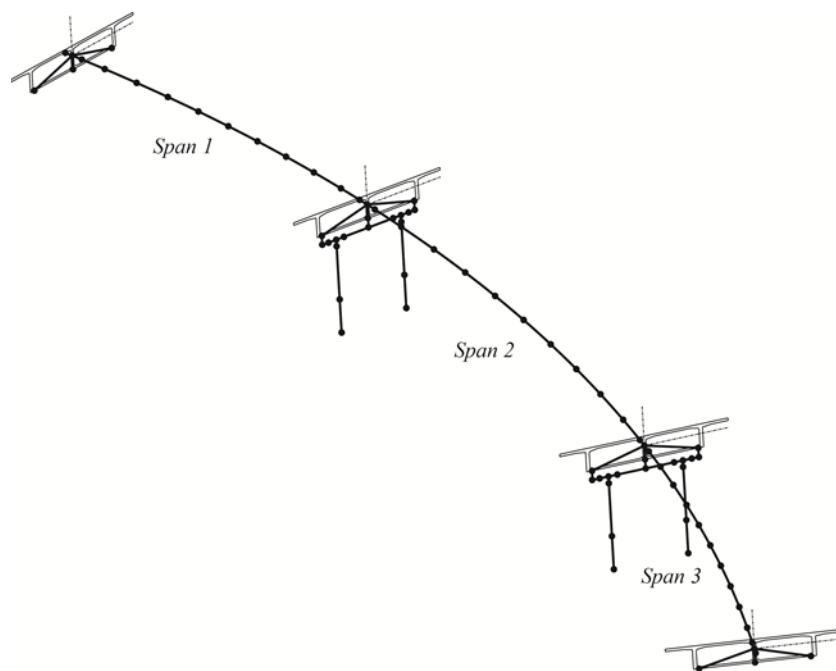


Figure 7.11 – 3D Model for Bridge in Design Example 2

The bridge of design example 2 is also different from that of design example 1 in that it is supported by three bearings at the piers and abutments. Figure 7.12 shows a cross section of the bridge at the pier. Figure 7.13 shows the layout of nodes and members at the piers. Rigid elements are used to replicate the rigidity that the superstructure diaphragms add at the pier. Other rigid members are used to account for the thickness of the substructure members and output convenience.

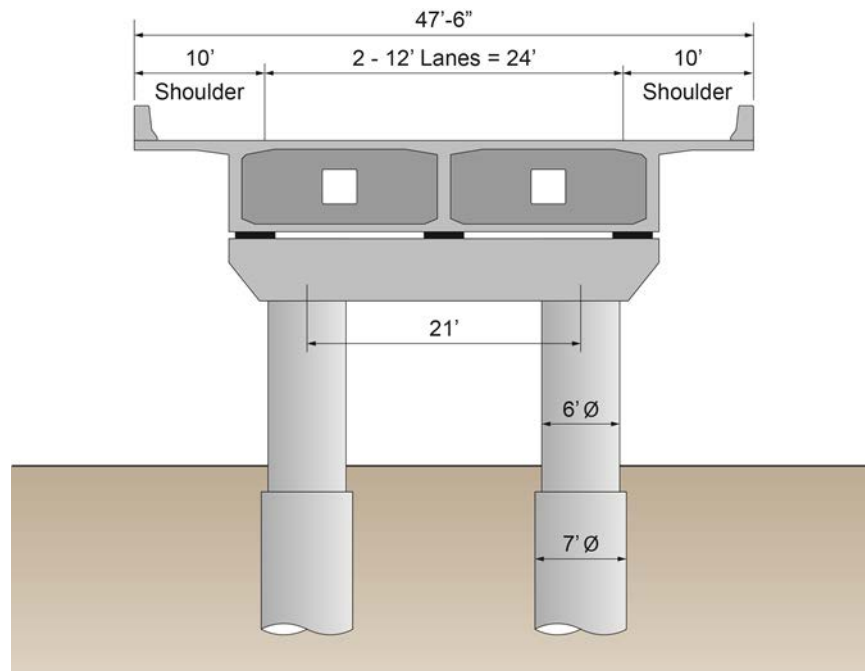


Figure 7.12 – Cross Section of Design Example 2 Bridge at the Piers

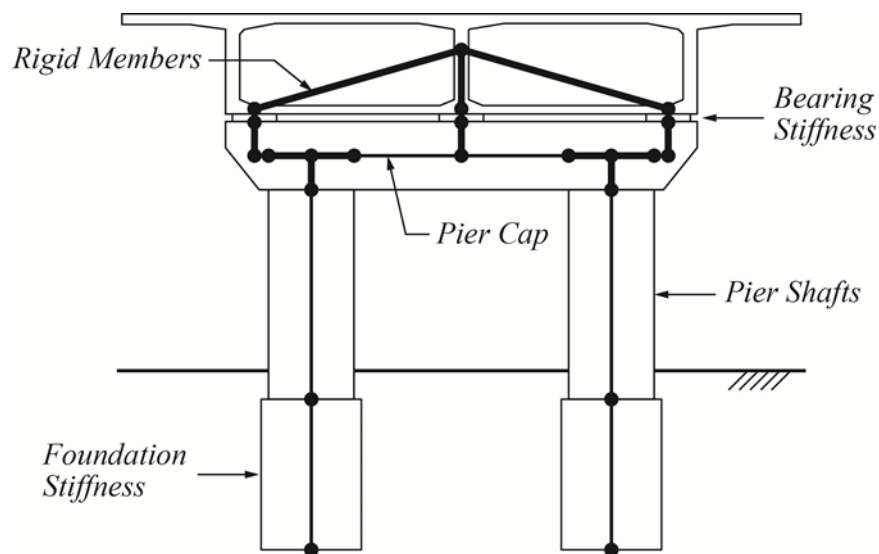


Figure 7.13 – 3D Model for Bridge in Design Example 2 at the Piers

Computerized stiffness solutions of three-dimensional spine girders that incorporate bridge curvature represent the members with element stiffness matrices similar to those of two-dimensional analyses. Two additional cross section characteristics are required to define these members: the moment of inertia about the element vertical axis (for transverse flexure), and the torsional constant, J , that is used to model the element torsional stiffness.

Torsional moments applied to closed cross sections such as concrete box girder bridges are, in the first order, resisted by a flow of shear around the perimeter of the closed section. Figure 7.14 shows a single cell box girder subjected to a torsional moment M_t . The shear flow around the box girder is defined by the variable “q”, with units force per length.

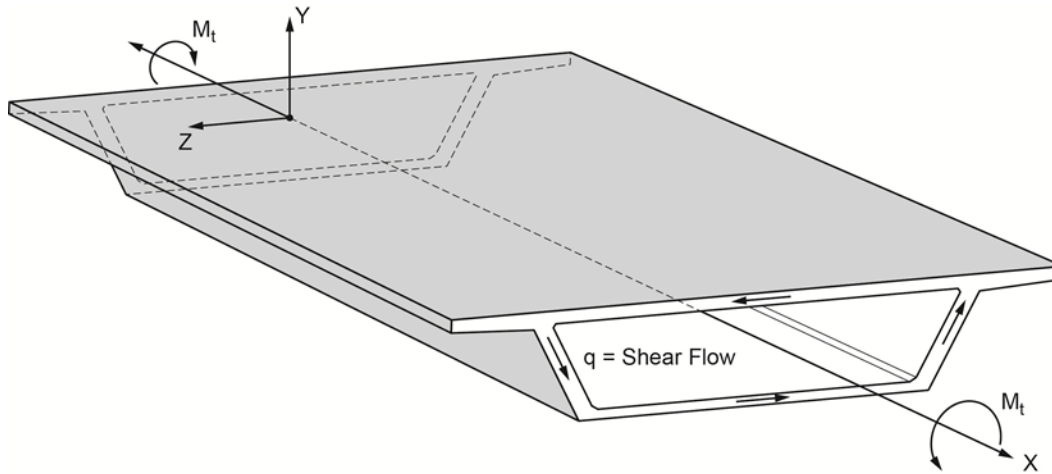


Figure 7.14 –Torsion in a Single Cell Box Girder

Appendix B to this manual presents a detailed development of the torsional behavior of closed, hollow cross sections. From that development, the shear flow is found to be constant around the closed section and related to the torsional moment by:

(Eqn. 7.1)
$$q = \frac{M_t}{2A_o}$$

Where A_o is the area enclosed within a perimeter defined by the median lines of the closed section elements (webs, top slab, and bottom slab). The corresponding shear stress in the members of the closed section is found by dividing the shear flow by the member thickness:

(Eqn. 7.2)
$$\tau = \frac{M_t}{2A_o t(s)}$$

The torsional constant for the single cell closed hollow section is:

(Eqn. 7.3)
$$J = \frac{4A_o^2}{\oint \frac{ds}{t(s)}}$$

The denominator in equation 7.3 is the integral of length along the median perimeter divided by the thickness of the members comprising the closed hollow section. For box girder cross sections where the members are distinct and linear, equation 7.3 can be written as:

(Eqn. 7.4)

$$J = \frac{4A_o^2}{\sum_{i=1}^n \frac{s_i}{t_i}}$$

Where, the closed loop integral is replaced with a discrete summation.

For cross section comprised of multiple closed hollow cells, torsional moments are resisted by shear flow around all of the cells. Figure 7.15 shows the equilibrium of external torsional moment and internal shear flow in a two-cell box girder superstructure.

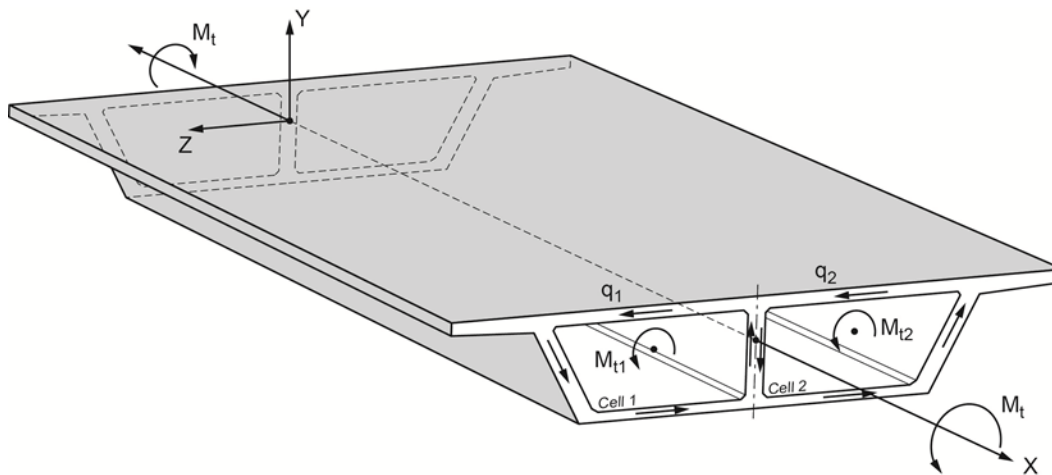


Figure 7.15 –Torsion in a Two-Cell Box Girder

The torsional moment is in equilibrium with the sum of the shear flows multiplied by their enclosed medial area:

(Eqn. 7.5)

$$M_t = 2 \sum_{i=1}^n A_{oi} q_i$$

Evaluation of the shear flow in each cell must include the effects of the shear flow in adjacent cells, as influenced by members that are shared in common. Equations B.44 in appendix B shows the relationship between cross section rotation of a single box girder cell and shear flow:

(Eqn. 7.6)

$$\theta = \frac{q}{2GA_o} \oint \frac{ds}{t(s)}$$

Including the effects of shear flow in common members, equation 7.6 can be expressed for each cell of the box girder as:

(Eqn. 7.7)

$$\theta_1 = \frac{1}{2GA_{o1}} \left(q_1 \oint \frac{ds}{t(s)} - q_2 \int_{12} \frac{ds}{t(s)} \right)$$

(Eqn 7.8)

$$\theta_2 = \frac{1}{2GA_{o2}} \left(q_2 \oint \frac{ds}{t(s)} - q_1 \int_{21} \frac{ds}{t(s)} \right)$$

Compatibility of deformations requires that the rotations of the individual cells are equal to each other and are equal to the rotation of the cross section, so that:

$$(Eqn. 7.9) \quad \theta_1 = \theta_2 = \theta$$

Equations 7.7 and 7.8 can be written as a system of simultaneous equations which include the equality of equation 7.9:

$$(Eqn. 7.10) \quad \delta_1(q_1) + \delta_{12}(q_2) = 2GA_{o1}\theta$$

$$(Eqn. 7.11) \quad \delta_{21}(q_1) + \delta_2(q_2) = 2GA_{o2}\theta$$

Where the shape constants (δ) of the expression are:

$$(Eqns. 7.12) \quad \delta_1 = \oint_1 \frac{ds}{t(s)} \quad \delta_2 = \oint_2 \frac{ds}{t(s)} \quad \delta_{12} = \delta_{21} = -\int_{12} \frac{ds}{t(s)}$$

Solution for the shear flows in equations 7.10 and 7.11 can be made in terms of the cross section rotation. The relationship between applied torsional moment and cross section rotation is developed in appendix B as:

$$(Eqn. 7.13) \quad M_t = GJ\theta$$

Equilibrium between applied torsional moment and shear flow in the cells (equation 7.5) can be expressed for the two-cell box girder as:

$$(Eqn. 7.14) \quad M_t = 2A_{o1}q_1 + 2A_{o2}q_2$$

Equating equations 7.13 and equation 7.14 leads to the calculation of the torsional constant for the cross section.

Example: Consider the cross section of design example 1 in appendix C. The dimensions of the cross section, enclosed cell areas for torsion, and idealized thin wall member thickness and lengths are shown in figure 7.16.

The system of simultaneous equations that needs to be solved for the four-cell box girder is:

$$\delta_1(q_1) + \delta_{12}(q_2) + \delta_{13}(q_3) + \delta_{14}(q_4) = 2GA_{o1}\theta$$

$$\delta_{21}(q_1) + \delta_2(q_2) + \delta_{23}(q_3) + \delta_{24}(q_4) = 2GA_{o2}\theta$$

$$\delta_{31}(q_1) + \delta_{32}(q_2) + \delta_3(q_3) + \delta_{34}(q_4) = 2GA_{o3}\theta$$

$$\delta_{41}(q_1) + \delta_{42}(q_2) + \delta_{43}(q_3) + \delta_4(q_4) = 2GA_{o4}\theta$$

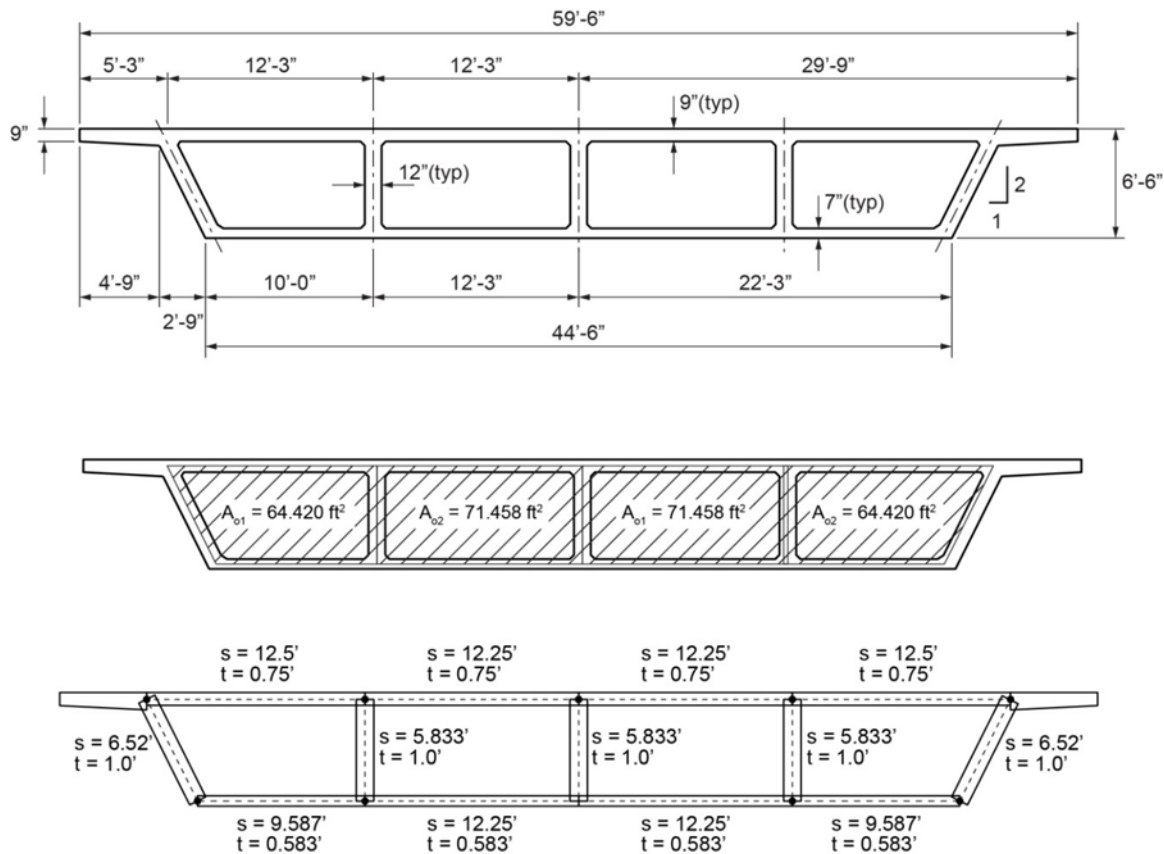


Figure 7.16 – Cross Section of Bridge in Example 1, Appendix C

These equations are modified to discount the influence of cells that are not adjoining:

$$\delta_1(q_1) + \delta_{12}(q_2) + 0 + 0 = 2GA_{o1}\theta$$

$$\delta_{21}(q_1) + \delta_2(q_2) + \delta_{23}(q_3) + 0 = 2GA_{o2}\theta$$

$$0 + \delta_{32}(q_2) + \delta_3(q_3) + \delta_{34}(q_4) = 2GA_{o3}\theta$$

$$0 + 0 + \delta_{43}(q_3) + \delta_4(q_4) = 2GA_{o4}\theta$$

Using the cross section geometry, and noting symmetry, the shape constants are:

$$\delta_1 = \delta_4 = 45.46$$

$$\delta_2 = \delta_3 = 49.00$$

$$\delta_{12} = \delta_{21} = \delta_{23} = \delta_{32} = \delta_{34} = \delta_{43} = -5.833$$

$$q_1 = q_4 \quad q_2 = q_3$$

Again noting the symmetry of the section, the system of four simultaneous equations can be reduced to two equations:

$$\delta_1(q_1) + \delta_{12}(q_2) = 2GA_{o1}\theta$$

$$\delta_{21}(q_1) + \delta_2(q_2) + \delta_{23}(q_2) = 2GA_{o2}\theta$$

Or,

$$45.46(q_1) - 5.833(q_2) = 128.84G\theta$$

$$-5.833(q_1) + 49.00(q_2) - 5.833(q_2) = 142.92G\theta$$

From which,

$$q_1 = 0.8823q_2$$

$$q_2 = 3.759G\theta$$

$$q_1 = 3.317G\theta$$

Considering equilibrium, and symmetry:

$$M_t = GJ\theta = 2(2A_{o1}q_1 + 2A_{o2}q_2)$$

$$GJ\theta = 2[2(64.42)3.317 + 2(71.46)3.759]G\theta$$

$$J = 1929.2 \text{ ft}^4$$

7.2.4 Other Three-Dimensional Analyses

Bridges containing spans with large central angles (> 34 degrees) are one type of concrete box girder superstructure that requires analysis by methods beyond three-dimensional frame (spine beam) analyses. There are other concrete box girder bridge types that warrant more rigorous three-dimensional analyses, the two most common of these are:

- Bridges with Variable Skew Supports—Bridges, straight or curved, with orientation of supports different from right angles to supported cross sections are said to have skewed supports. Bridges with skew supports exhibit different distributions of flexural stresses and shear forces than those in similar bridges with radial supports. LRFD Article 4.6.2.2 presents live load distribution factor corrections for bridges with consistently skewed supports. Special modeling is required to capture flexure and shear behavior when adjacent skewed supports are significantly different.
- Two-Cell Box Girder Bridges—The LRFD live load distribution equations do not address bridges with less than three cells. Bridges with two cells require additional analysis to determine the distribution of live load effects with the box girder superstructure. These bridges may be straight or curved, and with or without skew supports.

The most common methods of analyzing the bridge types described above are by grillage or shell finite elements. Grillage methods subdivide the box girder cross section into a series of longitudinal and transverse three-dimensional beam elements with characteristics such, that

when analyzed together, replicate bridge deck behavior with appropriate accuracy. Figure 7.17 shows the development of nodal locations for a grillage analysis of the superstructure of design example 2 in appendix D. Figure 7.18 shows a perspective of a grillage model for that bridge.

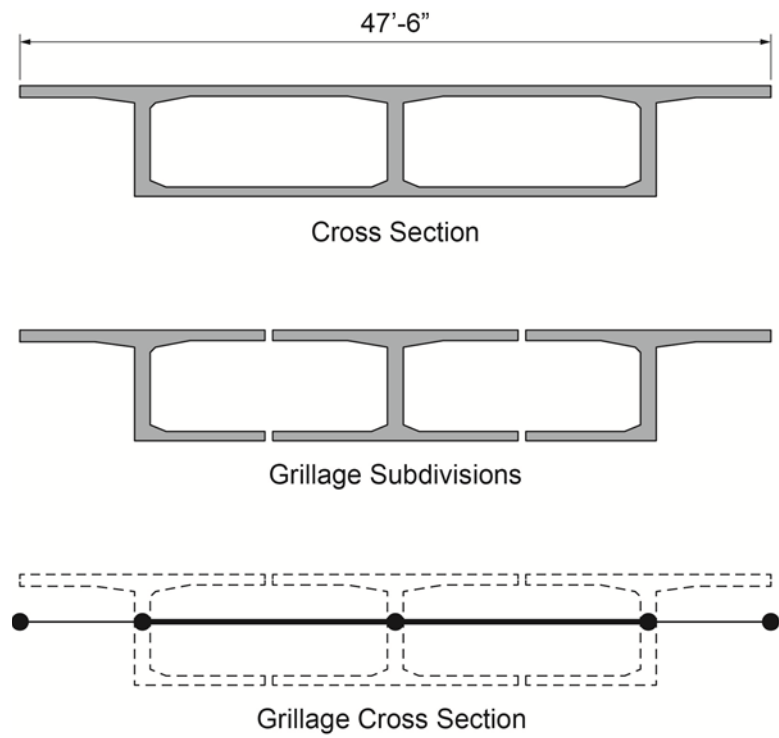


Figure 7.17 – Grillage Model Development for Design Example 2

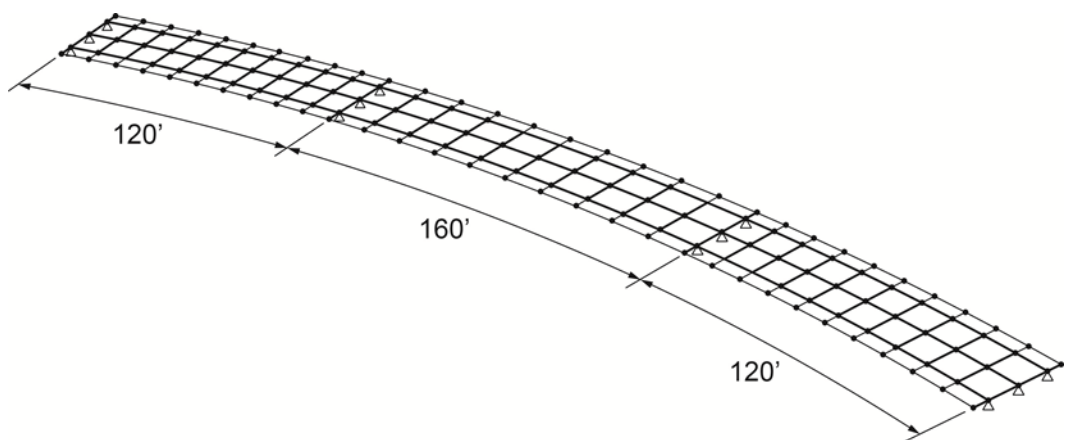


Figure 7.18 – Grillage Model Design Example 2

Grillage methods of analysis are relatively easy to develop using general purpose three-dimensional analysis software. The quality of the results of the analysis, however, can vary significantly depending on the distribution of members in the grillage. Chapter 5 of E.C. Hambly’s book “Bridge Deck Behavior” (1998 reprint of the 1991 2nd Edition, ISBN 0-419-17260-

2) is an excellent reference to consult when developing a grillage analysis of a concrete box girder bridge.

Finite element methods of analyzing box girder superstructures are typically performed using three-dimensional shell elements. For this manual, shell elements are defined as those that exhibit in-plane membrane behavior and out-of-plane flexure and shear behavior. Finite element methods using shell elements model the continuum of the bridge, reducing the influence of mesh choices in grillage methods. That is not to say that they are free from inappropriate modeling choices, such as inappropriate element aspect ratios or ineffective model discretization. Thus, care must be taken when developing the model. Many FEM software packages have powerful graphical modeling interfaces and/or allow for ease in importing model geometry developed in a CAD environment.

Figure 7.19 shows the cross section of the finite element model that was used to find live load distribution factors for the bridge in design example 2 in appendix D. The model was generated by copying elements along the 600' horizontal curve radius to produce one foot long elements along the centerline of the bridge.

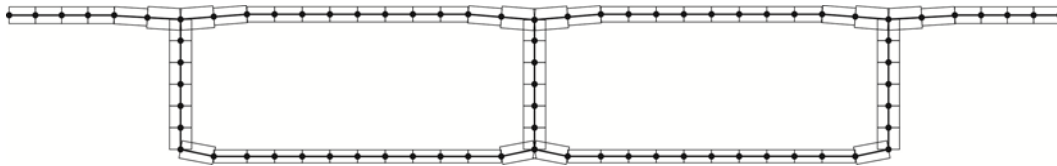


Figure 7.19 – Cross Section of Shell Element FEM Model for Design Example 2

The reader is encouraged to read NCRP Report 620 “Development of Design Specifications for Horizontally Curved Concrete Box-Girder Bridges” (2008) for further information regarding the analysis and design of curved box girder bridges.

7.3 Strength Limit Verification—Flexure

Cross sections along the length of the box girder superstructure must satisfy LRFD flexural requirements at strength limit states. The number of cross sections verified should sufficiently capture the effects of support conditions, individual span lengths within continuous units, changes in post-tensioning tendon geometry, and cross section changes, if present.

The basic equation for factored flexural resistance of a cross section in a box girder bridge is presented in LRFD Equation 5.7.3.2.1-1.

$$\text{(Eqn. 7.15)} \quad M_r = \phi M_n$$

Where, M_r = factored flexural resistance
 M_n = nominal flexural resistance
 ϕ = resistance factor as specified in Article 5.5.4.2

Expressing this relationship in terms of the fundamental equation of LRFD (Equation 1.3.2.1-1) results in:

$$(Eqn. 7.16) \quad \sum \eta_i \gamma_i M_i \leq \phi M_n = M_r$$

Where, M_i = bending moment resulting from a force effect or superimposed deformation
 γ_i = load factor
 η_i = load modifier relating to ductility, redundancy, and operational classification

Load factors for the various force effects and superimposed deformations are found in LRFD Article 3.4.1. The majority of the load factor information is found in Tables 3.4.1-1, 3.4.1-2, and 3.4.1-3.

The load modifier (η) is defined in LRFD Equations 1.3.2.1-2 and 1.3.2.1-3. Both of these equations contain a form of the following expression:

$$(Eqn. 7.17) \quad \eta_i = \eta_D \eta_R \eta_I$$

Where, η_D = factor relating to ductility
 η_R = factor relating to redundancy
 η_I = factor relating to importance

For strength limit verifications, each of these three factors vary between 0.95 and 1.05 depending on conditions described in Articles 1.3.3, 1.3.4, and 1.3.5. For concrete post-tensioned box girder bridges designed in accordance with LRFD Specifications and typical operational importance, the load modifiers are:

$$(Eqns. 7.18) \quad \eta_D = 1.0 \quad \eta_R = 1.0 \quad \eta_I = 1.0$$

A load modifier related to redundancy (η_R) equal to 1.0 is valid for both simple span and continuous concrete post-tensioned box girder bridges. Though simple span girders do not exhibit an external redundancy with regard to longitudinal flexure, there are multiple internal load paths to justify increasing load effects.

Equation 7.16 can then be modified to:

$$(Eqn. 7.19) \quad M_r = \phi M_n \geq \sum \gamma_i M_i$$

7.3.1 Factored Loads for Longitudinal Flexure

Loads for bridge design specified by the LRFD Specifications are described in Article 3.3.2. Those loads that act to produce bending moments in the superstructure of a concrete box girder bridge are:

- DC = dead load of structural components and nonstructural components
- DW = dead load of wearing surface and utilities
- LL = vehicular live load
- IM = vehicular dynamic allowance
- PS = secondary moments from post-tensioning
- CR = bending moments caused by concrete creep
- SH = bending moments caused by concrete shrinkage

- TU = bending moment caused by uniform temperature rise or fall
- TG = bending moments caused by thermal gradient (positive or negative)

Dynamic load allowances are defined in AASHTO LRFD Article 3.6.2. Load effects caused by the application of truck and tandem loads are to be increased by a dynamic load allowance equal to:

$$\text{(Eqn. 7.20)} \quad \text{Dynamic Load Allowance} = \left(1 + \frac{33}{100}\right) = 1.33$$

Moments PS, CR, SH, and TU are defined in Article 3.12 as force effects due to superimposed deformations. The secondary post-tensioning moments (PS) are those caused by the restraining effect of adjacent spans and integral substructures (see section 6.6). Considering construction of complete continuous units in a single phase, the moments caused by concrete creep, concrete shrinkage, and uniform thermal changes are induced only when the substructure is integral with the superstructure. The shortening/extension of the bridge deck displaces the piers, which in turn, induces bending moments in the superstructure (see sections 6.8, 6.9, and 6.10). For typical bridges on bearings, moments produced by concrete creep, concrete shrinkage and uniform temperature change are equal to zero.

The LRFD Specifications define five strength limit state load combinations (Strength I through Strength V). Of these five load combinations, those with wind (Strength III and Strength V) are not likely to govern with regard to maximum superstructure bending moment. The three remaining strength load combinations can be expressed as:

Strength I: (Eqn. 7.21)

$$\sum \gamma_i M_i = 1.25(M_{DC}) + 1.5(M_{DW}) + 1.75(M_{LL+IM}) + 0.5(M_{TU}) + 1.0(M_{PS} + M_{CR} + M_{SH})$$

Strength II: (Eqn. 7.22)

$$\sum \gamma_i M_i = 1.25(M_{DC}) + 1.5(M_{DW}) + 1.35(M_{LL+IM}) + 0.5(M_{TU}) + 1.0(M_{PS} + M_{CR} + M_{SH})$$

Strength IV: (Eqn. 7.23)

$$\sum \gamma_i M_i = 1.5(M_{DC}) + 1.5(M_{DW}) + 0.5(M_{TU}) + 1.0(M_{PS} + M_{CR} + M_{SH})$$

For bridges on bearings, these simplify to:

Strength I: (Eqn. 7.24)

$$\sum \gamma_i M_i = 1.25(M_{DC}) + 1.5(M_{DW}) + 1.75(M_{LL+IM})$$

Strength II: (Eqn. 7.25)

$$\sum \gamma_i M_i = 1.25(M_{DC}) + 1.5(M_{DW}) + 1.35(M_{LL+IM})$$

Strength IV: (Eqn. 7.26)

$$\sum \gamma_i M_i = 1.5(M_{DC}) + 1.5(M_{DW})$$

The Strength II limit state is intended for special owner-specified design vehicles and/or permit vehicles use to evaluate bridges. These vehicles vary with transportation agencies. The engineer should consult individual agency requirements and ensure that the newly designed bridge adequately carries these vehicles. For this manual, the information presented uses the LRFD design notional loading in the Strength I and Strength IV limit states.

Example: Using the three-span bridge in example 1 found in appendix C, whose analysis model is shown in figure 7.7, compute factored bending moments at selected locations within the bridge.

The bending moment results from analysis by the BD2 computer program in units of foot-kips are:

Loading	0.42L Span 1 Node 8	1.0L Span 1 Left of Node 16	0.0L Span 2 Right of Node 16	0.5L Span 1 Node 25
DC	15,125	-26,585	-29,178	17,761
DW	1,339	-2,353	-2,583	1,572
LL+I	12,306	-11,348	-13,778	11,795
TU	2,165	-5,067	-2,622	2,622
PS	1,964	4,594	9,834	9,799
CR	1,161	2,717	-1,543	-1,543
SH	-2,642	-6,181	3,618	3,618

Table 7.1 – Example Bridge 1 Bending Moments (ft-kips)

Using the load factors of equation 7.21 and 7.23 the factored moment combinations for Strength Limit States I and IV are:

Strength Case	0.42L Span 1 Node 8	1.0L Span 1 Left of Node 16	0.0L Span 2 Right of Node 16	0.5L Span 1 Node 25
I	44,016	-58,023	-53,861	58,386
IV	26,262	-44,811	-37,044	42,185

Table 7.2 – Example Bridge 1 Bending Moments (ft-kips)

7.3.2 Flexural Resistance

7.3.2.1 Strain Compatibility

LRFD Article 5.7.3 provides guidance and requirements for the design of prestressed concrete flexural members at strength limit states. Equations leading to the computation of flexural resistance for both rectangular sections and t-beam sections are presented in LRFD Article 5.7.3. This manual presents the more general approach presented in Article 5.7.3.2.5, in which strain compatibility throughout the depth of the member is considered for determining internal forces under ultimate conditions.

Consider the rectangular prestressed concrete beam shown in figure 7.20. The beam, with height of h and width of b , is reinforced with a single layer of prestressing steel with a total area of steel equal to A_{ps} , located a distance d_p from the extreme compression fiber. The bending moment M_n is the nominal resistance of the cross section in flexure. The nominal flexural resistance is produced by the internal couple of compression in the concrete and tension in the prestressing steel, acting along their lines of action.

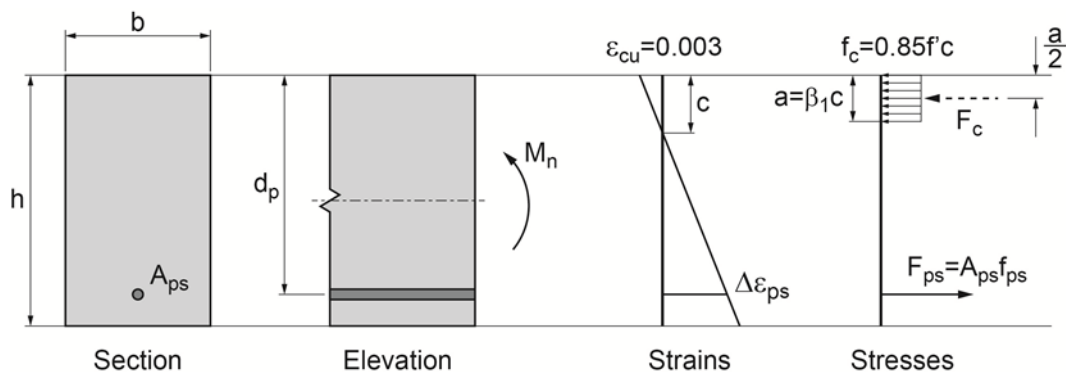


Figure 7.20 – Flexural Resistance by Strain Compatibility

Figure 7.20 shows a strain diagram over the depth of the member. LRFD Article 5.7.2 provides guidelines for establishing the strain diagram:

- The diagram is linear over the depth of the beam.
- The diagram passes through a neutral axis at depth (c) from the extreme compression fiber.
- The ultimate strain in the concrete (ϵ_{cu}) at the extreme compression fiber is equal to 0.003 in/in.

It is important to note that the prestressing steel only provides resistance in the internal equilibrium shown in figure 7.20. This is different from considering the prestressing force as a load effect in the summation of stresses at service limit states. The difference is seen in the strain in the prestressing steel at nominal flexural resistance. The strain on which the stress in the prestressing steel is computed is the sum of the strain at the effective level of stress in the prestressing plus the change in strain resulting from strain compatibility. This can be expressed as:

(Eqn. 7.27)
$$\epsilon_{ps} = \epsilon_{pe} + \Delta\epsilon_{ps}$$

Where, ϵ_{ps} = strain in prestressing steel (in/in)
 ϵ_{pe} = effective strain in prestressing at time of loading (in/in)
 $\Delta\epsilon_{ps}$ = change in strain in prestressing as a result of loading (in/in)

Where the change in strain is provided by similar triangles:

$$(Eqn. 7.28) \quad \Delta\epsilon_{ps} = \epsilon_{cu} \left(\frac{d_p}{c} - 1 \right) = 0.003 \left(\frac{d_p}{c} - 1 \right)$$

7.3.2.2 Material Stresses and Internal Forces

Figure 7.20 also shows the stress and resultant forces developed in the cross section at nominal resistance. The compressive force in the concrete is found by integrating concrete stresses from the neutral axis to the extreme compression fiber. Forces in the prestressing steel are found by multiplying the stress in the steel times the area of the reinforcing steel. Material stress-strain relationships, such as those presented in chapter 2 of this manual, for both concrete and reinforcing steel are required to compute these internal forces.

To simplify the computation of the resultant compressive force in the concrete, the LRFD Specifications permit the use of an equivalent rectangular stress block (Whitney's Stress Block). Details of the rectangular stress block as defined in LRFD Article 5.7.2.2 are shown in figure 7.21.

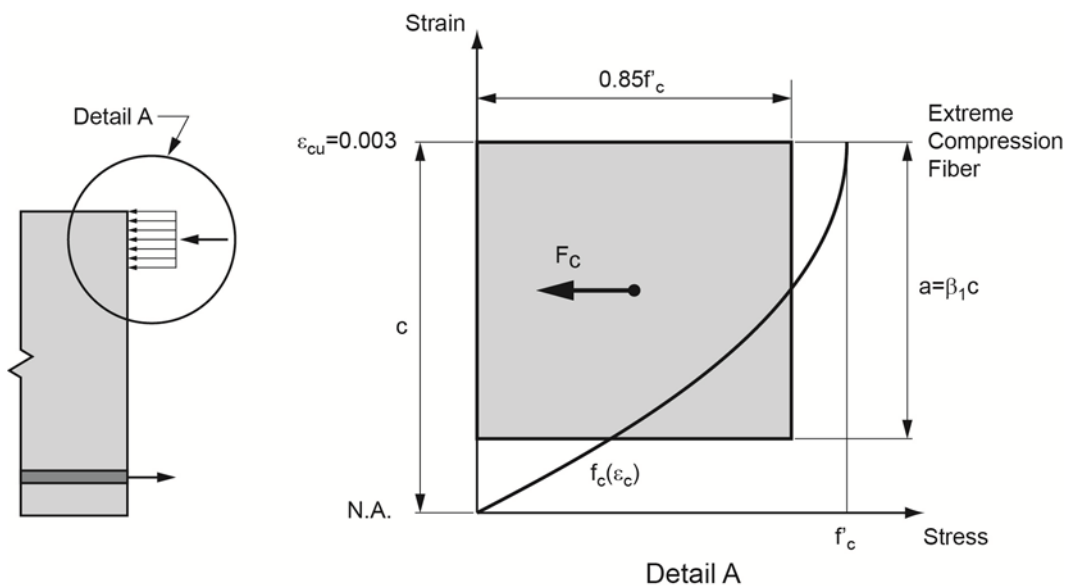


Figure 7.21 – Rectangular Stress Block to Represent Concrete Compression

The actual distribution of concrete stress is replaced by a constant stress equal to 85 percent of the 28-day concrete strength. The depth of the block (a), measured from the extreme compression fiber, is taken as a percentage of the neutral axis depth (c):

$$(Eqn. 7.29) \quad a = \beta_1 c$$

The relationship between the depth of the stress block and the neutral axis depth is a function of concrete strength. The parameter β_1 is taken as 0.85 for concrete strengths equal to, or less than, 4.0 ksi. For greater strengths the parameter is reduced at a rate of 0.05 per 1.0 ksi increase in concrete strength above 4.0 ksi, with a lower bound of 0.65. In equation form this is expressed as:

$$(Eqn. 7.30) \quad \beta_1 = 0.85 - 0.05(f'_c - 4.0) \geq 0.65$$

The computation of the resultant tensile force in the prestressing steel also relies on a representation of the material's stress-strain relationship. Figure 7.22 shows the comparison of typical stress strain relationships for mild reinforcing and prestressing strand presented in figure 2.10 of this manual.

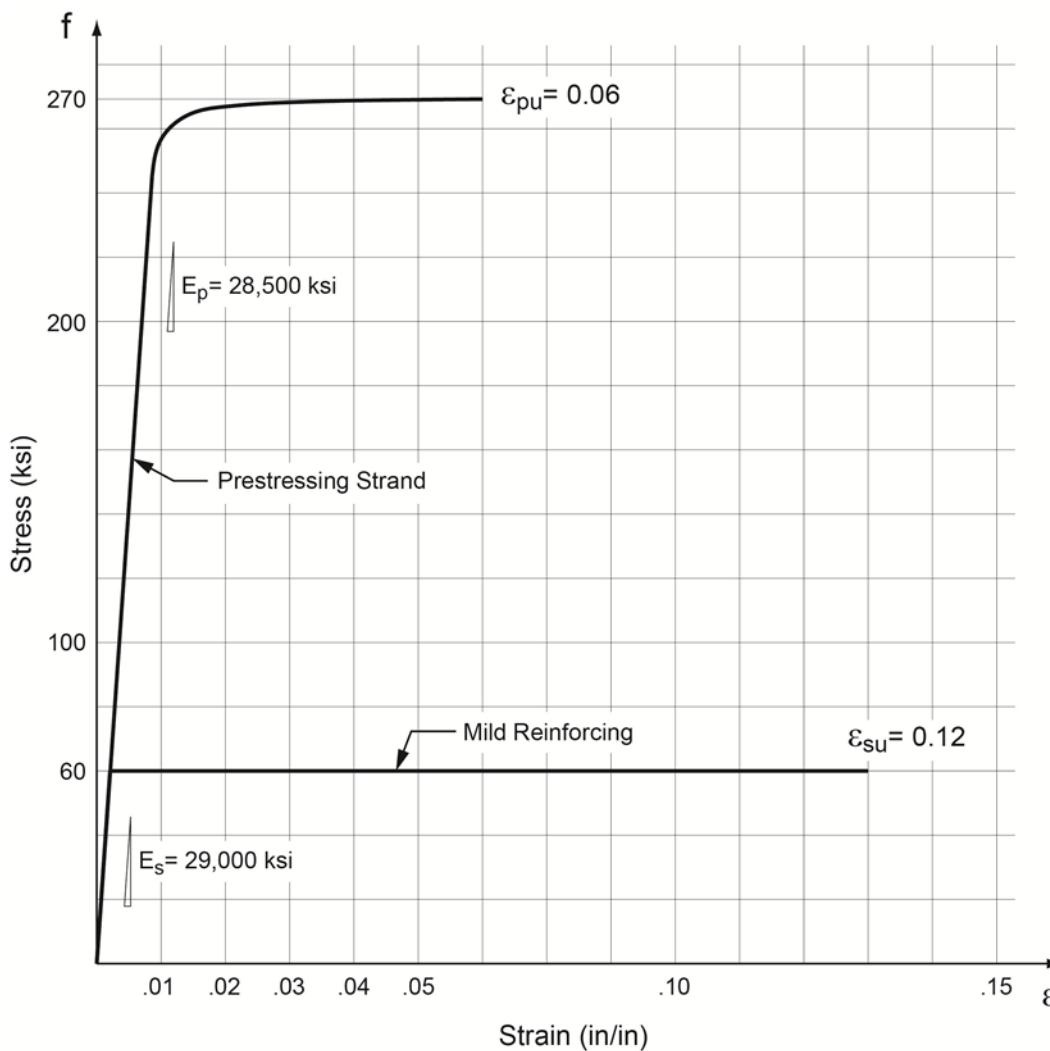


Figure 7.22 – Comparison of Typical Stress-Strain Relationships for Prestressing Strand and Mild Reinforcing

Mild reinforcing exhibits a bilinear relationship with a well-defined yield strain. The relationship of strains and stresses in the prestressing steel are assumed linear for stresses up to 90

percent of the ultimate strength of the strand. Beyond this level of stress the relationship is highly nonlinear.

LRFD Article 5.7.3.1 provides an equation to determine the stress in the prestressing steel at nominal resistance for cross sections where it is appropriate to lump the prestressing steel into a single level (as shown in figure 7.20) and where the effective stress in prestressing steel is not less than 50 percent of specified tensile strength of the prestressing steel. The LRFD expression for stress in the prestressing steel under these conditions is:

$$(Eqn. 7.31) \quad f_{ps} = f_{pu} \left(1 - k \frac{c}{d_p} \right)$$

Where, f_{ps} = average stress in prestressing steel at nominal resistance (ksi)
 f_{ps} = specified tensile strength of prestressing steel (ksi)
 c = depth from extreme compression fiber to the neutral axis (in)
 d_p = depth from extreme compression fiber to the centroid of the steel (in)

The parameter k in equation 7.31 relates the stress in the prestressing steel to the type of prestressing steel that is being used. This variation is related to the ratio of the yield stress of the prestressing steel to its specified tensile strength:

$$(Eqn. 7.32) \quad k = 2 \left(1.04 - \frac{f_{py}}{f_{pu}} \right)$$

LRFD Table C5.7.3.1.1-1 provides values for the ratio of stresses in equation 7.32. The great majority of prestressing steel used for cast-in-place concrete box girder construction is low relaxation steel with a specified tensile strength of 270 ksi. The corresponding values from Table C5.7.3.1.1-1 are:

$$(Eqns. 7.33) \quad \frac{f_{py}}{f_{pu}} = 0.9 \quad k = 0.28$$

So that for 270 ksi, low relaxation steel,

$$(Eqn. 7.34) \quad f_{ps} = 270 \left(1 - 0.28 \frac{c}{d_p} \right)$$

When the arrangement of prestressing steel is such that the steel cannot be lumped into a single layer, another relationship between prestressing steel strain and stress must be used. An often used source for estimating the stress in the prestressing steel is found in the Precast Concrete Institute Design Manual. Figure 7.23 shows a reproduction of the stress-strain relationship presented in Design Aid 11.2.5 of the PCI Design Handbook, 6th Edition.

Up to a strain of 0.0086, the stress in the prestressing steel varies linearly as a function of the modulus of elasticity of the steel—in this case 7-wire strand. This level of strain corresponds to a stress of approximately 90 percent of the specified strength of the strand for the case of 270 ksi steel. When the strain in 270 ksi steel is greater than 0.0086 the relationship between stress and strain is:

(Eqn. 7.35)
$$f_{ps} = 270 - \frac{0.04}{\epsilon_{ps} - 0.007} \quad (ksi)$$

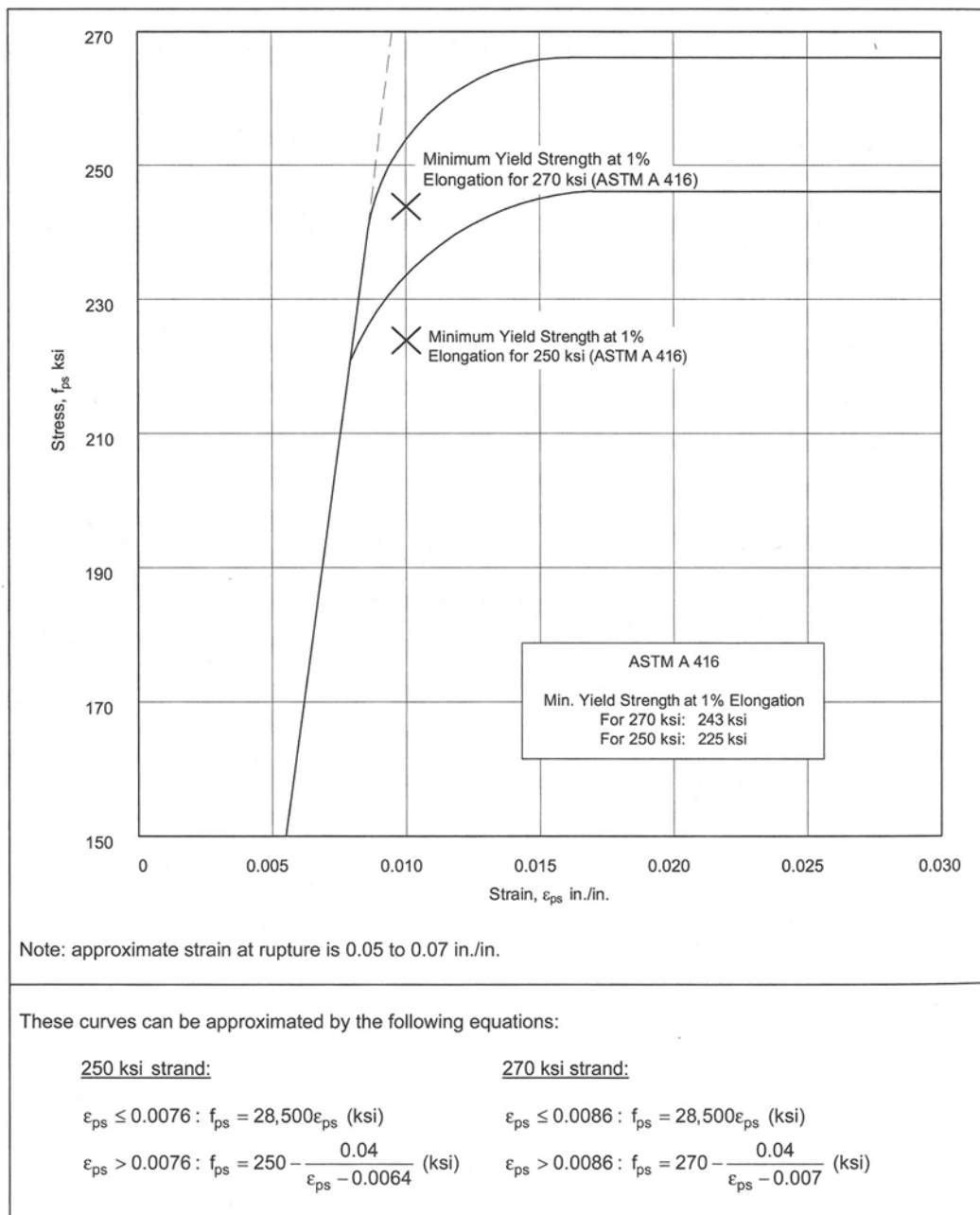


Figure 7.23 –Stress-Strain Relationships for Prestressing Strand (PCI Design Handbook, 6th Ed.)

7.3.2.3 Internal Equilibrium

With material strains and stresses computed, the internal equilibrium of the cross section is considered. For the beam shown in figure 7.20, with a single layer of prestressing reinforcing, the horizontal equilibrium is expressed as:

$$(Eqn. 7.36) \quad \sum F: 0.85f'_c ba - A_{ps}f_{ps} = 0$$

The condition of a net horizontal force is met through the choosing of the correct neutral axis depth. When the condition is met, the flexural resistance of the cross section can be found by summing moments about the centroid of the resultant concrete force:

$$(Eqn. 7.37) \quad \sum M: M_n = A_{ps}f_{ps} \left(d - \frac{a}{2} \right)$$

The equation above considers the fundamental case of one layer of prestressing. Post-tensioned concrete box girder bridges may have post-tensioning tendons that need to be considered at individual levels. In addition, this method of construction also provides for longitudinal mild reinforcing in the top and bottom slabs that can provide additional flexural resistance. Figure 7.24 shows a cross section with these additional elements.

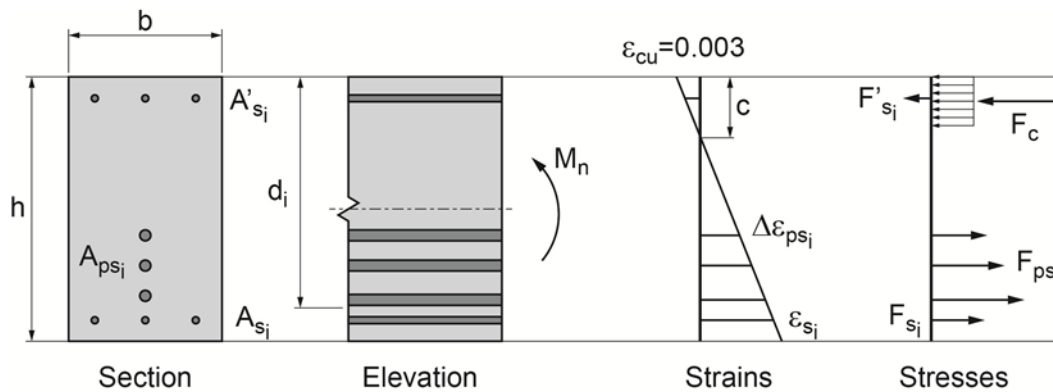


Figure 7.24 – Flexural Resistance with Multiple Layers of Prestressing Steel and Mild Reinforcing

Horizontal equilibrium for the cross section in figure 7.24 can be written as:

$$(Eqn. 7.38) \quad \sum F: 0.85f'_c ba + \sum A'_s (f_s - 0.85f'_c) - \sum A_{ps}f_{ps} - \sum A_s f_s = 0$$

The nominal resistance can be found by summing moments about the top of the beam:

$$(Eqn. 7.39)$$

$$\sum M: M_n = \sum A_{ps}f_{ps} (d_{ps}) + \sum A_s f_s (d_s) - \sum A'_s (f_s - 0.85f'_c) (d'_s) - 0.85f'_c ba \left(\frac{a}{2} \right)$$

The reduction of stress in the compressive reinforcement is a subtraction from the concrete stress block that occupies the same area as the compressive reinforcing. It is accounted for with the compressive reinforcing for computational ease. With the flexural resistance computed, the conditions of equation 7.19 must be met, expressed here as:

(Eqn. 7.40)
$$M_u \leq \phi M_n$$

7.3.3 Resistance Factors (ϕ)

Resistance factors (ϕ), sometimes referred to as capacity reduction factors, for prestressed concrete members vary as a function of the controlling behavior of the member with regard to specific compression and tension limits. For compression controlled behavior, the resistance factor is 0.75. For tension controlled behavior the resistance factor is 1.0. Between code specified limitations in strain that define the limits of this behavior, the resistance factor is taken as a linear ratio between 0.75 and 1.0 (see figure 7.25) defined in LRFD Equation 5.5.4.2.1-1:

(Eqn. 7.41)
$$0.75 \leq \phi = 0.75 + \frac{0.25(\epsilon_t - \epsilon_{cl})}{(\epsilon_{tl} - \epsilon_{cl})} \leq 1.0$$

Where, ϵ_t = net tensile strain in the extreme tension steel at nominal resistance
 ϵ_{cl} = compression-controlled strain limit in the extreme tension steel
 ϵ_{tl} = tension-controlled strain limit in the extreme tension steel

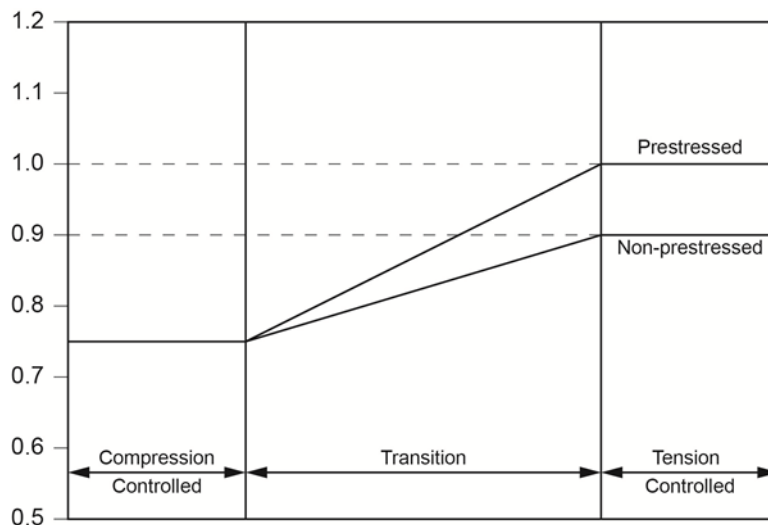


Figure 7.25 – Transition of Resistance Factors from Compression Controlled to Tension Controlled

The commentary to Article 5.5.4.2 includes a discussion of cross sections reinforced with a combination of prestressed reinforcing and mild reinforcing. With regard to resistance factor, a cross section is considered as being prestressed when mild reinforcing is used to provide additional flexural capacity, provided that the cross section was designed as a prestressed section under service limit state requirements.

Some discernment is required when selecting the resistance factors for prestressed concrete members. For the vast majority of superstructure flexure cases for cast-in-place box girder

bridges, the resistance factor will be equal to 1.0. This should not be inferred, however, because of the initial level of strain in the prestressing steel. The tensile-controlled strain limit of 0.005 would represent a stress in the prestressing steel of 142.5 ksi, using a modulus of elasticity of the steel of 28,500 ksi. This is less than the effective stresses in the tendons under service limit state conditions. What should be considered is the change in prestressing strain in the calculation of flexural resistance. When the change of strain is greater than 0.005, the resistance factor of 1.0 is appropriate. Again, this is the case for the great majority of prestressed concrete superstructures.

7.3.4 Limits of Reinforcing

LRFD Article 5.7.3.3.2 provides minimum reinforcement requirements for prestressed concrete members at strength limit states. Two criteria are presented to assure that the flexural resistance is greater than the cracking strength of the cross section, avoiding possible brittle failures. In equation form, the minimum reinforcing in the cross section must be greater than the lesser of:

$$\text{(Eqn. 7.42)} \quad M_r \geq 1.33M_u$$

Or,

$$\text{(Eqn. 7.43)} \quad M_r \geq M_{cr}$$

Where M_{cr} is the cracking moment of the cross section. The cracking strength is determined by LRFD Equation 5.7.3.3.2-1.

$$\text{(Eqn. 7.44)} \quad M_{cr} = \gamma_3 \left[(\gamma_1 f_r + \gamma_2 f_{cpe}) S_c - M_{dnc} \left(\frac{S_c}{S_{nc}} - 1 \right) \right]$$

This equation accommodates cross sections made of flexural members made composite with a concrete deck slab. The equation can be simplified for concrete box girder bridges with monolithically cast cross sections ($S_c/S_{nc}=1$) to:

$$\text{(Eqn. 7.45)} \quad M_{cr} = \gamma_3 \left[(\gamma_1 f_r + \gamma_2 f_{cpe}) S \right]$$

Where,

- γ_1 = flexural cracking variability factor (= 1.6 for non-segmental bridges)
- γ_2 = prestress variability factor (= 1.1 for bonded tendons)
- γ_3 = ratio of yield strength to ultimate strength (= 1.00 for prestressed bridges)
- S = cross section modulus corresponding to the extreme fiber for which the cracking moment is being computed.
- f_{cpe} = compressive stress in concrete due to effective prestressing forces only(after all losses) at extreme fiber of section where tensile stress is caused by external applied loads (ksi)
- M_{dnc} = total unfactored dead load moment acting on the monolithic or noncomposite section (kip-in)

Using the applicable values for the gamma coefficients (γ), the resulting equation is then:

$$(Eqn. 7.46) \quad M_{cr} = (1.6f_r + 1.1f_{cpe})S$$

The modulus of rupture to be used in computing the rupture moment in these equations is found in LRFD Article 5.4.2.6. For normal weight concretes with a 28-day strength less than 15.0 ksi, the rupture stress is:

$$(Eqn. 7.47) \quad f_r = 0.24\sqrt{f'_c}$$

Example: Using the three-span bridge in the previous example, find the moment controlling the LRFD minimum reinforcement requirements at the Pier 1.

The factored moment at the left of Node 25 in the previous example was:

$$M_u = -58,023 \text{ ft-kips}$$

The stress at the extreme fiber under the action of the prestressing only is (See example 1 in appendix C):

$$f_{cpe} = 174.8 \text{ ksf}$$

The modulus of rupture is:

$$f_r = 0.24\sqrt{5.0}(144) = 77.3 \text{ ksf}$$

The resulting cracking moment at this location is:

$$M_{cr} = (1.6(77.3) + 1.1(174.8)) \left(\frac{643.7}{2.732} \right) = 74,445 \text{ ft-kips}$$

This moment is compared to 13 percent of the governing factored moment:

$$1.33M_u = 1.33|-58,023| = 77,171 \text{ ft-kips}$$

As this moment is larger than the cracking moment, the resistance of the cross section must be:

$$M_r \geq 77,171 \text{ ft-kips}$$

Note that change in the sign convention of the example problem to an absolute value of the moments for calculating resistance requirements.

7.3.5 Procedure

Figure 7.26 shows a flow chart that describes the verification of a prestressed concrete cross section at strength limit state for flexure. Two iterative loops are embedded in the flow chart. The inner loop is for the appropriate selection of the depth of the neutral axis, which converges when horizontal equilibrium of the cross section is reached. The outer loop is for the verification that the reduced nominal capacity is greater than the factored loads. Mild reinforcing can be considered to add needed flexural capacity. Additional prestressing steel can be added as long as service limit state verifications remain valid. If these two approaches do not lead to sufficient flexural capacity, more significant changes, such as increased depth of the cross section, may be required.

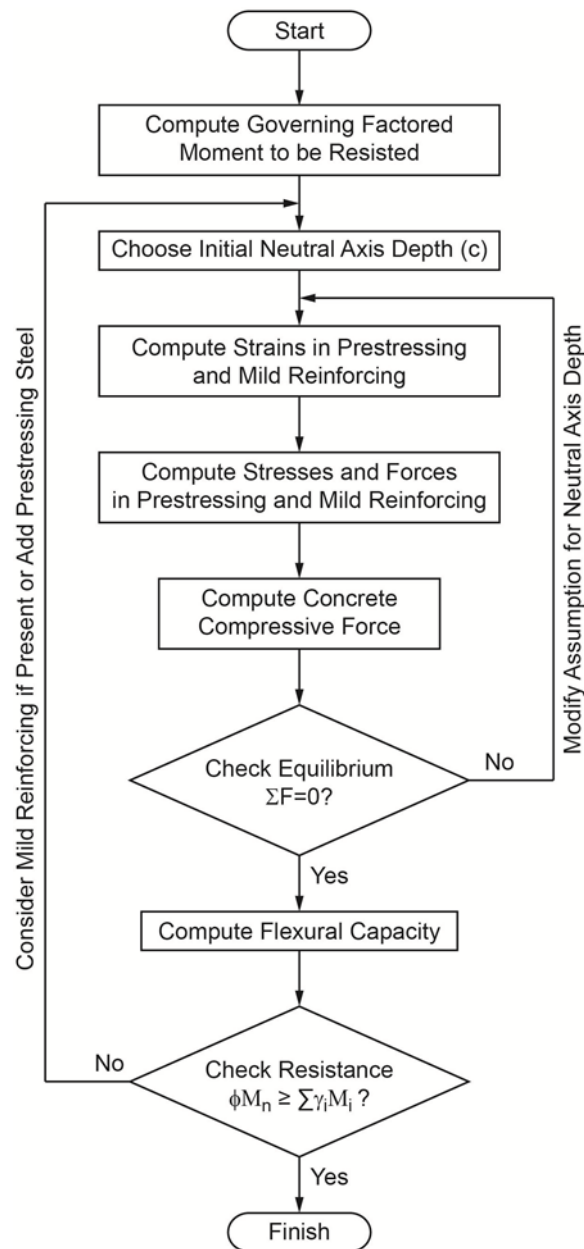


Figure 7.26 – Flow Chart for Verification of Flexure at the Strength Limit State

Example: Using the three-span bridge in the previous example, verify the flexure strength limit state at the mid-span of the 160' central span.

Figure 7.27 shows the cross section of the box girder bridge of this example along with the idealized cross section with regard to longitudinal flexure. Figure 7.28 shows the location of the 15 (3 per web), 19-strand tendons at mid-span.

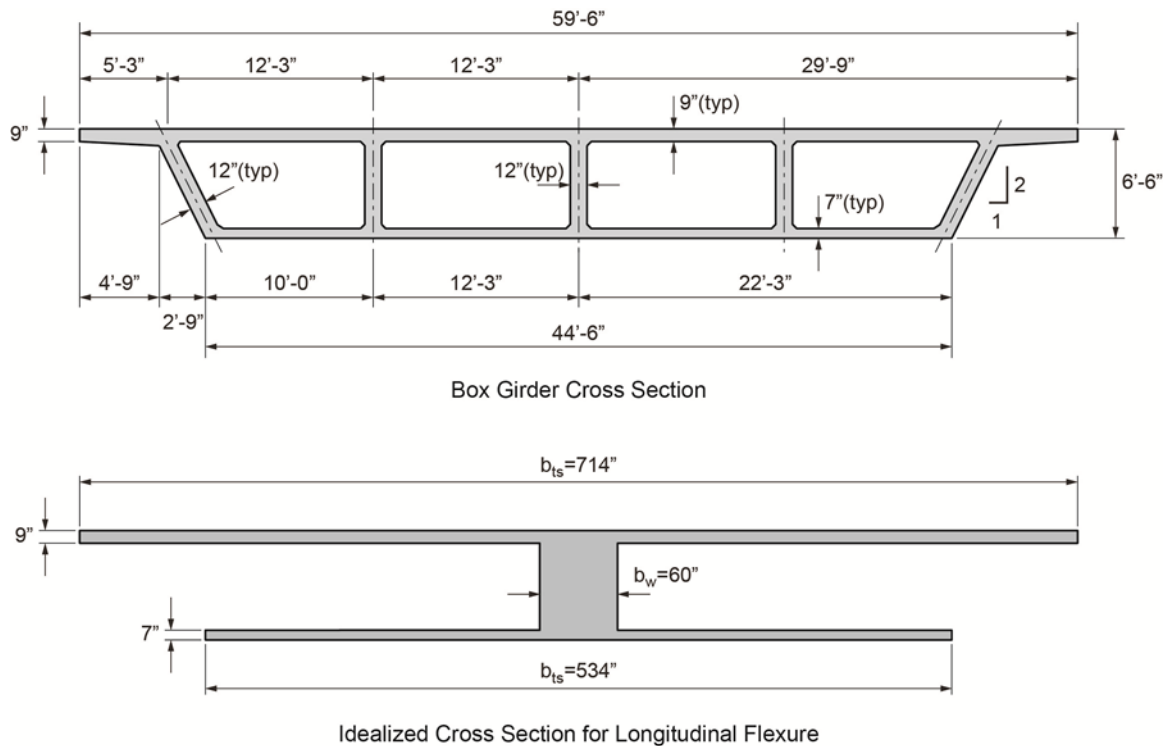


Figure 7.27 – Idealized Cross Section For Longitudinal Flexure

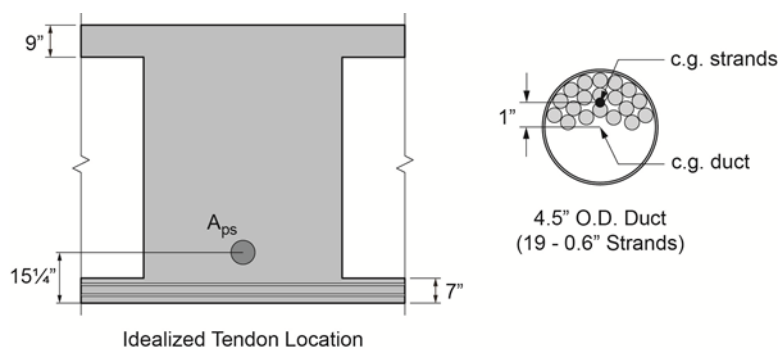


Figure 7.28 – Location of Prestressing Reinforcing in Idealized Cross Section

Parameters:

$$\begin{aligned}
 f'_c &= 5.0 \text{ ksi} \\
 b_{ts} &= 714'' \\
 b_w &= 62.8''
 \end{aligned}$$

$$d_p = 78'' - 7.75'' - 6.5'' - 1'' = 62.75''$$

$$A_{ps} = 15(19 \times 0.217) = 61.845 \text{ in}^2$$

The factored moment at Node 25 in the previous example was:

$$M_u = 58,386 \text{ ft} - \text{kips}$$

Determine the moment for minimum reinforcing based on the lesser of the cracking moment or 133 percent of the factored moment.

The stress at the extreme fiber under the action of the prestressing only is (See example 1 in appendix C):

$$f_{cpe} = 165.1 \text{ ksf}$$

The modulus of rupture is:

$$f_r = 0.24\sqrt{5.0}(144) = 77.3 \text{ ksf}$$

The resulting cracking moment at this location is:

$$M_{cr} = (1.6(77.3) + 1.1(165.06)) \left(\frac{643.7}{3.768} \right) = 52,146 \text{ ft} - \text{kips}$$

This moment is compared to 133 percent of the factored moment or:

$$1.33M_u = 77,653 \text{ ft} - \text{kips}$$

The cracking moment of 52,146 ft-kips is less than the increased factored moment and is the moment required for minimum reinforcing. This minimum moment is less than the factored moment of 58,386 ft-kips, so the design moment is the factored moment.

The depth of the neutral axis from the extreme compression fiber (top of top slab at this cross section) is determined by iteration and axial force equilibrium checks. After some iteration, assume a neutral axis depth of 6.86 inches:

$$c = 6.86 \text{ inches}$$

The ratio of depth of the rectangular stress block to the neutral axis is:

$$\beta_1 = 0.85 - 0.05(5.0 - 4.0) = 0.8$$

So that the depth of the rectangular stress block is:

$$a = 0.8(6.86) = 5.488 \text{ inches}$$

The change in the prestressing steel strain is:

$$\Delta \varepsilon_{ps} = 0.003 \left(\frac{62.75}{6.86} - 1 \right) = 0.02444 \text{ in / in}$$

Assuming an effective strain in the prestressing steel of 63 percent of the ultimate strength of the strand, the total strain in the prestressing steel is:

$$\varepsilon_{ps} = \left(\frac{0.63(270)}{28,500} + 0.02444 \right) = 0.03041 \text{ in / in}$$

Using equation 7.35 of this Manual for determining stress in the prestressing steel:

$$f_{ps} = 270 - \frac{0.04}{0.03041 - 0.007} = 268.29 \text{ ksi}$$

The force in the prestressing is:

$$F_{ps} = 268.29(61.845) = 16,592 \text{ kips}$$

The force in the rectangular compression block is:

$$F_c = 0.85(5.0)714(5.488) = 16,653 \text{ kips} \approx F_{ps}$$

The summation of the forces in the cross section are essentially zero, so the nominal flexural resistance can be found by summing moments about the center of the compression block:

$$\sum M : M_n = 16,592 \left(62.75 - \frac{5.488}{2} \right) \left(\frac{1}{12} \right) = 82,968 \text{ ft-kips}$$

The level of change in stress in the strands is such that the section is compression controlled, so that the resistance factor is 1.0. The reduced nominal capacity is such that the strength limit state is satisfied:

$$58,386 \leq (1.0)83,096 = 83,096$$

Example: Determine the nominal flexural capacity of the cross section of the previous example considering mild reinforcing in the bottom slab. Use No. 4 bars top and bottom of the bottom slab at a spacing of 12 inches.

The area of mild reinforcing is:

$$A_s = 44(2)(0.2 \text{ in}^2) = 17.6 \text{ in}^2$$

The yield strain of the mild reinforcing is equal to:

$$\varepsilon_s = \frac{60}{29,000} = 0.00207 \text{ in / in}$$

By inspection, the yield strain will be reached for reinforcing located in the bottom slab of this example problem. Assuming a neutral axis depth of 7.27", the depth of the rectangular stress block is:

$$a = 0.8(7.27) = 5.816 \text{ inches}$$

$$\Delta\varepsilon_{ps} = 0.003 \left(\frac{62.75}{7.27} - 1 \right) = 0.02289 \text{ in / in}$$

$$\varepsilon_{ps} = \left(\frac{0.63(270)}{28,500} + 0.02289 \right) = 0.02886 \text{ in / in}$$

$$f_{ps} = 270 - \frac{0.04}{0.02886 - 0.007} = 268.17 \text{ ksi}$$

$$F_{ps} = 268.17(61.845) = 16,585 \text{ kips}$$

Checking equilibrium in the cross section:

$$\sum F: 0.85(5.0)714(5.816) - 16,585 - 60.0(17.6) = 7.7 \text{ kips} \approx 0.0$$

Summing moments about the top of the cross section:

$$\sum M: M_n = \left(16,585(62.75) + 1,056(74.5) - 0.85(5)(714)(5.816) \left(\frac{5.816}{2} \right) \right) \left(\frac{1}{12} \right)$$

$$M_n = 89,005 \text{ ft-kips}$$

This represents an increase in nominal flexural capacity of 7 percent. A similar example could be performed including the top slab longitudinal reinforcing. The location of the steel relative to the resulting neutral axis does not significantly increase positive flexural capacity for this cross section.

7.4 Strength Limit Verification—Shear

The verification of the webs of post-tensioned concrete box girder bridge superstructures at strength limit states requires the combination of several analyses and design steps. LRFD Article 5.8.1.5, repeated below, defines the scope of verifying the webs of curved box girder superstructures.

5.8.1.5—Webs of Curved Post-Tensioned Box Girder Bridges

Curved post-tensioned box girders having an overall clear height, h_c , in excess of 4 ft shall be designed for the following combined effects before and after losses:

- The combined effects of global shear resulting from vertical shear and torsion,
- Transverse web regional bending resulting from lateral prestress force, and
- Transverse web bending from vertical loads and transverse post-tensioning.

Though Article 5.8.1.5 lists the design components for curved box girder bridges, the webs of all box girder bridges must be designed for the first and third bulleted items – global shear and transverse flexure.

The transverse analysis and design of concrete box girder bridges (bulleted item 3) is presented in chapter 8 of this manual. Chapter 9, section 9.1 of this manual presents information related to regional bending in the webs. This section of the manual presents information related to the evaluation of the effects of global shear resulting from shear and torsion.

7.4.1 LRFD Design Procedures for Shear and Torsion

The AASHTO LRFD specifications specifies two design procedures (models) for verifying shear at strength limit states. These two models are the Sectional Model, presented in LRFD Article 5.8.3, and the Strut-and-Tie Model, detailed in LRFD Article 5.6.3. The application of these methods is determined by the behavior of the member in the region being verified. The LRFD Specifications defines two behavioral regions:

- Flexural Regions (LRFD Article 5.8.1.1)—Locations in reinforced or prestressed concrete members where plane sections can be assumed to remain plane under loading. In flexural regions the response of the section depends only upon the sectional force effects—moment, shear, axial load, and torsion—and not on how the force effects are introduced into the member.
- Regions near Discontinuities (LRFD Article 5.8.1.2)—Locations where the assumptions of plane sections remaining plane cannot be appropriately applied. Examples of these regions are locations of abrupt change in cross section, openings, dapped ends, deep beams, and corbels.

The LRFD Specifications, with the limitations presented in paragraph 2 of LRFD Article 5.8.1.1, state that either the Sectional Model or the Strut-and-Tie Model can be used to verify shear at strength limit states in flexural regions. The commentary presented in LRFD Article C5.8.1.1 states that design using the Strut-and-Tie Model generally produces designs that are less

conservative than those designed using the Sectional Model. The LRFD Specifications require that the Strut-and-Tie Method be used for the design of regions near discontinuities.

The behavior of post-tensioned concrete box girder bridges, with regard to shear associated with the longitudinal superstructure design, are consistent with the LRFD definition of a flexural region. As a result, this manual presents information related to the Sectional Model design procedure.

7.4.2 General Requirements

Cross sections along the length of the superstructure must satisfy LRFD requirements for shear and torsion at strength limit states. LRFD Article 5.8.2.1 provides equations that define the resistance with regard to shear and torsion with respect to cross section nominal capacities. The resistance with regard to shear is provided in LRFD Equation 5.8.2.1-2:

$$\text{(Eqn. 7.48)} \quad V_r = \phi V_n$$

Where, V_r = factored shear resistance
 V_n = nominal shear resistance
 ϕ = resistance factor as specified in Article 5.5.4.2

Extending this equation with regard to applied loads, the resistance with regard to shear must be greater than the summation factored load effects:

$$\text{(Eqn. 7.49)} \quad V_r = \phi V_n \geq \sum \gamma_i V_i$$

Where, V_i = shear resulting from a force effect or superimposed deformations
 γ_i = load factor applicable to force effect or superimposed deformations

An equation similar equation 7.15 is provided for torsion in LRFD Equation 5.8.2.1-1:

$$\text{(Eqn. 7.50)} \quad T_r = \phi T_n$$

Where, T_r = factored torsional resistance
 T_n = nominal torsional resistance
 ϕ = resistance factor as specified in Article 5.5.4.2

Again, extending this equation with regard to applied loads, the torsional resistance must be greater than the summation of the factored torsional effects:

$$\text{(Eqn. 7.51)} \quad T_r = \phi T_n \geq \sum \gamma_i T_i$$

Where, T_i = torsional moment resulting from a force effect or superimposed deformation
 γ_i = load factor applicable to force effect or superimposed deformation

When the factored torsional moment is small with regard to the torsional moment required to crack the cross section, the effects of torsion do not need to be considered in the verification of the box girder webs. LRFD Equation 5.8.2.1-3 requires that if the factored torsional moment is

greater than or equal to one fourth of the torsional cracking moment, the effects of torsion must be considered in the design.

Minimum shear and torsion resistance is ensured through the requirement for minimum transverse reinforcing in LRFD Article 5.8.2.5.

7.4.3 Sectional Model Nominal Shear Resistance

Shear design of reinforced and prestressed concrete girders in the AASHTO LRFD specifications in flexural regions has long been based on a truss analogy. Figure 7.29 shows a typical parallel chord truss for a constant depth beam. The beam is loaded with a concentrated vertical load at mid-span. The vertical force is carried to the supports through successive inclined compression struts. Vertical tension members lift the vertical component at the bottom of a diagonal strut to the top of the adjacent inclined strut. The horizontal component of the diagonal strut is held in equilibrium by the compressive forces in top chord members and tensile forces in the bottom chord members.

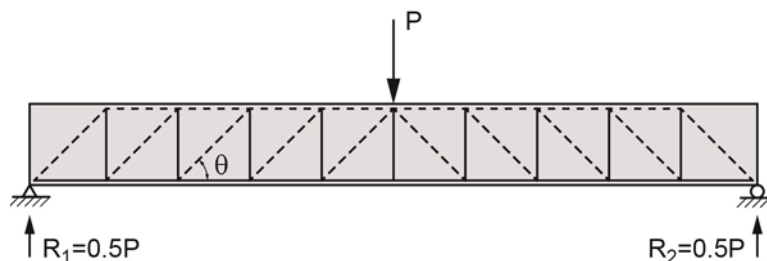


Figure 7.29 – Web Width based on Horizontal Widths

Using truss analogies for shear design of reinforced concrete beams has its origins in the beginning of the last century. Early applications used shear reinforcing to carry the entire shear forces predicted in the vertical tension members of the truss. Orientation of the inclined compressive struts (θ) for these early solutions was typically 45 degrees from horizontal.

Later testing of concrete beams reinforced using truss analogies revealed shear strengths greater than that provided by the reinforcing alone (V_s in LRFD). The additional shear resistance was observed to be a somewhat complex combination of behaviors that were a function of the magnitude and nature of beam cracking under ultimate loads. Tests of this nature led to the empirical development of a shear resisting mechanism associated with the girder concrete (V_c in LRFD).

Still later work in the 1980's advanced the estimation of the concrete contribution from a purely empirically based solution to a more analytical approach using the Modified Compression Field Theory (MCFT). The MCFT methods still have an empirical component, but one based only on the nature of reinforced webs to resist in-plane forces. The LRFD Specifications provide both empirically based and MCFT based methods for determining the component of shear resistance provided by the girder concrete.

The nominal shear resistance of a reinforced or prestressed concrete member with transverse reinforcing is presented as the lesser of that predicted by LRFD Equations 5.8.3.3-1 and 5.8.3.3-2:

$$(Eqn. 7.52) \quad V_n = V_c + V_s + V_p$$

(Eqn. 7.53)
$$V_n = 0.25f'_c b_v d_v + V_p$$

- Where,
- V_c = shear resistance provided by the cross section concrete
 - V_s = shear resistance provided by transverse reinforcing
 - V_p = shear resistance provided by the component of the effective prestressing force in the direction of the applied shear
 - b_v = the effective web width (LRFD Article 5.8.2.9)
 - d_v = the effective shear depth (LRFD Article 5.8.2.9)

The three components of resistance will be discussed in the following sections. This section continues by providing more detail with regard to girder dimensions to be used for shear design.

7.4.3.1 Effective Web Width

LRFD Article 5.8.2.9 defines the effective web width as being measured parallel to the neutral axis. A literal interpretation of this article is depicted in figure 7.30 for the cross section of design example 1. The widths of all webs in this cross section, vertical and inclined, are 12 inches perpendicular to their axes. A horizontal cut along the neutral axis would cross the vertical webs with their 12-inch widths. The horizontal cut through the inclined webs would see horizontal widths, b_h , equal to 13.42 inches for a web slope of 2:1. The total web width along the horizontal cut is then 62.84 inches.

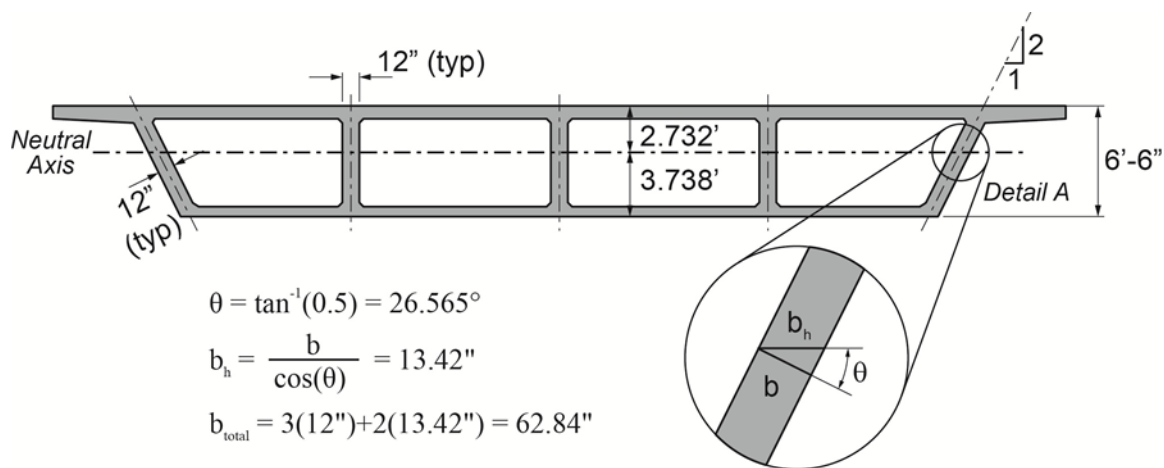


Figure 7.30 – Web Width based on Horizontal Widths

Unfortunately, the web width computed above is inconsistent with the internal equilibrium of shear flow around the cross section with regard to the inclined webs. Consider the cross section of the single cell box girder with inclined webs shown in figure 7.31. A shear force, V , is applied to the cross section. The inclination of the webs requires that the sum of the shear flow in the inclined webs is:

(Eqn. 7.54)
$$V_{web} = \frac{V}{\cos(\theta)}$$

The vector summation of this force and a horizontal force in the top slab resolves to one half of the applied shear force.

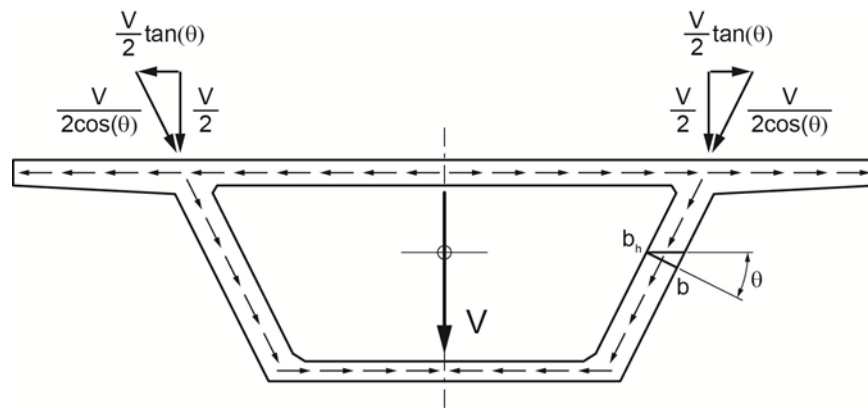


Figure 7.31 – Shear Flow in Single Cell Box Girder

The resulting shear stress acting on the web is then:

$$(Eqn. 7.55) \quad \tau = \frac{V}{\cos(\theta)} \left(\frac{Q}{I \cdot 2b_h} \right)$$

Noting that:

$$(Eqn. 7.56) \quad b = b_h \cos(\theta)$$

Reduces Equation 7.55 to:

$$(Eqn. 7.57) \quad \tau = \frac{VQ}{I \cdot 2b}$$

Thus, vertical shear forces are related to web widths perpendicular to their inclined axes. Extending these considerations to the cross section shown in figure 7.30, it can be argued that the appropriate web width should be 60 inches as opposed to the 62.84 inches of width along a horizontal cut through the webs. Using the horizontal width would lead to limit state verifications that are approximately 5 percent unconservative. By comparison, the verifications of the single cell box girder, using a similar web slope, would be unconservative by 11 percent. The engineer should give appropriate consideration to the web width used for each cross section.

In addition to the previous discussion, the effective web width must include reductions in width to account for ducts embedded in the webs. Figure 7.32 shows one web of the box girder of design example 1. Also shown is the shear stress distribution for a given vertical shear force and a detail of the flow of shear around ducts. To accommodate the shear flow concentrations, LRFD Article 5.8.2.9 requires a subtraction of one half of the duct diameter for loads applied to the bridge when the duct is ungrouted and a subtraction of one fourth of the diameter for loads applied after the duct is grouted.

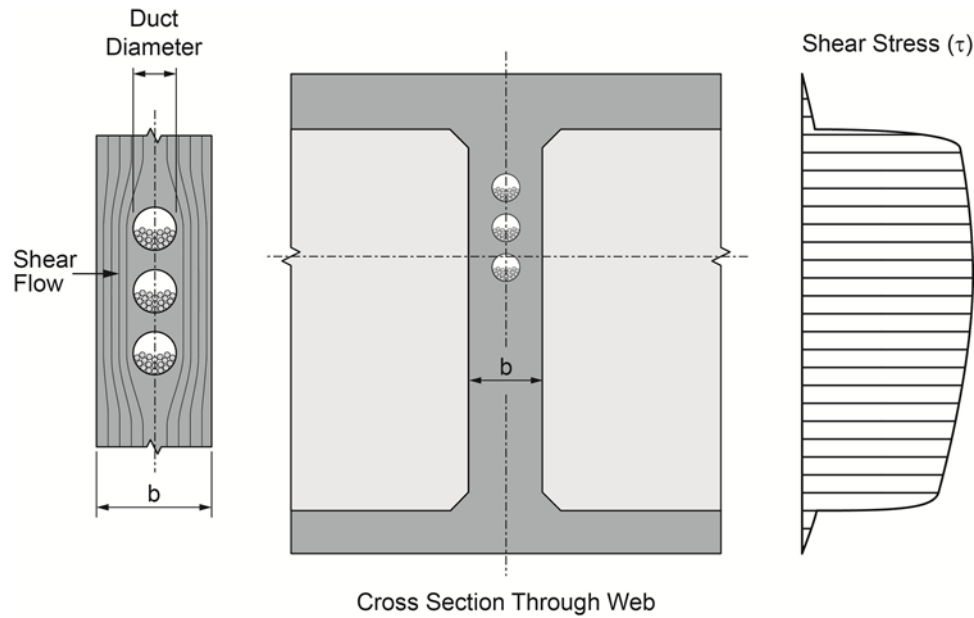


Figure 7.32 – Shear Stress and Shear Flow Around Ducts

7.4.3.2 Effective Shear Depth

The effective depth for shear, d_v , is required to be at least equal to the distance between the centroids of compression in the concrete and tension in the tensile elements. Figure 7.33 shows one of the webs of the cross section of the box girder of design example 1 at one of the interior supports. The centroid of the compression in the concrete was determined as the center of gravity of the stress block at nominal loading. The corresponding tension force passes through the center of gravity of the post-tensioning tendons.

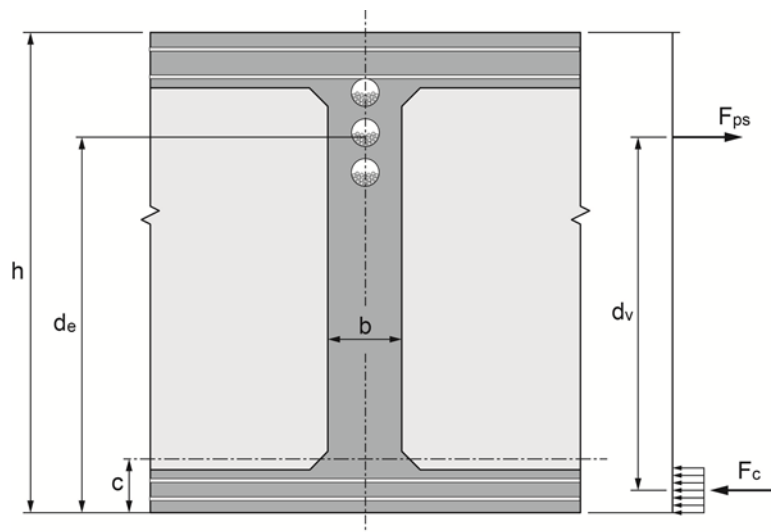


Figure 7.33 – Effective Depth for Shear Calculations

The minimum effective shear depth can be found as the nominal moment capacity of the section divided by either the internal compressive or tensile force:

$$(Eqn. 7.58) \quad d_v = \frac{M_n}{F_s + F_{ps}} = \frac{M_n}{F_c}$$

The effective shear depth need not be taken less than 90 percent of the depth measured from the extreme compression fiber to the centroid of the prestressing steel, d_e , or 72 percent of the overall depth of the box girder.

7.4.4 Shear Resistance from Concrete (V_c)

The LRFD Specifications provide three different methods for determining the concrete contribution of shear resistance in reinforced and prestressed concrete members in flexural regions. Method 1 and Method 2 are based on the Modified Compression Field Theory. Method 3, included in AASHTO LRFD specifications for many years, is more empirically derived from shear testing of prestressed girders. The applicability of the three methods is:

- Method 1 (LRFD Article 5.8.3.1)—for non-prestressed members.
- Method 2 (LRFD Article 5.8.3.4.2 or LRFD Appendix B5)—for both prestressed and non-prestressed members, with or without shear reinforcing.
- Method 3 (LRFD Article 5.8.3.4.3)—for both prestressed and non-prestressed concrete members where there is no net axial tensile load and minimum shear reinforcing is provided.

Since the concern of this manual is post-tensioned concrete box girder bridges, this section presents the LRFD requirements for Methods 2 and 3. (Method 1, though not a focus of this manual, can be viewed as a special case within Method 2.)

7.4.4.1 Method 2 (Simplified MCFT)

Method 2 for computing the contribution of the concrete to cross section nominal shear resistance is based on design procedures derived from the Modified Compression Field Theory. Three primary parameters are used to evaluate concrete shear resistance in this method:

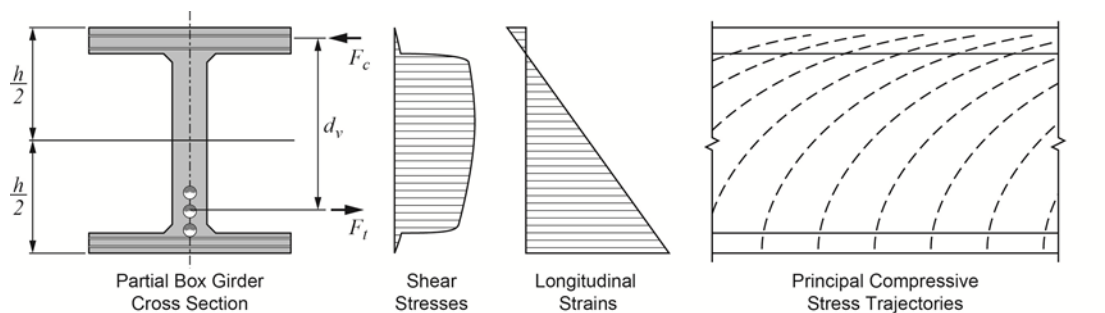
- θ = angle, from horizontal, of the inclination of the diagonal compressive strut
- β = factor indicating ability of diagonally cracked concrete subjected to in-plane shear and normal stresses to transmit tension.
- ϵ_x = longitudinal strain in the web of the member

These three parameters are interdependent in the MCFT, with no direct solution available for the wide range of possible girder variables. As a result, the first implementation of MCFT in LRFD presented an iterative approach to evaluating these parameters. This iterative approach is now provided in LRFD Appendix B5 of LRFD. Beginning in 2008, LRFD offered a simplified, non-iterative solution for these parameters. This simplified approach is presented in the Manual.

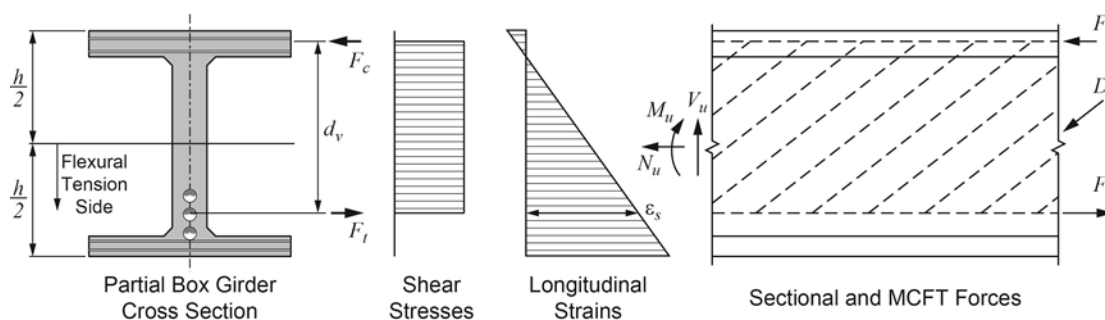
The LRFD application of MCFT is based on a set of assumptions in modeling actual girder shear behavior. The top of figure 7.34 depicts a portion of a box girder cross section and

shows shear stress distributions, longitudinal strains and principal compressive stress trajectories. The bottom of figure 7.34 shows the LRFD behavior assumed in design procedures using MCFT. Three significant assumptions are:

- The distribution of shear stress over the depth of the section is taken as the value at mid-depth of the girder using MCFT methods and the computed longitudinal strain at mid-depth. Shear stresses are uniformly distributed over the rectangular area that has a height of d_v and width of b_v , as calculated in the previous sections.
- The direction of principal compressive stresses remains constant over the height d_v .
- The web is modeled by one biaxial member.



Actual Stresses and Strains by Elastic Analysis



Stresses, Strains and Sectional Forces for MCFT

Figure 7.34 –Actual vs. MCFT Girders

In the LRFD approach to MCFT shear design, the sectional forces shown in the bottom right of figure 7.34 are placed in equilibrium with forces in an idealized model comprised of compression and tension flanges and the web. The forces in these three elements are calculated as follows:

- The sectional bending moment, M_u , is the resisted force in the flanges multiplied by the lever arm, d_v , between them.
- The sectional axial force, N_u , is resisted by forces in the flanges, one-half assumed to be carried by each flange.
- The sectional shear force, V_u , is resisted by the inclined compression strut force, D , which is resolved into horizontal and vertical components. The vertical component of the force is equal to the factored sectional shear force less the value of any vertical component of prestressing acting at the section. The horizontal component is resisted by tension in the flanges.

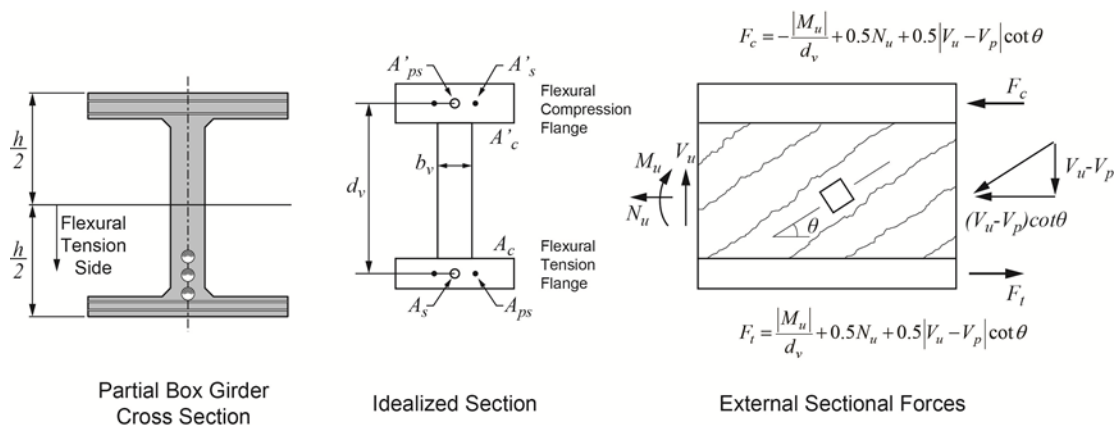


Figure 7.35 – MCFT Forces and Longitudinal Strain

The assumed resistance equilibrium for Method 2 is shown above in figure 7.35. Evaluating these forces acting at the center of the tensile force, allows the computation of the strain in the tensile element, ϵ_s , which is needed to evaluate the beta and theta terms. The strain is predicted by LRFD Equation 5.8.3.4.2-4:

$$\text{(Eqn. 7.59)} \quad \epsilon_s = \frac{\left(\frac{|M_u|}{d} + 0.5N_u + |V_u - V_p| - A_{ps}f_{po} \right)}{\left(E_s A_s + E_p A_{ps} \right)}$$

Where, f_{po} = average stress in prestressing steel or $0.7f_{pu}$

An important difference between the simplified and iterative MCFT approaches in Method 2 is seen in equation 7.59. The longitudinal strain, ϵ_s , at the level of the tensile force is used for the simplified approach. The iterative approach presented in LRFD Appendix B5 uses the average longitudinal strain in the section. A longitudinal strain of $\epsilon_s/2$ is used, which assumes that the strain at the level of the center of compression is small.

Equation 7.59 includes another adjustment to produce the simplified version of Method 2. By equilibrium, the horizontal component of the compressive strut force divided into the two flanges should be:

$$\text{(Eqn. 7.60)} \quad F = 0.5(V_u - V_p) \cot \theta$$

The simplified Method 2 fixes the angle θ in this equation such that its cotangent is equal to 2.0 ($\theta \approx 26.6^\circ$). This reduces the equation for horizontal components in the flanges to:

$$\text{(Eqn. 7.61)} \quad F = V_u - V_p$$

In using equation 7.61 the following considerations should be applied:

- The absolute value of the factored moment, $|M_u|$, acting with the factored shear, V_u , should not be taken less than $|V_u - V_p|$ multiplied by the shear depth, d_v .

- The areas of reinforcing bars and prestressing steel not fully developed at the cross section under consideration should be reduced in proportion to their lack of full development.
- If the longitudinal strain, ϵ_s , calculated by equation 7.61 is negative, it can either be taken equal to zero or recomputed by equation 7.61 where the denominator is replaced with $(E_s A_s + E_p A_{ps} + E_c A_c)$. A_c in this revised denominator is the area of concrete on the flexural side of the member. However, ϵ_s should not be taken less than -0.4×10^{-3} .
- If the axial tension is large enough to crack the flexural compression face of the section, the value calculated by equation 7.61 should be doubled.
- β and θ may be calculated with values of ϵ_s larger than that predicted by equation 7.61. However, ϵ_s should not be taken greater than 6.0×10^{-3} .

With the sectional forces resolved into the idealized cross section and the longitudinal strain computed, the shear resistance contributed by the concrete can be determined. LRFD Article 5.8.3.3 defines this contribution for the simplified form of Method 2:

$$\text{(Eqn. 7.62)} \quad V_c = 0.0316\beta\sqrt{f'_c}b_v d_v$$

The parameter β , for the simplified approach, is defined in LRFD Article 5.8.3.4.2. When the minimum required web (transverse) reinforcing is provided, β is defined as:

$$\text{(Eqn. 7.63)} \quad \beta = \frac{4.8}{(1 + 750\epsilon_s)}$$

In most cases, the transverse requirements at the critical sections of post-tensioned concrete box girders will require more than the minimum shear reinforcing requirements. This reinforcing is often used throughout the span to simplify the tying of reinforcing steel. The spacing of this reinforcing could be increased where demand is lower, even to that less than the minimum requirements. In this case, the LRFD Specifications provides an equation for β when the minimum amount of transverse reinforcing is not provided. In all cases, the minimum transverse reinforcing spacing requirements must be met.

Note: It is interesting to be aware of the forms that AASHTO LRFD equations take as a result of using consistent units. In the case of equation 7.62 the units are ksi for the concrete strength and inches for b_v and d_v . The parameter β has no units. Historically, the concrete contribution to shear resistance was first expressed as a function of the concrete strength in psi. Later, this contribution was defined as a multiple of the square root of the concrete strength (again in psi), with that multiple typically ranging between a factor of 2 and 4. This multiple is now expressed as the β term, with the constant of 0.0316 added for consistent units of ksi. Though more cumbersome in appearance, it may be that equation is better understood from the historical perspective as:

$$V_c = \beta \left(0.0316\sqrt{f'_c} \right) b_v d_v = \beta \sqrt{f'_c} b_v d_v \left(\frac{1}{\sqrt{1000}} \right)$$

The concrete strength term in the last expression of this equation is in psi. The engineer is encouraged to consider other LRFD equations of similar form in order to retain the historical development of the code.

7.4.4.2 Method 3 (Historical Empirical)

Past editions of the AASHTO Standard Specifications for Bridge Design included an approach to shear design based on the nature of girder cracking initiation. Figure 7.36 shows a portion of a continuous concrete girder with zones that generally define two types of shear cracks and their typical general locations. At the ends of girders and near points of contraflexure girder bending is small and web cracking initiates by principle tensile stresses in the webs large enough to crack the concrete. In regions of significant flexure girders can crack vertically on the tension faces as a result of longitudinal flexural stresses greater than the tensile capacity of the concrete. If cracking continues into the webs, the effect of shear stresses in these regions can change the direction of these cracks in the webs to be inclined shear cracks.

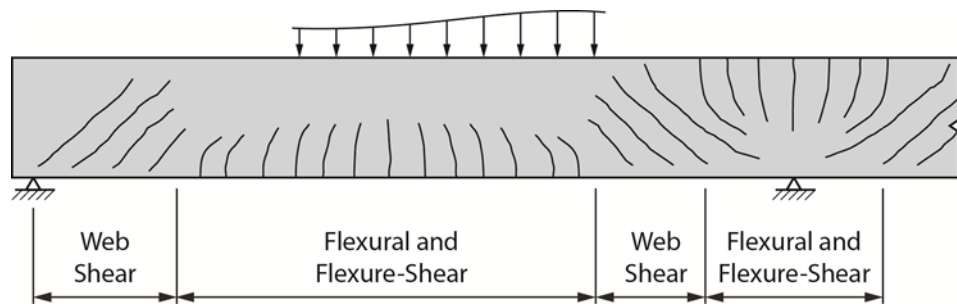


Figure 7.36 – Types and Locations of Reinforced and Prestressed Girder Cracking

The contribution of the concrete in Method 3 is different depending on the type of cracking likely to be found. Two resistance expressions, one for each type of cracking, are defined in LRFD Article 5.8.3.4.3. This article requires that concrete resistance for each expression be evaluated, and the lesser of the two be used for design.

In regions of web shear cracking, the expression for the shear capacity of the concrete is determined from LRFD Equation 5.8.3.4.3-3:

$$(Eqn. 7.64) \quad V_{cw} = \left(0.06\sqrt{f'_c} + 0.30f_{pc} \right) b_v d_v + V_p$$

Where: f_{pc} = compressive stress at the center of gravity of the cross section after all losses (ksi)

The first term of equation 7.64 represents, in the form of a shear force, a principle tension in the web required to offset the axial compression from the post-tensioning and a conservative estimate of the tensile strength of the concrete. This combination of terms was empirically derived. The second term of equation 7.64 represents the vertical component of the post-tensioning at the section. When equation 7.64 governs the evaluation of the concrete resistance, V_p in equation 7.52 (LRFD Equation 5.8.3.3-1) is set equal to zero.

In regions of flexure-shear cracking, the expression for the shear capacity of the concrete is determined from LRFD Equation 5.8.3.4.3-1:

$$(Eqn. 7.65) \quad V_{ci} = 0.02\sqrt{f'_c} b_v d_v + V_d + \frac{V_i M_{cre}}{M_{max}} \geq 0.06\sqrt{f'_c} b_v d_v$$

Where: V_d = shear force at section due to the unfactored combination of DC and DW (kips)
 V_i = factored shear force at section due to externally applied loads occurring simultaneously with M_{max} (kips)
 M_{cre} = moment causing flexural cracking moment at section due to externally applied loads (kip-in)
 M_{max} = moment causing flexural cracking moment at section due to externally applied loads (kip-in)

The second and third terms of equation 7.65 represent a shear force consistent with a bending moment that causes cracking at the section. The first term of equation 7.65 is an empirically derived expression that accounts for an increase concrete resistance developed as the flexure crack transforms into a shear crack.

7.4.5 Shear Resistance from Transverse (Web) Reinforcing Steel (V_s)

The contribution to the nominal shear capacity of a cross section from transverse (web) reinforcing is based on the number and orientation of the transverse reinforcing relative to the design length of shear crack. Figure 7.37 shows a portion of a girder cracked by shear. The reinforcing in this figure is oriented vertically and is spaced along the length of the girder at a spacing s . At each bar location there is a resisting force equal to the area of the reinforcing times the yield strength. (The area of reinforcing would be the total of all bars in all webs for a multi-cell box girder where a spine beam analysis and global forces are used without distinction for specific distribution factors to the webs.)

Whether Method 2 (Simplified MCFT) or Method 3 (Historical Empirical) are used to determine the contribution of the concrete in resisting shear, the shear depth, d_v , multiplied by the cotangent of the inclination of the diagonal strut is used to determine the number of bars participating to resist shear at the section.

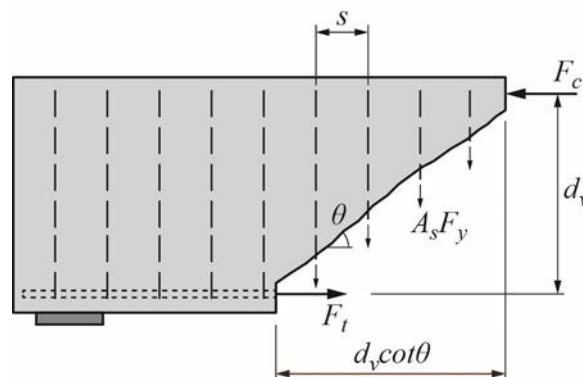


Figure 7.37 – Contribution of Shear Reinforcing to Nominal Shear Resistance

The general expression for the shear contribution of the transverse reinforcing is determined by LRFD Equation 5.8.3.4.3-3:

$$(Eqn. 7.66) \quad V_s = \frac{A_v f_y d_v (\cot \theta + \cot \alpha) \sin \alpha}{s}$$

Where: A_v = area of transverse reinforcement within distance s (in²)
 f_y = minimum yield strength of reinforcing bars (ksi)
 d_v = effective shear depth, taken as the distance between the resultants of the tensile and compressive forces due to flexure; it need not be taken less than the greater of $0.9d_e$ or $0.72h$, where d_e is the distance from the extreme compression fiber to the centroid of the tensile force in the tensile reinforcement, and where h is the overall depth of the member (in)
 s = spacing of reinforcing bars (in)
 θ = angle of inclination of diagonal compressive stresses (degrees)
 α = angle of inclination of the transverse reinforcing from the longitudinal reinforcing

When the transverse reinforcing is placed vertically ($\alpha = 90^\circ$ as shown in figure 7.37), equation 7.66 simplifies to:

$$(Eqn. 7.67) \quad V_s = \frac{A_v f_y d_v \cot \theta}{s}$$

The angle θ that defines the orientation of the diagonal compressive strut is calculated differently in Method 2 and Method 3. When Method 2 is used, the inclination of the compressive strut is equal to:

$$(Eqn. 7.68) \quad \theta = 29 + 3500 \varepsilon_s$$

When Method 3 is used to determine concrete resistance, one of two values for the inclination of the compressive strut, in terms of its cotangent, must be used. If the resistance determined by web cracking (V_{cw}) is greater than that determined by flexure-shear cracking (V_{ci}), the cotangent of the inclination of the compressive strut is taken as:

$$(Eqn. 7.69) \quad \cot \theta = 1.0$$

When V_{ci} is greater than V_{cw} the cotangent of the inclination of the compressive strut is taken as:

$$(Eqn. 7.70) \quad \cot \theta = 1.0 + \left(\frac{f_{pc}}{\sqrt{f'_c}} \right) \leq 1.8$$

7.4.6 Shear Resistance from Vertical Component of Effective Prestressing (V_p)

The shear resistances provided by components of the effective prestressing force in tendons are determined from the geometry of the tendons. For the relatively small variations in tendon profiles in cast-in-place concrete box girder superstructures, the contribution of the prestressing to shear resistance can be taken as:

$$(Eqn. 7.71) \quad V_p = A_{ps} f_{ps} \tan \omega$$

Where: ω = the angle of the tendon at the cross section relative to horizontal (degrees)

Depending on the tendon geometry, the component in the direction of the applied shear can increase or reduce nominal cross section resistance. Tendon components acting against the applied shear force will increase cross section resistance. Tendon components acting with the applied shear force will decrease cross section resistance. Remember that V_p is equal to zero when using Method 3 for determining the concrete shear contribution.

Figure 7.38 shows a simple span post-tensioned beam with a parabolic tendon profile originally presented in figure 3.13.

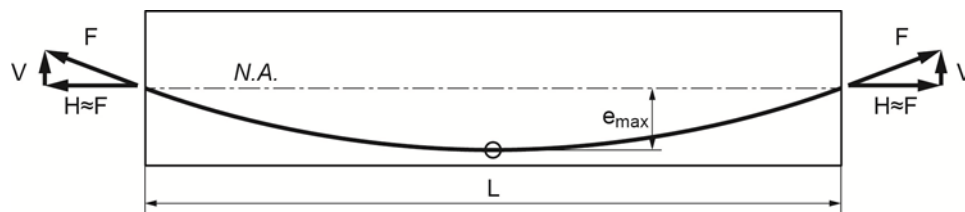


Figure 7.38 – Simple Span Beam with Parabolically Draped Tendon

The eccentricity of the tendon along the length of the tendon was found to be:

(Eqn. 7.71)
$$e(x) = -\frac{4e_{\max}x^2}{L^2} + \frac{4e_{\max}x}{L}$$

The slope of the tendon profile is found by taking the derivative of the equation for eccentricity:

(Eqn. 7.72)
$$\text{slope}(x) = \frac{d}{dx}e(x) = -\frac{8e_{\max}x}{L^2} + \frac{4e_{\max}}{L}$$

The maximum vertical component of the prestressing force, also the resistance provided by the prestressing, is the maximum shear times the effective prestressing force:

(Eqn. 7.73)
$$V_p = \frac{4e_{\max}}{L} F_{\text{eff}}$$

Figures 7.39 and 7.40 show typical draped tendon profiles typically used for continuous post-tensioned box girder bridges. These tendon profiles were previously presented in figures 3.19 and 20. The profiles of these tendons were developed as parabolic segments with slopes compatible with adjacent parabolic segments at their joining.

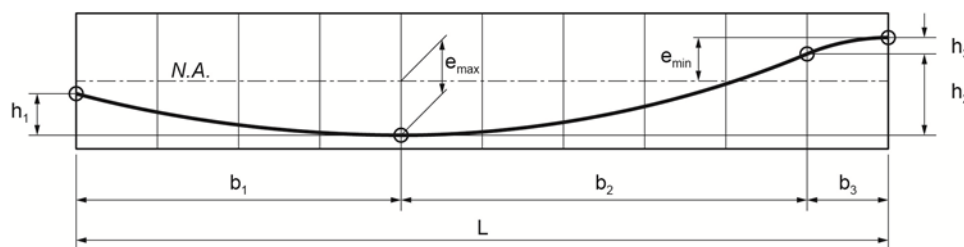


Figure 7.39 – Typical Tendon Profile for an End Span of a Continuous Unit

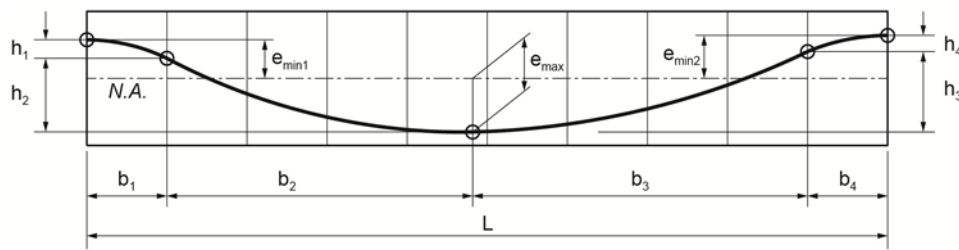


Figure 7.40 – Typical Tendon Profile for an Interior Span of a Continuous Unit

The definition of the parameters of the parabolic segments, presented in chapter 3, is shown in figure 7.41.

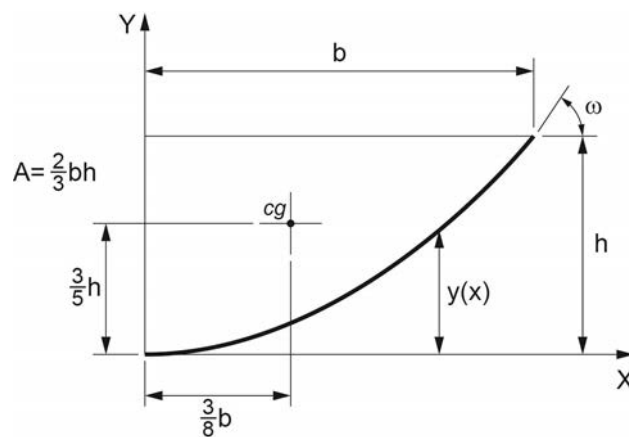


Figure 7.41 – Tendon Profile Parabolic Segment

The elevation of the tendon profile at a horizontal distance from the origin is given as:

(Eqn. 7.74)
$$y = \frac{h}{b^2} x^2$$

The slope of the tendon profile is:

(Eqn. 7.75)
$$\frac{dy}{dx} = \frac{2h}{b^2} x$$

And the angle of the tendon profile at the end of the parabolic segment is:

(Eqn. 7.76)
$$\omega = \frac{dy}{dx}(b) = \frac{2h}{b} (\text{radians})$$

7.4.7 Longitudinal Reinforcing

Regardless of the method used for determining the contribution of the concrete in resisting shear, sufficient tensile capacity in the longitudinal reinforcing is required to appropriately

develop the shear capacity of the cross section. That is to say, the horizontal component of the compression strut in the web has to be resisted by longitudinal tension reinforcement. LRFD Article 5.8.3.5 provides the requirements for the tensile force:

$$(Eqn. 7.77) \quad A_s f_y + A_{ps} f_{ps} \geq \frac{|M_u|}{d_v \phi_f} + 0.5 \frac{N_u}{\phi_c} + \left(\left| \frac{V_u}{\phi_v} - V_p \right| - 0.5 V_s \right) \cot \theta$$

Where: V_s = shear resistance provided by the transverse reinforcing, except that V_s shall not be taken greater than V_u/ϕ

If this inequality is not met, either the transverse or the longitudinal reinforcement must be increased.

7.4.8 Torsion Reinforcing

When torsional forces are large enough to warrant inclusion in design (LRFD Article 5.8.2.1), the transverse reinforcing provided in the webs shall be the sum of that required for shear and for that required for the concurrent torsion. The nominal torsional resistance is presented in LRFD Article 5.8.3.6.2:

$$(Eqn. 7.78) \quad T_n = \frac{2A_o A_t f_y \cot \theta}{s}$$

Where: A_o = area enclosed by the shear flow path around the box girder (in²)
 A_t = total area of transverse torsion reinforcing in the exterior web of the box girder (in²)

The LRFD Specifications also include requirements for the longitudinal reinforcing when torsion is included in the design. For box girders, the longitudinal reinforcing for torsion, in addition to that required for flexure, is:

$$(Eqn. 7.79) \quad A_l = \frac{T_n p_h}{2A_o f_y}$$

Where: p_h = perimeter of the centerline of the transverse reinforcement located in the outer most webs and top and bottom slabs (in)

The longitudinal reinforcing is to be distributed around the outer-most webs and top and bottom slab of the box girder.

Chapter 8—Transverse Analysis

8.1 Introduction

The cross section of a concrete box girder bridge is designed to resist bending moments acting transverse to the longitudinal direction of the bridge span. Transverse analyses are performed to evaluate transverse bending moments resulting from both permanent and live loads. Permanent loads include self weight, barrier rails, sidewalks, wearing surfaces, and utilities that may be attached inside or outside of the box girder superstructure. Live loads are comprised of the AASHTO LRFD Design Truck and Design Tandem, located in design lanes arranged to produce maximum bending moments at critical sections. Figure 8.1 shows typical box girder superstructures, applied loads and likely critical sections. The results of the transverse analysis are used to design the transverse reinforcing and post-tensioning (if required) of the cantilever wings, top slab, webs, and bottom slab.

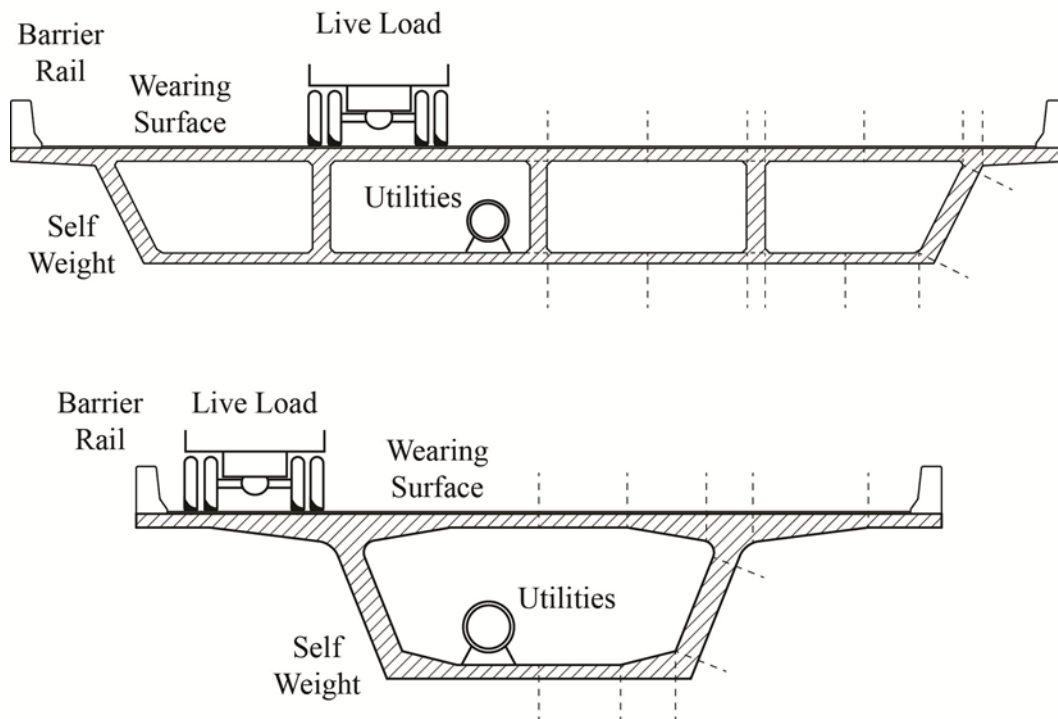


Figure 8.1 – Concrete Box Girder Cross Sections and Loads

8.2 Methods of Analysis

The magnitude and distribution of transverse bending moments due to permanent and live loads vary along the length of a span as a function of the deflection behavior of the box girder. Near supports, where girder deflections are restrained, localized bending moments remain relatively concentrated. Within the span, general longitudinal deflections reduce maximum transverse moments as they are distributed along a greater portion of the span.

AASHTO LRFD provides for three levels of analysis for determining transverse design moments:

- Empirical Method—This method, presented in LRFD Article 9.7, presents required top slab reinforcing for bridges meeting the criteria of Article 9.7.2.4. No guidance for reinforcing or forces in the remainder of the cross section are presented. The use of this method of analysis is not recommended for concrete box girders presented in this manual.
- Approximate Method—Article 4.6.2 presents an approximate method of analysis in where the deck is subdivided into strips perpendicular to the supporting elements (webs). Internal forces are determined first by structural analysis of a unit width of transverse cross section and then by dividing these force and moment results by the width of the strip to determine forces per foot along the superstructure.
- Refined Method—Article 4.6.3 permits the use of refined transverse analyses by methods listed in Article 4.4. One typical approach is to use three-dimensional finite elements methods with sufficient load cases to generate an envelope of transverse design moments. Most often, however, the practicality of detailing and constructing superstructures with uniform reinforcing and post-tensioning details typically overrides small quantity savings that refined methods offer.

This manual uses the Approximate Method for transverse analysis of the concrete box girder cross section, with additional considerations. Multi-cell box girder bridges with three or more cells and with web spacing not greater than 15 feet use the LRFD strip method to determine transverse moments resulting from concentrated wheel loads. Single-cell or dual-cell box girders, and multi-cell box girders with web spacing greater than 15 feet use a refined approach (as presented in section 8.5) to account for longitudinal distribution of concentrated wheel loads in determining the transverse live load moments. Live load moments are then combined with moments resulting from uniformly repeating loads for design.

8.3 Applicable AASHTO LRFD Specifications

AASHTO LRFD Articles governing the design of the concrete box girder cross sections are found in four different Sections of the code. The following subsections summarize the most relevant of these articles to facilitate transverse analysis and design.

8.3.1 Section 9—Deck and Deck Systems

Section 9 provides general guidance for the design of bridge decks. Requirements related to different design limit states are provided in Article 9.5:

9.5.2—Service Limit States

At service limit states, decks and deck systems shall be analyzed as fully elastic structures and shall be designed and detailed to satisfy the provisions of sections 5, 6, 7, and 8. ...

9.5.3—Fatigue and Fracture Limit State

Fatigue need not be investigated for :

- Concrete decks, ...

9.5.4—Strength Limit States

At strength limit states, decks and deck systems may be analyzed as either elastic or inelastic structures and shall be designed and detailed to satisfy the provisions of sections 5, 6, 7, and 8. ...

9.5.5—Extreme Event Limit States

Decks shall be designed for force effects transmitted by traffic and combination railings using loads, analysis procedures, and limit states specified in section 13. ...

Article 9.6 presents requirements particular to the analysis of bridge decks:

9.6.1—Method of Analysis

Approximate elastic methods of analysis specified in Article 4.6.2.1, refined methods specified in Article 4.6.3.2, or the empirical design of concrete slabs specified in Article 9.7 may be used for various limit states as permitted in Article 9.5.

9.6.2—Loading

Loads, load positions, tire contact area, and load combinations shall be in accordance with the provisions of section 3.

Article 9.7 contains requirements particular to concrete deck slabs:

9.7.1.1—Minimum Depth and Cover

Unless approved by the owner, the depth of a concrete deck, excluding any provision for grinding, grooving, and sacrificial surface, should not be less than 7.0 in.

Minimum cover shall be in accordance with the provisions of Article 5.12.3.

8.3.2 Section 3—Loads

Section 3 presents the various loadings and load combinations for bridge design. Article 3.6.1.3.3 directs that only the design axles (comprised of wheel loads) of the HL93 and design tandem need be used in transverse design:

3.6.1.3.3- Design Loads for Decks, Deck Systems, and the Top Slabs of Box Culverts

...Where the approximate strip method is used to analyze decks and top slabs of culverts, force effects shall be determined on the following basis:

- Where the slab spans primarily in the transverse direction, only the axles of the design truck of Article 3.6.1.2.2 or design tandem of Article 3.6.1.2.3 shall be applied to the deck slab or the top slab of box culverts. ...

Wheel loads shall be assumed to be equal within an axle unit, and amplification of the wheel loads due to centrifugal and braking forces need not be considered for the design of decks.

The live loads of the Design Truck and Design Tandem are shown in adjacent lanes in figure 8.2.

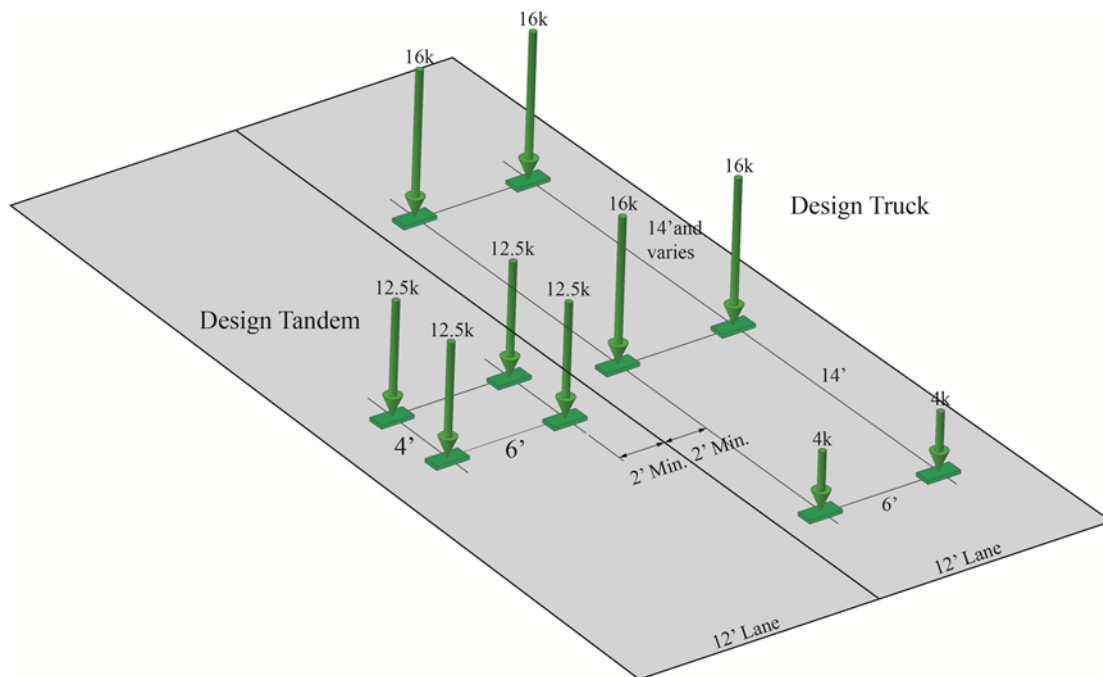


Figure 8.2 – AASHTO LRFD Design Truck and Design Tandem

Location of the applied wheel loads are in accordance with Article 3.6.1.3:

3.6.1.3—Application of Design Vehicular Live Loads

...Both the design lanes and the 10 ft loaded width in each lane shall be positioned to produce extreme force effects. The design truck or tandem shall be positioned transversely such that the center of any wheel load is not closer than:

For the design of the deck overhang—1.0 ft from the face of the curb or railing, and...

For the design of all other components—2.0 ft from the edge of the design lane. ...

Figure 8.3 shows an example loading with two lanes placed at the left side of a box girder cross section developed in chapter 5 (also design example 1 in appendix C). In this figure, the left most truck is located for design of the overhang. Respecting that, trucks are positioned within 10' loaded widths, and that loaded width is located within in the 12' lane, the left wheel of the adjacent truck is positioned no closer than 7' to the right wheel of truck on the left.

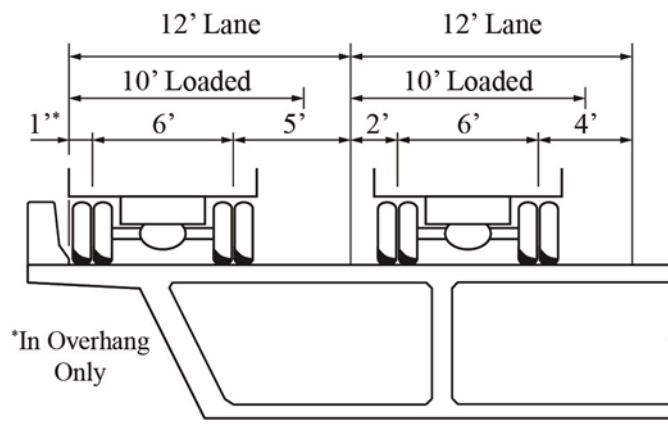


Figure 8.3 – Transverse Truck Placement

When web spacing is small, the application of the wheel loads as uniform pressures, as opposed to concentrated loads, can impact the top slab bending moments. The 16 kip HL93 truck wheel loads or 12.5 kip tandem wheel load may be distributed in accordance with Article 3.6.1.2.5:

3.6.1.2.5—Tire Contact Area

The tire contact area of a wheel consisting of one or two tires shall be assumed to be a single rectangle, whose width is 20.0 in and whose length is 10.0 in...

Figure 8.4 shows the tire contact area in the transverse direction of a concrete box girder bridge. The load width at the center of gravity of the top slab is equal to the 20" transverse tire contact dimension, further distributed at 45 degrees on either side over half of the slab thickness. The resulting loaded width is 20" plus the slab thickness.

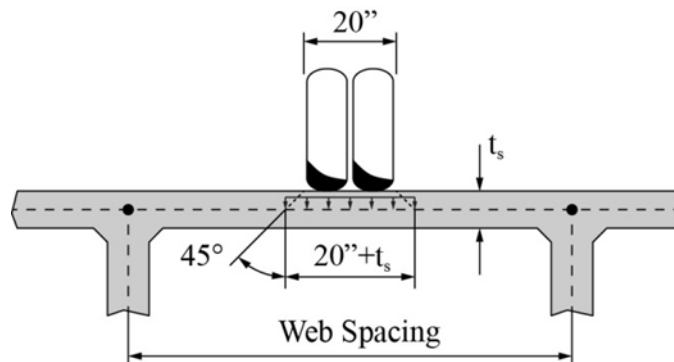


Figure 8.4 – Tire Contact Area in the Transverse Direction

An optional vertical design load for the overhanging slab (cantilever wing) of the box girder is provided in Article 3.6.1.3.4. This loading is shown in figure 8.5

3.6.1.3.4—Deck Overhang Load

For the design of deck overhangs with a cantilever, not exceeding 6.0 ft from the centerline of the exterior girder to the face of a structurally continuous concrete railing, the outside row of wheel loads may be replaced with a uniformly distributed line load of 1.0 klf intensity, located 1.0 ft from the face of the railing.

Horizontal loads on the overhang resulting from vehicle collisions with barriers shall be in accordance with the provisions of section 13.

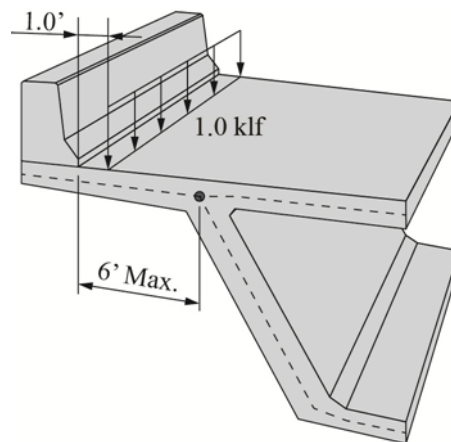


Figure 8.5 – Alternate Vertical Loading for Overhang Design

8.3.3 Section 4—Analysis

This manual uses the Approximate Method, or Strip Method, of analysis for the design of the transverse cross section of concrete box girder superstructures. Article 4.6.2 presents guidance for this analysis approach.

4.6.2.1—Decks

An approximate method of analysis in which the deck is subdivided into strips perpendicular to the supporting components shall be considered acceptable for decks other than:

- Fully filled and partially filled grids for which the provisions of Article 4.6.2.1.8 shall apply, and
- Top slabs of segmental concrete box girders for which the provisions of 4.6.2.9.4 shall apply.

Where the strip method is used, the extreme positive moment in any deck panel between girders shall be taken to apply to all positive moment regions. Similarly, the extreme negative moment over any beam or girder shall be taken to apply to all negative moment regions.

Figure 8.6 shows a perspective of the four-cell box girder developed in chapter 5 (design example problem 1, appendix C).

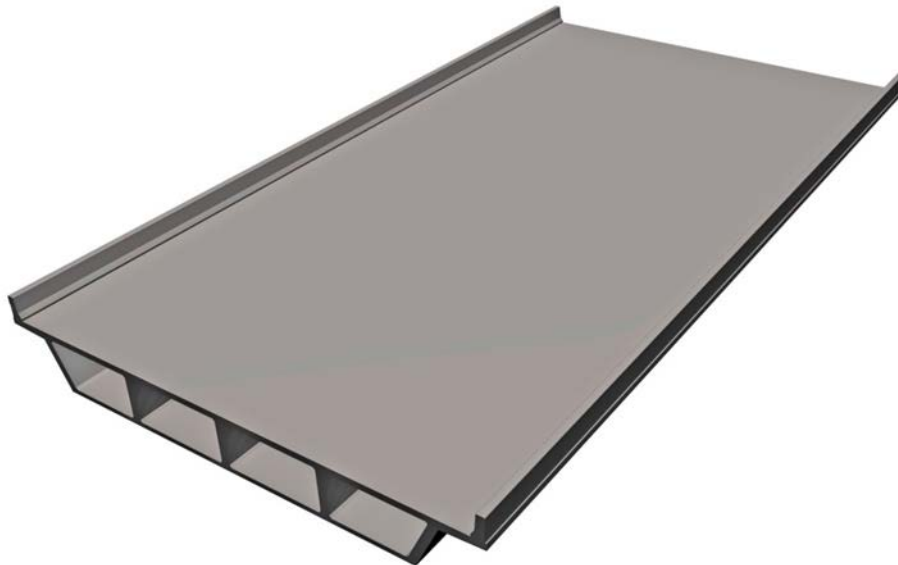


Figure 8.6 – Perspective of Multi-cell Box Girder

Figure 8.7 shows the transverse strip used for computing the longitudinal distribution of concentrated wheel loads.

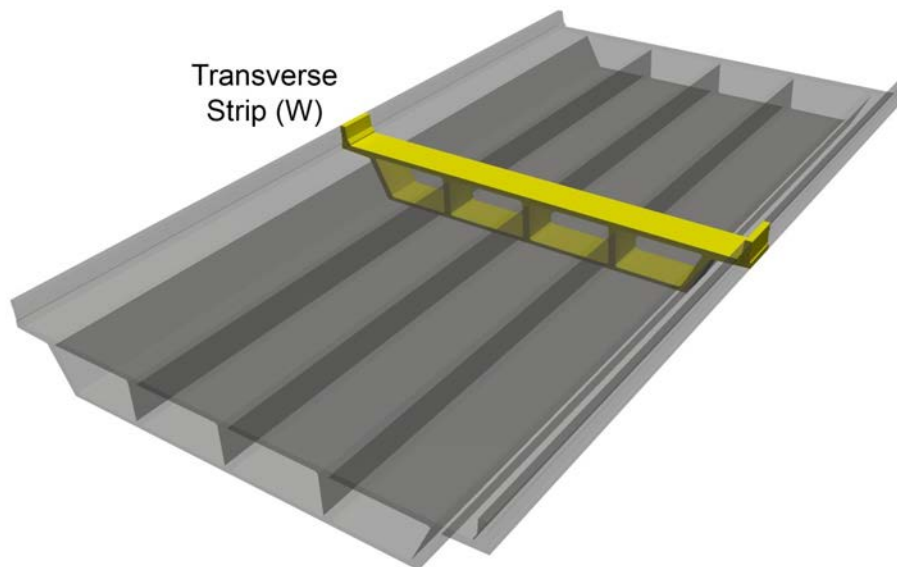


Figure 8.7 – Transverse Strip for Approximate Design Method

Figure 8.8 shows an example loading of the Design Truck in two lanes positioned to the left of the roadway width as depicted in cross section view in figure 8.3.

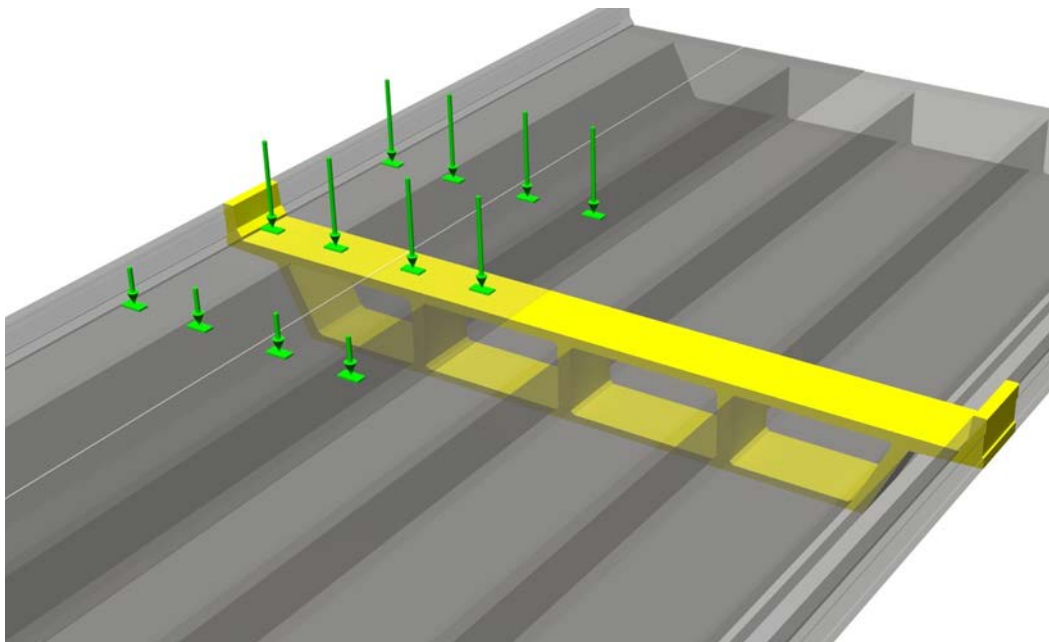


Figure 8.8 – Transverse Strip subjected to two Design Trucks as per Figure 8.3

The longitudinal length of the transverse strip is specified in Article 4.6.2.1.3:

4.6.2.1.3—Width of Equivalent Interior Strips

The width of the equivalent strip of a deck may be taken as specified in Table 4.6.2.1.3-1. ...

...The equivalent strips for decks that span primarily in the transverse direction shall not be subject to width limits....

Equations for the width of the transverse strip in the longitudinal direction from Table 4.6.2.2.1-1 for cast-in-place concrete box girder bridges are:

$$\text{(Eqn. 8.1)} \quad W = 45.0 + 10X \quad (\text{Overhang})$$

$$\text{(Eqn. 8.2)} \quad W = 26.0 + 6.6S \quad (\text{Positive Moment})$$

$$\text{(Eqn. 8.3)} \quad W = 48.0 + 3.0S \quad (\text{Negative Moment})$$

Where, S = spacing of supporting components (ft)
 X = distance from load to point of support (ft)
 W = width of transverse strip in the longitudinal length of transverse strip (in)

Article 4.6.2.1.7 requires that the transverse cross section of the box girder bridge be modeled for frame action.

4.6.2.1.7—Cross-Sectional Frame Action

Where decks are an integral part of box or cellular cross sections, flexural and/or torsional stiffnesses of supporting components of the cross section, i.e., the webs and bottom flange, are likely to cause significant force effects in the deck. Those components shall be included in the analysis of the deck.

If the length of a frame segment is modeled as the width of an equivalent strip, provisions of Articles 4.6.2.1.3, 4.6.2.1.5, and 4.6.2.1.6 may be used.

Article 4.6.2.1.6 presents that the critical sections for negative moments and shear of concrete box girders (Section Type “d” in Table 4.6.2.2.1-1) is at the face of the supporting component, the webs.

4.6.2.1.6—Calculation of Force Effects

...The design section for negative moments and shear forces, where investigated, may be taken as follows:

- For monolithic construction, closed steel boxes, closed concrete boxes, open concrete boxes without top flanges, and stemmed precast beams, i.e., cross sections (b), (c), (d), (e), (f), (g), (h), (i), and (j) from Table 4.2.6.2.2.1-1, at the face of the supporting component.

8.3.4 Section 13—Railing

Article 13 presents requirements for the design of overhangs (cantilever wings) with regard to vehicle crash loadings on barriers. The intent of the specifications is that overhangs have sufficient strength such that the barrier fails first with respect to the design forces. Article A13.4.1 presents two design cases to assure this intention is achieved. The third design case presented in this Article is the case of normal traffic loading.

A13.4.1—Design Cases

Bridge deck overhangs shall be designed for the following design cases considered separately:

Design Case 1: the transverse and longitudinal forces specified in Article A13.2—Extreme Event Load Combination II limit state

Design Case 2: the vertical forces specified in Article A13.2—Extreme Event Load Combination II limit state

Design Case 3: the loads, specified in Article 3.6.1, that occupy the overhang—Load Combination Strength I limit state

For Design Case 1 and 2, the load factor for dead load, γ_P , shall be taken as 1.0.

Extreme Event Load Combination II for the design of the overhang with regard to vehicle collision can be reduced to:

$$(Eqn. 8.4) \quad M_u = 1.0DC + 1.0DW + 0.5(LL + IM) + 1.0CV$$

Two cross sections of the overhang should be verified at this limit state: 1) at the face of the barrier and 2) at the root of the cantilevering overhang. The first section is subject to a small portion of overhang slab, the weight of the barrier rail, and collision forces. The second section includes the remainder of the overhang self weight and vertical wheel loads along the cantilever length. Figure 8.9 shows these two critical sections for the cross section of the overhang to be designed for the overhang presented for the cross section developed in chapter 5.

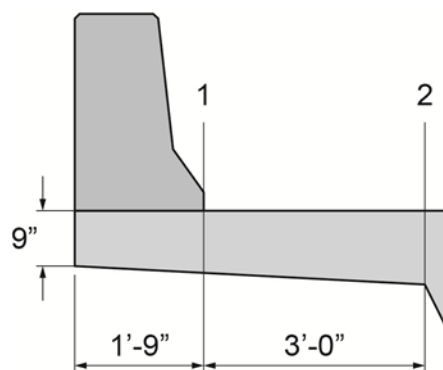


Figure 8.9 – Critical Sections for Overhang Design to Develop Barrier Railing

Design loads and dimensional considerations for Design Load Cases 1 and 2 specified in Article A13.4.1 are presented in Article A13.2. The magnitude of the loads and dimensional considerations are a function of the crash testing rating of the barrier railing used on the bridge. The superstructures of the design examples in this manual use concrete parapet type barrier railing with a TL-4 crash test rating. Design forces for this railing are taken from Table A13.2-1:

Design Forces and Designations	TL-4 Crash Test Level
F_t Transverse (kips)	54.0
F_L Longitudinal (kips)	18.0
F_v Vertical (kips) Down	18.0
L_t and L_L (ft)	3.5
L_v (ft)	18.0
H_e (min)(in.)	32.0
Minimum H Height of Rail (in.)	32.0

Table 8.1 – Railing Loads for TL-4 Barrier (from AASHTO LRFD Table A13.2-1)

There are some interesting considerations with regard to the application of Articles A13.4.1 and A13.2:

- Design Load Case 2 has implications with regard to Post-and-Beam railings, but will not govern for overhangs with concrete parapet barriers.
- The longitudinal loads shown in Table A13.2-1 also have implications with regard to Post-and-Beam railings, but are not meaningful with regard to bridges with concrete parapet barriers away from railing ends.
- Loads from Table A13.2-1 applied over the specified lengths plus a distribution of 45 degrees over the height of the barrier. This results in a width of application of the forces in Table A13.2-1 (also table 8.1) of the specified length plus twice the height of the barrier railing.

Articles A13.4.2 and A13.4.3 present alternate design approaches to Design Case 1 for bridges that use concrete parapet and post-and-beam rail. Article A13.4.2 is presented here for the very common concrete parapet type of barrier rail.

Article A13.4.2—Decks Supporting Concrete Parapet Railings

For Design Case 1, the deck overhang may be designed to provide a flexural resistance, M_s in kip-ft/ft which, acting coincident with the tensile force T in kip/ft, specified herein, exceeds M_c of the parapet at its base. The axial tensile force, T , may be taken as:

$$(Eqn. 8.5) \quad T = \frac{R_w}{L_c + 2H}$$

Where,

R_w = parapet resistance specified in Article A13.3.1(kips)

L_c = critical length of the yield line failure pattern (ft)

H = height of wall (ft)

T = tensile force per unit of deck length (kip/ft)

Design of the deck overhang for the vertical forces specified in Design Case 2 shall be based on the overhanging portion of the deck.

The parapet resistance, R_w , and critical length R_w , are taken from Article A13.3.1

$$(Eqn. 8.6) \quad R_w = \left(\frac{2}{2L_c - L_t} \right) \left(8M_b + 8M_w + \frac{M_c L_c^2}{H} \right)$$

$$(Eqn. 8.7) \quad L_c = \frac{L_t}{2} + \sqrt{\left(\frac{L_t}{2} \right)^2 + \frac{8H(M_b + M_w)}{M_c}}$$

Where,

F_t = transverse force specified in Table A13.2-1 assumed to be acting at top of a concrete wall (kips)

H = height of wall (ft)

L_c = critical length of yield line failure pattern (ft)

L_t = longitudinal length of distribution of impact force F_t (ft)

R_w = total transverse resistance of the railing (kips)

M_b = additional flexural resistance of beam in addition to M_w , if any, at top of wall (ft-k)

M_c = flexural resistance of cantilevered walls about an axis parallel to the longitudinal axis of the bridge (kip-ft/ft)

M_w = flexural resistance of the wall about its vertical axis (kip-ft/ft)

8.4 Strip Method Analysis for a Multi-Cell Box Girder Superstructure

This section presents the transverse analysis of the four-cell box girder used in the preliminary design presented in chapter 5 and in example problem 1 presented in appendix C.

8.4.1 The Transverse Model

The transverse analysis of the cross section shown in figure 8.9 is a two-dimensional solution that can be performed using either a 2D or 3D general-purpose frame analysis program. The three-dimensional analysis will typically require additional support conditions out of the model plane to provide needed analytical stability.

The analysis performed is a linear elastic analysis utilizing gross section properties of the concrete cross section. The top slabs, bottom slabs, webs, and overhangs are modeled as beam elements with depths equal to their representative thicknesses. The width of the beam elements “out of the plane of the page” is set equal to 1.0'. Node locations are provided at intersections of elements, changes in transverse member thickness, changes in transverse member orientation, and for convenience at locations of desired output.

Vertical support of the cross section model is with rigid supports at the bottom of the webs (Article 4.6.2.1.6 Paragraph 1). A horizontal support is placed rigidly to restrain the transverse movement of the bottom slab. A second horizontal support is provided to restrain the frame against side-sway, which better represents the torsional stiffness of the box girder with regard to transverse displacements.

Figure 8.10 shows the development of the cross section from transverse dimensions, to idealized members to the computer nodal analysis model for the cross section of Design Example 1.

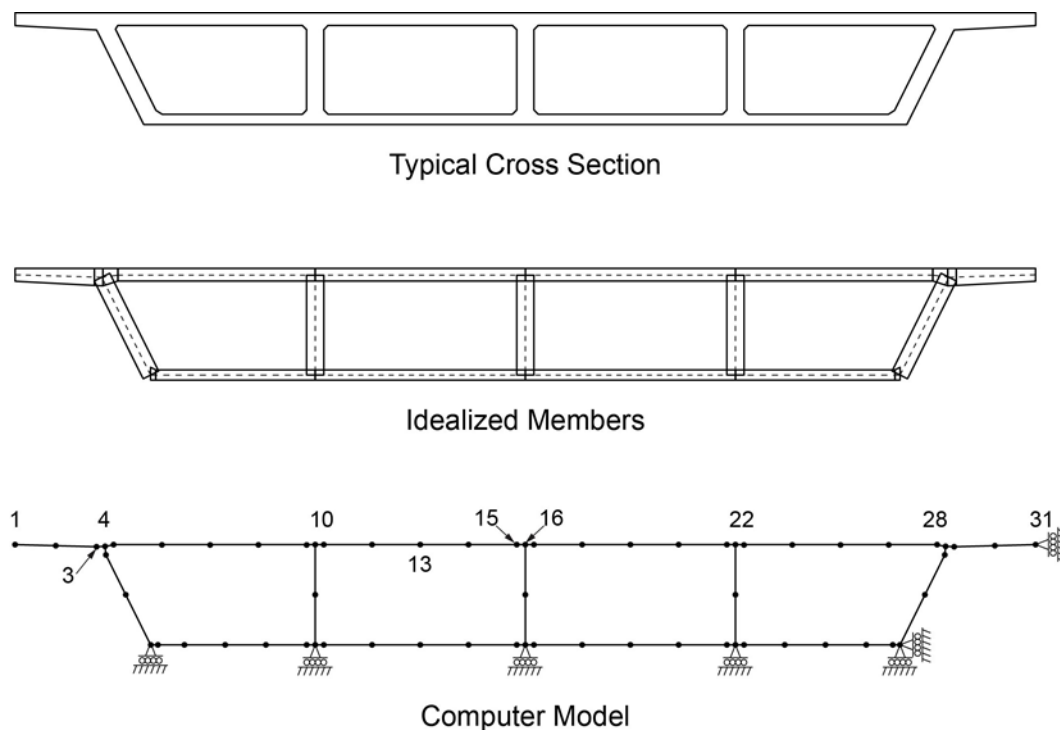


Figure 8.10 – Developing the Two-Dimensional Transverse Model

8.4.2 Transverse Bending Moment Results

Loads that uniformly repeat along the span can be applied directly to the analytical model without consideration for longitudinal distribution. These loads include self weight and superimposed dead loads such as barrier railing, wearing surfaces, and suspended utilities.

Figure 8.11 shows the bending moments from the self weight of the cross section. The analysis software used developed the applied loads internally based on the member cross section dimensions and the unit weight of the concrete. Figure 8.12 shows the effect of barrier railing weight 0.45 kips/foot, applied at the center of gravity of the barrier cross section. Figure 8.13 shows the bending moments resulting from the application of a 25 psf (or 25plf in the unit width model) wearing surface.

Small bending moments in webs and bottom slab members are not shown in some of the figures of this Section for clarity.

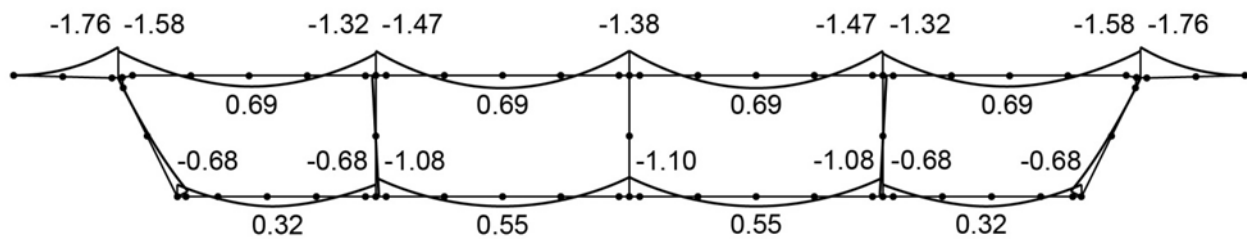


Figure 8.11 – Transverse Self Weight Moments (ft-kip/ft)

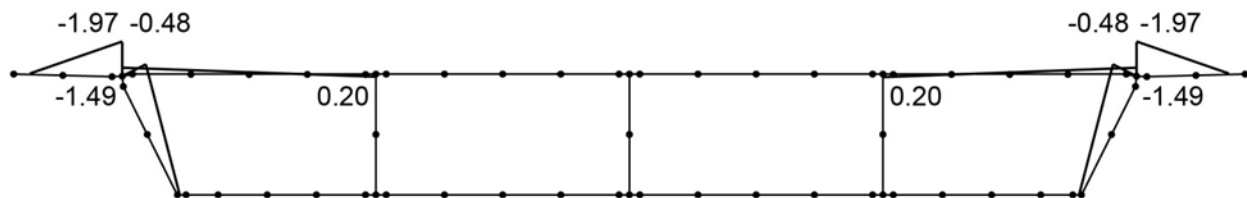


Figure 8.12 – Transverse Barrier Railing Moments (ft-kip/ft)

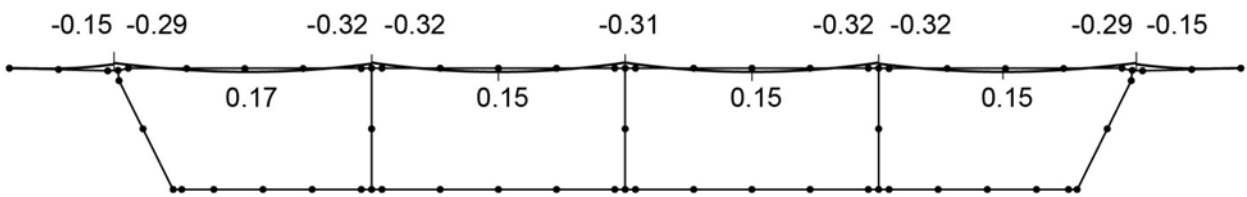


Figure 8.13 – Transverse Wearing Surface Moments (ft-kips/ft)

Live load moments are determined by positioning both the Design Truck and Tandem wheel loads in position to produce maximum transverse moments. Figures 8.14, 8.15 and 8.16 show the results of three load cases for the Design Truck. Figure 8.14 shows the position of one truck to produce maximum negative transverse bending at the inside face of the outer webs. Figure 8.15 shows two trucks positioned to produce maximum transverse negative moment at interior webs. Figure 8.16 shows the load case producing maximum positive moment in the top slab.

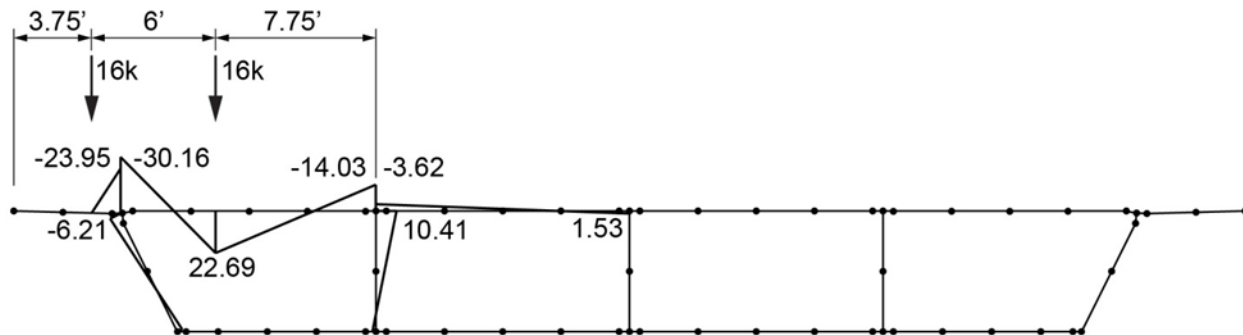


Figure 8.14 – Maximum Negative Design Truck Moment in Outer Web

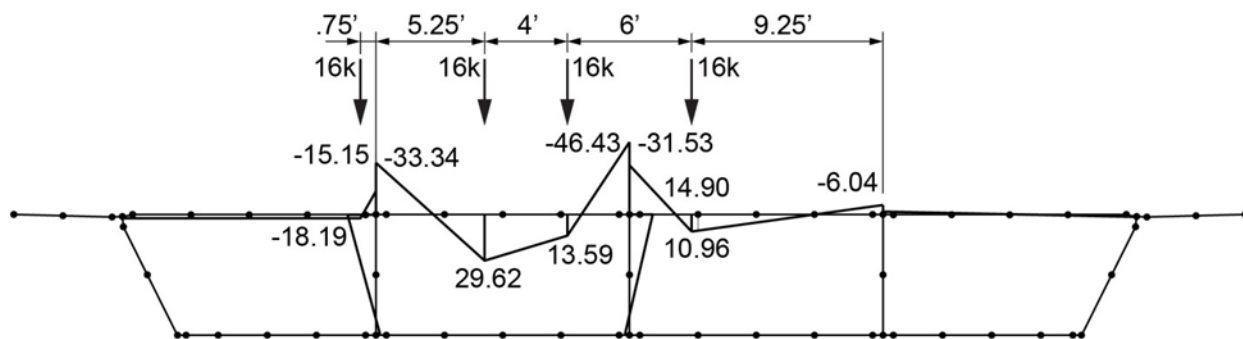


Figure 8.15 – Maximum Negative Design Truck Moment at Inner Web

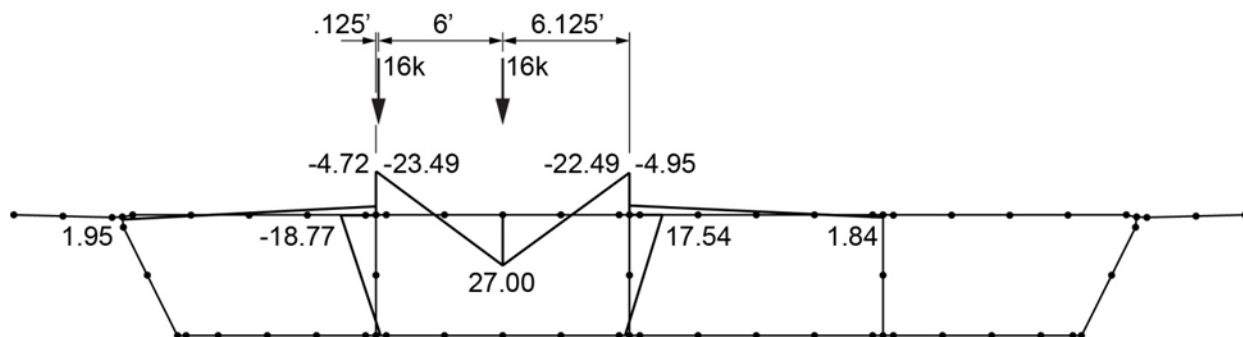


Figure 8.16 – Maximum Positive Design Truck Moment in Top Slab

8.4.3 Transverse Design Moments

Moment results for live load cases need to be magnified for impact and multiple presence factors, and then divided by the longitudinal length of the strips, W , based on equations 8.1, 8.2 and 8.3.

$$\text{(Eqn. 8.8)} \quad W = 45.0 + 10X = 45.0 + 100 = 65" = 5.42'$$

$$\text{(Eqn. 8.9)} \quad W = 26.0 + 6.6S = 26.0 + 6.6(12.25) = 106.85" = 8.90'$$

$$\text{(Eqn. 8.10)} \quad W = 48.0 + 3.0S = 48.0 + 3.0(12.25) = 84.75" = 7.06'$$

Bending moment results from the transverse analysis of example problem 1 at critical nodes in foot-kips/foot are:

Node	Type	Self Weight	Barrier	Wearing Surface	Live Load
3	Overhang (Neg)	-1.76	-1.97	-0.15	-32.00
13	Top Slab (Pos)	0.69	0.0	0.15	27.00
15	Top Slab (Neg)	-1.06	0.0	-0.24	-36.42

Table 8.2 – Transverse Bending Moment Results from Frame Analysis

Live Load bending moments are magnified by vehicle impact and multi-presence factors, and divided over their associated strip width.

The negative live load moment in the overhang at the face of the web is:

$$\text{(Eqn. 8.11)} \quad M_{\max}^- = \frac{1.33(1.2)(-32)}{5.42} = -9.42 \frac{ft-k}{ft}$$

It is interesting to note the magnitude of the overhang moment with regard to the moment caused by a 1 kip/foot load acting 1' from the face of the railing as permitted by Article 3.6.1.3.4. This moment would be approximately 1/3 of the moment predicted by the strength method:

$$\text{(Eqn. 8.12)} \quad M_{\max}^- = 1.33(1.2)(-2.0) = -3.19 \frac{ft-k}{ft}$$

The top slab maximum positive live load moment:

$$\text{(Eqn. 8.13)} \quad M_{\max}^+ = \frac{1.33(1.2)(27.00)}{8.90} = 4.84 \frac{ft-k}{ft}$$

The negative live load moment in the top slab at the face of the middle web:

$$\text{(Eqn. 8.14)} \quad M_{\max}^- = \frac{1.33(1.0)(-36.42)}{7.06} = -6.86 \frac{ft-k}{ft}$$

The resulting factored moments for the AASHTO LRFD Strength I case are then:

$$(Eqn. 8.15) \quad M_3 = 1.25(-1.76 - 1.97) + 1.5(-.15) + 1.75(-9.42) = -21.37 \frac{ft-k}{ft}$$

$$(Eqn. 8.16) \quad M_{13} = 1.25(0.69 + 0) + 1.5(.15) + 1.75(4.84) = 9.56 \frac{ft-k}{ft}$$

$$(Eqn. 8.17) \quad M_{15} = 1.25(-1.06 - 0) + 1.5(-.24) + 1.75(-6.86) = -13.69 \frac{ft-k}{ft}$$

The three critical cross sections are designed for the amount of required reinforcing per foot along the length of the bridge. Reinforcing for the maximum positive and maximum negative ultimate moments is used in each slab and over each web. Additional reinforcing may be required over the outer webs in order to develop the capacity of the barrier when subjected to vehicle collision forces.

8.5 Top Slab Transverse Bending Moment Results for a Single-Cell Box Girder

8.5.1 Introduction

Section 8.2 of this Manual presented limitations on the use of the LRFD Approximate Method for certain concrete box girder cross sections. The method can produce unconservative results when applied directly to single-cell girders, dual-cell girders, and multi-cell box girders with web spacing greater than 15 feet. Using a refined approach to account for longitudinal distribution of concentrated wheel loads in determining the transverse live load moments can produce the needed conservatism.

The approach taken is the same as specified in Article 4.6.2.9.4 for concrete box girders built segmentally. Differences in transverse behavior does not lie in the method of construction, but the fact that the majority of box girder bridges built segmentally are constructed with 2 webs (single cell) or 3 webs (dual cell), resulting in significant slab spans for most common roadway widths.

Figure 8.17 shows the cross section of a single-cell box girder that will be analyzed in this Section with regard to transverse flexure.

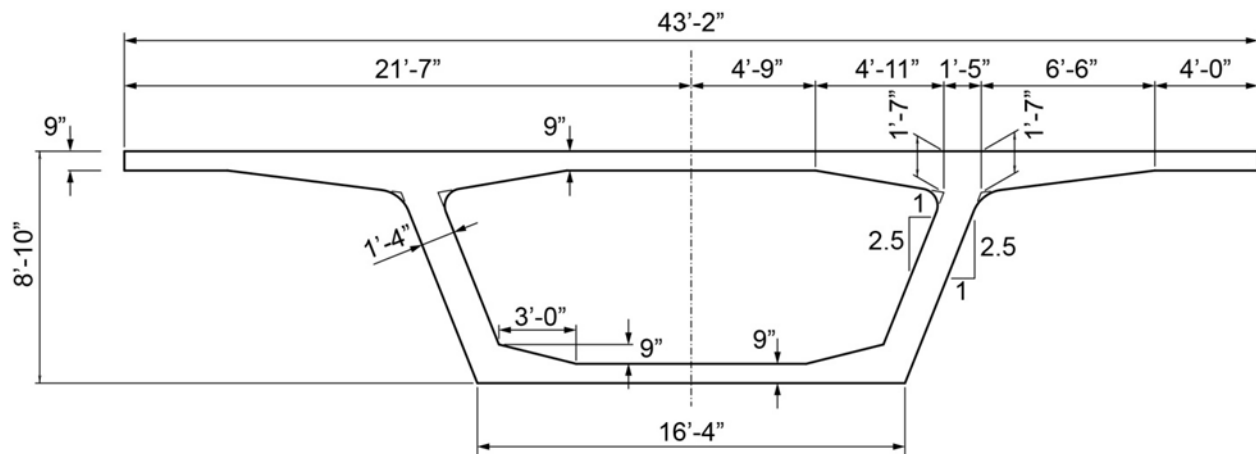


Figure 8.17 – Typical Single-Cell Box Girder Cross Section Defined at Mid-Span

Figure 8.18 shows a perspective of a span with the cross section under consideration. As before, a typical cross section with a unit length is identified in the span for a two-dimensional analysis in the plane of the cross section. The extracted typical section for analysis is shown in figure 8.19.

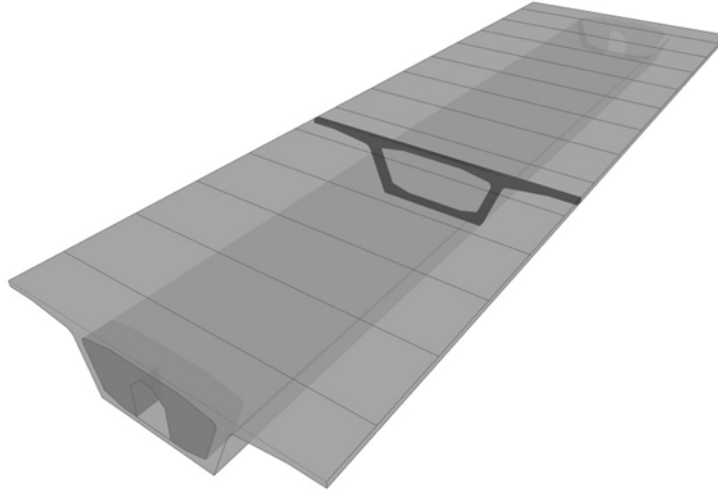


Figure 8.18 – Typical Single-Cell Box Girder Span with Cross Section Defined at Mid-Span



Figure 8.19 – One Foot Section of Typical Cross Section

The typical cross section is modeled using beam elements in a general two-dimensional structural analysis program. Figure 8.20 shows the transition from typical cross section, to idealized beam members, to a node and element layout for a typical analysis model. Special transverse modeling considerations include:

- a. The model shown in figure 8.20 shows beam elements extending to nodes at the top of web/cantilever/top slab intersection and the bottom of web/bottom slab intersection. Often, designers will model a portion of these intersecting members as rigid elements, as the size of the connection can be significant with regard to member length.

- b. Many precast single-cell box girder cross sections include linear or circular fillets at the cantilever/top of web and top slab/top of web connections. The choice of the critical sections for design of flexure at these sections is left to the discretion of engineer considering the particular geometry of the cross section.
- c. Vertical supports are placed under the webs as shown in the bottom sketch of figure 8.20. One horizontal support is required for model stability. A second horizontal support has been added to restrain side-sway of the two-dimensional model. This support helps account for the torsional rigidity of the box girder in the actual three-dimensional structure. This second horizontal support can be problematic for some load cases such as transverse post-tensioning. Use and placement of the second support is left to the discretion of the engineer.

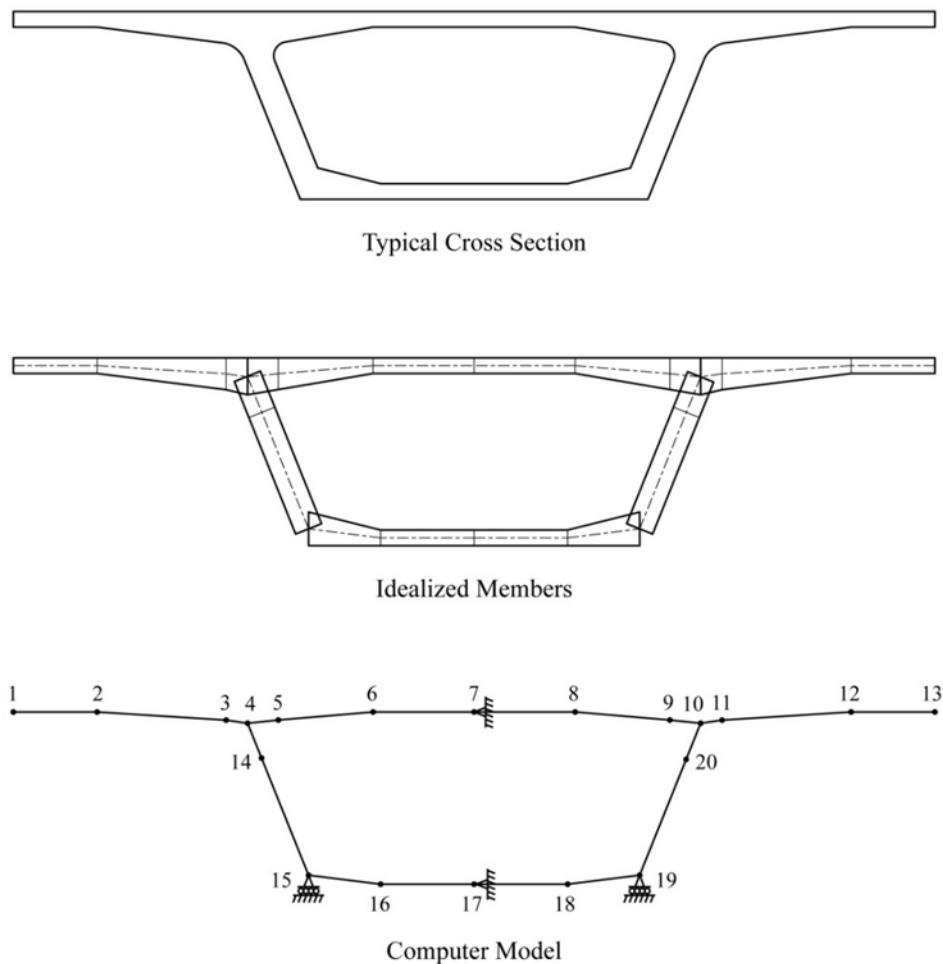


Figure 8.20 – Developing the Two-Dimensional Transverse Model

8.5.2 Analysis for Uniformly Repeating Loads

Transverse bending moments for loads that repeat uniformly along the span can be determined directly from the two-dimensional analysis mode. Self weight bending moments can typically be generated internally by the analysis software once the unit weight of the concrete has been

defined. The per-unit length values of superimposed dead loads are applied directly to the two-dimensional analysis model as either concentrated or distributed loads.

The typical cross section shown in figure 8.20 was analyzed for the following loads:

- Self Weight: Concrete unit weight = 150 lb/ft³
- Barrier Railing: $p = 0.420$ kips/ft (8" from edge of the cantilevers)
- Future Wearing Surface: 2" concrete, $p = .025$ kips/ft/ft

The transverse bending moments resulting from these three load cases are shown in figure 8.21.

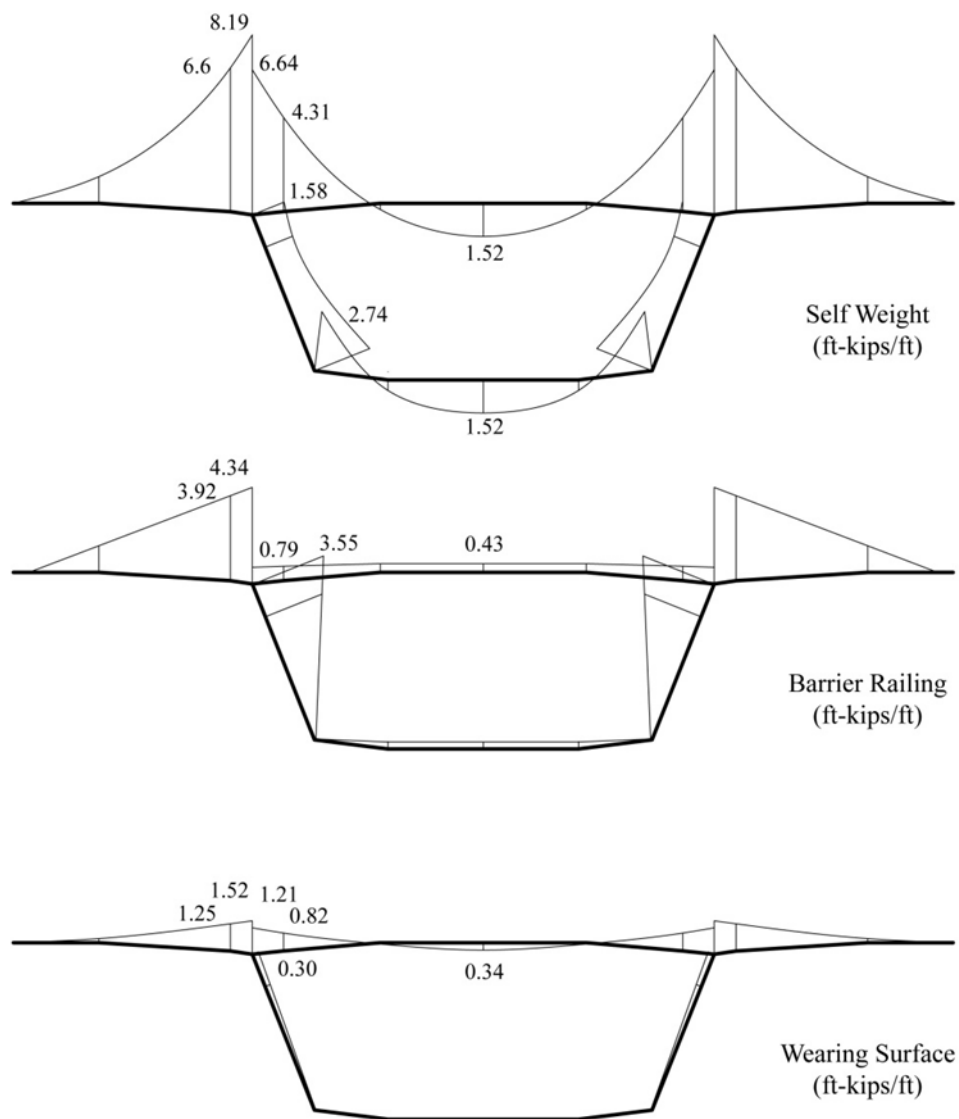


Figure 8.21 – Transverse Bending Moments for Uniformly Repeating Loads

8.5.3 Analysis for Concentrated Wheel Live Loads

Figure 8.22 shows the perspective of a single-cell box girder superstructure loaded with the Design Truck portion of the HL-93 notional load. Travel lanes, and the trucks/tandems within the lanes, are positioned in number and location in accordance with AASHTO LRFD requirements to produce maximum transverse bending moments at critical sections. The appropriate multi-presence factor of AASHTO LRFD Article 3.8.1.1.2 should be considered in choosing the number of design lanes to apply for a given critical section. Truck/tandem locations within the lanes should be in accordance with AASHTO LRFD Article 3.8.1.3.1.

Transverse bending moments resulting from the application of concentrated loads in the span are determined in a three step process:

1. Determine maximum transverse bending moments at critical sections of the cantilever wing and top slab considering these members as separate three-dimensional, fixed-end slab structures.
2. Use the two-dimensional model to distribute “fixed-end” slab moments around the cross section model.
3. Sum the fixed-end moments and redistributed moments to determine live load moments for design.

The fixed-end slab structures are typically analyzed using finite element methods or other tools such as influence surfaces. When modeled using finite elements, the slab structures are supported by full restraints at their intersection with the top of the webs. The longitudinal length of the slab structure should be sufficient to not impact transverse bending behavior. Slabs with shorter spans may warrant the application of wheel loads as surface loads. The areas over which the loads are distributed are the AASHTO LRFD Tire Contact Area (AASHTO LRFD Article 3.8.1.2.5) projected to the center of gravity of the top slab using a 45 degree distribution in both longitudinal and transverse directions. Bending moments computed in the examples included in this Section use influence surfaces and consider only the HL93 Design Truck.

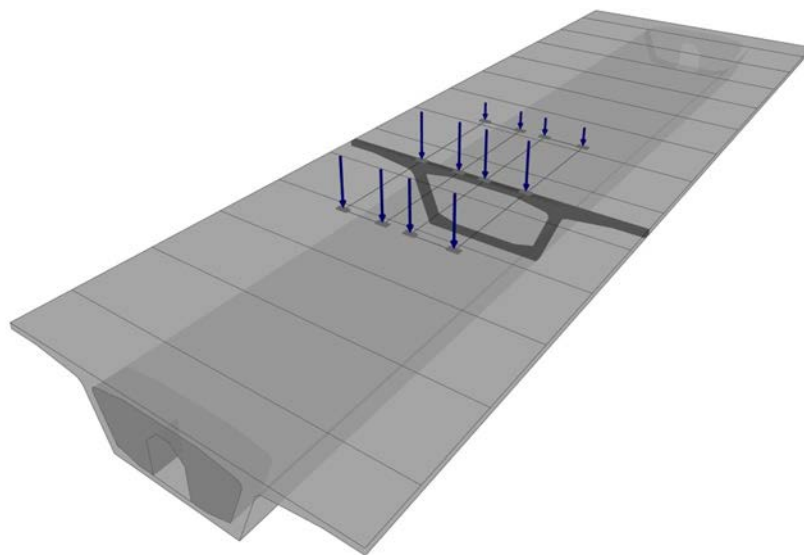


Figure 8.22 – Truck Loads on a Single-Cell Box Girder Span

8.5.4 Live Load Moments in Cantilever Wings.

The maximum fixed-end moment in the cantilever wing is determined by positioning the HL93 Truck one foot away from the face of the barrier railing in accordance with AASHTO LRFD Article 3.8.1.3.1. Figure 8.23 shows this loading on the cross section being analyzed. Figure 8.24 shows an influence surface for negative moment at the root of the cantilever, along the centerline of the influence surface. This figure also shows the location of wheel loads to produce the maximum fixed-end moment in the cantilever slab. The unfactored negative maximum bending moment found using this cantilever influence surface is 15.2 ft-kips without impact.

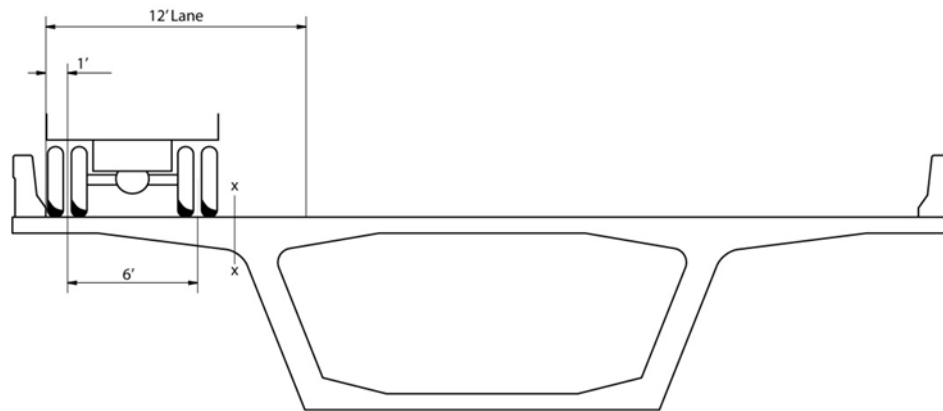


Figure 8.23 – Truck Location for Maximum Transverse Bending Moment at Root of Cantilever

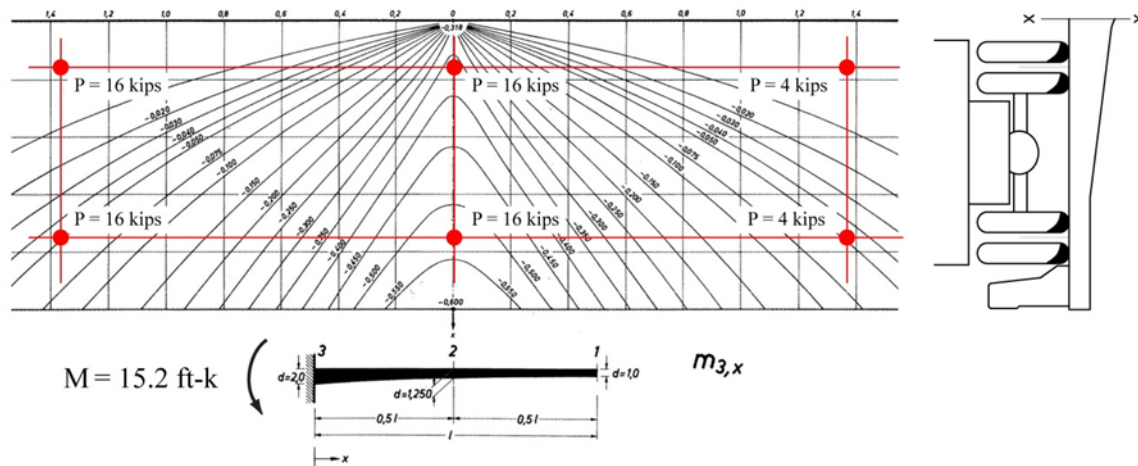


Figure 8.24 – Loaded Influence Surface for the Cantilever Wing.

Transverse bending moments in the other members of the cross section resulting from live load in the cantilever are determined by applying the cantilever moment to the cantilever/top slab/web intersection in the two-dimensional model. Figure 8.25 shows the distribution of 15.2 ft-kip cantilever moment around the cross section. Superimposing the cantilever moments with the distributed moments produces the final transverse bending moment diagram shown in figure 8.26.

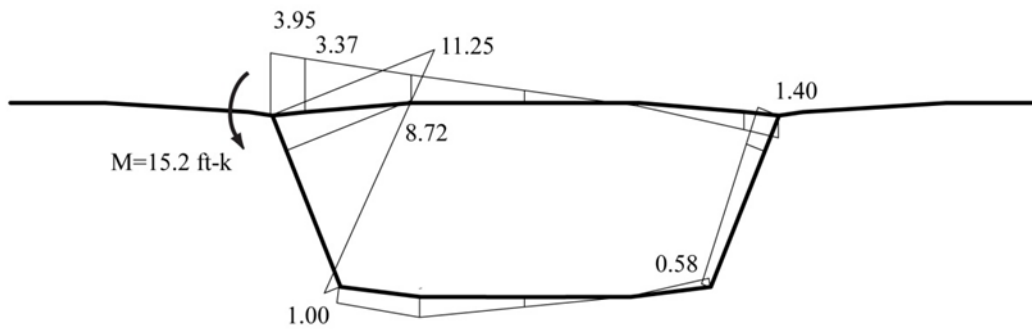


Figure 8.25 – Distribution of Cantilever Live Load Moments in the Cross Section

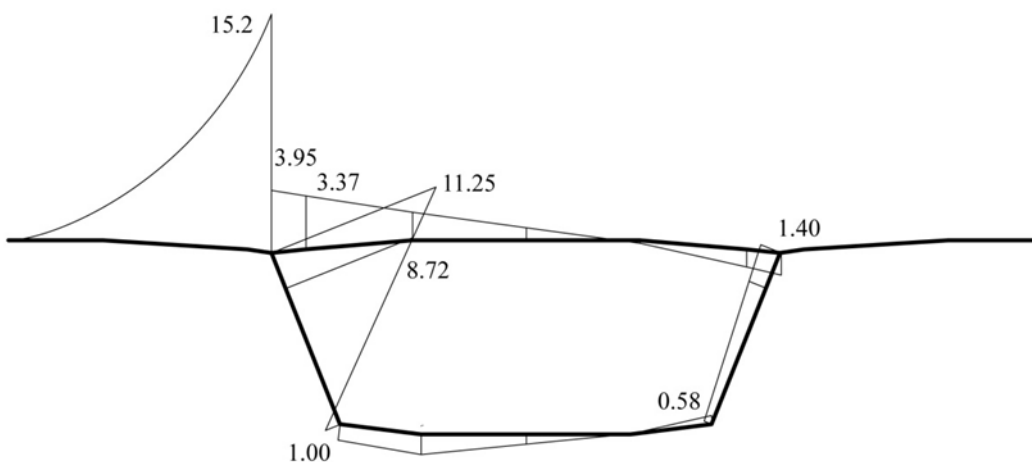


Figure 8.26 – Final Bending Moments for Live Load in Cantilever

The shape of the bending moment diagram in the loaded cantilever wing is approximate, as the influence surface used only provides the bending moment at the root of the cantilever. Plate solutions using finite element methods could be used to produce moments along the loaded cantilever.

8.5.5 Negative Live Load Moments in the Top Slab.

Negative live load moments in the top slab require positioning the Design Truck/Tandem for maximum negative effect at the end of the isolated top slab structure. In the cross section being studied, the maximum negative moment at the left end of the top slab is produced by locating one truck in the top slab and adding the effect of one truck in the cantilever wing. Figure 8.27 shows the locations of these two travel lanes. This loading arrangement can be evaluated as a superposition of the moments due to a truck in the cantilever shown in figure 8.24 and moments resulting from the single truck located between the webs as shown in figure 8.28 and figure 8.29.

The fixed-end moments for the top slab plate structure are determined using influence surfaces for a doubly fixed plate. Figure 8.28 shows the influence surface for the maximum negative

moment at the left end of the slab (10.3 ft-kips). Figure 8.29 shows the inverted influence surface used to compute the corresponding moment at the right end of the slab (5.1 ft-kips).

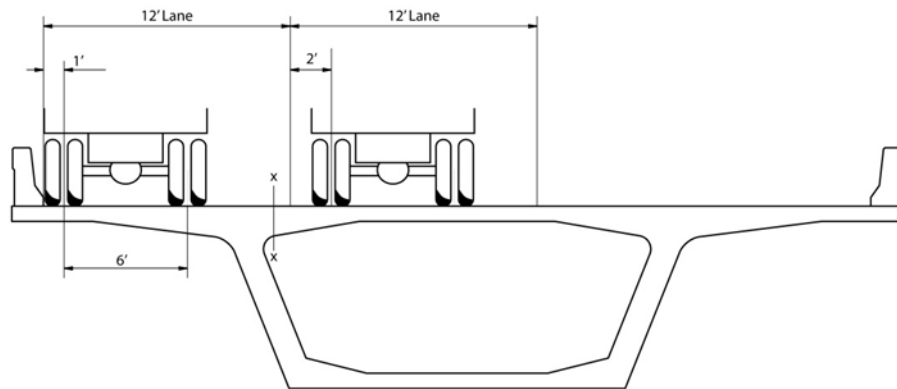


Figure 8.27 – Truck Location for Maximum Transverse Bending Moment at Middle of Top Slab

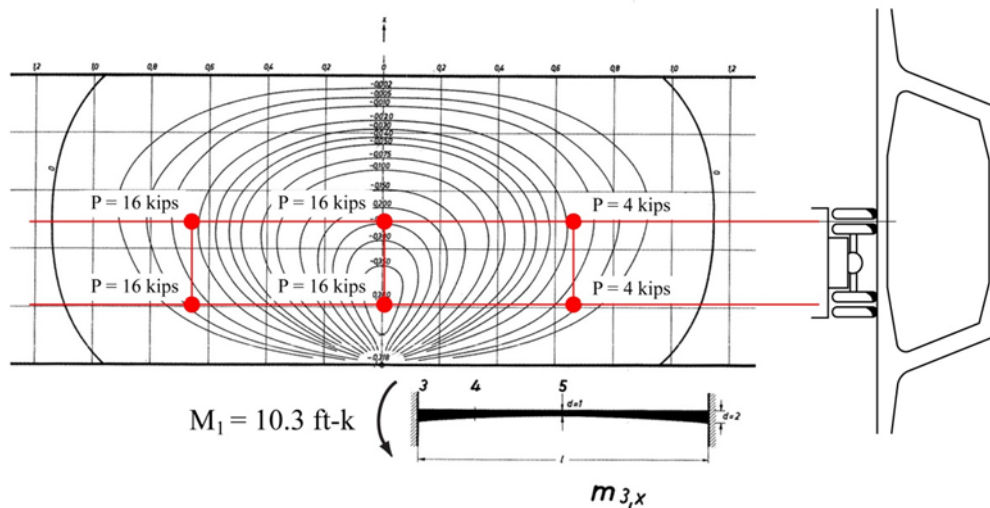


Figure 8.28 – Influence Surface for Maximum Negative Bending at the Left End of the Top Slab.

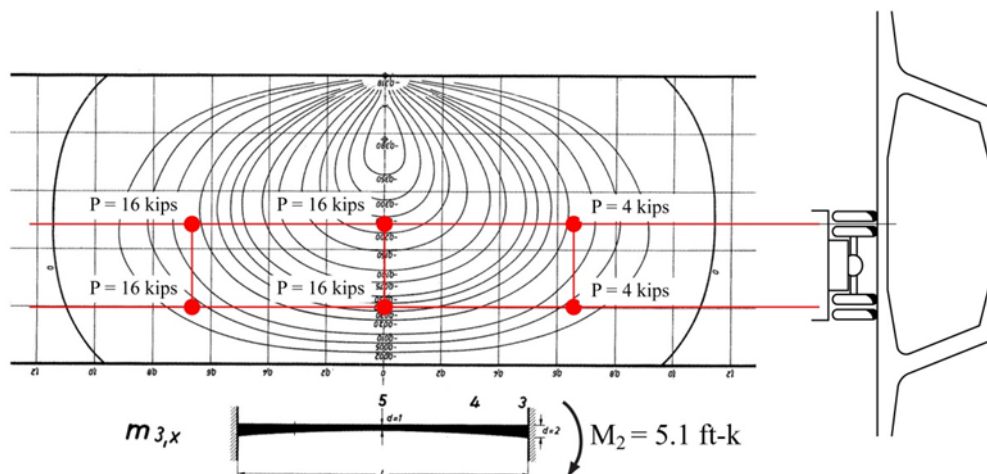


Figure 8.29 – Influence Surface for Maximum Negative Bending at the Right End of the Top Slab.

The two fixed-end moments can be “released” on the cross section by applying them as concentrated moments at the cantilever/top slab/web intersection. Figure 8.30 shows the results of the application of the concentrated couples on the two-dimensional analysis model. The concentrated couples, though applied as external loads, are actually internal fixed-end moments. When applied as external loads with signs opposite to the internally fixed-end moments, the moments in the unloaded members (webs and bottom slab) are the final moments due to the loading. The moments in the top slab represent the differential moments in the loaded member in moving from fixed-end conditions to the actual flexibility of the box girder. The final bending moment diagram, shown in figure 8.31, is determined by reducing the fixed-end moments by these differential moments.

The total negative moment at the left end of the top slab for Design Trucks arranged in two lanes as shown in figure 8.27 are found by summing the maximum moment from the distributed cantilever moment (figure 8.26) and the moment resulting from the truck in the top slab (figure 8.31). The moment at the left end of the top slab is:

$$(Eqn. 8.18) \quad M_{neg} = 3.95 + 8.09 = 12.04 \text{ ft-kips}$$

The results of this analysis are valid only at the location of known fixed moments and their redistributed differential moments. The shape of the top slab bending moment between the two known extremity moments is not an exact representation, but general in nature. Efforts have been made in past practice to develop approaches using equivalent forces in equilibrium with the extremity moments to determine bending moments within the top slab for a given loading. The results of these methods do not prove accurate or necessary for the design of the top slab.

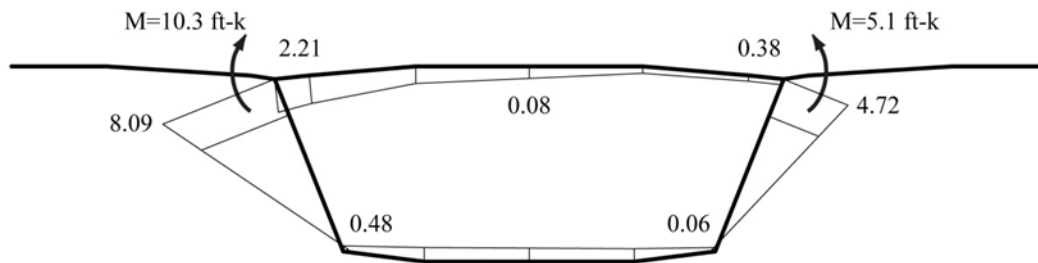


Figure 8.30 – Distribution of Fixed-End Live Load Moments for Maximum Negative Moment Case

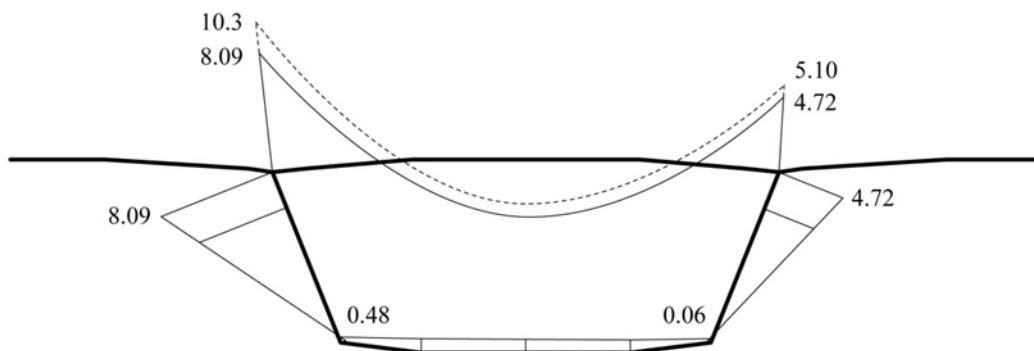


Figure 8.31 – Summed Live Load Moments for the Maximum Negative Moment Case

8.5.6 Positive Live Load Moments at Centerline of the Top Slab.

Positive live load moments at the centerline of the top slab are computed in a fashion similar to the negative moments at the ends of the slab, with one additional initial step. An influence surface for moment at the center of the isolated top slab structure, or a finite element model, is first used to determine the arrangement of loads to produce maximum positive moment. Fixed-end negative moments are then determined for this load arrangement and distributed around the cross section. The final positive moment at the centerline of the slab is the positive moment in the fixed-end top slab structure, increased by the release of the end moments.

Figure 8.32 shows the load arrangement for maximum positive bending moment at the center of the top slab. Figure 8.33 shows an influence surface for the maximum positive transverse bending moment at the center of the top slab for this loading arrangement. The value of this bending moment with fixed-end supports is 3.88 ft-kips. The fixed-end bending moments at the ends of the top slab structure for the same loading arrangement are 12.0 ft-kips at the left end and 11.1 ft-kips at the right end.

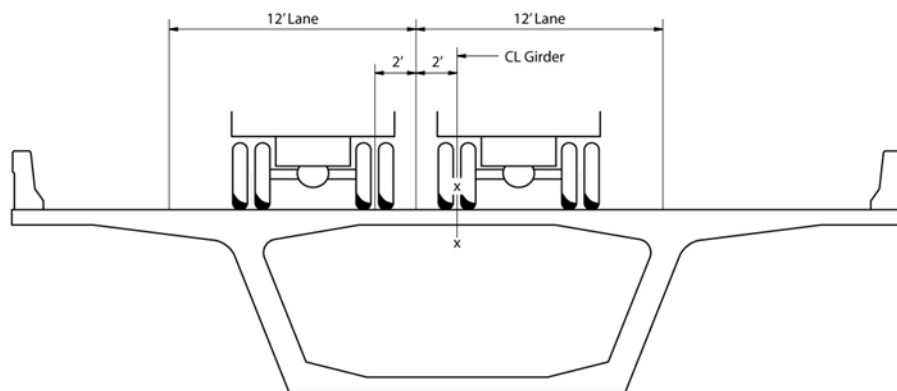


Figure 8.32 – Live Load Position for Maximum Positive Bending

These fixed-end moments are released on the cross section as presented in the previous Section. Figure 8.34 shows the differential moments, and figure 8.35 shows the summed values. The release of the fixed-end moments shifts the bending moment diagram in the top slab, increasing the bending moment at the centerline of the top slab. The fixed-end centerline moment increases from 3.88 ft-kips/ft to 5.08 ft-kips/ft. Again, the shape of the top slab bending moment diagram between known locations is only an approximation.

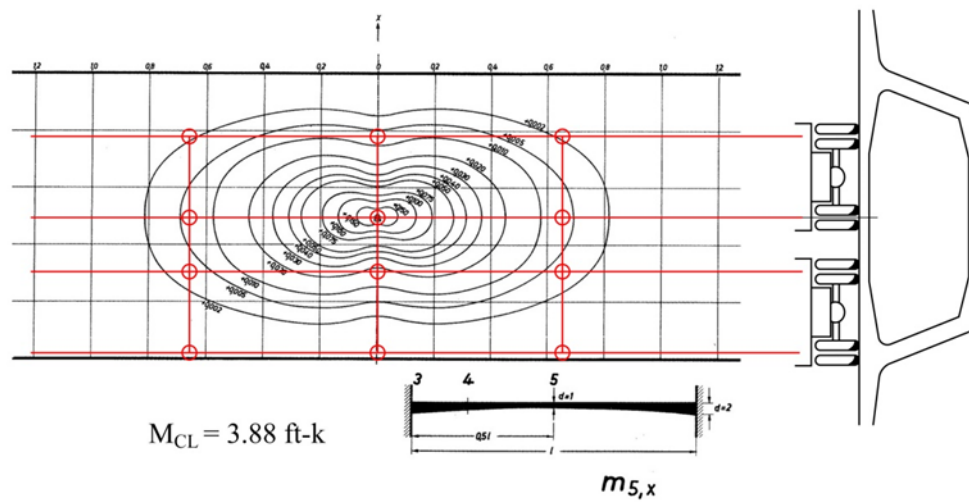


Figure 8.33 – Maximum Positive Moment in the Top Slab for Fixed-End Conditions

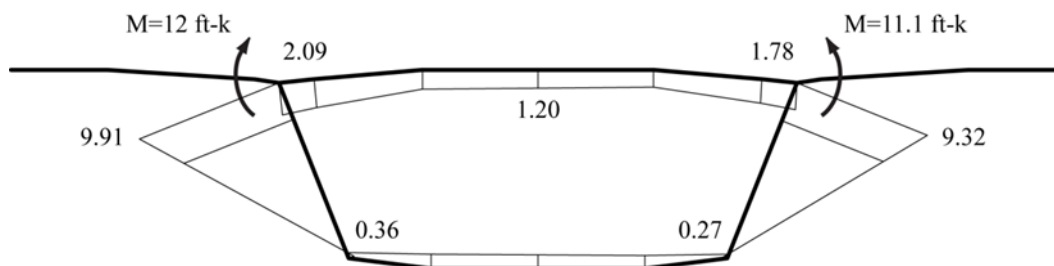


Figure 8.34 – Distribution of Fixed-End Live Load Moments for Maximum Negative Moment Case

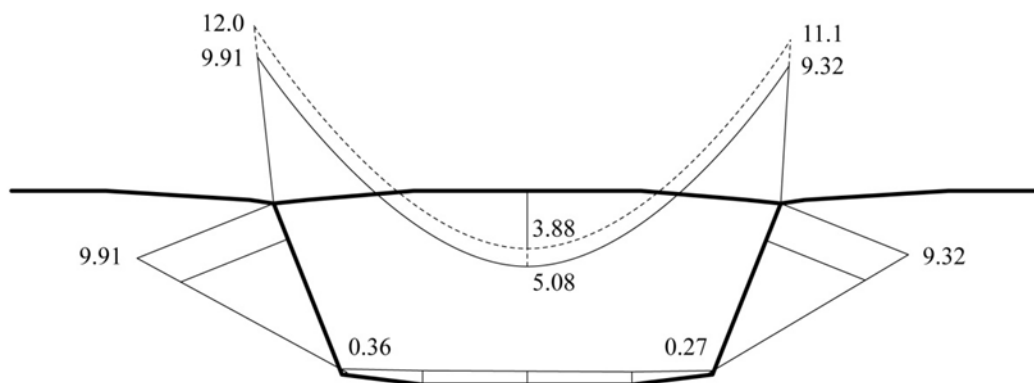


Figure 8.35 – Summed Live Load Moments for the Maximum Positive Moment Case

8.6 Transverse Post-Tensioning

8.6.1 Transverse Post-Tensioning Tendon Layouts

The cantilever wings and top slab of single-cell box girder superstructures are typically prestressed transversely with post-tensioning to offset tensile stresses resulting from permanent and live loads. Narrow precast box girders with widths of 16' or less, often used for single track transit systems, may not greatly benefit from transverse post-tensioning. Rails that carry normal operating train loads can be positioned adjacent to the webs, limiting top slab bending moments to values small enough to not require transverse post-tensioning.

LRFD Article 5.14.2.3.10a provides minimum cantilever wing and top slab thicknesses for segmental construction. Cast-in-place box girders with cross sections similar to segmentally constructed bridges should follow these provisions. The 15 foot top slab span length limitation for requiring transverse post-tensioning should be the total length from face of web to face of web (top slab with haunches).

Figure 8.35 shows a typical transverse post-tensioning tendon layout for the typical section studied in this section. The transverse tendons are typically comprised of 3 or 4 strands, either 0.5" or 0.6" diameter each, placed in oval shaped "flat" ducts. The profile of the tendons varies to provide needed eccentricity over the webs and at the centerline of the top slab. The perspective view in figure 8.35 shows three transverse tendons in a section of a single cell box girder superstructure.

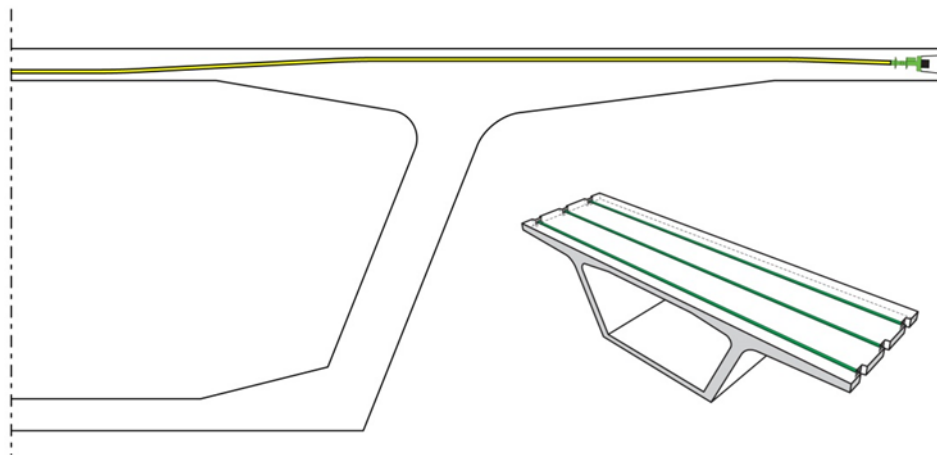


Figure 8.36 – Typical Transverse Tendon Layout.

8.6.2 Required Prestressing Force

The selection of the required prestressing force on a unit length basis is made by summing the moments at critical sections, evaluating each section's prestressing requirement, and choosing the greatest required force. AASHTO LRFD Service I is the appropriate limit state for transverse prestressing design based on permissible concrete tension (AASHTO LRFD Article 3.4.1). The load factors for permanent and live loads at this limit state are equal to 1.0.

Considering the example presented in this section, the summary of moments at the three sections studied are:

Section	Root of Cantilever	Edge of Top Slab	CL of Top Slab
Self Weight	-8.19	-8.64	1.52
Barrier Railing	-4.34	-0.79	-0.43
Wearing Surface	-1.52	-1.21	0.34
Live Load	-15.2	-12.04	5.08
Multi-Presence	1.20	1.00	1.00
Dynamic Allowance (IM)	1.33	1.33	1.33
Total Service I Moment	-38.4	-24.7	8.19

Table 8.3 – Transverse Bending Moment Results from Frame Analysis

The equations governing post-tensioning selection are:

$$\text{(Eqn. 8.19)} \quad F \geq \frac{-M + M_a}{\rho c_2 - e} \quad (\text{negative moment})$$

$$\text{(Eqn. 8.20)} \quad F \geq \frac{M - M_a}{\rho c_1 + e} \quad (\text{positive moment})$$

Where: M = Total applied service load moment
 M_a = Moment causing allowable tensile stress
 c_1 = Distance from neutral axis to extreme top fiber
 c_2 = Distance from neutral axis to extreme bottom fiber
 ρ = Cross section efficiency = 1/3 for a rectangular section
 e = Tendon eccentricity considering location of strands within the duct

The moment causing allowable tensile stress (M_a) is equal to the allowable tensile stress (f_a) multiplied by the section modulus ($S = bh^2/6$ for a rectangular section), or:

$$\text{(Eqn. 8.21)} \quad M_a = f_a \left(\frac{h^2}{6} \right)$$

The allowable transverse flexural stress in the top slab of a single-cell box girder is equal to $0.0948\sqrt{f'_c}$. Using 6 ksi concrete, the allowable stress would be 0.232 ksi (33.4 ksf). Solving for the prestress force requirements:

Section	Root of Cantilever	Edge of Top Slab	CL of Top Slab
Moment	-38.4	-24.7	8.19
$h/2 = c_1 = c_2$	0.87	0.87	0.369
Efficiency (ρ)	1/3	1/3	1/3
Eccentricity (e)	-0.60	-0.60	0.19
Moment Causing f_a	-18.9	-18.9	4.12
Required PT Force/ft	24.2	8.8	13.0

Table 8.4 – Transverse Bending Moment Results from Frame Analysis

Considering the limited example presented in this section, the governing cross section for required prestress force is the root of the cantilever. The prestress force required at this section is 24.2 kips/foot.

The final selection of the number and size of the post-tensioning tendons requires a study to determine the final force in the tendons. This work must include initial losses caused by friction, wobble and anchor set, and long term losses resulting from concrete creep and shrinkage, as well as prestressing steel relaxation. Secondary post-tensioning effects must be included when present. Several commercially available software packages include modeling of the actual geometry of post-tensioning tendons, automatic generation of internal forces due to tendon stressing, losses during stressing, and long-term, time-dependent loss calculations.

Depending on the tendon profile in the top slab, the flexural restraint provided by the webs can result in secondary prestressing moments. These moments should be included in the summation of service limit state moments when determining the required prestressing force. The final value of the secondary moments is a function of the resulting prestress demand, thwarting a direct solution and slightly complicating the final prestress force. For the example in this section, a concordant tendon profile that produced no secondary moments was used.

The selection of the required prestress force satisfies just a part of the design requirements for the cross section. Other tasks that need to be performed include:

- Tensile and compressive stress checks at all sections of the cantilever wings and top slab to verify appropriate service limit states.
- Reinforcing requirement checks in the top slab to verify appropriate strength limit states.
- Transverse bending moments in the webs combined with shear reinforcing requirements to select final web reinforcing.

8.6.3 Transverse Post-Tensioning Tendon Placement and Stressing

Figures 8.37 and 8.38 show various photographs of the installation and stressing of the transverse top slab tendons in the casting yard. Figure 8.37 shows the placement of the transverse flat duct within the reinforcing cage after positioning into the casting machine. Transverse ducts pass over the longitudinal tendons of this cantilever bridge and are connected to the anchorages which are fixed to the cantilever wing bulkhead during the concrete pour. The ducts shown are plastic (typically polypropylene) which provide an important layer of corrosion protection to the transverse post-tensioning strands. Vertical grout inspection ports are located at the top of the anchorages to permit post-grouting inspections within the tendon.



Figure 8.37 – Transverse Duct Placement in Casting Machine

The photograph on the left of figure 8.38 shows the stressing of a four strand tendon using a mono-strand stressing ram. The photograph of the right is a close-up of the transverse tendon anchorage and wedge block after stressing the two central strands. Following stressing and verification of tendon elongations by the Resident Engineer and/or Engineer of Record, strand “tails” are cut off, permanent grout caps are placed over the anchorages, the tendons are grouted, anchorage block-outs are filled with concrete, and protective coatings are applied.



*Figure 8.38 – Mono-Strand Stressing of a 4 Strand Tendon (left).
Anchorage After Stressing 2nd Strand (right).*

Chapter 9—Other Design Considerations

9.1 Effects of Curved Tendons

Alignments of post-tensioning tendons change direction as they pass through curved ducts cast into the surrounding concrete. Figure 9.1 shows two common forms of tendon path deviations used in post-tensioned concrete superstructures. The top of figure 9.1 shows a parabolic tendon deviation commonly used for vertical deviations in cast-in-place box girder bridges. Parabolic deviations exert a uniform load along the horizontal projected length of the tendon deviation. This uniform force is a function of tendon force, deviation length and tendon eccentricity. The bottom of figure 9.1 shows a tendon deviated along a circular arc. The force exerted by the tendon is a radial force proportional to tendon force and inversely proportional to the radius of the circular deviation. Circular arc deviations are often used in anchorage blisters and at deviations of external tendons.

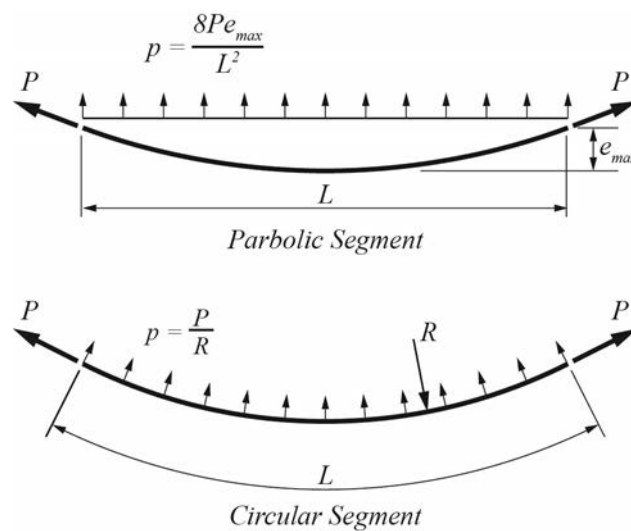


Figure 9.1 – Curved Tendon Deviations

Tendons with circular geometry also occur in webs of cast-in-place box girder bridges that curve to follow a horizontal circular alignment. Figure 9.2 shows a perspective of a section of curved multi-cell box girder superstructure. Radial forces inversely proportional to the radii of a particular web act towards the center of curvature as the tendons rise and fall along their vertical parabolic profile. The radial forces vary in each web as a function of web radius.

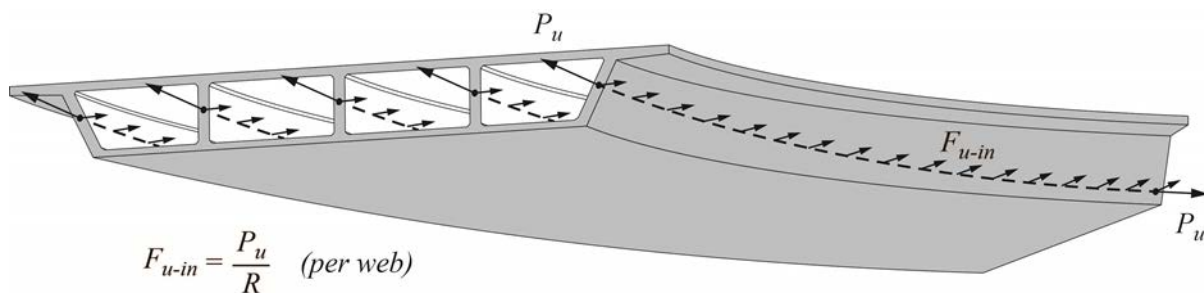


Figure 9.2 – Tendons in Curved Superstructures

The horizontal forces per unit length of superstructure load the webs of box girder bridges causing transverse bending moments that may increase the required amount of transverse reinforcing steel. The lateral tendon forces also cause local stresses in the webs that can lead to cover spalling and tendon pull-out. Figure 9.3 shows the deflected shape of a multi-cell box girder subjected to lateral loading resulting from tendons following horizontal curvature.

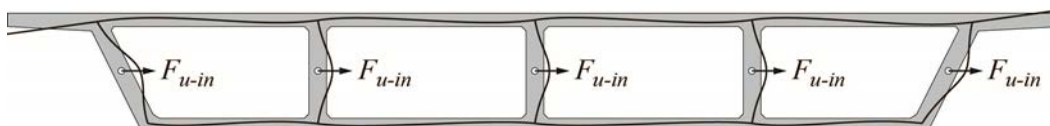


Figure 9.3 – Cross Section of Multi-Cell Box Girder with Lateral Tendon Loads

This Section addresses the design requirements for the radial effects associated with curved tendons in webs. Requirements for this subject are found in LRFD Article 5.10.4.3 which is a part of a larger LRFD Article 5.10.4 - Tendon Confinement.

9.1.1 In-Plane and Out-of-Plane Forces

The LRFD Specifications delineate between in-plane and out-of-plane effects when providing design requirements for the effects of curved tendons. The direction of in-plane and out-of-plane forces can change along the length of a tendon. Figure 9.4 shows a post-tensioning tendon that deviates direction through two circular curves. Curve 1 of the tendon lies in the $Y-Z$ plane. In-plane forces for the tendon in this location would be forces whose components act in the Y and/or Z direction. Out-of-plane forces for this portion of the tendon would be those acting in the $\pm X$ direction. After exiting Curve 1, the tendon deviates around Curve 2 which lies in the $X-Y$ plane. In-plane forces for this curve lie in the XY plane. Out-of-plane forces for this curve act in the $\pm Z$ direction.

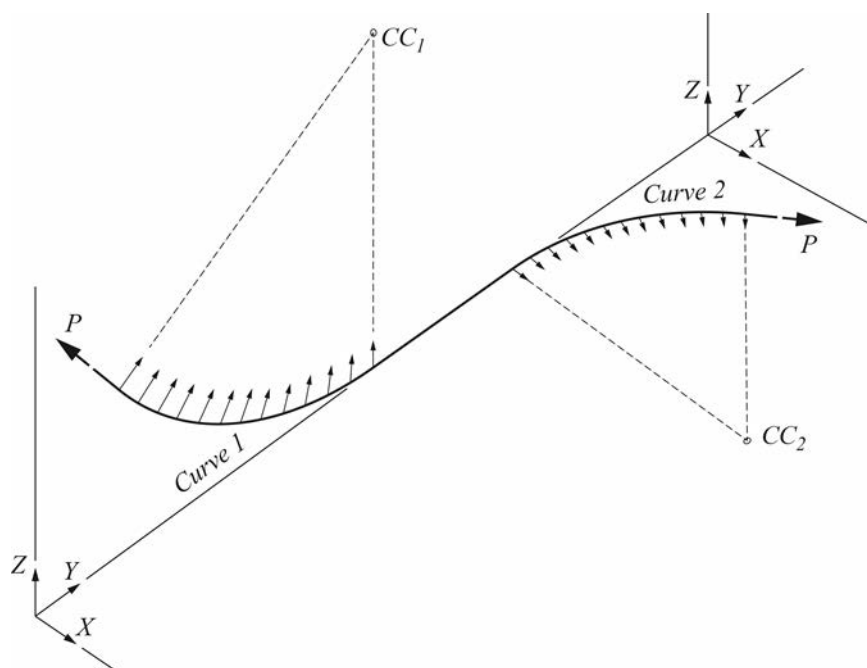


Figure 9.4 – Tendon Plane of Curvature

In-plane force in a region of circular curvature, presented in LRFD Article 5.10.4.3.1a, is shown in equation 9.1:

$$(Eqn. 9.1) \quad F_{u-in} = \frac{P_u}{R}$$

Where, F_{u-in} = the in-plane deviation force per unit length of tendon
 P_u = the factored tendon force = 1.2 times P_{jack} (LRFD Article 3.4.3.2)
 R = the in-plane radius of curvature of the tendon

Out-of-plane forces acting transverse to in-plane forces are the result of the spreading of the strands as they bear on the inside face of curved circular ducts. Figure 9.5 shows a section (at a profiled tendon high point) of a web of a concrete box girder bridge with a tendon curving to produce a downward in-plane curvature. When the tendon is stressed, the strands are drawn to the bottom of the duct where they create lateral stresses within the concrete.

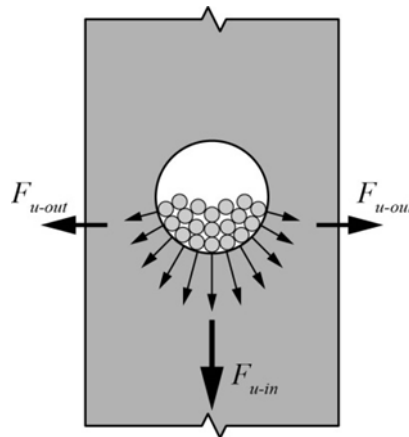


Figure 9.5 – In-Plane and Out-of-Plane Tendon Forces

In-plane force in a region of circular curvature, presented in LRFD Article 5.10.4.3.2, is shown in equation 9.2:

$$(Eqn. 9.2) \quad F_{u-out} = \frac{P_u}{\pi R}$$

Where, F_{u-out} = the out-of-plane force per unit length of tendon
 P_u = the factored tendon force = 1.2 times P_{jack} (LRFD Article 3.4.3.2)
 R = the in-plane radius of curvature of the tendon

Tendons in cast-in-place concrete box girder bridges are primarily placed to follow a series of parabolic curves in the vertical direction. These tendons produce in-plane forces in a plane defined by the vertical direction and the longitudinal axis of the bridge. At the same time, these tendons can be in webs that are cast to follow a horizontal bridge curvature, producing simultaneously acting in-plane forces in a horizontal plane. In theory, the in-plane force effects should be verified for both sets of in-plane forces. In reality, the in-plane forces in the vertical direction in webs of concrete box girder bridges are resisted by significant concrete as to negate concerns. For bridges following horizontal alignments with large radius curves, the in-plane forces acting transverse to the webs typically have only the web concrete cover acting to resist

tendon pullout. Supplemental duct ties are used to resist the in-plane forces for more tightly curved bridges.

9.1.2 AASHTO LRFD Design Approach

The requirements of LRFD Article 5.10.4.3 address the design of in-plane and out-of-plane force effects of post-tensioning tendons within webs of single-cell and multi-cell concrete box girder bridges. This manual presents these requirements in a slightly different arrangement as those presented in LRFD Article 5.10.4.3:

- Regional Effects—Flexure of the transverse cross section of the box girder superstructure, referred to in LRFD Specifications as Regional Bending (5.10.4.3.1d)
- Local Effects—Local flexure and shear behavior at locations of ducts and duct stacks in the webs. This includes Shear Resistance to Pull-out (5.10.4.3.1b) and Cracking of Cover Concrete (5.10.4.3.1c)
- Out-of-Plane Force Effects (5.10.4.3.2)

9.1.3 Regional Effects—Transverse (Regional) Bending

Consider the hypothetical case of a tendon following a circular arc within a concrete member whose area is concentrated as to be completely coincident with the tendon. Figure 9.6 shows this hypothetical case with the tendon shown separated from the concrete for clarity. The curved stressed tendon produces an inward radial force. The concrete is placed in compression at the tendon anchorages and its curvature induces an outwardly resisting radial load equal and opposite to the tendon force. The radial forces negate each other and the curved concrete member only shortens under the prestressing force.

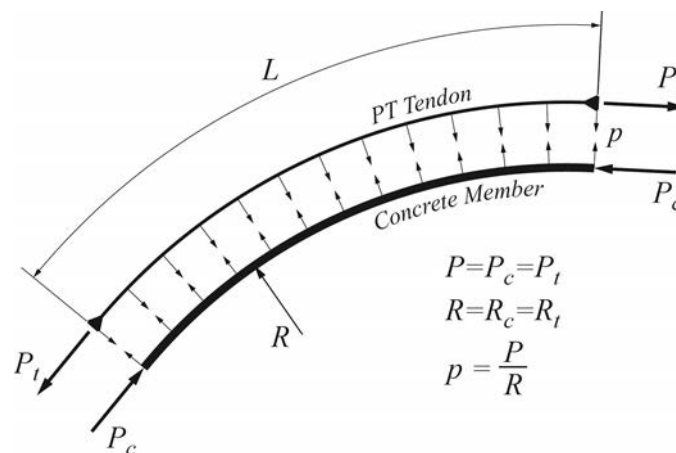


Figure 9.6 – Hypothetical Concrete Member Completely Coincident with a Tendon

Figure 9.7 shows a tendon following a circularly curving plate with a height of h_c . In this case, the post-tensioning tendon and area of the concrete member being prestressed are not coincident. The radial force produced by the post-tensioning tendon is equal to the tendon force divided by the radius of the curved member. Circumferential compression is produced in the curved plate that is in equilibrium with the prestressing force. This circumferential compression is distributed over the height of the plate and produces a distributed pressure in the plate radial

to the plate curvature. The member will shorten under the action of the prestressing force, but as the radial distributed force of the tendon is not coincident with the radial pressure produced in the concrete, the plate will bend radially.

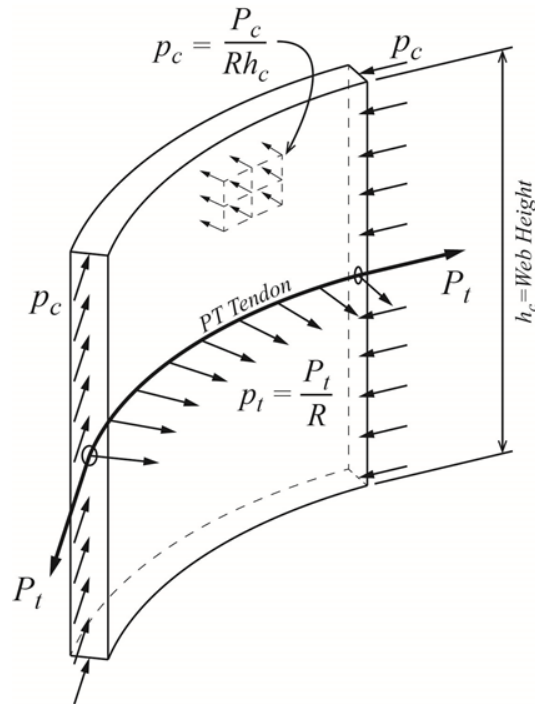


Figure 9.7 – Post-Tensioning a Curved Plate

The curved plate shown in figure 9.7 is free to deflect radially under the applied post-tensioning. The top and bottom of the plate will tend to deflect radially outward from the center of curvature, while deflections would tend to be inward at the elevation of the post-tensioning tendon. In concrete box girder construction the tops and bottoms of webs are restrained by their monolithic connections with the top and bottom slabs, producing transverse restraining moments as shown in figure 9.8.

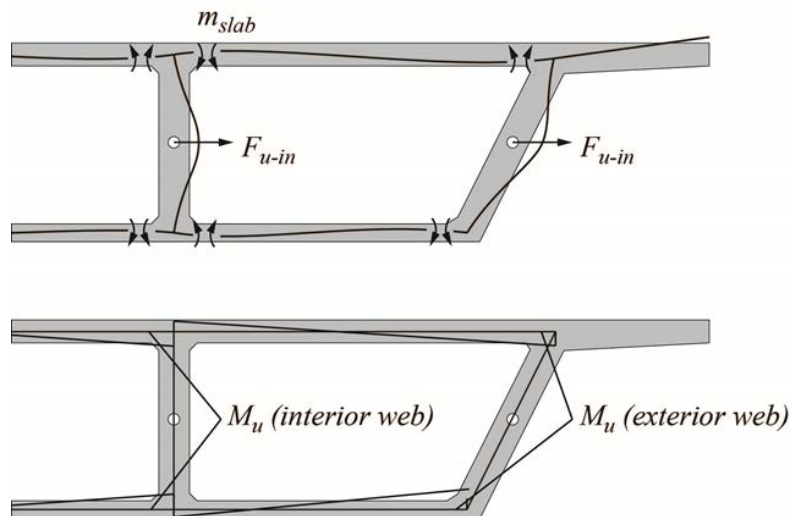


Figure 9.8 – Web Flexure Restrained by Top and Bottom Slabs

Transverse moments (Regional Bending in LRFD Article 5.10.4.3.1d) must be evaluated and combined with other transverse moments and shear requirements to determine the appropriate amount and placement of transverse reinforcing. The transverse moments from the in-plane radial forces could be determined by either a 2-dimensional analysis of a unit length of transverse cross section (as in chapter 8) or a more complex 3-dimensional finite element analysis. The LRFD Specifications offers a simplified approach to evaluating these transverse moments in the webs of box girder bridges. This approach first considers the web to be simply supported at its connection with the top and bottom slab, and loaded at mid-height of the web. A continuity factor is then applied to express end moments as a percentage of the maximum positive transverse bending moment in the simply supported beam.

Figure 9.9 shows a comparison of the LRFD simplified approach to moments developed by more detailed analysis performed on a transverse cross section of a box girder bridge. In the detailed analysis, the bending moments can be seen as the superposition of the concentrated post-tensioning force and the resisting radial force in the compressed concrete web. Figure 9.9 shows these component loads and their summation. The LRFD simplified approach is shown at the left of figure 9.9. The effects of the radial force produced in the compressed concrete web are not considered in the LRFD simplified approach.

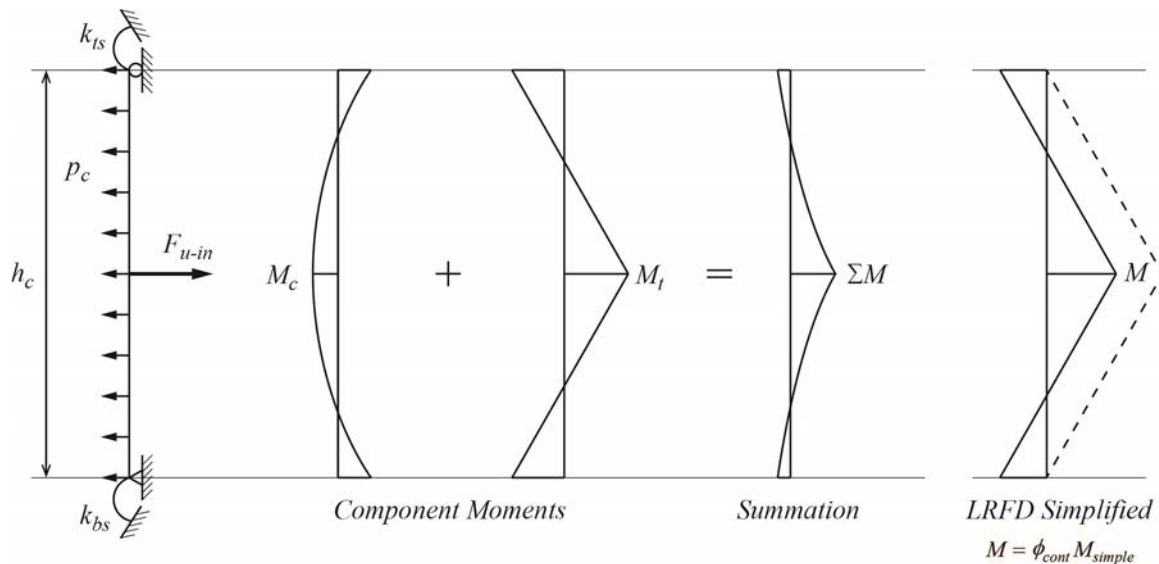


Figure 9.9 – Web Transverse (Regional) Bending Moments

The factored moment in using the LRFD simplified approach is:

$$(Eqn. 9.3) \quad M_u = \frac{\phi_{cont} F_{u-in} h_c}{4}$$

Where, ϕ_{cont} = continuity factor = 0.6 for interior webs and 0.7 for exterior webs
 h_c = span of the web between the top and bottom slabs, measured along the axis of the web

The span of the web for equation 9.3 is shown in figure 9.10. Only components of forces acting to produce bending in the direction transverse to the axis of the web needs to be considered. Though the height of the inclined outer web is taller than the vertical interior web in figure 9.10

by one over the cosine of the web slope, the force transverse to the web axis is the in-plane force multiplied by the cosine of the web slope. These two negate each other such that the regional bending in the outer web is only different from the inner web by the difference of the radii of the two webs.



Figure 9.10 – Web Height for Equation 9.3

9.1.4 Local Shear and Flexure in Webs

The webs of concrete box girder bridges must be verified with regard to local shear pull-out and flexure of cover concrete in the vicinity of ducts and duct banks. Figure 9.11 shows one interior web of a post-tensioned box girder bridge that contains three post-tensioning tendons arranged in a duct stack. The detail to the right in figure 9.11 is an enlargement of the duct stack. The dimensions shown are defined as:

- d_{duct} = outside diameter of the post-tensioning tendon duct (in)
- d_c = cover of the duct on towards the direction of curvature (in)
- s_{duct} = clear distance between tendon ducts in the vertical direction (in)
- h_{ds} = height of the duct stack (in)
- t_w = web width (in)

Ducts are considered stacked for flexure of the concrete cover when the clear distance between ducts (s_{duct}) is less than 1.5 inches. For shear resistance calculations, duct stacks include clear spacings greater than the diameter of the ducts.

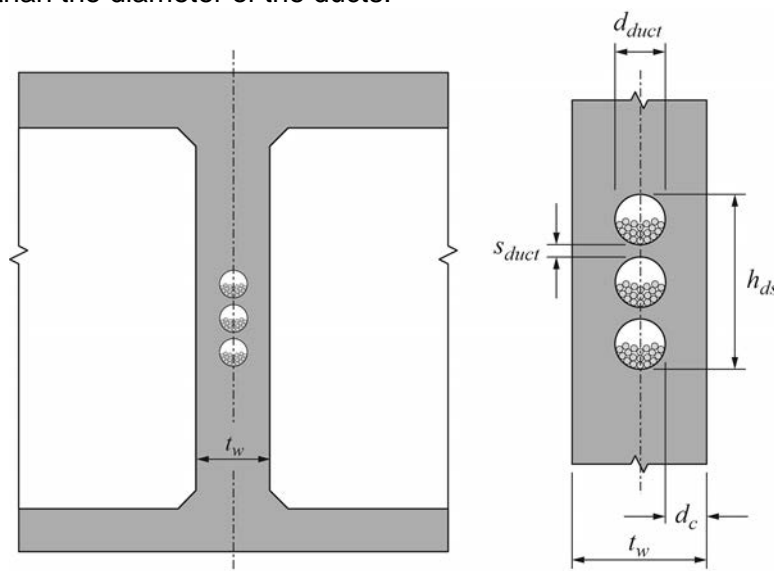


Figure 9.11 – Parameters for Local Shear and Flexure Design

9.1.4.1 Shear Resistance to Pull-out

In-plane tendon forces may cause tendons to pull-out of the webs towards the center of box girder curvature unless they are sufficiently embedded in web concrete or tied back to transverse reinforcing within the web. Resistance to tendon pull-out is provided by the shear capacity of the concrete in the webs on the side of the ducts towards the center of box girder curvature. The LRFD Specifications define the shear resistance as:

(Eqn. 9.4)
$$V_r = \phi V_n$$

In which the nominal capacity is defined by:

(Eqn. 9.5)
$$V_n = 0.15d_{eff}\sqrt{f'_{ci}}$$

- Where,
- V_n = nominal shear resistance of two shear planes per unit length (kips/in)
 - ϕ = resistance factor for shear = 0.75
 - f'_{ci} = concrete strength at time of prestressing (ksi)
 - d_{eff} = one-half of the effective length of the failure plane in shear and tension for a curved element (in)

The length of the shear failure plane (d_{eff}) varies as a function of the clear spacing (s_{duct}) between the tendons in a duct stack. For duct clear spacings less than the diameter of the duct ($s_{duct} < d_{duct}$), the effective length of the failure plane is defined by equation 9.6. The effective length of the failure plane for this case is shown in Figure 9.12. The detail to the left in figure 9.12 shows the special case of zero duct spacing. The detail to the right shows the general case for equation 9.6.

(Eqn. 9.6)
$$d_{eff} = d_c + \frac{d_{duct}}{4}$$

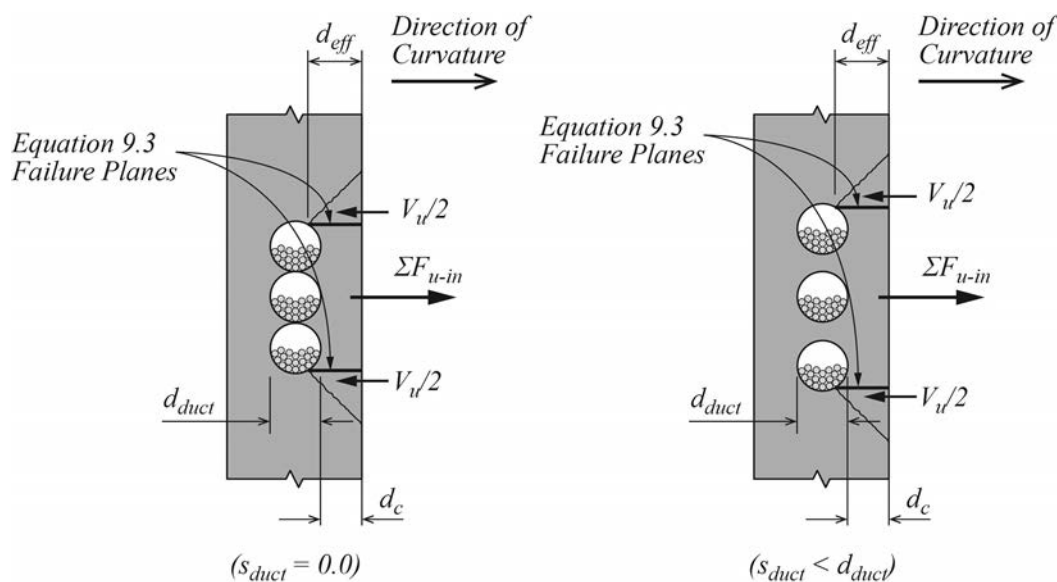


Figure 9.12 – Effective Length of Failure Plane for Equation 9.6

When the duct spacing is greater than or equal to the duct diameter, the definition of the effective length of the failure plane changes. In this case, the lesser value of equation 9.7 and 9.8 is used for d_{eff} . These two equations are shown graphically in figure 9.13.

$$(Eqn. 9.7) \quad d_{eff} = t_w - \frac{d_{duct}}{2}$$

$$(Eqn. 9.8) \quad d_{eff} = d_c + \frac{d_{duct}}{4} + \frac{\sum S_{duct}}{2}$$

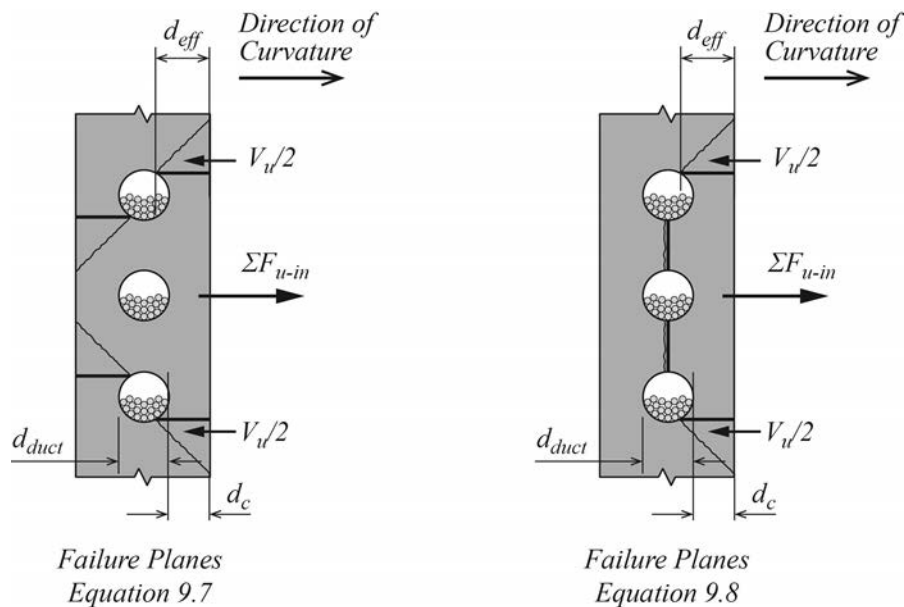


Figure 9.13 – Effective Length of Failure Plane for Equations 9.7 and 9.8

Procedure for verifying resistance to shear pull-out:

- Compute the factored in-plane force for all tendons in a web (equation 9.1).
- Compute the effective length of the failure plane for shear by equation 9.6, 9.7 or 9.8.
- Compute the shear resistance using equations 9.3 and 9.4.
- If the factored in-plane force is greater than the shear resistance, provide duct ties and stirrup similar to those shown in LRFD Figure C5.10.4.3.1b-1.
- As web radii vary, preform for each web in the cross section.

9.1.4.2 Cracking of Concrete Cover

Excessive in-plane force in a duct stack can cause cracking of the concrete cover. This cracking can negatively impact the long-term durability of the web and post-tensioning system. The LRFD Specifications requires a calculation of flexural stresses in an idealized beam of concrete cover that spans the duct stack as shown in figure 9.14. This calculation is required when the clear spacing between ducts is less than 1.5 inches. These flexural stresses are combined with flexural stresses from regional bending moments for evaluation.

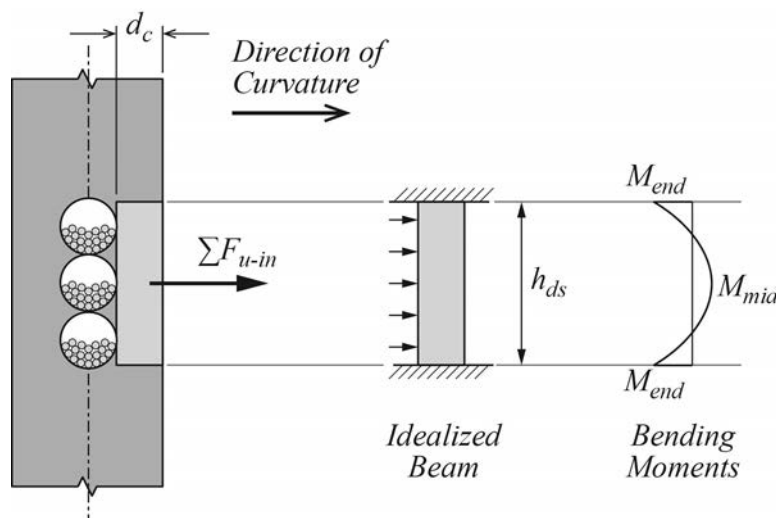


Figure 9.14 – Local Bending Moments for Evaluating Cracking of Concrete Cover

The bending moments in the beam of concrete cover are those of a fixed end beam subjected to a uniform load over its length. The magnitude of the uniform load is equal to the summation of the factored in-plane forces divided by the duct stack height. The resulting end and mid-point bending moments are:

(Eqn. 9.9)
$$M_{end} = \frac{\left(\frac{\sum F_{u-in}}{h_{ds}} \right) h_{ds}^2}{12}$$

(Eqn. 9.10)
$$M_{mid} = \frac{\left(\frac{\sum F_{u-in}}{h_{ds}} \right) h_{ds}^2}{24}$$

The stresses from the local and regional bending in the web are computed and compared to a permissible cracking stress given as:

(Eqn. 9.11)
$$f_{cr} = \phi f_r = 0.85 \left(0.24 \sqrt{f'_{ci}} \right)$$

Procedure for verifying cracking of concrete cover:

- Compute the factored in-plane force for all tendons in a web (equation 9.1).
- Compute local bending moments from equations 9.9 and 9.10.
- Compute the stresses in the beam of concrete cover.
- Combine stresses resulting from regional bending with those from local bending.
- Compare the stresses to the permissible cracking stress from equation 9.11
- If the stresses are greater than the permissible cracking stress, provide duct ties and stirrup similar to those shown in LRFD Figure C5.10.4.3.1b-1 (Caltrans recommends duct ties when the bridge horizontal radius is less than 800').
- As web radii vary, preform for each web in the cross section.

9.1.5 Out-of-Plane Force Effects

Equation 9.2 defines the out-of-plane force effects resulting from the vertical deviation of post-tensioning tendons. For straight bridges, the requirements of equations 9.3 and 9.4 should be met with regard to out-of-plane forces, or duct ties should be provided. In bridges with horizontal curvature, the out-of-plane force effects should be added to the in-plane force effects for the design procedures described in sections 9.1.3 and 9.1.4 of this manual.

9.2 End Anchorage Zones

The anchorages of the post-tensioning tendons for cast-in-place box girder bridges are typically located at the end of continuous units of the superstructure. Figure 9.15 shows details commonly found at the end of post-tensioned box girder bridge.

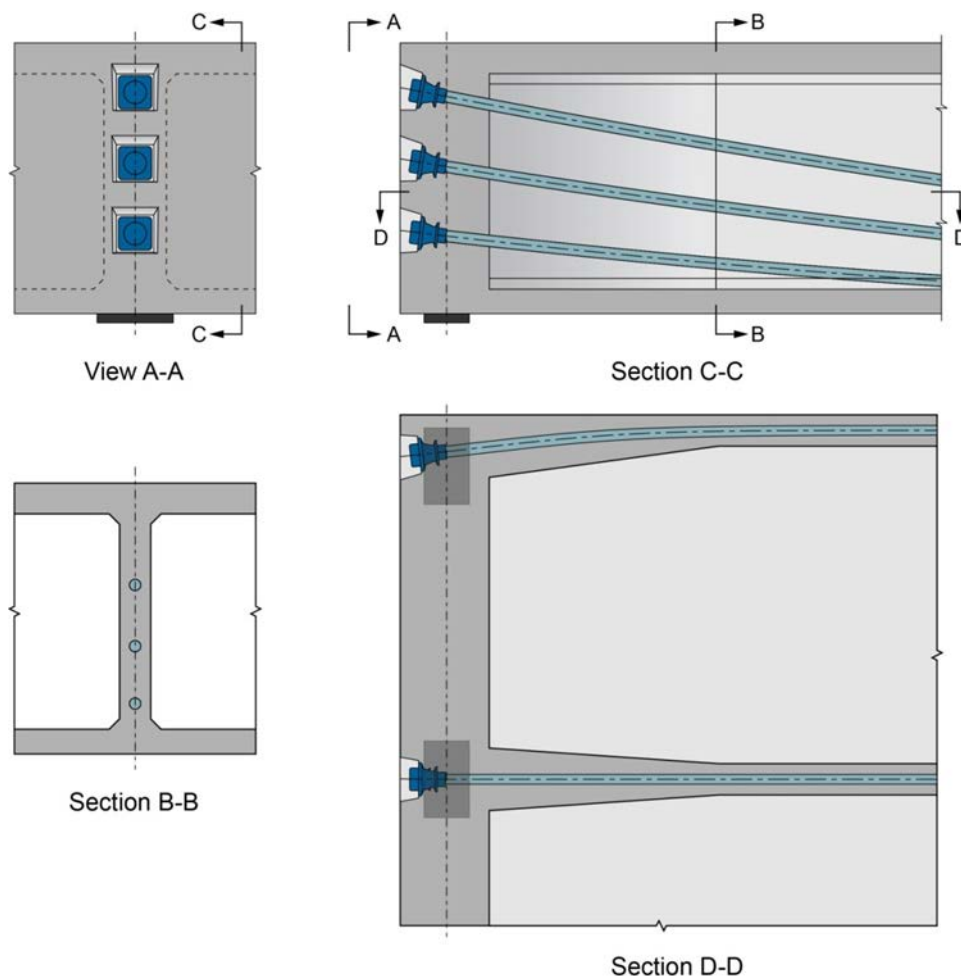


Figure 9.15 – Details of End of Post-Tensioned Box Girder Bridge

The LRFD Article 5.10.9 provides design direction for the development of post-tensioning tendon anchorage zones. The concentrated force applied through the anchorage causes bursting forces in a local zone directly behind the anchorage. The post-tensioning forces are further distributed through a general zone until the beam behavior is achieved. The resistances

required in the local and general zones are determined by strut-and-tie modeling. Figure 5.16 shows a side elevation of one web of a post-tensioned concrete box girder bridge, possible strut-and-tie modeling, and end zone reinforcing steel.

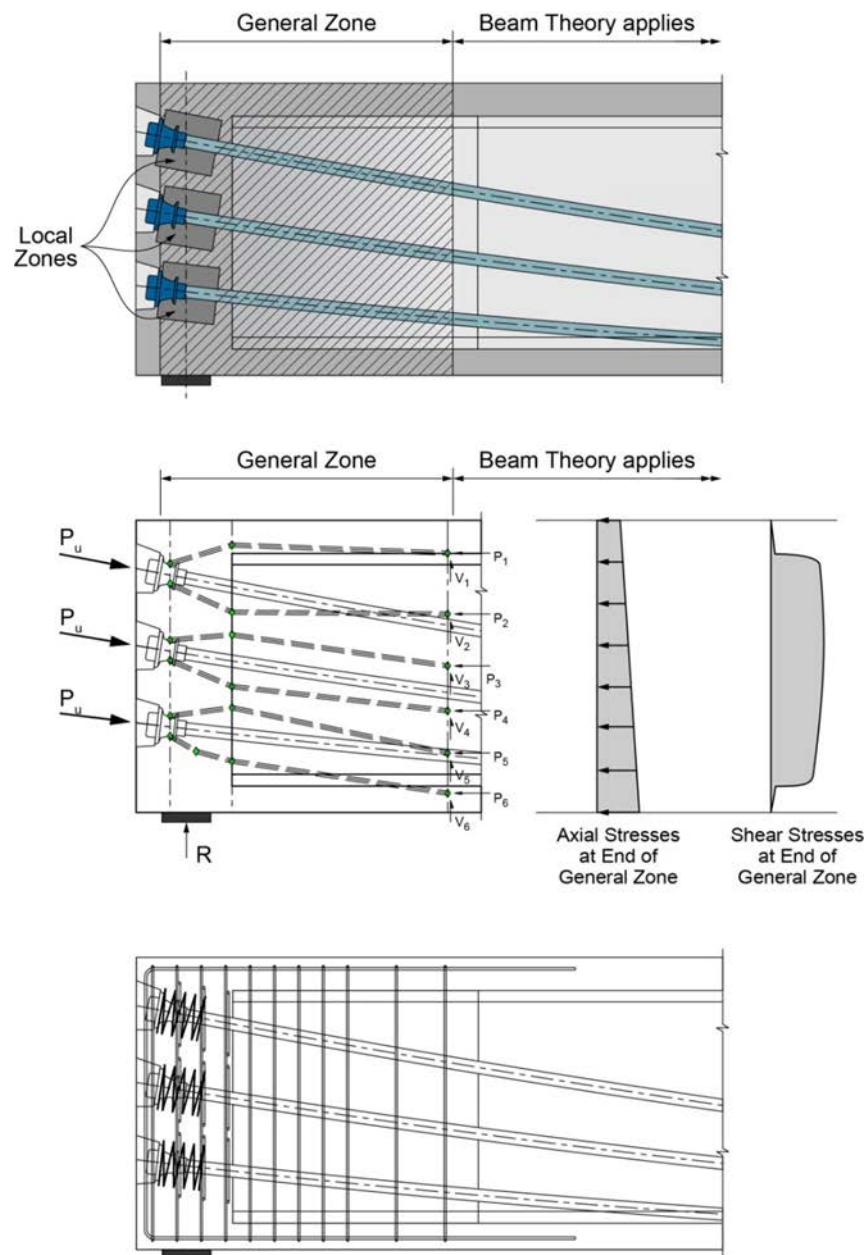


Figure 9.16 – End Zone Design Development

The specifics of designing anchorage zones are not presented in this manual. The reader is directed to FHWA Publication No. FHWA-NHI-07-035 “Load and Resistance Factor Design (LRFD) for Highway Superstructures”, Volume 3 “Concrete Bridge Superstructure Design”, Section 2.6.4 “Post-Tensioning Anchor Zones” for more detailed design information. Another excellent resource is Caltran’s Memo To Designers 11-25 Anchorage Zone Design (October 2012). This document can be found at: <http://www.dot.ca.gov/hq/esc/techpubs/manual/bridgemanuals/bridge-memo-to-designer/page/Section%2011/11-25.pdf>

9.3 Diaphragms at Supports

Box girder sections at piers, expansion joints and abutments contain diaphragms to stiffen and strengthen the typical cross section and to transfer loads from the superstructure to the supporting substructure. Diaphragms work to transfer shear forces in the webs to the bridge bearings, stiffen the box girder with regard to torsion, and provide a location for anchoring post-tensioning tendons. This section develops basic load carrying considerations for diaphragm design.

9.3.1 Single-Cell Box Girder Transfer of Vertical Shear to Bearings

Figure 9.17 shows a fundamental arrangement of a vertical web box girder supported by bearings on a pier. In this arrangement, the pier is sufficiently wide to allow the bearings to be placed directly below the axes of the vertical webs. The diaphragm in this arrangement sees no force under the action of vertical loads.

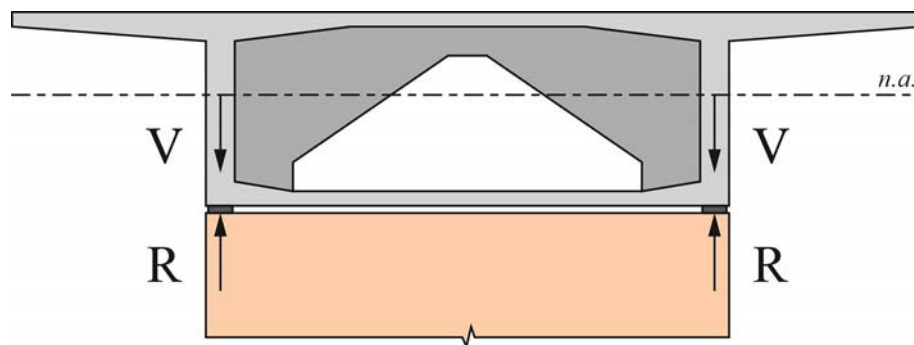


Figure 9.17 – Concentric Web/Bearing Orientation

Using the diaphragm to transfer vertical forces, the bearings spacing may be reduced and the width of the pier cap greatly reduced. This narrowing of the pier cap provides significant cost reduction and can greatly enhance aesthetics. Figure 9.18 shows this bearing configuration for the case of the vertical web box girder. Using strut and tie modeling, the horizontal forces developed by the eccentricity of the web to the bearing can be computed. Though occurring over some depth of the box girder, the transverse reinforcing or post-tensioning used to resist the horizontal forces is typically placed near the top of the diaphragm, detailed to fully develop the width of the webs.

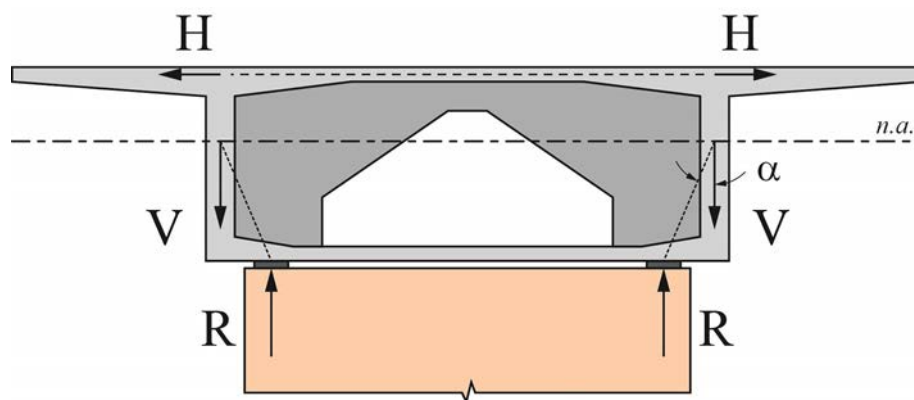


Figure 9.18 – Eccentric Web/Bearing Orientation

In addition to horizontal transverse tensions, figure 9.19 shows two other force transfer mechanisms that need to be investigated when the line of action of the web is eccentric to the bearings. Shear friction at the interface of the web and diaphragm, as shown in the sketch on the left in figure 9.19, should be evaluated and reinforced for in accordance with AASHTO LRFD requirements. Locally, web reinforcing at the bottom of the web is subjected to a direct tension (seen to the right in figure 9.19) that should be included in the web reinforcing selection at the piers and abutments.

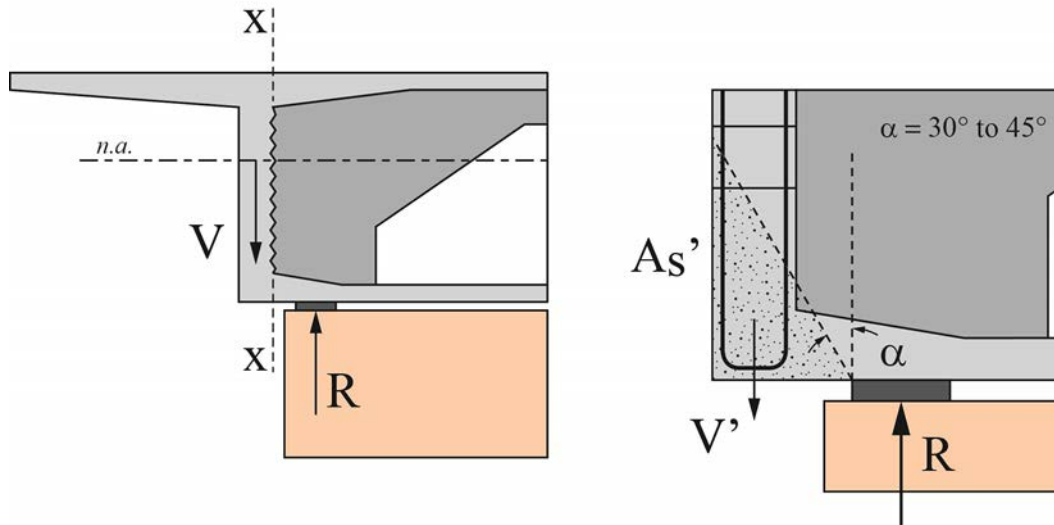


Figure 9.19 – General Shear Friction and Localized Direct Tension

Further cost savings and improved aesthetics are achieved in box girder construction through the use of inclined webs. Figure 9.20 shows the impact on transverse horizontal forces when inclined webs are used. The combination of web slope and bearing offset work to increase transverse horizontal force in the diaphragm.

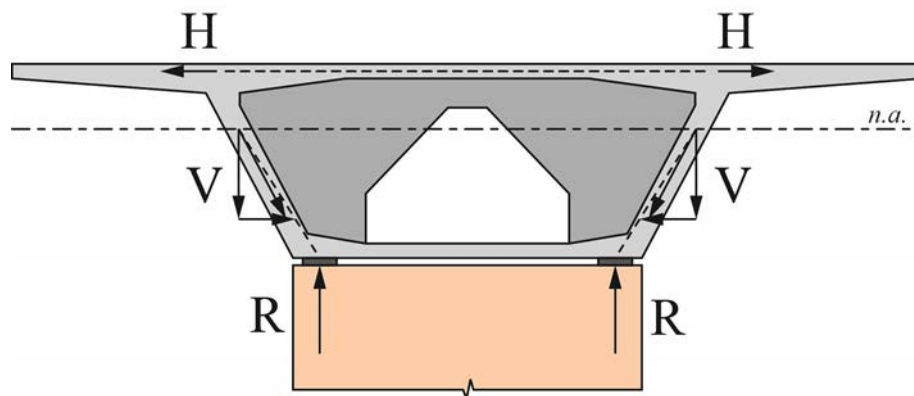


Figure 9.20 – Vertical Force Transfer with Inclined Webs

As with the case of the vertical web box girders, the bearing spacing can be further reduced in bridges with inclined webs to again reduce substructure costs and improve aesthetics. Figure 9.21 depicts a box girder with significant eccentricity between the web line of action and bearings. In this instance, transverse post-tensioning is used to “lift” the web forces to the top of the diaphragm where they are then transferred to the bearings.

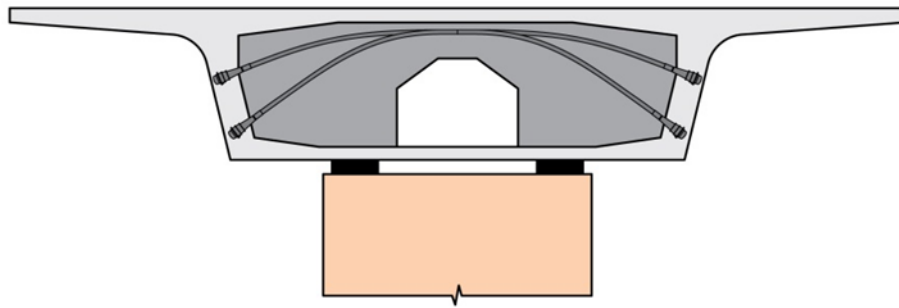


Figure 9.21 – Transverse Post-Tensioning in Diaphragms

9.3.2 Single-Cell Box Girder Transfer of Torsion to Bearings

Forces acting on the superstructure eccentric to the center of torsion will produce torsional moments in the box girder superstructure (see appendix B for further information). The torsional moments are resisted in shear flow around the closed box section. The shear flow and resulting shear stress due to torsion are given by:

(Eqn. 9.12)
$$q = \frac{M_t}{2A_o}$$

(Eqn. 9.13)
$$\tau_i = \frac{q}{t_i} = \frac{M_t}{2A_o t_i}$$

- Where:
- M_t = applied torsional moment (force-length)
 - A_o = area bounded by the median line of the wall thickness
 - t_i = Thickness of the i^{th} member of the cross section (length)
 - q = shear flow (force/length)
 - τ_i = shear stress in the i^{th} member of the cross section (force/length²)

Figure 9.22 shows the concept of shear flow and the limits of A_o . The equations presented here, along with those typically used for the torsional stiffness of a box girder superstructure, are simplified from more complete expressions that include the effect of the cantilever wings. Generally speaking, for most box girder bridges, this behavior is small and may be neglected.

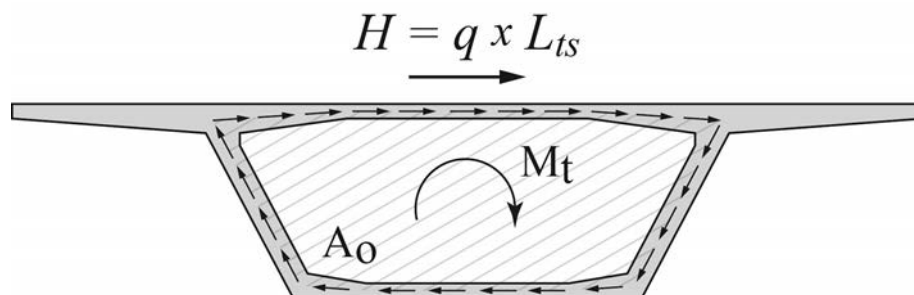


Figure 9.22 – Shear Flow Resulting from Torsional Forces

Torsional moments along a span are transferred to the substructure at the bearings. The shear flow in the top slab caused by the torsional moment reaction produces a horizontal force in the top slab as shown in figure 9.22. Diaphragms located at the piers are detailed to resist the horizontal force in the top slab, and maintain the integrity of the transverse cross section of the superstructure. Figure 9.23 and figure 9.24 show two common configurations of torsion resisting diaphragms. The diaphragm in figure 9.23 resists torsion in an “A-shaped” configuration, while figure 9.24 resists torsion in a “V-shaped” layout. The tension and compression components are evaluated by strut-and-tie models. Tension forces are resisted by either mild reinforcing or inclined post tensioning. Compressive forces are verified to establish minimum torsion diaphragm concrete dimensions.

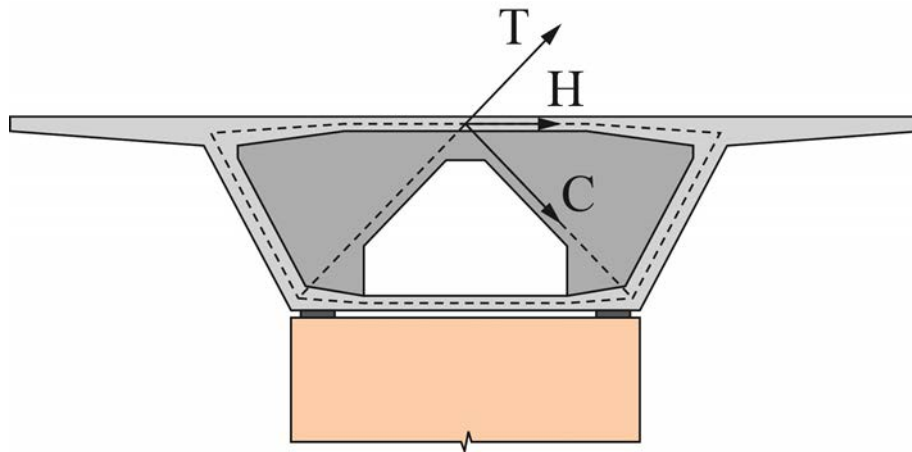


Figure 9.23 - A-shaped Torsion Diaphragm

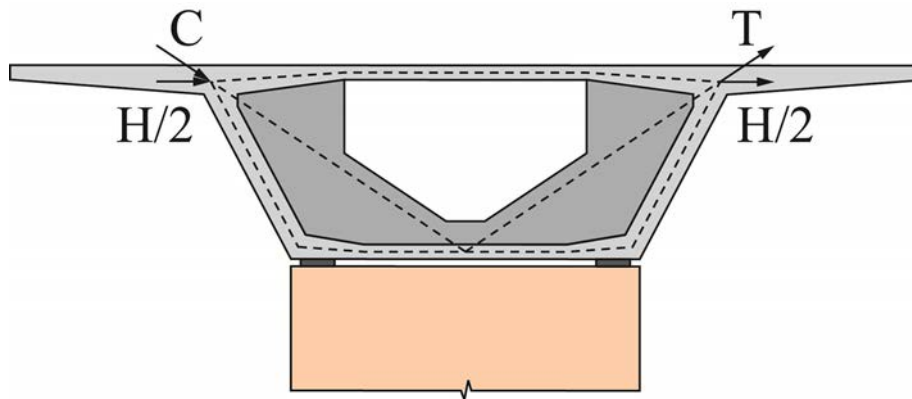


Figure 9.24 – V-shaped Torsion Diaphragm

9.3.3 Multi-Cell Box Girder Diaphragms

Diaphragms of multi-cell box girder bridges are often solid sections within the box girder, with longitudinal thickness sufficient to accept and develop the reinforcing from integrally cast columns. If no access is provided through the diaphragm generally access hatches have to be provided in the soffitt of each box cell for each span. Transverse span-to-depth ratios of the

diaphragms between supporting columns is usually such that a strut-and-tie analysis is appropriate for determining reinforcing.

Figure 9.25 shows one possible strut-and-tie layout for the diaphragms of the bridge of design example 1 in appendix C. The forces applied to this model are the summation of shear forces in the webs. The web forces are applied in halves at the top and bottom of the struts aligned with the webs. (This loading pattern is discussed in a 2007 Transportation Research Board article entitled “LRFD Design of Integral Bent Caps” by Zayati, Ibrahim and Hida.) In this example the diaphragm is simply supported for simplicity of computing the support reactions and member forces.

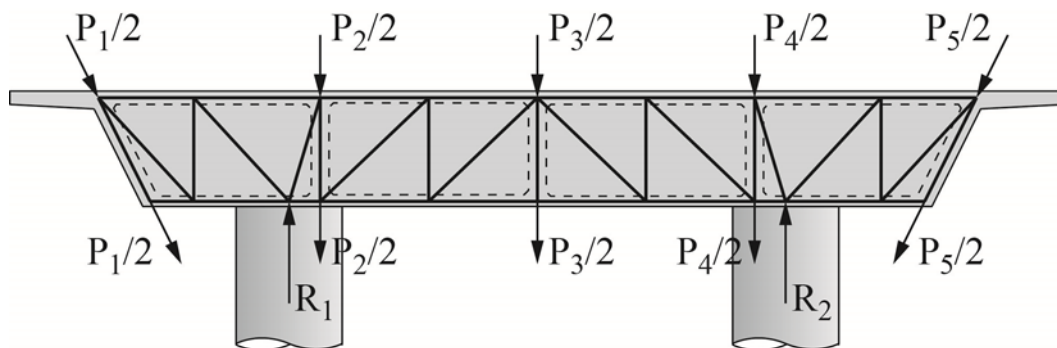


Figure 9.25 – Possible Strut-and-Tie Layout for Diaphragm of Design Example 1

Figure 9.26 shows another possible strut-and-tie layout for the diaphragms of the bridge of design example 1. The alignment of members near the center of compression and tension zones in the columns allow for the monolithic connection behavior of the columns to be captured.

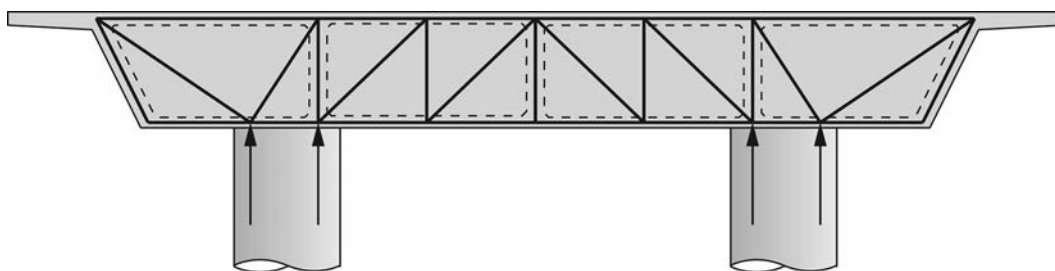


Figure 9.26 – Strut-and-Tie Layout Considering Monolithic Column Connection

Appendix A—Analysis of Two-Dimensional Indeterminate Structures by the Flexibility Method

1. Introduction

Analysis of continuous bridge superstructures is primarily preformed using stiffness based computer solutions that solve the following general equation:

$$\text{(Eqn. A.1)} \quad [F] = [K][X]$$

Where: [F] = vector of forces
[K] = global structure stiffness matrix
[X] = vector of nodal displacements/rotations

The similar general expression in terms of the structure flexibility is:

$$\text{(Eqn. A.2)} \quad [X] = [D][F]$$

Where: [D] = global structure flexibility matrix

The development of computerized stiffness solutions, over computerized flexibility solutions, grew as a result of several factors. Stiffness solutions lent themselves to more efficient programming, an important feature in the early days of computing where CPU costs were very expensive. Stiffness methods also fit well with the predominant hand method of solving indeterminate structures, e.g. the Hardy Cross Method of Moment Distribution.

Hand solutions for solving indeterminate structures by flexibility methods have also been in use for some time. Calperyron produced his Theorem of Three Moments in the 1850's. However, a generalized flexibility method of indeterminate structural analysis, complementary to Moment Distribution, was not generally a part of the American engineer's educational experience.

Flexibility solutions of indeterminate structures did, however, continue to develop outside of the U.S. In the 1960's, Muller and Mathivat summarized a general flexibility method called the Method of Joint Flexibilities (or the Flexibility Method).

Both the Method of Moment Distribution and the Flexibility Method rely on the same basic assumptions of linear elastic behavior, generalized beam deflection equations, and superposition. In practice the two methods are easily understood and have their own advantages:

Moment Distribution—Distributing fixed end moments to find final continuity moments.
Flexibility Method—Restraining simple span rotations to find final continuity moments.

The Flexibility Method is a very useful tool when coupled with numerical techniques for finding simple beam end rotations, such as the Conjugate-Beam Method or Newmark's Method of Numerical Integration. This is especially true for determining continuity bending moments such as secondary moments due to post-tensioning, where simple span rotations can be quickly found by equivalent loading or integration of the curvature diagram defined by F_e/EI .

The Flexibility Method presented in this appendix is that similar to that produced by Muller and Mathivat. This method will serve as the basic analysis method for this Manual.

2. Definition of the Problem

Consider a continuous beam defined by members spanning between supports as shown in figure A.1. Nodes are located at the supports and are lettered g through n . Span ij defines the member that spans between nodes i and j . Nodes i and j , along with the other nodes of the structure, are fixed against displacement but are free to rotate. This one-degree of freedom per node indeterminate structure is to be analyzed to by determining member end (continuity) moments.

The top diagram in figure A.1 shows the continuous beam subjected to the load $p(x)$ in Span ij . This load produces shear forces and bending moments in the continuous beam as shown in the second and third diagrams in figure A.1. The shear forces vary in Span ij because of the loads present in that span. The shear forces in the adjacent unloaded spans are constant and only a function of making equilibrium within the member end moments. Likewise, the bending moments in Span ij are related to the continuity moments and loading within that span, where the moments in adjacent unloaded spans are only related to the member end moments.

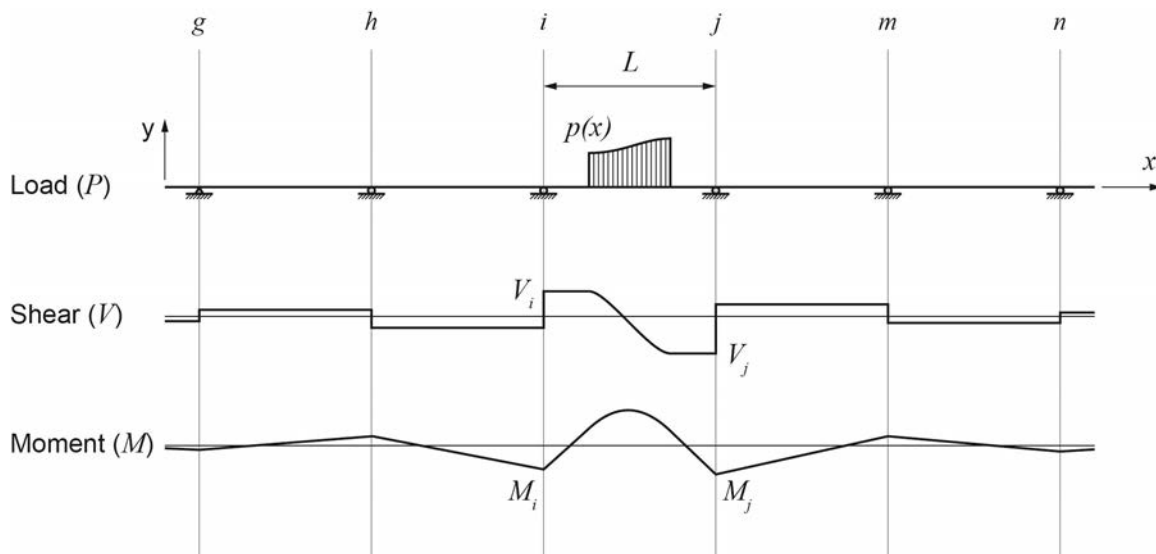


Figure A.1 – Continuous Beam Load, Shear and Moment Diagrams

The Flexibility Method is used to solve for continuity moments in each individually loaded span. Loaded members are first isolated from the structure and end moments determined based on known flexibilities of adjacent restraining spans. The continuity moments are distributed throughout the adjacent spans with distribution and carry-over factors. The complete analysis of a structure loaded in multiple spans is then solved by summing continuity moments of the individual spans.

3. Sign Convention

Positive sign conventions for the Flexibility Method presented in this appendix are shown in figure A.2. Positive bending moments cause tensile stresses on the bottom of the beam (beam designer's sign convention). Positive rotations at the ends of the beams are counter-clockwise.

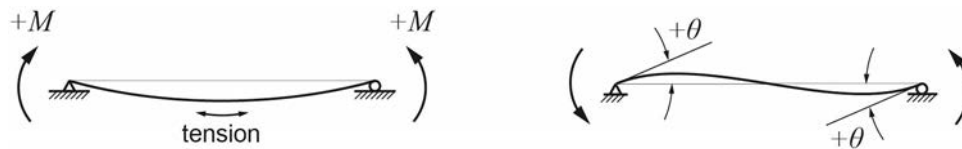


Figure A.2 – Bending Moment and Rotation Sign Convention

4. Simple Span Beam Characteristics

Figure A.3 shows a simple span beam subjected to a bending moment, $M(x)$, and resulting end rotations ω_i and ω_j .

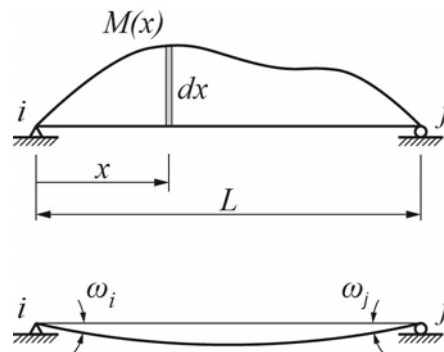


Figure A.3 – Equations for End Rotations of Simple Beams.

The end rotations of simple span beams can be expressed by Bresse’s formulae:

(Eqn. A.3)
$$\omega_i = -\frac{1}{L} \int_0^L \frac{M}{EI} (L-x) dx$$

(Eqn. A.4)
$$\omega_j = \frac{1}{L} \int_0^L \frac{Mx}{EI} dx$$

Simple span beam characteristics for the Flexibility Method are defined as the rotations of the beam ends under the action of unit moments applied at the beam ends, as shown in figures A.4 and A.5.

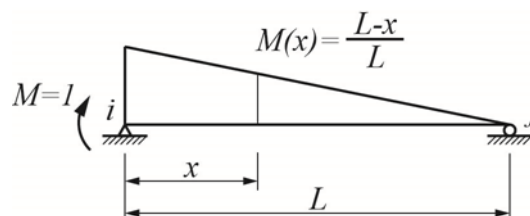


Figure A.4 – Bending Moment Diagram for Unit Moment at Node i.

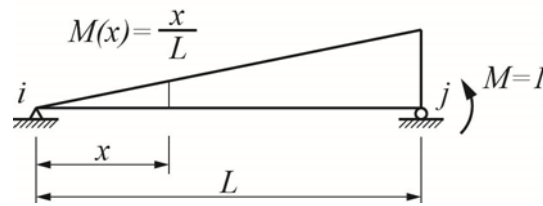


Figure A.5 – Bending Moment Diagram for Unit Moment at Node *j*.

Applying a unit moment at node *i* results in the rotations:

(Eqn. A.5)
$$\omega_i = -\frac{1}{L^2} \int_0^L \frac{(L-x)^2}{EI} dx = a$$

(Eqn. A.6)
$$\omega_j = \frac{1}{L^2} \int_0^L \frac{x(L-x)}{EI} dx = b$$

Applying a unit moment at node *j* results in the rotations:

(Eqn. A.7)
$$\omega_j = \frac{1}{L^2} \int_0^L \frac{x^2}{EI} dx = c$$

(Eqn. A.8)
$$\omega_i = -\frac{1}{L^2} \int_0^L \frac{x(L-x)}{EI} dx = -b$$

Coefficients *a*, *b*, and *c* are the simple span beam characteristics required in the Flexibility Method. The coefficients are always positive and graphically expressed these coefficients are:

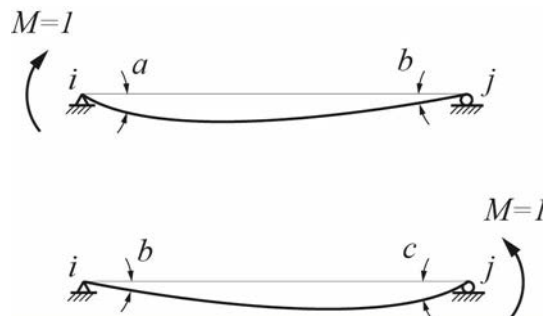


Figure A.6 – Simple Span Beam Characteristics

For a beam with constant inertia:

(Eqn. A.9)
$$a = c = \frac{L}{3EI}$$

(Eqn. A.10)
$$b = \frac{L}{6EI}$$

5. Definition of Support Flexibility and Member Flexibility Coefficients

The development of the Flexibility Method begins with isolating the individual spans and defining their behavior as a function of the span characteristics and the rotational restraints offered by adjacent spans. Consider Span ij which is defined between nodes i and j as shown in figure A.7. Span ij is part of an indeterminate planar structure as previously described. Other members are connected to nodes i and j in this structure are Span ih and Span jm .

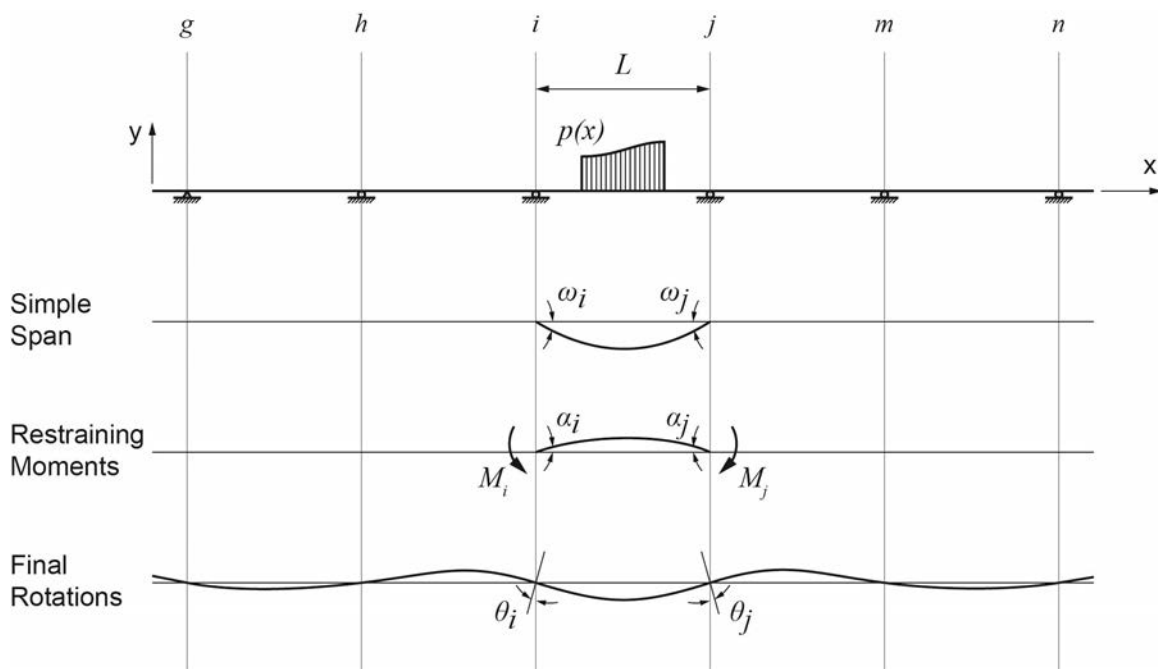


Figure A.7 – Span ij in a Continuous Structure.

If Span ij was simply supported it would deflect freely and the rotations of the extremities would be the simple span rotations ω_i and ω_j shown in the second sketch of figure A.7. The adjacent connecting members, Span ih and Span jm , restrain these rotations, producing moments M_i and M_j . The simple span rotations caused by the continuity moments M_i and M_j are α_i and α_j . The final end rotations are the values θ_i and θ_j which represent the difference between the simple span rotations resulting from loads (ω) and the simple span rotations resulting from continuity moments (α).

Assuming linear elastic behavior and non-deformable connections between the members, Span ij behaves as if each extremity was restrained by a rotational spring simulating the actual connecting members, Span ih and Span jm . The isolated Span ij with equivalent end rotational springs is shown in figure A.11.

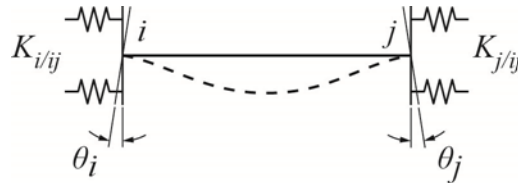


Figure A.8 – Isolating Span ij

The coefficients $K_{i/ij}$ and $K_{j/ij}$, are called the Support Flexibility Constants, and represent the flexibilities that the Span ij feels as a result of its connectivity with the adjacent spans. The flexibility of a support is a positive number varying between zero and infinity (0 and ∞). The constants are equal to zero when the end of the beam is completely fixed. A simply supported beam end has a support flexibility constant of infinity.

The relationship between end rotations and end moments are:

$$\theta_i = M_i K_{i/ij}$$

(Eqns. A.11)

$$\theta_j = -M_j K_{j/ij}$$

The support flexibilities $K_{i/ij}$ and $K_{j/ij}$ are related to the flexibility of the adjacent spans connected to Span ij at nodes i and j . Figure A.9 shows the unloaded adjacent spans with compatible rotations θ_i and θ_j , subjected to the end moments m_i and m_j . Figure A.10 isolates the two adjacent members Span hi and Span jm . The coefficients $k_{ih/i}$ and $k_{jm/j}$, are called the member flexibility constants of the adjacent member spans. They are defined by the span characteristics and the support flexibilities at the far ends of the spans.

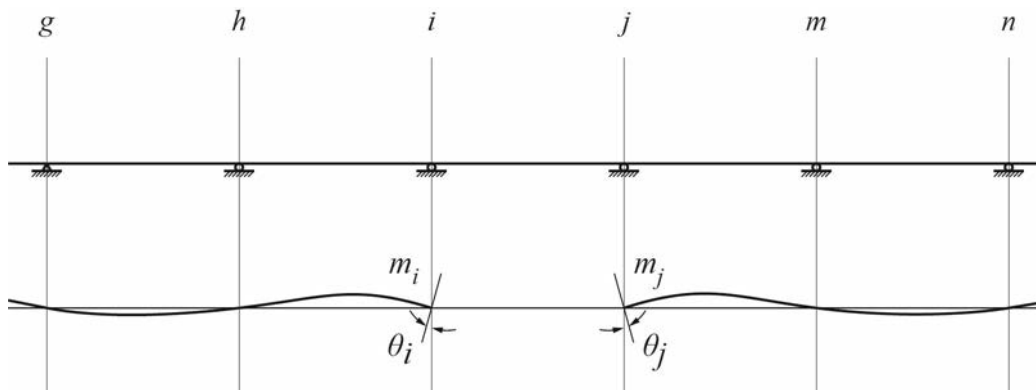


Figure A.9 – Compatible rotations of adjacent members

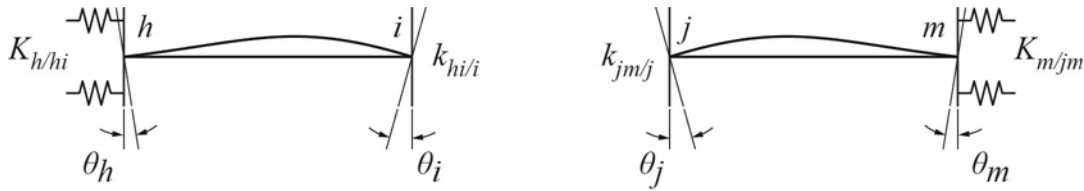


Figure A.10 – Adjacent Member Flexibilities

The relationship between end rotations and end moments are:

$$\theta_i = m_i k_{hi/i}$$

(Eqns. A.12)

$$\theta_j = -m_j k_{jm/j}$$

Setting equations A.11 and A.12 equal to each other we see that:

$$K_{i/ij} = k_{hi/i}$$

(Eqns. A.13)

$$K_{j/jm} = k_{jm/j}$$

The equality of the support flexibilities with the adjacent member flexibilities, as shown in equations A.13, are true for the case of continuous beams with only one span framing into Span *ij*. When several members frame into nodes *i* and *j*, the summation of moments result in:

$$M_i = \frac{\theta_i}{K_{i/ij}} = \sum_{h \neq j} m_i = \sum_{h \neq j} \frac{\theta_i}{k_{hi/i}}$$

(Eqn. A.14)

$$M_j = -\frac{\theta_j}{K_{j/ij}} = \sum_{m \neq i} m_j = -\sum_{m \neq i} \frac{\theta_j}{k_{jm/j}}$$

(Eqn. A.15)

From these expressions, the general relationships between support and adjacent beam end flexibilities are:

$$\frac{1}{K_{i/ij}} = \sum_{h \neq j} \frac{1}{k_{hi/i}}$$

(Eqns. A.16)

$$\frac{1}{K_{j/ij}} = \sum_{m \neq i} \frac{1}{k_{jm/j}}$$

6. Relationship between Support Flexibility Constants and Continuity Bending Moments

The next step in the development of the Flexibility Method is to express continuity bending moments as a result of restraining side spans in relation to the flexibilities that those spans provide through Support Flexibility Constants.

By superposition, we define the final rotations in the continuous beam as the summation of the simple span rotations under the action of the applied loads and the rotations resulting from the continuity moments:

$$\theta_i = \omega_i + \alpha_i$$

(Eqns. A.17)

$$\theta_j = \omega_j + \alpha_j$$

Knowing beam characteristics for Span ij (a , b , and c) the rotations of the simple span beam resulting from the continuity moments can be written as:

$$\alpha_i = -aM_i - bM_j$$

(Eqns. A.18)

$$\alpha_j = bM_i + cM_j$$

Combining equations A.17 and A.18 the final rotations are:

$$\theta_i = \omega_i - aM_i - bM_j$$

(Eqns. A.19)

$$\theta_j = \omega_j + bM_i + cM_j$$

Recalling that the final rotations in the continuous beam are also defined to be equal to the continuity moment times the support flexibility constant (equation A.11), we can write:

$$K_{i/ij}M_i = \omega_i - aM_i - bM_j$$

(Eqns. A.20)

$$-K_{j/ij}M_j = \omega_j + bM_i + cM_j$$

Solving for the continuity moments M_i and M_j we find:

$$M_i = \frac{(c + K_{j/ij})\omega_i + b\omega_j}{(a + K_{i/ij})(c + K_{j/ij}) - b^2}$$

(Eqns. A.21)

$$M_j = -\frac{b\omega_i + (a + K_{i/ij})\omega_j}{(a + K_{i/ij})(c + K_{j/ij}) - b^2}$$

For the special case of a beam fixed against rotations at both ends, $K_{i/ij}$ and $K_{j/ij}$ equal zero, and:

$$M_i = \frac{c\omega_i + b\omega_j}{ac - b^2}$$

(Eqns. A.22)

$$M_j = -\frac{b\omega_i + a\omega_j}{ac - b^2}$$

Comparing equations A.21 and A.22, the elastically restrained span is equivalent to a perfectly fixed span having the effective flexibilities of:

$$a' = a + K_{i/ij}$$

(Eqns. A.23)

$$b' = b$$

$$c' = c + K_{j/ji}$$

For a span perfectly fixed and with constant inertia, the coefficients of flexibility are equal to those of equations A.9 and A.10 and equations A.21 can be reduced to:

$$M_i = \frac{2EI}{L}(2\omega_i + \omega_j)$$

(Eqns. A.24)

$$M_j = -\frac{2EI}{L}(\omega_i + 2\omega_j)$$

7. Relationships between Support Joint Flexibilities and Member End Flexibilities

Determining the support constants $K_{i/ij}$ and $K_{j/ji}$ requires the determination of the member end flexibilities $k_{ih/i}$ and $k_{jm/j}$ of the members connecting the Span ij to the structure. Consider Span hi which is to the left of Span ij .

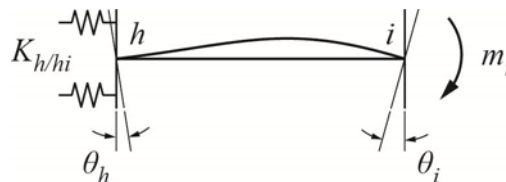


Figure A.11 – Member End Flexibility for Span hi

Apply a moment m_i at the i end of Span ih . The resulting end moments in relation to end rotations are:

$$\theta_h = K_{h/hi} m_h$$

(Eqns. A.25)

$$\theta_i = k_{hi/i} m_i$$

The end rotations in terms of the beam characteristics are:

$$\theta_h = -am_h - bm_i$$

(Eqns. A.26)

$$\theta_i = bm_h + cm_i$$

Equating equations A.25 and A.26:

$$K_{h/hi} m_h = -am_h - bm_i$$

(Eqns. A.27)

$$k_{hi/i} m_i = bm_h + cm_i$$

Solving for $k_{hi/i}$:

$$k_{hi/i} = c - \frac{b^2}{a + K_{h/hi}}$$

(Eqn. A.28)

If we perform the same analysis for Span jm , which is to the right of Span ij , we can solve for $k_{jm/j}$:

$$k_{jm/j} = a - \frac{b^2}{c + K_{m/jm}}$$

(Eqn. A.29)

In developing a solution for all spans of the structure, we will require the member end flexibilities at either end of each span. For convenience, therefore, we will write the relationships between member end flexibility and support flexibility in a more generic form in terms of Span ij :

$$k_{ij/i} = a - \frac{b^2}{c + K_{j/ij}}$$

(Eqn. A. 30)

$$k_{ij/j} = c - \frac{b^2}{a + K_{i/ij}}$$

(Eqn. A. 31)

Consider two special conditions of known boundary conditions:

- a. For a member simple supported at the i end, the flexibility of the support $K_{i/ij}$ is equal to infinity and the member end flexibility reduces to:

(Eqn. A.32)
$$k_{ij|j} = c$$

- b. When the i end of the member is fixed, the flexibility of the support $K_{i|ij}$ is equal to zero and the member flexibility becomes:

(Eqn. A.33)
$$k_{ij|j} = c - \frac{b^2}{a + K_{i|ij}}$$

8. Carry Over Factors

In the previous section we developed the member end flexibilities as a function of beam characteristics and the support flexibility at the other end of the beam. The top of figure A.12 shows this modeling for Span ij . The bottom figure shows the moment diagram when there are no loads in the span. It is convenient to express the ratio of the moment at the i end of Span ij to the moment at the j end. For this reason, we define the Carry Over Factor as the ratio of m_i to m_j .

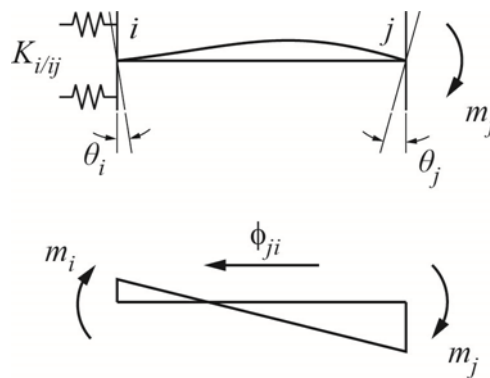


Figure A.12 – Carry Over Factor from j to i

Equating the end rotations at i to those of the restraining side span to the left of i :

(Eqn. A.34)
$$K_{i|ij} m_i = -am_i - bm_j$$

Rearranging and combining like terms:

(Eqn. A.35)
$$(a + K_{i|ij}) m_i = -bm_j$$

From this we can define the Carry Over Factor from i to j :

(Eqn. A.36)
$$\phi_{ji} = \frac{m_i}{m_j} = -\frac{b}{a + K_{i|ij}}$$

Considering Span in the opposite direction, as if it were a member restraining the right end of a loaded span, we would find:

$$(Eqn. A.37) \quad \phi_{ij} = \frac{m_j}{m_i} = -\frac{b}{c + K_{jlij}}$$

Consider two special conditions of known boundary conditions:

- a. For a member simple supported at the i end, the flexibility of the support K_{iij} is equal to infinity and the Carry Over Factor is equal to zero. This is intuitive, as there is no adjacent member connected at i to attract any bending moment.
- b. When the both ends of the member are fixed, the flexibility of the supports is equal to zero and the Carry Over Factors are:

$$(Eqns. A.38) \quad \phi_{ij} = -\frac{b}{c}$$

$$\phi_{ji} = -\frac{b}{a}$$

If this span has constant inertia over its length:

$$(Eqn. A.39) \quad \phi_{ij} = \phi_{ji} = -\frac{1}{2}$$

9. Continuity Moments Expressed by Carry Over Factors

The Carry Over Factors developed in the previous section can be substituted into the relationships for bending moment as a function of beam characteristics and joint support flexibilities (equations A.21) to produce the following simplified expressions:

$$(Eqn. A.40) \quad M_i = -\frac{\phi_{ji}}{b} \left(\frac{\omega_i - \phi_{ij}\omega_j}{1 - \phi_{ij}\phi_{ji}} \right)$$

$$M_j = \frac{\phi_{ij}}{b} \left(\frac{\omega_j - \phi_{ji}\omega_i}{1 - \phi_{ij}\phi_{ji}} \right)$$

For a symmetric span symmetrically loaded,

$$(Eqn. A.41) \quad \omega_{ij} = -\omega_{ji} = \omega$$

$$M_i = -\frac{\phi_{ji}}{b} \left(\frac{1 + \phi_{ij}}{1 - \phi_{ij}\phi_{ji}} \right) \omega$$

(Eqns. A.42)

$$M_j = -\frac{\phi_{ij}}{b} \left(\frac{1 + \phi_{ji}}{1 - \phi_{ij}\phi_{ji}} \right) \omega$$

For a symmetric span, symmetrically loaded, with symmetrical support flexibilities,

$$K_{i/ij} = K_{j/ij}$$

(Eqns. A.43)

$$\phi_{ij} = \phi_{ji} = \phi$$

(Eqn. A.44)

$$M_i = M_j = -\left(\frac{\phi}{1 + \phi} \right) \frac{\omega}{b}$$

For a span hinged at support i ,

$$\phi = 0$$

(Eqns. A.45)

$$M_{ij} = 0$$

(Eqn. A.46)

$$M_j = -\frac{\phi_{ij}}{b} \omega_j$$

10. Distribution Coefficients of Moments at Nodes.

In equations 14, 15 and 16 of section 5, we considered the development of the support flexibilities when multiple members frame into node i and all work to restrain Span ij . Bending moments developed by the restraining members must be distributed between the elements which frame together at node i .

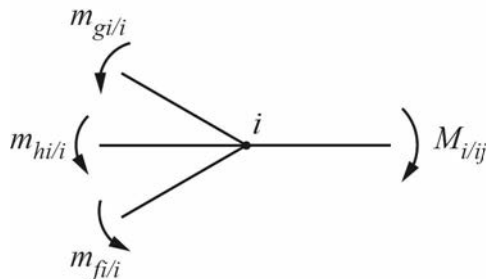


Figure A.13 – Moment Equilibrium at Node i

$$(Eqn. A.47) \quad \theta_i = K_{i/ij} M_{i/ij}$$

$$(Eqn. A.48) \quad \theta_i = k_{hi/i} m_{hi/i}$$

$$(Eqn. A.49) \quad \lambda_{ih} = \frac{m_{hi/i}}{M_{i/ij}} = \frac{K_{i/ij}}{k_{hi/i}}$$

Remembering that stiffnesses are the inverse of flexibility

$$(Eqn. A.50) \quad \lambda_{ih} = \frac{K_{i/ij}}{k_{hi/i}} = \frac{1}{\frac{k_{hi/i}}{K_{i/ij}}} = \frac{r_{hi/i}}{R_{i/ij}} = \frac{r_{hi/i}}{\sum_{h \neq j} r_{hi/i}}$$

The distribution of bending moments at nodes is therefore, proportional to the relative stiffness of the elements framing at joint i .

11. Solving the Structure

We have seen that any Span ij is defined by the member characteristics and the Support Flexibilities $K_{i/ij}$ and $K_{j/ij}$. The span is first isolated from the structure and analyzed for the applied loads to determine continuity moments. The distribution of the continuity moments to other elements framing into the supports is made in proportion to their relative stiffnesses using distribution factors. The moments at the far end of adjacent spans is found through the carry-over factors.

For plane frame structures (open systems) the solution begins at a known boundary condition, such as an end span whose extremity is free to rotate. The needed coefficients are then determined first working left to right from the known boundary condition at the left, and then work right to left from the known boundary condition at the right.

In the case of closed systems, such as the cross section of a box girder bridge, the determination of the support flexibilities can be made by successive approximations of one support and then calculating the others in order. Typically, few analyses around closed structure are required to have the assumed value converge to that derived by the analysis.

12. Summary of Equations

Support Flexibilities:

$$(Eqn. A.51) \quad K_{i/ij} = \frac{\theta_i}{M_{i/ij}}$$

$$(Eqn. A.52) \quad K_{j/ij} = \frac{\theta_j}{M_{j/ij}}$$

Member Flexibilities:

$$(Eqn. A.53) \quad k_{ij/i} = a - \frac{b^2}{c + K_{j/ij}}$$

$$(Eqn. A.54) \quad k_{ij/j} = c - \frac{b^2}{a + K_{i/ij}}$$

Carry-Over Factors:

$$(Eqn. A.55) \quad \phi_{ij} = -\frac{b}{c + K_{j/ij}}$$

$$(Eqn. A.56) \quad \phi_{ji} = -\frac{b}{a + K_{i/ij}}$$

End Moments of the Loaded Span:

$$(Eqn. A.57) \quad M_i = -\frac{\phi_{ji}}{b} \left(\frac{\omega_i - \phi_{ij}\omega_j}{1 - \phi_{ij}\phi_{ji}} \right)$$

$$(Eqn. A.58) \quad M_j = \frac{\phi_{ij}}{b} \left(\frac{\omega_j - \phi_{ji}\omega_i}{1 - \phi_{ij}\phi_{ji}} \right)$$

Distribution Factors:

$$(Eqn. A.59) \quad \lambda_{ih} = \frac{\frac{1}{k_{hi/i}}}{\frac{1}{K_{i/ij}} + \sum_{h \neq j} \frac{1}{k_{hi/i}}} = \frac{1}{\frac{1}{K_{i/ij}} + \sum_{h \neq j} \frac{1}{k_{hi/i}}} = \frac{K_{i/ij}}{k_{hi/i}}$$

13. Example – Flexibility Analysis of a 3 Span Continuous Beam

The three-span example bridge being developed in this Section is shown schematically in figure A.14. The cross section of the superstructure of the box girder is shown in figure 5.9 in chapter 5 of this manual.

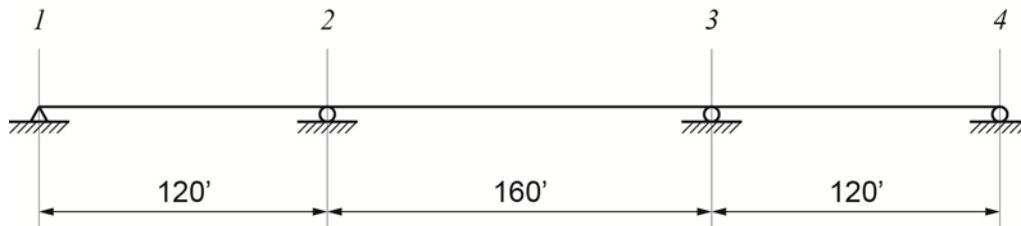


Figure A.14 – Model of 3-Span Bridge for Example 1

13.1 Span Properties and Characteristic Flexibilities

The cross section properties of the box girder superstructure shown in figure 5.9 in chapter 5 of this manual are:

$$I = 643.7 \text{ ft}^4$$

$$A = 99.45 \text{ ft}^2$$

$$c_1 = 2.732 \text{ ft}$$

$$c_2 = 3.768 \text{ ft}$$

$$\rho = 0.6288$$

$$Q_0 = 118.1 \text{ ft}^3$$

The characteristic flexibilities for the 120' Span are:

$$Ea = Ec = \frac{L}{3I} = \frac{120}{3(643.7)} = 0.06214$$

$$Eb = \frac{L}{6I} = \frac{120}{6(643.7)} = 0.03107$$

The characteristic flexibilities for the 160' Span are:

$$Ea = Ec = \frac{L}{3I} = \frac{160}{3(643.7)} = 0.08285$$

$$Eb = \frac{L}{6I} = \frac{160}{6(643.7)} = 0.041425$$

13.2 Analysis Left to Right

$$K_{1/12} = \infty \quad k_{12/2} = c - \frac{b^2}{a + K_{1/12}} = 0.06214 - \frac{(0.03107)^2}{0.06214 + \infty} = 0.06214$$

$$K_{2/23} = \frac{1}{\frac{1}{0.06214}} = 0.06214$$

$$k_{23/3} = c - \frac{b^2}{a + K_{2/23}} = 0.08285 - \frac{(0.041425)^2}{0.08285 + 0.06214} = 0.07101$$

$$K_{3/34} = \frac{1}{\frac{1}{0.07101}} = 0.07101$$

13.3 Analysis Right to Left

$$K_{4/43} = \infty \quad k_{34/3} = a - \frac{b^2}{c + K_{4/43}} = 0.06214 - \frac{(0.03107)^2}{0.06214 + \infty} = 0.06214$$

$$K_{3/23} = \frac{1}{\frac{1}{0.06214}} = 0.06214$$

$$k_{23/2} = a - \frac{b^2}{c + K_{3/23}} = 0.08285 - \frac{(0.041425)^2}{0.08285 + 0.06214} = 0.07101$$

$$K_{2/12} = \frac{1}{\frac{1}{0.07101}} = 0.07101$$

13.4 Carry-Over Factors

For the Superstructure:

$$\phi_{12} = -\frac{b}{c + K_{2/12}} = -\frac{0.03107}{0.06214 + 0.07101} = -0.2333$$

$$\phi_{21} = -\frac{b}{a + K_{1/12}} = -\frac{0.03107}{0.06214 + \infty} = 0.0$$

$$\phi_{23} = -\frac{b}{c + K_{3/23}} = -\frac{0.041425}{0.08285 + .06214} = -0.2857 \quad (= \phi_{32} \text{ by symmetry})$$

$$\phi_{34} = -\frac{b}{c + K_{4/34}} = -\frac{0.03107}{0.06214 + \infty} = 0.0 \quad \phi_{43} = -\frac{b}{a + K_{3/34}} = -\frac{0.03107}{0.06214 + .07101} = -0.2333$$

13.5 Effect of a Unit Uniform Load

The beam end rotations when loaded by a downward acting unit uniform load are:

$$E\omega_i = -E\omega_j = -\frac{L^3}{24I}$$

The beam characteristics of the 120' end spans are:

$$E\omega_i = -E\omega_j = -\frac{120^3}{24(643.7)} = -111.9$$

The beam characteristics of the 160' center span is:

$$E\omega_i = -E\omega_j = -\frac{160^3}{24(643.7)} = -265.1$$

The moments in Span 1 are:

$$M_{12} = 0.0 \quad M_{21} = -\frac{\phi_{12}}{b}(\omega_2) = -\frac{-0.2333}{.03107}(-111.9) = -840 \text{ ft-kips}$$

The end moments in Span 2 are:

$$M_{23} = -\frac{\phi_{32}}{b} \left(\frac{\omega_2 - \phi_{23}\omega_3}{1 - \phi_{23}\phi_{32}} \right) = -\frac{0.2857}{0.041425} \left(\frac{-265.1 - (-0.2857)(265.1)}{1 - (-0.2857)(-0.2857)} \right) = -1422 \text{ ft-kips}$$

The other end moments in Span 2 and 3 are known by symmetry:

$$M_{32} = -1422 \text{ ft-kips} \quad M_{34} = -840 \text{ ft-kips} \quad M_{43} = 0.0$$

The bending moments diagrams for the load in each span and the total of all moments is shown in figure 5.11.

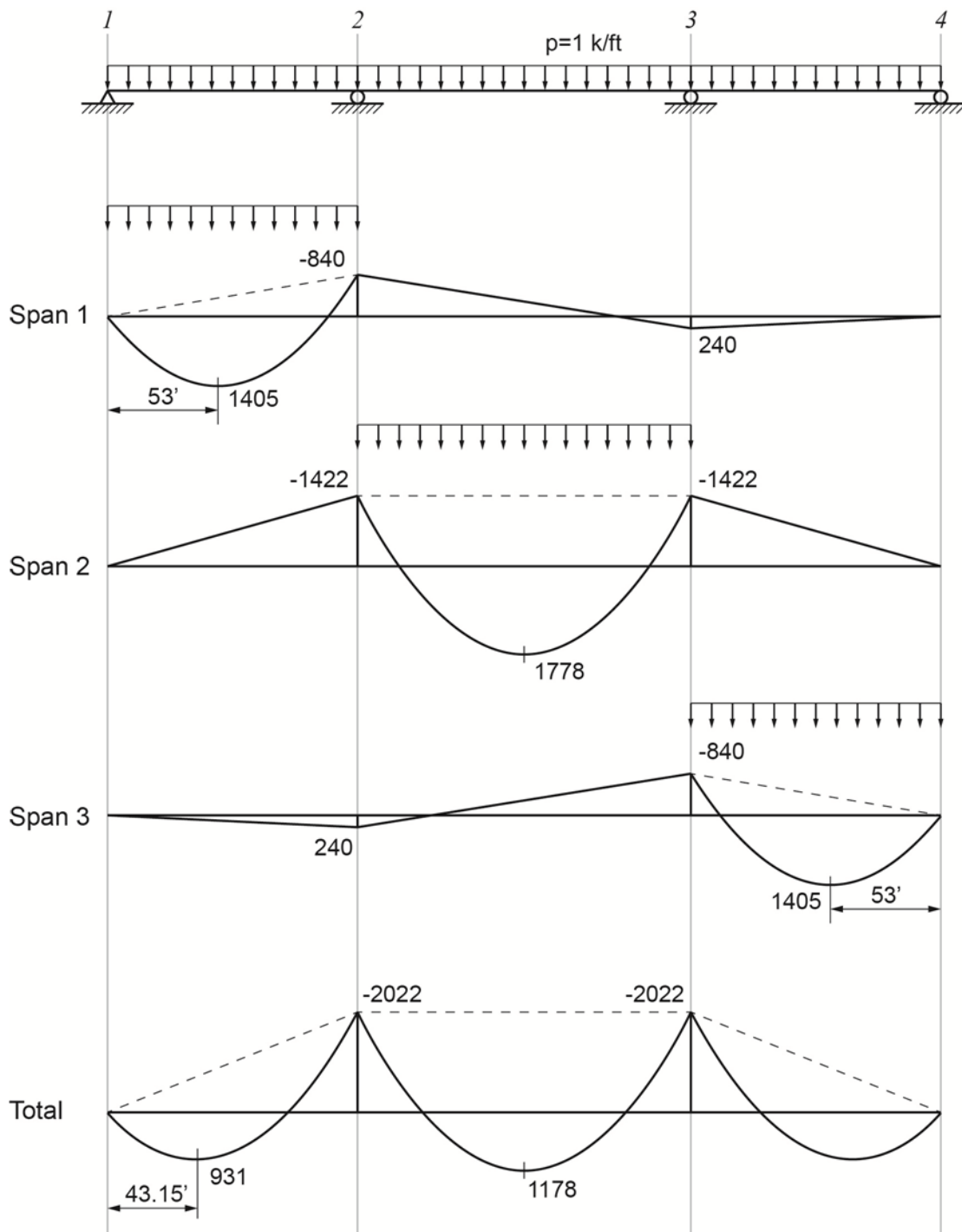


Figure A.15 – Moment Diagram for a Unit Uniform Load

14. Frames Braced Against Side-Sway

The previous analysis considered a three-span beam horizontally restrained by a hinged support at the left end of the beam. Now consider a framed structure where the beam is integrally connected to supporting columns as shown in figure A.16. The columns, designated by the node number of the beam at the top of the column and the letter at the base of the column, are fixed at the base.

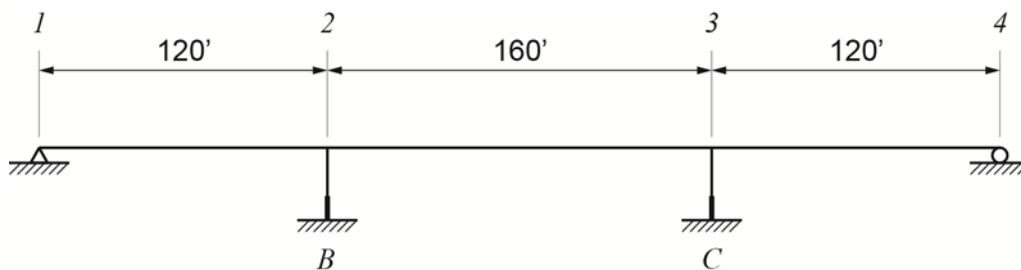


Figure A.16 – Moment Diagram for a Unit Uniform Load

Figure A.17 shows an individual column, applied pier top forces Q and M , and the resulting pier top rotations and deflections. Column characteristic flexibilities are required in order to define top of pier lateral and rotational flexibilities.

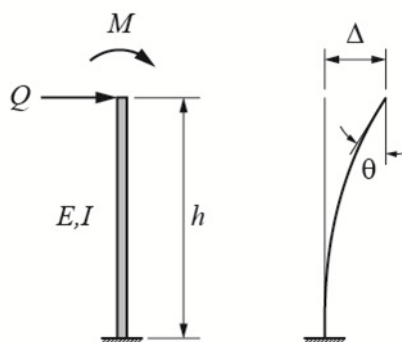


Figure A.17 – Cantilever Column

The general equations for pier top displacements are:

$$\theta = \int_0^h \frac{M(x)}{EI(x)} dx \qquad \Delta = \int_0^h \frac{M(x)}{EI(x)} x dx$$

(Eqns. A.60)

For a moment M applied at the top of the pier:

$$\theta = \frac{Mh}{EI} \qquad \Delta = \frac{Mh^2}{2EI}$$

(Eqns. A.61)

For a force Q applied at the top of the pier:

$$(Eqns. A.62) \quad \theta = \frac{Qh^2}{2EI} \quad \Delta = \frac{Qh^3}{3EI}$$

For unit forces and moments the rotations and displacements become the pier flexibilities summarized as:

$$(Eqns. A.63) \quad A = \frac{h}{EI} \quad B = \frac{h^2}{2EI} \quad C = \frac{h^3}{3EI}$$

The equations describing the rotation and deflection at the top of the pier are expressed as:

$$(Eqn. A.64) \quad \theta = AM + BQ$$

$$(Eqn. A.65) \quad \Delta = BM + CQ$$

For the case of a framed braced against side-sway, the lateral deflection equals zero:

$$(Eqn. A.66) \quad -BM = CQ$$

$$(Eqn. A.67) \quad Q = -\frac{B}{C}M$$

Substituting equation A.67 into A.64:

$$(Eqn. A.68) \quad \theta = AM + B\left(-\frac{B}{C}M\right)$$

Rearranging terms:

$$(Eqn. A.69) \quad \theta = \left(A - \frac{B^2}{C}\right)M$$

From which we define the pier top rotational flexibility as:

$$(Eqn. A.70) \quad k_{pier} = \frac{\theta}{M} = A - \frac{B^2}{C}$$

We can also compute a carry-over factor from the top to the bottom of the pier by considering equilibrium:

$$(Eqn. A.71) \quad M_{base} = M_{top} + Qh$$

Substituting equation A.67 into A.71:

$$(Eqn. A.72) \quad M_{base} = M_{top} + \left(-\frac{B}{C} M_{top} \right) h$$

$$(Eqn. A.73) \quad \phi = \frac{M_{base}}{M_{top}} = 1 - \frac{B}{C} h$$

For a pier of constant inertia:

$$(Eqn. A.74) \quad \phi = 1 - \left(\frac{h^2}{2EI} \right) \left(\frac{3EI}{h^3} \right) h = -0.5$$

With the pier top rotational flexibility and the carry-over factor from the top to the bottom of the pier, the framed structure braced against side-sway can be solved.

15. Multiple Pier Elements

The flexibility of the supporting piers can vary with height. Gradual variations, such as linear tapers of pier width are accounted for in the development of basic flexibility characteristics beginning with equation A.60. Abrupt changes in column properties or where foundation elements are modeled with equivalent vertical members, as shown in figure A.18, are treated using the following relationships:

$$(Eqn. A.75) \quad EA = \sum EA_i$$

$$(Eqn. A.76) \quad EB = \sum EB_i + \sum EA_i(h - z_i)$$

$$(Eqn. A.77) \quad EC = \sum EC_i + 2\sum EB_i(h - z_i) + \sum EA_i(h - z_i)^2$$

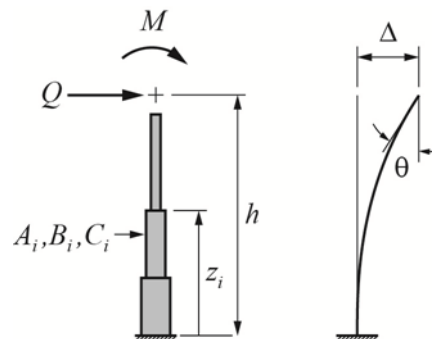


Figure A.18 – Column with Multiple Elements

16. Side-Sway Correction

Figure A.19 shows the lateral displacement for a column rigidly connected to superstructure girder.

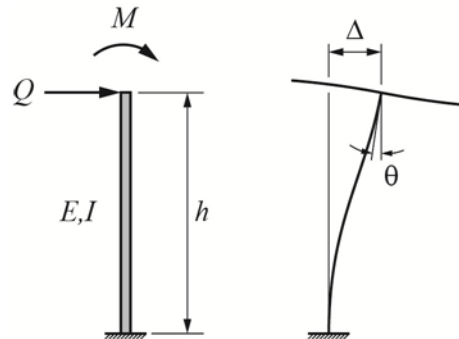


Figure A.19 – Column in a Rigid Frame

For a unit lateral displacement, the general equations of deflection given in equations A.66 and A.67 become:

$$(Eqn. A.78) \quad \theta = AM + BQ = -KM$$

$$(Eqn. A.79) \quad \Delta = BM + CQ = 1$$

Where K is the joint flexibility provided by the restraining superstructure:

$$(Eqn. A.80) \quad K_{j/jn} = \frac{1}{\frac{1}{k_{ij/j}} + \frac{1}{k_{jk/j}}}$$

Solving equation A.78 for Q, substituting the results into equation A.79, and rearranging, the moment at the top of the pier from the unit lateral displacement is:

$$(Eqn. A.81) \quad M = -\frac{B}{C} \left(\frac{1}{k + K} \right)$$

Solving for the shear in the column:

$$(Eqn. A.82) \quad Q = -\left(\frac{K + A}{B} \right) M$$

By equilibrium, the moment at the bottom of the column is:

$$(Eqn. A.83) \quad M_{bottom} = M_{top} - Qh$$

Side-sway corrections are made by restraining shears for the frame braced against side-sway and then applying the release of the sway by adding the moments due to side-sway scaled to have equity with the base shear.

17. Example Problem with Side-Sway

The three-span bridge being designed in example 1 is shown schematically in figure A.20. The piers consist of two, 6' diameter columns at supports B and C. Each concrete column is supported by a 7' diameter drilled shaft. The equivalent length of drilled shaft based on the soil characteristics at this site has been determined to be 10'. The modulus of elasticity of all concrete is assumed constant for this example.

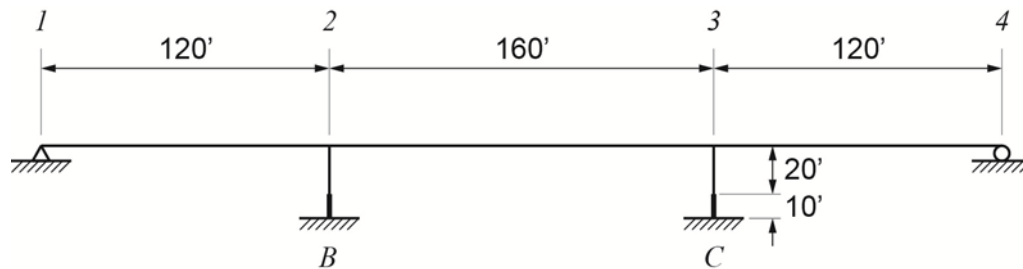


Figure A.20 – Model of 3-Span Bridge for Example 1

17.1 Span Properties and Characteristic Flexibilities

The moment of inertia for the superstructure is:

$$I = 643.7 \text{ ft}^4$$

The characteristic flexibilities for the 120' Span are:

$$Ea = Ec = \frac{L}{3I} = \frac{120}{3(643.7)} = 0.06214$$

$$Eb = \frac{L}{6I} = \frac{120}{6(643.7)} = 0.03107$$

The characteristic flexibilities for the 160' Span are:

$$Ea = Ec = \frac{L}{3I} = \frac{160}{3(643.7)} = 0.08285$$

$$Eb = \frac{L}{6I} = \frac{160}{6(643.7)} = 0.041425$$

17.2 Column and Drilled Shaft Characteristic Flexibilities

The gross moment of inertias for the 7' diameter drilled shafts and the 6' diameter columns are (2 columns at each support):

$$I_d = 2 \times \frac{\pi(7)^4}{64} = 235.7 \text{ ft}^4 \qquad I_c = 2 \times \frac{\pi(6)^4}{64} = 127.2 \text{ ft}^4$$

The characteristic flexibilities for the 10' Drilled Shafts are:

$$EA_f = \frac{L_d}{I_d} = \frac{10}{(235.7)} = 0.04243$$

$$EB_f = \frac{L_d^2}{2I_d} = \frac{10^2}{2(235.7)} = 0.2121$$

$$EC_f = \frac{L_d^3}{3I_d} = \frac{10^3}{3(235.7)} = 1.414$$

The characteristic flexibilities for the 20' Columns are:

$$EA_c = \frac{L_c}{I_c} = \frac{20}{(127.2)} = 0.1572$$

$$EB_c = \frac{L_c^2}{2I_c} = \frac{20^2}{2(127.2)} = 1.572$$

$$EC_c = \frac{L_c^3}{3I_c} = \frac{20^3}{3(127.2)} = 20.96$$

The combined flexibilities for the column/drilled shaft foundations at the top of the rigid connection at the center of gravity of the bridge deck are:

$$EA = EA_f + EA_c$$

$$EA = 0.1572 + 0.04243 = 0.1996$$

$$EB = EB_f + EB_c + EA_f(z - z_f) + EA_c(z - z_c)$$

$$EB = 0.2121 + 1.572 + 0.04243(33.768 - 10) + 0.1572(33.768 - 30) = 3.385$$

$$EC = EC_f + EC_c + EC_f + 2EB_f(z - z_f) + 2EB_c(z - z_c) + EA_f(z - z_f)^2 + EA_c(z - z_c)^2$$

$$EC = 1.414 + 20.96 + 2(0.2121)(33.768 - 10) + 2(1.572)(33.768 - 30)$$

$$+ 0.04243(33.768 - 10)^2 + 0.1572(33.768 - 30)^2 = 70.50$$

The combined pier top flexibilities when sidesway is restrained are:

$$Ek_p = EA - \frac{(EB)^2}{EC} = 0.1996 - \frac{(3.385)^2}{70.50} = 0.03707$$

17.3 Analysis Left to Right

$$K_{1/12} = \infty$$

$$k_{12/2} = c - \frac{b^2}{a + K_{1/12}} = 0.06214 - \frac{(0.03107)^2}{0.06214 + \infty} = 0.06214$$

$$k_{2B/2} = 0.03707$$

$$K_{2/23} = \frac{1}{\frac{1}{0.06214} + \frac{1}{.03707}} = 0.02322$$

$$k_{23/3} = c - \frac{b^2}{a + K_{2/23}} = 0.08285 - \frac{(0.041425)^2}{0.08285 + 0.02322} = 0.06667$$

$$k_{3C/3} = 0.03707$$

$$K_{3/34} = \frac{1}{\frac{1}{0.06667} + \frac{1}{.03707}} = 0.02382$$

17.4 Analysis Right to Left

$$K_{4/34} = \infty$$

$$k_{34/3} = a - \frac{b^2}{c + K_{4/34}} = 0.06214 - \frac{(0.03107)^2}{0.06214 + \infty} = 0.06214$$

$$k_{3C/3} = 0.03707$$

$$K_{3/23} = \frac{1}{\frac{1}{0.06214} + \frac{1}{.03707}} = 0.02322$$

$$k_{23/2} = a - \frac{b^2}{c + K_{3/23}} = 0.08285 - \frac{(0.041425)^2}{0.08285 + 0.02322} = 0.06667$$

$$k_{2B/2} = 0.03707$$

$$K_{2/21} = \frac{1}{\frac{1}{0.06667} + \frac{1}{.03707}} = 0.02382$$

17.5 Carry-Over Factors

For the Superstructure:

$$\phi_{12} = -\frac{b}{c + K_{2/21}} = -\frac{0.03107}{0.06214 + .02382} = -0.3615 \quad \phi_{21} = -\frac{b}{a + K_{1/12}} = -\frac{0.03107}{0.06214 + \infty} = 0.0$$

$$\phi_{23} = \phi_{32} = -\frac{b}{c + K_{3/32}} = -\frac{0.041425}{0.08285 + .02322} = -0.3905$$

$$\phi_{34} = -\frac{b}{c + K_{4/43}} = -\frac{0.03107}{0.06214 + \infty} = 0.0 \quad \phi_{43} = -\frac{b}{c + K_{3/34}} = -\frac{0.03107}{0.06214 + .02382} = -0.3615$$

For the Substructure:

$$\phi_{2B} = \phi_{3C} = 1 - \left(\frac{EB}{EC} \right) L = 1 - \left(\frac{3.385}{70.50} \right) 33.768 = -0.6213$$

17.6 Distribution Factors

Moment at 2 end of member 21:

$$d_{23} = \frac{\frac{1}{k_{23/2}}}{\frac{1}{k_{23/2}} + \frac{1}{k_{2B/2}}} = \frac{\frac{1}{0.06667}}{\frac{1}{0.06667} + \frac{1}{.03707}} = 0.3573$$

$$d_{2B} = \frac{\frac{1}{k_{2B/2}}}{\frac{1}{k_{23/2}} + \frac{1}{k_{2B/2}}} = \frac{\frac{1}{0.03707}}{\frac{1}{0.06667} + \frac{1}{.03707}} = 0.6427$$

Moment at 2 end of member 23:

$$d_{21} = \frac{\frac{1}{k_{12/2}}}{\frac{1}{k_{12/2}} + \frac{1}{k_{2B/2}}} = \frac{\frac{1}{0.06214}}{\frac{1}{0.06214} + \frac{1}{.03707}} = 0.3737$$

$$d_{2B} = \frac{\frac{1}{k_{2B/2}}}{\frac{1}{k_{12/2}} + \frac{1}{k_{2B/2}}} = \frac{\frac{1}{0.03707}}{\frac{1}{0.06214} + \frac{1}{.03707}} = 0.6263$$

Moment at 3 end of member 32 (by symmetry):

$$d_{34} = 0.3737$$

$$d_{3C} = 0.6263$$

Moment at 3 end of member 34 (by symmetry):

$$d_{32} = 0.3573$$

$$d_{2B} = 0.6427$$

The distribution of moments at the top of Column 2B to the adjacent spans are:

$$d_{21} = \frac{\frac{1}{k_{12/2}}}{\frac{1}{k_{12/2}} + \frac{1}{k_{23/2}}} = \frac{\frac{1}{0.06214}}{\frac{1}{0.06214} + \frac{1}{.06667}} = 0.5176$$

$$d_{23} = \frac{\frac{1}{k_{23/2}}}{\frac{1}{k_{12/2}} + \frac{1}{k_{23/2}}} = \frac{\frac{1}{0.06667}}{\frac{1}{0.06214} + \frac{1}{.06667}} = 0.4824$$

For a moment at the top of Column 3C (by symmetry):

$$d_{32} = 0.4824$$

$$d_{34} = 0.5176$$

17.7 End Moments for Unit Uniform Load

The beam end rotations when loaded by a downward acting unit uniform load are:

$$E\omega_i = -E\omega_j = -\frac{L^3}{24I}$$

The beam characteristics of the 120' end spans are:

$$E\omega_i = -E\omega_j = -\frac{120^3}{24(643.7)} = -111.9$$

The beam characteristics of the 160' center span is:

$$E\omega_i = -E\omega_j = -\frac{160^3}{24(643.7)} = -265.1$$

The moments in Span 1 are:

$$M_{12} = 0.0$$

$$M_{21} = -\frac{\phi_{12}}{b}(\omega_2) = -\frac{-0.3615}{.03107}(-1111.9) = -1302 \text{ ft-kips}$$

The end moments in Span 2 are:

$$M_{23} = -\frac{\phi_{32}}{b} \left(\frac{\omega_2 - \phi_{23}\omega_3}{1 - \phi_{23}\phi_{32}} \right) = \frac{-0.3905}{0.041425} \left(\frac{-265.1 - (-0.3905)(265.1)}{1 - (-0.3905)(-0.3905)} \right) = -1797 \text{ ft-kips}$$

The end moments in Span 3 (by Symmetry),

$$M_{32} = -1797 \text{ ft-kips} \quad M_{34} = -1302 \text{ ft-kips} \quad M_{43} = 0.0$$

17.8 Distribute End Moments across the Structure

Carry-Over Factors are applied to compute the moments at the adjacent supports.

Load in Span 1:

$$M_{12} = 0$$

$$M_{21} = -1302$$

$$M_{23} = d_{23}M_{21} = 0.3573(-1302) = -465$$

$$M_{2B} = d_{2B}M_{21} = 0.6427(-1302) = -837$$

$$M_{32} = \phi_{23}M_{23} = -0.3905(-465) = 182$$

$$M_{B2} = \phi_{2B}M_{2B} = -0.6213(-837) = 520$$

$$M_{34} = d_{34}M_{32} = 0.3737(182) = 68$$

$$M_{3C} = d_{3C}M_{32} = 0.6263(182) = 114$$

$$M_{43} = 0$$

$$M_{C3} = \phi_{3C}M_{3C} = -0.6213(114) = -71$$

Load in Span 2:

$$M_{23} = -1797$$

$$M_{32} = -1797$$

$$M_{21} = d_{21}M_{23} = 0.3737(-1797) = -672$$

$$M_{2B} = d_{2B}M_{23} = 0.6263(-1797) = -1125$$

$$M_{12} = 0$$

$$M_{B2} = \phi_{2B}M_{2B} = -0.6213(-1125) = 699$$

$$M_{34} = d_{34}M_{32} = 0.3737(-1797) = -672$$

$$M_{3C} = d_{3C}M_{32} = 0.6263(-1797) = -1125$$

$$M_{43} = 0$$

$$M_{C3} = \phi_{3C}M_{3C} = -0.6213(-1125) = 699$$

Load in Span 3: $M_{43} = 0$

$$M_{34} = -1302$$

$$M_{32} = d_{32}M_{34} = 0.3573(-1302) = -465$$

$$M_{3C} = d_{3C}M_{34} = 0.6427(-1302) = -837$$

$$M_{23} = \phi_{32}M_{32} = -0.3905(-465) = 182$$

$$M_{C3} = \phi_{3C}M_{3C} = -0.6213(-837) = 520$$

$$M_{21} = d_{21}M_{23} = 0.3737(182) = 68$$

$$M_{2B} = d_{2B}M_{23} = 0.6263(182) = 114$$

$$M_{12} = 0$$

$$M_{B2} = \phi_{2B}M_{2B} = -0.6213(114) = -71$$

17.9 Effect of a Unit Uniform Load

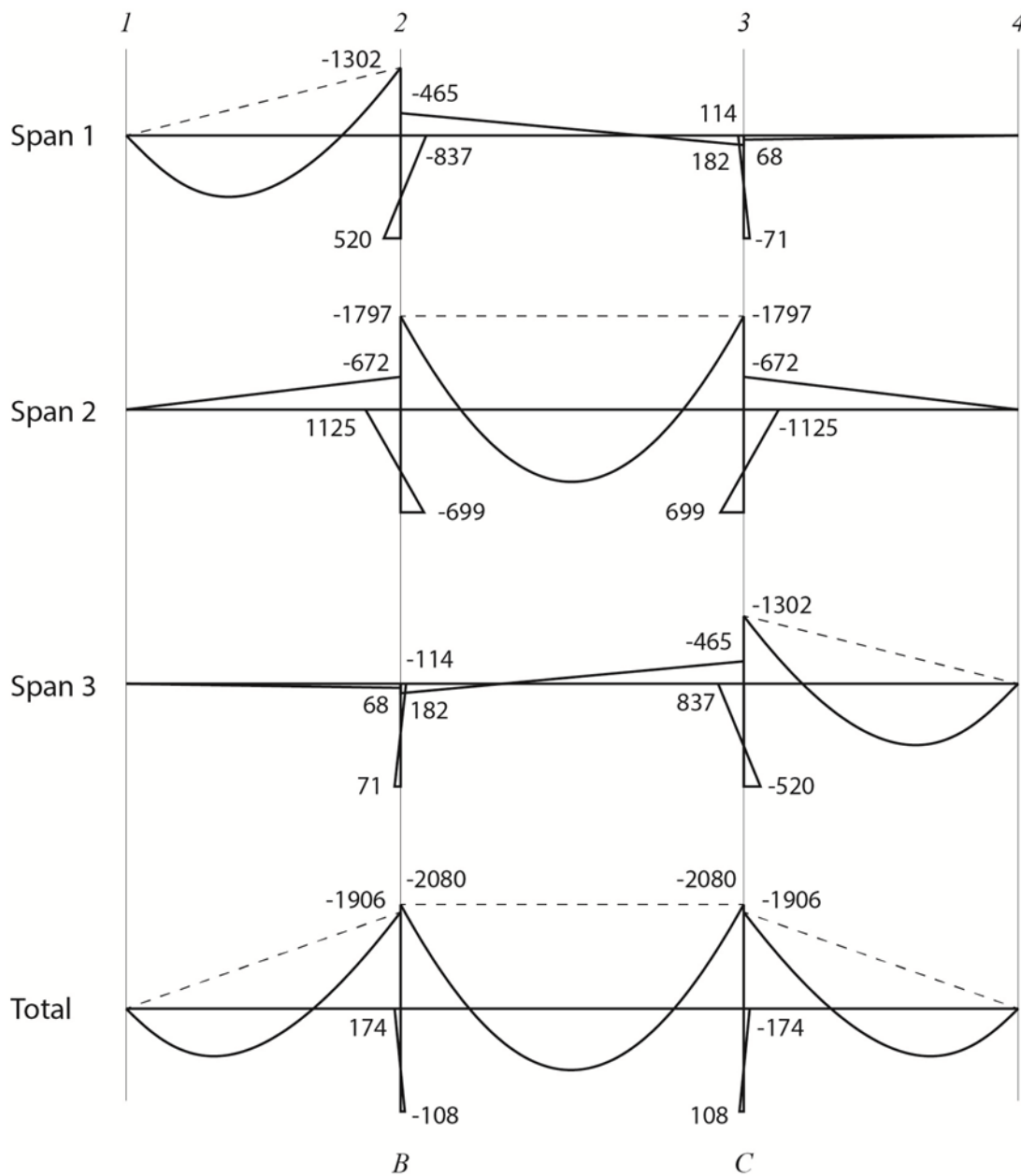


Figure A.21 – Moment Diagram for a Unit Uniform Load

17.10 Side-Sway Correction

For a unit lateral displacement of a top of the piers (see appendix A):

$$M = -\frac{B}{C} E\Delta \left(\frac{1}{k+K} \right)$$

$$Q = -\left(\frac{K+A}{B} \right) M$$

From the analysis above:

$$k_p = 0.03707$$

$$k_{23/2} = 0.06667$$

$$k_{21/2} = 0.06214$$

From which we derive:

$$K_{2/2B} = \frac{1}{\frac{1}{k_{23/2}} + \frac{1}{k_{21/2}}} = 0.03216$$

And the distribution factors for moments in the piers:

$$d_{21} = 0.5176$$

$$d_{32} = 0.4824$$

$$d_{23} = 0.4824$$

$$d_{34} = 0.5176$$

The bending moment and shear force developed at the top of each pier as each pier is displaced a unit dimension while the second pier is stationary are:

$$M_{top} = -\frac{3.385}{70.50} (617,300)(1) \left(\frac{1}{0.03707 + 0.03216} \right) = -428,126 \text{ ft} - \text{kips}$$

$$Q = -\left(\frac{0.03216 + 0.1996}{3.385} \right) (-428,126) = 29,312.4 \text{ kips}$$

By equilibrium, the moment at the bottom of the column is (h=33.768'):

$$M_{bottom} = M_{top} - Qh = 561,695 \text{ ft} - \text{kips}$$

Figure A.22 shows the distribution of the bending moments around the frame for Pier 2B, Pier 3C, and the sum of the bending moments for a unit side-sway. The base shear created for this unit side-sway is:

$$Q = 2 \left(\frac{593,077 + 478,636}{33.768} \right) = 63,475 \text{ kips / ft}$$

Side-sway corrections are made by restraining shears for the frame braced against side-sway and then applying the release of the sway by adding the moments due to side-sway scaled to have equity with the base shear.

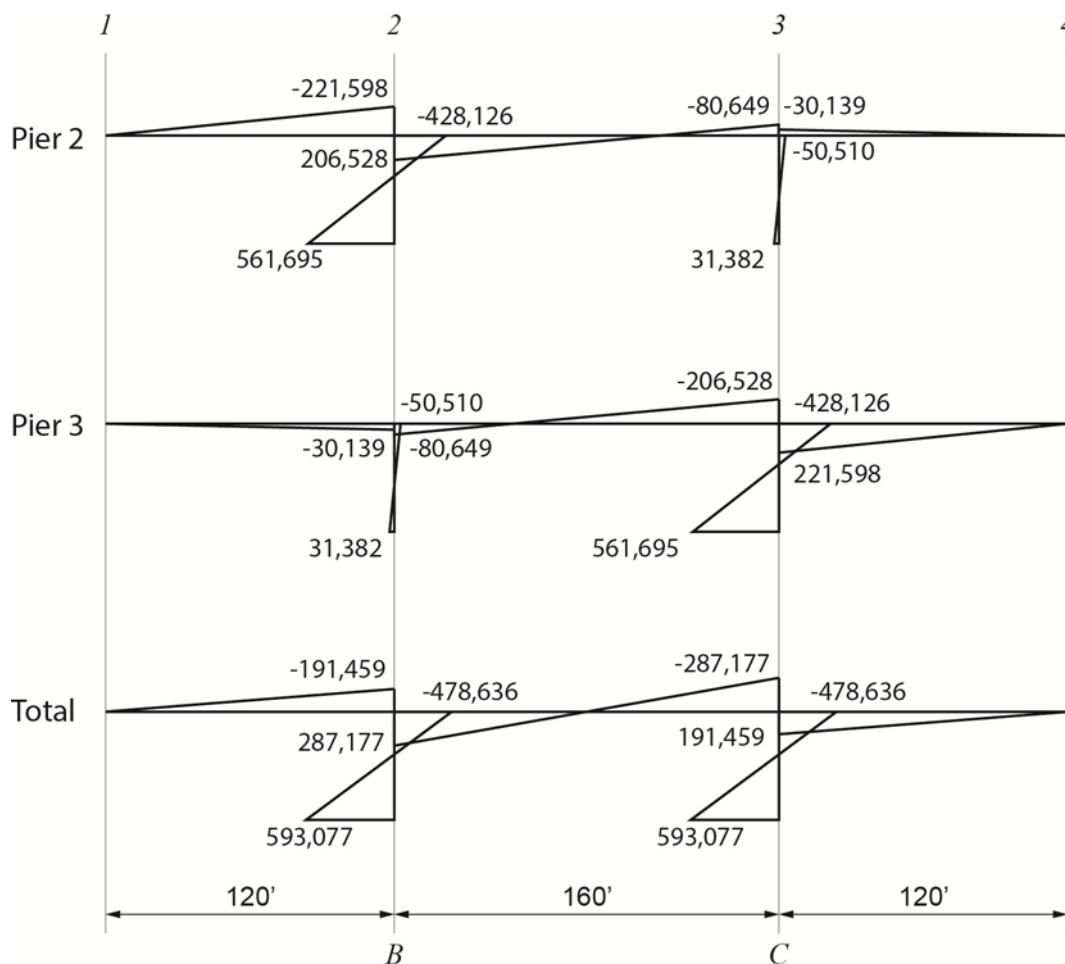


Figure A.22 – Moment Diagram for a Unit Lateral Side-Sway

Appendix B—Torsion

This Appendix presents information related to the torsional characteristics of box girder bridges. A review of torsion in a solid circular bar is first presented to establish basic concepts. This information is then extended to the torsional behavior of a thin wall closed shape, specifically, the single-cell box girder. Lastly, torsional characteristics of multiple-cell box girders are presented.

1. Torsion in a Circular Shaft

The circular shaft is unique with regard to torsion in that the relationship between torsional moment and rotation can be determined directly from kinematics, equilibrium, and constitutive laws. Consider a circular shaft shown in figure B.1 with length L and outside radius R . Radius r denotes the location of point p within the cross section of the bar. The bar is assumed to be comprised of a perfectly elastic, homogeneous and isotropic material. The circular bar is subjected to an externally applied torsional moment M_t at one end which is resisted by an equal and opposite torsional moment at the opposite end. The application and restraint of the torsional moments is such that regions of discontinuity in torsional deformations are not created at the ends of the bar. The resulting nature of torsional deformation is constant throughout the length of the bar.

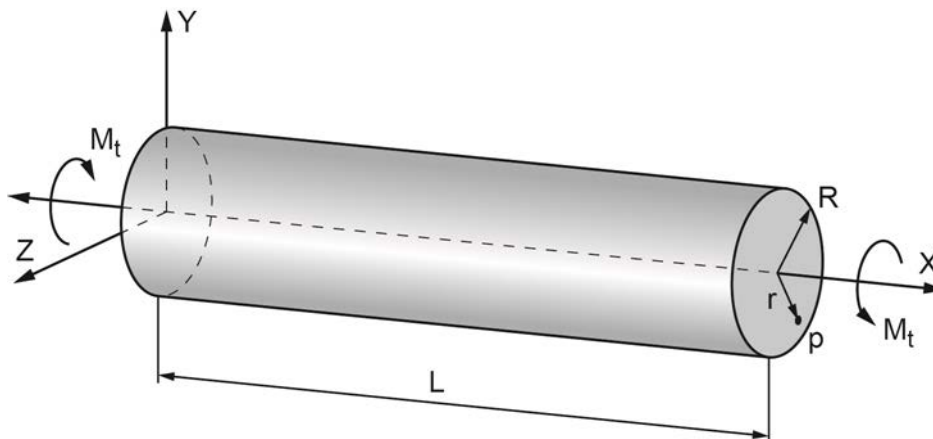


Figure B.1 – Circular Bar Subjected to Torsional Moment

Concepts of equilibrium and compatibility of deformations are investigated to determine how a series of points within a cross section displace under the action of a torsional moment. Figure B.2 presents the circular bar of figure B.1 subdivided into distinct segments of length Δx . Equilibrium requires that when the segments of the beam in figure B.2 are separated, the externally applied torsional moment, M_t , must be acting equally and oppositely at either end of all segments.

As the same torsional moment is applied to each segment, each segment will deform in the same manner. The kinematics of the individual segments must be such that there is compatibility of the shape of radial lines when the segments are reassembled. Figures B.3, B.4, and B.5 kinematically consider three different options for the deformations of radial lines. In all

cases, the twist on the exterior surface of the bar in these three figures is equal. The plane ABCD defines a plane through the center of the bar.

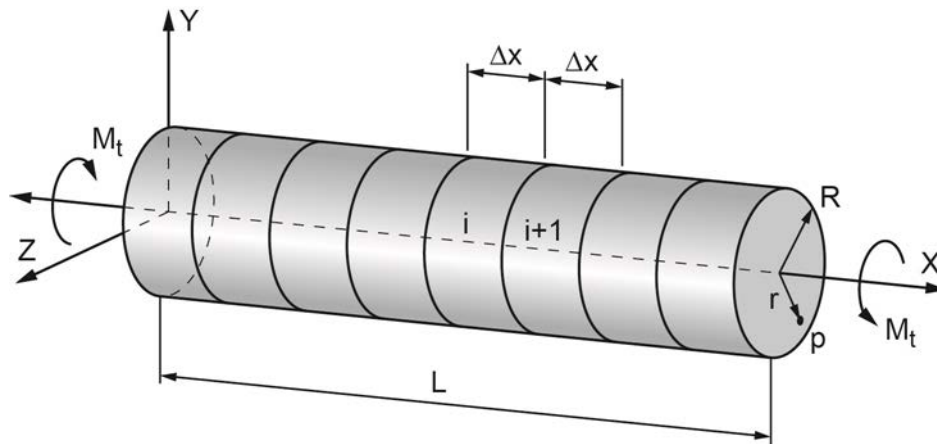


Figure B.2 – Segmented Circular Bar

Figure B.3 shows a non-linear deformation of radial lines in which the rate of displacement diminishes with distance from the center of twist. The deformed lines B'C' and A'D' in both element i and i+1 are consistent for the direction of the applied torsional moments. Inspection of the deformed radial lines at the interface of segments i and i+1 reveals that geometric compatibility will not allow the reassembly of the two segments when a differential rotation is applied to align point E' to B' and point H' to C'.

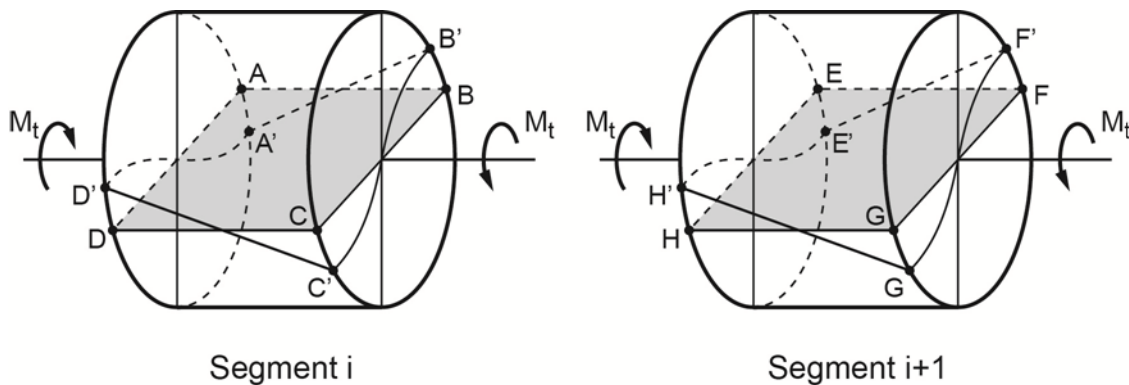


Figure B.3 – Kinematic Study I

Figure B.4 shows a second form of non-linear deformation of radial lines in which the rate of displacement increases with distance from the center of twist. As with the previous case, the radial lines at the interface of segments i and i+1 cannot be re-joined while respecting geometric compatibility.

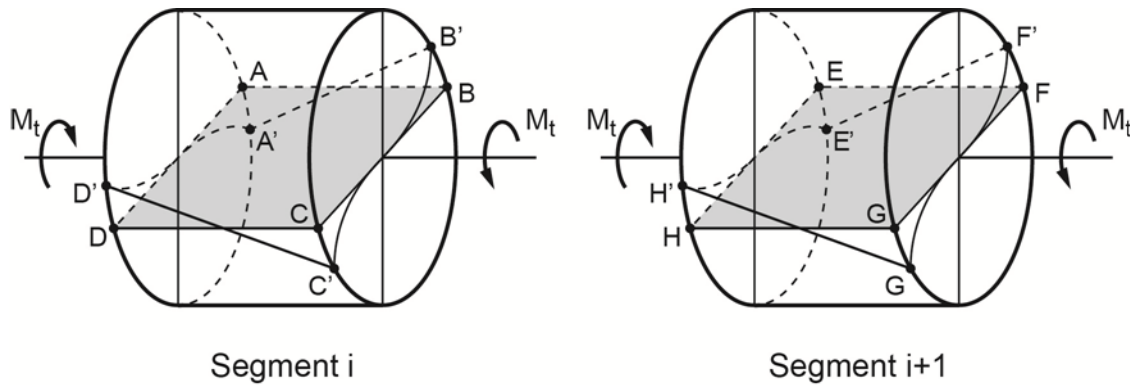


Figure B.4 – Kinematic Study 2

Figure B.5 presents a third alternative of the deformed shape of radial lines within cross sections of the circular bar. In this alternative, the rate of displacement is constant across the diameter of the bar. The resulting shape B'C' and A'D' is linear. A rigid body rotation of the i+1 segment allows it to be rejoined to the ith segment.

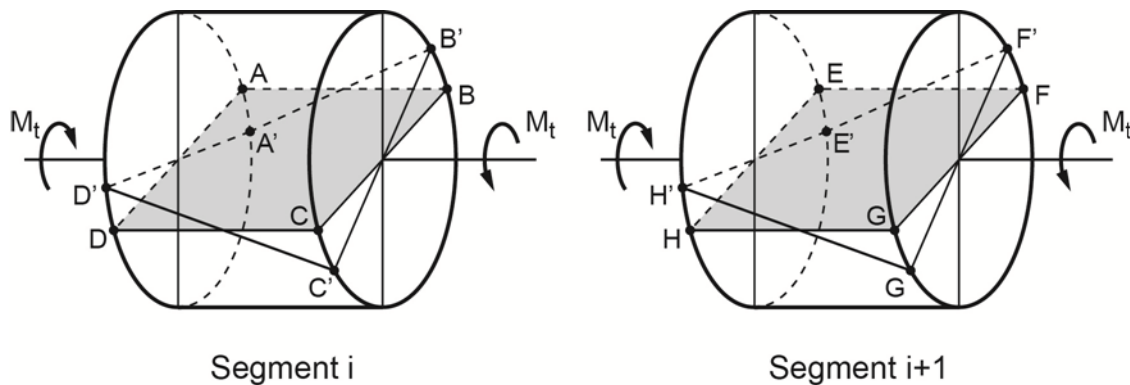


Figure B.5 – Kinematic Study 3

The linear displacement of radial lines within the cross sections of a circular bar has important implications. Figure B.6 shows a circular bar subjected to a torsional moment. The figure shows a radial plane abcd and the deformed plane a'b'c'd'. The maximum rotation at the end of the beam is denoted ϕ . The previous kinematic study indicates that ϕ varies linearly along the length of the bar. A rate of change of twist, θ , can be defined as:

(Eqn. B.1)
$$\theta = \frac{\phi}{L}$$

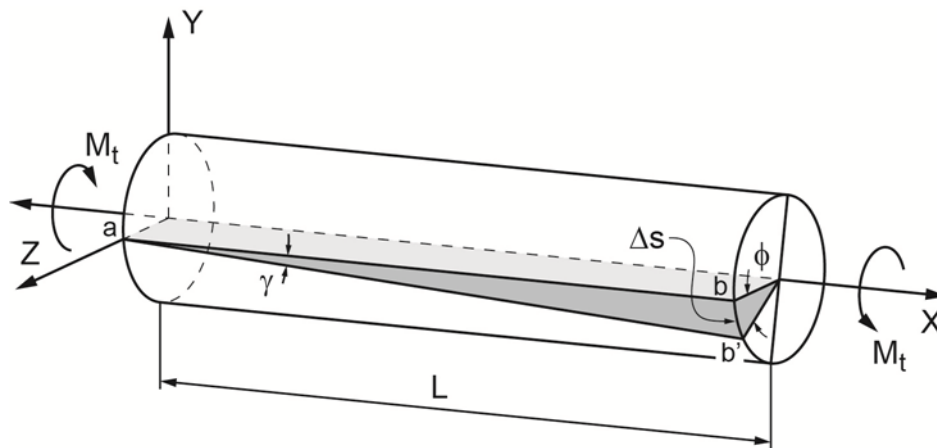


Figure B.6 – Linear Twisting of the Circular Bar

Shear strain, γ , is also shown in figure B.6. It is defined as the circumferential displacement of a point in a cross section divided by the length of the bar to the cross section under consideration. The maximum shear strain, on the outer surface of the bar, at the end of the bar is:

(Eqn. B.2)
$$\gamma = \frac{\Delta s}{L}$$

The linear displacement radial lines of the cross section coupled with the assumed material characteristics imply a linear distribution of shear stress within the cross section of the bar as shown in figure B.7. Equilibrium within the bar requires that, for small rotations, longitudinal shear stresses in the bar are also present. Shear stress on an element of the exterior surface of the bar is shown in figure B.7. Shear stresses are zero along the center of twist and maximum at the exterior radius of the bar.

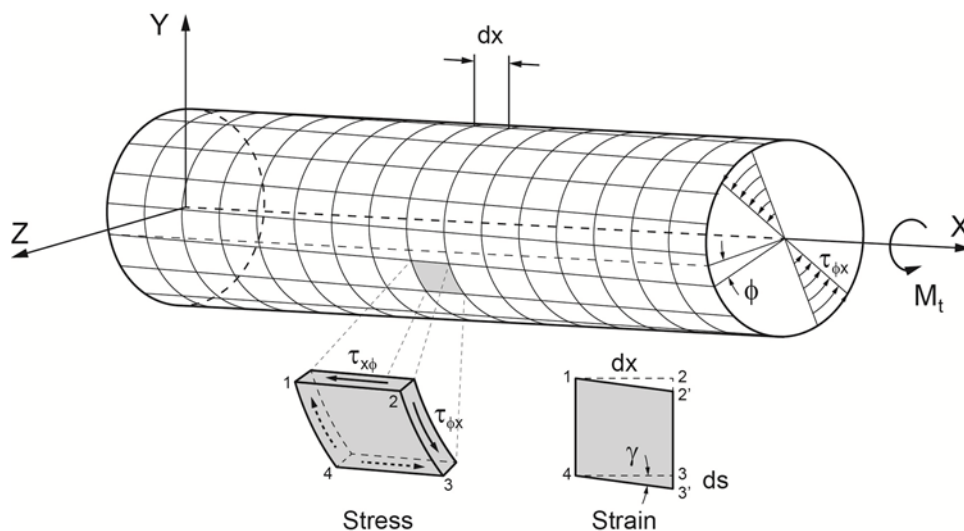


Figure B.7 – Shear Stresses and Shear Strains in the Circular Bar

Continuing with the development of relationships between applied torsional moment and resulting rotations, consider a distinct element of length dx of the bar shown in figure B.8.

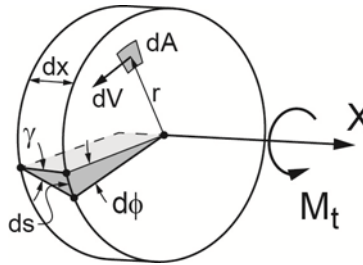


Figure B.8 – Element of the Circular Bar

Previously defined equations can be rewritten for the element of the bar shown in figure B.8. The rate of twist becomes:

$$\text{(Eqn. B.3)} \quad \theta = \frac{d\phi}{dx}$$

And the strain is defined as:

$$\text{(Eqn. B.4)} \quad \gamma = \frac{ds}{dx}$$

It can also be seen in figure B.8 that the displacement ds over the length dx is equal to:

$$\text{(Eqn. B.5)} \quad ds = rd\phi$$

Substituting equation B.5 into equation B.4,

$$\text{(Eqn. B.6)} \quad \gamma = \frac{rd\phi}{dx}$$

Substituting equation B.3 into equation B.6,

$$\text{(Eqn. B.7)} \quad \gamma = r\theta$$

This equation says that the shear strain at any distance from the center of twist is the rate of twist multiplied by the radial distance, with a maximum shear strain at the outer surface of the circular bar.

Considering now the linear elastic behavior of the bar, the shear stress shown in figure B.7 is related to strain by Hooke's Law:

$$\text{(Eqn. B.8)} \quad \tau_{\phi x} = \tau_{x\phi} = \tau = G\gamma$$

Substituting the expression for shear strain in equation B.7 into equation B.8 we find:

$$\text{(Eqn. B.9)} \quad \tau = Gr\theta$$

Consider the equilibrium between the externally applied torsional moment and the resisting shear stress in the plane of a cross section within the bar. As shown in figure B.8, call the shear stress acting over a small element of surface area dA a force dV . The magnitude of the force is:

$$(Eqn. B. 10) \quad dV = \tau dA$$

The element of torsional moment caused by the force dV is

$$(Eqn. B. 11) \quad dM_t = dV(r) = \tau dA(r)$$

Integrating the incremental torsional moments over the cross sectional area yields

$$(Eqn. B. 12) \quad M_t = \int_A dM_t = \int_A \tau r dA = \int_A (Gr\theta)r dA$$

Or,

$$(Eqn. B.13) \quad M_t = G\theta \int_A r^2 dA$$

The integral represents a cross section characteristic known as the torsional constant J :

$$(Eqn. B. 14) \quad J = \int_A r^2 dA$$

For the unique case of the circular bar, the torsional constant equals the polar moment of inertia:

$$(Eqn. B.15) \quad J = I_p = \int_A r^2 dA = I_x + I_y$$

For a solid circular shaft the polar moment of inertia is:

$$(Eqn. B.16) \quad I_p = \frac{\pi r^4}{2} = \frac{\pi d^4}{32}$$

So, we relate the torsional moment to rotation as follows:

$$(Eqn. B.17) \quad M_t = GJ\theta$$

$$(Eqn. B.18) \quad \theta = \frac{M_t}{GJ}$$

$$(Eqn. B.19) \quad \phi = \frac{M_t L}{GJ}$$

The shear stress becomes:

$$(Eqn. B.20) \quad \tau = \frac{M_t r}{J}$$

The relationships between torsional moment, rotation, and shear stress are consistent with those found by a Saint Venant Semi-Inverse solution incorporating Prandtl's Stress Function to more easily address boundary conditions. The fundamental assumptions of Saint Venant Torsion are:

- Cross sections of the bar are assumed to rotate as rigid bodies.
- Warping of the cross sections is not restricted, but warping at any point in the cross section is constant along the length of the bar.

2. Torsion in a Closed Thin-Walled Shaft

The approach taken for developing torsional characteristics of the circular bar are extended to a hollow closed shaft as shown in figure B.9. The length of the shaft is L and the thickness of the wall of the shaft is t . The derivation of the torsional constant for the thin-walled shaft is based on Saint Venant shear and the assumption that the wall thickness is small compared to the overall dimensions of the cross section.

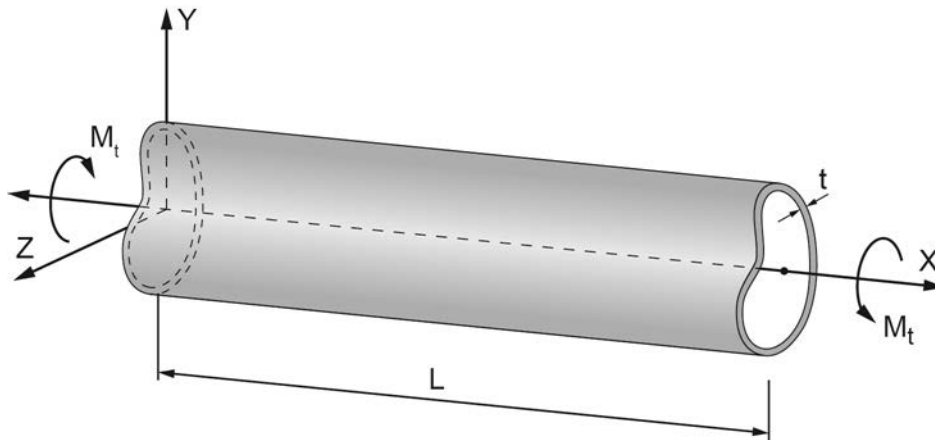


Figure B.9 – Closed Thin-Wall Shaft

The torsional moment applied to the closed thin-wall shaft will produce shear stress around shaft's the cross section. Figure B.10 shows an element of the shaft shown in figure B.9 with length dx . It is convenient to define a system of coordinates where the local x axis is oriented in the direction of the global X axis, the s axis is tangential to the centerline of the wall at any location within the cross section, and the n axis is normal to the local tangent. The shear stresses produced by the torsional moment on the cross section are then labeled τ_{xs} .

It is also convenient, for reasons about to be seen, to introduce the concept of shear flow, q . The shear flow is an expression of the shear stress integrated over the thickness of the wall.

$$(Eqn. B.21) \quad q = \int_{-t(s)/2}^{t(s)/2} \tau_{xs} \, dn$$

Assuming a linear variation in shear stress across the wall thickness, the expression for shear flow becomes:

(Eqn. B.22)
$$q = \left(\frac{\tau_{xsi} + \tau_{xso}}{2} \right) t(s)$$

Where the shear stresses in equation B.22 are the shear stresses at the inner face and outer face of the wall. The assumption of a thin wall simplifies this equation to an expression where the shear stress is assumed constant over the thickness of the wall:

(Eqn. B.23)
$$q = \tau_{xs} t(s)$$

In each of these expressions the wall thickness t is assumed to be variable along the s axis.

Figure B.10 includes a segment of the hollow cross section, of width dx and length ds , subjected to the incremental forces of shear flow. Tangential shear flow is labeled q_{xs} . Equilibrium of the segment requires the presence of incremental shear flow forces in the longitudinal direction, labeled q_{sx} . As there is no net longitudinal force applied to the shaft, equilibrium of the segment in the longitudinal direction also requires that the incremental shear flow forces q_{sx} must be equal and opposite. Satisfaction of these two conditions of equilibrium means, that while shear stresses vary as a function of wall thickness at the point where shear stresses are being considered, shear flow is constant around the hollow thin-walled cross section.

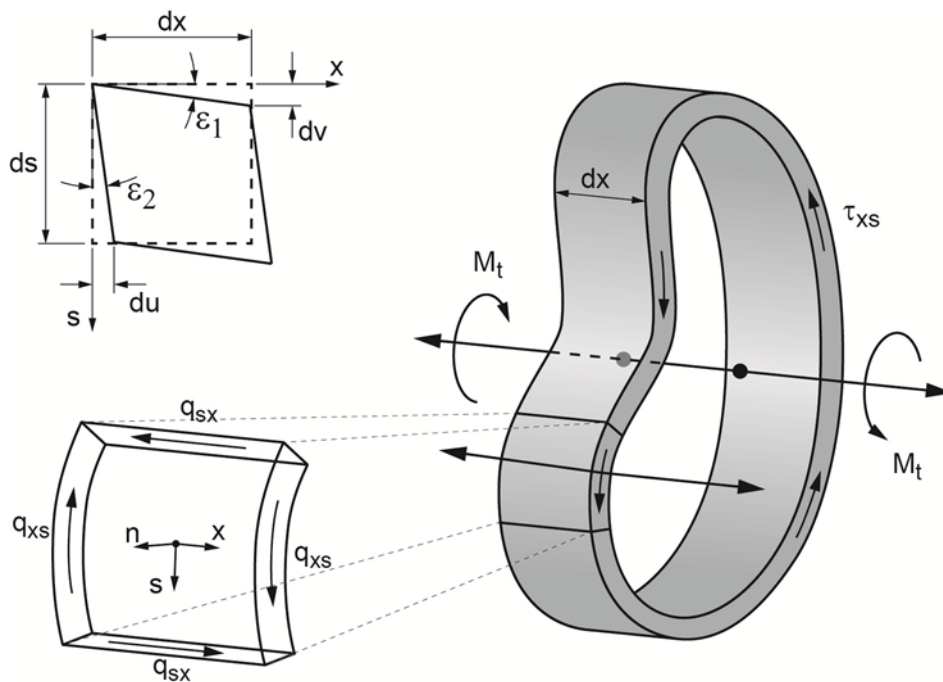


Figure B.10 – Segment of Closed, Thin-Wall Shaft

The shear flow around the cross section must be in equilibrium with the applied torsional moment. Figure B.11 shows an end view of the cross section of the hollow thin-walled shaft with an applied torsional moment M_t .

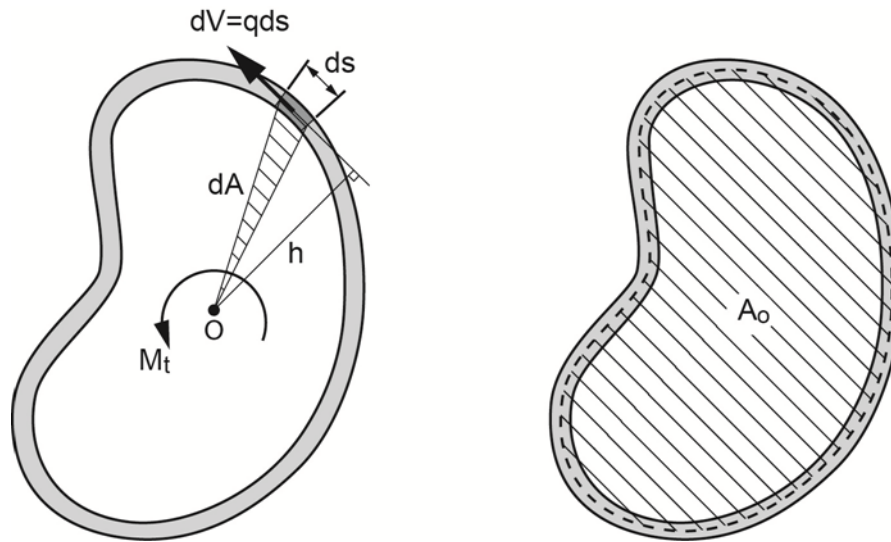


Figure B.11 – Equilibrium in the Cross Section of the Thin Wall Closed Shaft

The tangential force caused by the shear flow over ds is:

(Eqn. B. 24)
$$dV = qds$$

The torsional moment caused by this force is:

(Eqn. B. 25)
$$dM_t = dV(h) = qds(h)$$

The dimension h is the perpendicular distance from the line of action of dV to the center of rotation. Define a differential area dA as the triangle enclosed by rays from the center of rotation to the beginning and end of element ds . The area of the triangle is:

(Eqn. B.26)
$$dA = \frac{1}{2}(h)ds$$

Solving equations B.24 and B.25 for $(h)ds$ and setting them equal to each other produces:

(Eqn. B.27)
$$2dA = \frac{dM_t}{q}$$

Or,

(Eqn. B. 28)
$$dM_t = 2qdA$$

The torsional moment is found by integrating this equation around the median line of the wall thickness:

(Eqn. B.29)
$$M_t = 2q \oint dA = q \oint (h)ds$$

Or,

$$(Eqn. B. 30) \quad M_t = 2qA_o$$

Where A_o is the area bounded by the median line of the wall thickness. This expression can be written into two other convenient forms:

$$(Eqn. B.31) \quad q = \frac{M_t}{2A_o}$$

$$(Eqn. B.32) \quad \tau = \frac{M_t}{2A_o t(s)}$$

Consider now the kinematics of an element on the wall of the thin tube. Figure B.10 also includes a sketch of the deformation of an element of the hollow thin-walled shaft. The torsional load leads to displacements of the element in the x direction (u) and s direction (v). The shear strain in this element is defined as:

$$(Eqn. B.33) \quad \gamma_{xs} = \frac{du}{ds} + \frac{dv}{dx}$$

Where,

$$(Eqn. B.34) \quad \gamma_{xs} = \varepsilon_{xs1} + \varepsilon_{xs2} = \frac{du}{ds} + \frac{dv}{dx}$$

Applying Hooke's Law, shear stress divided by the shear modulus can be substituted for strain:

$$(Eqn. B.35) \quad \frac{\tau_{xs}}{G} = \frac{du}{ds} + \frac{dv}{dx}$$

This equation can be rearranged to solve for the axial displacement du :

$$(Eqn. B.36) \quad du = \left(\frac{\tau_{xs}}{G} - \frac{dv}{dx} \right) ds$$

As there is no longitudinally applied load, equilibrium with the applied external forces requires that the sum of all longitudinal displacements must be equal to zero, or:

$$(Eqn. B.37) \quad \oint du = 0$$

Equation B.36 can be substituted into equation B.37 to give:

$$(Eqn. B.38) \quad \oint \left(\frac{\tau_{xs}}{G} - \frac{dv}{dx} \right) ds = 0$$

For small angles, the tangential displacement dv is also equal to the differential twist multiplied by the perpendicular dimension from the center of twist, h :

$$(Eqn. B. 39) \quad dv = d\phi(h)$$

Inserting equation B.39 into B.38 and rearranging:

$$(Eqn. B.40) \quad \oint \frac{\tau_{xs}}{G} ds = \oint \frac{d\phi}{dx}(h) ds$$

Substituting the rate of twist as defined in equation B.3 into this expression yields:

$$(Eqn. B.41) \quad \oint \frac{\tau_{xs}}{G} ds = \theta \oint (h) ds$$

Twice the area enclosed by the centerline of the wall thickness can be substituted for the integral on the right side of this expression to produce:

$$(Eqn. B.42) \quad \oint \frac{\tau_{xs}}{G} ds = 2A_o\theta$$

The shear stress in the integral on the left side of this expression can be replaced with the shear flow divided by the wall thickness. Multiplying both sides of the resulting equation by the shear modulus produces:

$$(Eqn. B.43) \quad q \oint \frac{ds}{t(s)} = 2GA_o\theta$$

This equation can be rearranged to produce a relationship between the rate of twist and shear flow:

$$(Eqn. B.44) \quad \theta = \frac{q}{2GA_o} \oint \frac{ds}{t(s)}$$

The work developed in this and the previous section resulted in two expressions for the torsional moment. equation B.17 and B.30 state:

$$(Eqns. B.17 and B.30) \quad M_t = GJ\theta \quad M_t = 2qA_o$$

Equating these two equations and solving for the rate of twist produces:

$$(Eqn. B. 45) \quad \theta = \frac{2qA_o}{GJ}$$

Now equations B.44 and B.45 can be set equal to each other:

(Eqn. B.46)
$$\frac{2qA_o}{GJ} = \frac{q}{2GA_o} \oint \frac{ds}{t(s)}$$

And finally, the torsional constant for the hollow thin-walled shaft can be determined:

(Eqn. B.47)
$$J = \frac{4A_o^2}{\oint \frac{ds}{t(s)}}$$

For concrete box girder sections, the closed loop integral in the denominator of equation B.47 is often more conveniently expressed as a discrete summation. The equation for the torsion constant then becomes:

(Eqn. B.48)
$$J = \frac{4A_o^2}{\sum_{i=1}^n \frac{s_i}{t_i}}$$

Where, s_i is the length, and t_i the thickness of, each of the n individual elements comprising the closed cross section.

Example 1: Consider the cross section of a single-cell box girder used in chapter 8, Transverse Analysis. The dimensions of the cross section are shown in figure B.12. Figure B.13 shows the idealized thin wall members of the box along with their lengths and average thicknesses.

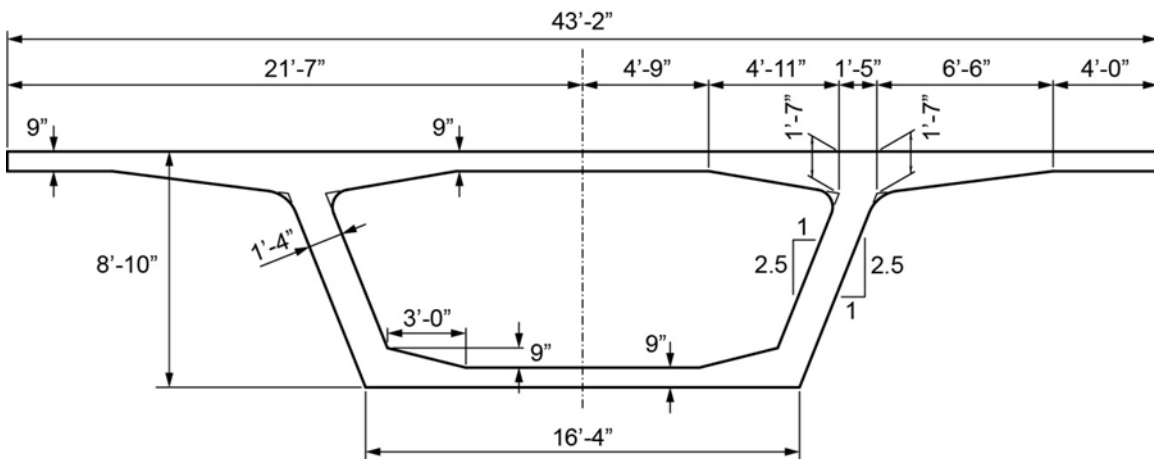


Figure B.12 –Example Single Cell Box Girder

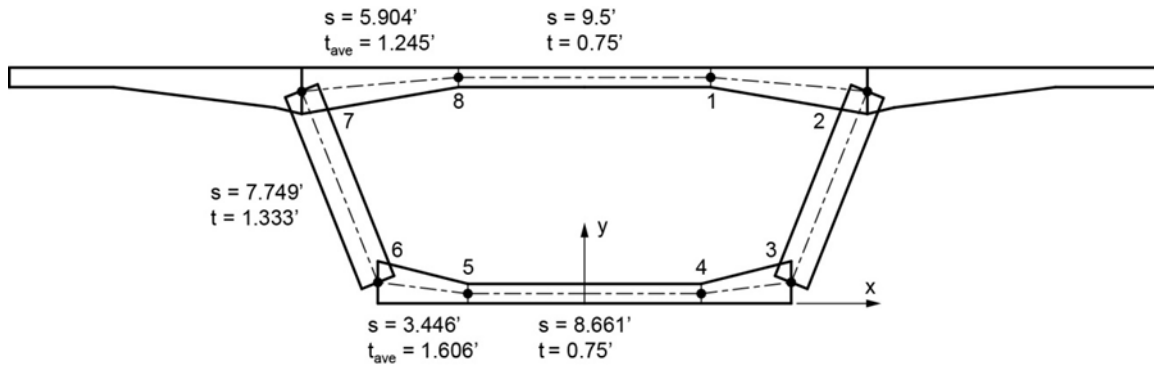


Figure B.13 – Idealized Thin-Walled Members

The coordinates of points 1 through 8 are shown in table B.1. The dimensions of the thin wall members and a computation of equation B.48 denominator is shown in table B.2.

Point	x	y
1	4.75	8.4583
2	10.6326	7.9598
3	7.7545	0.7646
4	4.3306	0.375
5	-4.3306	0.375
6	-7.7545	0.7646
7	-10.6326	7.9598
8	-4.75	8.4583

Table B.1 – Coordinates of Points Defining the Thin-Walled Section

Element	S (ft)	t (ft)	s/t
8-1	9.5	0.75	12.667
1-2	5.904	1.245	4.742
2-3	7.749	1.333	5.813
3-4	3.446	1.606	2.146
4-5	8.661	0.75	11.548
5-6	3.446	1.606	2.146
6-7	7.749	1.333	5.813
7-8	5.904	1.245	4.742
		Sum	49.617

Table B.2 – Thin-Walled Section Member Dimensions

The results for the area enclosed by the mid-line of the thin-walled section and the summation of member lengths divided by their average thicknesses are:

$$A_o = 144.68 \text{ ft}^2$$

$$\sum_{i=1}^8 \frac{s_i}{t_i} = 49.617 \text{ ft}$$

$$J = \frac{4(144.68)^2}{49.617} = 1687.5 \text{ ft}^4$$

Note that the cantilever wings do contribute to the torsional constant for the cross section shown in figure B.13. This value of this contribution is, however, small with regard to the contribution of the closed cell, and is typically not considered. In an instance where it was considered, thin open appendages to a closed cell would add torsional constant with the equation for a thin cross section which is:

$$(Eqn. B.49) \quad J = \frac{b(t)^3}{3}$$

The total torsional constant would then be:

$$(Eqn. B.50) \quad J = \frac{4A_o^2}{\sum_{i=1}^n \frac{s_i}{t_i}} + \sum_{k=1}^m \frac{b_k(t_k)^3}{3}$$

Where m is the number of open appended thin wall sections with depth b_k and thickness t_k . For the example problem above, the average thickness of the cantilever wings is 1.035' and the length of the cantilever is 10.952'. The resulting contribution of the torsional constant is:

$$J = 2 \left(\frac{10.952(1.035)^3}{3} \right) = 8.095 \text{ ft}^4$$

This value represents approximately 0.5 percent of the torsional constant of the closed section.

3. Torsion Multi-Cell Box Girder

Torsional moments applied to box girder cross sections comprised of multiple closed cells will be resisted by the sum of shear flows around the individual cells. Compatibility of deformation of the cross section requires that all cells will rotate the same amount when loaded in torsion. This is based on the assumption that the width of the cross section is small with regard to the span length. Care should be taken when the ratio of span length to box girder width is less than four. In wide bridges, torsional moments tend to be resisted by differential bending in the outer webs.

Figure B.14 shows a typical two-cell box girder superstructure cross section. The applied torsional moment, M_t , is resisted by the sum of torsional moments in each of the cells. The moments in the cells produce shear flows q_1 in Cell 1 and q_2 in Cell 2.

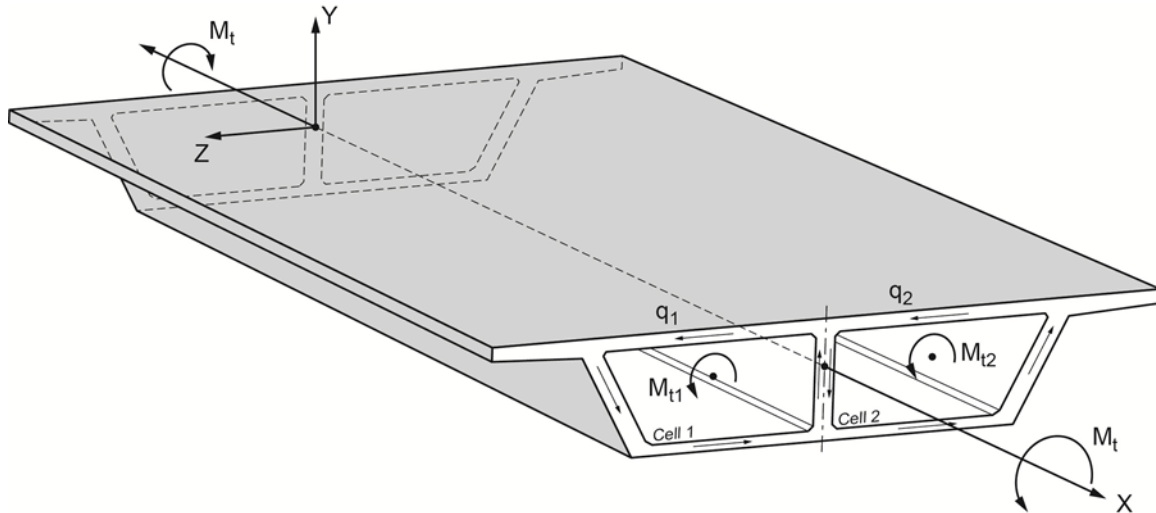


Figure B.14 – Two-Cell Box Girder Superstructure

In the previous section the relationship between applied torsional moment and shear flow in a single-cell closed shape was presented in equation 30:

(Eqn. B.30)
$$M_t = 2A_o q$$

For the case of a two-cell structure, this relationship becomes:

(Eqn. B.51)
$$M_t = 2A_{o1}q_1 + 2A_{o2}q_2$$

Or, for any number of cells:

(Eqn. B.52)
$$M_t = 2 \sum_{i=1}^n A_{oi} q_i$$

Equation B.44, repeated below, presents an expression for the rate of twist as a function of the member dimensions:

(Eqn. B.44)
$$\theta = \frac{q}{2GA_o} \oint \frac{ds}{t(s)}$$

As the shear flows from adjacent cells will impact the shear flow of a particular cell in members that are shared in common, a statically indeterminate solution is required to solve for the individual shear flows.

The rotations of the two cells are expressed as the net shear flows:

$$(Eqn. B.53) \quad \theta_1 = \frac{1}{2GA_{o1}} \left(q_1 \oint \frac{ds}{t(s)} - q_2 \int_{12} \frac{ds}{t(s)} \right)$$

$$(Eqn. B.54) \quad \theta_2 = \frac{1}{2GA_{o2}} \left(q_2 \oint \frac{ds}{t(s)} - q_1 \int_{21} \frac{ds}{t(s)} \right)$$

Where, the open integral portions in the equations are the shear flow in the common members multiplied by the lengths of the adjoining sections divided by their thicknesses.

Compatibility of deformations requires that:

$$(Eqn. B. 55) \quad \theta_1 = \theta_2 = \theta$$

This allows us to rewrite equations B.53 and B.54 as:

$$(Eqn. B. 56) \quad \delta_1(q_1) + \delta_{12}(q_2) = 2GA_{o1}\theta$$

$$(Eqn. B. 57) \quad \delta_{21}(q_1) + \delta_2(q_2) = 2GA_{o2}\theta$$

Where the shape constants are defined as,

$$(Eqn. B.58) \quad \delta_1 = \oint_1 \frac{ds}{t(s)}$$

$$(Eqn. B.59) \quad \delta_2 = \oint_2 \frac{ds}{t(s)}$$

And,

$$(Eqn. B.60) \quad \delta_{12} = \delta_{21} = - \int_{12} \frac{ds}{t(s)}$$

$$(Eqn. B.61) \quad \begin{bmatrix} \delta_1 & \delta_{12} \\ \delta_{21} & \delta_2 \end{bmatrix} \begin{bmatrix} q_1 \\ q_2 \end{bmatrix} = 2G\theta \begin{bmatrix} A_{o1} \\ A_{o2} \end{bmatrix}$$

The shear flows, q_1 and q_2 , can be solved in terms of the constant $G\theta$. The torsional constant can then be found remembering the relationship between torsional moment and rate of twist presented in equation B.17 and repeated here:

$$(Eqn. B. 17) \quad M_t = GJ\theta$$

Example 2: Determine the torsional constant, J , for the cross section of the two-cell box girder shown in figure B.15.

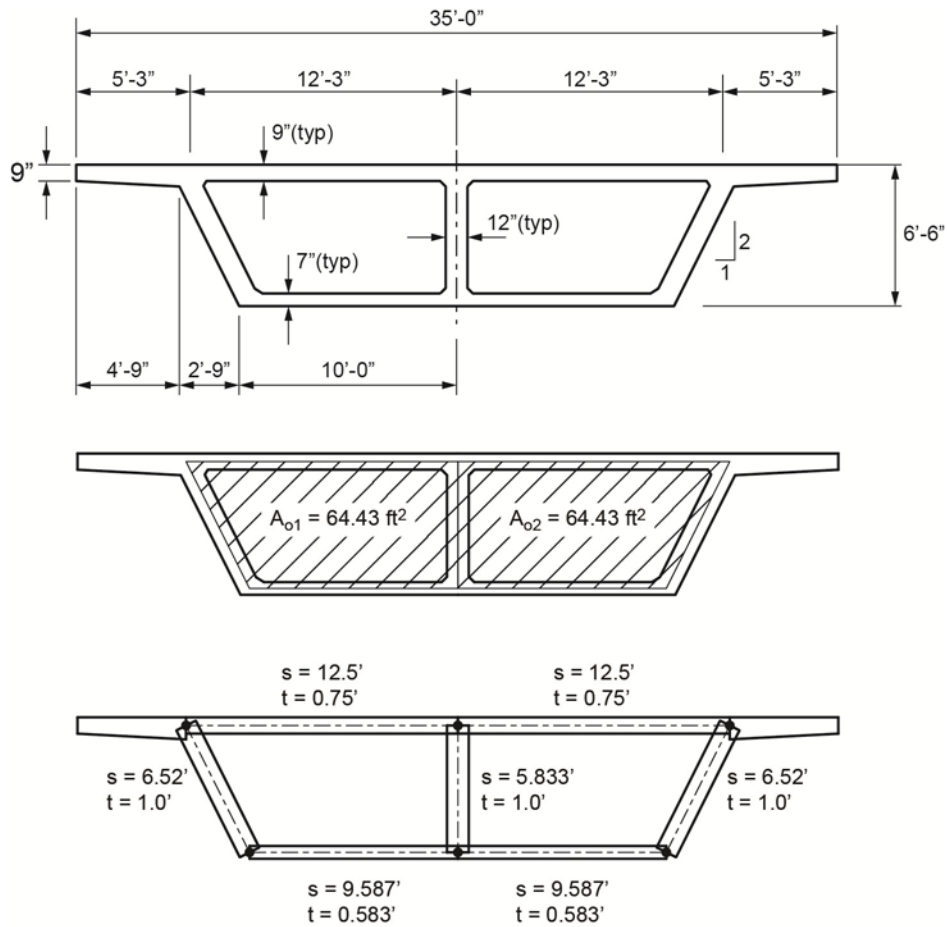


Figure B.15 –Example Two-Cell Box Girder

Evaluating the shape constants:

$$\delta_1 = \delta_2 = 45.456$$

$$\delta_{12} = \delta_{21} = -5.833$$

Equations B.56 and B.57 become

$$45.456(q_1) - 5.833(q_2) = 128.84G\theta$$

$$-5.833(q_1) + 45.456(q_2) = 128.84G\theta$$

From which the shear flows are solved in terms of $G\theta$:

$$q_1 = q_2 = 3.2516G\theta$$

Considering torsional equilibrium:

$$M_t = GJ\theta = 2A_{o1}q_1 + 2A_{o2}q_2$$

Or,

$$GJ\theta = [2(64.42)3.2516 + 2(64.42)3.2516]G\theta$$

From which the torsional constant is found:

$$J = 837.9 \text{ ft}^4$$

The symmetry of this two-cell box girder cross section would, by inspection, would lead to the conclusion that there is no net shear flow in the center web. The result is that the torsional constant for this special condition would be the same as if the center web did not exist. Computing the torsional constant from equation B.47 verifies this condition.

$$A_o = 128.84 \text{ ft}^2$$

$$\sum_{i=1}^8 \frac{s_i}{t_i} = 79.26 \text{ ft}$$

$$J = \frac{4A_o^2}{\oint \frac{ds}{t(s)}} = \frac{4(128.84)^2}{79.26} = 837.9 \text{ ft}^4$$

Example 3: Consider the cross section of a four-cell box girder shown in figure B.16. Figure B.16 also shows the idealized thin wall members of the box along with their lengths and average thicknesses.

The system of simultaneous equations that needs to be solved for the four-cell box girder is:

$$\delta_1(q_1) + \delta_{12}(q_2) + \delta_{13}(q_3) + \delta_{14}(q_4) = 2GA_{o1}\theta$$

$$\delta_{21}(q_1) + \delta_2(q_2) + \delta_{23}(q_3) + \delta_{24}(q_4) = 2GA_{o2}\theta$$

$$\delta_{31}(q_1) + \delta_{32}(q_2) + \delta_3(q_3) + \delta_{34}(q_4) = 2GA_{o3}\theta$$

$$\delta_{41}(q_1) + \delta_{42}(q_2) + \delta_{43}(q_3) + \delta_4(q_4) = 2GA_{o4}\theta$$

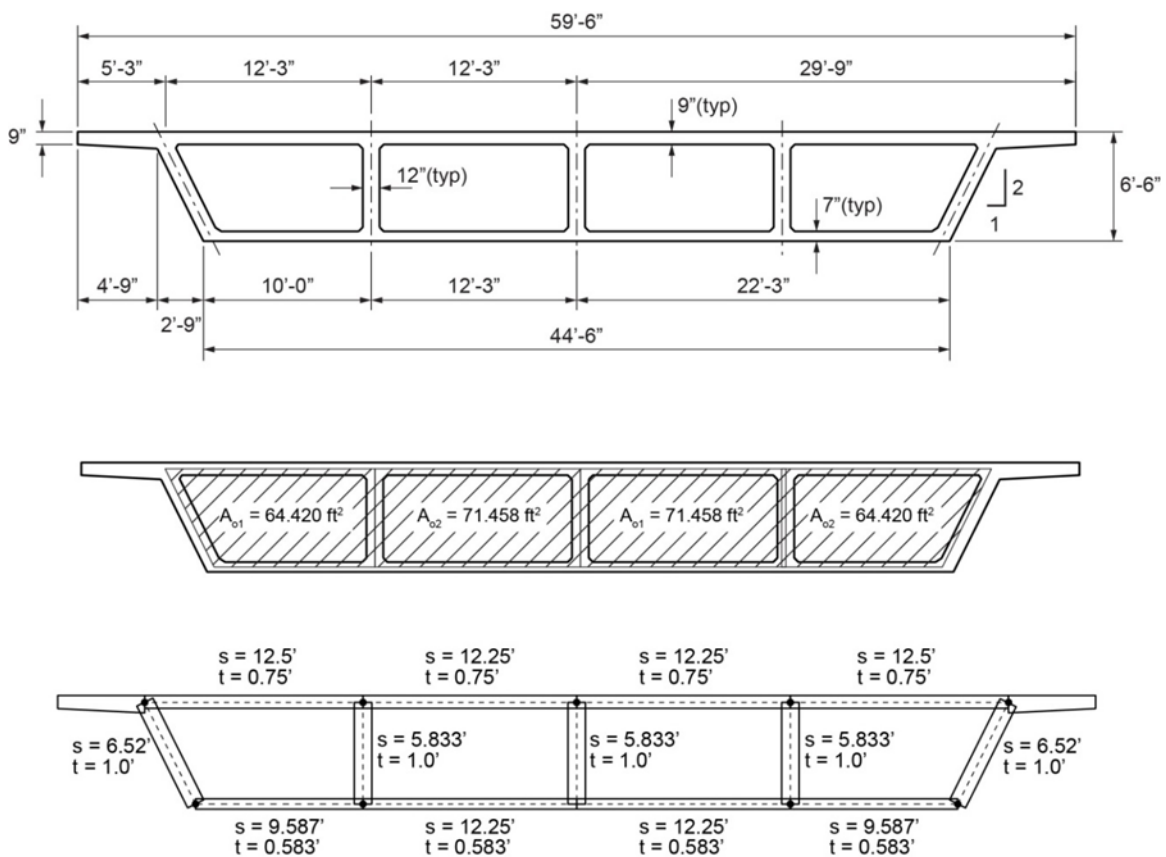


Figure B.16 – Example Four-Cell Box Girder

These equations are modified to discount the influence of cells that are not adjoining:

$$\delta_1(q_1) + \delta_{12}(q_2) + 0 + 0 = 2GA_{o1}\theta$$

$$\delta_{21}(q_1) + \delta_2(q_2) + \delta_{23}(q_3) + 0 = 2GA_{o2}\theta$$

$$0 + \delta_{32}(q_2) + \delta_3(q_3) + \delta_{34}(q_4) = 2GA_{o3}\theta$$

$$0 + 0 + \delta_{43}(q_3) + \delta_4(q_4) = 2GA_{o4}\theta$$

From the cross section geometry, and noting symmetry:

$$\delta_1 = \delta_4 = 45.46$$

$$\delta_2 = \delta_3 = 49.00$$

$$\delta_{12} = \delta_{21} = \delta_{23} = \delta_{32} = \delta_{34} = \delta_{43} = -5.833$$

$$q_1 = q_4 \quad q_2 = q_3$$

Based on the symmetry of the section, the system of four simultaneous equations reduces to two:

$$\begin{aligned}\delta_1(q_1) + \delta_{12}(q_2) &= 2GA_{o1}\theta \\ \delta_{21}(q_1) + \delta_2(q_2) + \delta_{23}(q_2) &= 2GA_{o2}\theta\end{aligned}$$

Or,

$$\begin{aligned}45.46(q_1) - 5.833(q_2) &= 128.84G\theta \\ -5.833(q_1) + 49.00(q_2) - 5.833(q_2) &= 142.92G\theta\end{aligned}$$

From which,

$$\begin{aligned}q_1 &= 0.8823q_2 \\ q_1 &= 3.317G\theta \\ q_2 &= 3.759G\theta\end{aligned}$$

Considering equilibrium:

$$\begin{aligned}M_t = GJ\theta &= 2A_{o1}q_1 + 2A_{o2}q_2 \\ GJ\theta &= 2[2(64.42)3.317 + 2(71.46)3.759]G\theta\end{aligned}$$

$$J = 1929.2 \text{ ft}^4$$

Comparing this to the torsional characteristic of the outside perimeter of the bridge only:

$$A_o = 271.76 \text{ ft}^2$$

$$\sum_{i=1}^8 \frac{s_i}{t_i} = 153.91 \text{ ft}$$

$$J = 1919.4 \text{ ft}^4$$

This represents a 0.6 percent increase in torsional characteristic.

Example 1—Multi-Cell Box Girder Bridge

1. Introduction

This example demonstrates the use of the AASHTO LRFD Design Specifications in the design of a cast-in-place, post-tensioned concrete, multi-cell box girder bridge. The design of the supporting substructure is not included in this manual.

The bridge considered in this example is shown in figure C.1. The length of the three-span bridge from the centerline of the bearings at the abutments is 400', comprised of 120' side spans and a 160' center span. The bridge is straight, following a tangent alignment, and has no skew. In elevation, the bridge is symmetrical in all ways about the centerline of the center span.

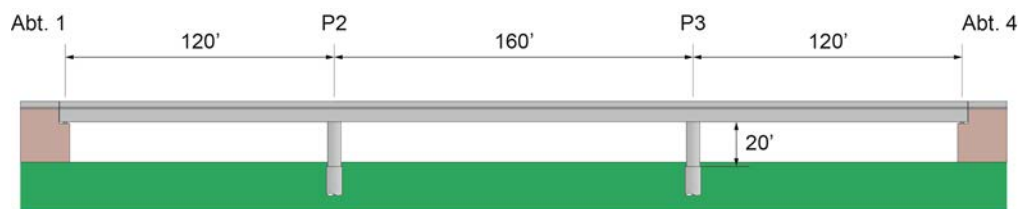


Figure C.1 – Elevation of Example 1 Bridge

Figure C.2 shows a transverse cross section taken through the bridge. The 4-cell box girder bridge carries three 12' wide traffic lanes, two 10' shoulders, and two 1'-9" barriers, for a total out-to-out width of 59'-6".

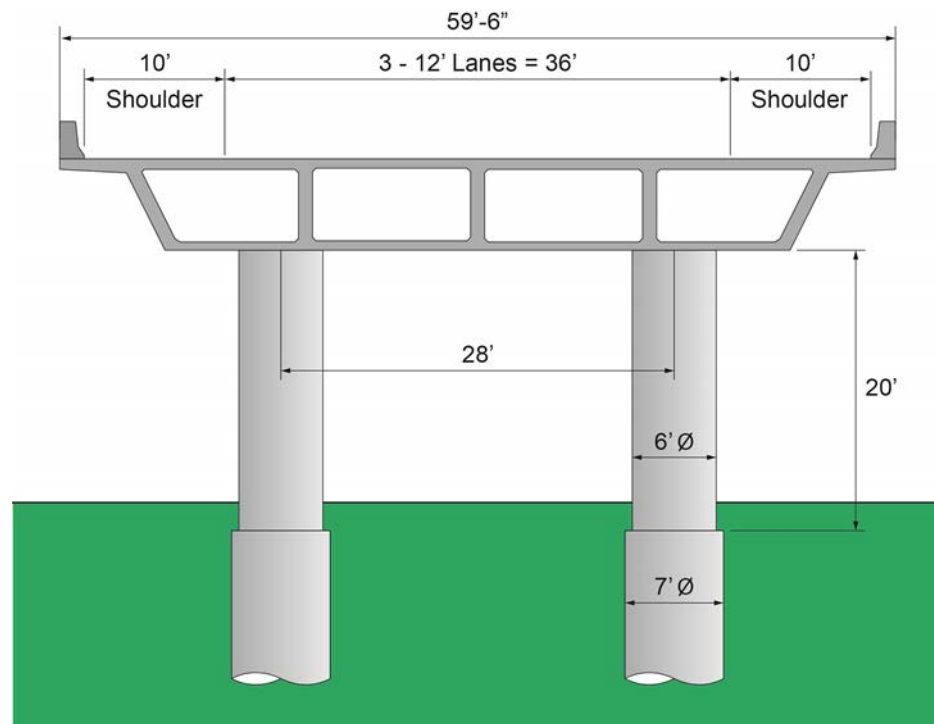


Figure C.2 – Cross Section through Example 1 Bridge

Pier 2 and Pier 3 are each comprised of two cylindrical columns with a diameter of 6'-0". The columns are cast monolithic with the superstructure. The columns are 20' in height, measured from the top of foundations to the base of the superstructure. The foundations consist of 7'-0" diameter mono-shafts supporting each of the columns. For this example, it is assumed that the supporting soil provides an equivalent point of fixity 10' below the top of the mono-shafts for all force effects. The distance from the base of the superstructure to the point of fixity is 30'.

Summary of Bridge Geometry:

Bridge length between abutment bearings	= 400'
Span arrangement	= 120'-160'-120'
Roadway Width (3-12' lanes, 2-10' shoulders)	= 56'-0"
Width of Barrier Railing	= 1'-9"
Overall Bridge Width	= 59'-6"

2. Material Characteristics

2.1. Concrete

The initial and 28-day concrete strengths for the superstructure and substructure are:

$$f'_{ci} = 3500 \text{ psi} = 3.5 \text{ ksi}$$

$$f'_c = 5000 \text{ psi} = 5.0 \text{ ksi}$$

[3.5.1] The unit weight of the concrete is defined below. Note that the unit weight used for the self-weight calculations includes an additional weight for the reinforcement.

$$w_c = 145 \text{ pcf} = 0.145 \text{ kcf}$$

$$w_{c,DC} = w_c + 5 \text{ pcf} = 150 \text{ pcf} = 0.150 \text{ kcf}$$

[C5.4.2.4-1] The modulus of elasticity for normal weight concrete, where $w_c = 0.145 \text{ kcf}$, can be taken as:

$$E_c = 1820\sqrt{f'_c} = 1820\sqrt{5} = 4070 \text{ ksi} = 586000 \text{ ksf}$$

2.2 Reinforcing Steel

[5.4.3] The yield strength and modulus of elasticity are:

$$f_y = 60 \text{ ksi}$$

$$E_s = 29000 \text{ ksi}$$

2.3 Prestressing Steel

[5.4.4] The 0.6 inch diameter low-relaxation prestressing strand is used in this example with the following properties:

$$A_{ps} = 0.217 \text{ in}^2 / \text{strand}$$

$$f_{pu} = 270 \text{ ksi}$$

$$f_{py} = 0.9 f_{pu} = 243 \text{ ksi}$$

$$E_{ps} = 28500 \text{ ksi}$$

3. Cross Section Properties

The typical cross section dimensions are shown in figure C.3. The cross section dimensions are constant over the length of the bridge:

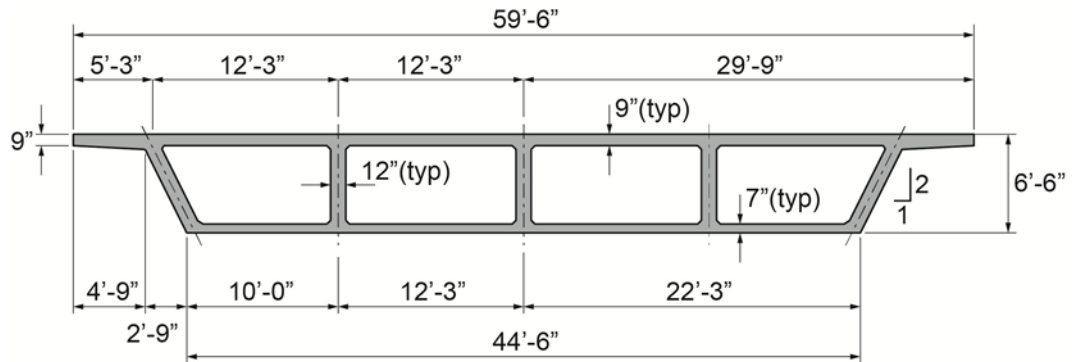


Figure C.3 – Cross Section Dimensions

The properties of the typical superstructure cross section are:

A	= cross sectional area	= 99.45 ft ²
I_x	= moment of inertia	= 643.75 ft ⁴
H	= height of section	= 6.5 ft
c_1	= top of section to centroid	= 2.732 ft
c_2	= bottom of section to centroid	= 3.768 ft

The gross section properties of the substructure elements are used in this design example:

A_c	= area for two columns	= 56.55 ft ²
I_{xc}	= moment of inertia for two columns	= 127.24 ft ⁴
A_p	= area for two monshafts	= 76.97 ft ²
I_{xp}	= moment of inertia for two monshafts	= 235.72 ft ⁴

4. LRFD General Design Equation

[1.3.2.1-1]

The AASHTO LRFD Design Specification's general design equation is:

$$\sum \eta_i \gamma_i Q_i \leq \phi R_n = R_r$$

where,

- η_i = load modifying factor for ductility, redundancy, and operational importance
- γ_i = load factor
- Q_i = force effect
- ϕ = resistance factor
- R_n = nominal resistance
- R_r = factored resistance

[1.3.2.1-2],
[1.3.2.1-3]

The load modifier, η_i , takes on two forms. The first is for loads in which a maximum value of γ_i is appropriate, the second is in which a minimum value of γ_i is appropriate.

$$\eta_i = \eta_D \eta_R \eta_I \geq 0.95$$

$$\eta_i = \frac{1}{\eta_D \eta_R \eta_I} \leq 1.0$$

where,

- η_D = ductility factor
- η_R = redundancy factor
- η_I = operational importance factor

[1.3.3],
[1.3.4],
[1.3.5]

Since the purpose of this example is to illustrate a conventional design on a typical bridge,

$$\eta_D = \eta_R = \eta_I = 1.0$$

$$\therefore \eta_i = 1.0$$

Note that the load modifying factors are project and design specific and may not equal 1.0 in actual designs.

5. Live Load Distribution Factors

[4.6.2.2]

The AASHTO LRFD Design Specifications provide live load distribution tables that can be used on structures that meet the requirements of section 4.6.2.2. There are two methods of applying the live load distribution factors to cast-in-place multi-cell box girders. The first method is to apply the distribution factors to each web as an individual girder. According to the AASHTO LRFD specifications, the “notional shape” of the web and the tributary areas of the top and bottom slabs shall be taken to form a girder. This method would have two designs, one for the interior girders and one for the exterior girders.

The second method is the “whole-width” method. A cast-in-place multi-cell box girder bridge may be designed as a whole-width structure using the live load distribution factors for interior girders multiplied by the number of webs in the cross section. This is the method chosen for this design example.

[C3.6.1.1.2]

Note that in the development of the distribution factor equations the multiple presence factors were considered and included.

Live Load Distribution Factor variables:

$$\begin{aligned}
 L &= \text{length of span (ft)}^* \\
 DF &= \text{distribution factor} \\
 N_L &= \text{number of lanes} \\
 N_w &= \text{number of webs} &= 5 \\
 N_c &= \text{number of cells} &= 4 \\
 S &= \text{web spacing (ft)} &= 12.25 \text{ ft} \\
 d &= \text{depth of beam (in)} &= 78 \text{ in}
 \end{aligned}$$

[c4.6.2.2.1-1]

* For positive moment, negative moment, and shear, L is the length of the span for the section considered. For negative moment between points of contraflexure under uniform loading, L is the average length of two adjacent spans.

[4.6.2.2.2b-1]

Distribution of live loads for moment in interior beams:

– One design lane loaded

$$DF = \left(1.75 + \frac{S}{3.6}\right) \left(\frac{1}{L}\right)^{0.35} \left(\frac{1}{N_c}\right)^{0.45}$$

$$DF_{Span\ 2\ M\pm} = \left(1.75 + \frac{12.25}{3.6}\right) \left(\frac{1}{160}\right)^{0.35} \left(\frac{1}{4}\right)^{0.45} = 0.467$$

$$DF_{Spans\ 1\ \&\ 3\ M\pm} = \left(1.75 + \frac{12.25}{3.6}\right) \left(\frac{1}{120}\right)^{0.35} \left(\frac{1}{4}\right)^{0.45} = 0.517$$

$$DF_{Piers\ 2\ \&\ 3\ M-} = \left(1.75 + \frac{12.25}{3.6}\right) \left(\frac{1}{140}\right)^{0.35} \left(\frac{1}{4}\right)^{0.45} = 0.490$$

– Two or more design lanes loaded (note these factors control over one lane)

$$DF = \left(\frac{13}{N_c}\right)^{0.3} \left(\frac{S}{5.8}\right) \left(\frac{1}{L}\right)^{0.25}$$

$$DF_{Spans\ 1\ \&\ 3\ M\pm} = \left(\frac{13}{4}\right)^{0.3} \left(\frac{12.25}{5.8}\right) \left(\frac{1}{120}\right)^{0.25} = 0.909$$

$$DF_{Piers\ 2\ \&\ 3\ M-} = \left(\frac{13}{4}\right)^{0.3} \left(\frac{12.25}{5.8}\right) \left(\frac{1}{140}\right)^{0.25} = 0.874$$

$$DF_{Span\ 2\ M\pm} = \left(\frac{13}{4}\right)^{0.3} \left(\frac{12.25}{5.8}\right) \left(\frac{1}{160}\right)^{0.25} = 0.846$$

Number of lanes for whole width section

$$N_L = N_w \cdot DF$$

$$N_{L\ Spans\ 1\ \&\ 3\ M\pm} = 5 \cdot 0.909 = 4.544$$

$$N_{L\ Piers\ 2\ \&\ 3\ M-} = 5 \cdot 0.874 = 4.372$$

$$N_{L\ Span\ 2\ M\pm} = 5 \cdot 0.846 = 4.229$$

[4.6.2.2.3a-1] Distribution of live loads for shear in interior beams:

– One design lane loaded

$$DF = \left(\frac{S}{9.5}\right)^{0.6} \left(\frac{d}{12L}\right)^{0.1}$$

$$DF_{Spans\ 1\ \&\ 3} = \left(\frac{12.25}{9.5}\right)^{0.6} \left(\frac{78}{12 \cdot 120}\right)^{0.1} = 0.870$$

$$DF_{Span\ 2} = \left(\frac{12.25}{9.5}\right)^{0.6} \left(\frac{78}{12 \cdot 160}\right)^{0.1} = 0.846$$

– Two or more design lanes loaded (note these factors control over one lane)

$$DF = \left(\frac{S}{7.3}\right)^{0.9} \left(\frac{d}{12L}\right)^{0.1}$$

$$DF_{Spans\ 1\ \&\ 3} = \left(\frac{12.25}{7.3}\right)^{0.9} \left(\frac{78}{12 \cdot 120}\right)^{0.1} = 1.190$$

$$DF_{Span\ 2} = \left(\frac{12.25}{7.3}\right)^{0.9} \left(\frac{78}{12 \cdot 160}\right)^{0.1} = 1.157$$

Number of lanes for whole width section

$$N_L = N_w \cdot DF$$

$$N_{L \text{ Spans } 1 \& 3} = 5 \cdot 1.190 = 5.952$$

$$N_{L \text{ Span } 2} = 5 \cdot 1.157 = 5.783$$

6. Modeling, Analysis and Results

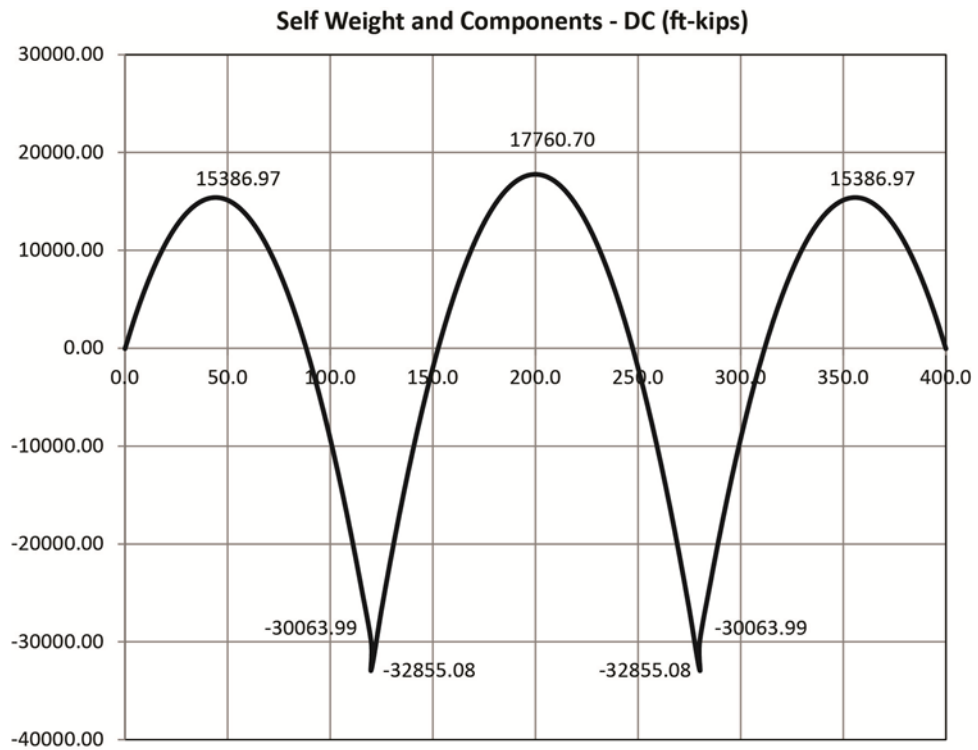


Figure C.4 – Self Weight and Component Bending Moments

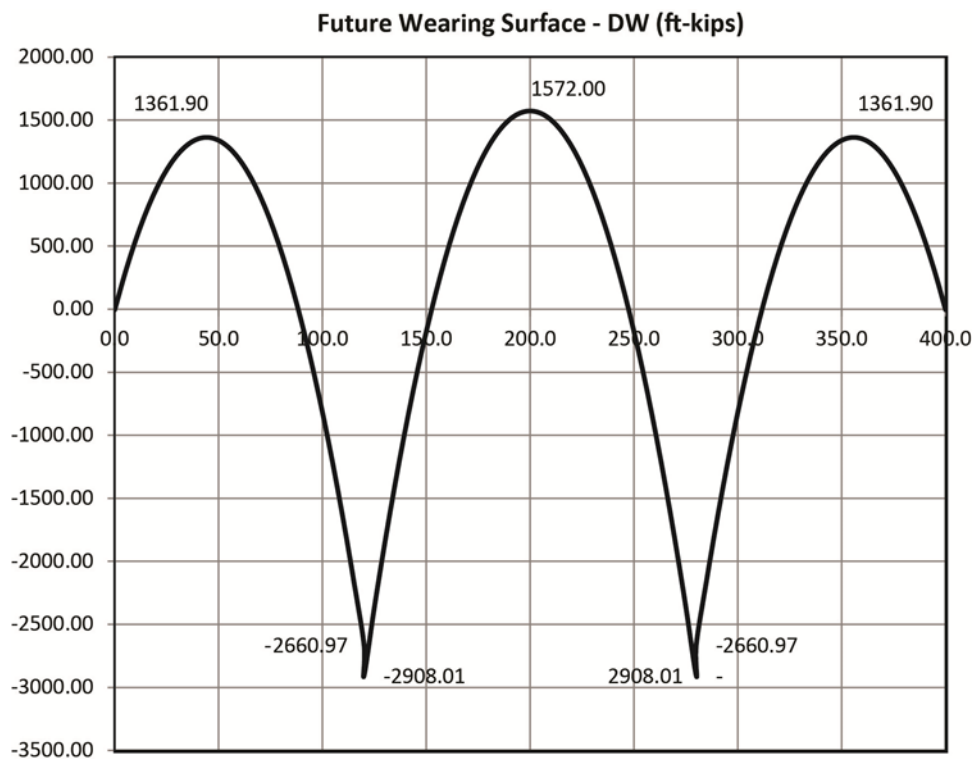


Figure C.5 – Future Wearing Surface Bending Moments

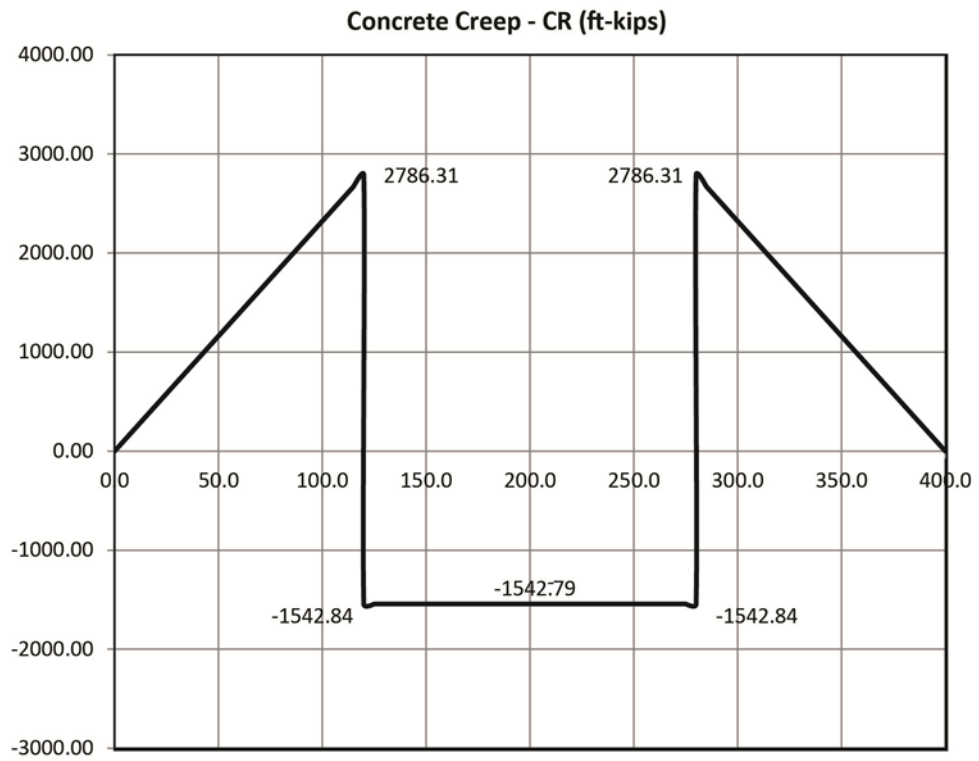


Figure C.6 – Concrete Creep Bending Moments

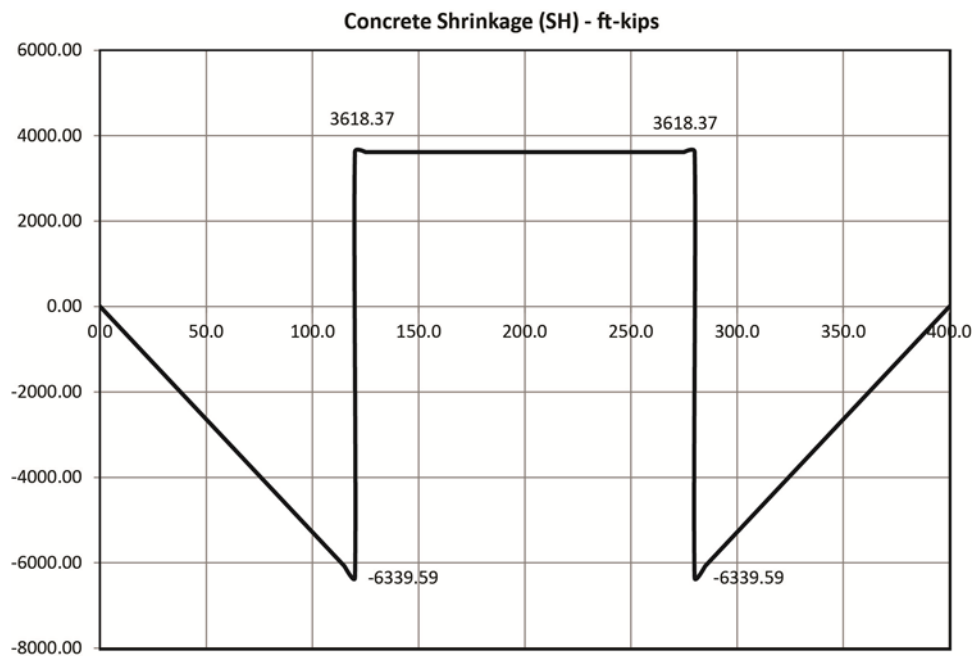


Figure C.7 – Concrete Shrinkage Bending Moments

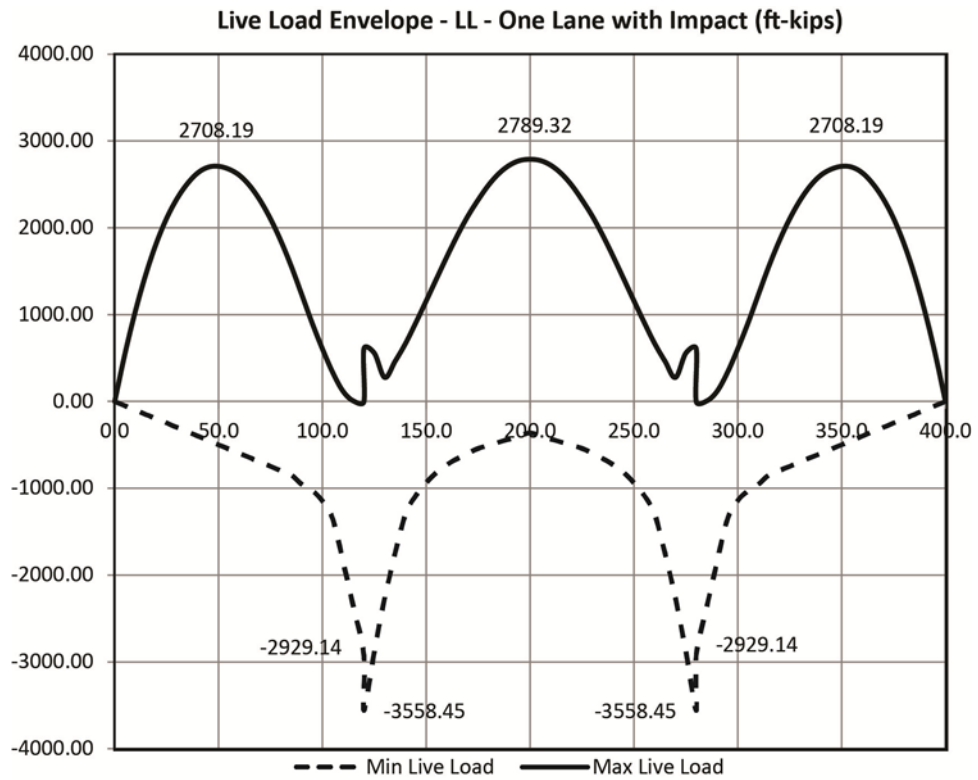


Figure C.8 – Live Load Envelope Bending Moments

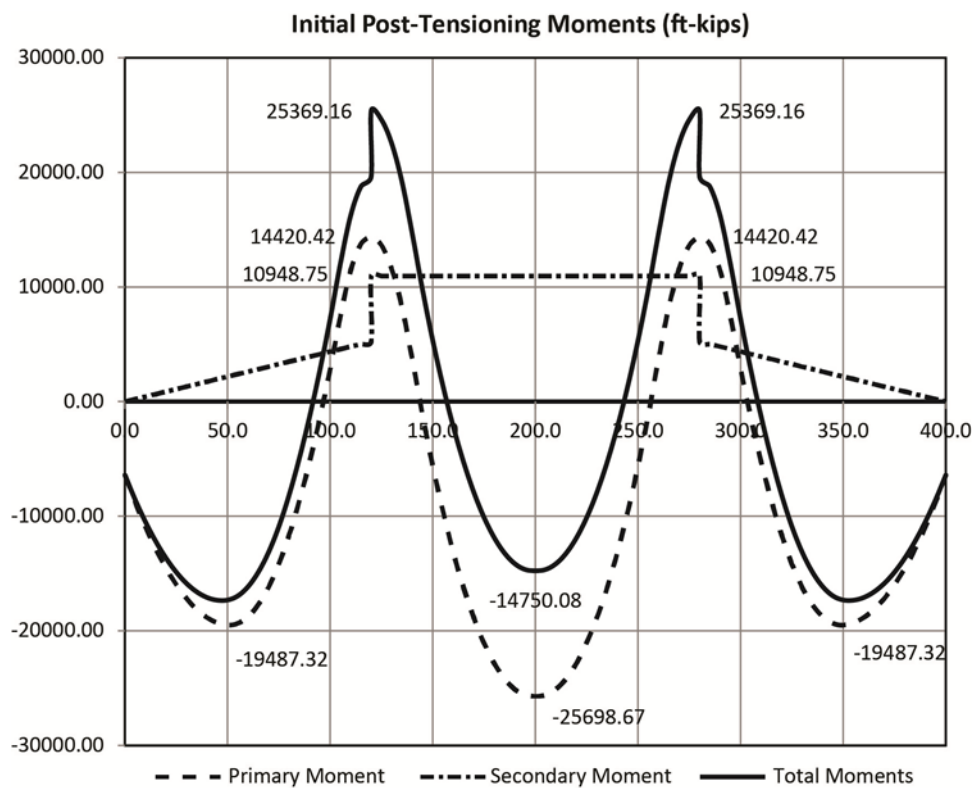


Figure C.9 – Initial Post-Tensioning Bending Moments

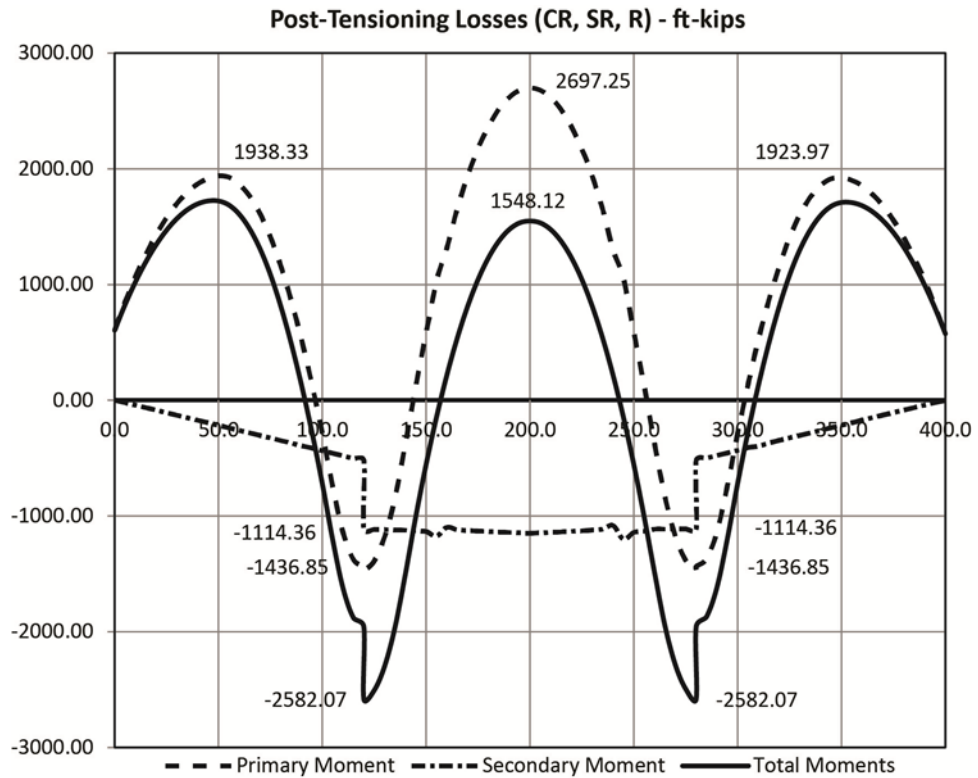


Figure C.10 – Bending Moments for Post-Tensioning Losses

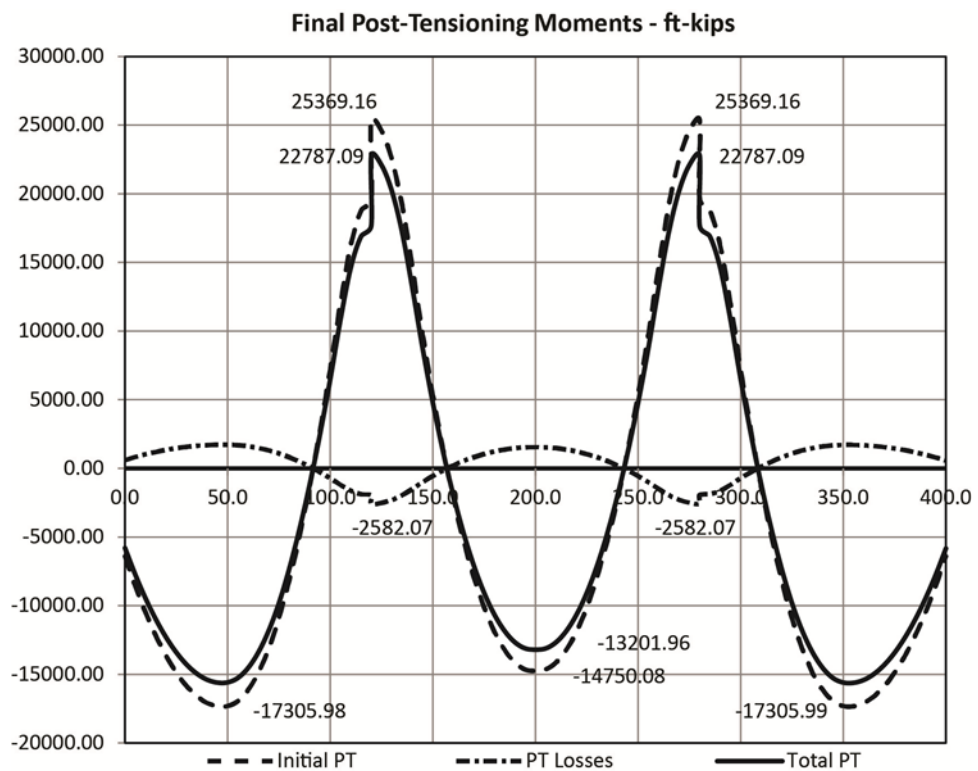


Figure C.11 – Final Post-Tensioning Moments

7. Flexural Design

There are two flexural designs required by the AASHTO LRFD specifications for prestressed concrete: flexural designs at the Service Limit State and at the Strength Limit State.

7.1 Service Limit State

[3.4.1]

There are two load combinations for the Service Limit State: Service I and Service III. The Service I load combination is used to check against maximum allowable compression in the superstructure and Service III is used to check against maximum allowable tension.

[3.4.1-1]

Load Combination Limit State	DC	DW	CR+SH	PS	TU	TG	LL+I
Service I	1.0	1.0	1.0	1.0	1.0	0.5	1.0
Service III	1.0	1.0	1.0	1.0	1.0	0.5	0.8

Table C.1 – Service Limit State Load Factors

[5.9.4]

The maximum allowable compressive stresses are:

- $0.6f'_{ci}$ for temporary stresses at the time of tendon stressing.
- $0.45f'_c$ due to prestressing and permanent loads after all time dependent effects and losses.
- $0.6f'_c$ due to prestressing, permanent, and transient loads after all time dependent effects and losses.

The maximum allowable tensile stresses are:

- $0.24\sqrt{f'_{ci}}$ (ksi) for temporary stresses at the time of tendon stressing ($7.5\sqrt{f'_{ci}}$ for units in psi).
- $0.019\sqrt{f'_c}$ (ksi) for stresses after all time dependent effects and losses ($6\sqrt{f'_c}$ for units in psi).

Temporary initial stress check:

The controlling point for compressive stresses is located in the bottom of the section at the down-station face of the diaphragm at Pier 2 (node 249).

$$f_{i\text{ }bm} = 1.0DC + 1.0PS_{\text{initial}} = -155.6ksf + (-1.3ksf)$$

$$f_{i\text{ }bm} = -156.9ksf > -0.6 \cdot 3.5ksi = -2.1ksi = -302.4ksf$$

$$f_{i\text{ }top} = 112.8ksf + (-194.3ksf) = -81.5ksf$$

$$f_{i\text{ }top} = -81.5ksf < 7.5\sqrt{3500\text{psi}} = 443.7\text{psi} = 63.9ksf$$

Final compression stress check, permanent loads:

The controlling point is located in the bottom of the section at the downstation face of the diaphragm at Pier 2 (node 249).

$$f_{p \text{ btm}} = 1.0DC + 1.0DW + 1.0(CR + SH) + 1.0PS$$

$$f_{p \text{ btm}} = -155.6 + (-13.8) + (15.9 - 36.2) + (-1.0) = -190.7 \text{ksf}$$

$$f_{f \text{ tension top}} = -190.7 \text{ksf} > -0.45 \cdot 5 \text{ksi} = -2.25 \text{ksi} = -324 \text{ksf}$$

Final compression stress check, all loads:

The controlling point is located in the bottom of the section at the downstation face of the diaphragm at Pier 2 (node 249). Use Service I load combination.

$$f_{f \text{ comp btm}} = f_{p \text{ btm}} + 1.0TU + 0.5TG + 1.0(LL + I)$$

$$f_{f \text{ comp btm}} = -190.7 - 29.7 + 0.5 \cdot (-15.2) - 60.1 = -288.1 \text{ksf}$$

$$f_{f \text{ comp btm}} = -288.1 \text{ksf} > -0.6 \cdot 5 \text{ksi} = -3.0 \text{ksi} = -432 \text{ksf}$$

Final tensile stress check, all loads:

The controlling point is located in the top of the section at the midspan of Span 2 (node 266). Use Service III load combination

$$f_{f \text{ tension top}} = f_{p \text{ top}} + 1.0TU + 0.5TG + 0.8(LL + I)$$

$$f_{f \text{ tension top}} = 112.8 + 10.0 - 11.5 + 26.2 - 174.8 + 21.5 + 0.5 \cdot 46.1 + 0.8 \cdot 43.5$$

$$f_{f \text{ tension top}} = 42.1 \text{ksf} < 6\sqrt{5000 \text{psi}} = 424.3 \text{psi} = 61.1 \text{ksf}$$

The table below contains a summary of the stress checks every ten feet along the superstructure.

Node	Distance (ft)	$> -0.6 f'_{ci}$		$> -0.45 f'_c$		Service I $> -0.6 f'_e$		Service III $< 6 \sqrt{f'_c}$	
		Bottom	Top	Bottom	Top	Bottom	Top	Bottom	Top
		(ksf)	(ksf)	(ksf)	(ksf)	Min	Min	Max	Max
150	0								
151	2.5	-146.4	-87.0	-130.4	-79.0	-137.8	-138.7	-122.0	-62.0
152	10	-138.0	-94.2	-119.1	-88.3	-128.3	-165.8	-93.3	-68.1
154	20	-130.4	-101.3	-109.0	-97.0	-120.9	-193.1	-64.7	-73.1
156	30	-126.5	-105.8	-103.9	-102.4	-119.9	-212.5	-45.2	-74.4
158	40	-126.1	-107.6	-103.7	-103.8	-125.5	-223.2	-33.5	-72.0
160	50	-129.1	-107.1	-108.2	-102.1	-136.3	-226.9	-30.9	-66.2
162	60	-133.3	-105.7	-115.6	-98.1	-149.6	-224.9	-35.3	-58.1
240	70	-136.0	-105.6	-123.4	-94.3	-163.3	-219.2	-44.1	-50.5
242	80	-135.0	-105.8	-129.5	-89.4	-175.6	-209.2	-54.6	-41.5
244	90	-131.6	-106.3	-135.3	-83.3	-187.3	-194.9	-68.3	-31.7
246	100	-127.7	-107.2	-142.4	-76.5	-202.9	-180.0	-83.6	-19.2
248	110	-129.9	-103.3	-156.8	-63.9	-233.7	-161.9	-102.9	3.4
249	117	-156.9	-81.5	-190.7	-37.2	-288.1	-135.6	-135.7	42.1
250	120								
251	123	-134.4	-91.2	-137.4	-63.4	-237.9	-150.8	-89.7	7.1
252	130	-99.1	-114.3	-96.6	-90.7	-177.1	-172.3	-55.2	-31.8
254	140	-82.9	-122.8	-70.6	-106.6	-129.2	-195.2	-21.5	-60.4
256	150	-85.7	-119.2	-63.4	-110.4	-112.7	-207.9	-4.5	-69.6
258	160	-87.1	-116.7	-56.6	-113.8	-99.9	-220.4	12.4	-76.4
260	170	-87.4	-115.0	-50.6	-116.8	-90.7	-231.7	27.5	-81.3
262	180	-86.7	-114.1	-45.5	-119.2	-83.3	-240.6	39.8	-85.0
264	190	-85.1	-113.7	-41.2	-120.8	-77.2	-246.3	48.6	-87.7
266	200	-83.2	-113.6	-38.5	-121.3	-72.8	-248.0	52.6	-89.2
336	210	-85.1	-113.7	-41.2	-120.8	-77.2	-246.3	48.6	-87.7
338	220	-86.7	-114.1	-45.5	-119.2	-83.3	-240.6	39.8	-85.0
340	230	-87.4	-115.0	-50.6	-116.7	-90.7	-231.6	27.5	-81.2
342	240	-87.1	-116.7	-56.6	-113.8	-99.9	-220.4	12.4	-76.4
344	250	-85.7	-119.2	-63.4	-110.4	-112.7	-207.9	-4.5	-69.6
346	260	-82.9	-122.8	-70.5	-106.6	-129.1	-195.2	-21.4	-60.4
348	270	-99.1	-114.3	-96.5	-90.7	-177.0	-172.3	-55.1	-31.8
349	277	-134.4	-91.2	-137.4	-63.4	-237.9	-150.8	-89.7	7.1
350	280								
351	283	-156.9	-81.5	-190.7	-37.2	-288.1	-135.6	-135.7	42.1
352	290	-129.9	-103.3	-156.7	-63.9	-233.6	-161.9	-102.8	3.4
354	300	-127.7	-107.2	-142.3	-76.5	-202.8	-180.0	-83.5	-19.2
356	310	-131.6	-106.3	-135.3	-83.3	-187.3	-194.9	-68.3	-31.7
358	320	-135.0	-105.8	-129.5	-89.4	-175.6	-209.2	-54.6	-41.5
360	330	-136.0	-105.6	-123.4	-94.2	-163.3	-219.1	-44.1	-50.4
362	340	-133.3	-105.7	-115.7	-98.1	-149.7	-224.9	-35.4	-58.1
440	350	-129.1	-107.1	-108.3	-102.1	-136.4	-226.9	-31.0	-66.2
442	360	-126.1	-107.6	-103.7	-103.7	-125.5	-223.1	-33.5	-71.9
444	370	-126.5	-105.8	-104.0	-102.3	-120.0	-212.4	-45.3	-74.3
446	380	-130.4	-101.3	-109.1	-96.9	-121.0	-193.0	-64.8	-73.0
448	390	-138.0	-94.2	-119.3	-88.1	-128.5	-165.6	-93.5	-67.9
449	397.5	-146.4	-87.0	-130.6	-78.8	-138.0	-138.5	-122.2	-61.8
450	400								

Table C.2 – Service Limit State Flexural Verifications

7.2 Strength Limit State

[3.4.1] There is one basic load combination used to check the Strength Limit State for cast-in-place segmental superstructure: Strength I.

[3.4.1-1]

Load Combination Limit State	DC	DW	CR+SH	PS	TU	TG	LL+I
Strength I	1.25	1.5	1.0	1.0	0.5	0.0	1.75

Table C.3 – Strength Limit State Load Factors

Where, PS represents the secondary moment caused by post-tensioning (note, it does not include the primary moment due to post-tensioning)

[1.3.2.1-1],
[5.7.3.2],
[5.7.3.3.2]

The factored flexural resistance, M_r , must be greater than the Strength I load combination, M_u (ultimate moment), and the minimum reinforcement requirement. The minimum reinforcement requirement states that the flexural resistance must at least equal to $1.33M_u$ or the cracking moment, M_{cr} , whichever is less. This can be summarized by the following equation:

$$M_r = \phi M_n \geq \max(M_u, \min(1.33M_u, M_{cr}))$$

7.2.1 Factored Design Moment

The location with the largest demand to capacity ratio, d/c , is the negative moment at the downstation face of the diaphragm at Pier 2 (node 249). The summation of the Strength I load combination is:

$$M_{DC} = -26585 \text{ ft} - \text{kips}$$

$$M_{DW} = -2353 \text{ ft} - \text{kips}$$

$$M_{CR+SH} = 2717 - 6181 = -3464 \text{ ft} - \text{kips}$$

$$M_{PS} = 4594 \text{ ft} - \text{kips}$$

$$M_{TU} = -5067 \text{ ft} - \text{kips}$$

$$M_{LL+I} = -11348 \text{ ft} - \text{kips}$$

$$\rightarrow M_u = -58024 \text{ ft} - \text{kips}$$

[5.7.3.3.2]

Minimum reinforcement calculation

$$1.33M_u = -77171 \text{ ft} - \text{kips}$$

$$M_{cr} = \gamma_3 \left[(\gamma_1 f_r + \gamma_2 f_{cpe}) S_c \right]$$

where,

$$\begin{aligned} \gamma_1 &= 1.6 & \gamma_2 &= 1.1 \\ \gamma_3 &= 1.0 & f_r &= 7.5\sqrt{5000 \text{ psi}} = 530 \text{ psi} = 76.4 \text{ ksf} \\ f_{cpe} &= 174.8 \text{ ksf} & S_c &= 235.6 \text{ ft}^3 \end{aligned}$$

$$\rightarrow M_{cr} = -74099 \text{ ft} - \text{kips}$$

The absolute value of the cracking moment is less than the absolute value of $1.33M_u$, and this value is greater than the absolute value of the factored moment, M_u . Thus, the design moment is M_{cr} .

7.2.2 Factored Flexural Resistance

[5.7.3.2.2-1] The nominal flexural resistance for flanged sections:

$$M_n = A_{ps} f_{ps} \left(d_p - \frac{a}{2} \right) + 0.85 f'_c (b - b_w) h_f \left(\frac{a}{2} - \frac{h_f}{2} \right)$$

For rectangular sections, $b_w = b$ making the second part of the above equation drop to zero. Note that the equation is modified from AASHTO LRFD neglecting the contributions from mild reinforcement.

The nominal moment calculated at the downstation face of the diaphragm at Pier 2 (node 249). The following can be obtained from the section dimensions:

[5.7.3.2.2] $a = c\beta_1$

[5.7.3.1.1-3]
$$c = \frac{A_{ps} f_{pu} - 0.85 f'_c (b - b_w) h_f}{0.85 f'_c \beta_1 b_w + k A_{ps} \frac{f_{pu}}{d_p}}$$

where,

$$A_{ps} = 5 \cdot 3 \cdot 19 \cdot 0.217 \text{ in}^2 = 61.845 \text{ in}^2$$

$$f_{pu} = 270 \text{ ksi}$$

$$f'_c = 5 \text{ ksi}$$

$$b = 44.5 \text{ ft} = 534 \text{ in}$$

$$b_w = 5.2361 \text{ ft} = 62.833 \text{ in}$$

$$h_f = 7 \text{ in}$$

[C5.7.3.1.1-1] $k = 0.28$

$$d_p = 5.03625 \text{ ft} = 60.435 \text{ in}$$

$$[5.7.2.2] \quad \beta_1 = \begin{cases} 0.85, & f'_c \leq 4 \text{ ksi} \\ 0.85 - (0.05/\text{ksi})(f'_c - 4 \text{ ksi}), & 4 \text{ ksi} < f'_c < 8 \text{ ksi} \\ 0.65, & f'_c \geq 8 \text{ ksi} \end{cases}$$

$$\beta_1 = 0.85 - (0.05/\text{ksi})(5 \text{ ksi} - 4 \text{ ksi}) = 0.80$$

Solve for c and determine if the section is rectangular or T-section.

$$c = \frac{61.845 \text{ in}^2 \cdot 270 \text{ ksi} - 0.85 \cdot 5 \text{ ksi} (534 \text{ in} - 62.833 \text{ in}) 7 \text{ in}}{0.85 \cdot 5 \text{ ksi} \cdot 0.80 \cdot 62.833 \text{ in} + 0.28 \cdot 61.845 \text{ in}^2 \cdot \frac{270 \text{ ksi}}{60.435 \text{ in}}} = 9.213 \text{ in}$$

If the value of $a \leq h_f$, then the section is rectangular, otherwise it is considered a T-section.

$$a = 0.80 \cdot 9.213 \text{ in} = 7.370 \text{ in} = 0.6142 \text{ ft} > h_f = 7 \text{ in} = 0.5833 \text{ ft}$$

Therefore, this is a T-section.

[5.7.3.1] The average stress in prestressing steel:

$$f_{ps} = f_{pu} \left(1 - k \frac{c}{d_p} \right) = 270 \text{ ksi} \left(1 - 0.28 \frac{9.213 \text{ in}}{60.435 \text{ in}} \right) = 258.475 \text{ ksi}$$

[5.5.4.2] The resistance (reduction) factor:

$$0.75 \leq \phi = 0.583 + 0.25 \left(\frac{d_p}{c} - 1 \right) \leq 1.0$$

$$\phi = 0.583 + 0.25 \left(\frac{60.435}{9.213} - 1 \right) > 1.0$$

$$\rightarrow \phi = 1.0$$

Calculate the flexural resistance, ϕM_n , for negative bending.

$$\phi M_n = -1.0 \cdot \left(61.845 \text{ in}^2 \cdot 258.475 \text{ ksi} \left(5.03625 \text{ ft} - \frac{0.6142 \text{ ft}}{2} \right) + 0.85 \cdot 5 \text{ ksi} (534 \text{ in} - 62.833 \text{ in}) 7 \text{ in} \left(\frac{0.6142 \text{ ft}}{2} - \frac{0.5833 \text{ ft}}{2} \right) \right)$$

$$\phi M_n = -75814 \text{ ft} - \text{kips}$$

Therefore, the flexural resistance is greater than the flexural demand:

$$|\phi M_n| \geq |M_{cr}|$$

$$75814 \text{ ft} - \text{kips} > 74099 \text{ ft} - \text{kips}$$

The demand to capacity ratio, d/c :

$$d/c \leq 1.0$$

$$\frac{-74099 \text{ ft} - \text{kips}}{-75814 \text{ ft} - \text{kips}} = 0.977 < 1.0$$

The above calculations show that the down station face of the diaphragm at Pier 2 (node 249) is adequately designed for the flexural demand at that location.

The table below contains a summary of the flexural strength design checks at typical critical locations along the superstructure.

Node			160	249	251	266	349	351	440
Location			~ 0.4 L	Pier 2		0.5 L	Pier 3		~ 0.6 L
Distance		(ft)	50	117	123	200	277	283	350
DC		(ft-kips)	15125	-26585	-29178	17761	-29178	-26585	15125
DW		(ft-kips)	1339	-2353	-2583	1572	-2583	-2353	1339
CR		(ft-kips)	1161	2717	-1543	-1543	-1543	2717	1161
SH		(ft-kips)	-2642	-6181	3618	3618	3618	-6181	-2642
PS		(ft-kips)	1964	4594	9834	9799	9836	4595	1966
TU	Rise	(ft-kips)	2165	5067	-2622	-2622	-2622	5067	2165
	Fall	(ft-kips)	-2165	-5067	2622	2622	2622	-5067	-2165
LL+I	Min	(ft-kips)	-2264	-11348	-13778	-1530	-13778	-11348	-2264
	Max	(ft-kips)	12306	14	2438	11795	2438	14	12306
M_u	Min	(ft-kips)	16354	-58024	-51237	32445	-51234	-58022	16355
	Max	(ft-kips)	44017	-33074	-25482	58387	-25479	-33072	44018
$1.33M_u$	Min	(ft-kips)		-77171	-68145		-68141	-77169	
	Max	(ft-kips)	58542			77655			58544
M_{cr}	Min	(ft-kips)		-74099	-78573		-78573	-74099	
	Max	(ft-kips)	57672			52147			57691
Design Moment	Min			M_{cr}	$1.33M_u$		$1.33M_u$	M_{cr}	
	Max		M_{cr}			M_u			M_{cr}
	Min	(ft-kips)		-74099	-68145		-68141	-74099	
	Max	(ft-kips)	57672			58387			57691
fM_n	Min	(ft-kips)	-27327	-75814	-75622	-11740	-75622	-75814	-27327
	Max	(ft-kips)	67604	18917	19105	81151	19105	18917	67604
d/c ratio	Min			0.977	0.901		0.901	0.977	
	Max		0.853			0.719			0.853

Table C.4 – Flexural Strength Design Verifications

8. Shear and Torsion Design – Strength Limit State

Like the flexural design, the Strength I Limit State load combination is used for the shear and torsion design. It can be found in table 4.2-1 in section 4.

The factored shear resistance must be greater than the Strength I load combination, V_u (ultimate shear).

$$\phi V_n \geq V_u$$

8.1 Torsion Members

[5.8.2.1]

According to the AASHTO LRFD specifications, torsion may not be neglected if:

$$T_u > 0.25\phi T_{cr}$$

where,

$$T_{cr} = 0.125\sqrt{f'_c} \frac{A_{cp}^2}{p_c} \sqrt{1 + \frac{f_{pc}}{0.125\sqrt{f'_c}}}$$

However, by inspection, torsion need not be investigated for this design example. Due to the bridge being straight, live loading is the only cause for torsion. No dead, miscellaneous, or other loads cause torsion in the superstructure. As outlined above in section 2 of this design example, this bridge meets the requirements to utilize the live load distribution tables in the AASHTO LRFD specifications.

Torsional effects are inherently included in the distribution factor equations. The purpose of a live load distribution factor is to capture the maximum possible vertical shear load on a web due to live loading. This can be done by altering the number of specified live loads and its transverse position on the cross section to create the maximum shear effect on the web of interest. Torsion affects the vertical shear loads in the webs and is subsequently captured by this process.

Therefore, torsion may be neglected in the following calculations of the shear design. See design example 2 for a procedure of designing for torsional effects.

8.2 Factored Design Shear

The AASHTO LRFD specifications specifies that the critical section for shear design can be located a distance d_v from the support or point of discontinuity. The highest shear demand and critical section is located just upstation to Pier 2, a distance d_v (4.68 ft) from the diaphragm (node 252) (see section 8.3 for calculation of d_v).

The summation of the Strength I load combination is:

$$V_{DC} = 1143.92 \text{ kips}$$

$$V_{DW} = 101.25 \text{ kips}$$

$$V_{CR+SH} = V_{PS} = V_{TU} = 0$$

$$V_{LL+I} = 801.89 \text{ kips}$$

$$\rightarrow V_u = 2985.08 \text{ kips}$$

where,

V_{PS} = the shear due to secondary post-tensioning effects

8.3 Factored Shear Resistance

A prestressed concrete beam fails under shear along diagonal cracks. There are two types of diagonal cracks that form: Type I and Type II. The first type is known as flexure-shear cracks and the second as web-shear cracks. The flexure-shear cracks start as a nearly vertical flexural cracks on the tension face that later, under a shear demand, spread into diagonal shear cracks toward the compression face. Flexure-shear cracks are common in beams with low prestressing force near midspan. Web-shear cracks form near the neutral axis of the section in the web and spread diagonally. This type of cracking is caused by tension in the web called principal tensile stresses and can be found near supports.

[5.8.3.3] The AASHTO LRFD specification states the nominal shear resistance to be the following:

$$V_n = V_c + V_s$$

[5.8.3.4] The shear resistance may be determined using one of three methods outlined in the AASHTO LRFD specification. Method 1 is for nonprestressed sections only. Method 2 is the general procedure for prestressed and nonprestressed members. And Method 3 is the simplified procedure for prestressed and nonprestressed members.

[5.8.3.4.3] This design example uses the Simplified Procedure outlined in the AASHTO LRFD specifications. The concrete contribution, V_c , of the nominal shear resistance is the minimum of V_{ci} and V_{cw} , the flexure-shear resistance and web-shear resistance respectively.

$$V_c = \min(V_{ci}, V_{cw})$$

The nominal shear resistance to combined flexure and shear can be obtained from the following equation (units in *kips* and *in*):

$$V_{ci} = 0.02\sqrt{f'_c}b_vd_v + V_o$$

The above equation can be separated into two parts. The second term, V_o , is the shear that occurs at the section when a flexural crack forms. The first term is an empirical formula that represents the additional shear force required to transform the flexural crack into an inclined shear crack.

The second term is often separated into two parts as follows:

$$V_o = V_d + V_{cr} = V_d + V_i \frac{M_{cre}}{M_{max}}$$

where,

$$\begin{aligned} V_d &= \text{unfactored dead loads (DC + DW)} \\ M_{cre} &= \text{the moment required to crack the section above the dead loads} \\ M_{max} &= \text{the maximum factored moment less the unfactored dead loads} \\ V_i &= \text{the factored shear concurrent to the maximum moment less the dead load} \end{aligned}$$

[5.8.3.4.3-1] Therefore, the nominal shear resistance to combined flexure and shear and its lower limit can be written (units in kips and in):

$$V_{ci} = 0.02\sqrt{f'_c}b_vd_v + V_d + V_i \frac{M_{cre}}{M_{max}} \geq 0.06\sqrt{f'_c}b_vd_v$$

[5.8.2.9] The effective web width, b_v , is the sum of the web widths less $\frac{1}{4}$ the diameter of the grouted ducts or $\frac{1}{2}$ the diameter of the ungrouted ducts:

$$b_v = 5 \cdot 1.0 \text{ ft} - 5 \cdot (0.25 \cdot 0.375 \text{ ft}) = 4.53125 \text{ ft}$$

[5.8.2.9] The effective shear depth, d_v , can be defined by:

$$d_v = \max \left(\frac{M_n}{A_{ps}f_{ps}}, 0.9d_e, 0.72h \right)$$

[C5.8.2.9-1] where,

$$\frac{M_n}{A_{ps}f_{ps}} = \left| \frac{-73605 \text{ ft} - \text{kips}}{0.4295 \text{ ft}^2 \cdot 258.24 \text{ ksi} \cdot 144 \frac{\text{in}^2}{\text{ft}^2}} \right| = 4.61 \text{ ft}$$

[5.8.2.9-2] $0.9d_e = 0.9 \frac{A_{ps}f_{ps}d_p}{A_{ps}f_{ps}} = 0.9d_p = 0.9 \cdot 4.90 \text{ ft} = 4.41 \text{ ft}$

$$0.72h = 0.72 \cdot 6.5 \text{ ft} = 4.68 \text{ ft}$$

$$\rightarrow d_v = 0.72h = 4.68 \text{ ft}$$

The unfactored dead load, V_d , is:

$$V_d = V_{DC} + V_{DW} = 1143.92 + 101.25 = 1245.17 \text{ kips}$$

The factored maximum moment (negative flexure near pier) and the shear that acts concurrent to the moment from externally applied loads (M_{max} and V_i respectively) are:

$$M_{max} = M_u - M_d = M_u - M_{DC+DW} = -41624 - (-25746) = -15878 \text{ ft-kips}$$

$$V_i = 889.16 \text{ kips}$$

Note that M_{max} and V_i contain the secondary post-tensioning effects.

As defined above, M_{cre} is the moment required, above that caused by dead loads, to crack the section. Before looking at the code equation, it is known that the moment required to crack a concrete section is:

$$M_{cr} = S \left(f_r + \frac{P_{PT}}{A} \right)$$

where:

- S = section modulus
- f_r = modulus of rupture, or the stress at which the concrete cracks
- P_{PT} = axial force from post-tensioning (including secondary effects)
- A = cross sectional area

Therefore, when the section cracks in flexure, the applied factored moments must equal the cracking moment.

$$S \left(f_r + \frac{P_{PT}}{A} \right) = 1.25M_{DC} + 1.5M_{DW} + M_{CR+SH} + M_{PT} + 0.5M_{TU} + 1.75M_{LL+I}$$

Knowing:

$$M_u = 1.25M_{DC} + 1.5M_{DW} + M_{CR+SH} + M_{PS} + 0.5M_{TU} + 1.75M_{LL+I}$$

where,

- M_{PS} = moment from secondary post-tensioning effects
- M_P = moment primary post-tensioning effects

$$S \left(f_r + \frac{P_p}{A} + \frac{P_{PS}}{A} \right) = M_u + M_p$$

$$S \left(f_r + \frac{P_p}{A} - \frac{M_p}{S} + \frac{P_{PS}}{A} \right) = M_u$$

$$S \left(f_r + f_p + \frac{P_{PS}}{A} \right) = M_u$$

$$S \left(f_r + f_p + \frac{P_{PS}}{A} - \frac{M_d}{S} \right) = M_u - M_d$$

[5.8.3.4.3-2] Therefore, the equation for the cracking moment, M_{cre} , is written as:

$$M_{cre} = S_i \left(f_r + f_{cpe} - \frac{M_{dnc}}{S_{nc}} \right)$$

[5.4.2.6] where,

$$f_r = 0.20\sqrt{f'_c} = 0.20\sqrt{5\text{ksi}} = -0.447\text{ksi} = -64.40\text{ksf}$$

$$f_{cpe} = f_p + \frac{P_{PS}}{A} = -143.96\text{ksf}$$

$$M_{dnc} = M_d = -25746\text{ft} - \text{kips}$$

$$S_c = S_{nc} = \frac{I_x}{y_{ct}} = 235.63\text{ft}^3$$

at the top of the section.

$$M_{cre} = 235.63\text{ft}^3 \left(-64.40\text{ksf} - 143.96\text{ksf} - \frac{-25746\text{ft} - \text{kips}}{235.63\text{ft}^3} \right)$$

$$\rightarrow M_{cre} = -23350\text{ft} - \text{kips}$$

For the V_{ci} equation to apply, the following must be true:

$$\frac{M_{cre}}{M_{max}} \leq 1.0 \rightarrow \frac{23350}{15878} > 1.0$$

The purpose of the V_{ci} equation is to determine the concrete's resistance to a flexural shear crack. If, in this case, the section does not crack in flexure, V_{ci} does not apply and V_{cw} controls.

[5.8.3.4.3-3] The nominal shear resistance to excessive principal tension is:

$$V_{cw} = (0.06\sqrt{f'_c} + 0.30f_{pc})b_v d_v + V_p$$

The compressive stress at the centroid of the section, f_{pc} , is:

$$f_{pc} = 96.22ksf \text{ (compression)}$$

[C5.8.2.3] The vertical component of the prestressing force, V_p , is as follows (positive when resisting the applied shear):

$$V_p = 360.40kips$$

Therefore:

$$V_{cw} = (0.06\sqrt{5ksi} \cdot 144 \frac{in^2}{ft^2} + 0.30 \cdot 96.22ksf) 4.53 ft \cdot 4.68 ft + 360.40kips$$

$$V_{cw} = 1382.22kips$$

section is:

$$V_s = \frac{V_u}{\phi} - V_c$$

[C5.8.3.3-1] The shear reinforcement required to provide the above shear resistance is:

$$A_v = \frac{V_s}{f_y d_v \cot \theta} = \frac{V_u / \phi - V_c}{f_y d_v \cot \theta}$$

**[5.5.4.2.1],
[5.8.3.4.3-4]**

where,

$$\phi = 0.90$$

$$f_y = 60ksi$$

$$\cot \theta = 1.0 + 3 \left(\frac{f_{pc}}{\sqrt{f'_c}} \right) \leq 1.8$$

$$\cot \theta = 1.8$$

$$\rightarrow A_v \geq \frac{2985.08kips / 0.90 - 1382.22kips}{60ksi \cdot 4.68 ft \cdot 1.8} = 3.83 in^2 / ft$$

Divided evenly among the 5 webs:

$$A_v = 0.77 \text{ in}^2/\text{ft}$$

[5.8.2.5-1]

The minimum required reinforcement for the entire cross section is:

$$A_{v_min} \geq 0.0316 \sqrt{f'_c} \frac{b_v}{f_y} = 0.0316 \sqrt{5 \text{ksi}} \frac{4.53125 \text{ft} \cdot 144 \text{in}^2}{60 \text{ksi}} = 0.77 \text{ in}^2/\text{ft}$$

Therefore, use #5 bars spaced at 9 inches on each face of each web.

$$A_v = \frac{5 \cdot 2 \cdot 0.31 \text{in}^2}{9/12 \text{ft}} = 4.13 \text{ in}^2/\text{ft}$$

The table below contains a summary of the shear strength design at every 20 feet. Note that #4 bars at 12 inches is the lowest reinforcement used. This is due to engineering judgment.

Node	Distance (ft)	V_u (kips)	V_c (kips)	$V_{s \text{ req}}$ (kips)	$A_{v \text{ req}}$ per web (in ² /ft)	Bar Area (in ²)	@ (in)	$A_{v \text{ prov}}$ per web (in ² /ft)
150	0							
152	7.18	1946	1434	728	0.288	0.20	12	0.40
154	20	1456	1330	288	0.114	0.20	12	0.40
158	40	726	979	0	0.000	0.20	12	0.40
162	60	-1059	1244	0	0.000	0.20	12	0.40
242	80	-1768	1576	389	0.154	0.20	12	0.40
246	100	-2465	1875	865	0.342	0.20	12	0.40
248	112.32	-2882	1508	1694	0.670	0.31	9	0.83
250	120							
252	127.68	2985	1382	1935	0.765	0.31	9	0.83
254	140	2576	1851	1011	0.400	0.20	12	0.40
258	160	1902	1601	512	0.203	0.20	12	0.40
262	180	1229	1286	79	0.031	0.20	12	0.40
266	200	569	1027	0	0.000	0.20	12	0.40
338	220	-1229	1286	79	0.031	0.20	12	0.40
342	240	-1902	1601	512	0.203	0.20	12	0.40
346	260	-2576	1852	1011	0.400	0.20	12	0.40
348	277.32	-2985	1382	1934	0.765	0.31	9	0.83
350	280							
352	292.68	2882	1508	1694	0.670	0.31	9	0.83
354	300	2465	1875	864	0.342	0.20	12	0.40
358	320	1768	1576	388	0.154	0.20	12	0.40
362	340	1059	918	0	0.000	0.20	12	0.40
442	360	-726	1161	0	0.000	0.20	12	0.40
446	380	-1456	1330	288	0.114	0.20	12	0.40
448	392.82	-1946	1434	728	0.288	0.20	12	0.40
450	400							

Table C.5 – Summary of Shear Design at Strength Limit State

9. Principal Tensile Stresses

[5.8.5]

The AASHTO-LRFD Design Specifications state that the principal stresses in the webs shall be analyzed for all segmental bridges. It does not give direction on non-segmental concrete box girder bridges. However, it is a good design check and the calculation of principal stresses is included in this example.

The principal tensile stresses shall be calculated using the long-term residual axial stress and the maximum shear stress. The Service III Limit State load combination is used for both axial and shear stresses. The load combination can be found in table 4.1-1 in section 4.

The thermal gradient loading is not considered in the calculation of principal stresses. The purpose of thermal gradient is to check longitudinal stresses under special thermal effects. Axial stresses resulting from temperature and live loading are also not included since they are not long-term loadings.

The critical section with the maximum principal tensile stress is located just upstation to Pier 2, a distance of d_v (4.68 ft) from the diaphragm (node 252). See section 5 above for the calculation of d_v .

From general mechanics of materials, the shear stress can be taken as:

$$\tau = \frac{VQ}{Ib}$$

where,

$$\begin{aligned} V &= \text{vertical shear in section} \\ &= V_{DC} + V_{DW} + V_{PS} + V_{CR+SH} + V_{TU} + 0.8 \cdot V_{LL+I} \\ &= 1526 \text{ kips} \\ Q &= \text{first moment of the area} = 118.12 \text{ ft}^3 \\ I &= \text{section moment of inertia} = 643.75 \text{ ft}^4 \\ b &= \Sigma \text{ web widths less } \frac{1}{4} \text{ duct } \emptyset = 4.53125 \text{ ft} \end{aligned}$$

$$\rightarrow \tau = \frac{1526 \text{ kips} \cdot 118.12 \text{ ft}^3}{643.75 \text{ ft}^4 \cdot 4.53125 \text{ ft}} = 61.81 \text{ ksf}$$

9.1 Mohr's Circle

The Mohr's circle is a graphical representation of the state of plane stress at a given point. The abscissa and ordinate represent the normal and shear stress components respectively. Below is a graph of Mohr's circle and points M , N , and C .

$$\sigma = \sigma_x \cos^2 \alpha + \sigma_y \sin^2 \alpha$$

$$\tau = \frac{1}{2} (\sigma_y - \sigma_x) \sin 2\alpha$$

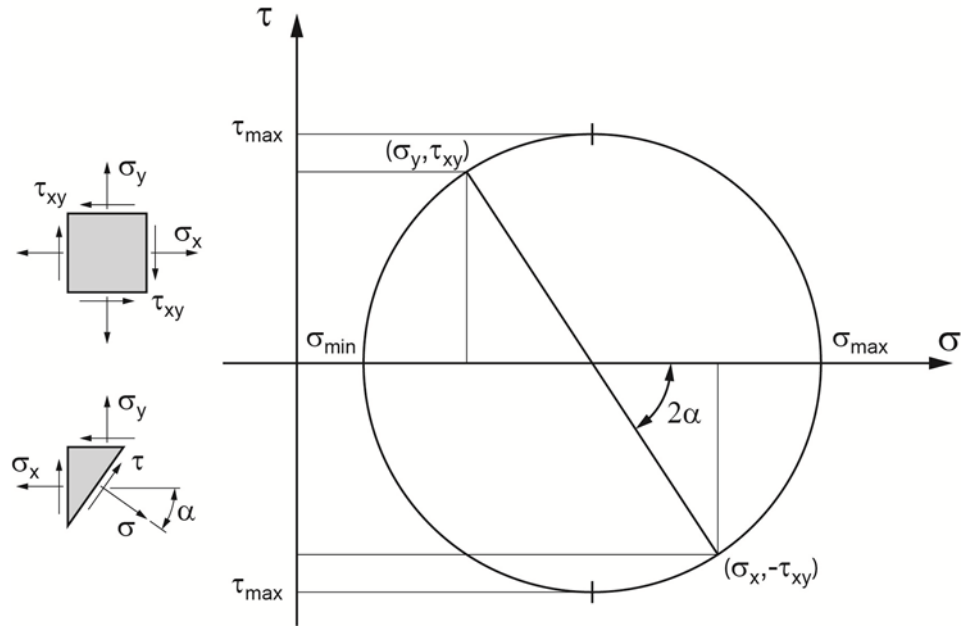


Figure C.12 – Mohr's Circle

The normal stress at point *M* is the axial stress on the section at the neutral axis. The stresses used

$$\sigma_x = \sigma_{DC} + \sigma_{DW} + \sigma_{PS} + \sigma_{CR+SH} = -93.52ksf$$

$$\sigma_y = 0$$

$$\tau_{xy} = -61.81ksf$$

The Mohr's circle representation of this state of stress is:

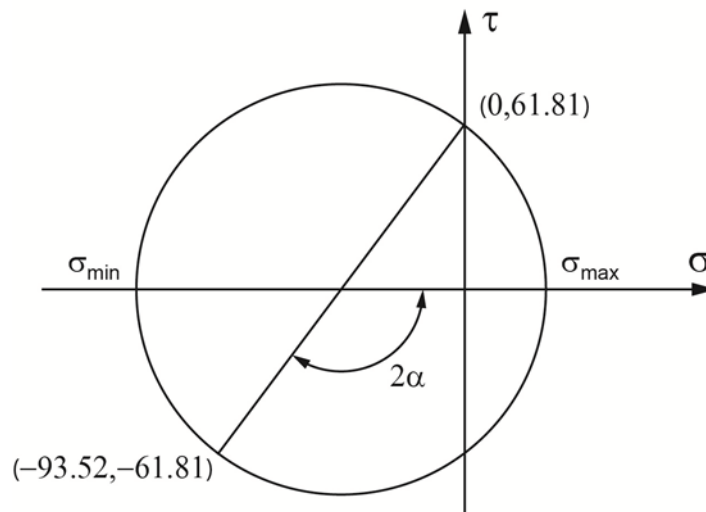


Figure C.13 – State of Stress at Node 252

For the case of no vertical compression ($s_y=0$), the radius, R , of Mohr's circle can be expressed as:

$$R = \sqrt{\left(\frac{\sigma_x}{2}\right)^2 + \tau_{xy}^2} = \sqrt{(-46.76)^2 + 61.81^2} = 77.50ksf$$

$$\rightarrow \sigma_{max} = \frac{\sigma_x}{2} + R = -46.76 + 77.50 = 30.74ksf$$

[5.9.4.2.2-1]

The maximum permissible principal tension is $3.5\sqrt{f'_c}$ (psi) ($0.110\sqrt{f'_c}$ for units in ksi).

$$\sigma_{max} = 30.74ksf = 213.5psi = 3.02\sqrt{f'_c} \text{ (psi)} \leq 3.5\sqrt{f'_c} \text{ (psi)}$$

$$f'_c = 5000psi$$

The table below contains a summary of the principal tension check at a distance d_v (4.68 ft) from each diaphragm. These are the critical locations for each span in this example. Note that this is not always true for every bridge or bridge type.

Node	Distance (ft)	τ		σ	$\sigma/2$ (ksf)	Radius (ksf)	σ_{max} (ksf)	$\sqrt{f'_c}$
		Min (ksf)	Max (ksf)	COG (ksf)				
150	0							
152	7.18	7.1	32.9	-101	-50.5	60.3	9.8	0.96
248	112.32	-56.4	-27.2	-103	-51.3	76.2	24.9	2.45
250	120							
252	127.68	33.8	61.8	-94	-46.8	77.5	30.7	3.02
348	277.32	-61.8	-33.8	-94	-46.8	77.5	30.7	3.02
350	285							
352	292.68	27.2	56.3	-103	-51.3	76.2	24.9	2.45
448	392.82	-32.9	-7.1	-101	-50.5	60.3	9.8	0.96
450	400							

Table C.6 – Principal Tensile Stress Summary

10. Transverse Design

[5.8.1.5] The transverse design of a multicell concrete box girder bridge may be split into four sections: the deck design, overhang design, web design, and bottom slab design. Web bending need only be considered for curved post-tensioned box girder bridges with a depth of more than 4 feet. Since this example is straight and has relatively short bay widths, transverse web bending may be neglected.

The three sections below are designed with mild reinforcement. Therefore, the transverse reinforcement is the cover steel, or the outer layer of reinforcement. The longitudinal mild reinforcement will be placed inside the transverse reinforcement for temperature and shrinkage effects.

[5.12.3] The distance, d , from the compression face to the center of the tension reinforcement is dependent on the concrete cover. The following are the minimum covers used for this example:

Deck surface	=	2.5 in
Exterior other than above	=	2.0 in
Interior other than above	=	1.5 in

10.1 Deck Design

[4.6.2]
[4.6.2.1.7] This example uses the Approximate Method outlined in the AASHTO LRFD specifications. A cross-sectional frame model one foot in length is used to determine the design loads per unit length for the deck. This type of model captures the flexural and torsional stiffnesses of the supporting webs and bottom slab in a multi-cell box girder.

One or more axles (representing lanes of traffic) are placed on the deck and moved transversely to maximize the moments. The minimum distance between the wheels of two adjacent axles is four feet. The resulting moments are divided by the strip width calculated from AASHTO LRFD Table 4.6.2.1.3-1 to obtain the live load moment per unit length of bridge.

10.1.1 Minimum Reinforcing

As shown previously in the Flexural Strength section of this example, the design moment is:

[5.7.3.3.2]
$$M_r \geq \min(1.33M_u, M_{cr})$$

And the cracking moment is:

$$M_{cr} = \gamma_3 \gamma_1 f_r S_c$$

where,

$$\gamma_1 = 1.6$$

$$\gamma_3 = 0.67$$

$$f_r = 7.5\sqrt{5000 \text{ psi}} = 530 \text{ psi} = 0.53 \text{ ksi}$$

$$S_c = \frac{I_x}{y_c} = \frac{bh^2}{6} = \frac{12 \text{ in}(9 \text{ in})^2}{6} = 162 \text{ in}^3$$

$$M_{cr} = 0.67 \cdot 1.6 \cdot 0.53 \text{ ksi} \cdot 162 \text{ in}^3 \cdot \frac{\text{ft}}{12 \text{ in}} = 7.67 \text{ ft} - \text{kips}$$

10.1.2 Negative Moment (max) @ 6 inches from CL of web

Strength I load combination

$$M_u = 1.25M_{DC} + 1.5M_{DW} + 1.75M_{LL+I}$$

$$M_{DC} = -1.06 \text{ ft} - \text{kips} / \text{ft} \quad (\text{center web})$$

$$M_{DW} = -0.24 \text{ ft} - \text{kips} / \text{ft}$$

The moment due to live loading is:

[4.6.2.1.3-1]

$$M_{LL+I} = \frac{LL + I}{48 \text{ in} + 3.0 \text{ in} / \text{ft} \cdot S} = \frac{-48.44 \text{ ft} - \text{kips}}{(48 + 3.0 \cdot 12.25 \text{ ft}) / 12}$$

$$M_{LL+I} = -6.86 \text{ ft} - \text{kips} / \text{ft}$$

Therefore,

$$\rightarrow M_u = -13.69 \text{ ft} - \text{kips} / \text{ft}$$

Considering the minimum reinforcement requirement above:

$$M_u \geq M_{cr}$$

[5.7.3]

The following formulae are needed to determine the required flexural reinforcement:

$$\frac{M_u}{\phi} \leq M_n$$

$$M_n = A_s f_y \left(d - \frac{a}{2} \right)$$

$$a = c \beta_1 = \frac{A_s f_y}{0.85 f'_c b}$$

Manipulation of the above formulae gives the required area of flexural reinforcement:

$$A_s = \frac{0.85 f'_c b d - \sqrt{(0.85 f'_c b d)^2 - 1.7 f'_c b M_u / \phi}}{f_y}$$

where,

$$\phi = 0.90$$

$$f'_c = 5 \text{ ksi}$$

$$f_y = 60 \text{ ksi}$$

$$b = 12 \text{ in}$$

$$d = h - \text{cover} - \frac{1}{2} \text{ bar} = 9 - 2.5 - 0.5 \cdot 1 = 6 \text{ in}$$

$$\rightarrow A_s = 0.54 \text{ in}^2 / \text{ft}$$

Therefore, use #5 bars at 6 inches.

10.1.3 Positive Moment @ CL of interior cell

Strength I load combination

$$M_{DC} = 0.69 \text{ ft} - \text{kips} / \text{ft}$$

$$M_{DW} = 0.15 \text{ ft} - \text{kips} / \text{ft}$$

The moment due to live loading is:

[4.6.2.1.3-1]

$$M_{LL+I} = \frac{LL + I}{26 \text{ in} + 6.6 \text{ in} / \text{ft} \cdot S} = \frac{43.10 \text{ ft} - \text{kips}}{(26 + 6.6 \cdot 12.25 \text{ ft}) / 12}$$

$$M_{LL+I} = 4.84 \text{ ft} - \text{kips} / \text{ft}$$

Therefore,

$$\rightarrow M_u = 9.56 \text{ ft} - \text{kips}/\text{ft}$$

Considering the minimum reinforcement requirement above:

$$M_u \geq M_{cr}$$

Therefore with $d = 7 \text{ in}$:

$$A_s = 0.31 \text{ in}^2/\text{ft}$$

For simplicity, use the same reinforcement used in the top: #5 bars at 6 inches

10.2 Overhang (Wing) Design

[A13.4]

The deck overhang, or wing, must be designed to resist the maximum of three design cases given in Section A13. According to the AASHTO LRFD specifications, the flexural resistance, M_s , of the wing shall exceed.

- The transverse vehicular collision forces under Extreme Event II load combination limit state.
- The vertical vehicular collision force forces under Extreme Event II load combination limit state.
- The loads that occupy the overhang under the Strength I load combination limit state.

[3.4.1-1]

Load Combination Limit State	DC	DW	CR+SH	LL+I	CT
Extreme Event II	1.0	1.0	1.0	0.5	1.0
Strength I	1.25	1.5	1.25	1.75	0

Table C.7 – Load Factors for Overhang Design

This design example does not cover the design of a barrier. Instead, It is assumed that a 32" tall barrier of test level TL-4 is used. It has a self-weight of 0.45 kips/ft and its center of gravity is located 1'-0" from its inside face. The three moment capacities (horizontal moment, vertical moment, and additional beam moment respectively) needed in the following calculations are given as:

$$M_c = 24.90 \text{ ft} - \text{kips}/\text{ft}$$

$$M_w = 45.54 \text{ ft} - \text{kips}$$

$$M_b = 0$$

See Figure CA13.3.1-1 in the AASHTO LRFD Design Specifications for a depiction of each moment.

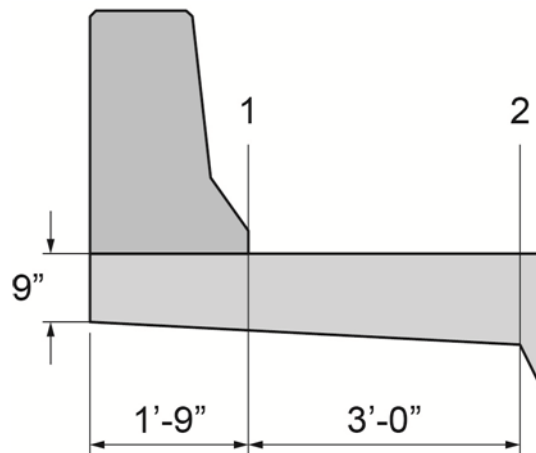


Figure C.14 – Overhang Design Sections

The above figure shows the two sections that need to be designed for this example. The first section will include design cases 1 and 2. The second section will include all three design cases.

10.2.1 Section 1: Overhang design at the face of the barrier

Case 1:

[A13.4.2]

For design case 1, overhang, or wing, of a box girder bridge must be design to simultaneously exceed the moment capacity, M_c , at the barrier’s base as well as the tensile force, T , from the barrier. In other words, it must be designed to resist railing collision forces given in section A13.

Calculate the dead load moments:

$$M_{slab_1} = \frac{wl_1^2}{2} + \frac{W_1l_1}{3}$$

where,

$$l_1 = 1.75 \text{ ft}$$

$$w = 0.75 \text{ ft}^2 (0.150 \text{ kcf}) = 0.1125 \text{ klf}$$

$$W_1 = \frac{1.75}{4.75} \cdot 0.25 \text{ ft} \cdot 1 \text{ ft} (-0.150 \text{ kcf}) \frac{1.75 \text{ ft}}{2} = 0.0121 \text{ kips}$$

$$\rightarrow M_{slab_1} = -\frac{0.1125 \text{ klf} (1.75 \text{ ft})^2}{2} - \frac{0.0121 \text{ kips} \cdot 1.75 \text{ ft}}{3} = -0.18 \text{ ft} - \text{kips} / \text{ft}$$

$$M_{barrier_1} = -0.45 \text{ kips} (1.0 \text{ ft}) = -0.45 \text{ ft} - \text{kips} / \text{ft}$$

$$\rightarrow M_{DC} = -0.45 - 0.18 = -0.63 \text{ ft} - \text{kips} / \text{ft}$$

Extreme Event II load combination:

$$M_{u1} = -M_c + 1.0M_{DC}$$

$$M_{u1} = -24.90 + 1.0(-0.63) = -25.53 \text{ ft} - \text{kips} / \text{ft}$$

[A13.4.2-1] Tensile force from the barrier is defined as:

$$T = \frac{R_w}{L_c + 2H}$$

[A13.3.1-2] where,

$$L_c = \frac{L_t}{2} + \sqrt{\left(\frac{L_t}{2}\right)^2 + \frac{8H(M_b + M_w)}{M_c}}$$

$$L_t = 3.5 \text{ ft}$$

$$H = 32 \text{ in} = 2.667 \text{ ft}$$

$$\rightarrow L_c = 8.24 \text{ ft}$$

[A13.3.1-1]

$$R_w = \left(\frac{2}{2L_c - L_t}\right) \left(8M_b + 8M_w + \frac{M_c L_c^2}{H}\right) = 153.81 \text{ kips}$$

$$\rightarrow T_1 = \frac{153.81 \text{ kips}}{8.24 \text{ ft} + 2 \cdot 2.667 \text{ ft}} = 11.33 \text{ kips} / \text{ft}$$

Calculate the factored flexural resistance, ϕM_s . It can be seen from the figure and calculations below that the collision tensile force, T , decreases the moment resistance of the section.

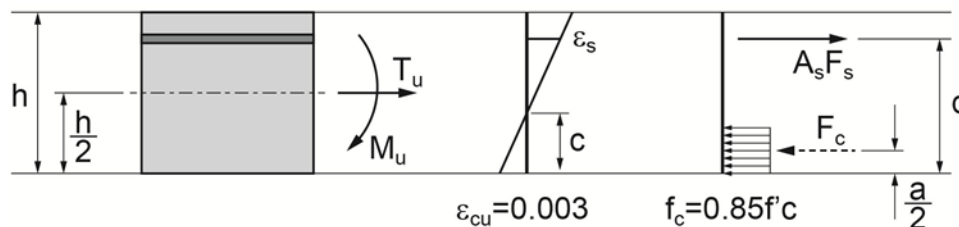


Figure C.15 – Equilibrium at Strength Limit State

Take Moment about the compression force, C .

$$\frac{M_u}{\phi} \leq M_s = A_s f_y \left(d - \frac{a}{2}\right) - T \left(\frac{h}{2} - \frac{a}{2}\right)$$

and,

$$C = 0.85 f'_c \beta_1 c b = 0.85 f'_c a b$$

$$C = A_s f_y - T$$

Therefore,

$$a = \frac{A_s f_y - T}{0.85 f'_c b}$$

Plug a into the moment equation above and solve for the required area of reinforcement, A_s , where:

$$f_y = 60 \text{ksi}$$

$$f'_c = 5 \text{ksi}$$

$$\phi = 0.90$$

$$b = 12 \text{in}$$

$$h = 9 \text{in} + 3 \text{in} \cdot \frac{1.75}{4.75} = 10.11 \text{in} \quad d = 10.11 - 2.5 - 0.5 \cdot 1 = 7.11 \text{in}$$

$$T = 11.33 \text{kips}$$

$$M_u = 25.53 \text{ft-kips/ft} = 306.36 \text{in-kips/ft}$$

$$\rightarrow A_s = 0.98 \text{in}^2/\text{ft}$$

Assume the bottom reinforcement carries half of the collision tensile force.

$$A_s = \frac{1}{2} \cdot \frac{T}{\phi f_y} = 0.10 \text{in}^2/\text{ft}$$

Use #7 bars at 6 inches for the top reinforcement and #4 bars at 12 inches for the bottom.

Case 2:

[A13.3.1-1]

According to AASHTO, a vertical downward force of 18 *kips* is to be distributed over 18 *ft* of the TL-4 barrier. This equates to 1 *klf*. If we assume this load acts at the center of gravity of the barrier, the moment it produces on the overhang is 1 *ft-kips/ft*. Note that this moment is less than the effects in design case 1 and we may skip this design case.

Case 3:

Note that design case 3 does not include any loads that are not included in design case 1. Therefore, we may neglect this case at this section.

10.2.2 Section 2: Overhang design at the outside face of the web

Case 1:

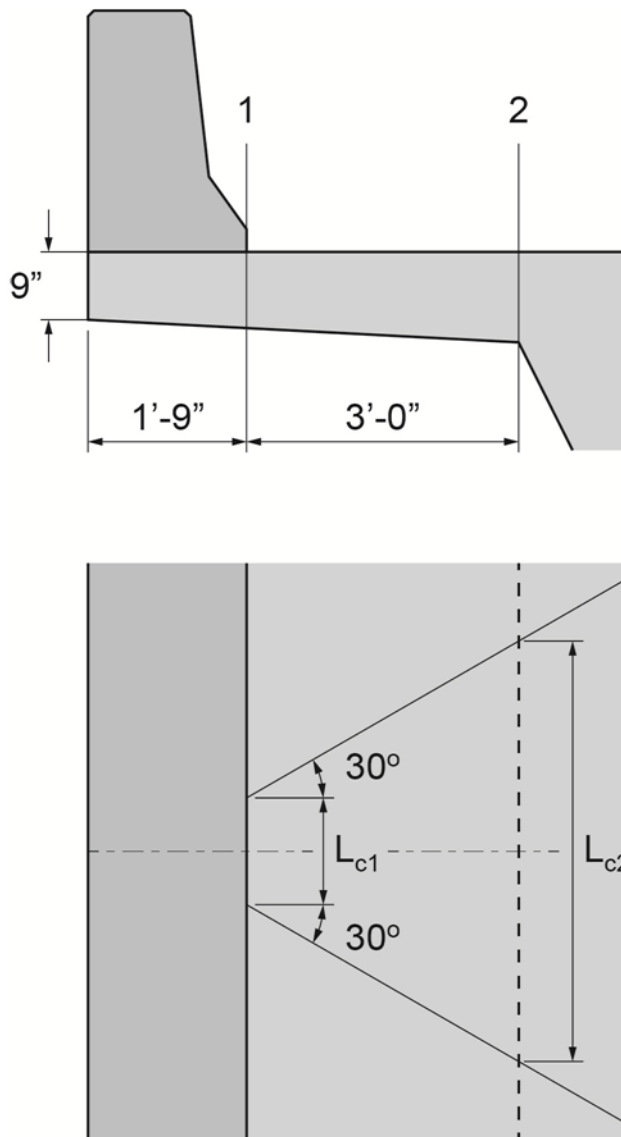


Figure C.16 – Length of Loaded Areas

As depicted in the figure above, loads distribute over larger lengths the farther the section is from the load application. Assume the distribution length, L_c , increases at a 30° angle.

$$M_{c_2} = \frac{M_{c_1} L_c}{L_c + 2x \tan 30^\circ} = \frac{24.90 \text{ ft} - \text{kips} / \text{ft} \cdot 8.24 \text{ ft}}{8.24 \text{ ft} + 2 \cdot 3 \text{ ft} \cdot \tan 30^\circ} = 17.53 \text{ ft} - \text{kips} / \text{ft}$$

$$T_2 = \frac{T_1 L_c}{L_c + 2x \tan 30^\circ} = \frac{11.33 \text{ kips} / \text{ft} \cdot 8.24 \text{ ft}}{8.24 \text{ ft} + 2 \cdot 3 \text{ ft} \cdot \tan 30^\circ} = 7.98 \text{ kips}$$

Calculate the dead load moments:

$$M_{slab_2} = \frac{wl_2^2}{2} + \frac{W_2l_2}{3}$$

where,

$$l_2 = 4.75 \text{ ft}$$

$$w = 0.75 \text{ ft}^2 (-0.150 \text{ kcf}) = -0.1125 \text{ klf}$$

$$W_2 = 0.25 \text{ ft} \cdot 1 \text{ ft} (-0.150 \text{ kcf}) \frac{4.75 \text{ ft}}{2} = -0.0891 \text{ kips}$$

$$\rightarrow M_{slab_2} = -\frac{0.1125 \text{ klf} (4.75 \text{ ft})^2}{2} - \frac{-0.0891 \text{ kips} \cdot 4.75 \text{ ft}}{3} = -1.41 \text{ ft} - \text{kips} / \text{ft}$$

$$M_{barrier_2} = -0.45 \text{ kips} / \text{ft} (1.0 \text{ ft} + 3.0 \text{ ft}) = -1.80 \text{ ft} - \text{kips} / \text{ft}$$

$$\rightarrow M_{DC} = -1.41 - 1.80 = -3.21 \text{ ft} - \text{kips} / \text{ft}$$

The moment due to 25 psf wearing surface is:

$$M_{DW} = -0.025 \text{ ksf} \cdot 3 \text{ ft} (0.5 \cdot 3 \text{ ft}) = -0.1125 \text{ ft} - \text{kips} / \text{ft}$$

The moment due to live loading is:

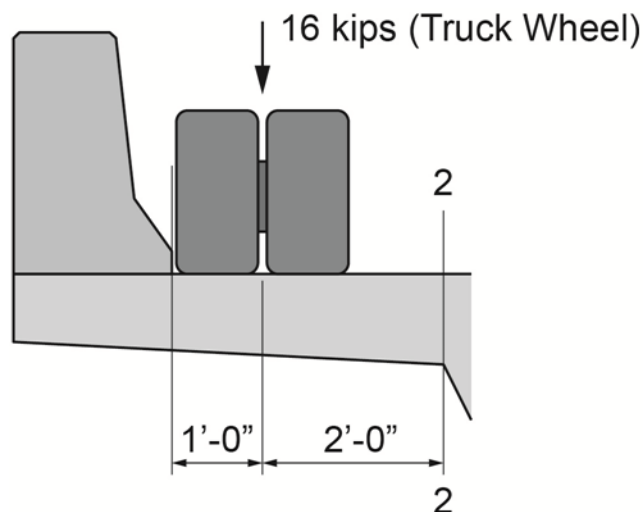


Figure C.17 – Live Load on Overhang

$$M_{LL} = -\frac{mPx}{w_s}$$

[3.6.1.1.2-1] where,

$$\begin{aligned}
 m &= \text{multiple presence factor} && = 1.2 \\
 P &= \text{AASHTO Truck wheel load} && = 16 \text{ kips} \\
 x &= \text{distance from load to support} && = 2 \text{ ft} \\
 w_s &= \text{width of equivalent strip (in)} && = 45 + 10x
 \end{aligned}$$

$$\rightarrow M_{LL} = -\frac{mPx}{45/12 \text{ ft} + 10x/12} = -\frac{1.2 \cdot 16 \text{ kips} \cdot 2 \text{ ft}}{45/12 \text{ ft} + 10 \cdot 2 \text{ ft}/12} = -7.09 \text{ ft} - \text{kips}/\text{ft}$$

[3.4.1-1] Extreme Event II load combination:

$$\begin{aligned}
 M_{u_2} &= -M_c + 1.0M_{DC} + 1.0M_{DW} + 0.5M_{LL+I} \\
 M_{u_2} &= -17.53 + 1.0(-3.21) + 1.0(-0.1125) + 0.5(1.33 \cdot -7.09) \\
 M_{u_2} &= -25.57 \text{ ft} - \text{kips}/\text{ft}
 \end{aligned}$$

Case 2:

Note that design case 2 at this section is similar to section 1 and does not need to be investigated.

Case 3:

Strength I load combination:

$$\begin{aligned}
 M_{u_2 \text{ Strength I}} &= 1.25M_{DC} + 1.5M_{DW} + 1.75M_{LL+I} \\
 M_{u_2 \text{ Strength I}} &= 1.25(-3.21) + 1.5(-0.1125) + 1.75(1.33 \cdot -7.09) \\
 M_{u_2 \text{ Strength I}} &= -20.68 \text{ ft} - \text{kips}/\text{ft} \\
 |M_{u_2}| &> |M_{u_1}| > |M_{u_2 \text{ Strength I}}|
 \end{aligned}$$

Note that the collision tensile force is less at section 2 than at section 1, the moment is of equivalent magnitude, and the section is much greater in depth. Therefore the same reinforcement may be used for the entire overhang.

Verify the area of reinforcement, A_s , required. Use the same moment equation used at Section 1 where:

$$\begin{aligned}
 f_y &= 60 \text{ ksi} & f'_c &= 5 \text{ ksi} \\
 \phi &= 0.90 & b &= 12 \text{ in} \\
 h &= 12 \text{ in} & d &= 12 - 2.5 - 0.5 \cdot 1 = 9.0 \text{ in} \\
 T &= 7.98 \text{ kips} & M_u &= 25.57 \text{ ft} - \text{kips}/\text{ft} = 306.84 \text{ in} - \text{kips}/\text{ft} \\
 \rightarrow A_s &= 0.74 \text{ in}^2/\text{ft}
 \end{aligned}$$

10.3 Bottom Slab Design**10.3.1 Minimum Reinforcement Cracking Moment**

$$M_{cr} = \gamma_3 \gamma_1 f_r S_c = 0.67 \cdot 1.6 \cdot 0.53 \text{ksi} \cdot \frac{1 \text{ft} (7 \text{in})^2}{6} = 4.64 \text{ft} - \text{kips}$$

10.3.2 Negative Moment

$$M_u = 1.25 M_{DC} = 1.25(-0.84) = -1.05 \text{ft} - \text{kips} / \text{ft}$$

Considering the minimum reinforcement requirement above:

$$M_u \leq M_{cr}$$

$$\rightarrow M_u = 1.33(-1.05) = -1.40 \text{ft} - \text{kips} / \text{ft}$$

Using the same formula presented in section 7.1 above, solve for required negative area of reinforcement for negative flexure where $d = 5 \text{ in}$:

$$A_s = 0.06 \text{in}^2 / \text{ft}$$

10.3.3 Positive Moment

$$M_u = 1.25 M_{DC} = 1.25 \cdot 0.55 = 0.69 \text{ft} - \text{kips} / \text{ft}$$

Considering the minimum reinforcement requirement above:

$$M_u \leq M_{cr}$$

$$\rightarrow M_u = 1.33 \cdot 0.69 = 0.92 \text{ft} - \text{kips} / \text{ft}$$

Solve for required area of reinforcement for positive flexure where $d = 4.5 \text{ in}$:

$$A_s = 0.05 \text{in}^2 / \text{ft}$$

10.3.4 Minimum reinforcement for shrinkage and temperature:

$$0.11 \text{in}^2 / \text{ft} \leq A_s \leq 0.60 \text{in}^2 / \text{ft}$$

$$A_s \geq \frac{1.30bh}{2(b+h)f_y}$$

where,

$$b = 11.25 \text{ft} = 135 \text{in}$$

$$h = 7 \text{in}$$

$$f_y = 60 \text{ksi}$$

$$A_s \geq 0.07 \text{in}^2 / \text{ft} \rightarrow A_s \geq 0.11 \text{in}^2 / \text{ft}$$

Therefore, the minimum required reinforcement for shrinkage and temperature controls. Notice that this requires a minimum of # 3 bars spaced at 12 inches. This is very light.

Due to engineering experience and judgment, use #5 bars at 12 inches for the top of the bottom slab and #4 bars at 12 inches for the bottom.

Example 2—Curved Two-Cell Box Girder Bridge

1. Introduction

This Design example is a curved, 3-span concrete box girder with three webs. The top slab of the bridge is 47'-6" wide, with a travelled way dimension of 44'-0", between the faces of the curbs. The span lengths are 120'-0", 160'-0", and 120'-0" measured along the centerline of the bridge. The radius of curvature of the centerline of bridge is 600'-0". It is assumed that the substructure supports are bearings on individual columns beneath each web at the piers and similar bearings beneath each web at the abutments. As a result, the substructure effectively provides full vertical and torsional fixity at each pier and abutment, while allowing longitudinal movement, so that thermal rise and fall, creep, and shrinkage shortening do not have an appreciable effect on the superstructure.

The bridge is assumed to require the following concrete covers to the reinforcing:

- 2 ½ inches—Top of top slab.
- 2 inches—Other external surfaces.
- 1 ½ inches—Internal surfaces.

It is assumed to be located in a moderate corrosion environment.

The spacing of the three, 1'-0"-thick, vertical webs is 16'-0". The bottom slab is thus 33'-0" wide. Also, the cantilevers of the top slab, beyond the centerline of the exterior webs, are 7'-6". The top slab is thickened at the web locations, and is assumed to be transversely post-tensioned, as discussed in section 2.

Figure D.1 shows a perspective of the bridge studied in this design example.



Figure D.1 – Curved Bridge of Design Example 2

An elevation view of the bridge for this design example is shown in figure D.2.

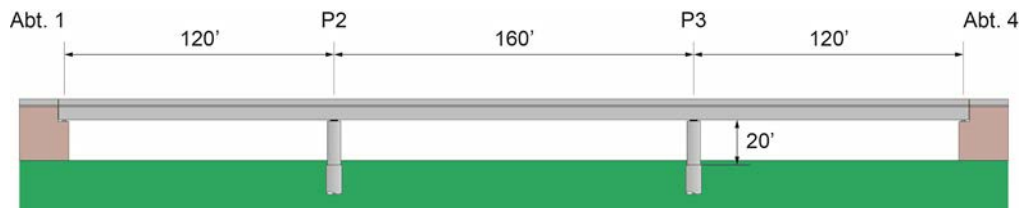


Figure D.2 – Elevation of Example 2 Bridge

Figure D.3 shows a transverse cross section taken through the bridge. The 2-cell box girder bridge carries two 12' wide traffic lanes, two 10', and 1'-9" barriers, for a total out-to-out width of 47'-6".

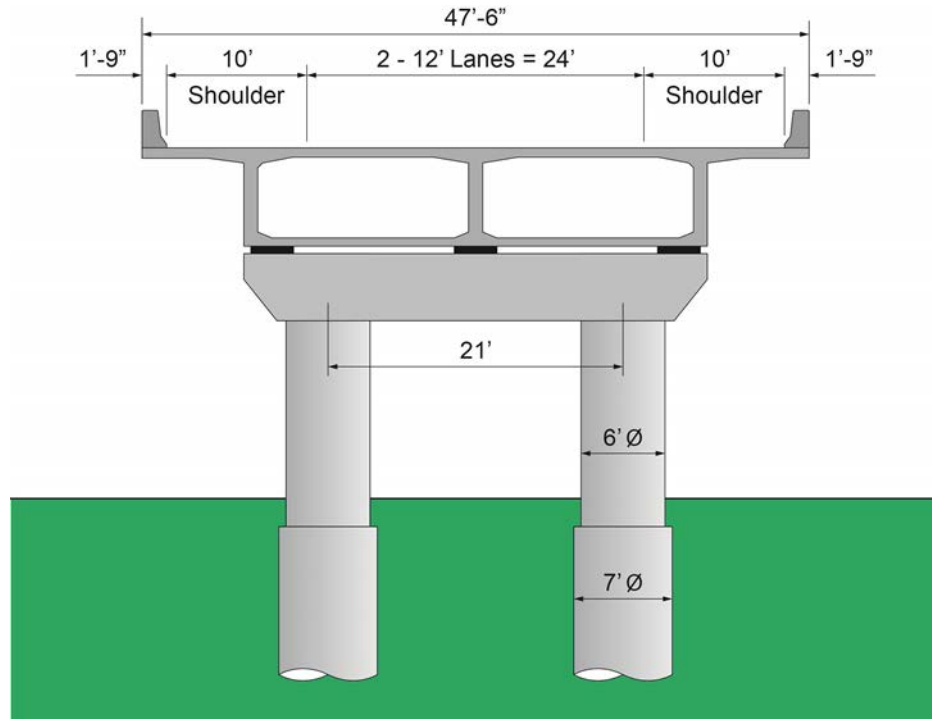


Figure D.3 – Cross Section through Example 2 Bridge

Pier 2 and Pier 3 are each comprised of two cylindrical columns 6'-0" in diameter connected by a transverse pier cap. The box girder superstructure is supported by bearings placed on the pier cap. The columns are 20' in height, measured from the top of foundations to the base of the superstructure. The foundations for this design example consist of 7'-0" diameter mono-shafts. For this example, it is assumed that the supporting soil provides an equivalent point of fixity 10' below the top of the mono-shafts for all force effects. The distance from the base of the superstructure to the point of fixity is 30'.

2. Material Characteristics

2.1. Concrete

The initial and 28-day concrete strengths for the superstructure and substructure are:

$$f'_{ci} = 4500 \text{ psi} = 4.5 \text{ ksi}$$

$$f'_c = 6000 \text{ psi} = 6.0 \text{ ksi}$$

[3.5.1] The unit weight of the concrete is defined below. Note that the unit weight used for the self-weight calculations includes an additional weight for the reinforcement.

$$w_c = 145 \text{ pcf} = 0.145 \text{ kcf}$$

$$w_{c,DC} = w_c + 5 \text{ pcf} = 150 \text{ pcf} = 0.150 \text{ kcf}$$

[C5.4.2.4-1] The modulus of elasticity for normal weight concrete, where $w_c = 0.145 \text{ kcf}$, can be taken as:

$$E_c = 1820\sqrt{f'_c} = 1820\sqrt{5} = 4070 \text{ ksi} = 586000 \text{ ksf}$$

2.2 Reinforcing Steel

[5.4.3] The yield strength and modulus of elasticity are:

$$f_y = 60 \text{ ksi}$$

$$E_s = 29000 \text{ ksi}$$

2.3 Prestressing Steel

[5.4.4] The 0.6 inch diameter low-relaxation prestressing strand is used in this example with the following properties:

$$A_{ps} = 0.217 \text{ in}^2 / \text{strand}$$

$$f_{pu} = 270 \text{ ksi}$$

$$f_{py} = 0.9 f_{pu} = 243 \text{ ksi}$$

$$E_{ps} = 28500 \text{ ksi}$$

3. Cross Section Properties

The typical cross section dimensions are shown in figure D.4. The cross section dimensions are constant over the length of the bridge:

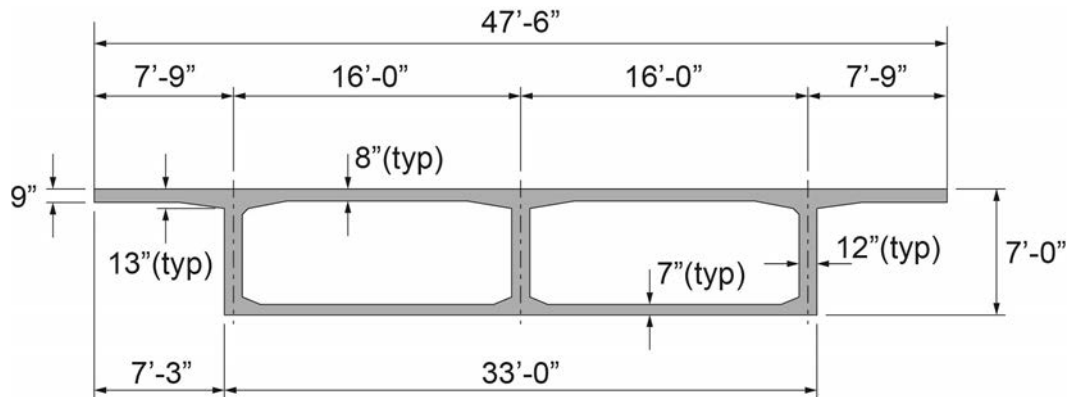


Figure D.4 – Cross Section Dimensions

The properties of the typical superstructure cross section are:

A	= cross sectional area	= 73.36 ft ²
I_x	= moment of inertia	= 572.7 ft ⁴
H	= height of section	= 7.0 ft
y_{ct}	= top of section to centroid	= 2.255 ft
y_{cv}	= bottom of section to centroid	= 4.745 ft

The gross section properties of the substructure elements are used in this design example:

A_c	= area for two columns	= 56.55 ft ²
I_{xc}	= moment of inertia for two columns	= 127.24 ft ⁴
A_p	= area for two monshafts	= 56.55 ft ²
I_{xp}	= moment of inertia for two monshafts	= 127.24 ft ⁴

4. LRFD General Design Equation

[1.3.2.1-1]

The AASHTO LRFD Design Specification's general design equation is:

$$\sum \eta_i \gamma_i Q_i \leq \phi R_n = R_r$$

where,

- η_i = load modifying factor for ductility, redundancy, and operational importance
- γ_i = load factor
- Q_i = force effect
- ϕ = resistance factor
- R_n = nominal resistance
- R_r = factored resistance

[1.3.2.1-2],
[1.3.2.1-3]

The load modifier, η_i , takes on two forms. The first is for loads in which a maximum value of γ_i is appropriate, the second is in which a minimum value of γ_i is appropriate.

$$\eta_i = \eta_D \eta_R \eta_I \geq 0.95$$

$$\eta_i = \frac{1}{\eta_D \eta_R \eta_I} \leq 1.0$$

where,

- η_D = ductility factor
- η_R = redundancy factor
- η_I = operational importance factor

[1.3.3],
[1.3.4],
[1.3.5]

Since the purpose of this example is to illustrate a conventional design on a typical bridge,

$$\eta_D = \eta_R = \eta_I = 1.0$$

$$\therefore \eta_i = 1.0$$

Note that the load modifying factors are project and design specific and may not equal 1.0 in actual designs.

5. Transverse Design

The transverse analysis for this structure was accomplished using the method described under LRFD 4.6.2.9.4. This method is a simple way to accurately calculate the contribution of the webs and bottom slab to the top slab bending, as well as calculate the web and bottom slab bending. For the top slab, which is a transversely prestressed member, both service and strength limit states are checked. The webs and bottom slab, which are not prestressed transversely, are designed at the strength limit state as reinforced members. Because the superstructure is symmetrical, the results will be reported for half the top and bottom slabs, the center web, and one exterior web.

Figure D.5 shows the transverse model of the bridge, made for the BDII program, a program that allows the post tensioning tendons to be input and calculates the time-dependent effects of creep and shrinkage. The properties of this model assume it is 1'-0" long. The transverse post-tensioning is 1-0.6" dia. strand in the 1'-0" long model, which equates to 4-strand tendons spaced at 4'-0" along the bridge.

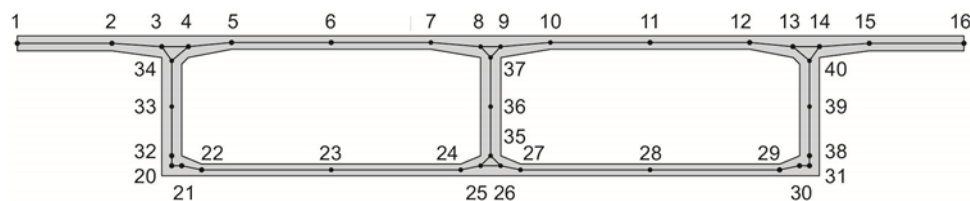


Figure D.5 – Frame Model for Transverse Analysis

Seven live load cases were developed by positioning trucks on the cross section to maximize the following moments:

- Negative Moment, Node 3
- Positive Moment, Node 6
- Negative Moment, Node 4
- Negative Moment, Node 8
- Negative Moment, Node 5
- Negative Moment, Node 7
- Negative Moment, Node 2

[3.6.1.1.2]

In this example, all of the maximum moments were created by a single truck on the cross section, due to the 1.2 multiple presence factor for a single lane from LRFD 3.6.1.1.2. Because a single truck produces the maximum top slab moments, the positions of the trucks which maximize the negative moment at nodes 3, 4, and 8 also produce maximum bending in the adjacent webs.

Influence surfaces are then used to calculate the Fixed End Moments at the end of each slab span for each load case. Also, the maximum moment for a beam with fixed ends at nodes 5, 6, and 7 were determined when those were the nodes of interest.

Once these fixed end moments are calculated for each load case, they are input into the BDII model, which calculates the redistributed moments for each load case. The redistributed moments are then added to the moments with fixed ends to calculate the final live load moments at a node.

The step-by-step process of calculating the positive bending (tension on the bottom) live loads at Node 6 will be shown as an example:

The loading producing maximum positive bending at Node 6 is shown in figure D.6.

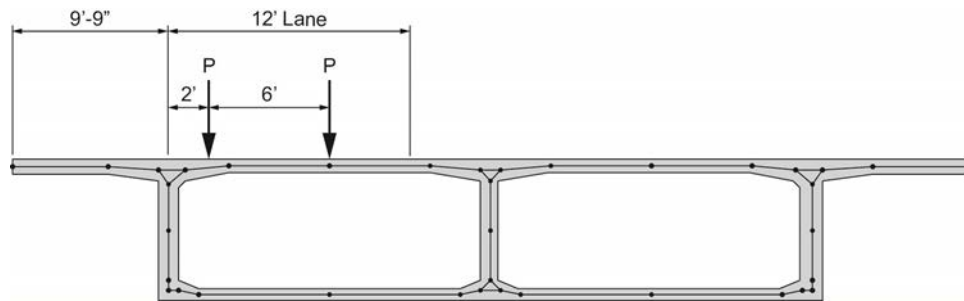


Figure D.6 – Load Location for Maximum Positive Flexure at Node 6

Then, influence surfaces are used to calculate the values of the fixed end moments at Nodes 4 and 8 for this loading, as well as the moment with fixed ends at Node 6. These moments at Points 4,6,and 8 are shown in the following table:

Node	FEM (ft-kips)
4	-14.1
6	5.1
8	6.3

Table D.1 – Fixed End Moments for Maximum Flexure at Node 6

The BDII transverse plane frame model is loaded with the fixed end moments at Nodes 4 and 8 in order to determine their redistribution as a result of the flexibility of the adjoining top slab. The result of interest due to this load case is only the redistributed moment at Node 6, which is +0.6 ft-kips/ft.

The design positive Live Load Moment at Node 6 is then:

$$5.1 + 0.6 = 5.7 \text{ ft-kips / ft}$$

Similarly, the maximum Live load effects are found on other nodes in the cross section and are shown in table D.2. Note that for the top and bottom slabs,

positive moments create tension on the bottom. For the webs, positive moments create tension on the inside of the exterior webs and the right side of the center web. Also, an influence surface was unavailable for Node 2, so a plate model of the cantilever overhang was created, and truck wheels were placed on the model to give the maximum live load moment at that node.

Node	MLL + (ft-kips)	MLL - (ft-kips)
1	0.0	0.0
2	n/a	-3.7
3	n/a	-9.5
4	n/a	-12.4
5	n/a	-3.1
6	5.7	n/a
7	n/a	-3.3
8	n/a	-12.9
21	0.1	-0.1
22	0.3	-0.5
23	0.1	-0.3
24	0.0	-0.3
25	0.5	-0.4
32	0.5	-1.0
33	4.6	-7.6
34	6.7	-11.0
35	1.2	-1.2
36	6.4	-6.4
37	9.9	-9.9

Table D.2 – Design Live Load Moments

Once the Live load moments are calculated, they are combined with dead load and PT forces in service and strength load groups.

Service Load Groups for Top Slab

Because the top slab is a prestressed member, the Service Limit State that must be checked at the time of tendon stressing and after all losses have occurred. The Service I load combination is used to check both the allowable tension and compression for transverse analysis, using only the truck loads, and no lane loads.

The Service I load factors simplify to those shown in table D.3 for this structure.

Load Combination	DC	DW	CR + SH	PS	LL+I
Service I	1.0	1.0	1.0	1.0	1.0

Table D.3 – Service Limit State Load Factors

[3.4.1]
[4.6.2.9.4]

[5.9.4]

The maximum allowable compressive stresses are:

- $0.6f'_{ci}$ for temporary stresses at the time of tendon stressing.
- $0.45f'_c$ due to prestressing and permanent loads after all time dependent effects and losses.
- $0.6f'_c$ due to prestressing, permanent, and transient loads after all time dependent effects and losses.

The maximum allowable tensile stresses are:

- $0.24\sqrt{f'_{ci}}$ (ksi) for temporary stresses at the time of tendon stressing ($7.5\sqrt{f'_{ci}}$ for units in psi).
- $0.0948\sqrt{f'_c}$ (ksi) for stresses after all time dependent effects and losses ($3.0\sqrt{f'_c}$ for units in psi).

Temporary Initial Stress Check

The top slab stresses at stressing of PT are shown below in table D.4. With 6ksi concrete, the allowable stress in compression is -518ksf, and the allowable tension stress is +33ksf. The reported stresses are well below these limits.

Node	f top (ksf)	f bot (ksf)
1	0.0	0.0
2	-56.3	-45.3
3	-61.4	-9.2
4	-78.3	8.4
5	-79.5	-33.9
6	-20.9	-92.6
7	-65.3	-47.8
8	-69.6	-0.4

Table D.4 – Top Slab Stresses at Stressing of PT

Stresses After All Time Dependent Losses

The stresses due to dead load, PT, creep, and shrinkage after all losses are shown in table D.5.

Node	f top (ksf)	f bot (ksf)
1	0.0	0.0
2	-31.0	-63.4
3	-39.0	-26.7
4	-66.9	2.8
5	-67.4	-36.7
6	-21.4	-82.7
7	-61.1	-42.7
8	-62.2	-2.0

Table D.5 – Top Slab Stresses due to DC, DW, CR, SH after all losses

Combining the stresses from table D.5, above, with those from the Live load design moments shown in table D.2 yields the following final stresses, shown in table D.6 below:

Node	Max Tension		Max Compression	
	f top (ksf)	f bot (ksf)	f top (ksf)	f bot (ksf)
1	0.0	0.0	0.0	0.0
2	8.5	-63.4	-31.0	-102.9
3	9.6	-26.7	-39.0	-75.3
4	-3.5	2.8	-66.9	-60.6
5	-25.6	-36.7	-67.4	-78.5
6	-21.4	-5.8	-98.3	-82.7
7	-16.6	-42.7	-61.1	-87.2
8	3.8	-2.0	-62.2	-68.0

Table D.6 – Top Slab Stresses From Service I (Compression) and Service III (Tension) Load Combinations

Strength Limit State for Transverse Analysis

All members must be designed for the Strength Limit State. For the top slab, this amounts to a check for the post-tensioning layout determined in the Service Limit State design. For the bottom slab, reinforcing will be determined based on this work. The required web reinforcing for bending will be determined in this stage, but will eventually be combined with that required for longitudinal shear and torsion.

The Strength I load factors simplify to those shown in table D.7 for this structure.

[3.4.1]

Load Combination	DC	DW	CR + SH	PS	LL+I
Strength I	1.25	1.5	1.0	1.0	1.75

Table D.7 – Strength I Load Factors for Transverse Analysis

The ultimate applied moments are calculated from the output of the BDII program (for all except live loads) and the live load moments shown in table D.2. Once combined using the above load factors, the ultimate moments for each node in the cross section are as shown in table D.8

Node	$M_u +$ (k-ft)	$M_u -$ (k-ft)
1	0.0	0.0
2	-4.3	-10.7
3	-8.6	-25.2
4	-1.7	-23.4
5	0.6	-4.8
6	12.4	2.5
7	0.6	-5.2
8	-2.1	-24.7
21	-0.8	-1.1
22	0.4	-1.0
23	1.5	0.8
24	-1.9	-2.4
25	-2.1	-3.7
32	2.7	0.0
33	12.7	-8.6
34	17.9	-13.1
35	2.1	-2.1
36	11.2	-11.2
37	17.3	-17.3

Table D.8 – Ultimate Moments for Transverse Design

The ultimate resistance of the top slab will be calculated separately from the resistance of the bottom slab and webs. As mentioned previously, the Strength Limit State calculations of the prestressed top slab serve as a check of the Service Level design. However, for the webs and bottom slab, reinforcing requirements will be determined using this Strength Limit State design.

Top Slab Resistance

The top slab resistance is calculated using LRFD 5.7.3

[C5.7.3.1.1-1]

$$k = 0.28$$

[5.7.2.2]

$$\beta_1 = 0.75$$

[5.5.4.2] $A_{ps} = 0.217in^2$

[5.7.3.3.2] $\phi = 0.583 + 0.25\left(\frac{d_t}{c} - 1\right)$

[5.4.2.6] $f_r = 84.7ksf$

Table D.9 presents the ultimate capacity of the top slab. In the table, the neutral axis and the stress in the prestressing at ultimate are calculated using 5.7.3.1.1-4 and 5.7.3.1.1-1, respectively. The ultimate capacity is calculated using 5.7.3.2.2-1, without considering mild reinforcing (though it could be considered, if necessary).

[5.7.3]

Node	H (in)	dp (in)	c (in)	f _{ps} (ksi)	φ	φM _n (k-ft)
1	9.00	4.50	1.18	250.1	1.00	18.3
2	9.00	4.86	1.19	251.5	1.00	-20.1
3	13.00	9.02	1.23	259.7	1.00	-40.2
4	13.00	9.02	1.23	259.7	1.00	-40.2
5	8.00	4.00	1.17	247.9	1.00	-16.0
6	8.00	5.56	1.20	253.7	1.00	23.4
7	8.00	4.00	1.17	247.9	1.00	-16.0
8	13.00	9.02	1.23	259.7	1.00	-40.2

Table D.9 – Ultimate Capacity of the Top Slab

The minimum reinforcing provisions of 5.7.3.3.2 should be satisfied, as well. In this case, φM_n is greater than 1.33·M_u in all cases, thus 5.7.3.3.2 is satisfied. The comparison is shown in table D.10.

[5.7.3.3.22]

Node	φM _n (k-ft)	1.33·M _u (k-ft)
1	18.3	0.0
2	-20.1	-14.3
3	-40.2	-33.6
4	-40.2	-31.1
5	-16.0	-6.4
6	23.4	16.5
7	-16.0	-6.9
8	-40.2	-32.8

Table D.10 – φM_n vs. 1.33·M_u

Required Reinforcing in Bottom Slab and Webs

[5.8.1.5]

The bottom slab reinforcing is sized for $1.33 \cdot M_u$ to accommodate minimum reinforcing requirements. However, since the web reinforcing will ultimately be combined with the longitudinal shear reinforcing and regional bending reinforcing from post-tensioning (see section 6), the minimum reinforcing requirements will be satisfied for the webs. table D.11 shows positive bending reinforcement requirements, and table D.12 shows negative bending requirements.

[5.7.3]

	Node	As/s (in ² /ft)	d (in)	a (in)	ϕ	ϕM_n (+) (k-ft)	$1.33 \cdot M_u$ (k-ft)
Bottom Slab	21	N/A	9.625	0.00	0.9	N/A	N/A
	22	0.030	4.625	0.03	0.9	0.6	0.5
	23	0.095	4.625	0.09	0.9	2.0	2.0
	24	N/A	4.625	0.00	0.9	N/A	N/A
	25	N/A	9.625	0.00	0.9	N/A	N/A
Ext. Webs	32	0.060	10.125	0.06	0.9	2.7	N/A
	33	0.283	10.125	0.28	0.9	12.7	N/A
	34	0.400	10.125	0.39	0.9	17.9	N/A
Int. Web	35	0.047	10.125	0.05	0.9	2.1	N/A
	36	0.248	10.125	0.24	0.9	11.2	N/A
	37	0.388	10.125	0.38	0.9	17.3	N/A

Table D.11 – Positive Bending Reinforcement, Bottom Slab and Webs

[5.7.3]

	Node	As/s (in ² /ft)	d (in)	a (in)	ϕ	ϕM_n (-) (k-ft)	$1.33 \cdot M_u$ (k-ft)
Bottom Slab	21	0.035	9.625	0.03	0.9	-1.5	-1.5
	22	0.070	4.625	0.07	0.9	-1.4	-1.3
	23	N/A	4.625	0.00	0.9	N/A	N/A
	24	0.155	4.625	0.15	0.9	-3.2	-3.2
	25	0.115	9.625	0.11	0.9	-5.0	-4.9
Ext. Webs	32	0.010	10.125	0.00	0.9	0.0	N/A
	33	0.190	10.125	0.19	0.9	-8.6	N/A
	34	0.292	10.125	0.29	0.9	-13.1	N/A
Int. Web	35	0.047	10.125	0.05	0.9	-2.1	N/A
	36	0.248	10.125	0.24	0.9	-11.2	N/A
	37	0.388	10.125	0.38	0.9	-17.3	N/A

Table D.12 – Negative Bending Reinforcement, Bottom Slab and Webs

The controlling amounts of reinforcing are highlighted in the above tables. For positive bending in the bottom slab, the point at the center of the bottom slab controls. Likewise, for negative moment in the bottom slab, the locations near the center web control. In all cases, the required reinforcing in the bottom slab is less than 0.2 in²/ft, which means #4 bars at 1'-0" spacing will be adequate.

The web reinforcing for bending is controlled by the reinforcing at the top of the web, as expected. The reinforcing required for bending in the center web is symmetrical. Also, note that more reinforcing is required on the inside faces than is required on the outside faces of the exterior webs. This web reinforcing demand will be added to that required for shear and torsion as well as regional bending later in the calculations.

Overhang Design

[13.6.2]
[A13.4.2]

The deck overhang of a box girder bridge must be designed to withstand impact on the barrier and to withstand normal (Strength 1) traffic loads, though not concurrently. There are three design cases given in LRFD A13.4.1. Case 1 includes lateral load on the barrier which produces moment and tension in the overhang. Case 2 is a vertical impact on the barrier, and Case 3 is the design accomplished in section 2, with wheel loads on the deck.

Case 1:

[A13.4.1]

The strength of the deck must simultaneously exceed the moment capacity, M_c , of the barrier as well as the tensile force, T , from the barrier. The flexural resistance, M_s , of the overhang is designed using the Extreme Event II load combination limit state shown below:

[3.4.1]

Load Combination Limit State	DC	DW	CR+SH	PS	TU	TG	LL+I
Extreme Event II	1.0	1.0	1.0	1.0	0	0	0.5

Table D.13 – Extreme Event II Load Factors

Typically, barriers are standard designs, and for this problem, a TL-4, 32 inch high barrier will be used. The three moment capacities needed in the following calculations are given as:

[A13.3.1]

$$M_c = -24.90 \text{ ft} - \text{kips} / \text{ft}$$

$$M_w = 45.54 \text{ ft} - \text{kips}$$

$$M_b = 0$$

Also given are the weight of the barrier at 0.45kips/ft and its center of gravity, 1'-0" from its inside face.

For this bridge, the capacity of the slab must be checked at three locations:

- At the inside face of the barrier.
- At the point where the slab bottom surface changes slope (Node 2 in the transverse model).

- At the face of the web (Node 3 in the transverse model).

Case 1, Inside Face of Barrier:

1.75ft from the end of the slab:

- PT is at the center of the slab at this location.
- Slab is 9 inches thick.
- Top cover is 2.5 inches to the longitudinal (top layer) of reinforcing, which is #5 bars.

Calculate the dead load moments:

$$M_{DC} = M_{slab} + M_{barrier}$$

$$M_{Slab} = \frac{-0.75 \text{ ft} (1.75 \text{ ft})^2}{2} \cdot 0.150 \frac{\text{kips}}{\text{ft}^3} = -0.17 \frac{\text{ft} - \text{kips}}{\text{ft}}$$

$$M_{barrier} = -0.45 \frac{\text{kips}}{\text{ft}} \cdot 1.0 \text{ ft} = -0.45 \frac{\text{ft} - \text{kips}}{\text{ft}}$$

$$M_{DC} = -0.17 - 0.45 = -0.62 \frac{\text{ft} - \text{kips}}{\text{ft}}$$

$$M_{u1} = -M_c + 1.0M_{DC}$$

$$M_{u1} = -25.5 \frac{\text{ft} - \text{kips}}{\text{ft}}$$

Tensile force from the barrier is defined as:

$$[A13.4.2-1] \quad T = \frac{R_w}{L_c + 2H}$$

where,

$$[A13.3.1] \quad L_c = \frac{L_t}{2} + \sqrt{\left(\frac{L_t}{2}\right)^2 + \frac{8H(M_b + M_w)}{M_c}}$$

$$L_t = 3.5 \text{ ft}$$

$$H = 32 \text{ in} = 2.667 \text{ ft}$$

$$\rightarrow L_c = 8.24 \text{ ft}$$

$$R_w = \left(\frac{2}{2L_c - L_t}\right) \left(8M_b + 8M_w + \frac{M_c L_c^2}{H}\right) = 153.8 \text{ kips}$$

$$\rightarrow T = \frac{153.8 \text{ kips}}{8.24 \text{ ft} + 2 \cdot 2.667 \text{ ft}} = 11.3 \text{ kips/ft}$$

The reinforcing required to carry the tension will be split between the top and bottom layers. The amount required for tension is:

$$A_s = \frac{1}{2} \cdot \frac{T}{\phi f_y} = \frac{11.3 \frac{kips}{ft}}{2 \cdot 0.9 \cdot 60ksi} = 0.104 in^2/ft$$

Use #4 at 1'-0" transverse in the bottom = 0.2in²/ft.

For bending, try #5's and #4's alternated, each at 1'-0", along with the post-tensioning (4 strand tendons spaced at 4'-0"). Subtract the amount of reinforcing required for tension in the top layer.

$$A_s = 0.31in^2 + 0.20in^2 - 0.104in^2 = 0.406 \frac{in^2}{ft}$$

[5.7.3.1]

$$c = \frac{0.217in^2 \cdot 270ksi + 0.406in^2 \cdot 60ksi}{0.85 \cdot 6ksi \cdot 0.75 \cdot 12in + 0.28 \cdot 0.217in^2 \left(\frac{270ksi}{4.5in} \right)} = 1.67in$$

$$f_{ps} = 270ksi \left(1 - 0.28 \left(\frac{1.67in}{4.5in} \right) \right) = 241.9ksi$$

[5.7.3.2]

$$\begin{aligned} \phi M_n &= -0.217in^2 \cdot 241.9ksi \cdot \left(4.5in - \frac{0.75 \cdot 1.67in}{2} \right) \\ &- 0.406in^2 \cdot 60ksi \left(5.56in - \frac{0.75 \cdot 1.67in}{2} \right) = -323.5in - kips = -27.0ft - kips \end{aligned}$$

Case 1, Node 2:

4.75 ft from the end of the slab:

- PT is 5.07 in above the bottom of the slab at this location.
- Slab is 9 in thick.
- Assume distribution length, L_c , increases at a 30 degree angle.
- Ignore vertical live load during an impact event.

Calculate the dead load moments:

$$M_{DC} = M_{slab} + M_{barrier}$$

$$M_{slab} = \frac{-0.75ft(4.75ft)^2}{2} \cdot 0.150 \frac{kips}{ft^3} = -1.3 \frac{ft - kips}{ft}$$

$$M_{barrier} = -0.45 \frac{kips}{ft} \cdot 4.0ft = -1.8 \frac{ft - kips}{ft}$$

$$M_{DC} = -1.3 - 1.8 = -3.1 \frac{ft - kips}{ft}$$

$$M_{DW} = M_{overlay}$$

$$M_{DW} = \frac{-0.25ksf(3ft)^2}{2} = -0.11ft - kips$$

Calculate the impact forces:

$$M_c = -24.9ft - kips \left(\frac{7.35ft}{7.35ft + 2 \cdot 3ft \tan 30^\circ} \right) = -16.9ft - kips$$

$$\rightarrow M_u = -3.1 - 0.11 - 16.9 = -20.1ft - kips$$

[A13.4.2-1]

$$T = \frac{R_w}{L_c + 2H + 2x \tan 30^\circ}$$

$$T = \frac{153.8kips}{8.24ft + 2 \cdot 2.667ft + 2 \cdot 3ft \cdot \tan 30^\circ} = 9.0 \frac{kips}{ft}$$

For tension, required A_s per layer is $0.08in^2/ft$. The #4's at 1'-0" standard transverse reinforcing satisfies this demand, at $0.2in^2/ft$.

Recalling from section 2 the capacity at Node 2 for transverse bending using the post-tensioning only,

$$\phi M_n = -20.1ft - kips$$

$\phi M_n = M_u$ for the post-tensioning alone. Thus, the #5's may be cut off near Node 2. Run half of the #5's 1ft beyond Node 2, and cut the others at Node 2.

Case 1, Face of Web (Node 3):

Impact reinforcing at the face of the web is acceptable by inspection, since it was acceptable at Node 2, the #5's at 1'-0" are continuous, the PT continues to move up, and the overhang continues to deepen, all while the applied moment continues to spread and decrease.

Case 2:

[T A13.2-1]

Case 2 does not control, since the $F_v=18kip$ vertical load distributed over $L_v=18ft$ does not control over a wheel load in the overhang or Case 1.

Longitudinal Slab and Web Reinforcing

The top and bottom slabs act as one-way members, carrying forces in the transverse direction. A summary of the reinforcing to this point is:

- Top slab, top, transverse reinforcing: #4 at 1'-0", with additional #5 at 1'-0" in overhang.
- Top slab, top longitudinal reinforcing: #5 at 1'-0" except over the piers, where additional #5 at 1'-0" are used for negative moment capacity.
- Bottom slab, transverse reinforcing: #4 at 1'-0", top and bottom.

It remains to calculate the bottom longitudinal reinforcing for the top slab and both mats of longitudinal reinforcing for the bottom slab, as well as the longitudinal reinforcing in the webs. In each case, the reinforcing is controlled by temperature and shrinkage requirements.

For the top slab, bottom mat, using the thickest portion of the slab:

[5.10.8]

$$0.11 \text{ in}^2/\text{ft} \leq A_s \leq 0.60 \text{ in}^2/\text{ft}$$

$$A_s \geq \frac{1.30bh}{2(b+h)f_y}$$

where,

$$b = 47.5 \text{ ft} = 570 \text{ in}$$

$$h = 13 \text{ in}$$

$$f_y = 60 \text{ ksi}$$

$$A_s = 0.137 \frac{\text{in}^2}{\text{ft}}$$

Use #4 bars at 1'-0", which is 0.2 in²/ft.

For the bottom slab, the results will be lower. However, use #4 bars at 1'-0", which is 0.2 in²/ft for the longitudinal reinforcing in each face.

Similarly, for the longitudinal reinforcing in the webs, which are 1'-0" thick,

$$A_s = 0.107 \frac{\text{in}^2}{\text{ft}} \rightarrow 0.11 \frac{\text{in}^2}{\text{ft}}$$

Use #4 bars at 1'-0", $A_s=0.2 \text{ in}^2/\text{ft}$.

6. Live Load Distribution

[4.6.2.2.1]

LRFD 4.6.2.2.1 discusses the conditions for calculation of distribution factors. It is found that this cross section does not meet the requirements for use of 4.6.2.2.2, since the number of cells (N_c) is less than 3, and the spacing of the webs (S) is greater than 13ft. Thus, the number of lanes of live load for design is calculated by creating a finite element model of the bridge, as discussed in AASHTO LRFD Article 4.6.3.

[4.6.2.2.2]

[4.6.2.2.3]

[4.6.3]

The model finite element model uses plates for the top and bottom slabs, rigidly connected to beams representing the webs of the box girder. It is loaded with live load in positions to create maximum moments and shears for the following locations, for both the center and exterior webs:

- End Span—Maximum Positive Bending.
- Center Span—Maximum Positive Bending.
- End Span and Center Span—Maximum Negative Bending.
- End Span—Shear at Abutment.
- End Span—Shear at Pier.
- Center Span—Shear at Pier.

[3.6.1.1.2-1]

The effects for one, two and three lanes loaded are studied, each with the appropriate multiple presence factors applied. In interpreting results for the finite element model, it is important to determine how much of the top and bottom slabs are attributed to each web by calculating the amount of top and bottom slab that creates the same center of gravity for each web as for the entire cross section.

The results show that for bending, 3 lanes loaded creates the maximum longitudinal bending in each web for each case, while for shear, 2 lanes loaded creates maximum shear in each web for each case.

These results were compared to a single lane loaded on a straight bridge, to calculate the number of lanes carried by each web for each case. Table D.14 shows the results of the bending investigation, and table D.15 shows the results for shear.

Center Web			Exterior Web	
End Span (+)	Center Span (+)	Negative	End Span (+)	Center Span (+)
0.91	0.91	0.93	0.86	0.87

Table D.14 – Number of Lanes per Web - Bending

Center Web			Exterior Web		
End Span @ Abut.	End Span @ P1	Span 2 @ P1	End Span @ Abut	End Span @ P1	Span 2 @ P1
1.30	1.20	1.18	1.24	1.11	1.14

Table D.15 – Number of Lanes per Web - Shear

[3.6.1.1.1]

[3.6.1.1.2]

All of the results are fairly consistent for bending, with the largest number of lanes carried by the center web in negative bending. Therefore, this analysis uses $3 \times 0.93 = 2.79$ lanes of live load for bending, including the 0.85 multiple presence factor. This is an increase of 9.4 percent over the 3 lanes times 0.85 multiple presence factor the bridge can carry according to LRFD, where $3 \times 0.85 = 2.55$ lanes.

For shear, two different values are chosen, because the variation among the cases is greater than it is for bending. At the abutments (and in the ends of the end spans), a value of 1.30 lanes per web is used, for a total of $3 \times 1.30 = 3.9$ lanes. At other locations, a value of 1.20 lanes per web is used, for a total of $3 \times 1.20 = 3.6$ lanes.

Note that the bridge can be loaded in the longitudinal model without regard to live load torsion, since torsion is implicitly included in the above loadings.

7. Modeling

As discussed in the introduction, this example has supports beneath each web, which are considered to fix the bridge for superstructure torsion and transverse displacement, but it is free to shorten and lengthen. Thus, the superstructure can be separated from the substructure for analysis purposes.

[4.6.3.4]

Once the total number of design lanes is known, the bridge can be modeled as a spine beam with straight segments along the curve for all types of loads.

The curvature is within the limits discussed in LRFD 4.6.1, since the largest central angle is as follows, and is less than the 34° limit:

[4.6.1.2.3]

$$CentralAngle = \frac{160ft}{600ft} = 0.2667rad = 15.27^\circ$$

Where the span length along the centerline of the box is 160ft, and the radius of the centerline is 600ft.

For Dead Loads and PT, the bridge is modeled in a three-dimensional program that allows the actual curved geometry to be modeled, as well as the input of the post-tensioning tendons along their paths, and calculates their effects, including time-dependent changes. The model is made up of straight segments, with nodes every 5 ft, beginning at the centerline of bearings at the abutments. It has the properties of the gross cross section.

[5.9.5.4.1]

The post-tensioning modeled is three, 19 x 0.6” strand tendons per web, draped so that they are low at the midspan and high at the piers. At the abutments, the tendons are spread to allow room for the anchorages, but otherwise, they are parallel, with 2” clear between the ducts.

It should be noted that for this type of bridge a time-dependent program is not necessary, and LRFD 5.9.5 may be used to estimate the post-tensioning losses.

Live loads, which cannot be run in the time-dependent program, are calculated using a separate three-dimensional finite element program, with the same spine beam type layout as the one used for dead load. Several cases were run, representing the above-calculated numbers of lanes.

Member forces and stresses were then taken from these two models to check Service and Strength Load Groups for flexure and shear.

8. Flexural Design

There are two flexural designs required by the AASHTO LRFD specifications for prestressed concrete: flexural designs at the Service Limit State and at the Strength Limit State.

8.1 Service Limit State

[3.4.1]

There are two load combinations for the Service Limit State: Service I and Service III. The Service I load combination is used to check against maximum allowable compression in the superstructure and Service III is used to check against maximum allowable tension. Table D.16 shows the Service I and Service III load combinations.

[3.4.1-1]

Load Combination	DC	DW	CR + SH	PS	TG	LL+I
Service I	1.0	1.0	1.0	1.0	.0.5	1.0
Service III	1.0	1.0	1.0	1.0	0.5	0.8

Table D.16 – Service Load Combinations

[5.9.4]

The maximum allowable compressive stresses are:

- $0.6 f'_{ci}$ for temporary stresses at the time of tendon stressing.
- $0.45 f'_c$ due to prestressing and permanent loads after all time dependent effects and losses.
- $0.6 f'_c$ due to prestressing, permanent, and transient loads after all time dependent effects and losses.

The maximum allowable tensile stresses are:

- $0.24 \sqrt{f'_{ci}}$ (ksi) for temporary stresses at the time of tendon stressing ($7.5 \sqrt{f'_{ci}}$ for units in psi).

- $0.019\sqrt{f'_c}$ (*ksi*) for stresses after all time dependent effects and losses
($6\sqrt{f'_c}$ for units in *psi*).

Temporary Initial Stress Check:

At the time the post-tensioning is stressed, the controlling point for compressive stresses is located in the bottom of the section at the centerline of the pier (Node 26).

It should be noted that though there is a diaphragm at this section (which changes the section properties), the longitudinal stresses do not typically have room to spread significantly through the diaphragm. Thus, the typical section properties are used, and the stresses are taken at the centerline of the pier. However, they are conservatively taken for the peak moment at this location. That peak moment does not exist in reality, since the bearing has a length. Thus, if stresses due to the peak moment become critical, that bearing length can be accounted for and the design moments reduced somewhat.

At Node 26,

$$f_{bm} = 1.0(DC + PS)$$

$$f_{bm} = -133.4ksf > -0.6 \cdot 4.0ksi = -2.4ksi = -345.6ksf$$

At the time the post-tensioning is stressed, the output from the analysis shows there is no tension in the bridge.

Stresses after All Losses:

The controlling tension and compression in a post-tensioned structure is generally always after all long term losses have occurred. The relaxation of the post-tensioning, as well as shortening due to creep and shrinkage typically cause increases in tension at the top of the bridge over the piers, and at the bottom of the bridge at midspan. The compression at the bottom of the soffit at the piers typically increases over time, as well.

This effect can be seen in table D.17, which summarizes all dead load plus post-tensioning effects at the two midspan nodes as well as at the centerline of pier, both when the structure is opened to traffic as well as when all losses have taken place. The other loads remain constant over time, unless a future wearing surface is added, which will increase the differences between the stresses at the times shown.

Node	Location	Σ (DL + PT)	
		Open to Traffic (ksf)	After All Losses (ksf)
12	Bottom, in End Span	-88.4	-81.4
26	Top, at Pier	-35.9	-28.8
26	Bottom, at Pier	-163.8	-164.9
42	Bottom, in Main Span	-48.3	-40.9

Table D.17 – Change in Superstructure Stresses over Time

At the bottom at the centerline of pier (which is a compression point) the compression increases over time. At the other locations, which are checked against allowable tension, the compression decreases over time.

After all losses have occurred, the controlling point for compression is located in the bottom of the section at the center line of the pier (Node 26).

$$f_{bm} = 1.0(DC + DW + CR + SH + PS)$$

This is the same stress as shown in the above table.

$$f_{bm} = -164.9ksf > -0.45 \cdot 6ksi = -2.7ksi = -388.8ksf$$

Final Compression Stress Check, All Loads:

The controlling point is again located at the bottom of the section at the pier (Node 26). Use Service I load combination.

$$f_{bm} = 1.0(DC + DW + CR + SH + PS + LL + I) + 0.5 \cdot TG$$

$$f_{bm} = -241.0ksf > -0.6 \cdot 6ksi = -3.6ksi = -518.4ksf$$

Final Tensile Stress Check, All Loads:

The controlling point is located in the bottom of the section at the midspan of Span 2 (node 42). Use Service III load combination:

$$f_{btm} = 1.0(DC + DW + CR + SH + PS) + 0.5 \cdot TG + 0.8(LL + I)$$

$$f_{btm} = 35.4ksf < 6\sqrt{6000}psi = 465psi = 67ksf$$

The table below contains a summary of the stress checks every ten feet along the superstructure.

Node	Distance	Initial > - 345.6ksf		Permanent > - 518.4ksf		Service I > -0.6 f _c		Service III > $\frac{6\sqrt{f_c}}{f_c}$	
		Bottom (ksf)	Top (ksf)	Bottom (ksf)	Top (ksf)	Bottom (ksf)	Top (ksf)	Bottom (ksf)	Top (ksf)
2	0	-116.8	-73.2	-111.1	-64.1	-111.0	-122.3	-45.5	-118.0
4	10	-110.8	-78.7	-96.4	-75.6	-100.3	-150.5	-54.7	-83.5
6	20	-107.3	-82.5	-86.3	-83.9	-94.4	-172.1	-60.6	-57.4
8	30	-106.2	-84.6	-80.6	-89.2	-93.8	-187.3	-63.0	-39.7
10	40	-107.2	-85.2	-79.0	-91.6	-97.3	-196.5	-62.5	-29.8
12	50	-109.8	-84.7	-81.4	-91.2	-104.7	-199.9	-59.2	-27.2
14	60	-111.5	-84.9	-86.2	-89.2	-114.6	-199.1	-54.4	-30.4
16	70	-111	-86.2	-91.6	-86.9	-125.0	-195.3	-49.2	-36.8
18	80	-106.5	-87.9	-95.7	-83.7	-134.1	-188.3	-43.2	-44.9
20	90	-100.9	-90.2	-99.4	-79.6	-142.9	-177.8	-36.1	-55.6
22	110	-95	-92.7	-104.6	-74.4	-153.3	-164.4	-28.0	-69.8
24	100	-110.1	-80.3	-116.9	-64.4	-173.8	-147.4	-13.3	-89.7
26	120	-105.6	-80.8	-164.9	-28.8	-241.0	-113.4	33.0	-135.3
28	130	-75.2	-98.9	-105.8	-66.9	-161.3	-150.1	-16.4	-77.9
30	140	-73.2	-98.5	-79.2	-82.7	-118.8	-172.6	-41.0	-43.5
32	150	-75	-96.3	-69.4	-88.2	-99.5	-186.7	-51.8	-23.8
34	160	-75.7	-94.7	-60.9	-93.0	-88.7	-200.4	-57.9	-4.9
36	170	-75.5	-93.8	-53.6	-97.0	-80.5	-212.1	-62.4	11.2
38	180	-74.5	-93.3	-47.6	-100.0	-74.5	-220.6	-65.4	23.6
40	190	-73.1	-93.1	-43.2	-101.9	-70.0	-225.8	-67.3	31.9
42	200	-73.5	-93.1	-40.9	-102.6	-67.7	-227.5	-68.0	35.4
44	210	-74.9	-93.3	-43.6	-101.9	-70.4	-225.6	-67.3	31.4
46	220	-75.8	-93.8	-48.1	-100.0	-74.8	-220.5	-65.4	23.2
48	230	-75.9	-94.8	-54.0	-97.0	-80.8	-212.1	-62.5	10.8
50	240	-75.1	-96.4	-61.3	-93.1	-88.9	-200.5	-58.0	-5.2
52	250	-73.3	-98.7	-69.7	-88.3	-99.8	-186.9	-52.0	-24.1
54	260	-75.2	-99.2	-79.4	-82.8	-118.7	-172.8	-41.3	-43.6
56	270	-105.6	-81.1	-106.0	-67.1	-161.3	-150.4	-16.7	-77.9
58	280	-110.2	-80.5	-165.0	-29.1	-241.0	-113.7	32.7	-135.4
60	290	-95.1	-92.9	-117.0	-64.7	-173.9	-147.7	-13.6	-89.8
62	300	-101.1	-90.3	-104.7	-74.7	-153.5	-164.6	-28.1	-69.9
64	310	-106.7	-88	-99.6	-79.8	-143.2	-177.9	-36.2	-55.8
66	320	-111.2	-86.3	-95.9	-83.9	-134.5	-188.3	-43.2	-45.3
68	330	-111.6	-84.9	-91.6	-86.9	-125.1	-195.4	-49.2	-36.8
70	340	-109.9	-84.7	-86.3	-89.3	-114.7	-199.2	-54.5	-30.3
72	350	-107.2	-85.2	-81.5	-91.2	-104.7	-199.8	-59.2	-27.4
74	360	-106.2	-84.6	-79.0	-91.6	-97.2	-196.4	-62.5	-29.9
76	370	-107.3	-82.5	-80.6	-89.2	-93.8	-187.2	-63.0	-39.8
78	380	-110.8	-78.8	-86.4	-83.9	-94.4	-172.2	-60.6	-57.4
80	390	-116.7	-73.3	-96.5	-75.6	-99.4	-150.6	-55.2	-83.3
82	400	0	0	-111.3	-64.2	-109.1	-122.4	-46.7	-118.1

Table D.18 – Stress Summaries

8.2 Strength Limit State

There is one load combination used to check the strength limit state: Strength I.

[3.4.1]

Load Combination	DC	DW	CR + SH	PS	LL+I
Strength I	1.25	1.5	1.0	1.0	1.75

Table D.19 – Strength Limit State Design Factors

[1.3.2.1-1]
[5.7.3.2]

The factored flexural resistance, M_r , must be greater than the Strength I load combination, M_u (ultimate moment), and the minimum reinforcement requirement. The minimum reinforcement requirement states that the flexural resistance must at least equal $1.33M_u$ or the cracking moment, M_{cr} , whichever is less. This can be summarized by the following equation (using absolute values):

[5.7.3.3.2]

$$M_r = \phi M_n \geq \max(M_u, \min(1.33M_u, M_{cr}))$$

Factored Design Moment

The critical location is the negative moment at the centerline of Pier 2 (Node 26). The summation of the Strength I load combination is:

[3.4.1]

$$M_{DC} = -22324.6 \text{ ft} - \text{kips}$$

$$M_{DW} = -4057.5 \text{ ft} - \text{kips}$$

$$M_{CR+SH} = 21 + 0 = 21 \text{ ft} - \text{kips}$$

$$M_{PS} = 6068.9 \text{ ft} - \text{kips}$$

$$M_{LL+I} = -9593.2 \text{ ft} - \text{kips}$$

$$\rightarrow M_u = -44690.2 \text{ ft} - \text{kips}$$

Minimum reinforcement calculation

[5.7.3.3.2]

$$1.33 \cdot M_u = -59438.0 \text{ ft} - \text{kips}$$

$$M_{cr} = \gamma_3 \left[(\gamma_1 f_r + \gamma_2 f_{cpe}) S_c \right]$$

where,

$$\gamma_1 = 1.6$$

$$\gamma_3 = 1.0$$

$$f_{cpe} = 160.2 \text{ ksf}$$

$$\gamma_2 = 1.1$$

$$f_r = 7.5\sqrt{6000 \text{ psi}} = 588.2 \text{ psi} = 84.7 \text{ ksf}$$

$$S_c = 200.5 \text{ ft}^3$$

$$\rightarrow M_{cr} = -62504 \text{ ft} - \text{kips}$$

Therefore, at this location, the design moment is $1.33 \cdot M_u$. The absolute value of $1.33 \cdot M_u$ is less than the absolute value of M_{cr} , and this value is greater than the absolute value of the factored moment, M_u .

Factored Flexural Resistance

Nominal moment calculations will be shown at the critical location. First, the nominal moment capacity, M_n , will be calculated using prestressing only. If necessary, non-prestressed reinforcing will then be added to increase the capacity.

First, LRFD Equation 5.7.3.1.1-4 will be checked, to see if the section is rectangular or flanged, as discussed in LRFD 5.7.2.2. The following are known from the cross section dimensions, concrete strength, and post-tensioning layout at Node 26:

[5.7.2.2]
C5.7.3.1.1-1]

$$\beta_1 = 0.75 \quad k = 0.28$$

$$A_{ps} = 37.1 \text{ in}^2 \quad f_{pu} = 270 \text{ ksi} \quad d_p = 67.5 \text{ in} \quad b = 33 \text{ ft}$$

Using these values in equation 5.7.3.1.1-4,

$$c = 6.4 \text{ in}$$

and

$$a = 0.85 \cdot c = 5.44 \text{ in}$$

which is less than the bottom slab thickness of 7in, so the section can be treated as rectangular, and equation 5.7.3.1.1-4 is the correct one to use to determine the neutral axis location.

Next, we use equation 5.7.3.1.1-1 to find the stress in the prestressing at ultimate, and obtain:

$$f_{ps} = 262.8 \text{ ksi}$$

Before the capacity is calculated, find ϕ .

[5.5.4.2]

$$\phi = 0.583 + 0.25 \left(\frac{d_t}{c} - 1 \right) \leq 1.0$$

where,

$$d_t = d_p = 67.5in$$

$$\phi = 1.0$$

Knowing these values, we now use equation 5.7.3.2.2-1 to calculate the moment capacity ϕM_n , and obtain:

$$\phi M_n = -52279 ft - kips$$

Comparing ϕM_n to the design moment of $1.33 \cdot M_u$, we find that the calculated capacity is too low. Thus, we will determine if reasonable amount of mild reinforcing over the pier can increase the capacity sufficiently.

Try longitudinal #5 bars at 6 inch spacing in the top of the deck. The total number of bars is 95. Recalculate the above values, incorporating this reinforcing. The values of c , f_{ps} , and ϕ need to be checked before entering equation 5.7.3.2.2-1.

$$A_s = 95 \cdot 0.31 \frac{in^2}{bar} = 29.45in^2$$

$$f_s = 60ksi$$

Recalculating c and checking for rectangular behavior,

$$c = 7.6in$$

and

$$a = 0.85c = 6.46in$$

Thus, the section still behaves as rectangular. Continuing,

$$f_{ps} = 261.5ksi \quad \phi = 1.0$$

And the increased capacity, accounting for mild reinforcing is

$$\phi M_n = -63715 ft - kips$$

Which is greater than the design moment of

$$1.33 \cdot M_u = -59438.0 ft - kips$$

The following table contains a summary of the flexural strength design checks at typical critical locations along the superstructure.

Node		12	26	42
Location		~0.4 L	Pier 2	0.5 L
Distance	(ft)	50	120	200
DC	(ft-kips)	9962.5	-22324.6	12949.7
DW	(ft-kips)	1810.7	-4057.5	2353.6
CR	(ft-kips)	9.0	21.0	21.1
SH	(ft-kips)	0.0	0.0	0.0
PS	(ft-kips)	2522.4	6068.9	6082.5
LL+I	(ft-kips)	8448.2	-9593.2	9323.9
M _u	(ft-kips)	32485.0	-44690.2	42138.1
1.33M _u	(ft-kips)	43205.0	-59438.0	56043.6
M _{cr}	(ft-kips)	44047.2	-62507.7	41781.8
Design Moment		1.33M _u	1.33M _u	M _u
	(ft-kips)	43205.0	-59438.0	42138.1
φM _n	(ft-kips)	47323.7	-63714.7	55027.4

Table D.20 – Factored Moments

9. Web Design

Critical Section:

[5.8.3.2]

For shear and torsion design, it is unnecessary to calculate shear and torsion values closer than d_v to supports. LRFD 5.8.2.9 states

[5.8.2.9]

$$d_v = \max \left(\frac{M_n}{A_s \cdot f_y + A_{ps} \cdot f_{ps}}, 0.9d_e, 0.72h \right)$$

Where,

[5.8.2.9-2]

$$d_e = \frac{A_{ps} f_{ps} d_p + A_s f_y d_s}{A_{ps} f_{ps} + A_s f_y}$$

Near the abutments, it is clear that d_v=0.72h, since the post-tensioning is not near the extremities of the beam. Near the piers, we will calculate d_v using the properties at the centerline of the pier, for the purposes of determining where

the critical section is located. We know the following values from the ultimate moment calculations:

$$A_{ps} = 37.1in^2 \quad d_p = 67.5in \quad f_{ps} = 261.5ksi$$

$$A_s = 29.45in^2 \quad f_s = 60ksi \quad d_s = 80.5in$$

$$M_n = -63715ft - kips \quad h = 7ft$$

$$d_{v1} = \frac{M_n}{A_s \cdot f_y + A_{ps} \cdot f_{ps}} = 66.67in$$

$$d_{v2} = 0.9d_e = 66.0in$$

$$d_{v3} = 0.72h = 60.5in$$

Thus, the critical section could be taken as far away as 5.55 ft from the support. However, it is conservative to take the critical section closer to the support (since the section properties are constant and shear typically dominates the design over torsion), and there is a node at 5.00 ft. So, the critical section will be taken at 5.0 ft from the pier and abutments.

Since shear and torsion combine in an exterior web, they must be considered together. However, to this point, torsion has only been implicitly considered in the calculation of the number of design lanes performed in section 3. In that section, loads were placed on the bridge that maximized the shear in the center and exterior webs. The interior web controlled, and the number of lanes taken by the center web was multiplied by the number of webs to give a conservative number of design lanes for the bridge; 3.9 lanes near the abutments and 3.6 lanes elsewhere. These lanes are placed along the centerline of the bridge in the spine model.

[C5.8.2.1]

LRFD 5.8.2.1 provides a formula that calculates whether torsion needs to be considered in the design. If this formula shows that torsion needs to be considered, we will calculate the required shear and torsion reinforcing for two cases, and use the most conservative design:

- 1) Maximum torsion on the bridge with its concurrent shear from a load case that is derived from the standard LRFD Loading.
- 2) Maximum shear as calculated in section 3, along with its concurrent torsion (if torsion needs to be considered for this case).

Determine the number of lanes that produce the maximum torsion for Case 1), above. Using the description of lanes and the transverse placement of loads in LRFD 3.6.1.1 and 3.6.1.2:

[3.6.1.1]

- Eccentricity for 1 Lane = 17 ft.
- Eccentricity for 2 Lanes = 11 ft.
- Eccentricity for 3 Lanes = 5 ft.

[3.6.1.2]

The controlling case is found by using number of lanes and multiple presence factors:

$$1\text{Lane} = 1Ln \cdot 17\text{ft} \cdot 1.2 = 20.4Ln \cdot \text{ft}$$

$$2\text{Lanes} = 2Ln \cdot 11\text{ft} \cdot 1.0 = 22Ln \cdot \text{ft}$$

$$3\text{Lanes} = 3Ln \cdot 5\text{ft} \cdot 0.85 = 12.75Ln \cdot \text{ft}$$

Thus, two Lanes controls for maximum torsion.

The finite element spine model is then used to compute the live load shear and torsion for two lanes positioned as close to the barrier as possible. The time dependent model gives dead load and PT forces and stresses. Once these are known, T_u and T_{cr} can be calculated and LRFD 5.8.2.1 can be entered to find whether torsion is critical for Case 1).

Constants used include the following:

[5.5.4.2.1]

$$\phi = 0.9$$

[5.8.2.9]

$$b_v = \text{web} - 0.25 \cdot \text{duct} \phi = 12\text{in} - 0.25 \cdot 4.5\text{in} = 10.875\text{in}$$

[5.8.2.1]

$$A_o = 203.2\text{ft}^2$$

The following table shows the calculation of T_{cr} and compares it to T_u according to LRFD 5.8.2.1-3. T_u is calculated according to LRFD 3.4.1. The two locations where torsion must be considered, shown in bold, are near the piers in the center span.

[5.8.2.1-4]

[3.4.1]

Node	f_{pc} (ksf)	T_{cr} (k-ft)	T_{DC} (k-ft)	T_{DW} (k-ft)	T_{CR} (k-ft)	T_{PT} (k-ft)	T_{LL+I} (k-ft)	T_u (k-ft)	$0.25\phi T_{cr}$ (k-ft)
3	83.7	27647	555.0	100.9	0.0	225.2	2904	6153	6221
7	85.3	27820	340.9	62.0	-0.1	217.5	2316	4789	6259
11	86.8	27980	11.6	2.1	-0.3	164.4	1594	2971	6296
14	88.0	-28108	-222.3	-40.4	-0.6	93.4	1135	1740	-6324
17	89.0	-28215	-376.0	-68.3	-0.9	-8.2	-1605	-3390	-6348
21	87.2	-28023	-349.2	-63.5	-1.4	-191.6	-2242	-4649	-6305
25	85.1	-27798	-75.4	14.0	-2.1	-414.6	-2811	-5410	-6255
27	83.6	27636	398.3	72.4	2.6	699.8	3218	6940	6218
31	80.9	27343	690.6	125.5	1.9	536.9	2760	6420	6152
35	79.6	27200	596.8	108.5	1.1	373.7	2248	5218	6120
39	78.3	27057	264.0	48.0	0.4	191.4	1692	3554	6088
42	77.4	-26957	-53.9	-9.8	-0.1	42.8	1274	2190	-6065

Table D.21 – Verification of Torsion Considerations

Thus, we can develop a load case that requires that torsion be considered for at least some locations in the structure. As previously stated, the reinforcing for this load case will be compared to that required for Case 2) at node 27, where the difference between the applied torsion and the limit is greatest, according to the above table.

Shear reinforcing for these two cases will be calculated using the simplified procedure of LRFD 5.8.3.4.3.

Case 1), Node 27:

The Governing equation for shear says the capacity, which is made up of the strength of concrete plus reinforcing, must be greater than the factored load, or,

[5.8.3.3]
[5.8.3.4.3]

$$V_n = V_c + V_s \geq \frac{V_u}{\phi}$$

And

$$V_c = \min(V_{ci}, V_{cw})$$

where

[5.8.3.4.3]

$$V_{ci} = 0.02\sqrt{f'_c}b_v d_v + V_d + \frac{V_i M_{cre}}{M_{max}} \geq 0.06\sqrt{f'_c}b_v d_v$$

[5.8.3.4.3-1]

and

[5.8.3.4.3-3]

$$V_{cw} = (0.06\sqrt{f'_c} + 0.30f_{pc})b_v d_v + V_p$$

V_{ci} relates to the tendency of flexure cracks to become shear cracks, and involves the following terms:

[5.8.3.4.3-2]

- M_{max} , which is the ultimate moment under the maximum bending load case minus the bending due to unfactored dead load. For this load case, the live load moments are taken from the Case 1) loading, which is two lanes placed with as much eccentricity as possible.
- V_i , which is the shear concurrent with M_{max} .
- M_{cre} , which is the moment, in addition to unfactored dead load moment, required to bring the flexural stress up to the code defined cracking stress, as defined in LRFD Equation 5.8.3.4.3-2.

- V_d , which is the unfactored dead load shear.
- b_v and d_v , which have been previously defined.

V_{cw} relates to the tendency of the web to crack from principal tension:

- f_{pc} is the compressive stress in the section at the center of gravity.
- V_p is the shear from post-tensioning.
- b_v and d_v are as previously defined.

Calculate V_{ci} :

$$|M_{\max}| = |M_u - M_{DC} - M_{DW}| = 14322 \text{ ft} - \text{kips}$$

$$V_i = 950.4k \quad V_d = 975.3k \quad f_r = 0.20\sqrt{f'_c} = 70.5 \text{ ksf}$$

$$f_{cpe} = 157.0 \text{ ksf} \quad |M_{cre}| = 24290.0 \text{ ft} - \text{kips}$$

And,

$$V_{ci} = 2683.8k$$

For V_{cw} :

$$f_{pc} = 83.5 \text{ ksf}$$

And

$$V_{cw} = 801.0k$$

Thus,

$$V_c = V_{cw} = 801.0k$$

The applied shear, V_u , is calculated from applied dead and live loads for Case 1):

[3.4.1]

Node	V_{DC} (k)	V_{DW} (k)	V_{CR+SH} (k)	$V_{PT \text{ sec}}$ (k)	V_{LL+I} (k)	V_u (k)
27	825.3	150.0	0.0	0.0	287.0	1758.8

Table D.22 – Ultimate Shear at Node 27

The required shear strength from reinforcing is:

$$[5.8.3.3-1] \quad V_s = \frac{V_u}{\phi} - V_c = \frac{1758.8 \text{ kips}}{0.9} - 801.0 \text{ kips} = 1153.2 \text{ kips}$$

Using LRFD Equation 5.8.3.3-4 for V_s , and realizing that the reinforcing will be placed at 90° to the longitudinal axis:

$$[5.8.3.3-4] \quad V_s = \frac{A_v f_y d_v (\cot \theta)}{s}$$

To find the required reinforcing, solve the above for A_v/s , using known values.

$$\frac{A_v}{s} = \frac{V_s}{f_y d_v \cot \theta}$$

Where

$$V_s = 1153.2 \text{ kips} \quad f_y = 60 \text{ ksi} \quad d_v = 0.72h = 60.5 \text{ in}$$

$$[5.8.3.4.3-4] \quad \cot \theta = 1.0 + 3 \left(\frac{f_{pc}}{\sqrt{f'_c}} \right) = 1.7$$

solving,

$$\frac{A_v}{s} = 0.18687 \frac{\text{in}^2}{\text{in}} = 2.24 \frac{\text{in}^2}{\text{ft}}$$

Since there are 3 webs, and each web has 2 faces, this equates to $0.373 \text{ in}^2/\text{ft}\cdot\text{face}$.

For Case 1, the reinforcing for torsion must now be calculated. Note that the following equation gives the reinforcing required in one outside web:

$$[5.8.3.6.2-1] \quad T_n = \frac{T_u}{\phi} = \frac{2A_0 A_v f_y \cot \theta}{s}$$

From the previous calculations in this section, at Node 27:

$$T_u = 6940 \text{ ft} - \text{kips} \quad A_0 = 203.2 \text{ ft}^2$$

$$\cot \theta = 1.7 \quad \phi = 0.9$$

And we can calculate A_v/s for one web as:

$$\frac{A_v}{s} = \frac{6940 \text{ ft-kips}}{0.9 \cdot 2 \cdot 203.2 \text{ ft}^2 \cdot 60 \text{ ksi} \cdot 1.7} = 0.185 \frac{\text{in}^2}{\text{ft} \cdot \text{web}}$$

Now, summing the required reinforcing, the critical exterior web would require:

[5.8.3.6.1]
$$0.373 \frac{\text{in}^2}{\text{ft} \cdot \text{face}} + \frac{0.185 \frac{\text{in}^2}{\text{ft} \cdot \text{web}}}{2 \frac{\text{face}}{\text{web}}} = 0.465 \frac{\text{in}^2}{\text{ft} \cdot \text{face}}$$

For Case 1). Note that the reinforcing in the exterior webs would be made equal to this minimum, while the interior web could use 0.373 in²/face, for a total of 2.61 in²/ft in the bridge

Case 2), Node 27:

Case 2) utilizes the load distribution calculated in section 3, with the live load placed along the centerline of the bridge, as explained in that section. Thus, the only torsion is due to the fact that the bridge is curved.

All permanent load effects are the same for the two cases so only the live load varies between the two cases. The table below shows that torsion need not be explicitly considered with Case 2).

[3.4.1]
[5.8.2.1]

Node	f _{pc} (ksf)	T _{cr} (k-ft)	T _{DC} (k-ft)	T _{DW} (k-ft)	T _{CR} (k-ft)	T _{PT} (k-ft)	T _{LL+I} (k-ft)	T _u (k-ft)	0.25φT _{cr} (k-ft)
3	83.7	27647	555.0	100.9	0.0	225.2	694	2284	6221
7	85.3	27820	340.9	62.0	-0.1	217.5	565	1725	6259
11	86.8	27980	11.6	2.1	-0.3	164.4	288	685	6296
14	88.0	-28108	-222.3	-40.4	-0.6	93.4	-83	-390	-6324
17	89.0	-28215	-376.0	-68.3	-0.9	-8.2	-214	-957	-6348
21	87.2	-28023	-349.2	-63.5	-1.4	-191.6	-290	-1233	-6305
25	85.1	-27798	-75.4	14.0	-2.1	-414.6	-140	-736	-6255
27	83.6	27636	398.3	72.4	2.6	699.8	242	1732	6218
31	80.9	27343	690.6	125.5	1.9	536.9	478	2427	6152
35	79.6	27200	596.8	108.5	1.1	373.7	469	2104	6120
39	78.3	27057	264.0	48.0	0.4	191.4	303	1124	6088
42	77.4	-26957	-53.9	-9.8	-0.1	42.8	145	215	-6065

Table D.23 – Verification of Torsion Considerations

For Node 27 we find:

[5.8.3.4.3-1] V_{ci} , Case 2):

$$|M_{\max}| = |M_u - M_{DC} - M_{DW}| = 14266.5 \text{ ft} - \text{kips}$$

$$V_i = 950.4k \quad V_d = 975.3k \quad f_r = 0.20\sqrt{f'_c} = 70.5\text{kpsf}$$

$$f_{cpe} = 157.0\text{kpsf} \quad |M_{cre}| = 24290.0 \text{ ft} - \text{kips}$$

And,

$$V_{ci} = 2399.1\text{kips}$$

V_{cw} is the same as for Case 1), and

[5.8.3.4.3-3] $V_c = V_{cw} = 801.0\text{kips}$

The applied shear, V_u , is:

[3.4.1]

Node	V_{DC} (k)	V_{DW} (k)	V_{CR+SH} (k)	$V_{PT \text{ sec}}$ (k)	V_{LL+I} (k)	V_u (k)
27	825.3	150.0	0.0	0.0	510.8	2150.5

Table D.24 – Shear at Node 26

The required shear strength from reinforcing is:

[5.8.3.3-1]
$$V_s = \frac{V_u}{\phi} - V_c = \frac{2150.5\text{kips}}{0.9} - 801.0\text{kips} = 1588.4\text{kips}$$

Using LRFD Equation 5.8.3.3-4 for V_s , and realizing that the reinforcing will be placed at 90° to the longitudinal axis:

[5.8.3.3-4]
$$V_s = \frac{A_v f_y d_v (\cot \theta)}{s}$$

Solving the above for A_v/s , using known values:

$$\frac{A_v}{s} = \frac{1588.4\text{kips} \cdot 12 \frac{\text{in}}{\text{ft}}}{60\text{ksi} \cdot 60.5\text{in} \cdot 1.7} = 3.1 \frac{\text{in}^2}{\text{ft}}$$

Thus, at Node 27, the total amount of shear and torsion reinforcing in the bridge is equal to 2.61in²/ft for Case 1), and 3.1in²/ft for Case 2). Of the two nodes that required investigation of torsion under Case 1), the worst case did not control over Case 2), and it will be conservative to design the structure using the forces developed under section 3, as in Case 2.

9.1 Shear Design

Shear will be investigated at discreet points along the bridge. The symmetry of the spans will be considered, and only half of the bridge will be reported. Points for investigation are chosen at distances that would be meaningful for changes in shear reinforcing, in this case, at about 20 ft.

Applied Shear:

Dead Load and Post-Tensioning values are from the 3D, time-dependent model, and live load is from the spine beam and load cases discussed in section 3 and Case 2), above. The table below shows the calculation of V_u . Note that only shear due to secondary PT moments is considered.

[3.4.1]

Node	Distance (ft)	V_{DC} (k)	V_{DW} (k)	V_{CR} (k)	$V_{PT_{sec}}$ (k)	V_{LL+I} (k)	V_u (k-ft)
3	5	419.5	76.2	0.2	50.6	443.4	1465.3
7	25	199.4	36.2	0.2	50.6	326.3	925.3
11	45	-20.7	-3.8	0.2	50.6	223.4	410.3
14	60	-185.8	-33.8	0.2	50.6	-241.3	-654.1
17	75	-350.8	-63.8	0.2	50.6	-305.2	-1017.5
21	95	-570.9	-103.8	0.2	50.6	-396.5	-1512.4
25	115	-791.0	-143.8	0.2	50.6	-484.6	-2001.6
27	125	825.3	150.0	0.0	0.0	510.8	2150.5
31	145	605.2	110.0	0.0	0.0	428.7	1671.8
35	165	385.1	70.0	0.0	0.0	344.7	1189.6
39	185	165.1	30	0.0	0.0	262.7	711.0
42	200	0.0	0.0	0.0	0.0	201.2	352.1

Table D.25 – Ultimate Shear Forces

[5.8.3.4.3-1]

Calculate V_{ci} :

Using the same methodology and constants as above, the calculation of V_{ci} at the nodes is shown in the table below. Note that the absolute values of M_{cre} , M_{max} , V_i , and V_d are used in the calculation of V_{ci} .

Node	f_{cpe} (ksf)	M_{dnc} (k-ft)	S (ft ³)	M_{cre} (k-ft)	M_{max} (k-ft)	V_i (k)	V_d (k)	V_{ci} (k)
3	122.0	2608.0	138.2	23997.2	3784.7	748.3	495.9	5337.2
7	154.8	9939.6	138.2	21205.3	15077.2	517.4	235.8	1060.2
11	166.9	12058.3	138.2	20764.6	20283.6	259.8	-24.3	386.9
14	160.3	10225.4	138.2	21674.7	20570.5	-30.6	-219.3	348.2
17	133.6	5460.7	138.2	22756.7	18048.5	-186.8	-414.4	746.6
21	104.2	-5446.8	200.5	29591.6	-6688.1	-248.1	-674.5	1868.9
25	157.5	-21547.3	200.5	24176.8	-14600.3	-708.7	-934.6	2204.8
27	157.0	-21339.8	200.5	24290.0	-14266.5	779.5	975.3	2399.1
31	107.4	-4411.7	200.5	31273.5	-1720.3	446.7	715.2	8933.2
35	110.2	7318.0	138.2	17661.0	19847.7	525.4	455.1	1019.4
39	145.4	13837.2	138.2	16014.0	25570.1	320.6	195.1	492.5
42	151.7	15303.4	138.2	15411.9	26834.7	-42.1	0.0	290.1

Table D.26 – Concrete Shear Capacity, V_{ci}

[5.8.3.4.3-3]

Calculate V_{cw} :

The calculation of V_{cw} is performed, again, with the same constants as were used for the calculations performed at Node 27, above. V_p is the shear due to primary and secondary PT forces, and typically increases the capacity V_{cw} .

Node	F_{pc} (ksf)	V_p (k)	V_{cw} (k)
3	83.6	-279.8	913.5
7	85.2	-136.9	777.3
11	86.8	12.2	658.9
14	88.0	171.3	822.9
17	88.9	356.0	1011.5
21	87.2	589.6	1237.9
25	85.1	264.8	904.5
27	83.5	-167.7	801.0
31	80.8	-594.8	1217.1
35	79.6	-372.7	989.9
39	78.3	-157.1	768.8
42	77.4	0.0	608.2

Table D.27 – Concrete Shear Capacity, V_{cw}

[5.8.3.4.3]

[5.8.3.3-4]

The final table repeats V_{ci} and V_{cw} , calculates V_c , and calculates the required reinforcing in in²/ft. Note that at Nodes 7, 11, and 42, the minimum reinforcing value controls.

Node	V_{ci} (k)	V_{cw} (k)	V_c (k)	$\cot\theta$	Req'd V_s (k)	Req'd A_v/s (in ² /ft)
3	5337.2	913.5	913.5	1.7	714.7	1.4
7	1060.2	777.3	777.3	1.7	250.8	0.5
11	386.9	658.9	386.9	1.0	69.0	0.5
14	348.2	822.9	348.2	1.0	378.5	1.3
17	746.6	1011.5	746.6	1.0	383.9	1.3
21	1868.9	1237.9	1237.9	1.7	442.6	0.8
25	2204.8	904.5	904.5	1.7	1319.6	2.5
27	2399.1	801.0	801.0	1.7	1588.4	3.1
31	8933.2	1217.1	1217.1	1.7	640.5	1.3
35	1019.4	989.9	989.9	1.7	331.9	0.7
39	492.5	768.8	492.5	1.0	297.5	1.0
42	290.1	608.2	290.1	1.0	101.1	0.5

Table D.28 – Required Web Reinforcing for Shear

9.2 Regional Web Bending

[5.8.1.5]

LRFD 5.8.1.5 states that webs shall be reinforced for vertical shear and torsion, regional web bending, and transverse web bending due to vertical loads. The above Shear Design section calculated the reinforcing required from shear. Section 2 calculated the reinforcing required from web bending. What remains is to calculate the reinforcing required from regional web bending.

Regional web bending is bending that places tension and compression on the inside and outside faces of the webs, due to the radius of the bridge and, thus, the curvature of the tendons. It is partially resisted by the longitudinal compression in the web, which bends the web in the opposite direction. However, the resistance from the longitudinal compression is not accounted for in the following, since it is not mentioned in the AASHTO LRFD Bridge Design Specifications.

The regional web bending will be calculated using LRFD 5.10.4.3.1d. The values used will be those when the bridge is first opened to traffic, as that is the earliest time the web will be subjected to all three effects – shear, transverse bending, and regional bending. Thus, the design will be conservative because shear and transverse bending are taken when they are most critical (after all losses), and regional web bending is taken when it is most critical (at opening to traffic).

Observing the maximum force in the post-tensioning tendons at the time the bridge is opened to traffic, from the time-dependent program output:

$$P_{pt} = \frac{6800 \text{ kips}}{3 \text{ webs}} = 2266.7 \frac{\text{kips}}{\text{web}}$$

[3.4.3]

Calculating values for the webs, with the radius of the inside web equal to 584 ft, and the load factor of 1.2,

[5.10.4.3.1a]

$$F_{u-in} = \frac{1.2 \cdot 2266.7 \text{ kips}}{584 \text{ ft}} = 4.66 \frac{\text{kips}}{\text{ft}} \quad h_c = 4.75 \text{ ft}$$

For exterior webs,

[5.10.4.3.1d]

$$M_u = \frac{0.6 \cdot 4.66 \frac{\text{kips}}{\text{ft}} \cdot 4.75 \text{ ft}}{4} = 3.32 \frac{\text{ft} \cdot \text{kips}}{\text{ft}}$$

For the interior web,

$$M_u = \left(\frac{0.7}{0.6} \right) 3.32 = 3.87 \frac{\text{ft} \cdot \text{kips}}{\text{ft}}$$

No indication of a difference between positive and negative moments is given in LRFD, so the assumption is that these values apply to both. For the exterior webs, these regional forces work in the same direction, so they put the inside face in tension on one web, and the outside in tension on the other. The effects of transverse bending are not symmetrical on these webs, so the regional bending forces will be used as both positive and negative at all locations.

Table D.29 below shows the ultimate moments and required reinforcing for the general web bending due to the curved PT tendons:

[5.7.3.1]
[5.7.3.2]

Node	Positive Moment		Negative Moment	
	M _u (+) (k-ft)	As/s (in ² /ft)	M _u (-) (k-ft)	As/s (in ² /ft)
32	3.3	0.072	-3.3	0.072
33	3.3	0.072	-3.3	0.072
34	3.3	0.072	-3.3	0.072
35	0.0	0.000	-3.9	0.085
36	3.9	0.085	0.0	0.000
37	0.0	0.000	-3.9	0.085

Table D.29 - Regional Web Bending Due to PT Moments And Required Reinforcing

9.3 Total Web Reinforcing

The reinforcing for shear, transverse bending due to vertical loads, and regional web bending due to PT will now be combined to find the total reinforcing required in the webs. The shear reinforcing requirements vary along the bridge, and the bending reinforcing requirements vary from web to web and vertically along each web, as well as from face to face in each web. Also, the live loading that produces maximum shear in a given web will not produce maximum bending. The converse is also true, as a single truck

[5.8.1.5]

produces maximum web bending, but that loading produces shears that are approximately one-third of the maximum shear design case. The only constant amount is for the regional bending from PT lateral forces, because LRFD 5.10.4.3.1d presents only one formula. As the tendons travel up and down the webs, this value would also change. Thus, there are many variables to accommodate in calculating web reinforcing.

It remains to the engineer to select web reinforcing that is efficient, not only in material price but also to place. Too much variation in shear reinforcing (from web to web, top to bottom or face to face) presents opportunities for incorrect placement. Placing the same reinforcing in each web is logical, as is using the same reinforcing in each face of each web, because a single U-shaped bar can be used for reinforcing, in this case. This will also provide the same reinforcing from top to bottom in each web.

As discussed above, the exact amount of reinforcing used at each location would be very cumbersome to calculate, as each bending case would have a corresponding shear reinforcing requirement, and vice-versa. Thus, it is simple to use a method that relates only to the maximums required. The following combination formula has proven to simplify the calculations and be conservative.

$$A = \max(V + 0.5B + P, 0.5V + B + P, 0.7(V + B) + P)$$

Where,

- V = shear reinforcing required at a given location
- B = maximum transverse bending reinforcement at a given face and height
- P = regional web bending from PT loads
- A = area of reinforcing to use

The design zones along the bridge are simplest to quantify if the locations and shear reinforcing requirements from Section 6.1 are recalled. In the table below, Node 2 is the abutment, Node 26 is the pier, and Node 42 is the centerline of Span 2. Note that the values shown are for the entire bridge width (three webs, with two faces each):

Node	Distance (ft)	Req'd A_v/s (in ² /ft)
3	5	1.4
7	25	0.5
11	45	0.5
14	60	1.3
17	75	1.3
21	95	0.8
25	115	2.5
27	125	3.1
31	145	1.3
35	165	0.7
39	185	1.0
42	200	0.5

Table D.30 – Shear Reinforcing Requirements

Using the values from the above table, the design regions chosen are expressed in the following table:

Design Region	Begin Distance	End Distance	Shear Reinforcing
1	B/B	25	1.4
2	25	45	0.5
3	45	75	1.3
4	75	120	2.5
5	120	145	3.1
6	145	185	1.3
7	185	M/S	1.0

Table D.31 – Shear Reinforcing Design Regions

In the above table, B/B refers to Begin Bridge and M/S refers to Midspan of Span 2.

For each region above, the transverse bending and regional web bending must be added, in accordance with the combination formula.

The table below recalls and summarizes the reinforcing requirements for positive and negative bending in the webs due to transverse bending and regional bending from PT, found in sections 2 and 6.2. The node numbers refer to the transverse analysis model. Note that the reinforcing shown is for one face of a web.

	Node	Transverse		Regional	
		Positive As/s (in ² /ft)	Negative As/s (in ² /ft)	Positive As/s (in ² /ft)	Negative As/s (in ² /ft)
Ext. Webs	32	0.060	0.010	0.072	0.072
	33	0.283	0.190	0.072	0.072
	34	0.400	0.292	0.072	0.072
Int. Webs	35	0.047	0.047	0.000	0.085
	36	0.248	0.248	0.085	0.000
	37	0.388	0.388	0.000	0.085

Table D.32 – Web Bending Reinforcing Requirements

As an example, the reinforcing in Region 1 would be calculated as in the following, for each face of each web:

$$V = \frac{1.4 \frac{in^2}{ft}}{6 \text{ faces}} = 0.233 \frac{in^2}{ft \cdot face}$$

Then, the combination formula yields, at the exterior webs, at the top of the web (Node 34), for positive bending:

The maximum of:

$$A_1 = 0.233 \frac{in^2}{ft} + 0.5 \cdot 0.400 \frac{in^2}{ft} + 0.072 \frac{in^2}{ft} = 0.505 \frac{in^2}{ft}$$

$$A_2 = 0.5 \cdot 0.233 \frac{in^2}{ft} + 0.400 \frac{in^2}{ft} + .072 \frac{in^2}{ft} = 0.589 \frac{in^2}{ft}$$

$$A_3 = 0.7 \left(0.233 \frac{in^2}{ft} + 0.400 \frac{in^2}{ft} \right) + .072 \frac{in^2}{ft} = 0.515 \frac{in^2}{ft}$$

So, at this location, the design would require 0.589in²/ft on each of the six faces.

Likewise, at the interior web, at the top of the web(Node 37), for negative bending:

$$A_1 = 0.233 \frac{in^2}{ft} + 0.5 \cdot 0.388 \frac{in^2}{ft} + 0.085 \frac{in^2}{ft} = 0.512 \frac{in^2}{ft}$$

$$A_2 = 0.5 \cdot 0.233 \frac{in^2}{ft} + 0.388 \frac{in^2}{ft} + .085 \frac{in^2}{ft} = 0.590 \frac{in^2}{ft}$$

$$A_3 = 0.7 \left(0.233 \frac{in^2}{ft} + 0.388 \frac{in^2}{ft} \right) + .085 \frac{in^2}{in} = 0.520 \frac{in^2}{ft}$$

And the design value would be 0.590in²/ft. Since these two values are in the same design region, 0.590in²/ft would control and would become the design value for that region, if there were no other locations which required more reinforcing.

Similarly, using the combination formula to calculate the reinforcing requirements for both positive and negative moment at each point in exterior and interior webs for each design region leads to the following web reinforcing

[5.7.3.1]
[5.7.3.2]

Design Region	Required Distance	Use	Provided Reinforcing (in ² /ft)
1	0.590	#5@6"	0.620
2	0.515	#5@7"	0.531
3	0.581	#5@6"	0.620
4	0.696	#5@5"	0.744
5	0.796	#6@6"	0.880
6	0.581	#5@6"	0.620
7	0.556	#5@6"	0.620

Table D.33 – Final Web Reinforcing at Each Face of Each Web

9.4 Principal Tension

[5.8.5]

The LRFD Design Specifications state that the principal stresses in the webs shall be analyzed for all segmental bridges. It does not give direction on non-segmental concrete box girder bridges. However, it is a good design check and the calculation of principal stresses is included in this example, because such a check will help prevent web cracking at the service level.

The principal tensile stresses are calculated using the long-term residual axial stress and the maximum shear stress. The Service III Limit State load combination is used for both axial and shear stresses.

The critical section with the maximum principal tensile stress is located just upstation of Pier 2, a distance of d_v (approximately 5.0 ft) from the diaphragm (Node 27). See section 5 above for the calculation of d_v . In this case, as discussed in section 6, torsion need not be included. However, the principal tension will be calculated at the critical location including torsion, as an example of how to calculate the effects of torsion.

Shear Stress from Vertical Shear

From general mechanics of materials, the shear stress can be taken as:

$$\tau = \frac{VQ}{Ibn_w}$$

where,

$$\begin{aligned} V &= \text{vertical shear in section} \\ &= V_{DC} + V_{DW} + V_{PS} + V_{CR+SH} + 0.8 \cdot V_{LL+I} \\ &= 1216.3 \text{ kips} \\ Q &= \text{first moment of the area} = 96.0 \text{ ft}^3 \\ I &= \text{section moment of inertia} = 572.7 \text{ ft}^4 \\ b &= \text{web width less } \frac{1}{4} \text{ duct } \emptyset = 0.906 \text{ ft} \\ n_w &= \text{number of webs} = 3 \end{aligned}$$

$$\rightarrow \tau = \frac{1216.3 \text{ kips} \cdot 96.0 \text{ ft}^3}{572.7 \text{ ft}^4 \cdot 0.906 \text{ ft} \cdot 3} = 75.0 \text{ ksf}$$

This calculation assumes that the shear effects all webs equally, and is conservative due to the fact that the load distribution in section 3 calculated the largest load to one web (the center one, in this case) then applied this value to all the webs to get the total load on the bridge.

Shear Stress from Torsion

[C5.8.2.1]

According to section 6, torsion need not be included in this design. Calculations are presented here as an example only.

In a box girder, St. Venant Torsion (the dominant effect) produces shear in the exterior webs. In one exterior web it adds to the vertical shear, and in the other it subtracts from it. On the interior webs, the shears from this torsion cancel. Typically, when torsion is included, it is calculated in the critical web and the required reinforcing is used in all webs for simplicity of placement.

Mechanics of materials gives the shear flow around a box as:

$$q = \frac{T}{2A_o}$$

$$\begin{aligned} \text{where, } T &= \text{Torsion at the section} \\ &= T_{DC} + T_{DW} + T_{PS} + T_{CR+SH} + 0.8 \cdot T_{LL+I} \\ &= 1366.5 \text{ ft-kips} \end{aligned}$$

$$A_o = \text{as defined in LRFD 5.8.2.1} = 203.2 \text{ ft}^2$$

$$\rightarrow q_T = \frac{1366.5 \text{ ft} \cdot \text{kips}}{2 \cdot 203.2 \text{ ft}^2} = 3.36 \frac{\text{kips}}{\text{ft}}$$

This value has units of force per unit length, and represents the force acting along the web. To calculate the shear stress in the web, simply divide by the effective thickness of the web, b_v :

$$\tau_T = \frac{q_T}{b_v} = \frac{3.36 \frac{\text{kips}}{\text{ft}}}{0.906 \text{ ft}} = 3.7 \text{ ksf}$$

In this case, the shear stress due to torsion, 3.7ksf, is about 5 percent of the shear stress due to vertical shear, 75.0 ksf.

Mohr's Circle

Using Mohr's circle, the principal tension can be calculated at the neutral axis:

The normal stress at Node 27 is:

$$\sigma = \sigma_{DC} + \sigma_{DW} + \sigma_{PS} + \sigma_{CR+SH} = -83.5 \text{ ksf}$$

From Mohr's circle, the radius, R , and then the principal stress, σ_p , can be calculated with and without torsion.

With torsion,

$$R = \sqrt{\left(\frac{\sigma}{2}\right)^2 + (\tau + \tau_T)^2} = \sqrt{(-41.75)^2 + 78.7^2} = 89.1 \text{ ksf}$$

$$\rightarrow \sigma_p = \frac{\sigma}{2} + R = -41.75 + 89.1 = 47.4 \text{ ksf}$$

Without torsion,

$$R = \sqrt{\left(\frac{\sigma}{2}\right)^2 + (\tau)^2} = \sqrt{(-41.75)^2 + 75.0^2} = 85.8 \text{ ksf}$$

$$\rightarrow \sigma_p = \frac{\sigma}{2} + R = -41.75 + 85.8 = 44.1 \text{ ksf}$$

However, the maximum allowable principal tension is:

$$0.110\sqrt{f'_c} \text{ (ksi)} = 3.5\sqrt{f'_c} \text{ (psi)} = 39 \text{ (ksf)} \text{ for } 6000 \text{ psi concrete}$$

At this location, both with and without torsion included, the principal tension is greater than the allowable. In order to reduce the principal tension, several options are available:

- Increase the axial stress by adding post-tensioning.
- Increase the thickness of the webs locally.
- Increase the strength of the concrete.

Of the above solutions, locally thickening the webs is the simplest for a cast-in-place structure. The webs can be tapered from 1 ft thick at 10 ft from the pier to 1'-6" at the pier. Thus, at 5 ft from the pier, they will be 1'-3" thick, with $b_v=1.156$ ft.

The revised section properties at Nodes 27 and 25, with 1'-3" thick webs are:

$$A = 96.0 \text{ ft}^3$$

$$Q = 96.0 \text{ ft}^3$$

$$I = 572.7 \text{ ft}^4$$

$$B = 0.906 \text{ ft}$$

Recalculating the principal tension with the revised section at the critical location shows that the principal tension is now below the required value. Note that for such a modest, localized web thickening, it is unnecessary to recalculate the remainder of the design values.

The table below contains a summary of the principal tension check at the same locations that were used for shear. Torsion is not explicitly included.

Node	b_v (ft)	τ (ksf)	θ (ksf)	Radius (ksf)	θ_p (ksf)	$\sqrt{f'_c}$ (psi)
3	0.906	35.2	-83.6	54.7	12.9	1.15
7	0.906	22.2	-85.2	48.1	5.4	0.49
11	0.906	10.3	-86.8	44.6	1.2	0.11
14	0.906	14.9	-88.0	46.4	2.4	0.22
17	0.906	18.7	-88.9	48.2	3.8	0.34
21	0.906	24.8	-87.2	50.1	6.6	0.59
25	1.156	51.1	-83.1	65.9	24.3	2.22
27	1.156	58.8	-79.2	70.9	31.3	2.85
31	0.906	28.6	-80.8	49.5	9.1	0.81
35	0.906	22.1	-79.6	45.5	5.7	0.51
39	0.906	15.3	-78.3	42.0	2.9	0.26
42	0.906	9.9	-77.4	39.9	1.3	0.11

Table D.34 – Results of Principal Tension Check

9.5 Longitudinal Shear Reinforcing

[5.8.3.5]

The longitudinal reinforcing required for shear is calculated using values already known from the calculations. The table below shows that the prestressing alone is sufficient.

Node	M _u (k-ft)	d _v (ft)	V _u (k)	V _p (k)	V _s (k)	Cotθ	Required A _{ps} f _{ps} (k)	Provided A _{ps} f _{ps} (k)
3	6393	5.04	1465.3	279.8	714.7	1.7	2964	9741
7	25017	5.04	925.3	136.9	250.8	1.7	6285	9790
21	12135	5.04	1512.4	589.6	442.6	1.7	3922	9640
25	36148	5.04	2001.6	264.8	1319.6	1.7	9412	9748
27	35606	5.04	2150.5	167.7	1588.4	1.7	9506	9748
31	6132	5.04	1671.8	594.8	640.5	1.7	2807	9649

Table D.35 – Verification of Longitudinal Shear Reinforcing

9.6 Duct Pull-Out

[5.10.4.3]

Post-tensioning ducts in curved webs apply lateral pressure to the webs. In addition to the regional web bending discussed earlier, local forces must also be addressed.

Ducts are assumed to be supported in the center of a web. Thus, the cover to the ducts, d_c, in these calculations is 3.75 inches. It is also assumed that the tendons are stressed to 75 percent of their capacity, when the concrete strength is 4500 psi. The center-to-center spacing of the ducts is 6.5 inches, and the clear space between ducts is 2 inches.

[5.10.4.3.1b]

$$\phi V_n = \phi \cdot 0.15 d_{eff} \sqrt{f'_{ci}}$$

$$d_{eff} = 3.75in + \frac{4.5in}{4} = 4.875in$$

$$\phi V_n = 0.75 \cdot 0.15 \cdot 4.875in \cdot \sqrt{4.5ksi} = 1.16 \frac{kips}{in}$$

[5.10.4.3.1a]

$$F_{u-in} = \frac{P_u}{R} = \frac{1.2 \cdot 0.75 (3 \cdot 19str) 0.217 \frac{in^2}{str} \cdot 270ksi}{584ft \cdot 12 \frac{in}{ft}} = 0.428 \frac{kips}{in}$$

[5.10.4.3.2]

Out-of-plane forces must also be added to F_{u-in}. The minimum radius on a tendon occurs on the lowest tendon as it crosses the pier, and the average radius in that region is 162.2 ft. The out-of-plane force

$$F_{u-out} = \frac{P_u}{\pi R}$$

$$F_{u-out} = \frac{1.2 \cdot 0.75 (3 \cdot 19 \text{str}) 0.217 \frac{\text{in}^2}{\text{str}} \cdot 270 \text{ksi}}{\pi \cdot 162.2 \text{ft} \cdot 12 \frac{\text{in}}{\text{ft}}} = 0.48 \frac{\text{kips}}{\text{in}}$$

$$F_{u-TOTAL} = F_{u-in} + F_{u-out} = 0.428 \frac{\text{kips}}{\text{in}} + 0.48 \frac{\text{kips}}{\text{in}} = 0.91 \frac{\text{kips}}{\text{in}}$$

Thus, since $F_{u-TOTAL}$ is less than ϕV_n , no ties are necessary.

[5.10.4.3.1d]

The 2 inch clear duct spacing must also be checked against the in-plane radius of the vertical duct curvature, to insure that stressing a tendon does not cause a shear failure that crushes an adjacent duct. Using the previous value of $R=162.2$ ft,

$$d_{eff} = 2\text{in} + \frac{4.5\text{in}}{4} = 3.125\text{in}$$

$$\phi V_n = 0.75 \cdot 0.15 \cdot 3.125\text{in} \cdot \sqrt{4.5\text{ksi}} = 0.75 \frac{\text{kips}}{\text{in}}$$

$$F_{u-in} = \frac{1.2 \cdot 0.75 (19 \text{str}) 0.217 \frac{\text{in}^2}{\text{str}} \cdot 270 \text{ksi}}{162.2 \text{ft} \cdot 12 \frac{\text{in}}{\text{ft}}} = 0.51 \frac{\text{kips}}{\text{in}}$$

Thus, the 2 inch clear spacing between ducts will not require additional ties.